

c growth in the availability of powerful com-
EM community lacks a comprehensive text
il techniques used to solve EM problems. The
erical Techniques in Electromagnetics filled
e the reference of choice for thousands of en-
, and students.

the bestselling text reflects the continuing in-
and use of numerical techniques and incor-
nd refinements made in recent years. Most
are the improvements made to the standard
e-difference time-domain (FDTD) method and
ing boundary conditions in FDTD, finite elec-
on-line-matrix methods. The author also has
the method of lines.

ues in Electromagnetics with MATLAB®,
ues to teach readers how to pose, numeri-
olve EM problems, to give them the ability to
n-solving skills using a variety of methods,
for research in electromagnetism. Now the
en further toward providing a comprehen-
addresses all of the most useful computa-
blems and includes MATLAB code instead of

Numerical techniques



کتابخانه مرکزی

۶۳۰۹۷

ISBN: ۹۷۸-۱-۴۲۰۰-۶۳۰۹-۷
90000
9 781420 063097

THIRD
EDITION

Numerical Techniques in
Electromagnetics with MATLAB®

QC
760
.S24
2009



THIRD EDITION

Numerical Techniques in
ELECTROMAGNETICS
with MATLAB®

MATTHEW N. O. SADIQU

CRC Press
Taylor & Francis Group

THIRD EDITION

**Numerical Techniques in
ELECTROMAGNETICS
with MATLAB®**

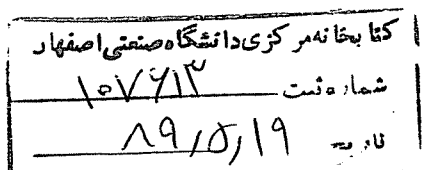
QC
460
S24
2009

49285
R

107613
~9/21/14

THIRD EDITION

Numerical Techniques in
ELECTROMAGNETICS
with MATLAB®



MATTHEW N. O. SADIQU

Prairie View A&M University
Texas, U.S.A.



CRC Press
Taylor & Francis Group
Boca Raton London New York

CRC Press is an imprint of the
Taylor & Francis Group, an Informa business

MATLAB® is a trademark of The MathWorks, Inc. and is used with permission. The MathWorks does not warrant the accuracy of the text or exercises in this book. This book's use or discussion of MATLAB® software or related products does not constitute endorsement or sponsorship by The MathWorks of a particular pedagogical approach or particular use of the MATLAB® software.

CRC Press
Taylor & Francis Group
6000 Broken Sound Parkway NW, Suite 300
Boca Raton, FL 33487-2742

© 2009 by Taylor & Francis Group, LLC
CRC Press is an imprint of Taylor & Francis Group, an Informa business

No claim to original U.S. Government works
Printed in the United States of America on acid-free paper
10 9 8 7 6 5 4 3 2

International Standard Book Number-13: 978-1-4200-6309-7 (Hardcover)

This book contains information obtained from authentic and highly regarded sources. Reasonable efforts have been made to publish reliable data and information, but the author and publisher cannot assume responsibility for the validity of all materials or the consequences of their use. The authors and publishers have attempted to trace the copyright holders of all material reproduced in this publication and apologize to copyright holders if permission to publish in this form has not been obtained. If any copyright material has not been acknowledged please write and let us know so we may rectify in any future reprint.

Except as permitted under U.S. Copyright Law, no part of this book may be reprinted, reproduced, transmitted, or utilized in any form by any electronic, mechanical, or other means, now known or hereafter invented, including photocopying, microfilming, and recording, or in any information storage or retrieval system, without written permission from the publishers.

For permission to photocopy or use material electronically from this work, please access www.copyright.com (<http://www.copyright.com/>) or contact the Copyright Clearance Center, Inc. (CCC), 222 Rosewood Drive, Danvers, MA 01923, 978-750-8400. CCC is a not-for-profit organization that provides licenses and registration for a variety of users. For organizations that have been granted a photocopy license by the CCC, a separate system of payment has been arranged.

Trademark Notice: Product or corporate names may be trademarks or registered trademarks, and are used only for identification and explanation without intent to infringe.

Visit the Taylor & Francis Web site at
<http://www.taylorandfrancis.com>

and the CRC Press Web site at
<http://www.crcpress.com>

Dedication

To my teacher

Carl A. Ventrice

and my parents

Ayisat and Solomon Sadiku

Contents

Preface	xiii
Author	xvii
1 Fundamental Concepts	1
1.1 Introduction	1
1.2 Review of Electromagnetic Theory	2
1.2.1 Electrostatic Fields	3
1.2.2 Magnetostatic Fields	4
1.2.3 Time-Varying Fields	5
1.2.4 Boundary Conditions	7
1.2.5 Wave Equations	7
1.2.6 Time-Varying Potentials	9
1.2.7 Time-Harmonic Fields	10
1.3 Classification of EM Problems	14
1.3.1 Classification of Solution Regions	14
1.3.2 Classification of Differential Equations	15
1.3.3 Classification of Boundary Conditions	18
1.4 Some Important Theorems	20
1.4.1 Superposition Principle	20
1.4.2 Uniqueness Theorem	21
References	23
Problems	23
2 Analytical Methods	27
2.1 Introduction	27
2.2 Separation of Variables	28
2.3 Separation of Variables in Rectangular Coordinates	30
2.3.1 Laplace's Equation	30
2.3.2 Wave Equation	34
2.4 Separation of Variables in Cylindrical Coordinates	39
2.4.1 Laplace's Equation	40
2.4.2 Wave Equation	42
2.5 Separation of Variables in Spherical Coordinates	53
2.5.1 Laplace's Equation	54
2.5.2 Wave Equation	59

2.6	Some Useful Orthogonal Functions	68
2.7	Series Expansion	78
2.7.1	Poisson's Equation in a Cube	78
2.7.2	Poisson's Equation in a Cylinder	79
2.7.3	Strip Transmission Line	82
2.8	Practical Applications	87
2.8.1	Scattering by Dielectric Sphere	87
2.8.2	Scattering Cross Sections	91
2.9	Attenuation Due to Raindrops	94
2.10	Concluding Remarks	102
	References	102
	Problems	103
3	Finite Difference Methods	119
3.1	Introduction	119
3.2	Finite Difference Schemes	120
3.3	Finite Differencing of Parabolic PDEs	123
3.4	Finite Differencing of Hyperbolic PDEs	129
3.5	Finite Differencing of Elliptic PDEs	132
3.5.1	Band Matrix Method	135
3.5.2	Iterative Methods	135
3.6	Accuracy and Stability of FD Solutions	142
3.7	Practical Applications I — Guided Structures	146
3.7.1	Transmission Lines	146
3.7.2	Waveguides	153
3.8	Practical Applications II — Wave Scattering (FDTD)	159
3.8.1	Yee's Finite Difference Algorithm	159
3.8.2	Accuracy and Stability	163
3.8.3	Lattice Truncation Conditions	163
3.8.4	Initial Fields	166
3.8.5	Programming Aspects	167
3.9	Absorbing Boundary Conditions for FDTD	181
3.10	Finite Differencing for Nonrectangular Systems	185
3.10.1	Cylindrical Coordinates	185
3.10.2	Spherical Coordinates	189
3.11	Numerical Integration	194
3.11.1	Euler's Rule	195
3.11.2	Trapezoidal Rule	196
3.11.3	Simpson's Rule	197
3.11.4	Newton-Cotes Rules	197
3.11.5	Gaussian Rules	199
3.11.6	Multiple Integration	202
3.12	Concluding Remarks	208
	References	210
	Problems	219

4	Variational Methods	235
4.1	Introduction	235
4.2	Operators in Linear Spaces	236
4.3	Calculus of Variations	238
4.4	Construction of Functionals from PDEs	242
4.5	Rayleigh-Ritz Method	245
4.6	Weighted Residual Method	252
4.6.1	Collocation Method	253
4.6.2	Subdomain Method	254
4.6.3	Galerkin Method	254
4.6.4	Least Squares Method	255
4.7	Eigenvalue Problems	261
4.8	Practical Applications	268
4.9	Concluding Remarks	275
	References	276
	Problems	280
5	Moment Methods	285
5.1	Introduction	285
5.2	Integral Equations	286
5.2.1	Classification of Integral Equations	286
5.2.2	Connection Between Differential and Integral Equations	287
5.3	Green's Functions	290
5.3.1	For Free Space	292
5.3.2	For Domain with Conducting Boundaries	295
5.4	Applications I — Quasi-Static Problems	308
5.5	Applications II — Scattering Problems	314
5.5.1	Scattering by Conducting Cylinder	314
5.5.2	Scattering by an Arbitrary Array of Parallel Wires	317
5.6	Applications III — Radiation Problems	323
5.6.1	Hallen's Integral Equation	325
5.6.2	Pocklington's Integral Equation	326
5.6.3	Expansion and Weighting Functions	326
5.7	Applications IV — EM Absorption in the Human Body	337
5.7.1	Derivation of Integral Equations	338
5.7.2	Transformation to Matrix Equation (Discretization)	341
5.7.3	Evaluation of Matrix Elements	342
5.7.4	Solution of the Matrix Equation	344
5.8	Concluding Remarks	355
	References	356
	Problems	362

6 Finite Element Method	379
6.1 Introduction	379
6.2 Solution of Laplace's Equation	380
6.2.1 Finite Element Discretization	380
6.2.2 Element Governing Equations	380
6.2.3 Assembling of All Elements	382
6.2.4 Solving the Resulting Equations	385
6.3 Solution of Poisson's Equation	388
6.3.1 Deriving Element-Governing Equations	398
6.3.2 Solving the Resulting Equations	399
6.4 Solution of the Wave Equation	400
6.5 Automatic Mesh Generation I — Rectangular Domains	402
6.6 Automatic Mesh Generation II — Arbitrary Domains	407
6.6.1 Definition of Blocks	409
6.6.2 Subdivision of Each Block	409
6.6.3 Connection of Individual Blocks	412
6.7 Bandwidth Reduction	413
6.8 Higher Order Elements	413
6.8.1 Pascal Triangle	419
6.8.2 Local Coordinates	420
6.8.3 Shape Functions	421
6.8.4 Fundamental Matrices	423
6.9 Three-Dimensional Elements	425
6.10 Finite Element Methods for Exterior Problems	435
6.10.1 Infinite Element Method	440
6.10.2 Boundary Element Method	440
6.10.3 Absorbing Boundary Condition	442
6.11 Finite-Element Time-Domain Method	442
6.12 Concluding Remarks	444
References	446
Problems	446
7 Transmission-Line-Matrix Method	465
7.1 Introduction	465
7.2 Transmission-Line Equations	467
7.3 Solution of Diffusion Equation	471
7.4 Solution of Wave Equations	471
7.4.1 Equivalence Between Network and Field Parameters	476
7.4.2 Dispersion Relation of Propagation Velocity	476
7.4.3 Scattering Matrix	479
7.4.4 Boundary Representation	481
7.4.5 Computation of Fields and Frequency Response	484
7.4.6 Output Response and Accuracy of Results	485
7.5 Inhomogeneous and Lossy Media in TLM	485
7.5.1 General Two-Dimensional Shunt Node	490
	492

7.5.2 Scattering Matrix	494
7.5.3 Representation of Lossy Boundaries	495
7.6 Three-Dimensional TLM Mesh	499
7.6.1 Series Nodes	500
7.6.2 Three-Dimensional Node	502
7.6.3 Boundary Conditions	507
7.7 Error Sources and Correction	515
7.7.1 Truncation Error	516
7.7.2 Coarseness Error	516
7.7.3 Velocity Error	517
7.7.4 Misalignment Error	517
7.8 Absorbing Boundary Conditions	517
7.9 Concluding Remarks	519
References	521
Problems	527
8 Monte Carlo Methods	535
8.1 Introduction	535
8.2 Generation of Random Numbers and Variables	536
8.3 Evaluation of Error	539
8.4 Numerical Integration	544
8.4.1 Crude Monte Carlo Integration	544
8.4.2 Monte Carlo Integration with Antithetic Variates	546
8.4.3 Improper Integrals	547
8.5 Solution of Potential Problems	549
8.5.1 Fixed Random Walk	549
8.5.2 Floating Random Walk	554
8.5.3 Exodus Method	557
8.6 Regional Monte Carlo Methods	571
8.7 Time-Dependent Problems	579
8.8 Concluding Remarks	585
References	586
Problems	592
9 Method of Lines	603
9.1 Introduction	603
9.2 Solution of Laplace's Equation	604
9.2.1 Rectangular Coordinates	604
9.2.2 Cylindrical Coordinates	611
9.3 Solution of Wave Equation	615
9.3.1 Planar Microstrip Structures	618
9.3.2 Cylindrical Microstrip Structures	627
9.4 Time-Domain Solution	632
9.5 Concluding Remarks	634
References	635

Problems	640
A Vector Relations	645
A.1 Vector Identities	645
A.2 Vector Theorems	645
A.3 Orthogonal Coordinates	646
B Programming in MATLAB	649
B.1 MATLAB Fundamentals	649
B.2 Using MATLAB to Plot	653
B.3 Programming with MATLAB	656
B.4 Functions	660
B.5 Solving Equations	661
B.6 Programming Hints	663
B.7 Other Useful MATLAB Commands	664
C Solution of Simultaneous Equations	665
C.1 Elimination Methods	665
C.1.1 Gauss's Method	666
C.1.2 Cholesky's Method	667
C.2 Iterative Methods	670
C.2.1 Jacobi's Method	670
C.2.2 Gauss-Seidel Method	672
C.2.3 Relaxation Method	673
C.2.4 Gradient Methods	674
C.3 Matrix Inversion	677
C.4 Eigenvalue Problems	678
C.4.1 Iteration (or Power) Method	680
C.4.2 Jacobi's Method	681
References	686
D Answers to Odd-Numbered Problems	687
Index	707

Preface

When I was first approached by CRC Press to work on the third edition of this book, I declined because I felt that not much had changed in computational electromagnetics since the second edition came out.

The art of computation of electromagnetic (EM) problems has grown exponentially for three decades due to the availability of powerful computer resources. In spite of this, the EM community has suffered without a suitable text on the computational techniques commonly used in solving EM-related problems. Although there have been monographs on one particular technique or another, the monographs are written for the experts rather than students. Only a few texts cover the major techniques and do that in a manner suitable for classroom use. It seems experts in this area are familiar with one or a few techniques but not many seem to be familiar with all the common techniques. This text attempts to fill that gap.

The text is intended for seniors or graduate students and may be used for a one-semester or two-semester course. The main requirements for students taking a course based on this text are introductory EM courses and knowledge of a high-level computer language. Because all the computer codes in the text are in MATLABTM, it is presumed that the students have basic knowledge of MATLAB. Although familiarity with linear algebra and numerical analysis is useful, it is not required.

In writing this book, three major objectives were borne in mind. First, the book is intended to teach students how to pose, numerically analyze, and solve EM problems. Second, it is designed to give them the ability to expand their problem-solving skills using a variety of available numerical methods. Third, it is meant to prepare graduate students for research in EM. The aim throughout has been simplicity of presentation so that the text can be useful for both teaching and self-study. In striving after simplicity, however, the reader is referred to the references for more information. Toward the end of each chapter, the techniques covered in the chapter are applied to real life problems. Since the applications of the technique are as vast as EM and author's experience is limited, the choice of application is selective.

The book is divided into nine chapters and four appendices. Chapter 1 covers some fundamental concepts in EM. Chapter 2 is intended to put numerical methods in a proper perspective. Analytical methods such as separation of variables and series expansion are covered. Chapter 3 discusses the finite difference methods and begins with the derivation of a difference equation from a partial differential equation (PDE) using forward, backward, and central differences. The finite-difference time-domain (FDTD) technique involving Yee's algorithm is presented and applied to scattering

problems. Numerical integration is covered using trapezoidal, Simpson's, Newton-Cotes rules, and Gaussian quadratures.

Chapter 4 on variational methods serves as a preparatory ground for the next two chapters: moment methods and finite element methods. Basic concepts such as inner product, self-adjoint operator, functionals, and Euler equation are covered. Chapter 5 on moment methods focuses on the solution of integral equations. Chapter 6 on the finite element method covers the basic steps involved in using the finite element. Solutions of Laplace's, Poisson's, and wave equations using the finite element method are covered.

Chapter 7 is devoted to transmission-line-matrix or modeling (TLM). The method is applied to diffusion and scattering problems. Chapter 8 is about Monte Carlo methods, which include fixed random walk, floating random walk, and the exodus method. Chapter 9 is on the method of lines.

Appendix A is on vector relations, while Appendix B provides basic programming in MATLAB. Appendix C briefly covers direct and iterative procedures for solving simultaneous equations. Appendix D provides answers to odd-numbered problems.

Since the publication of the second edition, there have been increased awareness and utilization of numerical techniques. Many graduate curricula now include courses in numerical analysis of EM problems. However, not much has changed in computational electromagnetics. A major noticeable change is in the FDTD method. The method seems to have attracted much attention and many improvements are being made to the standard algorithm. This edition adds noticeable changes in Section 6.11 on the finite-element time-domain method and in Section 8.7 on how to apply Monte Carlo methods to solve time-dependent problems.

Acknowledgments

I want to thank Richard Allred for converting all the FORTRAN codes in the previous editions to MATLAB. I also owe special thanks to Dr. Sudarshan Nelatury for helping in the conversion. I would like to acknowledge the support of Dr. Kendall Harris, dean of the College of Engineering, and Dr. John Attia, head of the Department of Electrical and Computer Engineering, at Prairie View A&M University. I am also grateful to the staff at CRC Press for their interest, commitment, support, and production of the third edition. I express my profound gratitude to my wife, Kikelomo, and our daughters, Motunrayo, Ann, and Joyce, for their patience, sacrifices, understanding, and prayer.

A Note to Students

Before you embark on writing your own computer program or using the ones in this text, you should try to understand all relevant theoretical backgrounds. A computer is no more than a tool used in the analysis of a program. For this reason, you should be as clear as possible what the machine is really being asked to do before setting it off on several hours of expensive computations.

It has been well said by A.C. Doyle that "It is a capital mistake to theorize before you have all the evidence. It biases the judgment." Therefore, you should never trust the results of numerical computation unless they are validated, as least in part. You validate the results by comparing them with those obtained by previous investigators or with similar results obtained using a different approach, which may be analytical or numerical. For this reason, it is advisable that you become familiar with as many numerical techniques as possible.

The references provided at the end of each chapter are by no means exhaustive but are meant to serve as the starting point for further reading.

Author

Matthew N. O. Sadiku received his B.Sc. degree in 1978 from Ahmadu Bello University, Zaria, Nigeria, and his M.Sc. and Ph.D. degrees from Tennessee Technological University, Cookeville, Tennessee, in 1982 and 1984, respectively. From 1984 to 1988, he was an assistant professor at Florida Atlantic University, where he did graduate work in computer science. From 1988 to 2000, he was at Temple University, Philadelphia, Pennsylvania, where he became a full professor. From 2000 to 2002, he was with Lucent/Avaya, Holmdel, New Jersey, as a system engineer and with Boeing Satellite Systems as a senior scientist. He is presently a professor at Prairie View A&M University, Prairie View, Texas.

He is the author of over 180 professional papers and 30 books including *Elements of Electromagnetics* (Oxford, 4th ed., 2007), *Fundamentals of Electric Circuits* (McGraw-Hill, 4th ed., 2009, with C. Alexander), *Numerical Techniques in Electromagnetics* (CRC, 3rd ed., 2009), and *Metropolitan Area Networks* (CRC Press, 1995). Some of his books have been translated into Korean, Chinese (and Chinese Long Form in Taiwan), Italian, Portuguese, and Spanish. He was the recipient of the 2000 McGraw-Hill/Jacob Millman Award for outstanding contributions in the field of electrical engineering.

His current research interests are in the areas of numerical modeling of electromagnetic systems and computer communication networks. He is a registered professional engineer and a senior member of the Institute of Electrical and Electronics Engineers (IEEE). He has been the IEEE Region 2 Student Activities Committee Chairman. He has been an associate editor for *IEEE Transactions on Education*.

Chapter 1

Fundamental Concepts

If the only tool you have is a hammer, all problems begin to look like nails.

-Abraham Maslow

1.1 Introduction

Scientists and engineers use several techniques in solving continuum or field problems. Loosely speaking, these techniques can be classified as experimental, analytical, or numerical. Experiments are expensive, time consuming, sometimes hazardous, and usually do not allow much flexibility in parameter variation. However, every numerical method, as we shall see, involves an analytic simplification to the point where it is easy to apply the numerical method. Notwithstanding this fact, the following methods are among the most commonly used in electromagnetics (EM).

A. Analytical methods (exact solutions)

- (1) separation of variables
- (2) series expansion
- (3) conformal mapping
- (4) integral solutions, e.g., Laplace and Fourier transforms
- (5) perturbation methods

B. Numerical methods (approximate solutions)

- (1) finite difference method
- (2) method of weighted residuals
- (3) moment method
- (4) finite element method
- (5) transmission-line modeling
- (6) Monte Carlo method
- (7) method of lines

Application of these methods is not limited to EM-related problems; they find applications in other continuum problems such as in fluid, heat transfer, and acoustics [1].

As we shall see, some of the numerical methods are related and they all generally give approximate solutions of sufficient accuracy for engineering purposes. Since our objective is to study these methods in detail in the subsequent chapters, it may be premature to say more than this at this point.

The need for numerical solution of electromagnetic problems is best expressed in the words of Paris and Hurd: "Most problems that can be solved formally (analytically) have been solved."¹ Until the 1940s, most EM problems were solved using the classical methods of separation of variables and integral equation solutions. Besides the fact that a high degree of ingenuity, experience, and effort were required to apply those methods, only a narrow range of practical problems could be investigated due to the complex geometries defining the problems.

Numerical solution of EM problems started in the mid-1960s with the availability of modern high-speed digital computers. Since then, considerable effort has been expended on solving practical, complex EM-related problems for which closed form analytical solutions are either intractable or do not exist. The numerical approach has the advantage of allowing the actual work to be carried out by operators without a knowledge of higher mathematics or physics, with a resulting economy of labor on the part of the highly trained personnel.

Before we set out to study the various techniques used in analyzing EM problems, it is expedient to remind ourselves of the physical laws governing EM phenomena in general. This will be done in Section 1.2. In Section 1.3, we shall become acquainted with different ways EM problems are categorized. The principle of superposition and the uniqueness theorem will be covered in Section 1.4.

1.2 Review of Electromagnetic Theory

The whole subject of EM unfolds as a logical deduction from eight postulated equations, namely, Maxwell's four field equations and four medium-dependent equations [2]–[4]. Before we briefly review these equations, it may be helpful to state two important theorems commonly used in EM. These are the divergence (or Gauss's) theorem,

$$\oint_S \mathbf{F} \cdot d\mathbf{S} = \int_V \nabla \cdot \mathbf{F} dv \quad (1.1)$$

¹Basic Electromagnetic Theory, D.T. Paris and F.K. Hurd, McGraw-Hill, New York, 1969, p. 166.

1.2. REVIEW OF ELECTROMAGNETIC THEORY

and Stokes's theorem

$$\oint_L \mathbf{F} \cdot d\mathbf{l} = \int_S \nabla \times \mathbf{F} \cdot d\mathbf{S} \quad (1.2)$$

Perhaps the best way to review EM theory is by using the fundamental concept of electric charge. EM theory can be regarded as the study of fields produced by electric charges at rest and in motion. Electrostatic fields are usually produced by static electric charges, whereas magnetostatic fields are due to motion of electric charges with uniform velocity (direct current). Dynamic or time-varying fields are usually due to accelerated charges or time-varying currents.

1.2.1 Electrostatic Fields

The two fundamental laws governing these electrostatic fields are Gauss's law,

$$\oint \mathbf{D} \cdot d\mathbf{S} = \int \rho_v dv \quad (1.3)$$

which is a direct consequence of Coulomb's force law, and the law describing electrostatic fields as conservative,

$$\oint \mathbf{E} \cdot d\mathbf{l} = 0 \quad (1.4)$$

In Equations (1.3) and (1.4),

\mathbf{D} = the electric flux density (in coulombs/meter²)

ρ_v = the volume charge density (in coulombs/meter³)

\mathbf{E} = the electric field intensity (in volts/meter)

The integral form of the laws in Equations (1.3) and (1.4) can be expressed in the differential form by applying Equation (1.1) to Equation (1.3) and Equation (1.2) to Equation (1.4). We obtain

$$\nabla \cdot \mathbf{D} = \rho_v \quad (1.5)$$

and

$$\nabla \times \mathbf{E} = 0 \quad (1.6)$$

The vector fields \mathbf{D} and \mathbf{E} are related as

$$\mathbf{D} = \epsilon \mathbf{E} \quad (1.7)$$

where ϵ is the dielectric permittivity (in farads/meter) of the medium. In terms of the electric potential V (in volts), \mathbf{E} is expressed as

$$\mathbf{E} = -\nabla V \quad (1.8)$$

or

$$V = - \int \mathbf{E} \cdot d\mathbf{l} \quad (1.9)$$

Combining Equations (1.5), (1.7), and (1.8) gives Poisson's equation:

$$\nabla \cdot \epsilon \nabla V = -\rho_v \quad (1.10a)$$

or, if ϵ is constant,

$$\boxed{\nabla^2 V = -\frac{\rho_v}{\epsilon}} \quad (1.10b)$$

When $\rho_v = 0$, Equation (1.10) becomes Laplace's equation:

$$\nabla \cdot \epsilon \nabla V = 0 \quad (1.11a)$$

or for constant ϵ

$$\boxed{\nabla^2 V = 0} \quad (1.11b)$$

1.2.2 Magnetostatic Fields

The basic laws of magnetostatic fields are Ampere's law

$$\oint_L \mathbf{H} \cdot d\mathbf{l} = \int_S \mathbf{J}_e \cdot d\mathbf{S} \quad (1.12)$$

which is related to Biot-Savart law, and the law of conservation of magnetic flux (also called Gauss's law for magnetostatics)

$$\oint_S \mathbf{B} \cdot d\mathbf{S} = 0 \quad (1.13)$$

where

- \mathbf{H} = the magnetic field intensity (in amperes/meter)
- \mathbf{J}_e = the electric current density (in amperes/meter²)
- \mathbf{B} = the magnetic flux density (in tesla or webers/meter²)

Applying Equation (1.2) to Equation (1.12) and Equation (1.1) to Equation (1.13) yields their differential forms as

$$\nabla \times \mathbf{H} = \mathbf{J}_e \quad (1.14)$$

and

$$\nabla \cdot \mathbf{B} = 0 \quad (1.15)$$

The vector fields \mathbf{B} and \mathbf{H} are related through the permeability μ (in henries/meter) of the medium as

$$\mathbf{B} = \mu \mathbf{H} \quad (1.16)$$

1.2. REVIEW OF ELECTROMAGNETIC THEORY

Also, \mathbf{J}_e is related to \mathbf{E} through the conductivity σ (in mhos/meter) of the medium as

$$\mathbf{J}_e = \sigma \mathbf{E} \quad (1.17)$$

This is usually referred to as point form of Ohm's law. In terms of the magnetic vector potential \mathbf{A} (in Wb/meter)

$$\mathbf{B} = \nabla \times \mathbf{A} \quad (1.18)$$

Applying the vector identity

$$\nabla \times (\nabla \times \mathbf{F}) = \nabla(\nabla \cdot \mathbf{F}) - \nabla^2 \mathbf{F} \quad (1.19)$$

to Equations (1.14) and (1.18) and assuming Coulomb gauge condition ($\nabla \cdot \mathbf{A} = 0$) leads to Poisson's equation for magnetostatic fields:

$$\boxed{\nabla^2 \mathbf{A} = -\mu \mathbf{J}_e} \quad (1.20)$$

When $\mathbf{J}_e = 0$, Equation (1.20) becomes Laplace's equation

$$\boxed{\nabla^2 \mathbf{A} = 0} \quad (1.21)$$

1.2.3 Time-Varying Fields

In this case, electric and magnetic fields exist simultaneously. Equations (1.5) and (1.15) remain the same whereas Equations (1.6) and (1.14) require some modification for dynamic fields. Modification of Equation (1.6) is necessary to incorporate Faraday's law of induction, and that of Equation (1.14) is warranted to allow for displacement current. The time-varying EM fields are governed by physical laws expressed mathematically as

$$\nabla \cdot \mathbf{D} = \rho_v \quad (1.22a)$$

$$\nabla \cdot \mathbf{B} = 0 \quad (1.22b)$$

$$\nabla \times \mathbf{E} = -\frac{\partial \mathbf{B}}{\partial t} - \mathbf{J}_m \quad (1.22c)$$

$$\nabla \times \mathbf{H} = \mathbf{J}_e + \frac{\partial \mathbf{D}}{\partial t} \quad (1.22d)$$

where

$\mathbf{J}_m = \sigma^* \mathbf{H}$ is the magnetic conductive current density (in volts/square meter)

σ^* = the magnetic resistivity (in ohms/meter)

These equations are referred to as Maxwell's equations in the generalized form. They are first-order linear coupled differential equations relating the vector field

quantities to each other. The equivalent integral form of Equation (1.22) is

$$\oint_S \mathbf{D} \cdot d\mathbf{S} = \int_v \rho_v dv \quad (1.23a)$$

$$\oint_S \mathbf{B} \cdot d\mathbf{S} = 0 \quad (1.23b)$$

$$\oint_L \mathbf{E} \cdot d\mathbf{l} = - \int_S \left(\frac{\partial \mathbf{B}}{\partial t} + \mathbf{J}_m \right) \cdot d\mathbf{S} \quad (1.23c)$$

$$\oint_L \mathbf{H} \cdot d\mathbf{l} = \int_S \left(\mathbf{J}_e + \frac{\partial \mathbf{D}}{\partial t} \right) \cdot d\mathbf{S} \quad (1.23d)$$

In addition to these four Maxwell's equations, there are four medium-dependent equations:

$$\mathbf{D} = \epsilon \mathbf{E} \quad (1.24a)$$

$$\mathbf{B} = \mu \mathbf{H} \quad (1.24b)$$

$$\mathbf{J}_e = \sigma \mathbf{E} \quad (1.24c)$$

$$\mathbf{J}_m = \sigma^* \mathbf{M} \quad (1.24d)$$

These are called *constitutive relations* for the medium in which the fields exist. Equations (1.22) and (1.24) form the eight postulated equations on which EM theory unfolds itself. We must note that in the region where Maxwellian fields exist, the fields are assumed to be

- (1) single valued,
- (2) bounded, and
- (3) continuous functions of space and time with continuous derivatives.

It is worthwhile to mention two other fundamental equations that go hand-in-hand with Maxwell's equations. One is the Lorentz force equation

$$\mathbf{F} = Q(\mathbf{E} + \mathbf{u} \times \mathbf{B}) \quad (1.25)$$

where \mathbf{F} is the force experienced by a particle with charge Q moving at velocity \mathbf{u} in an EM field; the Lorentz force equation constitutes a link between EM and mechanics. The other is the continuity equation

$$\nabla \cdot \mathbf{J} = - \frac{\partial \rho_v}{\partial t} \quad (1.26)$$

which expresses the conservation (or indestructibility) of electric charge. The continuity equation is implicit in Maxwell's equations (see Example 1.2). Equation (1.26) is not peculiar to EM. In fluid mechanics, where \mathbf{J} corresponds with velocity and ρ_v with mass, Equation (1.26) expresses the law of conservation of mass.

1.2.4 Boundary Conditions

The material medium in which an EM field exists is usually characterized by its constitutive parameters σ , ϵ , and μ . The medium is said to be *linear* if σ , ϵ , and μ are independent of \mathbf{E} and \mathbf{H} or nonlinear otherwise. It is *homogeneous* if σ , ϵ , and μ are not functions of space variables or inhomogeneous otherwise. It is *isotropic* if σ , ϵ , and μ are independent of direction (scalars) or anisotropic otherwise.

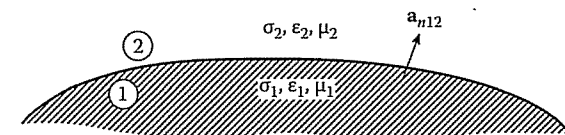


Figure 1.1
Interface between two media.

The boundary conditions at the interface separating two different media 1 and 2, with parameters $(\sigma_1, \epsilon_1, \mu_1)$ and $(\sigma_2, \epsilon_2, \mu_2)$ as shown in Figure 1.1, are easily derived from the integral form of Maxwell's equations. They are

$$E_{1t} = E_{2t} \text{ or } (\mathbf{E}_1 - \mathbf{E}_2) \times \mathbf{a}_{n12} = 0 \quad (1.27a)$$

$$H_{1t} - H_{2t} = K \text{ or } (\mathbf{H}_1 - \mathbf{H}_2) \times \mathbf{a}_{n12} = \mathbf{K} \quad (1.27b)$$

$$D_{1n} - D_{2n} = \rho_s \text{ or } (\mathbf{D}_1 - \mathbf{D}_2) \cdot \mathbf{a}_{n12} = \rho_s \quad (1.27c)$$

$$B_{1n} - B_{2n} = 0 \text{ or } (\mathbf{B}_1 - \mathbf{B}_2) \cdot \mathbf{a}_{n12} = 0 \quad (1.27d)$$

where \mathbf{a}_{n12} is a unit normal vector directed from medium 1 to medium 2, subscripts 1 and 2 denote fields in regions 1 and 2, and subscripts t and n , respectively, denote tangential and normal components of the fields. Equations (1.27a) and (1.27d) state that the tangential components of \mathbf{E} and the normal components of \mathbf{B} are continuous across the boundary. Equation (1.27b) states that the tangential component of \mathbf{H} is discontinuous by the surface current density \mathbf{K} on the boundary. Equation (1.27c) states that the discontinuity in the normal component of \mathbf{D} is the same as the surface charge density ρ_s on the boundary.

In practice, only two of Maxwell's equations are used [Equations (1.22c) and (1.22d)] when a medium is source-free ($\mathbf{J} = 0, \rho_v = 0$) since the other two are implied (see Problem 1.4). Also, in practice, it is sufficient to make the tangential components of the fields satisfy the necessary boundary conditions since the normal components implicitly satisfy their corresponding boundary conditions.

1.2.5 Wave Equations

As mentioned earlier, Maxwell's equations are coupled first-order differential equations which are difficult to apply when solving boundary-value problems. The difficulty is overcome by decoupling the first-order equations, thereby obtaining the wave equation, a second-order differential equation which is useful for solving problems.

To obtain the wave equation for a linear, isotropic, homogeneous, source-free medium ($\rho_v = 0, \mathbf{J} = 0$) from Equation (1.22), we take the curl of both sides of Equation (1.22c). This gives

$$\nabla \times \nabla \times \mathbf{E} = -\mu \frac{\partial}{\partial t} (\nabla \times \mathbf{H}) \quad (1.28)$$

From (1.22d),

$$\nabla \times \mathbf{H} = \epsilon \frac{\partial \mathbf{E}}{\partial t}$$

since $\mathbf{J} = 0$, so that Equation (1.28) becomes

$$\nabla \times \nabla \times \mathbf{E} = -\mu \epsilon \frac{\partial^2 \mathbf{E}}{\partial t^2} \quad (1.29)$$

Applying the vector identity

$$\nabla \times \nabla \times \mathbf{F} = \nabla(\nabla \cdot \mathbf{F}) - \nabla^2 \mathbf{F} \quad (1.30)$$

in Equation (1.29),

$$\nabla(\nabla \cdot \mathbf{E}) - \nabla^2 \mathbf{E} = -\mu \epsilon \frac{\partial^2 \mathbf{E}}{\partial t^2}$$

Since $\rho_v = 0, \nabla \cdot \mathbf{E} = 0$ from Equation (1.22a), and hence we obtain

$$\boxed{\nabla^2 \mathbf{E} - \mu \epsilon \frac{\partial^2 \mathbf{E}}{\partial t^2} = 0} \quad (1.31)$$

which is the time-dependent vector Helmholtz equation or simply wave equation. If we had started the derivation with Equation (1.22d), we would obtain the wave equation for \mathbf{H} as

$$\boxed{\nabla^2 \mathbf{H} - \mu \epsilon \frac{\partial^2 \mathbf{H}}{\partial t^2} = 0} \quad (1.32)$$

Equations (1.31) and (1.32) are the equations of motion of EM waves in the medium under consideration. The velocity (in m/s) of wave propagation is

$$u = \frac{1}{\sqrt{\mu \epsilon}} \quad (1.33)$$

where $u = c \approx 3 \times 10^8$ m/s in free space. It should be noted that each of the vector equations in (1.31) and (1.32) has three scalar components, so that altogether we have six scalar equations for E_x, E_y, E_z, H_x, H_y , and H_z . Thus each component of the wave equations has the form

$$\nabla^2 \Psi - \frac{1}{u^2} \frac{\partial^2 \Psi}{\partial t^2} = 0 \quad (1.34)$$

which is the scalar wave equation.

1.2.6 Time-Varying Potentials

Although we are often interested in electric and magnetic field intensities (\mathbf{E} and \mathbf{H}), which are physically measurable quantities, it is often convenient to use auxiliary functions in analyzing an EM field. These auxiliary functions are the scalar electric potential V and vector magnetic potential \mathbf{A} . Although these potential functions are arbitrary, they are required to satisfy Maxwell's equations. Their derivation is based on two fundamental vector identities (see Problem 1.1),

$$\nabla \times \nabla \Phi = 0 \quad (1.35)$$

and

$$\nabla \cdot \nabla \times \mathbf{F} = 0 \quad (1.36)$$

which an arbitrary scalar field Φ and vector field \mathbf{F} must satisfy. Maxwell's equation (1.22b) along with Equation (1.36) is satisfied if we define \mathbf{A} such that

$$\boxed{\mathbf{B} = \nabla \times \mathbf{A}} \quad (1.37)$$

Substituting this into Equation (1.22c) gives

$$-\nabla \times \left(\mathbf{E} + \frac{\partial \mathbf{A}}{\partial t} \right) = 0$$

Since this equation has to be compatible with Equation (1.35), we can choose the scalar field V such that

$$\mathbf{E} + \frac{\partial \mathbf{A}}{\partial t} = -\nabla V$$

or

$$\boxed{\mathbf{E} = -\nabla V - \frac{\partial \mathbf{A}}{\partial t}} \quad (1.38)$$

Thus, if we knew the potential functions V and \mathbf{A} , the fields \mathbf{E} and \mathbf{B} could be obtained from Equations (1.37) and (1.38). However, we still need to find the solution for the potential functions. Substituting Equations (1.37) and (1.38) into Equation (1.22d) and assuming a linear, homogeneous medium,

$$\nabla \times \nabla \times \mathbf{A} = \mu \mathbf{J} + \epsilon \mu \frac{\partial}{\partial t} \left(-\nabla V - \frac{\partial \mathbf{A}}{\partial t} \right)$$

Applying the vector identity in Equation (1.30) leads to

$$\nabla^2 \mathbf{A} - \nabla(\nabla \cdot \mathbf{A}) = -\mu \mathbf{J} + \mu \epsilon \nabla \frac{\partial^2 \mathbf{A}}{\partial t^2} + \mu \epsilon \nabla \frac{\partial V}{\partial t} \quad (1.39)$$

Substituting Equation (1.38) into Equation (1.22a) gives

$$\nabla \cdot \mathbf{E} = \frac{\rho}{\epsilon} = -\nabla^2 V - \frac{\partial(\nabla \cdot \mathbf{A})}{\partial t}$$

or

$$\nabla^2 V + \frac{\partial}{\partial t} \nabla \cdot \mathbf{A} = -\frac{\rho_v}{\epsilon} \quad (1.40)$$

According to the Helmholtz theorem of vector analysis, a vector is uniquely defined if and only if both its curl and divergence are specified. We have only specified the curl of \mathbf{A} in Equation (1.37); we may choose the divergence of \mathbf{A} so that the differential equations (1.39) and (1.40) have the simplest forms possible. We achieve this in the so-called *Lorentz condition*:

$$\nabla \cdot \mathbf{A} = -\mu\epsilon \frac{\partial V}{\partial t} \quad (1.41)$$

Incorporating this condition into Equations (1.39) and (1.40) results in

$$\boxed{\nabla^2 \mathbf{A} - \mu\epsilon \frac{\partial^2 \mathbf{A}}{\partial t^2} = -\mu \mathbf{J}} \quad (1.42)$$

and

$$\boxed{\nabla^2 V - \mu\epsilon \frac{\partial^2 V}{\partial t^2} = -\frac{\rho_v}{\epsilon}} \quad (1.43)$$

which are inhomogeneous wave equations. Thus Maxwell's equations in terms of the potentials V and \mathbf{A} reduce to the three equations (1.41) to (1.43). In other words, the three equations are equivalent to the ordinary form of Maxwell's equations in that potentials satisfying these equations always lead to a solution of Maxwell's equations for \mathbf{E} and \mathbf{B} when used with Equations (1.37) and (1.38). Integral solutions to Equations (1.42) and (1.43) are the so-called *retarded* potentials

$$\mathbf{A} = \int \frac{\mu[\mathbf{J}]dv}{4\pi R} \quad (1.44)$$

and

$$V = \int \frac{[\rho_v]dv}{4\pi\epsilon R} \quad (1.45)$$

where R is the distance from the source point to the field point, and the square brackets denote ρ_v and \mathbf{J} are specified at a time $R(\mu\epsilon)^{1/2}$ earlier than for which \mathbf{A} or V is being determined.

1.2.7 Time-Harmonic Fields

Up to this point, we have considered the general case of arbitrary time variation of EM fields. In many practical situations, especially at low frequencies, it is sufficient to deal with only the steady-state (or equilibrium) solution of EM fields when produced

by sinusoidal currents. Such fields are said to be sinusoidal time-varying or time-harmonic; that is, they vary at a sinusoidal frequency ω . An arbitrary time-dependent field $\mathbf{F}(x, y, z, t)$ or $\mathbf{F}(\mathbf{r}, t)$ can be expressed as

$$\boxed{\mathbf{F}(\mathbf{r}, t) = \operatorname{Re} [\mathbf{F}_s(\mathbf{r})e^{j\omega t}]} \quad (1.46)$$

where $\mathbf{F}_s(\mathbf{r}) = \mathbf{F}_s(x, y, z)$ is the phasor form of $\mathbf{F}(\mathbf{r}, t) = \mathbf{F}(x, y, z, t)$ and is in general complex, $\operatorname{Re}[\cdot]$ indicates "taking the real part of" quantity in brackets, and ω is the angular frequency (in rad/s) of the sinusoidal excitation. The EM field quantities can be represented in phasor notation as

$$\begin{bmatrix} \mathbf{E}(\mathbf{r}, t) \\ \mathbf{D}(\mathbf{r}, t) \\ \mathbf{H}(\mathbf{r}, t) \\ \mathbf{B}(\mathbf{r}, t) \end{bmatrix} = \operatorname{Re} \left\{ \begin{bmatrix} \mathbf{E}_s(\mathbf{r}) \\ \mathbf{D}_s(\mathbf{r}) \\ \mathbf{H}_s(\mathbf{r}) \\ \mathbf{B}_s(\mathbf{r}) \end{bmatrix} e^{j\omega t} \right\} \quad (1.47)$$

Using the phasor representation allows us to replace the time derivations $\partial/\partial t$ by $j\omega$ since

$$\frac{\partial e^{j\omega t}}{\partial t} = j\omega e^{j\omega t}$$

Thus Maxwell's equations, in sinusoidal steady state, become

$$\nabla \cdot \mathbf{D}_s = \rho_{vs} \quad (1.48a)$$

$$\nabla \cdot \mathbf{B}_s = 0 \quad (1.48b)$$

$$\nabla \times \mathbf{E}_s = -j\omega \mathbf{B}_s - \mathbf{J}_{ms} \quad (1.48c)$$

$$\nabla \times \mathbf{H}_s = \mathbf{J}_{es} + j\omega \mathbf{D}_s \quad (1.48d)$$

We should observe that the effect of the time-harmonic assumption is to eliminate the time dependence from Maxwell's equations, thereby reducing the time-space dependence to space dependence only. This simplification does not exclude more general time-varying fields if we consider ω to be one element of an entire frequency spectrum, with all the Fourier components superposed. In other words, a nonsinusoidal field can be represented as

$$\mathbf{F}(\mathbf{r}, t) = \operatorname{Re} \left[\int_{-\infty}^{\infty} \mathbf{F}_s(\mathbf{r}, \omega) e^{j\omega t} d\omega \right] \quad (1.49)$$

Thus the solutions to Maxwell's equations for a nonsinusoidal field can be obtained by summing all the Fourier components $\mathbf{F}_s(\mathbf{r}, \omega)$ over ω . Henceforth, we drop the subscript s denoting phasor quantity when no confusion results.

Replacing the time derivative in Equation (1.34) by $(j\omega)^2$ yields the scalar wave equation in phasor representation as

$$\nabla^2 \Psi + k^2 \Psi = 0 \quad (1.50)$$

where k is the propagation constant (in rad/m), given by

$$k = \frac{\omega}{u} = \frac{2\pi f}{u} = \frac{2\pi}{\lambda} \quad (1.51)$$

We recall that Equations (1.31) to (1.34) were obtained assuming that $\rho_v = 0 = \mathbf{J}$. If $\rho_v \neq 0 \neq \mathbf{J}$, Equation (1.50) will have the general form (see Problem 1.5)

$$\boxed{\nabla^2 \Psi + k^2 \Psi = g} \quad (1.52)$$

We notice that this Helmholtz equation reduces to

(1) Poisson's equation

$$\nabla^2 \Psi = g \quad (1.53)$$

when $k = 0$ (i.e., $\omega = 0$ for static case).

(2) Laplace's equation

$$\nabla^2 \Psi = 0 \quad (1.54)$$

when $k = 0 = g$.

Thus Poisson's and Laplace's equations are special cases of the Helmholtz equation. Note that function Ψ is said to be *harmonic* if it satisfies Laplace's equation.

Example 1.1

From the divergence theorem, derive Green's theorem

$$\int_v (U \nabla^2 V - V \nabla^2 U) dv = \oint_s \left(U \frac{\partial V}{\partial n} - V \frac{\partial U}{\partial n} \right) \cdot d\mathbf{S}$$

where $\frac{\partial \Phi}{\partial n} = \nabla \Phi \cdot \mathbf{a}_n$ is the directional derivative of Φ along the outward normal to S . \square

Solution

In Equation (1.1), let $\mathbf{F} = U \nabla V$, then

$$\int_v \nabla \cdot (U \nabla V) dv = \oint_s U \nabla V \cdot d\mathbf{S} \quad (1.55)$$

But

$$\begin{aligned} \nabla \cdot (U \nabla V) &= U \nabla \cdot \nabla V + \nabla V \cdot \nabla U \\ &= U \nabla^2 V + \nabla U \cdot \nabla V \end{aligned}$$

1.2. REVIEW OF ELECTROMAGNETIC THEORY

Substituting this into Equation (1.55) gives *Green's first identity*:

$$\int_v (U \nabla^2 V + \nabla U \cdot \nabla V) dv = \oint_s U \nabla V \cdot d\mathbf{S} \quad (1.56)$$

By interchanging U and V in Equation (1.56), we obtain

$$\int_v (V \nabla^2 U + \nabla V \cdot \nabla U) dv = \oint_s V \nabla U \cdot d\mathbf{S} \quad (1.57)$$

Subtracting Equation (1.57) from Equation (1.56) leads to *Green's second identity* or *Green's theorem*:

$$\int_v (U \nabla^2 V - V \nabla^2 U) dv = \oint_s (U \nabla V - V \nabla U) \cdot d\mathbf{S} \quad \blacksquare$$

Example 1.2

Show that the continuity equation is implicit (or incorporated) in Maxwell's equations. \square

Solution

According to Equation (1.36), the divergence of the curl of any vector field is zero. Hence, taking the divergence of Equation (1.22d) gives

$$0 = \nabla \cdot \nabla \times \mathbf{H} = \nabla \cdot \mathbf{J} + \frac{\partial}{\partial t} \nabla \cdot \mathbf{D}$$

But $\nabla \cdot \mathbf{D} = \rho_v$ from Equation (1.22a). Thus,

$$0 = \nabla \cdot \mathbf{J} + \frac{\partial \rho_v}{\partial t}$$

which is the continuity equation. \blacksquare

Example 1.3

Express

(a) $\mathbf{E} = 10 \sin(\omega t - kz) \mathbf{a}_x + 20 \cos(\omega t - kz) \mathbf{a}_y$ in phasor form.

(b) $\mathbf{H}_s = (4 - j3) \sin x \mathbf{a}_x + \frac{e^{j10^\circ}}{x} \mathbf{a}_z$ in instantaneous form. \square

Solution

(a) We can express $\sin \theta$ as $\cos(\theta - \pi/2)$. Hence,

$$\begin{aligned} \mathbf{E} &= 10 \cos(\omega t - kz - \pi/2) \mathbf{a}_x + 20 \cos(\omega t - kz) \mathbf{a}_y \\ &= \operatorname{Re} [(10e^{-jkz} e^{-j\pi/2} \mathbf{a}_x + 20e^{-jkz} \mathbf{a}_y) e^{j\omega t}] \\ &= \operatorname{Re} [\mathbf{E}_s e^{j\omega t}] \end{aligned}$$

Thus,

$$\begin{aligned}\mathbf{E}_s &= 10e^{-jkz}e^{-j\pi/2}\mathbf{a}_x + 20e^{-jkz}\mathbf{a}_y \\ &= (-j10\mathbf{a}_x + 20\mathbf{a}_y)e^{-jkz}\end{aligned}$$

(b) Since

$$\begin{aligned}\mathbf{H} &= \operatorname{Re} [\mathbf{H}_s e^{j\omega t}] \\ &= \operatorname{Re} \left[5 \sin x e^{j(\omega t - 36.87^\circ)} \mathbf{a}_x + \frac{1}{x} e^{j(\omega t + 10^\circ)} \mathbf{a}_z \right] \\ &= \left[5 \sin x \cos(\omega t - 36.87^\circ) \mathbf{a}_x + \frac{1}{x} \cos(\omega t + 10^\circ) \mathbf{a}_z \right]\end{aligned}$$

1.3 Classification of EM Problems

Classifying EM problems will help us later to answer the question of what method is best for solving a given problem. Continuum problems are categorized differently depending on the particular item of interest, which could be one of these:

- (1) the solution region of the problem,
- (2) the nature of the equation describing the problem, or
- (3) the associated boundary conditions.

(In fact, the above three items define a problem uniquely.) It will soon become evident that these classifications are sometimes not independent of each other.

1.3.1 Classification of Solution Regions

In terms of the solution region or problem domain, the problem could be an interior problem, also variably called an inner, closed, or bounded problem, or an exterior problem, also variably called an outer, open, or unbounded problem.

Consider the solution region R with boundary S , as shown in Figure 1.2. If part or all of S is at infinity, R is exterior/open, otherwise R is interior/closed. For example, wave propagation in a waveguide is an interior problem, whereas wave propagations in free space — scattering of EM waves by raindrops, and radiation from a dipole antenna — are exterior problems.

A problem can also be classified in terms of the electrical, constitutive properties (σ, ϵ, μ) of the solution region. As mentioned in Section 1.2.4, the solution region could be linear (or nonlinear), homogeneous (or inhomogeneous), and isotropic (or anisotropic). We shall be concerned, for the most part, with linear, homogeneous, isotropic media in this text.

1.3. CLASSIFICATION OF EM PROBLEMS

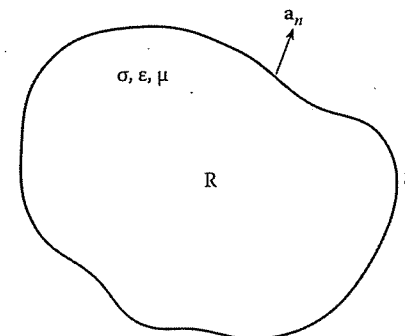


Figure 1.2
Solution region R with boundary S .

1.3.2 Classification of Differential Equations

EM problems are classified in terms of the equations describing them. The equations could be differential or integral or both. Most EM problems can be stated in terms of an operator equation

$$L\Phi = g \quad (1.58)$$

where L is an operator (differential, integral, or integro-differential), g is the known excitation or source, and Φ is the unknown function to be determined. A typical example is the electrostatic problem involving Poisson's equation. In differential form, Equation (1.58) becomes

$$-\nabla^2 V = \frac{\rho_v}{\epsilon} \quad (1.59)$$

so that $L = -\nabla^2$ is the Laplacian operator, $g = \rho_v/\epsilon$ is the source term, and $\Phi = V$ is the electric potential. In integral form, Poisson's equation is of the form

$$V = \int \frac{\rho_v dv}{4\pi\epsilon r^2} \quad (1.60)$$

so that

$$L = \int \frac{dv}{4\pi r^2}, \quad g = V, \quad \text{and} \quad \Phi = \rho_v/\epsilon$$

In this section, we shall limit our discussion to differential equations; integral equations will be considered in detail in Chapter 5.

As observed in Equations (1.52) to (1.54), EM problems involve linear, second-order differential equations. In general, a second-order partial differential equation (PDE) is given by

$$a \frac{\partial^2 \Phi}{\partial x^2} + b \frac{\partial^2 \Phi}{\partial x \partial y} + c \frac{\partial^2 \Phi}{\partial y^2} + d \frac{\partial \Phi}{\partial x} + e \frac{\partial \Phi}{\partial y} + f \Phi = g$$

or simply

$$a\Phi_{xx} + b\Phi_{xy} + c\Phi_{yy} + d\Phi_x + e\Phi_y + f\Phi = g \quad (1.61)$$

The coefficients, a , b , and c in general are functions of x and y ; they may also depend on Φ itself, in which case the PDE is said to be *nonlinear*. A PDE in which $g(x, y)$ in Equation (1.61) equals zero is termed *homogeneous*; it is *inhomogeneous* if $g(x, y) \neq 0$. Notice that Equation (1.61) has the same form as Equation (1.58), where L is now a differential operator given by

$$L = a\frac{\partial^2}{\partial x^2} + b\frac{\partial^2}{\partial x \partial y} + c\frac{\partial^2}{\partial y^2} + d\frac{\partial}{\partial x} + e\frac{\partial}{\partial y} + f \quad (1.62)$$

A PDE in general can be associated with both boundary values and initial values. PDEs whose boundary conditions are specified are called *steady-state equations*. If only initial values are specified, they are called *transient equations*.

Any linear second-order PDE can be classified as elliptic, hyperbolic, or parabolic depending on the coefficients a , b , and c . Equation (1.61) is said to be

elliptic if $b^2 - 4ac < 0$ hyperbolic if $b^2 - 4ac > 0$ parabolic if $b^2 - 4ac = 0$
--

$$(1.63)$$

The terms *hyperbolic*, *parabolic*, and *elliptic* are derived from the fact that the quadratic equation

$$ax^2 + bxy + cy^2 + dx + ey + f = 0$$

represents a hyperbola, parabola, or ellipse if $b^2 - 4ac$ is positive, zero, or negative, respectively. In each of these categories, there are PDEs that model certain physical phenomena. Such phenomena are not limited to EM but extend to almost all areas of science and engineering. Thus the mathematical model specified in Equation (1.61) arises in problems involving heat transfer, boundary-layer flow, vibrations, elasticity, electrostatic, wave propagation, and so on.

Elliptic PDEs are associated with steady-state phenomena, i.e., boundary-value problems. Typical examples of this type of PDE include Laplace's equation

$$\frac{\partial^2 \Phi}{\partial x^2} + \frac{\partial^2 \Phi}{\partial y^2} = 0 \quad (1.64)$$

and Poisson's equation

$$\frac{\partial^2 \Phi}{\partial x^2} + \frac{\partial^2 \Phi}{\partial y^2} = g(x, y) \quad (1.65)$$

where in both cases $a = c = 1, b = 0$. An elliptic PDE usually models an interior problem, and hence the solution region is usually closed or bounded as in Figure 1.3 (a).

1.3. CLASSIFICATION OF EM PROBLEMS

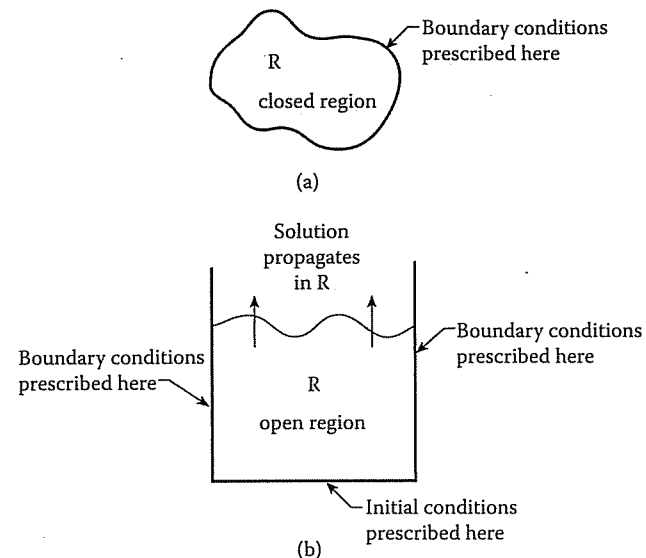


Figure 1.3
 (a) Elliptic, (b) parabolic, or hyperbolic problem.

Hyperbolic PDEs arise in propagation problems. The solution region is usually open so that a solution advances outward indefinitely from initial conditions while always satisfying specified boundary conditions. A typical example of hyperbolic PDE is the wave equation in one dimension

$$\frac{\partial^2 \Phi}{\partial x^2} = \frac{1}{u^2} \frac{\partial^2 \Phi}{\partial t^2} \quad (1.66)$$

where $a = u^2, b = 0, c = -1$. Notice that the wave equation in (1.50) is not hyperbolic but elliptic since the time-dependence has been suppressed and the equation is merely the steady-state solution of Equation (1.34).

Parabolic PDEs are generally associated with problems in which the quantity of interest varies slowly in comparison with the random motions which produce the variations. The most common parabolic PDE is the diffusion (or heat) equation in one dimension

$$\frac{\partial^2 \Phi}{\partial x^2} = k \frac{\partial \Phi}{\partial t} \quad (1.67)$$

where $a = 1, b = 0 = c$. Like hyperbolic PDE, the solution region for parabolic PDE is usually open, as in Figure 1.3 (b). The initial and boundary conditions typically associated with parabolic equations resemble those for hyperbolic problems except that only one initial condition at $t = 0$ is necessary since Equation (1.67) is only first order in time. Also, parabolic and hyperbolic equations are solved using similar techniques, whereas elliptic equations require different techniques.

Note that (1) since the coefficients a , b , and c are in general functions of x and y , the classification of Equation (1.61) may change from point to point in the solution region, and (2) PDEs with more than two independent variables (x, y, z, t, \dots) may not fit as neatly into the classification above. A summary of our discussion so far in this section is shown in Table 1.1.

Table 1.1 Classification of Partial Differential Equations

Type	Sign of $b^2 - 4ac$	Example	Solution Region
Elliptic	-	Laplace's equation: $\Phi_{xx} + \Phi_{yy} = 0$	Closed
Hyperbolic	+	Wave equation: $u^2 \Phi_{xx} = \Phi_{tt}$	Open
Parabolic	0	Diffusion equation: $\Phi_{xx} = k\Phi_t$	Open

The type of problem represented by Equation (1.58) is said to be *deterministic* since the quantity of interest can be determined directly. Another type of problem where the quantity is found indirectly is called *nondeterministic* or *eigenvalue*. The *standard eigenproblem* is of the form

$$L\Phi = \lambda\Phi \quad (1.68)$$

where the source term in Equation (1.58) has been replaced by $\lambda\Phi$. A more general version is the *generalized eigenproblem* having the form

$$L\Phi = \lambda M\Phi \quad (1.69)$$

where M , like L , is a linear operator for EM problems. In Equations (1.68) and (1.69), only some particular values of λ called *eigenvalues* are permissible; associated with these values are the corresponding solutions Φ called *eigenfunctions*. Eigenproblems are usually encountered in vibration and waveguide problems where the eigenvalues λ correspond to physical quantities such as resonance and cutoff frequencies, respectively.

1.3.3 Classification of Boundary Conditions

Our problem consists of finding the unknown function Φ of a partial differential equation. In addition to the fact that Φ satisfies Equation (1.58) within a prescribed solution region R , Φ must satisfy certain conditions on S , the boundary of R . Usually these boundary conditions are of the Dirichlet and Neumann types. Where a boundary has both, a mixed boundary condition is said to exist.

(1) Dirichlet boundary condition:

$$\Phi(\mathbf{r}) = 0, \quad \mathbf{r} \text{ on } S \quad (1.70)$$

1.3. CLASSIFICATION OF EM PROBLEMS

(2) Neumann boundary condition:

$$\frac{\partial \Phi(\mathbf{r})}{\partial n} = 0, \quad \mathbf{r} \text{ on } S, \quad (1.71)$$

i.e., the normal derivative of Φ vanishes on S .

(3) Mixed boundary condition:

$$\frac{\partial \Phi(\mathbf{r})}{\partial n} + h(\mathbf{r})\Phi(\mathbf{r}) = 0, \quad \mathbf{r} \text{ on } S, \quad (1.72)$$

where $h(\mathbf{r})$ is a known function and $\frac{\partial \Phi}{\partial n}$ is the directional derivative of Φ along the outward normal to the boundary S , i.e.,

$$\frac{\partial \Phi}{\partial n} = \nabla \Phi \cdot \mathbf{a}_n \quad (1.73)$$

where \mathbf{a}_n is a unit normal directed out of R , as shown in Figure 1.2. Note that the Neumann boundary condition is a special case of the mixed condition with $h(\mathbf{r}) = 0$.

The conditions in Equation (1.70) to (1.72) are called *homogeneous boundary conditions*. The more general ones are the inhomogeneous.

(1) Dirichlet:

$$\Phi(\mathbf{r}) = p(\mathbf{r}), \quad \mathbf{r} \text{ on } S \quad (1.74)$$

(2) Neumann:

$$\frac{\partial \Phi(\mathbf{r})}{\partial n} = q(\mathbf{r}), \quad \mathbf{r} \text{ on } S \quad (1.75)$$

(3) Mixed:

$$\frac{\partial \Phi(\mathbf{r})}{\partial n} + h(\mathbf{r})\Phi(\mathbf{r}) = w(\mathbf{r}), \quad \mathbf{r} \text{ on } S \quad (1.76)$$

where $p(\mathbf{r})$, $q(\mathbf{r})$, and $w(\mathbf{r})$ are explicitly known functions on the boundary S . For example, $\Phi(0) = 1$ is an inhomogeneous Dirichlet boundary condition, and the associated homogeneous counterpart is $\Phi(0) = 0$. Also $\Phi'(1) = 2$ and $\Phi'(1) = 0$ are, respectively, inhomogeneous and homogeneous Neumann boundary conditions. In electrostatics, for example, if the value of electric potential is specified on S , we have Dirichlet boundary condition, whereas if the surface charge ($\rho_s = D_n = \epsilon \frac{\partial V}{\partial n}$) is specified, the boundary condition is Neumann. The problem of finding a function Φ that is harmonic in a region is called a *Dirichlet problem* (or *Neumann problem*) if Φ (or $\frac{\partial \Phi}{\partial n}$) is prescribed on the boundary of the region.

It is worth observing that the term *homogeneous* has been used to mean different things. The solution region could be homogeneous meaning that σ , ϵ , and μ are constant within R ; the PDE could be homogeneous if $g = 0$ so that $L\Phi = 0$; and the boundary conditions are homogeneous when $p(\mathbf{r}) = q(\mathbf{r}) = w(\mathbf{r}) = 0$.

Example 1.4

Classify these equations as elliptic, hyperbolic, or parabolic:

$$(a) 4\Phi_{xx} + 2\Phi_x + \Phi_y + x + y = 0$$

$$(b) e^x \frac{\partial^2 V}{\partial x^2} + \cos y \frac{\partial^2 V}{\partial x \partial y} - \frac{\partial^2 V}{\partial y^2} = 0.$$

State whether the equations are homogeneous or inhomogeneous. \square

Solution

(a) In this PDE, $a = 4, b = 0 = c$. Hence

$$b^2 - 4ac = 0,$$

i.e., the PDE is parabolic. Since $g = -x - y$, the PDE is inhomogeneous.

(b) For this PDE, $a = e^x, b = \cos y, c = -1$. Hence

$$b^2 - 4ac = \cos^2 y + 4e^x > 0$$

and the PDE is hyperbolic. Since $g = 0$, the PDE is homogeneous. \blacksquare

1.4 Some Important Theorems

Two theorems are of fundamental importance in solving EM problems. These are the principle of superposition and the uniqueness theorem.

1.4.1 Superposition Principle

The principle of superposition is applied in several ways. We shall consider two of these.

If each member of a set of functions $\Phi_n, n = 1, 2, \dots, N$, is a solution to the PDE $L\Phi = 0$ with some prescribed boundary conditions, then a linear combination

$$\Phi_N = \Phi_0 + \sum_{n=1}^N a_n \Phi_n \quad (1.77)$$

also satisfies $L\Phi = g$.

Given a problem described by the PDE

$$L\Phi = g \quad (1.78)$$

1.4. SOME IMPORTANT THEOREMS

subject to the boundary conditions

$$M_1(s) = h_1$$

$$M_2(s) = h_2$$

\vdots

$$M_N(s) = h_N, \quad (1.79)$$

as long as L is linear, we may divide the problem into a series of problems as follows:

$$\begin{array}{llll} L\Phi_0 = g & L\Phi_1 = 0 & \cdots & L\Phi_N = 0 \\ M_1(s) = 0 & M_1(s) = h_1 & \cdots & M_1(s) = 0 \\ M_2(s) = 0 & M_2(s) = 0 & \cdots & M_2(s) = 0 \\ \vdots & \vdots & & \vdots \\ M_N(s) = 0 & M_N(s) = 0 & \cdots & M_N(s) = h_N \end{array} \quad (1.80)$$

where $\Phi_0, \Phi_1, \dots, \Phi_N$ are the solutions to the reduced problems, which are easier to solve than the original problem. The solution to the original problem is given by

$$\Phi = \sum_{n=0}^N \Phi_n \quad (1.81)$$

1.4.2 Uniqueness Theorem

This theorem guarantees that the solution obtained for a PDE with some prescribed boundary conditions is the only one possible. For EM problems, the theorem may be stated as follows: If in any way a set of fields (\mathbf{E}, \mathbf{H}) is found which satisfies simultaneously Maxwell's equations and the prescribed boundary conditions, this set is unique. Therefore, a field is uniquely specified by the sources (ρ_v, \mathbf{J}) within the medium plus the tangential components of \mathbf{E} or \mathbf{H} over the boundary.

To prove the uniqueness theorem, suppose there exist two solutions (with subscripts 1 and 2) that satisfy Maxwell's equations

$$\nabla \cdot \epsilon \mathbf{E}_{1,2} = \rho_v \quad (1.82a)$$

$$\nabla \cdot \mathbf{H}_{1,2} = 0 \quad (1.82b)$$

$$\nabla \times \mathbf{E}_{1,2} = -\mu \frac{\partial \mathbf{H}_{1,2}}{\partial t} \quad (1.82c)$$

$$\nabla \times \mathbf{H}_{1,2} = \mathbf{J} + \sigma \mathbf{E}_{1,2} + \epsilon \frac{\partial \mathbf{E}_{1,2}}{\partial t} \quad (1.82d)$$

If we denote the difference of the two fields as $\Delta\mathbf{E} = \mathbf{E}_2 - \mathbf{E}_1$ and $\Delta\mathbf{H} = \mathbf{H}_2 - \mathbf{H}_1$, $\Delta\mathbf{E}$ and $\Delta\mathbf{H}$ must satisfy the source-free Maxwell's equations, i.e.,

$$\nabla \cdot \epsilon \Delta\mathbf{E} = 0 \quad (1.83a)$$

$$\nabla \cdot \Delta\mathbf{H} = 0 \quad (1.83b)$$

$$\nabla \times \Delta\mathbf{E} = -\mu \frac{\partial \Delta\mathbf{H}}{\partial t} \quad (1.83c)$$

$$\nabla \times \Delta\mathbf{H} = \sigma \Delta\mathbf{E} + \epsilon \frac{\partial \Delta\mathbf{E}}{\partial t} \quad (1.83d)$$

Dotting both sides of Equation (1.83d) with $\Delta\mathbf{E}$ gives

$$\Delta\mathbf{E} \cdot \nabla \times \Delta\mathbf{H} = \sigma |\Delta\mathbf{E}|^2 + \epsilon \nabla \mathbf{E} \cdot \frac{\partial \Delta\mathbf{E}}{\partial t} \quad (1.84)$$

Using the vector identity

$$\mathbf{A} \cdot (\nabla \times \mathbf{B}) = \mathbf{B} \cdot (\nabla \times \mathbf{A}) - \nabla \cdot (\mathbf{A} \times \mathbf{B})$$

and Equation (1.83c), Equation (1.84) becomes

$$\nabla \cdot (\Delta\mathbf{E} \times \Delta\mathbf{H}) = -\frac{1}{2} \frac{\partial}{\partial t} (\mu |\Delta\mathbf{H}|^2 + \epsilon |\Delta\mathbf{E}|^2) - \sigma |\Delta\mathbf{E}|^2$$

Integrating over volume v bounded by surface S and applying divergence theorem to the left-hand side, we obtain

$$\oint_S (\Delta\mathbf{E} \times \Delta\mathbf{H}) \cdot d\mathbf{S} = -\frac{\partial}{\partial t} \int_v \left[\frac{1}{2} \epsilon |\Delta\mathbf{E}|^2 + \frac{1}{2} \mu |\Delta\mathbf{H}|^2 \right] dv - \int_v \sigma |\Delta\mathbf{E}| dv \quad (1.85)$$

showing that $\Delta\mathbf{E}$ and $\Delta\mathbf{H}$ satisfy the Poynting theorem just as $\mathbf{E}_{1,2}$ and $\mathbf{H}_{1,2}$. Only the tangential components of $\Delta\mathbf{E}$ and $\Delta\mathbf{H}$ contribute to the surface integral on the left side of Equation (1.85). Therefore, if the tangential components of \mathbf{E}_1 and \mathbf{E}_2 or \mathbf{H}_1 and \mathbf{H}_2 are equal over S [thereby satisfying Equation (1.27)], the tangential components of $\Delta\mathbf{E}$ and $\Delta\mathbf{H}$ vanish on S . Consequently, the surface integral in Equation (1.85) is identically zero, and hence the right side of the equation must vanish also. It follows that $\Delta\mathbf{E} = 0$ due to the second integral on the right side, and hence also $\Delta\mathbf{H} = 0$ throughout the volume. Thus $\mathbf{E}_1 = \mathbf{E}_2$ and $\mathbf{H}_1 = \mathbf{H}_2$, confirming that the solution is unique.

The theorem just proved for time-varying fields also holds for static fields as a special case. In terms of electrostatic potential V , the uniqueness theorem may be stated as follows: A solution to $\nabla^2 V = 0$ is uniquely determined by specifying either the value of V or the normal component of ∇V at each point on the boundary surface. For a magnetostatic field, the theorem becomes: A solution of $\nabla^2 \mathbf{A} = 0$ (and $\nabla \cdot \mathbf{A} = 0$) is uniquely determined by specifying the value of \mathbf{A} or the tangential component of $\mathbf{B} = (\nabla \times \mathbf{A})$ at each point on the boundary surface.

References

- [1] K.H. Huebner and E.A. Thornton, *The Finite Element Method for Engineers*. New York: John Wiley and Sons, 1982, Chap. 3, pp. 62–107.
- [2] J.A. Kong, *Electromagnetic Wave Theory*. New York: John Wiley and Sons, 1986, Chap. 1, pp. 1–41.
- [3] R.E. Collins, *Foundations of Microwave Engineering*. New York: McGraw-Hill, 1966, Chap. 2, pp. 11–63.
- [4] M.N.O. Sadiku, *Elements of Electromagnetics*, 4th ed., New York: Oxford Univ. Press, 2007, Chap. 9, pp. 385–427.

Problems

- 1.1 In a coordinate system of your choice, prove that
 - (a) $\nabla \times \nabla \Phi = 0$,
 - (b) $\nabla \cdot \nabla \times \mathbf{F} = 0$,
 - (c) $\nabla \times \nabla \times \mathbf{F} = \nabla(\nabla \cdot \mathbf{F}) - \nabla^2 \mathbf{F}$,
 where Φ and \mathbf{F} are scalar and vector fields, respectively.
- 1.2 If U and V are scalar fields, show that

$$\oint_L U \nabla V \cdot d\mathbf{l} = - \oint_L V \nabla U \cdot d\mathbf{l}$$
- 1.3 If $U(x, y, z)$ and $V(x, y, z)$ are two continuous functions with continuous derivatives over a smooth closed surface, show that

$$\int_S (U \nabla V) \cdot d\mathbf{S} = \int_v (U \nabla^2 V + \nabla U \cdot \nabla V) dv$$
- 1.4 Show that in a source-free region ($\mathbf{J} = 0, \rho_v = 0$), Maxwell's equations can be reduced to the two curl equations.

- 1.5 In deriving the wave equations (1.31) and (1.32), we assumed a source-free medium ($\mathbf{J} = 0, \rho_v = 0$). Show that if $\rho_v \neq 0, \mathbf{J} \neq 0$, the equations become

$$\nabla^2 \mathbf{E} - \frac{1}{c^2} \frac{\partial^2 \mathbf{E}}{\partial t^2} = \nabla(\rho_v/\epsilon) + \mu \frac{\partial \mathbf{J}}{\partial t},$$

$$\nabla^2 \mathbf{H} - \frac{1}{c^2} \frac{\partial^2 \mathbf{H}}{\partial t^2} = -\nabla \times \mathbf{J}$$

What assumptions have you made to arrive at these expressions?

- 1.6 Starting with Maxwell's equations, show that

$$(a) \nabla \times \nabla \times \mathbf{H} + \mu \epsilon \frac{\partial^2 \mathbf{H}}{\partial t^2} = \nabla \times \mathbf{J}$$

$$(b) \nabla \times \nabla \times \mathbf{E} + \mu \epsilon \frac{\partial^2 \mathbf{E}}{\partial t^2} = -\mu \frac{\partial \mathbf{J}}{\partial t}$$

- 1.7 Given the total electromagnetic energy

$$W = \frac{1}{2} \int_v (\mathbf{E} \cdot \mathbf{D} + \mathbf{H} \cdot \mathbf{B}) dv$$

show from Maxwell's equations that

$$\frac{\partial W}{\partial t} = - \oint_s (\mathbf{E} \times \mathbf{H}) \cdot d\mathbf{S} - \int_v \mathbf{E} \cdot \mathbf{J} dv$$

- 1.8 Determine whether the fields

$$\mathbf{E} = 20 \sin(\omega t - kz) \mathbf{a}_x - 10 \cos(\omega t + kz) \mathbf{a}_y$$

$$\mathbf{H} = \frac{k}{\omega \mu_0} [-10 \cos(\omega t + kz) \mathbf{a}_x + 20 \sin(\omega t - kz) \mathbf{a}_y],$$

where $k = \omega \sqrt{\mu_0 \epsilon_0}$, satisfy Maxwell's equations.

- 1.9 In free space, the electric flux density is given by

$$\mathbf{D} = D_0 \cos(\omega t + \beta z) \mathbf{a}_x$$

Use Maxwell's equation to find \mathbf{H} .

- 1.10 In free space, a source radiates the magnetic field

$$\mathbf{H}_s = H_0 \frac{e^{-j\beta\rho}}{\sqrt{\rho}} \mathbf{a}_\phi$$

where $\beta = \omega \sqrt{\mu_0 \epsilon_0}$. Determine \mathbf{E}_s .

- 1.11 In a homogeneous, lossless, source-free medium,

$$\mathbf{E}_s = \mathbf{E}_o e^{-j\beta z} \mathbf{a}_x$$

$$\mathbf{H}_s = \frac{E_o}{\eta} e^{-j\beta z} \mathbf{a}_x$$

Find β and η for which \mathbf{E} and \mathbf{H} satisfy Maxwell's equations.

- 1.12 The field of the TE₁₂ mode of a rectangular waveguide for $0 < x < a, 0 < y < b$ is

$$H_x = -\frac{\beta a}{\pi} H_o \sin\left(\frac{\pi x}{a}\right) \sin(\omega t - \beta z)$$

$$H_y = 0$$

$$H_z = H_o \cos\left(\frac{\pi x}{a}\right) \cos(\omega t - \beta z)$$

Determine the surface current densities that are required at $x = 0, x = a, y = 0, y = b$ to sustain the field.

- 1.13 In free space, the following electric field vector exists.

$$\mathbf{E} = \cos(\omega t - \beta z) \mathbf{a}_x$$

- (a) Does the field vector satisfy the wave equation

$$\left(\nabla^2 - \mu_0 \epsilon_0 \frac{\partial^2}{\partial t^2} \right) \mathbf{E} = 0$$

- (b) What is the relationship between ω and β ?

- (c) Find the magnetic field vector corresponding to the electric field vector.

- 1.14 An electric dipole of length L in free space has a field given in spherical system (r, θ, ϕ) as

$$\mathbf{H}_s = \frac{IL}{4\pi r} \sin\theta \left(\frac{1}{r} + j\beta \right) e^{-j\beta r} \mathbf{a}_\phi$$

Find \mathbf{E}_s using Maxwell's equations.

- 1.15 Show that the electric field

$$\mathbf{E}_s = 20 \sin(k_x x) \cos(k_y y) \mathbf{a}_z,$$

where $k_x^2 + k_y^2 = \omega^2 \mu_0 \epsilon_0$, can be represented as the superposition of four propagating plane waves. Find the corresponding \mathbf{H}_s field.

- 1.16 (a) Express $I_s = e^{-jz} \sin \pi x \cos \pi y$ in instantaneous form.

- (b) Determine the phasor form of $V = 20 \sin(\omega t - 2x) - 10 \cos(\omega t - 4x)$

- 1.17 For each of the following phasors, determine the corresponding instantaneous form:

$$\begin{aligned}(a) \quad & \mathbf{A}_s = (\mathbf{a}_x + j\mathbf{a}_y)e^{-2jz} \\(b) \quad & \mathbf{B}_s = j10 \sin x \mathbf{a}_x + 5e^{-j12z-\pi/4} \mathbf{a}_z \\(c) \quad & \mathbf{C}_s = \frac{2}{j} e^{-j3x} \cos 2x + e^{3x-j4x}\end{aligned}$$

- 1.18 Show that a time-harmonic EM field in a conducting medium ($\sigma \gg \omega\epsilon$) satisfies the diffusion equation

$$\nabla^2 \mathbf{E}_s - j\omega\mu\sigma \mathbf{E}_s = 0$$

- 1.19 Show that the time-harmonic potential functions V_s and \mathbf{A}_s satisfy the following inhomogeneous wave equation

$$\begin{aligned}\nabla^2 V_s + k^2 V_s &= -\frac{\rho_{vs}}{\epsilon} \\ \nabla^2 \mathbf{A}_s + k^2 \mathbf{A}_s &= -\mu \mathbf{J}_s\end{aligned}$$

where $k^2 = \omega^2 \mu \epsilon$.

- 1.20 Classify the following PDEs as elliptic, parabolic, or hyperbolic.

$$\begin{aligned}(a) \quad & \Phi_{xx} + 2\Phi_{xy} + 5\Phi_{yy} = 0 \\(b) \quad & (y^2 + 1)\Phi_{xx} + (x^2 + 1)\Phi_{yy} = 0 \\(c) \quad & \Phi_{xx} - 2\cos x \Phi_{xy} - (3 + \sin^2 x)\Phi_{yy} - y\Phi_y = 0 \\(d) \quad & x^2\Phi_{xx} - 2xy\Phi_{xy} + y^2\Phi_{yy} + x\Phi_x + y\Phi_y = 0\end{aligned}$$

- 1.21 Repeat Problem 1.20 for the following PDEs.

$$(a) \quad \alpha \frac{\partial^2 \Phi}{\partial x^2} = \beta \frac{\partial \Phi}{\partial x} + \frac{\partial \Phi}{\partial t} \quad (\alpha, \beta = \text{constant})$$

which is called convective heat equation.

$$(b) \quad \nabla^2 \phi + \lambda \Phi = 0$$

which is the Helmholtz equation.

$$(c) \quad \nabla^2 \Phi + [\lambda - \rho(x)]\Phi = 0$$

which is the time-independent Schrodinger equation.

Chapter 2

Analytical Methods

And so, my fellow Americans: ask not what your country can do for you – ask what you can do for your country. My fellow citizens of the world: ask not what America will do for you, but what together we can do for the freedom of man.

-John F. Kennedy

2.1 Introduction

The most satisfactory solution of a field problem is an exact mathematical one. Although in many practical cases such an analytical solution cannot be obtained and we must resort to numerical approximate solution, an analytical solution is useful in checking solutions obtained from numerical methods. Also, one would hardly appreciate the need for numerical methods without first seeing the limitations of the classical analytical methods. Hence our objective in this chapter is to briefly examine the common analytical methods and thereby put numerical methods in proper perspective.

The most commonly used analytical methods in solving EM-related problems include

- (1) separation of variables
- (2) series expansion
- (3) conformal mapping
- (4) integral methods

Perhaps the most powerful analytical method is the separation of variables; it is the method that will be emphasized in this chapter. Since the application of conformal mapping is restricted to certain EM problems, it will not be discussed here. The interested reader is referred to Gibbs [1]. The integral methods will be covered in Chapter 5 and are fully discussed in [2].

2.2 Separation of Variables

The method of separation of variables (sometimes called the method of Fourier) is a convenient method for solving a partial differential equation (PDE). Basically, it entails seeking a solution which breaks up into a product of functions, each of which involves only one of the variables. For example, if we are seeking a solution $\Phi(x, y, z, t)$ to some PDE, we require that it has the product form

$$\Phi(x, y, z, t) = X(x)Y(y)Z(z)T(t) \quad (2.1)$$

A solution of the form in Equation (2.1) is said to be separable in x, y, z , and t . For example, consider the functions

- (1) $x^2yz \sin 10t$,
- (2) $xy^2 + \frac{z}{t}$,
- (3) $(2x + y^2)z \cos 10t$

(1) is completely separable, (2) is not separable, while (3) is separable only in z and t .

To determine whether the method of independent separation of variables can be applied to a given physical problem, we must consider the PDE describing the problem, the shape of the solution region, and the boundary conditions — the three elements that uniquely define a problem. For example, to apply the method to a problem involving two variables x and y (or ρ and ϕ , etc.), three things must be considered [3]:

- (i) The differential operator L must be separable, i.e., it must be a function of $\Phi(x, y)$ such that

$$\frac{L\{X(x)Y(y)\}}{\Phi(x, y)X(x)Y(y)}$$

is a sum of a function of x only and a function of y only.

- (ii) All initial and boundary conditions must be on constant-coordinate surfaces, i.e., $x = \text{constant}$, $y = \text{constant}$.
- (iii) The linear operators defining the boundary conditions at $x = \text{constant}$ (or $y = \text{constant}$) must involve no partial derivatives of Φ with respect to y (or x), and their coefficient must be independent of y (or x).

For example, the operator equation

$$L\Phi = \frac{\partial^2 \Phi}{\partial x^2} + \frac{\partial^2 \Phi}{\partial x \partial y} + \frac{\partial^2 \Phi}{\partial y^2}$$

violates (i). If the solution region R is not a rectangle with sides parallel to the x and y axes, (ii) is violated. With a boundary condition $\Phi = 0$ on a part of $x = 0$ and $\partial \Phi / \partial x = 0$ on another part, (iii) is violated.

With this preliminary discussion, we will now apply the method of separation of variables to PDEs in rectangular, circular cylindrical, and spherical coordinate

2.2. SEPARATION OF VARIABLES

systems. In each of these applications, we shall always take these three major steps:

- (1) separate the (independent) variables;
- (2) find particular solutions of the separated equations, which satisfy some of the boundary conditions;
- (3) combine these solutions to satisfy the remaining boundary conditions.

We begin the application of separation of variables by finding the product solution of the homogeneous scalar wave equation

$$\nabla^2 \Phi - \frac{1}{c^2} \frac{\partial^2 \Phi}{\partial t^2} = 0 \quad (2.2)$$

Solution to Laplace's equation can be derived as a special case of the wave equation. Diffusion or heat equation can be handled in the same manner as we will treat the wave equation. To solve Equation (2.2), it is expedient that we first separate the time dependence. We let

$$\Phi(\mathbf{r}, t) = U(\mathbf{r})T(t) \quad (2.3)$$

Substituting this in Equation (2.2),

$$T \nabla^2 U - \frac{1}{c^2} U T'' = 0$$

Dividing by UT gives

$$\frac{\nabla^2 U}{U} = \frac{T''}{c^2 T} \quad (2.4)$$

The left side is independent of t , while the right side is independent of \mathbf{r} ; the equality can be true only if each side is independent of both variables. If we let an arbitrary constant $-k^2$ be the common value of the two sides, Equation (2.4) reduces to

$$T'' + c^2 k^2 T = 0, \quad (2.5a)$$

$$\nabla^2 U + k^2 U = 0 \quad (2.5b)$$

Thus we have been able to separate the space variable \mathbf{r} from the time variable t . The arbitrary constant $-k^2$ introduced in the course of the separation of variables is called the *separation constant*. We shall see that in general the total number of independent separation constants in a given problem is one less than the number of independent variables involved.

Equation (2.5a) is an ordinary differential equation with solution

$$T(t) = a_1 e^{jckt} + a_2 e^{-jckt} \quad (2.6a)$$

or

$$T(t) = b_1 \cos(ckt) + b_2 \sin(ckt) \quad (2.6b)$$

Since the time dependence does not change with a coordinate system, the time dependence expressed in Equation (2.6) is the same for all coordinate systems. Therefore, we shall henceforth restrict our effort to seeking a solution to Equation (2.5b). Notice that if $k = 0$, the time dependence disappears and Equation (2.5b) becomes Laplace's equation.

2.3 Separation of Variables in Rectangular Coordinates

In order not to complicate things, we shall first consider Laplace's equation in two dimensions and later extend the idea to wave equations in three dimensions.

2.3.1 Laplace's Equation

Consider the Dirichlet problem of an infinitely long rectangular conducting trough whose cross section is shown in Figure 2.1. For simplicity, let three of its sides be

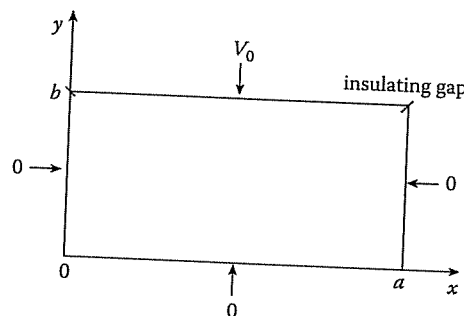


Figure 2.1
Cross section of the rectangular conducting trough.

maintained at zero potential while the fourth side is at a fixed potential V_o . This is a boundary value problem. The PDE to be solved is

$$\frac{\partial^2 V}{\partial x^2} + \frac{\partial^2 V}{\partial y^2} = 0 \quad (2.7)$$

subject to (Dirichlet) boundary conditions

$$V(0, y) = 0 \quad (2.8a)$$

$$V(a, y) = 0 \quad (2.8b)$$

$$V(x, 0) = 0 \quad (2.8c)$$

$$V(x, b) = V_o \quad (2.8d)$$

We let

$$V(x, y) = X(x)Y(y) \quad (2.9)$$

2.3. SEPARATION OF VARIABLES IN RECTANGULAR COORDINATES

Substitute this into Equation (2.7) and divide by XY . This leads to

$$\frac{X''}{X} + \frac{Y''}{Y} = 0$$

or

$$\frac{X''}{X} = -\frac{Y''}{Y} = \lambda \quad (2.10)$$

where λ is the separation constant. Thus the separated equations are

$$X'' - \lambda X = 0 \quad (2.11)$$

$$Y'' + \lambda Y = 0 \quad (2.12)$$

To solve the ordinary differential equations (2.11) and (2.12), we must impose the boundary conditions in Equation (2.8). However, these boundary conditions must be transformed so that they can be applied directly to the separated equations. Since $V = XY$,

$$V(0, y) = 0 \rightarrow X(0) = 0 \quad (2.13a)$$

$$V(a, y) = 0 \rightarrow X(a) = 0 \quad (2.13b)$$

$$V(x, 0) = 0 \rightarrow Y(0) = 0 \quad (2.13c)$$

$$V(x, b) = V_o \rightarrow X(x)Y(b) = V_o \quad (2.13d)$$

Notice that only the homogeneous conditions are separable. To solve Equation (2.11), we distinguish the three possible cases: $\lambda = 0$, $\lambda > 0$, and $\lambda < 0$.

Case 1: If $\lambda = 0$, Equation (2.11) reduces to

$$X'' = 0 \quad \text{or} \quad \frac{d^2 X}{dx^2} = 0 \quad (2.14)$$

which has the solution

$$X(x) = a_1 x + a_2 \quad (2.15)$$

where a_1 and a_2 are constants. Imposing the conditions in Equation (2.13a) and Equation (2.13b),

$$X(0) = 0 \rightarrow a_2 = 0$$

$$X(a) = 0 \rightarrow a_1 = 0$$

Hence $X(x) = 0$, a trivial solution. This renders case $\lambda = 0$ as unacceptable.

Case 2: If $\lambda > 0$, say $\lambda = \alpha^2$, Equation (2.11) becomes

$$X'' - \alpha^2 X = 0 \quad (2.16)$$

with the corresponding auxiliary equations $m^2 - \alpha^2 = 0$ or $m = \pm\alpha$. Hence the general solution is

$$X = b_1 e^{-\alpha x} + b_2 e^{\alpha x} \quad (2.17)$$

or

$$X = b_3 \sinh \alpha x + b_4 \cosh \alpha x \quad (2.18)$$

The boundary conditions are applied to determine b_3 and b_4 .

$$\begin{aligned} X(0) = 0 &\rightarrow b_4 = 0 \\ X(a) = 0 &\rightarrow b_3 = 0 \end{aligned}$$

since $\sinh \alpha x$ is never zero for $\alpha > 0$. Hence $X(x) = 0$, a trivial solution, and we conclude that case $\lambda > 0$ is not valid.

Case 3: If $\lambda < 0$, say $\lambda = -\beta^2$, Equation (2.11) becomes

$$X'' + \beta^2 X = 0 \quad (2.19)$$

with the auxiliary equation $m^2 + \beta^2 = 0$ or $m = \pm j\beta$. The solution to Equation (2.19) is

$$X = A_1 e^{j\beta x} + A_2 e^{-j\beta x} \quad (2.20a)$$

or

$$X = B_1 \sin \beta x + B_2 \cos \beta x \quad (2.20b)$$

Again,

$$\begin{aligned} X(0) = 0 &\rightarrow B_2 = 0 \\ X(a) = 0 &\rightarrow \sin \beta a = 0 = \sin n\pi \end{aligned}$$

or

$$\beta = \frac{n\pi}{a}, \quad n = 1, 2, 3, \dots \quad (2.21)$$

since B_1 cannot vanish for nontrivial solutions, whereas $\sin \beta a$ can vanish without its argument being zero. Thus we have found an infinite set of discrete values of λ for which Equation (2.11) has nontrivial solutions, i.e.,

$$\lambda = -\beta^2 = \frac{-n^2\pi^2}{a^2}, \quad n = 1, 2, 3, \dots \quad (2.22)$$

These are the eigenvalues of the problem and the corresponding eigenfunctions are

$$X_n(x) = \sin \beta x = \sin \frac{n\pi x}{a} \quad (2.23)$$

From Equation (2.22) note that it is not necessary to include negative values of n since they lead to the same set of eigenvalues. Also we exclude $n = 0$ since it yields

the trivial solution $X = 0$ as shown under Case 1 when $\lambda = 0$. Having determined λ , we can solve Equation (2.12) to find $Y_n(y)$ corresponding to $X_n(x)$. That is, we solve

$$Y'' - \beta^2 Y = 0, \quad (2.24)$$

which is similar to Equation (2.16), whose solution is in Equation (2.18). Hence the solution to Equation (2.24) has the form

$$Y_n(y) = a_n \sinh \frac{n\pi y}{a} + b_n \cosh \frac{n\pi y}{a} \quad (2.25)$$

Imposing the boundary condition in Equation (2.13c),

$$Y(0) = 0 \rightarrow b_n = 0$$

so that

$$Y_n(y) = a_n \sinh \frac{n\pi y}{a} \quad (2.26)$$

Substituting Equations (2.23) and (2.26) into Equation (2.9), we obtain

$$V_n(x, y) = X_n(x)Y_n(y) = a_n \sin \frac{n\pi x}{a} \sinh \frac{n\pi y}{a}, \quad (2.27)$$

which satisfies Equation (2.7) and the three homogeneous boundary conditions in Equations (2.8a), (2.8b), and (2.8c). By the superposition principle, a linear combination of the solutions V_n , each with different values of n and arbitrary coefficient a_n , is also a solution of Equation (2.7). Thus we may represent the solution V of Equation (2.7) as an infinite series in the function V_n , i.e.,

$$V(x, y) = \sum_{n=1}^{\infty} a_n \sin \frac{n\pi x}{a} \sinh \frac{n\pi y}{a} \quad (2.28)$$

We now determine the coefficient a_n by imposing the inhomogeneous boundary condition in Equation (2.8d) on Equation (2.28). We get

$$V(x, b) = V_o = \sum_{n=1}^{\infty} a_n \sin \frac{n\pi x}{a} \sinh \frac{n\pi b}{a}, \quad (2.29)$$

which is Fourier sine expansion of V_o . Hence,

$$a_n \sinh \frac{n\pi b}{a} = \frac{2}{b} \int_0^b V_o \sin \frac{n\pi x}{a} dx = \frac{2V_o}{n\pi} (1 - \cos n\pi)$$

or

$$a_n = \begin{cases} \frac{4V_o}{n\pi} \frac{1}{\sinh \frac{n\pi b}{a}}, & n = \text{odd}, \\ 0, & n = \text{even} \end{cases} \quad (2.30)$$

Substitution of Equation (2.30) into Equation (2.28) gives the complete solution as

$$V(x, y) = \frac{4V_o}{\pi} \sum_{n=\text{odd}}^{\infty} \frac{\sin \frac{n\pi x}{a} \sinh \frac{n\pi y}{a}}{n \sinh \frac{n\pi b}{a}} \quad (2.31a)$$

By replacing n by $2k - 1$, Equation (2.31a) may be written as

$$V(x, y) = \frac{4V_o}{\pi} \sum_{k=1}^{\infty} \frac{\sin \frac{n\pi x}{a} \sinh \frac{n\pi y}{a}}{n \sinh \frac{n\pi b}{a}}, \quad n = 2k - 1 \quad (2.31b)$$

2.3.2 Wave Equation

The time dependence has been taken care of in Section 2.2. We are left with solving the Helmholtz equation

$$\nabla^2 U + k^2 U = 0 \quad (2.5b)$$

In rectangular coordinates, Equation (2.5b) becomes

$$\frac{\partial^2 U}{\partial x^2} + \frac{\partial^2 U}{\partial y^2} + \frac{\partial^2 U}{\partial z^2} + k^2 U = 0 \quad (2.32)$$

We let

$$U(x, y, z) = X(x)Y(y)Z(z) \quad (2.33)$$

Substituting Equation (2.33) into Equation (2.32) and dividing by XYZ , we obtain

$$\frac{X''}{X} + \frac{Y''}{Y} + \frac{Z''}{Z} + k^2 = 0 \quad (2.34)$$

Each term must be equal to a constant since each term depends only on the corresponding variable; X on x , etc. We conclude that

$$\frac{X''}{X} = -k_x^2, \quad \frac{Y''}{Y} = -k_y^2, \quad \frac{Z''}{Z} = -k_z^2 \quad (2.35)$$

so that Equation (2.34) reduces to

$$k_x^2 + k_y^2 + k_z^2 = k^2 \quad (2.36)$$

Notice that there are four separation constants k , k_x , k_y , and k_z since we have four variables t , x , y , and z . But from Equation (2.36), one is related to the other three so that only three separation constants are independent. As mentioned earlier, the number of independent separation constants is generally one less than the number of independent variables involved. The ordinary differential equations in Equation (2.35) have solutions

$$X = A_1 e^{jk_x x} + A_2 e^{-jk_x x} \quad (2.37a)$$

2.3. SEPARATION OF VARIABLES IN RECTANGULAR COORDINATES

or

$$X = B_1 \sin k_x x + B_2 \cos k_x x, \quad (2.37b)$$

$$Y = A_3 e^{jk_y y} + A_4 e^{-jk_y y} \quad (2.37c)$$

or

$$Y = B_3 \sin k_y y + B_4 \cos k_y y, \quad (2.37d)$$

$$Z = A_5 e^{jk_z z} + A_6 e^{-jk_z z} \quad (2.37e)$$

or

$$Z = B_5 \sin k_z z + B_6 \cos k_z z, \quad (2.37f)$$

Various combinations of X , Y , and Z will satisfy Equation (2.5b). Suppose we choose

$$X = A_1 e^{jk_x x}, \quad Y = A_3 e^{jk_y y}, \quad Z = A_5 e^{jk_z z}, \quad (2.38)$$

then

$$U(x, y, z) = A e^{j(k_x x + k_y y + k_z z)} \quad (2.39)$$

or

$$U(\mathbf{r}) = A e^{j\mathbf{k} \cdot \mathbf{r}} \quad (2.40)$$

Introducing the time dependence of Equation (2.6a) gives

$$\Phi(x, y, z, t) = A e^{j(\mathbf{k} \cdot \mathbf{r} + \omega t)} \quad (2.41)$$

where $\omega = kc$ is the angular frequency of the wave and k is given by Equation (2.36). The solution in Equation (2.41) represents a plane wave of amplitude A propagating in the direction of the wave vector $\mathbf{k} = k_x \mathbf{a}_x + k_y \mathbf{a}_y + k_z \mathbf{a}_z$ with velocity c .

Example 2.1

In this example, we would like to show that the method of separation of variables is not limited to a problem with only one inhomogeneous boundary condition as presented in Section 2.3.1. We reconsider the problem of Figure 2.1, but with four inhomogeneous boundary conditions as in Figure 2.2(a). \square

Solution

The problem can be stated as solving Laplace's equation

$$\frac{\partial^2 V}{\partial x^2} + \frac{\partial^2 V}{\partial y^2} = 0 \quad (2.42)$$

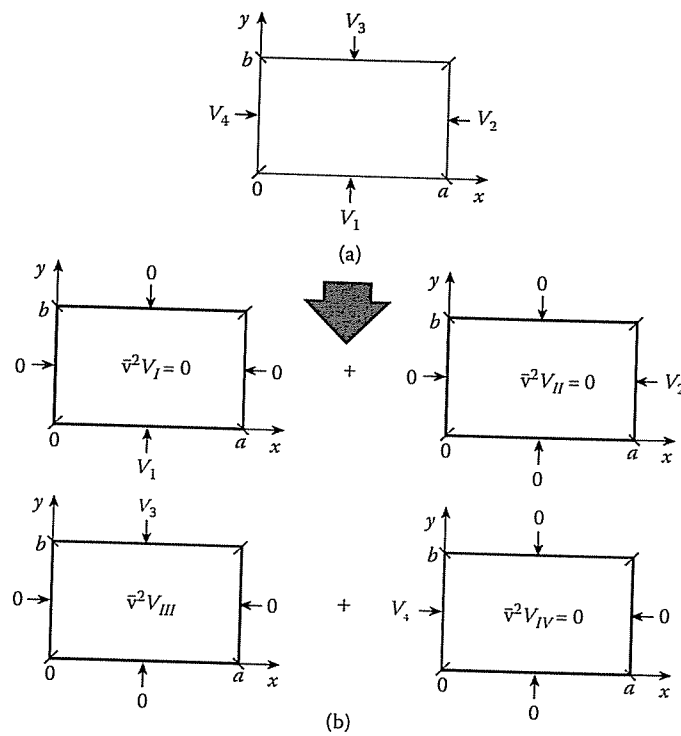


Figure 2.2

Applying the principle of superposition reduces the problem in (a) to those in (b).

subject to the following inhomogeneous Dirichlet conditions:

$$\begin{aligned} V(x, 0) &= V_1 \\ V(x, b) &= V_3 \\ V(0, y) &= V_4 \\ V(a, y) &= V_2 \end{aligned} \quad (2.43)$$

Since Laplace's equation is a linear homogeneous equation, the problem can be simplified by applying the superposition principle. If we let

$$V = V_I + V_{II} + V_{III} + V_{IV}, \quad (2.44)$$

we may reduce the problem to four simpler problems, each of which is associated with one of the inhomogeneous conditions. The reduced, simpler problems are illustrated in Figure 2.2 (b) and stated as follows:

$$\frac{\partial^2 V_I}{\partial x^2} + \frac{\partial^2 V_I}{\partial y^2} = 0 \quad (2.45)$$

2.3. SEPARATION OF VARIABLES IN RECTANGULAR COORDINATES

subject to

$$\begin{aligned} V_I(x, 0) &= V_1 \\ V_I(x, b) &= 0 \\ V_I(0, y) &= 0 \\ V_I(a, y) &= 0; \end{aligned} \quad (2.46)$$

$$\frac{\partial^2 V_{II}}{\partial x^2} + \frac{\partial^2 V_{II}}{\partial y^2} = 0 \quad (2.47)$$

subject to

$$\begin{aligned} V_{II}(x, 0) &= 0 \\ V_{II}(x, b) &= 0 \\ V_{II}(0, y) &= 0 \\ V_{II}(a, y) &= V_2; \end{aligned} \quad (2.48)$$

$$\frac{\partial^2 V_{III}}{\partial x^2} + \frac{\partial^2 V_{III}}{\partial y^2} = 0 \quad (2.49)$$

subject to

$$\begin{aligned} V_{III}(x, 0) &= 0 \\ V_{III}(x, b) &= V_3 \\ V_{III}(0, y) &= 0 \\ V_{III}(a, y) &= 0; \end{aligned} \quad (2.50)$$

and

$$\frac{\partial^2 V_{IV}}{\partial x^2} + \frac{\partial^2 V_{IV}}{\partial y^2} = 0 \quad (2.51)$$

subject to

$$\begin{aligned} V_{IV}(x, 0) &= 0 \\ V_{IV}(x, b) &= 0 \\ V_{IV}(0, y) &= V_4 \\ V_{IV}(a, y) &= 0; \end{aligned} \quad (2.52)$$

It is obvious that the reduced problem in Equations (2.49) and (2.50) with solution V_{III} is the same as that in Figure 2.1. The other three reduced problems are quite similar. Hence the solutions V_I , V_{II} , and V_{IV} can be obtained by taking the same steps

as in Section 2.3.1 or by a proper exchange of variables in Equation (2.31). Thus

$$V_I = \frac{4V_1}{\pi} \sum_{n=\text{odd}}^{\infty} \frac{\sin \frac{n\pi x}{a} \sinh \frac{n\pi(b-y)}{a}}{n \sinh \frac{n\pi b}{a}}, \quad (2.53)$$

$$V_{II} = \frac{4V_2}{\pi} \sum_{n=\text{odd}}^{\infty} \frac{\sin \frac{n\pi x}{b} \sinh \frac{n\pi y}{b}}{n \sinh \frac{n\pi a}{b}}, \quad (2.54)$$

$$V_{III} = \frac{4V_3}{\pi} \sum_{n=\text{odd}}^{\infty} \frac{\sin \frac{n\pi x}{a} \sinh \frac{n\pi y}{a}}{n \sinh \frac{n\pi b}{a}}, \quad (2.55)$$

$$V_{IV} = \frac{4V_4}{\pi} \sum_{n=\text{odd}}^{\infty} \frac{\sin \frac{n\pi(a-x)}{b} \sinh \frac{n\pi y}{b}}{n \sinh \frac{n\pi a}{b}} \quad (2.56)$$

We obtain the complete solution by substituting Equations (2.53) to (2.56) in Equation (2.44). ■

Example 2.2

Find the product solution of the diffusion equation

$$\Phi_t = k\Phi_{xx}, \quad 0 < x < 1, \quad t > 0 \quad (2.57)$$

subject to the boundary conditions

$$\Phi(0, t) = 0 = \Phi(1, t), \quad t > 0 \quad (2.58)$$

and initial condition

$$\Phi(x, 0) = 5 \sin 2\pi x, \quad 0 < x < 1 \quad \square \quad (2.59)$$

Solution

Let

$$\Phi(x, t) = X(x)U(t) \quad (2.60)$$

Substitute this into Equation (2.57) and divide by kXT to obtain

$$\frac{U'}{kU} = \frac{X''}{X} = \lambda$$

where λ is the separation constant. Thus

$$X'' - \lambda X = 0 \quad (2.61)$$

$$U' - \lambda k U = 0 \quad (2.62)$$

As usual, in order for the solution of Equation (2.61) to satisfy Equation (2.58), we must choose $\lambda = -\beta^2 = -n^2\pi^2$ so that $n = 1, 2, 3, \dots$ and

$$X_n(x) = \sin n\pi x \quad (2.63)$$

2.4. SEPARATION OF VARIABLES IN CYLINDRICAL COORDINATES

Equation (2.62) becomes

$$U' + kn^2\pi^2 U = 0,$$

which has solution

$$U_n(t) = e^{-kn^2\pi^2 t} \quad (2.64)$$

Substituting Equations (2.63) and (2.64) into Equation (2.60),

$$\Phi_n(x, t) = a_n \sin n\pi x \exp(-kn^2\pi^2 t)$$

where the coefficients a_n are to be determined from the initial condition in Equation (2.59). The complete solution is a linear combination of Φ_n , i.e.,

$$\Phi(x, t) = \sum_{n=1}^{\infty} a_n \sin n\pi x \exp(-kn^2\pi^2 t)$$

This satisfies Equation (2.59) if

$$\Phi(x, 0) = \sum_{n=1}^{\infty} a_n \sin n\pi x = 5 \sin 2\pi x \quad (2.65)$$

The coefficients a_n are determined as

$$a_n = \frac{2}{T} \int_0^1 5 \sin 2\pi x \sin n\pi x dx = \begin{cases} 5, & n = 2 \\ 0, & n \neq 0 \end{cases}$$

Alternatively, by comparing the middle term in Equation (2.65) with the last term, the two are equal only when $n = 2$, $a_n = 5$, otherwise $a_n = 0$. Hence the solution of the diffusion problem becomes

$$\Phi(x, t) = 5 \sin 2\pi x \exp(-4k\pi^2 t) \quad \square$$

2.4 Separation of Variables in Cylindrical Coordinates

Coordinate geometries other than rectangular Cartesian are used to describe many EM problems whenever it is necessary and convenient. For example, a problem having cylindrical symmetry is best solved in a cylindrical system where the coordinate variables (ρ, ϕ, z) are related as shown in Figure 2.3 and $0 \leq \rho \leq \infty$, $0 \leq \phi < 2\pi$, $-\infty \leq z \leq \infty$. In this system, the wave equation (2.5b) becomes

$$\nabla^2 U + k^2 U = \frac{1}{\rho} \frac{\partial}{\partial \rho} \left(\rho \frac{\partial U}{\partial \rho} \right) + \frac{1}{\rho^2} \frac{\partial^2 U}{\partial \phi^2} + \frac{\partial^2 U}{\partial z^2} + k^2 U = 0 \quad (2.66)$$

As we did in the previous section, we shall first solve Laplace's equation ($k = 0$) in two dimensions before we solve the wave equation.

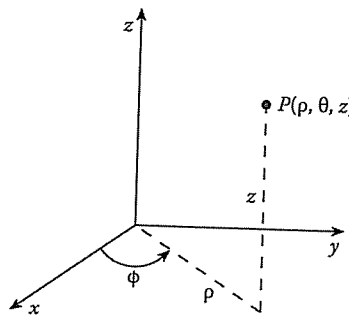


Figure 2.3
Coordinate relations in a cylindrical system.

2.4.1 Laplace's Equation

Consider an infinitely long conducting cylinder of radius a with the cross section shown in Figure 2.4. Assume that the upper half of the cylinder is maintained at potential V_0 while the lower half is maintained at potential $-V_0$. This is a Laplacian problem in two dimensions. Hence we need to solve for $V(\rho, \phi)$ in Laplace's equation

$$\nabla^2 V = \frac{1}{\rho} \frac{\partial}{\partial \rho} \left(\rho \frac{\partial V}{\partial \rho} \right) + \frac{1}{\rho^2} \frac{\partial^2 V}{\partial \phi^2} = 0 \quad (2.67)$$

subject to the inhomogeneous Dirichlet boundary condition

$$V(a, \phi) = \begin{cases} V_0, & 0 < \phi < \pi \\ -V_0, & \pi < \phi < 2\pi \end{cases} \quad (2.68)$$

We let

$$V(\rho, \phi) = R(\rho)F(\phi) \quad (2.69)$$

Substituting Equation (2.69) into Equation (2.67) and dividing through by RF/ρ^2 result in

$$\frac{\rho}{R} \frac{d}{d\rho} \left(\rho \frac{dR}{d\rho} \right) + \frac{1}{F} \frac{d^2 F}{d\phi^2} = 0$$

or

$$\frac{\rho^2}{R} \frac{d^2 R}{d\rho^2} + \frac{\rho}{R} \frac{dR}{d\rho} = -\frac{1}{F} \frac{d^2 F}{d\phi^2} = \lambda^2 \quad (2.70)$$

where λ is the separation constant. Thus the separated equations are

$$F'' + \lambda^2 F = 0 \quad (2.71a)$$

$$\rho^2 R'' + \rho R' - \lambda^2 R = 0 \quad (2.71b)$$

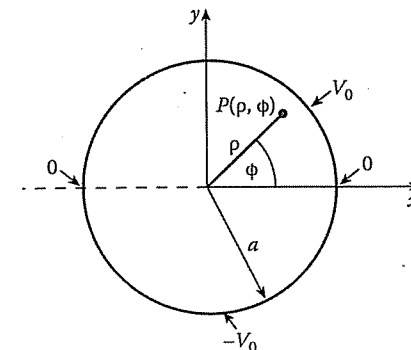


Figure 2.4
A two-dimensional Laplacian problem in cylindrical coordinates.

It is evident that Equation (2.71a) has the general solution of the form

$$F(\phi) = c_1 \cos(\lambda\phi) + c_2 \sin(\lambda\phi) \quad (2.72)$$

From the boundary conditions of Equation (2.68), we observe that $F(\phi)$ must be a periodic, odd function. Thus $c_1 = 0$, $\lambda = n$, a real integer, and hence Equation (2.72) becomes

$$F_n(\phi) = c_2 \sin n\phi \quad (2.73)$$

Equation (2.71b), known as the *Cauchy-Euler equation*, can be solved by making a substitution $\rho = e^u$ and reducing it to an equation with constant coefficients. This leads to

$$R_n(\rho) = c_3 \rho^n + c_4 \rho^{-n}, \quad n = 1, 2, \dots \quad (2.74)$$

Note that case $n = 0$ is excluded; if $n = 0$, we obtain $R(\rho) = \ln \rho + \text{constant}$, which is not finite at $\rho = 0$. For the problem of a coaxial cable, $a < \rho < b$, $\rho \neq 0$ so that case $n = 0$ is the only solution. However, for the problem at hand, $n = 0$ is not acceptable.

Substitution of Equations (2.73) and (2.74) into Equation (2.69) yields

$$V_n(\rho, \phi) = \sin n\phi (A_n \rho^n + B_n \rho^{-n}) \quad (2.75)$$

where A_n and B_n are constants to be determined. As usual, it is possible by the superposition principle to form a complete series solution

$$V(\rho, \phi) = \sum_{n=1}^{\infty} (A_n \rho^n + B_n \rho^{-n}) \sin n\phi \quad (2.76)$$

For $\rho < a$, inside the cylinder, V must be finite as $\rho \rightarrow 0$ so that $B_n = 0$. At $\rho = a$,

$$V(a, \phi) = \sum_{n=1}^{\infty} A_n a^n \sin n\phi = \begin{cases} V_0, & 0 < \phi < \pi \\ -V_0, & \pi < \phi < 2\pi \end{cases} \quad (2.77)$$

Multiplying both sides by $\sin m\phi$ and integrating over $0 < \phi < 2\pi$, we get

$$\int_0^\pi V_o \sin m\phi d\phi - \int_\pi^{2\pi} V_o \sin m\phi d\phi = \sum_{n=1}^{\infty} A_n a^n \int_0^{2\pi} \sin n\phi \sin m\phi d\phi$$

All terms in the right-hand side vanish except when $m = n$. Hence

$$\frac{2V_o}{n}(1 - \cos n\pi) = A_n a^n \int_0^{2\pi} \sin^2 \phi d\phi = \pi A_n a^n$$

or

$$A_n = \begin{cases} \frac{4V_o}{n\pi a^n}, & n = \text{odd} \\ 0, & n = \text{even} \end{cases} \quad (2.78)$$

Thus,

$$V(\rho, \phi) = \frac{4V_o}{\pi} \sum_{n=\text{odd}}^{\infty} \frac{\rho^n \sin n\phi}{na^n}, \quad \rho < a \quad (2.79)$$

For $\rho > a$, outside the cylinder, V must be finite as $\rho \rightarrow \infty$ so that $A_n = 0$ in Equation (2.76) for this case. By imposing the boundary condition in Equation (2.68) and following the same steps as for case $\rho < a$, we obtain

$$B_n = \begin{cases} \frac{4V_o a^n}{n\pi}, & n = \text{odd} \\ 0, & n = \text{even} \end{cases} \quad (2.80)$$

Hence,

$$V(\rho, \phi) = \frac{4V_o}{\pi} \sum_{n=\text{odd}}^{\infty} \frac{a^n \sin n\phi}{n\rho^n}, \quad \rho > a \quad (2.81)$$

2.4.2 Wave Equation

Having taken care of the time-dependence in Section 2.2, we now solve Helmholtz's equation (2.66), i.e.,

$$\frac{1}{\rho} \frac{\partial}{\partial \rho} \left(\rho \frac{\partial U}{\partial \rho} \right) + \frac{1}{\rho^2} \frac{\partial^2 U}{\partial \phi^2} + \frac{\partial^2 U}{\partial z^2} + k^2 U = 0 \quad (2.66)$$

Let

$$U(\rho, \phi, z) = R(\rho)F(\phi)Z(z) \quad (2.82)$$

Substituting Equation (2.82) into Equation (2.66) and dividing by RFZ/ρ^2 yields

$$\frac{\rho}{R} \frac{d}{d\rho} \left(\rho \frac{dR}{d\rho} \right) + \frac{\rho^2}{Z} \frac{d^2 Z}{dz^2} + k^2 \rho^2 = -\frac{1}{F} \frac{d^2 F}{d\phi^2} = n^2$$

where $n = 0, 1, 2, \dots$ and n^2 is the separation constant. Thus

$$F'' + n^2 F = 0 \quad (2.83)$$

and

$$\frac{\rho}{R} \frac{d}{d\rho} \left(\rho \frac{dR}{d\rho} \right) + \frac{\rho^2}{Z} \frac{d^2 Z}{dz^2} + k^2 \rho^2 = n^2 \quad (2.84)$$

Dividing both sides of Equation (2.84) by ρ^2 leads to

$$\frac{1}{\rho R} \frac{d}{d\rho} \left(\rho \frac{dR}{d\rho} \right) + \left(k^2 - \frac{n^2}{\rho^2} \right) = -\frac{1}{Z} \frac{d^2 Z}{dz^2} = \mu^2$$

where μ^2 is another separation constant. Hence

$$-\frac{1}{Z} \frac{d^2 Z}{dz^2} = \mu^2 \quad (2.85)$$

and

$$\frac{1}{\rho R} \frac{d}{d\rho} \left(\rho \frac{dR}{d\rho} \right) + \left(k^2 - \mu^2 - \frac{n^2}{\rho^2} \right) = 0 \quad (2.86)$$

If we let

$$\lambda^2 = k^2 - \mu^2, \quad (2.87)$$

the three separated equations (2.83), (2.85), and (2.86) become

$$F'' + n^2 F = 0, \quad (2.88)$$

$$Z'' + \mu^2 Z = 0, \quad (2.89)$$

$$\rho^2 R'' + \rho R' + (\lambda^2 \rho^2 - n^2) R = 0 \quad (2.90)$$

The solution to Equation (2.88) is given by

$$F(\phi) = c_1 e^{jn\phi} + c_2 e^{-jn\phi} \quad (2.91a)$$

or

$$F(\phi) = c_3 \sin n\phi + c_4 \cos n\phi \quad (2.91b)$$

Similarly, Equation (2.89) has the solution

$$Z(z) = c_5 e^{jn\mu} + c_6 e^{-jn\mu} \quad (2.92a)$$

or

$$Z(z) = c_7 \sin n\mu + c_8 \cos n\mu \quad (2.92b)$$

To solve Equation (2.90), we let $x = \lambda\rho$ and replace R by y ; $R' = \lambda y'$ and $R'' = \lambda^2 y''$ and Equation (2.90) becomes

$$x^2 y'' + xy' + (x^2 - n^2)y = 0 \quad (2.93)$$

This is called *Bessel's equation*. It has a general solution of the form

$$y(x) = b_1 J_n(x) + b_2 Y_n(x) \quad (2.94)$$

where $J_n(x)$ and $Y_n(x)$ are, respectively, *Bessel functions* of the first and second kinds of order n and real argument x . Y_n is also called the *Neumann function*. If x in Equation (2.93) is imaginary so that we may replace x by jx , the equation becomes

$$x^2 y'' + xy' - (x^2 + n^2)y = 0 \quad (2.95)$$

which is called *modified Bessel's equation*. This equation has a solution of the form

$$y(x) = b_3 I_n(x) + b_4 K_n(x) \quad (2.96)$$

where $I_n(x)$ and $K_n(x)$ are respectively *modified Bessel functions* of the first and second kind of order n . For small values of x , Figure 2.5 shows the sketch of some typical Bessel functions (or cylindrical functions) $J_n(x)$, $Y_n(x)$, $I_n(x)$, and $K_n(x)$.

To obtain the Bessel functions from Eqs (2.93) and (2.95), the method of Frobenius is applied. A detailed discussion is found in Kersten [4] and Myint-U [5]. For the Bessel function of the first kind,

$$y = J_n(x) = \sum_{m=0}^{\infty} \frac{(-1)^m (x/2)^{n+2m}}{m! \Gamma(n+m+1)} \quad (2.97)$$

where $\Gamma(k+1) = k!$ is the Gamma function. This is the most useful of all Bessel functions. Some of its important properties and identities are listed in Table 2.1. For the modified Bessel function of the second kind,

$$I_n(x) = j^{-n} J_n(jx) = \sum_{m=0}^{\infty} \frac{(x/2)^{n+2m}}{m! \Gamma(n+m+1)} \quad (2.98)$$

For the Neumann function, when $n > 0$,

$$\begin{aligned} Y_n(x) &= \frac{2}{\pi} J_n(x) \ln \frac{\gamma x}{2} - \frac{1}{\pi} \sum_{m=0}^{n-1} \frac{(n-m-1)!(x/2)^{2m-n}}{m!} \\ &\quad - \frac{1}{\pi} \sum_{m=0}^{\infty} \frac{(-1)^m (x/2)^{n+2m}}{m! \Gamma(n+m+1)} [p(m) + p(n+m)] \end{aligned} \quad (2.99)$$

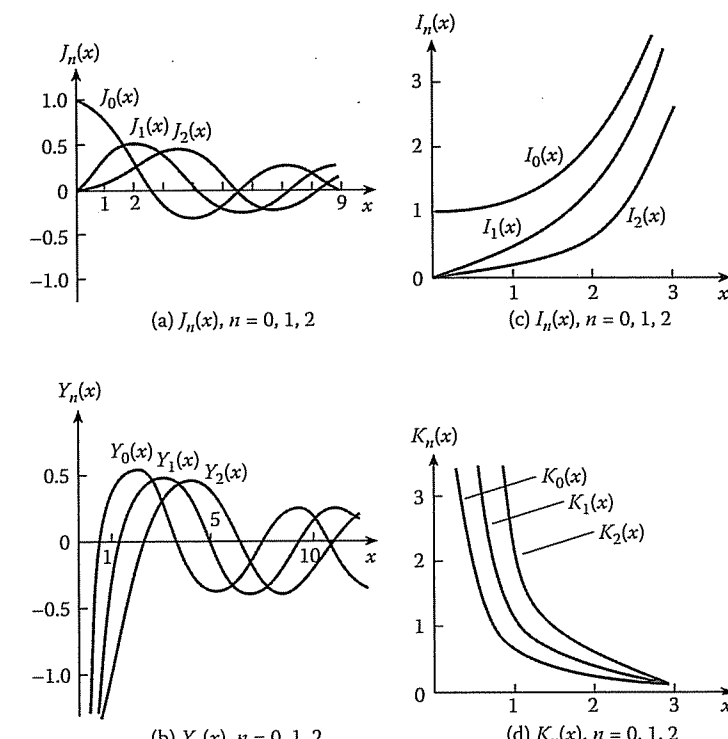


Figure 2.5
Bessel functions.

where $\gamma = 1.781$ is Euler's constant and

$$p(m) = \sum_{k=1}^m \frac{1}{k}, \quad p(0) = 0 \quad (2.100)$$

If $n = 0$,

$$Y_0(x) = \frac{2}{\pi} J_0(x) \ln \frac{\gamma x}{2} + \frac{2}{\pi} \sum_{m=0}^{\infty} \frac{(-1)^{m+1} (x/2)^{2m}}{(m!)^2} p(m) \quad (2.101)$$

For the modified Bessel function of the second kind,

$$K_n(x) = \frac{\pi}{2} j^{n+1} [J_n(jx) + j Y_n(jx)] \quad (2.102)$$

Table 2.1 Properties and Identities of Bessel Functions¹ $J_n(x)$

- (a) $J_{-n}(x) = (-1)^n J_n(x)$
 (b) $J_n(-x) = (-1)^n J_n(x)$
 (c) $J_{n+1}(x) = \frac{2n}{x} J_n(x) - J_{n-1}(x)$ (recurrence formula)

(d) $\frac{d}{dx} J_n(x) = \frac{1}{2} [J_{n-1}(x) - J_{n+1}(x)]$

(e) $\frac{d}{dx} [x^n J_n(x)] = x^n J_{n-1}(x)$

(f) $\frac{d}{dx} [x^{-n} J_n(x)] = -x^{-n} J_{n+1}(x)$

(g) $J_n(x) = \frac{1}{\pi} \int_0^\pi \cos(n\theta - x \sin\theta) d\theta, \quad n \geq 0$

(h) Fourier-Bessel expansion of $f(x)$:

$$f(x) = \sum_{k=1}^{\infty} A_k J_n(\lambda_k x), \quad n \geq 0$$

$$A_k = \frac{2}{[a J_{n+1}(\lambda_k a)]^2} \int_0^a x f(x) J_n(\lambda_k x) dx, \quad 0 < x < a$$

where λ_k are the positive roots in ascending order of magnitude of $J_n(\lambda_k a) = 0$.

(i) $\int_0^a \rho J_n(\lambda_i \rho) J_n(\lambda_j \rho) d\rho = \frac{a^2}{2} [J_{n+1}(\lambda_i a)]^2 \delta_{ij}$

where λ_i and λ_j are the positive roots of $J_n(\lambda a) = 0$.

¹ Properties (a) to (f) also hold for $Y_n(x)$.

If $n > 0$,

$$\begin{aligned} K_n(x) &= \frac{1}{2} \sum_{m=0}^{n-1} \frac{(-1)^m (n-m-1)! (x/2)^{2m-n}}{m!} \\ &+ (-1)^n \frac{1}{2} \sum_{m=0}^{\infty} \frac{(x/2)^{n+2m}}{m!(n+m)!} \left[p(m) + p(n+m) - 2 \ln \frac{\gamma x}{2} \right] \end{aligned} \quad (2.103)$$

and if $n = 0$,

$$K_0(x) = -I_0(x) \ln \frac{\gamma x}{2} + \sum_{m=0}^{\infty} \frac{(x/2)^{2m}}{(m!)^2} p(m) \quad (2.104)$$

Other functions closely related to Bessel functions are *Hankel functions* of the first and second kinds defined, respectively, by

$$H_n^{(1)}(x) = J_n(x) + j Y_n(x) \quad (2.105a)$$

$$H_n^{(2)}(x) = J_n(x) - j Y_n(x) \quad (2.105b)$$

2.4. SEPARATION OF VARIABLES IN CYLINDRICAL COORDINATES

Hankel functions are analogous to functions $\exp(\pm jx)$ just as J_n and Y_n are analogous to cosine and sine functions. This is evident from asymptotic expressions

$$J_n(x) \xrightarrow{x \rightarrow \infty} \sqrt{\frac{2}{\pi x}} \cos(x - n\pi/2 - \pi/4), \quad (2.106a)$$

$$Y_n(x) \xrightarrow{x \rightarrow \infty} \sqrt{\frac{2}{\pi x}} \sin(x - n\pi/2 - \pi/4), \quad (2.106b)$$

$$H_n^{(1)}(x) \xrightarrow{x \rightarrow \infty} \sqrt{\frac{2}{\pi x}} \exp[j(x - n\pi/2 - \pi/4)], \quad (2.106c)$$

$$H_n^{(2)}(x) \xrightarrow{x \rightarrow \infty} \sqrt{\frac{2}{\pi x}} \exp[-j(x - n\pi/2 - \pi/4)], \quad (2.106d)$$

$$I_n(x) \xrightarrow{x \rightarrow \infty} \frac{1}{\sqrt{2\pi x}} e^x, \quad (2.106e)$$

$$K_n(x) \xrightarrow{x \rightarrow \infty} \frac{1}{\sqrt{2\pi x}} e^{-x} \quad (2.106f)$$

With the time factor $e^{j\omega t}$, $H_n^{(1)}(x)$ and $H_n^{(2)}(x)$ represent inward and outward traveling waves, respectively, while $J_n(x)$ or $Y_n(x)$ represents a standing wave. With the time factor $e^{-j\omega t}$, the roles of $H_n^{(1)}(x)$ and $H_n^{(2)}(x)$ are reversed. For further treatment of Bessel and related functions, refer to the works of Watson [6] and Bell [7].

Any of the Bessel functions or related functions can be a solution to Equation (2.90) depending on the problem. If we choose $R(\rho) = J_n(x) = J_n(\lambda\rho)$ with Equations (2.91) and (2.92) and apply the superposition theorem, the solution to Equation (2.66) is

$$U(\rho, \phi, z) = \sum_n \sum_{\mu} A_{n\mu} J_n(\lambda\rho) \exp(\pm jn\phi \pm j\mu z) \quad (2.107)$$

Introducing the time dependence of Equation (2.6a), we finally get

$$\Phi(\rho, \phi, z, t) = \sum_m \sum_n \sum_{\mu} A_{mn\mu} J_n(\lambda\rho) \exp(\pm jn\phi \pm j\mu z \pm \omega t), \quad (2.108)$$

where $\omega = kc$.

Example 2.3

Consider the skin effect on a solid cylindrical conductor. The current density distribution within a good conducting wire ($\sigma/\omega\epsilon \gg 1$) obeys the diffusion equation

$$\nabla^2 J = \mu\sigma \frac{\partial J}{\partial t}$$

We want to solve this equation for a long conducting wire of radius a . □

Solution

We may derive the diffusion equation directly from Maxwell's equation. We recall that

$$\nabla \times \mathbf{H} = \mathbf{J} + \mathbf{J}_d$$

where $\mathbf{J} = \sigma \mathbf{E}$ is the conduction current density and $\mathbf{J}_d = \frac{\partial \mathbf{D}}{\partial t}$ is the displacement current density. For $\sigma/\omega\epsilon \gg 1$, \mathbf{J}_d is negligibly small compared with \mathbf{J} . Hence

$$\nabla \times \mathbf{H} \simeq \mathbf{J} \quad (2.109)$$

Also,

$$\nabla \times \mathbf{E} = -\mu \frac{\partial \mathbf{H}}{\partial t}$$

$$\nabla \times \nabla \times \mathbf{E} = \nabla \nabla \cdot \mathbf{E} - \nabla^2 \mathbf{E} = -\mu \frac{\partial}{\partial t} \nabla \times \mathbf{H}$$

Since $\nabla \cdot \mathbf{E} = 0$, introducing Equation (2.109), we obtain

$$\nabla^2 \mathbf{E} = \mu \frac{\partial \mathbf{J}}{\partial t} \quad (2.110)$$

Replacing \mathbf{E} with \mathbf{J}/σ , Equation (2.110) becomes

$$\nabla^2 \mathbf{J} = \mu \sigma \frac{\partial \mathbf{J}}{\partial t}, \quad (2.111)$$

which is the diffusion equation.

Assuming harmonic field with time factor $e^{j\omega t}$,

$$\nabla^2 \mathbf{J} = j\omega \mu \sigma \mathbf{J} \quad (2.112)$$

For infinitely long wire, Equation (2.112) reduces to a one-dimensional problem in cylindrical coordinates:

$$\frac{1}{\rho} \frac{\partial}{\partial \rho} \left(\rho \frac{\partial J_z}{\partial \rho} \right) = j\omega \mu \sigma J_z$$

or

$$\rho^2 J_z'' + \rho J_z' - j\omega \mu \sigma \rho^2 J_z = 0 \quad (2.113)$$

Comparing this with Equation (2.95) shows that Equation (2.113) is the modified Bessel equation of zero order. Hence the solution to Equation (2.113) is

$$J_z(\rho) = c_1 I_0(\lambda\rho) + c_2 K_0(\lambda\rho) \quad (2.114)$$

where c_1 and c_2 are constants and

$$\lambda = \sqrt{j\omega \mu \sigma} = j^{1/2} \frac{\sqrt{2}}{\delta} \quad (2.115)$$

and $\delta = \sqrt{\frac{2}{\sigma \mu \omega}}$ is the skin depth. Constant c_2 must vanish if J_z is to be finite at $\rho = 0$. At $\rho = a$,

$$J_z(a) = c_1 I_0(\lambda a) \rightarrow c_1 = J_z(a)/I_0(\lambda a)$$

Thus

$$J_z(\rho) = J_z(a) \frac{I_0(\lambda\rho)}{I_0(\lambda a)} \quad (2.116)$$

If we let $\lambda\rho = j^{1/2} \frac{\sqrt{2}}{\delta} \rho = j^{1/2} x$, it is convenient to replace

$$\begin{aligned} I_0(\lambda\rho) &= I_0(j^{1/2} x) = J_0(x e^{j3\pi/4}) \\ &= ber_0(x) + jbei_0(x) \end{aligned} \quad (2.117)$$

where ber_0 and bei_0 are ber and bei functions of zero order. Bei and bei functions are also known as *Kelvin functions*. For zero order, they are given by

$$ber_0(x) = \sum_{m=0}^{\infty} \frac{\cos(m\pi/2)(x/2)^{2m}}{(m!)^2}, \quad (2.118)$$

$$bei_0(x) = \sum_{m=0}^{\infty} \frac{\sin(m\pi/2)(x/2)^{2m}}{(m!)^2} \quad (2.119)$$

Using ber and bei functions, Equation (2.116) may be written as

$$J_z(\rho) = J_z(a) \frac{ber_0(x) + jbei_0(x)}{ber_0(y) + jbei_0(y)} \quad (2.120)$$

where $x = \sqrt{2}\rho/\delta$, $y = \sqrt{2}a/\delta$. \blacksquare

Example 2.4

A semi-infinitely long cylinder ($z \geq 0$) of radius a has its end at $z = 0$ maintained at $V_o(a^2 - \rho^2)$, $0 \leq \rho \leq a$. Find the potential distribution within the cylinder. \blacksquare

Solution

The problem is that of finding a function $V(\rho, z)$ satisfying the PDE

$$\nabla^2 V = \frac{\partial^2 V}{\partial \rho^2} + \frac{1}{\rho} \frac{\partial V}{\partial \rho} + \frac{\partial^2 V}{\partial z^2} = 0 \quad (2.121)$$

subject to the boundary conditions:

- (i) $V = V_o(a^2 - \rho^2)$, $z = 0$, $0 \leq \rho \leq a$,
- (ii) $V \rightarrow 0$ as $z \rightarrow \infty$, i.e., V is bounded,
- (iii) $V = 0$ on $\rho = a$,
- (iv) V is finite on $\rho = 0$.

Let $V = R(\rho)Z(z)$ and obtain the separated equations

$$Z'' - \lambda Z = 0 \quad (2.122a)$$

and

$$\rho^2 R'' + \rho R' + \lambda^2 \rho^2 R = 0 \quad (2.122b)$$

where λ is the separated constant. The solution to Equation (2.122a) is

$$Z_1 = c_1 e^{-\lambda z} + c_2 e^{\lambda z} \quad (2.123)$$

Comparing Equation (2.122b) with Equation (2.93) shows that $n = 0$ so that Equation (2.122b) is Bessel's equation with solution

$$R = c_3 J_0(\lambda\rho) + c_4 Y_0(\lambda\rho) \quad (2.124)$$

Condition (ii) forces $c_2 = 0$, while condition (iv) implies $c_4 = 0$, since $Y_0(\lambda\rho)$ blows up when $\rho = 0$. Hence the solution to Equation (2.121) is

$$V(\rho, z) = \sum_{n=0}^{\infty} A_n e^{-\lambda_n z} J_0(\lambda_n \rho) \quad (2.125)$$

where A_n and λ_n are constants to be determined using conditions (i) and (iii). Imposing condition (iii) on Equation (2.125) yields the transcendent equation

$$J_0(\lambda_n a) = 0 \quad (2.126)$$

Thus λ_n are the positive roots of $J_0(\lambda_n a)$. If we take λ_1 as the first root, λ_2 as the second root, etc., n must start from 1 in Equation (2.125). Imposing condition (i) on Equation (2.125), we obtain

$$V(\rho, 0) = V_o (a^2 - \rho^2) = \sum_{n=1}^{\infty} A_n J_0(\lambda_n \rho)$$

which is simply the Fourier-Bessel expansion of $V_o(a^2 - \rho^2)$. From Table 2.1, property (h),

$$A_n = \frac{2}{a^2 [J_1(\lambda_n a)]^2} \int_0^a \rho V_o (a^2 - \rho^2) J_0(\lambda_n \rho) d\rho \quad (2.127)$$

To evaluate the integral, we utilize property (e) in Table 2.1:

$$\int_0^a x^n J_{n-1}(x) dx = x^n J_n(x) \Big|_0^a = a^n J_n(a), \quad n > 0$$

By changing variables, $x = \lambda\rho$,

$$\int_0^a \rho^n J_{n-1}(\lambda\rho) d\rho = \frac{a^n}{\lambda} J_n(\lambda a) \quad (2.128)$$

If $n = 1$,

$$\int_0^a \rho J_0(\lambda\rho) d\rho = \frac{a}{\lambda} J_1(\lambda a) \quad (2.129)$$

Similarly, using property (e) in Table 2.1, we may write

$$\int_0^a \rho^3 J_0(\lambda\rho) d\rho = \int_0^a \frac{\rho^2}{\lambda} \frac{\partial}{\partial \rho} [\rho J_1(\lambda\rho)] d\rho$$

Integrating the right-hand side by parts and applying Equation (2.128),

$$\begin{aligned} \int_0^a \rho^3 J_0(\lambda\rho) d\rho &= \frac{a^3}{\lambda} J_1(\lambda a) - \frac{2}{\lambda} \int_0^a \rho^2 J_1(\lambda\rho) d\rho \\ &= \frac{a^3}{\lambda} J_1(\lambda a) - \frac{2a^2}{\lambda^2} J_2(\lambda a) \end{aligned}$$

$J_2(x)$ can be expressed in terms of $J_0(x)$ and $J_1(x)$ using the recurrence relations, i.e., property (c) in Table 2.1:

$$J_2(x) = \frac{2}{x} J_1(x) - J_0(x)$$

Hence

$$\int_0^a \rho^3 J_0(\lambda_n \rho) d\rho = \frac{2a^2}{\lambda_n^2} \left[J_0(\lambda_n a) + \left(\frac{a\lambda_n}{2} - \frac{2}{a\lambda_n} \right) J_1(\lambda_n a) \right] \quad (2.130)$$

Substitution of Equations (2.129) and (2.130) into Equation (2.127) gives

$$\begin{aligned} A_n &= \frac{2V_o}{a^2 [J_1(\lambda_n a)]^2} \left[\frac{4a}{\lambda_n^3} J_1(\lambda_n a) - \frac{2a^2}{\lambda_n^2} J_0(\lambda_n a) \right] \\ &= \frac{8V_o}{a\lambda_n^3 J_1(\lambda_n a)} \end{aligned}$$

since $J_0(\lambda_n a) = 0$ from Equation (2.126). Thus the potential distribution is given by

$$V(\rho, z) = \frac{8V_o}{a} \sum_{n=1}^{\infty} \frac{e^{-\lambda_n z} J_0(\lambda_n \rho)}{\lambda_n^3 J_1(\lambda_n a)}$$

Example 2.5

A plane wave $\mathbf{E} = E_o e^{j(\omega t - kx)} \mathbf{a}_z$ is incident on an infinitely long conducting cylinder of radius a . Determine the scattered field. \square

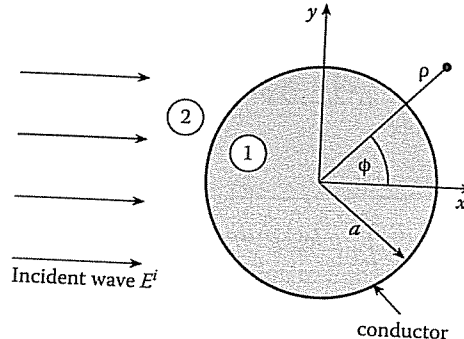


Figure 2.6
Scattering by a conducting cylinder.

Solution

Since the cylinder is infinitely long, the problem is two-dimensional as shown in Figure 2.6. We shall suppress the time factor $e^{j\omega t}$ throughout the analysis. For the sake of convenience, we need to express the plane wave in terms of cylindrical waves. We let

$$e^{-jx} = e^{-j\rho \cos \phi} = \sum_{n=-\infty}^{\infty} a_n J_n(\rho) e^{jn\phi} \quad (2.131)$$

where a_n are expansion coefficients to be determined. Since $e^{jn\phi}$ are orthogonal functions, multiplying both sides of Equation (2.131) by $e^{jm\phi}$ and integrating over $0 \leq \phi \leq 2\pi$ gives

$$\int_0^{2\pi} e^{-j\rho \cos \phi} e^{jm\phi} d\phi = 2\pi a_m J_m(\rho)$$

Taking the m th derivative of both sides with respect to ρ and evaluating at $\rho = 0$ leads to

$$2\pi \frac{j^{-m}}{2^m} = 2\pi a_m \frac{1}{2^m} \rightarrow a_m = j^{-m}$$

Substituting this into Equation (2.131), we obtain

$$e^{-jx} = \sum_{n=-\infty}^{\infty} j^{-n} J_n(\rho) e^{jn\phi}$$

(An alternative, easier way of obtaining this is using the generating function for $J_n(x)$ in Table 2.7.) Thus the incident wave may be written as

$$E_z^i = E_o e^{-jkx} = E_o \sum_{n=-\infty}^{\infty} (-j)^n J_n(k\rho) e^{jn\phi} \quad (2.132)$$

Since the scattered field E_z^s must consist of outgoing waves that vanish at infinity, it contains

$$J_n(k\rho) - j Y_n(k\rho) = H_n^{(2)}(k\rho)$$

Hence

$$E_z^s = \sum_{n=-\infty}^{\infty} A_n H_n^{(2)}(k\rho) e^{jn\phi} \quad (2.133)$$

The total field in medium 2 is

$$E_2 = E_z^i + E_z^s$$

while the total field in medium 1 is $E_1 = 0$ since medium 1 is conducting. At $\rho = a$, the boundary condition requires that the tangential components of E_1 and E_2 be equal. Hence

$$E_z^i(\rho = a) + E_z^s(\rho = a) = 0 \quad (2.134)$$

Substituting Equations (2.132) and (2.133) into Equation (2.134),

$$\sum_{n=-\infty}^{\infty} [E_o(-j)^n J_n(ka) + A_n H_n^{(2)}(ka)] e^{jn\phi} = 0$$

From this, we obtain

$$A_n = -\frac{E_o(-j)^n J_n(ka)}{H_n^{(2)}(ka)}$$

Finally, substituting A_n into Equation (2.133) and introducing the time factor leads to the scattered wave as

$$E_z^s = -E_o e^{j\omega t} \mathbf{a}_z \sum_{n=-\infty}^{\infty} (-j)^n \frac{J_n(ka) H_n^{(2)}(k\rho) e^{jn\phi}}{H_n^{(2)}(ka)} \quad \blacksquare$$

2.5 Separation of Variables in Spherical Coordinates

Spherical coordinates (r, θ, ϕ) may be defined as in Figure 2.7, where $0 \leq r \leq \infty$, $0 \leq \theta \leq \pi$, $0 \leq \phi < 2\pi$. In this system, the wave equation (2.5b) becomes

$$\begin{aligned} \nabla^2 U + k^2 U &= \frac{1}{r^2} \frac{\partial}{\partial r} \left(r^2 \frac{\partial U}{\partial r} \right) + \frac{1}{r^2 \sin \theta} \frac{\partial}{\partial \theta} \left(\sin \theta \frac{\partial U}{\partial \theta} \right) \\ &\quad + \frac{1}{r^2 \sin^2 \theta} \frac{\partial^2 U}{\partial \phi^2} + k^2 U = 0 \end{aligned} \quad (2.135)$$

As usual, we shall first solve Laplace's equation in two dimensions and later solve the wave equation in three dimensions.

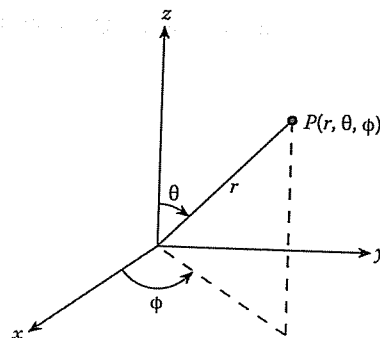


Figure 2.7
Coordinate relation in a spherical system.

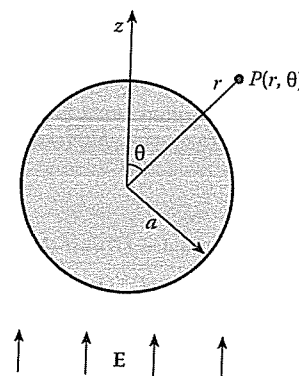


Figure 2.8
An uncharged conducting sphere in a uniform external electric field.

2.5.1 Laplace's Equation

Consider the problem of finding the potential distribution due to an uncharged conducting sphere of radius a located in an external uniform electric field as in Figure 2.8. The external electric field can be described as

$$\mathbf{E} = E_o \mathbf{a}_z \quad (2.136)$$

while the corresponding electric potential can be described as

$$V = - \int \mathbf{E} \cdot d\mathbf{l} = -E_o z$$

or

$$V = -E_o r \cos \theta \quad (2.137)$$

where $V(\theta = \pi/2) = 0$ has been assumed. From Equation (2.137), it is evident that V is independent of ϕ , and hence our problem is solving Laplace's equation in two dimensions, namely,

$$\nabla^2 V = \frac{1}{r^2} \frac{\partial}{\partial r} \left(r^2 \frac{\partial V}{\partial r} \right) + \frac{1}{r^2 \sin \theta} \frac{\partial}{\partial \theta} \left(\sin \theta \frac{\partial V}{\partial \theta} \right) = 0 \quad (2.138)$$

subject to the conditions

$$V(r, \theta) = -E_o r \cos \theta \quad \text{as } r \rightarrow \infty, \quad (2.139a)$$

$$V(a, \theta) = 0 \quad (2.139b)$$

We let

$$V(r, \theta) = R(r)H(\theta) \quad (2.140)$$

so that Equation (2.138) becomes

$$\frac{1}{R} \frac{d}{dr} (r^2 R') = -\frac{1}{H \sin \theta} \frac{d}{d\theta} (\sin \theta H') = \lambda \quad (2.141)$$

where λ is the separation constant. Thus the separated equations are

$$r^2 R'' + 2r R' - \lambda R = 0 \quad (2.142)$$

and

$$\frac{d}{d\theta} (\sin \theta H') + \lambda \sin \theta H = 0 \quad (2.143)$$

Equation (2.142) is the *Cauchy-Euler equation*. It can be solved by making the substitution $R = r^k$. This leads to the solution

$$R_n(r) = A_n r^n + B_n r^{-(n+1)}, \quad n = 0, 1, 2, \dots \quad (2.144)$$

with $\lambda = n(n+1)$. To solve Equation (2.143), we may replace H by y and $\cos \theta$ by x so that

$$\begin{aligned} \frac{d}{d\theta} &= \frac{dx}{d\theta} \frac{d}{dx} = -\sin \theta \frac{d}{dx} \\ \frac{d}{d\theta} \left(\sin \theta \frac{dy}{d\theta} \right) &= -\sin \theta \frac{d}{dx} \left(\sin \theta \frac{dy}{d\theta} \frac{dH}{dx} \right) \\ &= \sin \theta \frac{d}{dx} \left(\sin^2 \theta \frac{dy}{dx} \right) \\ &= \sqrt{1-x^2} \frac{d}{dx} \left[(1-x^2) \frac{dy}{dx} \right] \end{aligned}$$

Making these substitutions in Equation (2.143) yields

$$\frac{d}{dx} \left[(1-x^2) \frac{dy}{dx} \right] + n(n+1)y = 0$$

or

$$(1-x^2)y'' - 2xy' + n(n+1)y = 0 \quad (2.145)$$

which is the *Legendre differential equation*. Its solution is obtained by the method of Frobenius [5] as

$$y = c_n P_n(x) + d_n Q_n(x) \quad (2.146)$$

where $P_n(x)$ and $Q_n(x)$ are Legendre functions of the first and second kind, respectively.

$$P_n(x) = \sum_{k=0}^N \frac{(-1)^k (2n-2k)! x^{n-2k}}{2^n k! (n-k)! (n-2k)!} \quad (2.147)$$

where $N = n/2$ if n is even and $N = (n-1)/2$ if n is odd. For example,

$$P_0(x) = 1$$

$$P_1(x) = x = \cos \theta$$

$$P_2(x) = \frac{1}{2}(3x^2 - 1) = \frac{1}{4}(3\cos 2\theta + 1)$$

$$P_3(x) = \frac{1}{2}(5x^3 - 3x) = \frac{1}{8}(5\cos 3\theta + 3\cos \theta)$$

$$P_4(x) = \frac{1}{8}(35x^4 - 30x^2 + 3) = \frac{1}{64}(35\cos 4\theta + 20\cos 2\theta + 9)$$

$$P_5(x) = \frac{1}{8}(63x^5 - 70x^3 + 15x) = \frac{1}{128}(30\cos \theta + 35\cos 3\theta + 63\cos 5\theta)$$

Some useful identities and properties [5] of Legendre functions are listed in Table 2.2. The Legendre functions of the second kind are given by

$$\begin{aligned} Q_n(x) &= P_n(x) \left[\frac{1}{2} \ln \frac{1+x}{1-x} - p(n) \right] \\ &+ \sum_{k=1}^n \frac{(-1)^k (n+k)!}{(k!)^2 (n-k)!} p(k) \left[\frac{1-x}{2} \right]^k \end{aligned} \quad (2.148)$$

where $p(k)$ is as defined in Equation (2.100). Typical graphs of $P_n(x)$ and $Q_n(x)$ are shown in Figure 2.9. Q_n are not as useful as P_n since they are singular at $x = \pm 1$ (or $\theta = 0, \pi$) due to the logarithmic term in Equation (2.148). We use Q_n only when $x \neq \pm 1$ (or $\theta \neq 0, \pi$), e.g., in problems having conical boundaries that exclude the axis from the solution region. For the problem at hand, $\theta = 0, \pi$ is included so that the solution to Equation (2.143) is

$$H_n(\theta) = P_n(\cos \theta) \quad (2.149)$$

Table 2.2 Properties and Identities of Legendre Functions¹

- (a) For $n \geq 1$, $P_n(1) = 1$, $P_n(-1) = (-1)^n$,
- $P_{2n+1} = 0$, $P_{2n}(0) = (-1)^n \frac{(2n)!}{2^{2n}(n!)^2}$
- (b) $P_n(-x) = (-1)^n P_n(x)$
- (c) $P_n(x) = \frac{1}{2^n n!} \frac{d^n}{dx^n} (x^2 - 1)^n$, $n \geq 0$
(Rodriguez formula)
- (d) $(n+1)P_{n+1}(x) = (2n+1)xP_n(x) - nP_{n-1}(x)$, $n \geq 1$
(recurrence relation)
- (e) $P'_n(x) = xP'_{n-1}(x) + nP_{n-1}(x)$, $n \geq 1$
- (f) $P_n(x) = xP_{n-1}(x) + \frac{x^2-1}{n} P'_{n-1}(x)$, $n \geq 1$
- (g) $P'_{n+1}(x) - P'_{n-1}(x) = (2n+1)P_n(x)$, $n \geq 1$
- or $\int P_n(x) dx = \frac{P_{n+1}-P_{n-1}}{2n+1}$
- (h) Fourier-Legendre series expansion of $f(x)$:

$$f(x) = \sum_{n=0}^{\infty} A_n P_n(x), \quad -1 \leq x \leq 1$$

where

$$A_n = \frac{2n+1}{2} \int_{-1}^1 f(x) P_n(x) dx, \quad n \geq 0$$

If $f(x)$ is odd,

$$A_n = (2n+1) \int_0^1 f(x) P_n(x) dx, \quad n = 0, 2, 4, \dots$$

and if $f(x)$ is even,

$$A_n = (2n+1) \int_0^1 f(x) P_n(x) dx, \quad n = 1, 3, 5, \dots$$

(i) Orthogonality property

$$\int_{-1}^1 P_n(x) P_m(x) dx = \begin{cases} 0, & n \neq m \\ \frac{2}{2n+1}, & n = m \end{cases}$$

¹ Properties (d) to (g) are also valid for $Q_n(x)$.

Substituting Equations (2.144) and (2.149) into Equation (2.140) gives

$$V_n(r, \theta) = [A_n r^n + B_n r^{-(n+1)}] P_n(\cos \theta) \quad (2.150)$$

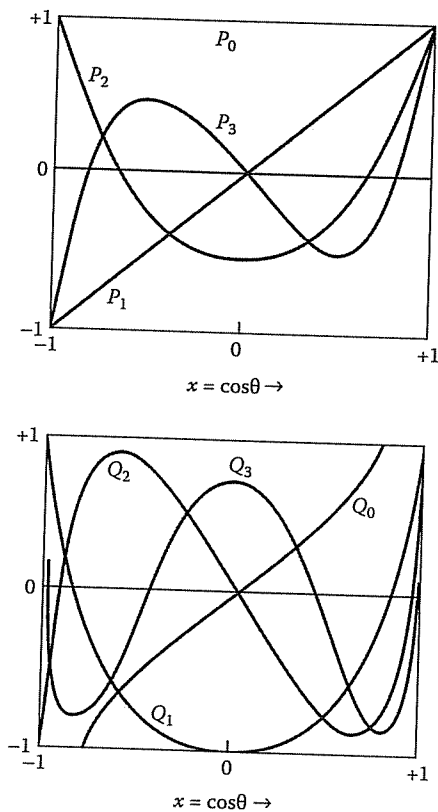


Figure 2.9

Typical Legendre functions of the first and second kinds.

To determine \$A_n\$ and \$B_n\$, we apply the boundary conditions in Equation (2.139). Since as \$r \rightarrow \infty\$, \$V = -E_o r \cos\theta\$, it follows that \$n = 1\$ and \$A_1 = -E_o\$, i.e.,

$$V(r, \theta) = \left(-E_o r + \frac{B_1}{r^2} \right) \cos\theta$$

Also since \$V = 0\$ when \$r = a\$, \$B_1 = E_o a^3\$. Hence the complete solution is

$$V(r, \theta) = -E_o \left(r - \frac{a^3}{r^2} \right) \cos\theta \quad (2.151)$$

The electric field intensity is given by

$$\begin{aligned} \mathbf{E} &= -\nabla V = -\frac{\partial V}{\partial r} \mathbf{a}_r - \frac{1}{r} \frac{\partial V}{\partial \theta} \mathbf{a}_\theta \\ &= E_o \left[1 + \frac{2a^3}{r^3} \right] \cos\theta \mathbf{a}_r + E_o \left[1 - \frac{a^3}{r^3} \right] \sin\theta \mathbf{a}_\theta \end{aligned} \quad (2.152)$$

2.5.2 Wave Equation

To solve the wave equation (2.135), we substitute

$$U(r, \theta, \phi) = R(r)H(\theta)F(\phi) \quad (2.153)$$

into the equation. Multiplying the result by \$r^2 \sin^2\theta / RH F\$ gives

$$\begin{aligned} \frac{\sin^2\theta}{R} \frac{d}{dr} \left(r^2 \frac{dR}{dr} \right) + \frac{\sin\theta}{H} \frac{d}{d\theta} \left(\sin\theta \frac{dH}{d\theta} \right) \\ + k^2 r^2 \sin^2\theta = -\frac{1}{F} \frac{d^2 F}{d\phi^2} \end{aligned} \quad (2.154)$$

Since the left-hand side of this equation is independent of \$\phi\$, we let

$$-\frac{1}{F} \frac{d^2 F}{d\phi^2} = m^2, \quad m = 0, 1, 2, \dots$$

where \$m\$, the first separation constant, is chosen to be nonnegative integer such that \$U\$ is periodic in \$\phi\$. This requirement is necessary for physical reasons that will be evident later. Thus Equation (2.154) reduces to

$$\frac{1}{R} \frac{d}{dr} \left(r^2 \frac{dR}{dr} \right) + k^2 r^2 = -\frac{1}{H \sin\theta} \frac{d}{d\theta} \left(\sin\theta \frac{dH}{d\theta} \right) + \frac{m^2}{\sin^2\theta} = \lambda$$

where \$\lambda\$ is the second separation constant. As in Equations (2.141) to (2.144), \$\lambda = n(n+1)\$ so that the separated equations are now

$$F'' + m^2 F = 0, \quad (2.155)$$

$$R'' + \frac{2}{r} R' + \left[k^2 - \frac{n(n+1)}{r^2} \right] R = 0, \quad (2.156)$$

and

$$\frac{1}{\sin\theta} \frac{d}{d\theta} (\sin\theta H') + \left[n(n+1) - \frac{m^2}{\sin^2\theta} \right] H = 0 \quad (2.157)$$

As usual, the solution to Equation (2.155) is

$$F(\phi) = c_1 e^{jm\phi} + c_2 e^{-jm\phi} \quad (2.158a)$$

or

$$F(\phi) = c_3 \sin m\phi + c_4 \cos m\phi \quad (2.158b)$$

If we let \$R(r) = r^{-1/2} \tilde{R}(r)\$, Equation (2.156) becomes

$$\tilde{R}'' + \frac{1}{r} \tilde{R}' + \left[k^2 - \frac{(n+1/2)^2}{r^2} \right] \tilde{R} = 0,$$

which has the solution

$$\tilde{R} = Ar^{1/2}z_n(kr) = BZ_{n+1/2}(kr) \quad (2.159)$$

Functions $z_n(x)$ are *spherical Bessel functions* and are related to ordinary Bessel functions $Z_{n+1/2}$ according to

$$z_n(x) = \sqrt{\frac{\pi}{2x}} Z_{n+1/2}(x) \quad (2.160)$$

In Equation (2.160), $Z_{n+1/2}(x)$ may be any of the ordinary Bessel functions of half-integer order, $J_{n+1/2}(x)$, $Y_{n+1/2}(x)$, $I_{n+1/2}(x)$, $K_{n+1/2}(x)$, $H_{n+1/2}^{(1)}(x)$, and $H_{n+1/2}^{(2)}(x)$, while $z_n(x)$ may be any of the corresponding spherical Bessel functions $j_n(x)$, $y_n(x)$, $i_n(x)$, $k_n(x)$, $h_n^{(1)}(x)$, and $h_n^{(2)}(x)$. Bessel functions of fractional order are, in general, given by

$$J_\nu(x) = \sum_{k=0}^{\infty} \frac{(-1)^k x^{2k+\nu}}{2^{2k+\nu} k! \Gamma(\nu+k+1)} \quad (2.161)$$

$$Y_\nu(x) = \frac{J_\nu(x) \cos(\nu\pi) - J_{-\nu}(x)}{\sin(\nu\pi)} \quad (2.162)$$

$$I_\nu(x) = (-j)^\nu J_\nu(jx) \quad (2.163)$$

$$K_\nu(x) = \frac{\pi}{2} \left[\frac{I_{-\nu} - I_\nu}{\sin(\nu\pi)} \right] \quad (2.164)$$

where $J_{-\nu}$ and $I_{-\nu}$ are, respectively, obtained from Equations (2.161) and (2.163) by replacing ν with $-\nu$. Although ν in Equations (2.161) to (2.164) can assume any fractional value, in our specific problem, $\nu = n + 1/2$. Since Gamma function of half-integer order is needed in Equation (2.161), it is necessary to add that

$$\Gamma(n+1/2) = \begin{cases} \frac{(2n)!}{2^{2n} n!} \sqrt{\pi}, & n \geq 0 \\ \frac{(-1)^n 2^{2n} n!}{(2n)!} \sqrt{\pi}, & n < 0 \end{cases} \quad (2.165)$$

Thus the lower-order spherical Bessel functions are as follows:

$$\begin{aligned} j_0(x) &= \frac{\sin x}{x}, & y_0(x) &= -\frac{\cos x}{x}, \\ h_0^{(1)}(x) &= \frac{e^{jx}}{jx}, & h_0^{(2)}(x) &= \frac{e^{-jx}}{-jx}, \\ i_0(x) &= \frac{\sinh x}{x}, & k_0(x) &= \frac{e^{-x}}{x}, \\ j_1(x) &= \frac{\sin x}{x^2} - \frac{\cos x}{x}, & y_1(x) &= -\frac{\cos x}{x^2} - \frac{\sin x}{x}, \\ h_1^{(1)} &= -\frac{(x+j)}{x^2} e^{jx}, & h_1^{(2)}(x) &= -\frac{(x-j)}{x^2} e^{-jx} \end{aligned}$$

Table 2.3 Properties and Identities of Spherical Bessel Functions

(a)	$z_{n+1} = \frac{(2n+1)}{x} z_n(x) - z_{n-1}(x)$	(recurrence relation)
(b)	$\frac{d}{dx} z_n(x) = \frac{1}{2n+1} [nz_{n-1} - (n+1)z_{n+1}(x)]$	
(c)	$\frac{d}{dx} [xz_n(x)] = -nz_n(x) + xz_{n-1}(x)$	
(d)	$\frac{d}{dx} [x^{n+1} z_n(x)] = -x^{n+1} z_{n-1}(x)$	
(e)	$\frac{d}{dx} [x^{-n} z_n(x)] = -x^{-n} z_{n+1}(x)$	
(f)	$\int x^{n+2} z_n(x) dx = x^{n+2} z_{n+1}(x)$	
(g)	$\int x^{1-n} z_n(x) dx = -x^{1-n} z_{n-1}(x)$	
(h)	$\int x^2 [z_n(x)]^2 dx = \frac{1}{2} x^3 [z_n(x) - z_{n-1}(x) z_{n+1}(x)]$	

Other $z_n(x)$ can be obtained from the series expansion in Equations (2.161) and (2.162) or the recurrence relations and properties of $z_n(x)$ presented in Table 2.3.

By replacing H in Equation (2.157) with $y, \cos\theta$ by x , and making other substitutions as we did for Equation (2.143), we obtain

$$(1-x^2)y'' - 2xy' + \left[n(n+1) - \frac{m^2}{1-x^2} \right] y = 0, \quad (2.166)$$

which is Legendre's associated differential equation. Its general solution is of the form

$$y(x) = a_{mn} P_n^m(x) + d_{mn} Q_n^m(x) \quad (2.167)$$

where $P_n^m(x)$ and $Q_n^m(x)$ are called associated Legendre functions of the first and second kind, respectively. Equation (2.146) is a special case of Equation (2.167) when $m = 0$. $P_n^m(x)$ and $Q_n^m(x)$ can be obtained from ordinary Legendre functions $P_n(x)$ and $Q_n(x)$ using

$$P_n^m(x) = [1-x^2]^{m/2} \frac{d^m}{dx^m} P_n(x) \quad (2.168)$$

and

$$Q_n^m(x) = [1-x^2]^{m/2} \frac{d^m}{dx^m} Q_n(x) \quad (2.169)$$

where $-1 < x < 1$. We note that

$$\begin{aligned} P_n^0(x) &= P_n(x), \\ Q_n^0(x) &= Q_n(x), \\ P_n^m(x) &= 0 \quad \text{for } m > n \end{aligned} \quad (2.170)$$

Typical associated Legendre functions are

$$\begin{aligned} P_1^1(x) &= (1-x^2)^{1/2} = \sin\theta, \\ P_2^1(x) &= 3x(1-x^2)^{1/2} = 3\cos\theta\sin\theta, \\ P_2^2(x) &= 3(1-x^2) = 3\sin^2\theta, \\ P_3^1(x) &= \frac{3}{2}(1-x^2)^{1/2}(5x-1) = \frac{3}{2}\sin\theta(5\cos\theta-1), \end{aligned}$$

$$\begin{aligned} Q_1^1(x) &= (1-x^2)^{1/2} \left[\frac{1}{2} \ln \frac{1+x}{1-x} + \frac{x}{1-x^2} \right], \\ Q_2^1 &= (1-x^2)^{1/2} \left[\frac{3x}{2} \ln \frac{1+x}{1-x} + \frac{3x^2-2}{1-x^2} \right], \\ Q_2^2 &= (1-x^2)^{1/2} \left[\frac{3}{2} \ln \frac{1+x}{1-x} + \frac{5x^2-3x^2}{[1-x^2]^2} \right] \end{aligned}$$

Higher-order associated Legendre functions can be obtained using Equations (2.168) and (2.169) along with the properties in Table 2.4. As mentioned earlier, $Q_n^m(x)$ is unbounded at $x = \pm 1$, and hence it is only used when $x = \pm 1$ is excluded. Substituting Equations (2.158), (2.159), and (2.167) into Equation (2.153) and applying superposition theorem, we obtain

$$U(r, \theta, \phi, t) = \sum_{n=0}^{\infty} \sum_{m=0}^n \sum_{\ell=0}^{\infty} A_{mn\ell} z_n(k_{m\ell} r) P_n^m(\cos\theta) \exp(\pm jm\phi \pm j\omega t) \quad (2.171)$$

Note that the products $H(\theta)F(\phi)$ are known as *spherical harmonics*.

Example 2.6

A thin ring of radius a carries charge of density ρ . Find the potential at (a) point $P(0, 0, z)$ on the axis of the ring, (b) point $P(r, \theta, \phi)$ in space. \square

Solution

Consider the thin ring as in Figure 2.10.

(a) From elementary electrostatics, at $P(0, 0, z)$

$$V = \int \frac{\rho dl}{4\pi\epsilon R}$$

where $dl = ad\phi$, $R = \sqrt{a^2+z^2}$. Hence

$$V = \int_0^{2\pi} \frac{\rho ad\phi}{4\pi\epsilon[a^2+z^2]^{1/2}} = \frac{a\rho}{2\epsilon[a^2+z^2]^{1/2}} \quad (2.172)$$

Table 2.4 Properties and Identities of Associated Legendre Functions¹

-
- (a) $P_m(x) = 0, \quad m > n$
- (b) $P_n^m(x) = \frac{(2n-1)xP_{n-1}^m(x)-(n+m-1)P_{n-2}^m(x)}{n-m}$
(recurrence relations for fixed m)
- (c) $P_n^m(x) = \frac{2(m-1)x}{(1-x^2)^{1/2}} P_n^{m-1}(x) - (n-m+2)(n+m-1)P_n^{m-2}(x)$
(recurrence relations for fixed n)
- (d) $P_n^m(x) = \frac{[1-x^2]^{m/2}}{2^n} \sum_{k=0}^{\lfloor \frac{m-n}{2} \rfloor} \frac{(-1)^k (2n-2k)! x^{n-2k-m}}{k!(n-k)!(n-2k-m)!}$
where $[t]$ is the bracket or greatest integer function, e.g., $[3.54] = 3$.
- (e) $\frac{d}{dx} P_n^m(x) = \frac{(n+m)P_{n-1}^m(x)-nxP_n^m(x)}{1-x^2}$
- (f) $\frac{d}{d\theta} P_n^m(x) = \frac{1}{2}[(n-m+1)(n+m)P_n^{m-1}(x) - P_n^{m+1}(x)]$
- (g) $\frac{d}{d\phi} P_n^m(x) = -\frac{mxP_n^m(x)}{1-x^2} + \frac{(1-x^2)^{m/2}}{2^n} \sum_{k=0}^{\lfloor \frac{m-n}{2} \rfloor} \frac{(-1)^k (2n-2k)! x^{n-2k-m-1}}{k!(n-k)!(n-2k-m)!}$
- (h) $\frac{d}{d\theta} P_n^m(x) = -(1-x^2)^{1/2} \frac{d}{dx} P_n^m(x)$
- (i) The series expansion of $f(x)$:
- $$f(x) = \sum_{n=0}^{\infty} A_n P_n^m(x),$$
- where $A_n = \frac{(2n+1)(n-m)!}{2(n+m)!} \int_{-1}^1 f(x) P_n^m(x) dx$
- (j) $\left. \frac{d^m}{dx^m} P_n(x) \right|_{x=1} = \frac{(n+m)!}{2^m m!(n-m)!}$
- $\left. \frac{d^m}{dx^m} P_n(x) \right|_{x=-1} = \frac{(-1)^{n+m}(n+m)!}{2^m m!(n-m)!}$
- (k) $P_n^{-m}(x) = (-1)^m \frac{(n-m)!}{(n+m)!} P_n^m(x), \quad m = 0, 1, \dots, n$
- (l) $\int_{-1}^1 P_n^m(x) P_n^m(x) dx = \frac{2}{2n+1} \frac{(n-m)!}{(n+m)!} \delta_{nk},$
where δ_{nk} is the Kronecker delta defined by $\delta_{nk} = \begin{cases} 0, & n \neq k \\ 1, & n = k \end{cases}$
-

¹ Properties (b) and (c) are also valid for $Q_n^m(x)$.

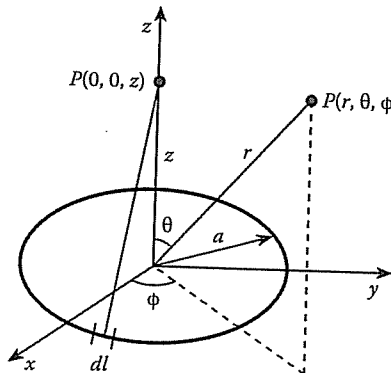


Figure 2.10
Charged ring of Example 2.6.

(b) To find the potential at $P(r, \theta, \phi)$, we may evaluate the integral for the potential as we did in part (a). However, it turns out that the boundary-value solution is simpler. So we solve Laplace's equation $\nabla^2 V = 0$, where $V(0, 0, z)$ must conform with the result in part (a). From Figure 2.10, it is evident that V is invariant with ϕ . Hence the solution to Laplace's equation is

$$V = \sum_{n=0}^{\infty} \left[A_n r^n + \frac{B_n}{r^{n+1}} \right] [A'_n P_n(u) + B'_n Q_n(u)]$$

where $u = \cos\theta$. Since Q_n is singular at $\theta = 0, \pi$, $B'_n = 0$. Thus

$$V = \sum_{n=0}^{\infty} \left[C'_n r^n + \frac{D'_n}{r^{n+1}} \right] P_n(u) \quad (2.173)$$

For $0 \leq r \leq a$, $D'_n = 0$ since V must be finite at $r = 0$.

$$V = \sum_{n=0}^{\infty} C'_n r^n P_n(u) \quad (2.174)$$

To determine the coefficients C'_n , we set $\theta = 0$ and equate V to the result in part (a). But when $\theta = 0$, $u = 1$, $P_n(1) = 1$, and $r = z$. Hence

$$V(0, 0, z) = \frac{a\rho}{2\epsilon[a^2+z^2]^{1/2}} = \frac{a\rho}{2\epsilon} \sum_{n=0}^{\infty} C_n z^n \quad (2.175)$$

Using the binomial expansion, the term $[a^2+z^2]^{1/2}$ can be written as

$$\frac{1}{a} \left[1 + \frac{z^2}{a^2} \right]^{-1/2} = \frac{1}{a} \left[1 - \frac{1}{2}(z/a)^2 + \frac{1 \cdot 3}{2 \cdot 4}(z/a)^4 - \frac{1 \cdot 3 \cdot 5}{2 \cdot 4 \cdot 6}(z/a)^6 + \dots \right]$$

Comparing this with the last term in Equation (2.175), we obtain

$$C_0 = 1, \quad C_1 = 0, \quad C_2 = -\frac{1}{2a^2}, \quad C_3 = 0, \\ C_4 = \frac{1 \cdot 3}{2 \cdot 4} \frac{1}{a^4}, \quad C_5 = 0, \quad C_6 = -\frac{1 \cdot 3 \cdot 5}{2 \cdot 4 \cdot 6} \frac{1}{a^6}, \dots$$

or in general,

$$C_{2n} = (-1)^n \frac{(2n)!}{[n!2^n]^2 a^{2n}}$$

Substituting these into Equation (2.174) gives

$$V = \frac{a\rho}{2\epsilon} \sum_{n=0}^{\infty} \frac{(-1)^n (2n)!}{[n!2^n]^2} (r/a)^{2n} P_{2n}(\cos\theta), \quad 0 \leq r \leq a \quad (2.176)$$

For $r \geq a$, $C'_n = 0$ since V must be finite as $r \rightarrow \infty$, and

$$V = \sum_{n=0}^{\infty} \frac{D'_n}{r^{n+1}} P_n(u) \quad (2.177)$$

Again, when $\theta = 0, u = 1, P_n(1) = 1, r = z$,

$$V(0, 0, z) = \frac{a\rho}{2\epsilon[a^2+z^2]^{1/2}} = \frac{a\rho}{2\epsilon} \sum_{n=0}^{\infty} D_n z^{-(n+1)} \quad (2.178)$$

Using the binomial expansion, the middle term $[a^2+z^2]^{-1/2}$ can be written as

$$\frac{1}{z} \left[1 + \frac{z^2}{a^2} \right]^{-1/2} = \frac{1}{z} \left[1 - \frac{1}{2}(a/z)^2 + \frac{1 \cdot 3}{2 \cdot 4}(a/z)^4 - \frac{1 \cdot 3 \cdot 5}{2 \cdot 4 \cdot 6}(a/z)^6 + \dots \right]$$

Comparing this with the last term in Equation (2.178), we obtain

$$D_0 = 1, \quad D_1 = 0, \quad D_2 = -\frac{a^2}{2}, \quad D_3 = 0, \\ D_4 = \frac{1 \cdot 3}{2 \cdot 4} a^4, \quad D_5 = 0, \quad D_6 = -\frac{1 \cdot 3 \cdot 5}{2 \cdot 4 \cdot 6} a^6, \dots$$

or in general,

$$D_{2n} = (-1)^n \frac{(2n)!}{[n!2^n]^2} a^{2n}$$

Substituting these into Equation (2.177) gives

$$V = \frac{a\rho}{2\epsilon r} \sum_{n=0}^{\infty} \frac{(-1)^n (2n)!}{[n!2^n]^2} (a/r)^{2n} P_{2n}(\cos\theta), \quad r \geq a \quad (2.179)$$

We may combine Equations (2.176) and (2.179) to get

$$V = \begin{cases} a \sum_{n=0}^{\infty} g_n(r/a)^{2n} P_{2n}(\cos\theta), & 0 \leq r \leq a \\ \sum_{n=0}^{\infty} g_n(a/r)^{2n+1} P_{2n}(\cos\theta), & r \geq a \end{cases}$$

where

$$g_n = (-1)^n \frac{\rho}{2\epsilon} \frac{2n!}{[n!2^n]^2}$$

Example 2.7

A conducting spherical shell of radius a is maintained at potential $V_o \cos 2\phi$; determine the potential at any point inside the sphere. \square

Solution

The solution to this problem is somewhat similar to that of the previous problem except that V is a function of ϕ . Hence the solution to Laplace's equation for $0 \leq r \leq a$ is of the form

$$V = \sum_{n=0}^{\infty} \sum_{m=0}^{\infty} (a_{mn} \cos m\phi + b_{mn} \sin m\phi) (r/a)^n P_n^m(\cos\theta)$$

Since $\cos m\phi$ and $\sin m\phi$ are orthogonal functions, $a_{mn} = 0 = b_{mn}$ except that $a_{n2} \neq 0$. Hence at $r = a$

$$V_o \cos 2\phi = \cos 2\phi \sum_{n=2}^{\infty} a_{n2} P_n^2(\cos\theta)$$

or

$$V_o = \sum_{n=2}^{\infty} a_{n2} P_n^2(x), \quad x = \cos\theta$$

which is the Legendre expansion of V_o . Multiplying both sides by $P_m^2(x)$ gives

$$\frac{2}{2n+1} \frac{(n+2)!}{(n-2)!} a_{n2} = V_o \int_{-1}^1 P_n^2(x) dx = V_o \int_{-1}^1 (1-x^2) \frac{d^2}{dx^2} P_n(x) dx$$

Integrating by parts twice yields

$$a_{n2} = V_o \frac{2n+1}{2} \frac{(n-2)!}{(n+2)!} \left(2P_n(1) - 2P_n(-1) - 2 \int_{-1}^1 P_n(x) dx \right)$$

Using the generating functions for $P_n(x)$ (see Table 2.7 and Example 2.10), it is readily shown that

$$P_n(1) = 1, \quad P_n(-1) = (-1)^n$$

Also

$$\int_{-1}^1 P_n(x) dx = \int_{-1}^1 P_0(x) P_n(x) dx = 0$$

by the orthogonality property of $P_n(x)$. Hence

$$a_{n2} = V_o (2n+1) \frac{(n-2)!}{(n+2)!} [1 - (-1)^n]$$

and

$$V = V_o \cos 2\phi \sum_{n=2}^{\infty} (2n+1) \frac{(n-2)!}{(n+2)!} [1 - (-1)^n] (r/a)^n P_n^2(\cos\theta)$$

Example 2.8

Express (a) the plane wave e^{jz} and (b) the cylindrical wave $J_0(\rho)$ in terms of spherical wave functions. \square

Solution

(a) Since $e^{jz} = e^{jr \cos\theta}$ is independent of ϕ and finite at the origin, we let

$$e^{jz} = e^{jr \cos\theta} = \sum_{n=0}^{\infty} a_n j_n(r) P_n(\cos\theta) \quad (2.180)$$

where a_n are the expansion coefficients. To determine a_n , we multiply both sides of Equation (2.180) by $P_m(\cos\theta) \sin\theta$ and integrate over $0 < \theta < \pi$:

$$\begin{aligned} \int_0^\pi e^{jr \cos\theta} P_m(\cos\theta) \sin\theta d\theta &= \sum_{n=0}^{\infty} a_n j_n(r) \int_{-1}^1 P_n(x) P_m(x) dx \\ &= \begin{cases} 0, & n \neq m \\ \frac{2}{2n+1} a_n j_n(r), & n = m \end{cases} \end{aligned}$$

where the orthogonality property (i) of Table 2.2 has been utilized. Taking the n th derivative of both sides and evaluating at $r = 0$ gives

$$j^n \int_0^\pi \cos^n \theta P_n(\cos\theta) \sin\theta d\theta = \frac{2}{2n+1} a_n \frac{d^n}{dr^n} j_n(r) \Big|_{r=0} \quad (2.181)$$

The left-hand side of Equation (2.181) yields

$$j^n \int_{-1}^1 x^n P_n(x) dx = \frac{2^{n+1} (n!)^2}{(2n+1)!} j^n \quad (2.182)$$

To evaluate the right-hand side of Equation (2.181), we recall that

$$j_n(r) = \sqrt{\frac{\pi}{2x}} J_{n+1/2}(r) = \sqrt{\frac{\pi}{2}} \sum_{m=0}^{\infty} \frac{(-1)^m r^{2m+n}}{m! \Gamma(m+n+3/2) 2^{2m+n+1/2}}$$

Hence

$$\left. \frac{d^n}{dr^n} j_n(r) \right|_{r=0} = \sqrt{\frac{\pi}{2}} \frac{n!}{\Gamma(n+3/2) 2^{n+1/2}} = \frac{2^n (n!)^2}{(2n+1)!} \quad (2.183)$$

Substituting Equations (2.182) and (2.183) into Equation (2.181) gives

$$a_n = j^n (2n+1)$$

Thus

$$e^{jz} = e^{jr \cos \theta} = \sum_{n=0}^{\infty} j^n (2n+1) j_n(r) P_n(\cos \theta) \quad (2.184)$$

(b) Since $J_0(\rho) = J_0(r \sin \theta)$ is even, independent of ϕ , and finite at the origin,

$$J_0(\rho) = J_0(r \sin \theta) = \sum_{n=0}^{\infty} b_n j_{2n}(r) P_{2n}(\cos \theta) \quad (2.185)$$

To determine the coefficients of expansion b_n , we multiply both sides by $P_m(\cos \theta) \sin \theta$ and integrate over $0 < \theta < \pi$. We obtain

$$\int_0^\pi J_0(r \sin \theta) P_m(\cos \theta) \sin \theta d\theta = \begin{cases} 0, & m \neq 2n \\ \frac{2b_n}{4n+1} j_{2n}(r), & m = 2n \end{cases}$$

Differentiating both sides $2n$ times with respect to r and setting $r = 0$ gives

$$b_n = \frac{(-1)^n (4n+1)(2n-1)!}{2^{2n-1} n!(n-1)!}$$

Hence

$$J_0(\rho) = \sum_{n=0}^{\infty} \frac{(-1)^n (4n+1)(2n-1)!}{2^{2n-1} n!(n-1)!} j_{2n}(r) P_{2n}(\cos \theta) \quad \blacksquare$$

2.6 Some Useful Orthogonal Functions

Orthogonal functions are of great importance in mathematical physics and engineering. A system of real functions $\Phi_n (n = 0, 1, 2, \dots)$ is said to be *orthogonal with weight w(x)* on the interval (a, b) if

$$\int_a^b w(x) \Phi_m(x) \Phi_n(x) dx = 0 \quad (2.186)$$

2.6. SOME USEFUL ORTHOGONAL FUNCTIONS

for every $m \neq n$. For example, the system of functions $\cos(nx)$ is orthogonal with weight 1 on the interval $(0, \pi)$ since

$$\int_0^\pi \cos mx \cos nx dx = 0, \quad m \neq n$$

Orthogonal functions usually arise in the solution of partial differential equations governing the behavior of certain physical phenomena. These include Bessel, Legendre, Hermite, Laguerre, and Chebyshev functions. In addition to the orthogonality properties in Equation (2.186), these functions have many other general properties, which will be discussed briefly in this section. They are very useful in series expansion of functions belonging to very general classes, e.g., Fourier-Bessel series, Legendre series, etc. Although Hermite, Laguerre, and Chebyshev functions are of less importance in EM problems than Bessel and Legendre functions, they are sometimes useful and therefore deserve some attention.

An arbitrary function $f(x)$, defined over interval (a, b) , can be expressed in terms of any complete, orthogonal set of functions:

$$f(x) = \sum_{n=0}^{\infty} A_n \Phi_n(x) \quad (2.187)$$

where the expansion coefficients are given by

$$A_n = \frac{1}{N_n} \int_a^b w(x) f(x) \Phi_n(x) dx \quad (2.188)$$

and the (weighted) norm N_n is defined as

$$N_n = \int_a^b w(x) \Phi_n^2(x) dx \quad (2.189)$$

Simple orthogonality results when $w(x) = 1$ in Equations (2.186) to (2.189).

Perhaps the best way to briefly describe the orthogonal functions is in table form. This is done in Tables 2.5 to 2.7. The differential equations giving rise to each function are provided in Table 2.5. The orthogonality relations in Table 2.6 are necessary for expanding a given arbitrary function $f(x)$ in terms of the orthogonal functions as in Equations (2.187) to (2.189). Most of the properties of the orthogonal functions can be proved using the generating functions of Table 2.7. To the properties in Tables 2.5 to 2.7 we may add the recurrence relations and series expansion formulas for calculating the functions for specific argument x and order n . These have been provided for $J_n(x)$ and $Y_n(x)$ in Table 2.1 and Equations (2.97) and (2.99), for $P_n(x)$ and $Q_n(x)$ in Table 2.2 and Equations (2.147) and (2.148), for $j_n(x)$ and $y_n(x)$ in Table 2.3 and Equation (2.160), and for $P_n^m(x)$ and $Q_n^m(x)$ in Table 2.4 and Equations (2.168) and (2.169). For Hermite polynomials, the series expansion formula is

$$H_n(x) = \sum_{k=0}^{[n/2]} \frac{(-1)^k n! (2x)^{n-2k}}{k! (n-2k)!} \quad (2.190)$$

Table 2.5 Differential Equations with Solutions

Equations	Solutions
$x^2y'' + xy' + (x^2 - n^2)y = 0$	$J_n(x)$ Bessel functions of the first kind $Y_n(x)$ Bessel functions of the second kind $H_n^{(1)}(x)$ Hankel functions of the first kind $H_n^{(2)}(x)$ Hankel functions of the second kind
$x^2y'' + xy' - (x^2 + n^2)y = 0$	$I_n(x)$ Modified Bessel functions of the first kind $K_n(x)$ Modified Bessel functions of the second kind
$x^2y'' + 2xy' + [x^2 - n(n+1)]y = 0$	$j_n(x)$ Spherical Bessel functions of the first kind $y_n(x)$ Spherical Bessel functions of the second kind
$(1-x^2)y'' - 2xy + n(n+1)y = 0$	$P_n(x)$ Legendre polynomials $Q_n(x)$ Legendre functions of the second kind
$(1-x^2)y'' - 2xy' + \left[n(n+1) - \frac{m^2}{1-x^2}\right]y = 0$	$P_n^m(x)$ Associated Legendre polynomials $Q_n^m(x)$ Associated Legendre functions of the second kind
$y'' - 2xy' + 2ny = 0$	$H_n(x)$ Hermite polynomials
$xy'' + (1-x)y' + ny = 0$	$L_n(x)$ Laguerre polynomials
$xy'' + (m+1-x)y' + ny = 0$	$L_n^m(x)$ Associated Laguerre polynomials
$(1-x^2)y'' - xy' + n^2y = 0$	$T_n(x)$ Chebyshev polynomials of the first kind $U_n(x)$ Chebyshev polynomials of the second kind

where $[n/2] = N$ is the largest even integer $\leq n/2$ or simply the greatest integer function. Thus,

$$H_0(x) = 1, \quad H_1(x) = 2x, \quad H_2(x) = 4x^2 - 2, \quad \text{etc.}$$

The recurrence relations are

$$H_{n+1}(x) = 2xH_n(x) - 2nH_{n-1}(x) \quad (2.191a)$$

2.6. SOME USEFUL ORTHOGONAL FUNCTIONS

Table 2.6 Orthogonality Relations

Functions	Relations
Bessel functions	$\int_0^a x J_n(\lambda_i x) J_n(\lambda_j x) dx = \frac{a^2}{2} [J_{n+1}(\lambda_i a)]^2 \delta_{ij}$ where λ_i and λ_j are the roots of $J_n(\lambda a) = 0$
Spherical Bessel functions	$\int_{-\infty}^{\infty} j_n(x) j_m(x) dx = \frac{\pi}{2n+1} \delta_{mn}$
Legendre polynomials	$\int_{-1}^1 P_n(x) P_m(x) dx = \frac{2}{2n+1} \delta_{mn}$
Associated Legendre polynomials	$\int_{-1}^1 P_n^k(x) P_m^k(x) dx = \frac{2(n+k)!}{(2n+1)(n-k)!} \delta_{mn}$ $\int_{-1}^1 \frac{P_n^m(x) P_n^k(x)}{1-x^2} dx = \frac{(n+m)!}{m(n-m)!} \delta_{mk}$
Hermite polynomials	$\int_{-\infty}^{\infty} e^{-x^2} H_n(x) H_m(x) dx = 2^n n! (\sqrt{\pi}) \delta_{mn}$
Laguerre polynomials	$\int_0^{\infty} e^{-x} L_n(x) L_m(x) dx = \delta_{mn}$
Associated Laguerre polynomials	$\int_0^{\infty} e^{-x} x^k L_n^k(x) L_m^k(x) dx = \frac{(n+k)!}{n!} \delta_{mn}$
Chebyshev polynomials	$\int_{-1}^1 \frac{T_n(x) T_m(x)}{(1-x^2)^{1/2}} dx = \begin{cases} 0, & m \neq n \\ \pi/2, & m = n \neq 0 \\ \pi, & m = n = 0 \end{cases}$
	$\int_{-1}^1 \frac{U_n(x) U_m(x)}{(1-x^2)^{1/2}} dx = \begin{cases} 0, & m \neq n \\ \pi/2, & m = n \neq 0 \\ \pi, & m = n = 0 \end{cases}$

and

$$H'_n(x) = 2nH_{n-1}(x) \quad (2.191b)$$

For Laguerre polynomials,

$$L_n(x) = \sum_{k=0}^n \frac{n!(-x)^k}{(k!)^2(n-k)!} \quad (2.192)$$

so that

$$L_0(x) = 1, \quad L_1(x) = -x + 1, \quad L_2(x) = \frac{1}{2!}(x^2 - 4x + 2), \quad \text{etc.}$$

The recurrence relations are

$$L_{n+1}(x) = (2n+1-x)L_n(x) - n^2 L_{n-1}(x) \quad (2.193a)$$

Table 2.7 Generating Functions

Functions	Generating function
	$R = [1 - 2xt + t^2]^{1/2}$
Bessel function	$\exp\left[\frac{x}{2}(t - \frac{1}{t})\right] = \sum_{n=-\infty}^{\infty} t^n J_n(x)$
Legendre polynomial	$\frac{1}{R} = \sum_{n=0}^{\infty} t^n P_n(x)$
Associated Legendre polynomial	$\frac{(2m)!(1-x^2)^{m/2}}{2^m m! R^{m+1}} = \sum_{n=0}^{\infty} t^n P_{n+m}^m(x)$
Hermite polynomial	$\exp(2tx - t^2) = \sum_{n=0}^{\infty} \frac{t^n}{n!} H_n(x)$
Laguerre polynomial	$\frac{\exp[-xt/(1-t)]}{1-t} = \sum_{n=0}^{\infty} t^n L_n(x)$
Associated Laguerre polynomial	$\frac{\exp[-xt/(1-t)]}{(1-t)^{m+1}} = \sum_{n=0}^{\infty} t^n L_n^m(x)$
Chebyshev polynomial	$\frac{1-t^2}{R^2} = T_0(x) + 2 \sum_{n=1}^{\infty} t^n T_n(x)$ $\frac{\sqrt{1-x^2}}{R^2} = \sum_{n=0}^{\infty} t^n U_{n+1}(x)$

and

$$\frac{d}{dx} L_n(x) = \frac{1}{x} [nL_n(x) - n^2 L_{n+1}(x)] \quad (2.193b)$$

For the associated Laguerre polynomials,

$$L_n^m(x) = (-1)^m \frac{d^m}{dx^m} L_{n+m}(x) = \sum_{k=0}^n \frac{(m+n)!(-x)^k}{k!(n-k)!(m+k)!} \quad (2.194)$$

so that

$$L_1^1(x) = -x + 2, \quad L_2^2(x) = \frac{x^2}{2} - 3x + 3, \quad L_2^2(x) = \frac{x^2}{2} - 4x + 6, \text{ etc.}$$

Note that $L_n^m(x) = 0$, $m > n$. The recurrence relations are

$$L_{n+1}^m(x) = \frac{1}{n+1} [(2n+m+1-x)L_n^m(x) - (n+m)L_{n-1}^m(x)] \quad (2.195)$$

2.6. SOME USEFUL ORTHOGONAL FUNCTIONS

For Chebyshev polynomials of the first kind,

$$T_n(x) = \sum_{k=0}^{[n/2]} \frac{(-1)^k n! x^{n-2k} (1-x^2)^k}{(2k)!(n-2k)!}, \quad -1 \leq x \leq 1 \quad (2.196)$$

so that

$$T_0(x) = 1, \quad T_1(x) = x, \quad T_2(x) = 2x^2 - 1, \text{ etc.}$$

The recurrence relation is

$$T_{n+1}(x) = 2xT_n(x) - T_{n-1}(x) \quad (2.197)$$

For Chebyshev polynomials of the second kind,

$$U_n(x) = \sum_{k=0}^N \frac{(-1)^{k-1} (n+1)! x^{n-2k+2} (1-x^2)^{k-1}}{(2k+1)!(n-2k+2)!}, \quad -1 \leq x \leq 1 \quad (2.198)$$

where $N = [\frac{n+1}{2}]$ so that

$$U_0(x) = 1, \quad U_1(x) = 2x, \quad U_2(x) = 4x^2 - 1, \text{ etc.}$$

The recurrence relation is the same as that in Equation (2.197).

For example, if a function $f(x)$ is to be expanded on the interval $(0, \infty)$, Laguerre functions can be used as the orthogonal functions with an exponential weighting function, i.e., $w(x) = e^{-x}$. If $f(x)$ is to be expanded on the interval $(-\infty, \infty)$, we may use Hermite functions with $w(x) = e^{-x^2}$. As we have noticed earlier, if $f(x)$ is defined on the interval $(-1, 1)$, we may choose Legendre functions with $w(x) = 1$. For more detailed treatment of these functions, see Bell [7] or Johnson and Johnson [8].

Example 2.9

Expand the function

$$f(x) = |x|, \quad -1 \leq x \leq 1$$

in a series of Chebyshev polynomials. \square

Solution

The given function can be written as

$$f(x) = \begin{cases} -x, & -1 \leq x < 0 \\ x, & 0 < x \leq 1 \end{cases}$$

Let

$$f(x) = \sum_{n=0}^{\infty} A_n T_n(x)$$

where A_n are expansion coefficients to be determined. Since $f(x)$ is an even function, the odd terms in the expansion vanish. Hence

$$f(x) = A_0 + \sum_{n=1}^{\infty} A_{2n} T_{2n}(x)$$

If we multiply both sides by $w(x) = \frac{T_{2m}}{\sqrt{1-x^2}}$ and integrate over $-1 \leq x \leq 1$, all terms in the summation vanish except when $m = n$. That is, from Table 2.6, the orthogonality property of $T_n(x)$ requires that

$$\int_{-1}^1 \frac{T_m(x)T_n(x)}{(1-x^2)^{1/2}} dx = \begin{cases} 0, & m \neq n \\ \pi/2, & m = n \neq 0 \\ \pi, & m = n = 0 \end{cases}$$

Hence

$$\begin{aligned} A_0 &= \frac{1}{\pi} \int_{-1}^1 \frac{f(x)T_0(x)}{(1-x^2)^{1/2}} dx = \frac{2}{\pi} \int_0^1 \frac{x}{(1-x^2)^{1/2}} dx = \frac{2}{\pi}, \\ A_{2n} &= \frac{2}{\pi} \int_{-1}^1 \frac{f(x)T_{2n}(x)}{(1-x^2)^{1/2}} dx = \frac{4}{\pi} \int_0^1 \frac{xT_{2n}}{(1-x^2)^{1/2}} dx \end{aligned}$$

Since $T_n(x) = \cos(n \cos^{-1} x)$, it is convenient to let $x = \cos \theta$ so that

$$\begin{aligned} A_{2n} &= \frac{4}{\pi} \int_{\pi/2}^0 \frac{\cos \theta \cos 2n\theta}{\sin \theta} (-\sin \theta d\theta) = \frac{4}{\pi} \int_0^{\pi/2} \cos \theta \cos 2n\theta d\theta \\ &= \frac{4}{\pi} \int_0^{\pi/2} \frac{1}{2} [\cos(2n+1)\theta + \cos(2n-1)\theta] d\theta = \frac{4}{\pi} \frac{(-1)^{n+1}}{4n^2 - 1} \end{aligned}$$

Hence

$$f(x) = \frac{2}{\pi} + \frac{4}{\pi} \sum_{n=1}^{\infty} \frac{(-1)^{n+1}}{4n^2 - 1} T_{2n}(x) \quad \blacksquare$$

Example 2.10

Evaluate $\frac{P_n^1(x)}{\sin \theta}$ at $x = 1$ and $x = -1$. \blacksquare

Solution

This example serves to illustrate how the generating functions are useful in deriving some properties of the corresponding orthogonal functions. Since

$$\frac{P_n^1(x)}{\sin \theta} = \frac{P_n^1(x)}{\sqrt{1-x^2}},$$

2.6. SOME USEFUL ORTHOGONAL FUNCTIONS

direct substitution of $x = 1$ or $x = -1$ gives $0/0$, which is indeterminate. But $P_n^1(x) = (1-x^2)^{1/2} \frac{d}{dx} P_n$ by definition. Hence

$$\frac{P_n^1(x)}{\sin \theta} = \frac{d}{dx} P_n,$$

i.e., the problem is reduced to evaluating dP_n/dx at $x = \pm 1$. We use the generating function for P_n , namely,

$$(1-2xt+t^2)^{-1/2} = \sum_{n=0}^{\infty} t^n P_n(x)$$

Differentiating both sides with respect to x ,

$$\frac{t}{(1-2xt+t^2)^{3/2}} = \sum_{n=0}^{\infty} t^n \frac{d}{dx} P_n \quad (2.199)$$

When $x = 1$,

$$\frac{1}{(1-t)^3} = \sum_{n=0}^{\infty} t^{n-1} \frac{d}{dx} P_n \Big|_{x=1} \quad (2.200)$$

But

$$(1-t)^{-3} = 1 + 3t + 6t^2 + 10t^3 + 15t^4 + \dots = \sum_{n=1}^{\infty} \frac{n}{2} (n+1) t^{n-1} \quad (2.201)$$

Comparing this with Equation (2.200) clearly shows that

$$\frac{d}{dx} P_n \Big|_{x=1} = n(n+1)/2$$

Similarly, when $x = -1$, Equation (2.199) becomes

$$\frac{1}{(1+t)^3} = \sum_{n=0}^{\infty} t^{n-1} \frac{d}{dx} P_n \Big|_{x=-1} \quad (2.202)$$

But

$$(1+t)^{-3} = 1 - 3t + 6t^2 - 10t^3 + 15t^4 - \dots = \sum_{n=1}^{\infty} (-1)^{n+1} \frac{n}{2} (n+1) t^{n-1}$$

Hence

$$\frac{d}{dx} P_n \Big|_{x=-1} = (-1)^{n+1} n(n+1)/2 \quad \blacksquare$$

Example 2.11

Write a program to generate Hermite functions $H_n(x)$ for any argument x and order n . Use the series expansion and recurrence formulas and compare your results. Take $x = 0.5, 0 \leq n \leq 15$. \square

Solution

The program is shown in Figure 2.11. Equation (2.190) is used for the series expansion method, while Equation (2.191a) with $H_0(x) = 1$ and $H_1(x) = 2x$ is used for the recurrence formula. Note that in the program, we have replaced n by $n - 1$ in Equation (2.191a) so that

$$H_n(x) = 2xH_{n-1}(x) - 2(n-1)H_{n-2}(x)$$

The result of the computation is in Table 2.8. In this case, the two methods give identical results. In general, the series expansion method gives results of greater accuracy since error in one computation is not propagated to the next as is the case when using recurrence relations.

Table 2.8 Results of the Program in Figure 2.11

N	Values of $H_n(x)$ for $x = 0.5, 0 \leq n \leq 15$		
	Series Expansion	Recurrence	Difference
0	1.00	1.00	0.00
1	1.00	1.00	0.00
2	-1.00	-1.00	0.00
3	-5.00	-5.00	0.00
4	1.00	1.00	0.00
5	44.00	44.00	0.00
6	31.00	31.00	0.00
7	-461.00	-461.00	0.00
8	-895.00	-895.00	0.00
9	6181.00	6181.00	0.00
10	22591.00	22591.00	0.00
11	-107029.00	-107029.00	0.00
12	-604031.00	-604031.00	0.00
13	1964665.00	1964665.00	0.00
14	17669472.00	17669472.00	0.00
15	-37341152.00	-37341148.00	-4.00

Generating functions such as this is sometimes needed in numerical computations. This example has served to illustrate how this can be done in two ways. Special techniques may be required for very large or very small values of x or n . \square

```

clear all; format compact; format short g; tic

%%%%%%%%%%%%% THIS PROGRAM GENERATES HERMITE'S FUNCTIONS HN(X) IN TWO WAYS USING:
% 1) SERIES EXPANSION
% 2) RECURRENCE RELATION
% THE TWO METHODS ARE COMPARED
% X = ARGUMENT (FIXED IN THIS PROGRAM)
% N = ORDER OF THE FUNCTION
%%%%%%%%%%%%%

```

```

X = 0.5; %Argument
NMAX = 15; %Order of Function

% METHOD 1: SERIES EXPANSION FORMULA Equation (2.190)
for N = 0:NMAX
    SUM = 0;
    FN = factorial(N);
    I = floor(N/2); %Greatest Integer Function
    for K = 0:I
        M = N - 2*K;
        FM = factorial(M);
        FK = factorial(K);
        SUM = SUM + ( ((-1)^K)*FN*((2*X)^M) )/( FK*FM );
    end
    HS(N+1) = SUM;
end

% METHOD 2: RECURRENCE FORMULA Equation (2.191a)
HR(1) = 1;
HR(2) = 2*X;
for k = 2:N
    n = k-1; %MATLAB HR vector starts at 1 while equation
              % subscript starts at 0
    HR(k+1) = 2*X*HR(k) - 2*(n)*HR(k-1);
end

Difference = HS-HR;

hdr = [{'N'}, {'Series Expansion'}, {'Recurrence'}, {'Difference'}];
output = [hdr; num2cell([(0:N)', HS', HR', Difference'])];
disp(['Values of Hn(x) for x = ', num2str(X), ', 0<=n<=', num2str(N)]);
disp(output)

```

Figure 2.11
Program for Hermite function $H_n(x)$.

2.7 Series Expansion

As we have noticed in earlier sections, partial differential equations can be solved with the aid of infinite series and, more generally, with the aid of series of orthogonal functions. In this section we apply the idea of infinite series expansion to those PDEs in which the independent variables are not separable or, if they are separable, the boundary conditions are not satisfied by the particular solutions. We will illustrate the technique in the following three examples.

2.7.1 Poisson's Equation in a Cube

Consider the problem

$$\nabla^2 V = \frac{\partial^2 V}{\partial x^2} + \frac{\partial^2 V}{\partial y^2} + \frac{\partial^2 V}{\partial z^2} = -f(x, y, z) \quad (2.203)$$

subject to the boundary conditions

$$\begin{aligned} V(0, y, z) &= V(a, y, z) = V(x, 0, z) = 0 \\ V(x, b, z) &= V(x, y, 0) = V(x, y, c) = 0 \end{aligned} \quad (2.204)$$

where $f(x, y, z)$, the source term, is given. We should note that the independent variables in Equation (2.203) are not separable. However, in Laplace's equation, $f(x, y, z) = 0$, and the variables are separable. Although the problem defined by Equations (2.203) and (2.204) can be solved in several ways, we stress the use of series expansion in this section.

Let the solution be of the form

$$V(x, y, z) = \sum_{m=1}^{\infty} \sum_{n=1}^{\infty} \sum_{p=1}^{\infty} A_{mnp} \sin \frac{m\pi x}{a} \sin \frac{n\pi y}{b} \sin \frac{p\pi z}{c} \quad (2.205)$$

where the triple sine series is chosen so that the individual terms and the entire series would satisfy the boundary conditions of Equation (2.204). However, the individual terms do not satisfy either Poisson's or Laplace's equation. Since the expansion coefficients A_{mnp} are arbitrary, they can be chosen such that Equation (2.205) satisfies Equation (2.203). We achieve this by substituting Equation (2.205) into Equation (2.203). We obtain

$$\begin{aligned} -\sum_{m=1}^{\infty} \sum_{n=1}^{\infty} \sum_{p=1}^{\infty} A_{mnp} (m\pi/a)^2 \sin \frac{m\pi x}{a} \sin \frac{n\pi y}{b} \sin \frac{p\pi z}{c} \\ -\sum_{m=1}^{\infty} \sum_{n=1}^{\infty} \sum_{p=1}^{\infty} A_{mnp} (n\pi/b)^2 \sin \frac{m\pi x}{a} \sin \frac{n\pi y}{b} \sin \frac{p\pi z}{c} \\ -\sum_{m=1}^{\infty} \sum_{n=1}^{\infty} \sum_{p=1}^{\infty} A_{mnp} (p\pi/c)^2 \sin \frac{m\pi x}{a} \sin \frac{n\pi y}{b} \sin \frac{p\pi z}{c} = -f(x, y, z) \end{aligned}$$

2.7. SERIES EXPANSION

Multiplying both sides by $\sin(i\pi x/a)\sin(j\pi y/b)\sin(k\pi z/c)$ and integrating over $0 < x < a, 0 < y < b, 0 < z < c$ gives

$$\begin{aligned} &\sum_{m=1}^{\infty} \sum_{n=1}^{\infty} \sum_{p=1}^{\infty} A_{mnp} [(m\pi/a)^2 + (n\pi/b)^2 + (p\pi/c)^2] \\ &\int_0^a \sin \frac{m\pi x}{a} \sin \frac{i\pi x}{a} dx \int_0^b \sin \frac{n\pi y}{b} \sin \frac{j\pi y}{b} dy \int_0^c \sin \frac{p\pi z}{c} \sin \frac{k\pi z}{c} dz \\ &= \int_0^a \int_0^b \int_0^c f(x, y, z) \sin \frac{i\pi x}{a} \sin \frac{j\pi y}{b} \sin \frac{k\pi z}{c} dx dy dz \end{aligned}$$

Each of the integrals on the left-hand side vanishes except when $m = i, n = j$, and $p = k$. Hence

$$\begin{aligned} &A_{mnp} [(m\pi/a)^2 + (n\pi/b)^2 + (p\pi/c)^2] \frac{a}{2} \cdot \frac{b}{2} \cdot \frac{c}{2} \\ &= \int_0^a \int_0^b \int_0^c f(x, y, z) \sin \frac{i\pi x}{a} \sin \frac{j\pi y}{b} \sin \frac{k\pi z}{c} dx dy dz \end{aligned}$$

or

$$\begin{aligned} A_{mnp} &= \frac{8}{abc} [(m\pi/a)^2 + (n\pi/b)^2 + (p\pi/c)^2]^{-1} \\ &\int_0^a \int_0^b \int_0^c f(x, y, z) \sin \frac{i\pi x}{a} \sin \frac{j\pi y}{b} \sin \frac{k\pi z}{c} dx dy dz \end{aligned} \quad (2.206)$$

Thus the series expansion solution to the problem is in Equation (2.205) with A_{mnp} given by Equation (2.206).

2.7.2 Poisson's Equation in a Cylinder

The problem to be solved is shown in Figure 2.12, which illustrates a cylindrical metal tank partially filled with charged liquid [9]. To find the potential distribution V in the tank, we let V_ℓ and V_g be the potential in the liquid and gas portions, respectively, i.e.,

$$V = \begin{cases} V_\ell, & 0 < z < b \\ V_g, & b < z < b+c \end{cases} \quad \begin{matrix} (\text{liquid}) \\ (\text{gas}) \end{matrix}$$

Thus we need to solve a two-dimensional problem:

$$\frac{1}{\rho} \frac{\partial}{\partial \rho} \left(\rho \frac{\partial V_\ell}{\partial \rho} \right) + \frac{\partial^2 V_\ell}{\partial z^2} = -\frac{\rho_v}{\epsilon}, \quad \text{for liquid space} \quad (2.207a)$$

$$\frac{1}{\rho} \frac{\partial}{\partial \rho} \left(\rho \frac{\partial V_g}{\partial \rho} \right) + \frac{\partial^2 V_g}{\partial z^2} = 0, \quad \text{for gas space} \quad (2.207b)$$

subject to

$$V = 0, \rho = a \quad (\text{at the wall})$$

$$V_g = V_\ell, z = b \quad (\text{at the gas-liquid interface})$$

$$\frac{\partial V_g}{\partial z} = \epsilon_r \frac{\partial V_\ell}{\partial z}, z = b \quad (\text{at the gas-liquid interface})$$

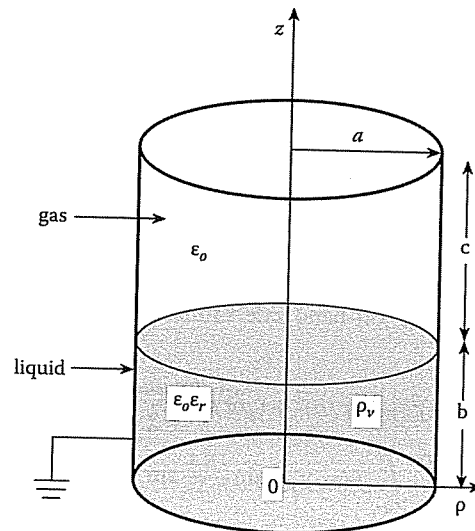


Figure 2.12
A cylindrical metal tank partially filled with charged liquid.

Applying the series expansion techniques, we let

$$V_\ell = \sum_{n=1}^{\infty} J_0(\lambda_n \rho) F_n(z) \quad (2.208a)$$

$$V_g = \sum_{n=1}^{\infty} J_0(\lambda_n \rho) [A_n \sinh[\lambda_n(b+c-z)] + B_n \cosh[\lambda_n(b+c-z)]] \quad (2.208b)$$

where $F_n(z)$, A_n , and B_n are to be determined.

At $z = b + c$, $V_g = 0$, which implies that $B_n = 0$. Hence, Equation (2.208b) becomes

$$V_g = \sum_{n=1}^{\infty} A_n J_0(\lambda_n \rho) \sinh[\lambda_n(b+c-z)] \quad (2.209)$$

Substituting Equation (2.208a) into (2.207a) yields

$$\sum_{n=1}^{\infty} J_0(\lambda_n \rho) [F_n'' - \lambda_n^2 F_n] = -\frac{\rho_v}{\epsilon}$$

If we let $F_n'' - \lambda_n^2 F_n = G_n$, then

$$\sum_{n=1}^{\infty} G_n J_0(\lambda_n \rho) = -\frac{\rho_v}{\epsilon} \quad (2.210)$$

At $\rho = a$, $V_g = V_\ell = 0$, which makes

$$J_0(\lambda_n a) = 0$$

2.7. SERIES EXPANSION

indicating that λ_n are the roots of J_0 divided by a . Multiplying Equation (2.210) by $\rho J_0(\lambda_m \rho)$ and integrating over the interval $0 < \rho < a$ gives

$$\sum_{n=1}^{\infty} G_n \int_0^a \rho J_0(\lambda_m \rho) J_0(\lambda_n \rho) d\rho = -\frac{\rho_v}{\epsilon} \int_0^a \rho J_0(\lambda_m \rho) d\rho$$

The left-hand side is zero except when $m = n$.

$$\int_0^a \rho J_0^2(\lambda_m \rho) d\rho = \frac{1}{2} a^2 [J_0^2(\lambda_n a) + J_1^2(\lambda_n a)] = \frac{a^2}{2} J_1^2(\lambda_n a)$$

since $J_0(\lambda_n a) = 0$. Also,

$$\int_0^a \rho J_0(\lambda_m \rho) d\rho = \frac{a}{\lambda_n} J_1(\lambda_n a)$$

Hence

$$G_n \frac{a^2}{2} J_1^2(\lambda_n a) = -\frac{\rho_v}{\epsilon} \frac{a}{\lambda_n} J_1(\lambda_n a)$$

or

$$G_n = -\frac{2\rho_v}{\epsilon a \lambda_n J_1(\lambda_n a)}$$

showing that G_n is a constant. Thus

$$F_n'' - \lambda_n^2 F_n = G_n$$

which is an inhomogeneous ordinary differential equation. Its solution is

$$F_n(z) = C_n \sinh(\lambda_n z) + D_n \cosh(\lambda_n z) - \frac{G_n}{\lambda_n^2}$$

But

$$F_n(0) = 0 \quad \rightarrow \quad D_n = \frac{G_n}{\lambda_n^2}$$

Thus

$$V_\ell = \sum_{n=1}^{\infty} J_0(\lambda_n \rho) \left[C_n \sinh(\lambda_n z) + \frac{G_n}{\lambda_n^2} [\cosh(\lambda_n z) - 1] \right] \quad (2.211)$$

Imposing the conditions at $z = b$, i.e.,

$$V_\ell(\rho, b) = V_g(\rho, b)$$

we obtain

$$A_n \sinh(\lambda_n c) = C_n \sinh(\lambda_n b) + \frac{G_n}{\lambda_n^2} [\cosh(\lambda_n b) - 1] \quad (2.212)$$

Also,

$$\left. \frac{\partial V_g}{\partial z} \right|_{z=b} = \epsilon_r \left. \frac{\partial V_\ell}{\partial z} \right|_{z=b}$$

gives

$$\lambda_n A_n \cosh(\lambda_n c) = -\epsilon_r \lambda_n C_n \cosh(\lambda_n b) - \frac{\epsilon_r G_n}{\lambda_n} \sinh(\lambda_n b) \quad (2.213)$$

Solving Equations (2.212) and (2.213), we get

$$A_n = \frac{2\rho_v}{R_n K_n} [\cosh(\lambda_n b) - 1]$$

$$C_n = \frac{2\rho_v}{R_n \epsilon_r} [\cosh(\lambda_n b) \cosh(\lambda_n c) + \epsilon_r \sinh(\lambda_n b) \sinh(\lambda_n c) - \cosh(\lambda_n c)]$$

where

$$K_n = \sinh(\lambda_n b) \cosh(\lambda_n c) + \epsilon_r \cosh(\lambda_n b) \sinh(\lambda_n c)$$

$$R_n = \epsilon_o a \lambda_n^3 J_1(\lambda_n a)$$

Substituting A_n and C_n in Equations (2.209) and (2.211), we obtain the complete solution as

$$V_\ell = \sum_{n=1}^{\infty} \frac{2\rho_v}{R_n \epsilon_r} J_0(\lambda_n \rho) \left[\frac{\sinh(\lambda_n z)}{K_n} [\cosh(\lambda_n b) \cosh(\lambda_n c) + \epsilon_r \sinh(\lambda_n b) \sinh(\lambda_n c) - \cosh(\lambda_n c)] - \cosh(\lambda_n z) + 1 \right] \quad (2.214a)$$

$$V_g = \sum_{n=1}^{\infty} \frac{2\rho_v}{R_n K_n} J_0(\lambda_n \rho) [\cosh(\lambda_n b) - 1] \sinh[\lambda_n(b + c - z)] \quad (2.214b)$$

2.7.3 Strip Transmission Line

Consider a strip conductor enclosed in a shielded box containing homogeneous medium as shown in Figure 2.13(a). If TEM mode of propagation is assumed, our problem is reduced to finding V satisfying Laplace's equation $\nabla^2 V = 0$. Due to symmetry, we need only consider one quarter-section of the line as in Figure 2.13(b). This quadrant can be subdivided into regions 1 and 2, where region 1 is under the center conductor and region 2 is not. We now seek solutions V_1 and V_2 for regions 1 and 2, respectively.

If $w >> b$, region 1 is similar to a parallel-plate problem. Thus, we have a one-dimensional problem similar to Equation (2.14) with solution

$$V_1 = a_1 y + a_2$$

Since $V_1(y=0) = V_0$ and $V_1(y=-b/2) = V_0$, $a_2 = 0$, $a_1 = -2V_0/b$. Hence

$$V_1(x, y) = \frac{-2V_0}{b} y \quad (2.215)$$

2.7. SERIES EXPANSION

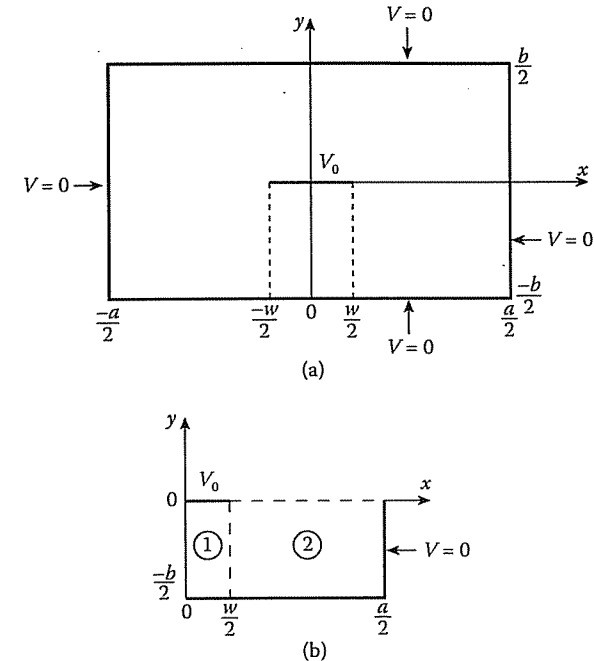


Figure 2.13
Strip line example.

For region 2, the series expansion solution is of the form

$$V_2(x, y) = \sum_{n=1,3,5}^{\infty} A_n \sin \frac{n\pi y}{b} \sinh \frac{n\pi}{b} (a/2 - x), \quad (2.216)$$

which satisfies Laplace's equation and the boundary condition along the box. Notice that the even-numbered terms could not be included because they do not satisfy the boundary condition requirements about line $y = 0$, i.e., $E_y(y=0) = -\partial V_2/\partial y|_{y=0} \neq 0$. To determine the expansion coefficients A_n in Equation (2.216), we utilize the fact that V must be continuous at the interface $x = w/2$ between regions 1 and 2, i.e.,

$$V_1(x = w/2, y) = V_2(x = w/2, y)$$

or

$$-\frac{2V_0 y}{b} = \sum_{n=\text{odd}}^{\infty} A_n \sin \frac{n\pi y}{b} \sinh \frac{n\pi}{2b} (a - w),$$

which is Fourier series. Thus,

$$A_n \sinh \frac{n\pi}{2b} (a - w) = -\frac{2}{b} \int_{-b/2}^{b/2} \frac{2V_0 y}{b} \sin \frac{n\pi y}{b} dy = -\frac{8V_0 \sin \frac{n\pi}{2}}{n^2 \pi^2}$$

Hence

$$A_n = -\frac{8V_o \sin \frac{n\pi}{2}}{n^2 \pi^2 \sinh \frac{n\pi}{2b}(a-w)} \quad (2.217)$$

It is instructive to find the capacitance per unit length C of the strip line using the fact that the energy stored per length is related to C according to

$$W = \frac{1}{2} C V_o^2 \quad (2.218)$$

where

$$W = \frac{1}{2} \int \mathbf{D} \cdot \mathbf{E} dv = \frac{1}{2} \epsilon \int |\mathbf{E}|^2 dv \quad (2.219)$$

For region 1,

$$\mathbf{E} = -\nabla V = -\frac{\partial V}{\partial x} \mathbf{a}_x - \frac{\partial V}{\partial y} \mathbf{a}_y = \frac{2V_o}{b} \mathbf{a}_y$$

Hence

$$W_1 = \frac{1}{2} \epsilon \int_{x=0}^{w/2} \int_{y=-b/2}^0 \frac{4V_o^2}{b^2} dy dx = \frac{\epsilon V_o^2 w}{2b} \quad (2.220)$$

For region 2,

$$E_x = -\frac{\partial V}{\partial x} = \sum \frac{n\pi}{b} A_n \cosh \frac{n\pi}{b}(a/2-x) \sin \frac{n\pi y}{b}$$

$$E_y = -\frac{\partial V}{\partial y} = -\sum \frac{n\pi}{b} A_n \sinh \frac{n\pi}{b}(a/2-x) \cos \frac{n\pi y}{b}$$

and

$$W_2 = \frac{1}{2} \epsilon \iint (E_x^2 + E_y^2) dx dy$$

$$= \frac{1}{2} \epsilon \int_{y=-b/2}^0 \int_{x=w/2}^{a/2} \sum_n \sum_m \frac{mn\pi^2}{b^2} A_n A_m \cdot$$

$$\left[\sinh^2 \frac{n\pi}{b}(a/2-x) \sinh^2 \frac{n\pi}{b}(a/2-x) \cos \frac{m\pi y}{b} \cos \frac{n\pi y}{b} \right.$$

$$\left. + \cosh^2 \frac{m\pi}{b}(a/2-x) \cosh^2 \frac{n\pi}{b}(a/2-x) \sin \frac{m\pi y}{b} \sin \frac{n\pi y}{b} \right] dx dy$$

where the double summation is used to show that we are multiplying two series which may have different indices m and n . Due to the orthogonality properties of sine and cosine functions, all terms vanish except when $m = n$. Thus

$$W_2 = \frac{1}{2} \epsilon \sum_{n=\text{odd}}^{\infty} \frac{n^2 \pi^2 A_n^2}{b^2} \cdot \frac{b/2}{2} \int_{w/2}^{a/2} \left[\sinh^2 \frac{n\pi}{b}(a/2-x) \right.$$

$$\left. + \cosh^2 \frac{n\pi}{b}(a/2-x) \right] dx$$

$$= \frac{1}{2} \epsilon \sum_{n=\text{odd}}^{\infty} \frac{n^2 \pi^2 A_n^2}{4b} \frac{b}{n\pi} \cosh \frac{n\pi}{2b}(a-w) \sinh \frac{n\pi}{2b}(a-w)$$

2.7. SERIES EXPANSION

Substituting for A_n gives

$$W_2 = \sum_{n=1,3,5}^{\infty} \frac{8\epsilon V_o^2}{n^3 \pi^3} \coth \frac{n\pi}{2b}(a-w) \quad (2.221)$$

The total energy in the four quadrants is

$$W = 4(W_1 + W_2)$$

Thus

$$C = \frac{2W}{V_o^2} = \frac{8}{V_o^2} (W_1 + W_2)$$

$$= \epsilon \left[\frac{4w}{b} + \frac{64}{\pi^3} \sum_{n=1,3,5}^{\infty} \frac{1}{n^3} \coth \frac{n\pi}{2b}(a-w) \right] \quad (2.222)$$

The characteristic impedance of the lossless line is given by

$$Z_o = \frac{\sqrt{\mu\epsilon}}{C} = \frac{\sqrt{\mu_r \epsilon_r}}{cC} = \sqrt{\frac{\mu}{\epsilon}} \frac{1}{C/\epsilon}$$

or

$$Z_o = \frac{120\pi}{\sqrt{\epsilon_r} \left[\frac{4w}{b} + \frac{64}{\pi^3} \sum_{n=1,3,5}^{\infty} \frac{1}{n^3} \coth \frac{n\pi}{2b}(a-w) \right]} \quad (2.223)$$

where $c = 3 \times 10^8$ m/s, the speed of light in a vacuum, and $\mu_r = 1$ is assumed.

Example 2.12

Solve the two-dimensional problem

$$\nabla^2 V = -\frac{\rho_s}{\epsilon_o}$$

where

$$\rho_s = x(y-1) \text{ nC/m}^2$$

subject to

$$V(x, 0) = 0, \quad V(x, b) = V_o, \quad V(0, y) = 0 = V(a, y) \quad \square$$

Solution

If we let

$$\nabla^2 V_1 = 0, \quad (2.224a)$$

subject to

$$V_1(x, 0) = 0, \quad V_1(x, b) = V_o, \quad V_1(0, y) = 0 = V(a, y) \quad (2.224b)$$

and

$$\nabla^2 V_2 = -\frac{\rho_s}{\epsilon_o}, \quad (2.225a)$$

subject to

$$V_2(x, 0) = 0, \quad V_2(x, b) = 0, \quad V_2(0, y) = 0 = V(a, y) \quad (2.225b)$$

By the superposition principle, the solution to the given problem is

$$V = V_1 + V_2 \quad (2.226)$$

The solution to Equation (2.224) is already found in Section 2.3.1, i.e.,

$$V_1(x, y) = \frac{4V_o}{\pi} \sum_{n=1,3,5}^{\infty} \frac{\sin \frac{n\pi x}{a} \sinh \frac{n\pi y}{a}}{n \sinh \frac{n\pi b}{a}} \quad (2.227)$$

The solution to Equation (2.225) is a special case of that of Equation (2.205). The only difference between this problem and that of Equations (2.203) and (2.204) is that this problem is two-dimensional while that of Equations (2.203) and (2.204) is three-dimensional. Hence

$$V_2(x, y) = \sum_{m=1}^{\infty} \sum_{n=1}^{\infty} A_{mn} \sin \frac{n\pi x}{a} \sin \frac{n\pi y}{b} \quad (2.228)$$

where, according to Equation (2.206), A_{mn} is given by

$$A_{mn} = \frac{4}{ab} [(m\pi/a)^2 + (n\pi/b)^2]^{-1} \times \int_0^b \int_0^a f(x, y) \sin \frac{n\pi x}{a} \sin \frac{n\pi y}{b} dx dy \quad (2.229)$$

But $f(x, y) = x(y-1)/\epsilon_0$ nC/m²,

$$\begin{aligned} & \int_0^b \int_0^a f(x, y) \sin \frac{n\pi x}{a} \sin \frac{n\pi y}{b} dx dy \\ &= \frac{10^{-9}}{\epsilon_o} \int_0^a x \sin \frac{n\pi x}{a} dx \int_0^b (y-1) \sin \frac{n\pi y}{b} dy \\ &= \frac{10^{-9}}{10^{-9}/36\pi} \left(-\frac{a^2 \cos m\pi}{m\pi} \right) \left(-\frac{b^2 \cos n\pi}{n\pi} + \frac{b}{n\pi} [\cos n\pi - 1] \right) \\ &= \frac{36\pi(-1)^{m+n} a^2 b^2}{mn\pi^2} \left(1 - \frac{1}{b} [1 - (-1)^n] \right) \end{aligned} \quad (2.230)$$

2.8. PRACTICAL APPLICATIONS

since $\cos n\pi = (-1)^n$. Substitution of Equation (2.230) into Equation (2.229) leads to

$$A_{mn} = [(m\pi/a)^2 + (n\pi/b)^2]^{-1} \frac{(-1)^{m+n} 144ab}{mn\pi} \left(1 - \frac{1}{b} [1 - (-1)^n] \right) \quad (2.231)$$

Substituting Equations (2.227) and (2.228) into Equation (2.226) gives the complete solution as

$$V(x, y) = \frac{4V_o}{\pi} \sum_{n=1,3,5}^{\infty} \frac{\sin \frac{n\pi x}{a} \sinh \frac{n\pi y}{a}}{n \sinh \frac{n\pi b}{a}} + \sum_{m=1}^{\infty} \sum_{n=1}^{\infty} A_{mn} \sin \frac{n\pi x}{a} \sin \frac{n\pi y}{b} \quad (2.232)$$

where A_{mn} is in Equation (2.231). ■

2.8 Practical Applications

The scattering of EM waves by a dielectric sphere, known as the Mie scattering problem due to its first investigator in 1908, is an important problem whose analytic solution is usually referred to in assessing some numerical computations. Though the analysis of the problem is more rigorous, the procedure is similar to that of Example 2.5, where scattering due to a conducting cylinder was treated. Our treatment here will be brief; for an in-depth treatment, consult Stratton [10].

2.8.1 Scattering by Dielectric Sphere

Consider a dielectric sphere illuminated by a plane wave propagating in the z direction and \mathbf{E} polarized in the x direction as shown in Figure 2.14. The incident wave is described by

$$\mathbf{E}^i = E_o e^{j(\omega t - kz)} \mathbf{a}_x \quad (2.233a)$$

$$\mathbf{H}^i = \frac{E_o}{\eta} e^{j(\omega t - kz)} \mathbf{a}_y \quad (2.233b)$$

The first step is to express this incident wave in terms of spherical wave functions as in Example 2.8. Since

$$\mathbf{a}_x = \sin \theta \cos \phi \mathbf{a}_r + \cos \theta \cos \phi \mathbf{a}_{\theta} - \sin \phi \mathbf{a}_{\phi},$$

the r -component of \mathbf{E}^i , for example, is

$$E_r^i = \cos \phi \sin \theta E_x^i = E_o e^{j\omega t} \frac{\cos \phi}{jkr} \frac{\partial}{\partial \theta} (e^{-jkr \cos \theta})$$

Introducing Equation (2.184),

$$E_r^i = E_o e^{j\omega t} \frac{\cos \phi}{jkr} \sum_{n=0}^{\infty} (-j)^n (2n+1) j_n(kr) \frac{\partial}{\partial \theta} P_n(\cos \theta)$$

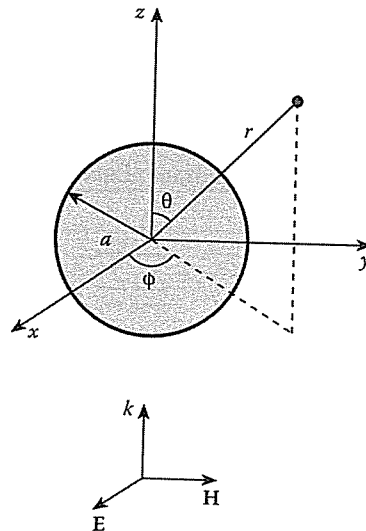


Figure 2.14
Incident EM plane wave on a dielectric sphere.

But

$$\frac{\partial P_n}{\partial \theta} = P_n^1$$

hence

$$E_r^i = E_o e^{j\omega t} \frac{\cos \phi}{jk r} \sum_{n=1}^{\infty} (-j)^n (2n+1) j_n(kr) P_n^1(\cos \theta) \quad (2.234)$$

where the $n = 0$ term has been dropped since $P_0^1 = 0$. The same steps can be taken to express E_θ^i and E_ϕ^i in terms of the spherical wave functions. The result is

$$\begin{aligned} \mathbf{E}^i &= \mathbf{a}_x E_o e^{j(\omega t - kz)} \\ &= E_o e^{j\omega t} \sum_{n=1}^{\infty} (-j)^n \frac{2n+1}{n(n+1)} [\mathbf{M}_n^{(1)}(k) + j \mathbf{N}_n^{(1)}(k)] \end{aligned} \quad (2.235a)$$

$$\begin{aligned} \mathbf{H}^i &= \mathbf{a}_y H_o e^{j(\omega t - kz)} \\ &= -\frac{k E_o}{\mu \omega} e^{j\omega t} \sum_{n=1}^{\infty} (-j)^n \frac{2n+1}{n(n+1)} [\mathbf{M}_n^{(1)}(k) - j \mathbf{N}_n^{(1)}(k)] \end{aligned} \quad (2.235b)$$

2.8. PRACTICAL APPLICATIONS

where

$$\begin{aligned} \mathbf{M}_n(k) &= \frac{1}{\sin \theta} z_n(kr) P_n^1(\cos \theta) \cos \phi \mathbf{a}_\theta \\ &\quad - z_n(kr) \frac{\partial P_n^1(\cos \theta)}{\partial \theta} \sin \phi \mathbf{a}_\phi \end{aligned} \quad (2.236)$$

$$\begin{aligned} \mathbf{N}_n(k) &= \frac{n(n+1)}{kr} z_n(kr) P_n^1(\cos \theta) \cos \phi \mathbf{a}_r \\ &\quad + \frac{1}{kr} \frac{\partial}{\partial r} [z_n(kr)] \frac{\partial P_n^1(\cos \theta)}{\partial \theta} \cos \phi \mathbf{a}_\theta \\ &\quad + \frac{1}{kr \sin \theta} \frac{\partial}{\partial r} [z_n(kr)] P_n^1(\cos \theta) \sin \phi \mathbf{a}_\phi \end{aligned} \quad (2.237)$$

The superscript (1) on the spherical vector functions \mathbf{M} and \mathbf{N} in Equation (2.235) indicates that these functions are constructed with spherical Bessel function of the first kind; i.e., $z_n(kr)$ in Equations (2.236) and (2.237) is replaced by $j_n(kr)$ when \mathbf{M} and \mathbf{N} are substituted in Equation (2.235).

The induced secondary field consists of two parts. One part applies to the interior of the sphere and is referred to as the transmitted field, while the other applies to the exterior of the sphere and is called the scattered field. Thus the total field outside the sphere is the sum of the incident and scattered fields. We now construct these fields in a fashion similar to that of the incident field. For the scattered field, we let

$$\mathbf{E}^s = E_o e^{j\omega t} \sum_{n=1}^{\infty} (-j)^n \frac{2n+1}{n(n+1)} [a_n \mathbf{M}_n^{(4)}(k) + j b_n \mathbf{N}_n^{(4)}(k)] \quad (2.238a)$$

$$\mathbf{H}^s = -\frac{k E_o}{\mu \omega} e^{j\omega t} \sum_{n=1}^{\infty} (-j)^n \frac{2n+1}{n(n+1)} [a_n \mathbf{M}_n^{(4)}(k) - j b_n \mathbf{N}_n^{(4)}(k)] \quad (2.238b)$$

where a_n and b_n are expansion coefficients and the superscript (4) on \mathbf{M} and \mathbf{N} shows that these functions are constructed with spherical Bessel function of the fourth kind (or Hankel function of the second kind); i.e., $z_n(kr)$ in Equations (2.236) and (2.237) is replaced by $h_n^{(2)}(kr)$ when \mathbf{M} and \mathbf{N} are substituted in Equation (2.238). The spherical Hankel function has been chosen to satisfy the radiation condition. In other words, the asymptotic behavior of $h_n^{(2)}(kr)$, namely,

$$h_n^{(2)}(kr) \sim j^{n+1} \frac{e^{-kr}}{kr}, \quad (2.239)$$

when combined with the time factor $e^{j\omega t}$, represents an outgoing spherical wave [see Equation (2.106d)]. Similarly, the transmitted field inside the sphere can be constructed as

$$\mathbf{E}' = E_o e^{j\omega t} \sum_{n=1}^{\infty} (-j)^n \frac{2n+1}{n(n+1)} [c_n \mathbf{M}_n^{(1)}(k_1) + j d_n \mathbf{N}_n^{(1)}(k_1)] \quad (2.240a)$$

$$\mathbf{H}' = -\frac{k E_o}{\mu \omega} e^{j\omega t} \sum_{n=1}^{\infty} (-j)^n \frac{2n+1}{n(n+1)} [c_n \mathbf{M}_n^{(1)}(k_1) - j d_n \mathbf{N}_n^{(1)}(k_1)] \quad (2.240b)$$

where c_n and d_n are expansion coefficients, k_1 is the propagation constant in the sphere. The functions $M_n^{(1)}$ and $N_n^{(1)}$ in Equation (2.240) are obtained by replacing $z_n(kr)$ in Equations (2.236) and (2.237) by $j_n(k_1 r)$; j_n is the only solution in this case since the field must be finite at the origin, the center of the sphere.

The unknown expansion coefficients a_n , b_n , c_n , and d_n are determined by letting the fields satisfy the boundary conditions, namely, the continuity of the tangential components of the total electric and magnetic fields at the surface of the sphere. Thus at $r = a$,

$$\mathbf{a}_r \times (\mathbf{E}^i + \mathbf{E}^s - \mathbf{E}') = 0 \quad (2.241a)$$

$$\mathbf{a}_r \times (\mathbf{H}^i + \mathbf{H}^s - \mathbf{H}') = 0 \quad (2.241b)$$

This is equivalent to

$$E_\theta^i + E_\theta^s = E_\theta', \quad r = a \quad (2.242a)$$

$$E_\phi^i + E_\phi^s = E_\phi', \quad r = a \quad (2.242b)$$

$$H_\theta^i + H_\theta^s = H_\theta', \quad r = a \quad (2.242c)$$

$$H_\phi^i + H_\phi^s = H_\phi', \quad r = a \quad (2.242d)$$

Substituting Equations (2.235), (2.238), and (2.240) into Equation (2.242), multiplying the resulting equations by $\cos\phi$ or $\sin\phi$ and integrating over $0 \leq \phi < 2\pi$, and then multiplying by $\frac{dP_m^1}{d\theta}$ and integrating over $0 \leq \theta \leq \pi$, we obtain

$$j_n(ka) + a_n h_n^{(2)}(ka) = c_n j_n(k_1 a) \quad (2.243a)$$

$$\mu_1 [kaj_n(ka)]' + a_n \mu_1 [kah_n^{(2)}(ka)]' = c_n \mu [k_1 a j_n(k_1 a)]' \quad (2.243b)$$

$$\mu_1 j_n(ka) + b_n \mu_1 h_n^{(2)}(ka) = d_n \mu j_n(k_1 a) \quad (2.243c)$$

$$k [kaj_n(ka)]' + b_n k [kah_n^{(2)}(ka)]' = d_n k_1 [k_1 a j_n(k_1 a)]' \quad (2.243d)$$

Solving Equations (2.243a) and (2.243b) gives a_n and c_n , while solving Equations (2.243c) and (2.243d) gives b_n and d_n . Thus, for $\mu = \mu_o = \mu_1$,

$$a_n = \frac{j_n(m\alpha)[\alpha j_n(\alpha)]' - j_n(\alpha)[m\alpha j_n(m\alpha)]'}{j_n(m\alpha)[\alpha h_n^{(2)}(\alpha)]' - h_n^{(2)}(\alpha)[m\alpha j_n(m\alpha)]'} \quad (2.244a)$$

$$b_n = \frac{j_n(\alpha)[m\alpha j_n(m\alpha)]' - m^2 j_n(m\alpha)[\alpha j_n(\alpha)]'}{h_n^{(2)}(\alpha)[m\alpha j_n(m\alpha)]' - m^2 j_n(m\alpha)[\alpha h_n^{(2)}(\alpha)]'} \quad (2.244b)$$

$$c_n = \frac{j/\alpha}{h_n^{(2)}(\alpha)[m\alpha j_n(m\alpha)]' - j_n(m\alpha)[\alpha h_n^{(2)}(\alpha)]'} \quad (2.244c)$$

$$d_n = \frac{j/\alpha}{h_n^{(2)}(\alpha)[m\alpha j_n(m\alpha)]' - m^2 j_n(m\alpha)[\alpha h_n^{(2)}(\alpha)]'} \quad (2.244d)$$

2.8. PRACTICAL APPLICATIONS

where $\alpha = ka = 2\pi a/\lambda$ and $m = k_1/k$ is the refractive index of the dielectric, which may be real or complex depending on whether the dielectric is lossless or lossy. The primes at the square brackets indicate differentiation with respect to the argument of the Bessel function inside the brackets, i.e., $[xz_n(x)]' = \frac{\partial}{\partial x}[xz_n(x)]$. To obtain Equations (2.244c) and (2.244d), we have made use of the Wronskian relationship

$$j_n(x) [x h_n^{(2)}(x)]' - h_n^{(2)}(x) [x j_n(x)]' = -j/x \quad (2.245)$$

If the dielectric is lossy and its surrounding medium is free space,

$$k_1^2 = \omega \mu_o (\omega \epsilon_1 - j\sigma), \quad k^2 = \omega^2 \mu_o \epsilon_0 \quad (2.246)$$

so that the (complex) refractive index m becomes

$$m = \frac{k_1}{k} = \sqrt{\epsilon_c} = \sqrt{\epsilon_r - j \frac{\sigma_1}{\omega \epsilon_o}} = m' - jm'' \quad (2.247)$$

The problem of scattering by a conducting sphere can be obtained as a special case of the problem considered above. Since the EM fields must vanish inside the conducting sphere, the right-hand sides of Equations (2.242a), (2.242b), (2.243a), and (2.243d) must be equal to zero so that ($c_n = 0 = d_n$)

$$a_n = -\frac{j_n(\alpha)}{h_n^{(2)}(\alpha)} \quad (2.248a)$$

$$b_n = -\frac{[\alpha j_n(\alpha)]'}{[\alpha h_n^{(2)}(\alpha)]'} \quad (2.248b)$$

Thus we have completed the Mie solution; the field at any point inside or outside the sphere can now be determined. We will now apply the solution to problems of practical interest.

2.8.2 Scattering Cross Sections

Often scattered radiation is most conveniently measured by the scattering cross section Q_{sca} (in meter²) which may be defined as the ratio of the total energy scattered per second W_s to the energy density P of the incident wave, i.e.,

$$Q_{\text{sca}} = \frac{W_s}{P} \quad (2.249)$$

The energy density of the incident wave is given by

$$P = \frac{E_o^2}{2\eta} = \frac{1}{2} E_o^2 \sqrt{\frac{\epsilon}{\mu}} \quad (2.250)$$

The scattered energy from the sphere is

$$W_s = \frac{1}{2} \operatorname{Re} \int_0^{2\pi} \int_0^\pi [E_\theta H_\phi^* - E_\phi H_\theta^*] r^2 \sin\theta d\theta d\phi$$

where the star sign denotes complex conjugation and field components are evaluated at far field ($r >> a$). By using the asymptotic expressions for spherical Bessel functions, we can write the resulting field components as

$$E_\theta^s = \eta H_\phi^s = -\frac{j}{kr} E_o e^{j(\omega t - kr)} \cos \phi S_2(\theta) \quad (2.251a)$$

$$-E_\phi^s = \eta H_\theta^s = -\frac{j}{kr} E_o e^{j(\omega t - kr)} \sin \phi S_1(\theta) \quad (2.251b)$$

where the amplitude functions $S_1(\theta)$ and $S_2(\theta)$ are given by [11]

$$S_1(\theta) = \sum_{n=1}^{\infty} \frac{2n+1}{n(n+1)} \left(\frac{a_n}{\sin \theta} P_n^1(\cos \theta) + b_n \frac{dP_n^1(\cos \theta)}{d\theta} \right) \quad (2.252a)$$

$$S_2(\theta) = \sum_{n=1}^{\infty} \frac{2n+1}{n(n+1)} \left(\frac{b_n}{\sin \theta} P_n^1(\cos \theta) + a_n \frac{dP_n^1(\cos \theta)}{d\theta} \right) \quad (2.252b)$$

Thus,

$$W_s = \frac{\pi E_o^2}{2k^2 \eta} \operatorname{Re} \int_0^\pi (|S_1(\theta)|^2 + |S_2(\theta)|^2) \sin \theta d\theta$$

This is evaluated with the help of the identities [10]

$$\begin{aligned} & \int_0^\pi \left(\frac{dP_n^1}{d\theta} \frac{dP_m^1}{d\theta} + \frac{1}{\sin^2 \theta} P_n^1 P_m^1 \right) \sin \theta d\theta \\ &= \begin{cases} 0, & n \neq m \\ \frac{2}{2n+1} \frac{(n+1)!}{(n-1)!} n(n+1), & n = m \end{cases} \end{aligned}$$

and

$$\int_0^\pi \left(\frac{dP_m^1}{d\theta} \frac{dP_n^1}{d\theta} + \frac{P_n^1}{\sin \theta} \frac{P_m^1}{d\theta} \right) \sin \theta d\theta = 0$$

We obtain

$$W_s = \frac{\pi E_o^2}{k^2 \eta} \sum_{n=1}^{\infty} (2n+1) (|a_n|^2 + |b_n|^2) \quad (2.253)$$

Substituting Equations (2.250) and (2.253) into Equation (2.249), the scattering cross section is found to be

$$\mathcal{Q}_{\text{sca}} = \frac{2\pi}{k^2} \sum_{n=1}^{\infty} (2n+1) (|a_n|^2 + |b_n|^2) \quad (2.254)$$

Similarly, the cross section for extinction \mathcal{Q}_{ext} (in meter²) is obtained [11] from the amplitude functions for $\theta = 0$, i.e.,

$$\mathcal{Q}_{\text{ext}} = \frac{4\pi}{k^2} \operatorname{Re} S(0)$$

2.8. PRACTICAL APPLICATIONS

or

$$\mathcal{Q}_{\text{ext}} = \frac{2\pi}{k^2} \operatorname{Re} \sum_{n=1}^{\infty} (2n+1) (a_n + b_n) \quad (2.255)$$

where

$$S(0) = S_1(0^\circ) = S_2(0^\circ) = \frac{1}{2} \sum_{n=1}^{\infty} (2n+1) (a_n + b_n) \quad (2.256)$$

In obtaining Equation (2.256), we have made use of

$$\left. \frac{P_n^1}{\sin \theta} \right|_{\theta=0} = \left. \frac{dP_n^1}{d\theta} \right|_{\theta=0} = n(n+1)/2$$

If the sphere is absorbing, the absorption cross section \mathcal{Q}_{abs} (in meter²) is obtained from

$$\mathcal{Q}_{\text{abs}} = \mathcal{Q}_{\text{ext}} - \mathcal{Q}_{\text{sca}} \quad (2.257)$$

since the energy removed is partly scattered and partly absorbed.

A useful, measurable quantity in radar communications is the radar cross section or back-scattering cross section σ_b of a scattering obstacle. It is a lump measure of the efficiency of the obstacle in scattering radiation back to the source ($\theta = 180^\circ$). It is defined in terms of the far zone scattered field as

$$\sigma_b = 4\pi r^2 \frac{|\mathbf{E}^s|^2}{E_o^2}, \quad \theta = \pi \quad (2.258)$$

From Equation (2.251),

$$\sigma_b = \frac{2\pi}{k^2} [|S_1(\pi)|^2 + |S_2(\pi)|^2]$$

But

$$-S_1(\pi) = S_2(\pi) = \frac{1}{2} \sum_{n=1}^{\infty} (-1)^n (2n+1) (a_n - b_n)$$

where we have used

$$\left. -\frac{P_n^1}{\sin \theta} \right|_{\theta=\pi} = \left. \frac{dP_n^1}{d\theta} \right|_{\theta=\pi} = (-1)^n n(n+1)/2$$

Thus

$$\sigma_b = \frac{\pi}{k^2} \left| \sum_{n=1}^{\infty} (-1)^n (2n+1) (a_n - b_n) \right|^2 \quad (2.259)$$

Similarly, we may determine the forward-scattering cross section ($\theta = 0^\circ$) as

$$\sigma_f = \frac{2\pi}{k^2} [|S_1(0)|^2 + |S_2(0)|^2]$$

Substituting Equation (2.256) into this yields

$$\sigma_f = \frac{\pi}{k^2} \left| \sum_{n=1}^{\infty} (2n+1) (a_n + b_n) \right|^2 \quad (2.260)$$

2.9 Attenuation Due to Raindrops

The rapid growth in demand for additional communication capacity has put pressure on engineers to develop microwave systems operating at higher frequencies. It turns out, however, that at frequencies above 10 GHz attenuation caused by atmospheric particles can reduce the reliability and performance of radar and space communication links. Such particles include oxygen, ice crystals, rain, fog, and snow. Prediction of the effect of these precipitates on the performance of a system becomes important. In this final subsection, we will examine attenuation and phase shift of an EM wave propagating through rain drops. We will assume that raindrops are spherical so that Mie rigorous solution can be applied. This assumption is valid if the rate intensity is low. For high rain intensity, an oblate spheroidal model would be more realistic [12].

The magnitude of an EM wave traveling through a homogeneous medium (with N identical spherical particles per unit volume) in a distance ℓ is given by $e^{-\gamma\ell}$, where γ is the attenuation coefficient given by [11]

$$\gamma = N Q_{\text{ext}}$$

or

$$\gamma = \frac{N\lambda^2}{\pi} \text{Re}S(0) \quad (2.261)$$

Thus the wave is attenuated by

$$A = 10 \log_{10} \frac{1}{e^{-\gamma\ell}} = \gamma\ell 10 \log_{10} e$$

or

$$A = 4.343\gamma\ell \quad (\text{in dB})$$

The attenuation per length (in dB/m) is

$$A = 4.343\gamma$$

or

$$A = 4.343 \frac{\lambda^2 N}{\pi} \text{Re}S(0) \quad (2.262)$$

Similarly, it can be shown [11] that the phase shift of the EM wave caused by the medium is

$$\Phi = -\frac{\lambda^2 N}{2\pi} \text{Im}S(0) \quad (\text{in radians/unit length})$$

or

$$\Phi = -\frac{\lambda^2 N}{2\pi} \text{Im}S(0) \frac{180}{\pi} \quad (\text{in deg/m}) \quad (2.263)$$

2.9. ATTENUATION DUE TO RAINDROPS

Table 2.9 Laws and Parsons' Drop-Size Distributions for Various Rain Rates

Drop Diameter (cm)	Rain Rate (mm/hour)								
	0.25	1.25	2.5	5	12.5	25	50	100	150
0.05	28.0	10.9	7.3	4.7	2.6	1.7	1.2	1.0	1.0
0.1	50.1	37.1	27.8	20.3	11.5	7.6	5.4	4.6	4.1
0.15	18.2	31.3	32.8	31.0	24.5	18.4	12.5	8.8	7.6
0.2	3.0	13.5	19.0	22.2	25.4	23.9	19.9	13.9	11.7
0.25	0.7	4.9	7.9	11.8	17.3	19.9	20.9	17.1	13.9
0.3		1.5	3.3	5.7	10.1	12.8	15.6	18.4	17.7
0.35		0.6	1.1	2.5	4.3	8.2	10.9	15.0	16.1
0.4		0.2	0.6	1.0	2.3	3.5	6.7	9.0	11.9
0.45			0.2	0.5	1.2	2.1	3.3	5.8	7.7
0.5				0.3	0.6	1.1	1.8	3.0	3.6
0.55					0.2	0.5	1.1	1.7	2.2
0.6						0.3	0.5	1.0	1.2
0.65							0.2	0.7	1.0
0.7									0.3

To relate attenuation and phase shift to a realistic rainfall rather than identical drops assumed so far, it is necessary to know the drop-size distribution for a given rate intensity. Representative distributions were obtained by Laws and Parsons [13] as shown in Table 2.9. To evaluate the effect of the drop-size distribution, suppose for a particular rain rate R , p is the percent of the total volume of water reaching the ground (as in Table 2.9), which consists of drops whose diameters fall in the interval centered in D cm ($D = 2a$), the number of drops in that interval is given by

$$N_c = pN(D) \quad (2.264)$$

The total attenuation and phase shift over the entire volume become

$$A = 0.4343 \frac{\lambda^2}{\pi} \cdot 10^6 \sum pN(D)\text{Re}S(0) \quad (\text{dB/km}) \quad (2.265)$$

$$\Phi = -\frac{9\lambda^2}{\pi^2} \cdot 10^6 \sum pN(D)\text{Im}S(0) \quad (\text{deg/km}) \quad (2.266)$$

where λ is the wavelength in cm and $N(D)$ is the number of raindrops with equivalent diameter D per cm^3 . The summations are taken over all drop sizes. In order to relate the attenuation and phase shift to the rain intensity measured in rain rate R (in mm/hour), it is necessary to have a relationship between N and R . The relationship obtained by Setzer [13], shown in Table 2.10, involves the terminal velocity u (in m/s)

of the rain drops, i.e.,

$$\begin{aligned} R &= u \cdot N \cdot \frac{4\pi a^3}{3} \quad (\text{volume of a drop}) \\ &= uN \frac{4\pi a^3}{3} \quad (\text{in m/s}) \end{aligned}$$

or

$$R = 6\pi Nu D^3 \cdot 10^5 \quad (\text{mm/hr})$$

Thus

$$N(D) = \frac{R}{6\pi u D^3} 10^{-5} \quad (2.267)$$

Substituting this into Equations (2.265) and (2.266) leads to

$$A = 4.343 \frac{\lambda^2}{\pi^2} R \sum \frac{p}{6u D^3} \operatorname{Re} S(0) \quad (\text{dB/km}) \quad (2.268)$$

$$\Phi = -90 \frac{\lambda^2}{\pi^3} R \sum \frac{p}{6u D^3} \operatorname{Im} S(0) \quad (\text{deg/km}), \quad (2.269)$$

where $N(D)$ is in per cm^3 , D and λ are in cm, u is in m/s, p is in percent, and $S(0)$ is the complex forward-scattering amplitude defined in Equation (2.256). The complex refractive index of raindrops [14] at 20°C required in calculating attenuation and phase shift is shown in Table 2.11.

Table 2.10 Raindrop Terminal Velocity

Radius (cm)	Velocity (m/s)
0.025	2.1
0.05	3.9
0.075	5.3
0.10	6.4
0.125	7.3
0.15	7.9
0.175	8.35
0.20	8.7
0.225	9.0
0.25	9.2
0.275	9.35
0.30	9.5
0.325	9.6

Example 2.13

For ice spheres, plot the normalized back-scattering cross section, $\sigma_b/\pi a^2$, as a function of the normalized circumference, $\alpha = 2\pi a/\lambda$. Assume that the refractive

2.9. ATTENUATION DUE TO RAINDROPS

Table 2.11 Refractive Index of Water at 20°C

Frequency (GHz)	Refractive Index ($m = m' - jm''$)
0.6	$8.960 - j0.1713$
0.8	$8.956 - j0.2172$
1.0	$8.952 - j0.2648$
1.6	$8.933 - j0.4105$
2.0	$8.915 - j0.5078$
3.0	$8.858 - j0.7471$
4.0	$8.780 - j0.9771$
6.0	$8.574 - j1.399$
11	$7.884 - j2.184$
16	$7.148 - j2.614$
20	$6.614 - j2.780$
30	$5.581 - j2.848$
40	$4.886 - j2.725$
60	$4.052 - j2.393$
80	$3.581 - j2.100$
100	$3.282 - j1.864$
160	$2.820 - j1.382$
200	$2.668 - j1.174$
300	$2.481 - j0.8466$

index of ice is independent of wavelength, making the normalized cross section for ice applicable over the entire microwave region. Take $m = 1.78 - j2.4 \times 10^{-3}$ at 0°C . \square

Solution

From Equation (2.259),

$$\sigma_b = \frac{\pi}{k^2} \left| \sum_{n=1}^{\infty} (-1)^n (2n+1) (a_n - b_n) \right|^2$$

Since $\alpha = ka$, the normalized back-scattering cross section is

$$\frac{\sigma_b}{\pi a^2} = \frac{1}{\alpha^2} \left| \sum_{n=1}^{\infty} (-1)^n (2n+1) (a_n - b_n) \right|^2 \quad (2.270)$$

Using this expression in conjunction with Equation (2.244), the section SCATTERING in the MATLAB code of Figure 2.15 was used as the main program to determine $\sigma_b/\pi a^2$ for $0.2 < \alpha < 4$. Details on the program will be explained in the next example. It suffices to mention that the maximum number of terms of the infinite series in Equation (2.270) was 10. It has been found that truncating the series at $n = 2\alpha$ provides sufficient accuracy. The plot of the normalized radar cross section versus α is shown in Figure 2.16. From the plot, we note that back-scattering oscillates between very large

```
%%%%%%
% MAIN PROGRAM
%
% FOR SPHERICAL RAIN DROPS, THIS PROGRAM CALCULATES ATTENUATION IN dB/KM
% AND PHASE SHIFT IN DEG/KM FOR A GIVEN RAIN RATE
%
% R = RAIN RATE IN MM/HR
% D = DROP DIAMETER IN CM
% F = FREQUENCY IN GHZ
% AT = ATTENUATION IN dB/KM
% PH = PHASE SHIFT IN DEG/KM
% V = TERMINAL VELOCITY OF RAIN DROPS
% P = PERCENT OF TOTAL VOLUME AS MEASURED
% M = COMPLEX REFRACTIVE INDEX OF WATER AT T = 20 C
% X = ALPHA = K*A

clear all; format compact; tic

%Inputs:
F = 11.0; %Frequency (GHz)
NMAX = 10; %Ideally inf but 10 is sufficient egn (2.256)

LAM = 30.0/F; % WAVELENGTH IN CM

% Raindrop Terminal Velocity Data
V=[2.1,3.9,5.3,6.4,7.3,7.9,8.35,8.7,9.0,9.2,9.35,9.5,9.6,9.6]; 

% Rain rate (mm/hr)
R=[0.25,1.25,2.5,5.0,12.5,25.0,50.0,100.0,150.0];

% Laws and Parsons drop-size distribution for various rain rate (% of total volume)
P=1/100*[28.0, 50.1, 18.2, 3.0, 0.7, 0 0 0 0 0 0 0 0;...
10.9, 37.1, 31.3, 13.5, 4.9, 1.5, 0.6, 0.2, 0 0 0 0 0 0 0;...
7.3, 27.8, 32.8, 19.0, 7.9, 3.3, 1.1, 0.6, 0.2, 0 0 0 0 0 0;...
4.7, 20.3, 31.0, 22.2, 11.8, 5.7, 2.5, 1.0, 0.5, 0.3, 0 0 0 0 0;...
2.6, 11.5, 24.5, 25.4, 17.3, 10.1, 4.3, 2.3, 1.2, 0.6, 0.2 0 0 0 0;...
1.7, 7.6, 18.4, 23.9, 19.9, 12.8, 8.2, 3.5, 2.1, 1.1, 0.5, 0.3 0 0 0;...
1.2, 5.4, 12.5, 19.9, 20.9, 15.6, 10.9, 6.7, 3.3, 1.8, 1.1, 0.5, 0.2, 0 0 0;...
1.0, 4.6, 8.8, 13.9, 17.1, 18.4, 15.0, 9.0, 5.8, 3.0, 1.7, 1.0, 0.7, 0 0 0;...
1.0, 4.1, 7.6, 11.7, 13.9, 17.7, 16.1, 11.9, 7.7, 3.6, 2.2, 1.2, 1.0, 0.3];;

f = [0.6 0.8 1 1.6 2 3 4 6 11 16 20 30 40 60 80 100 160 200 300];
% Refractive Index of Water at 20 degrees C, real and complex portions
mr= [8.96 8.956 8.952 8.933 8.915 8.858 8.78 8.574 7.884 7.148 6.614 5.581 4.886
4.052 3.581 3.282 2.82 2.668 2.481];
mi= [0.1713 0.2172 0.2648 0.4105 0.5078 0.7471 0.9771 1.399 2.184 2.614 2.78 2.848
2.725 2.393 2.100 1.864 1.382 1.174 0.8466];

% Interpolate refractive index of water to target frequency. F must be
% within the range of f.
mr_i = interp1(f,mr,F);
mi_i = interp1(f,mi,F);
M = mr_i - mi_i*i;
```

Figure 2.15

MATLAB program for Examples 2.13 and 2.14 (Continued).

2.9. ATTENUATION DUE TO RAINDROPS

```
N = 1:NMAX;
D = 0.05*(1:length(V));
SO = zeros(1,length(V));
SB = zeros(1,length(V));
for I = 1:length(V) %I sweeps rain drop diameter
    X = pi*D(I)/LAM;

    % CALCULATE THE SCATTERING COEFFICIENTS an and bn
    %
    % Spherical Bessel function of the first kind of order n
    J = sqrt(pi./(2*X)).*besselj(N+0.5,X);
    JD = -N.*sqrt(pi./(2*X)).*besselj(N+0.5,X)+ X.*sqrt(pi./(2*X)).*besselj(N+0.5-1,X);
    JM = sqrt(pi./(2*M*X)).*besselj(N+0.5,M*X);
    JMD= -N.*sqrt(pi./(2*M*X)).*besselj(N+0.5,M*X)+ M*X.*sqrt(pi./(2*M*X)).*besselj(N+0.5-1,M*X);
    H = sqrt(pi./(2*X)).*besselh(N+0.5,2,X);
    HD = -N.*sqrt(pi./(2*X)).*besselh(N+0.5,2,X)+X.*sqrt(pi./(2*X)).*besselh(N+0.5-1,2,X);

    A1 = JM.*JD - J.*JMD;
    A2 = JM.*HD - H.*JMD;
    B1 = J.*JMD - (M^2)*JM.*JD;
    B2 = H.*JMD - (M^2)*JM.*HD;
    an = A1./A2;
    bn = B1./B2;
    cn = i./(X*A2);
    dn = -i*M./(X*B2);

    % FORWARD SCATTERING AMPLITUDE FUNCTION S(0)
    SO(I) = sum((2*N+1).*(an+bn))/2;
    %
    % NORMALIZED RADAR CROSS-SECTION
    SB(I)=(abs( sum((2*N+1).*((-1).^(N)).*( an - bn )) )/X).^2;
end

AT = zeros(1,size(P,2));
PH = zeros(1,size(P,2));
for n = 1:size(P,2) % N sweeps rain rate
    %
    % CALCULATE ATTENUATION AND PHASE SHIFT
    ATO = real(SO).*P(:,n)./(6*D.^3.* V);
    AT(n) = 4.343*R(n)*(LAM/pi)^2*sum(AT0);

    PH0 = imag(SO).*P(:,n)./(6*D.^3.* V);
    PH(n) = 90.0*R(n)*(LAM/pi)^2/pi*sum(PH0);
end

disp(['Attenuation and Phase Shift at ',num2str(F),' GHz']);
hdr = {'Rain rate (mm/hr)'},{'Attenuation (dB/km)'},{'Phase shift (deg/km)'};
out = [hdr; num2cell([R', AT', PH'])];
disp(out);

figure(1),
semilogy(R,AT,'--'),
xlabel('rain rate (mm/hr)'), ylabel('Attenuation (dB/km)')
legend([num2str(F), ' GHz'], 'location', 'southeast')
```

Figure 2.15

(Cont.) MATLAB program for Examples 2.13 and 2.14.

and small values. If α is increased further, the normalized radar cross section increases rapidly. The unexpectedly large cross sections have been attributed to a lens effect; the ice sphere acts like a lens which focuses the incoming wave on the back side from which it is reflected backward in a concentrated beam. This is recognized as a crude description, but it at least permits visualization of a physical process which may have some reality.

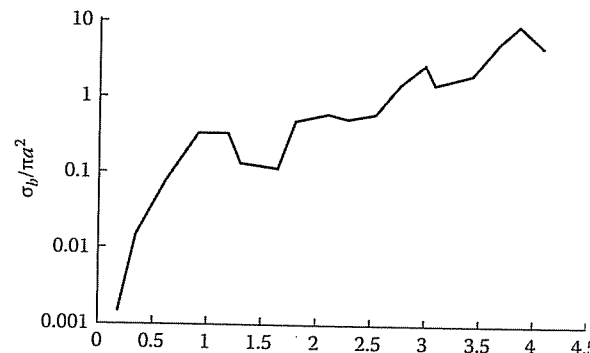


Figure 2.16
Normalized back-scattering (radar) cross sections $\alpha = 2\pi a/\lambda$ for ice at 0°C .

Example 2.14

Assuming the Laws and Parsons' rain drop-size distribution, calculate the attenuation in dB/km for rain rates of 0.25, 1.25, 2.5, 5.0, 12.5, 50.0, 100.0, and 150.0 mm/hr. Consider the incident microwave frequencies of 6, 11, and 30 GHz.

Solution

The MATLAB code developed for calculating attenuation and phase shift of microwaves due to rain is shown in Figure 2.15. The main program calculates attenuation and phase shift for given values of frequency and rain rate by employing Equations (2.268) and (2.269). For each frequency, the corresponding value of the refractive index of water at 20°C is taken from Table 2.11. The data in Tables 2.9 and 2.10 on the drop-size distributions and terminal velocity are incorporated in the main program.

MATLAB provides commands for calculating Bessel functions. The derivative of Bessel-Riccati function $[xz_n(x)]'$ is obtained from (see Problem 2.14)

$$[xz_n(x)]' = -nz_n(x) + xz_{n-1}(x)$$

where z_n is j_n , j_{-n} , y_n or $h_n(x)$. Subroutine GAMMA calculates $\Gamma(n + 1/2)$ using Equation (2.165), while subroutine FACTORIAL determines $n!$. All computations were done in double precision arithmetic, although it was observed that using single precision would only alter results slightly.

2.9. ATTENUATION DUE TO RAINDROPS

Typical results for 11 GHz are tabulated in Table 2.12. A graph of attenuation vs. rain rate is portrayed in Figure 2.17. The plot shows that attenuation increases with rain rate and conforms with the common rule of thumb. We must note that the underlying assumption of spherical raindrops renders the result as only a first order approximation of the practical rainfall situation.

Table 2.12 Attenuation and Phase Shift at 11 GHz

Rain Rate (mm/hr)	Attenuation (dB/km)	Phase Shift (deg/km)
0.25	2.56×10^{-3}	0.4119
1.25	1.702×10^{-3}	1.655
2.5	4.072×10^{-3}	3.040
5.0	9.878×10^{-3}	5.601
12.5	0.3155	12.58
25	0.7513	23.19
50	1.740	42.74
100	3.947	78.59
150	6.189	112.16

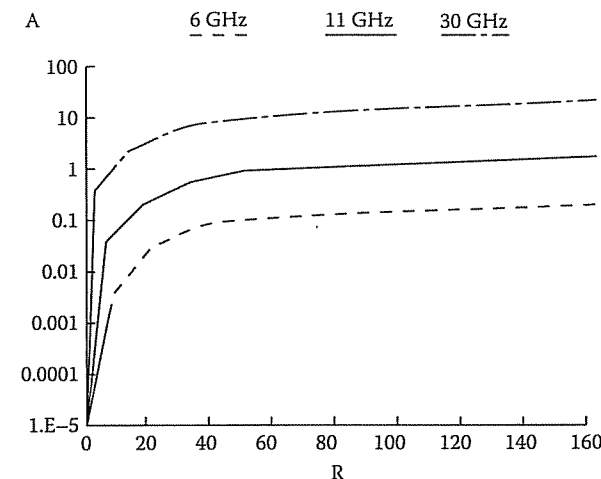


Figure 2.17
Attenuation vs. rain rate.

2.10 Concluding Remarks

We have reviewed analytic methods for solving partial differential equations. Analytic solutions are of major interest as test models for comparison with numerical techniques. The emphasis has been on the method of separation of variables, the most powerful analytic method. For an excellent, more in-depth exposition of this method, consult Myint-U [5]. In the course of applying the method of separation of variables, we have encountered some mathematical functions such as Bessel functions and Legendre polynomials. For a thorough treatment of these functions and their properties, Bell [7] and Johnson and Johnson [8] are recommended. The mathematical handbook by Abramowitz and Stegun [15] provides tabulated values of these functions for specific orders and arguments. A few useful texts on the topics covered in this chapter are also listed in the references.

As an example of real life problems, we have applied the analytical techniques developed in this chapter to the problem of attenuation of microwaves due to spherical raindrops. Spherical models have also been used to assess the absorption characteristics of the human skull exposed to EM plane waves [16]–[20] (see Problems 2.46 to 2.49).

We conclude this chapter by remarking that the most satisfactory solution of a field problem is an exact analytical one. In many practical situations, no solution can be obtained by the analytical methods, and one must therefore resort to numerical approximation or graphical or experimental solutions. (Experimental solutions are usually very expensive, while graphical solutions are not so accurate.) The remainder of this book will be devoted to a study of the numerical methods commonly used in EM.

REFERENCES

- [6] G.N. Watson, *Theory of Bessel Functions*. London: Cambridge University Press, 1966.
- [7] W.W. Bell, *Special Functions for Scientists and Engineers*. London: D. Van Nostrand, 1968.
- [8] D.E. Johnson and J.R. Johnson, *Mathematical Methods in Engineering and Physics*. Englewood Cliffs, NJ: Prentice-Hall, 1982.
- [9] K. Asano, "Electrostatic potential and field in a cylindrical tank containing charged liquid," *Proc. IEEE*, vol. 124, no. 12, Dec. 1977, pp. 1277–1281.
- [10] J.A. Stratton, *Electromagnetic Theory*. New York: McGraw-Hill, 1941, pp. 394–421, 563–573.
- [11] H.C. Van de Hulst, *Light Scattering of Small Particles*. New York: John Wiley, 1957, pp. 28–37, 114–136, 284.
- [12] J. Morrison and M.J. Cross, "Scattering of a plane electromagnetic wave by axisymmetric raindrops," *Bell Syst. Tech. J.*, vol. 53, no. 6, July–Aug. 1974, pp. 955–1019.
- [13] D.E. Setzer, "Computed transmission through rain at microwave and visible frequencies," *Bell Syst. Tech. J.*, vol. 49, no. 8, Oct. 1970, pp. 1873–1892.
- [14] M.N.O. Sadiku, "Refractive index of snow at microwave frequencies," *Appl. Optics*, vol. 24, no. 4, Feb. 1985, pp. 572–575.
- [15] M. Abramowitz and I.A. Stegun, *Handbook of Mathematical Functions*. New York: Dover, 1965.
- [16] C.H. Durney, "Electromagnetic dosimetry for models of humans and animals: A review of theoretical and numerical techniques," *Proc. IEEE*, vol. 68, no. 1, Jan. 1980, pp. 33–40.
- [17] M.A. Morgan, "Finite element calculation of microwave absorption by the cranial structure," *IEEE Trans. Bio. Engr.*, vol. BME-28, no. 10, Oct. 1981, pp. 687–695.
- [18] J.W. Hand, "Microwave heating patterns in simple tissue models," *Phys. Med. Biol.*, vol. 22, no. 5, 1977, pp. 981–987.
- [19] W.T. Joines and R.J. Spiegel, "Resonance absorption of microwaves by the human skull," *IEEE Trans. Bio. Engr.*, vol. BME-21, Jan. 1974, pp. 46–48.
- [20] C.M. Weil, "Absorption characteristics of multilayered sphere models exposed to UHF/microwave radiation," *IEEE Trans. Bio. Engr.*, vol. BME-22, no. 6, Nov. 1975, pp. 468–476.

References

- [1] W.J. Gibbs, *Conformal Transformation in Electrical Engineering*. London: Chapman & Hall, 1958.
- [2] N. Morita et al., *Integral Equation Methods for Electromagnetics*. Boston, MA: Artech House, 1990.
- [3] H.F. Weinberger, *A First Course in Partial Differential Equations*. New York: John Wiley, 1965, Chap. 5, pp. 63–116.
- [4] R.D. Kersten, *Engineering Differential Systems*. New York: McGraw-Hill, 1969, Chap. 5, pp. 66–106.
- [5] T. Myint-U, *Partial Differential Equations of Mathematical Physics*, 2nd ed., New York: North-Holland, 1980.

Problems

2.1 Consider the PDE

$$a\Phi_{xx} + b\Phi_{xy} + c\Phi_{yy} + d\Phi_x + e\Phi_y + f\Phi = 0$$

where the coefficients a, b, c, d, e , and f are in general functions of x and y . Under what conditions is the PDE separable?

2.2 Determine the distribution of electrostatic potential inside the conducting rectangular boxes with cross sections shown in Figure 2.18.

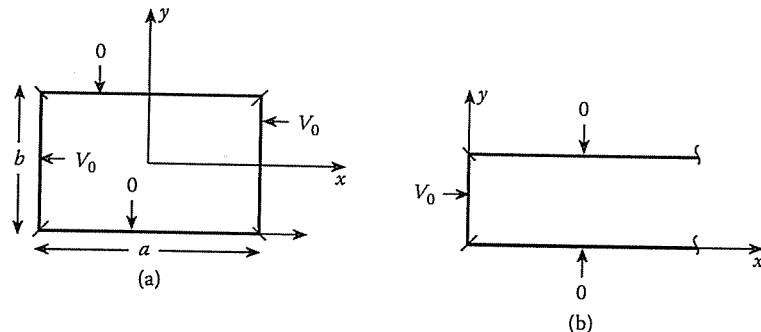


Figure 2.18
For Problem 2.2.

2.3 The cross sections of the cylindrical systems that extend to infinity in the z -direction are shown in Figure 2.19. The potentials on the boundaries are as shown. For each system, find the potential distribution.

2.4 Find the solution U of

(a) Laplace equation

$$\nabla^2 U = 0, \quad 0 < x, y < \pi$$

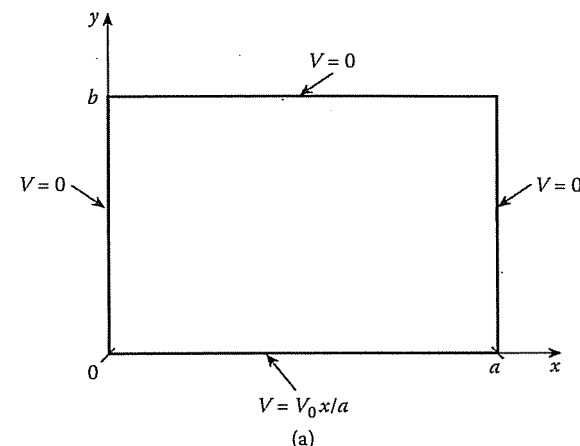
$$U_x(0, y) = 0 = U_x(x, y), \quad U(x, 0) = 0, \\ U(x, \pi) = x, \quad 0 < x < \pi$$

(b) Heat equation

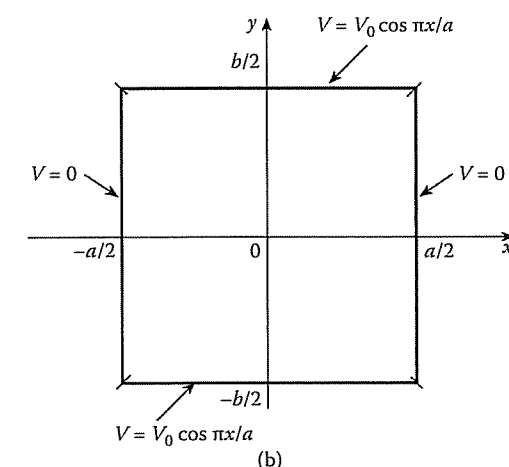
$$kU_{xx} = U_t, \quad 0 \leq x \leq 1, t > 0$$

$$U(0, t) = 0, t > 0, \quad U(1, t) = 1, t > 0$$

$$U(x, 0) = 0, \quad 0 \leq x \leq 1$$



(a)



(b)

Figure 2.19
For Problem 2.3.

(c) Wave equation

$$a^2 U_{xx} = U_{tt}, \quad 0 \leq x \leq 1, t > 0$$

$$U(0, t) = 0 = U(1, t), \quad t > 0$$

$$U(x, 0) = 0, \quad U_t(x, 0) = x$$

2.5 Find the solution Φ of

(a) Laplace equation

$$\nabla^2 \Phi = 0, \quad \rho \geq 1, 0 < \phi < \pi$$

$$\Phi(1, \phi) = \sin \phi, \quad \Phi(\rho, 0) = \Phi(\rho, \pi) = 0$$

(b) Laplace equation

$$\nabla^2 \Phi = 0, \quad 0 < \rho < 1, 0 < z < L$$

$$\Phi(\rho, \phi, 0) = 0 = \Phi(\rho, \phi, L), \quad \Phi(a, \phi, z) = 1$$

(c) Heat equation

$$\Phi_t = k \nabla^2 \Phi, \quad 0 \leq \rho \leq 1, -\infty < z < \infty, t > 0$$

$$\Phi(a, \phi, t) = 0, t > 0, \quad \Phi(\rho, \phi, 0) = \rho^2 \cos 2\phi, 0 \leq \phi < 2\pi$$

2.6 Obtain the solution to the one-dimensional heat equation

$$U_{xx} = U_t, \quad 0 < x < 1, \quad t > 0$$

Subject to the boundary conditions

$$U(0, t) = 0 = U(1, t), \quad t > 0$$

and initial condition

$$U(x, 0) = 100, \quad 0 < x < 1$$

2.7 Solve the two-dimensional heat equation

$$U_{xx} + U_{yy} = U_t, \quad 0 < x < 1, 0 < y < 1, t > 0$$

Boundary conditions:

$$U(0, y, t) = 0 = U(1, y, t), \quad 0 < y < 1, t > 0$$

$$U(x, 0, t) = 0 = U(x, 1, t), \quad 0 < x < 1, t > 0$$

Initial condition:

$$U(x, y, 0) = 10xy, \quad 0 < x < 1, 0 < y < 1$$

2.8 Solve the PDE

$$4 \frac{\partial^4 \Phi}{\partial x^4} + \frac{\partial^2 \Phi}{\partial t^2} = 0, \quad 0 < x < 1, t > 0$$

subject to the boundary conditions

$$\Phi(0, t) = 0 = \Phi(1, t) = \Phi_{xx}(0, t) = \Phi_{xx}(1, t)$$

and initial conditions

$$\Phi_t(x, 0) = 0, \quad \Phi(x, 0) = x$$

2.9 A cylinder similar to the one in Figure 2.20 has its ends $z = 0$ and $z = L$ held at zero potential. If

$$V(a, z) = \begin{cases} V_0 z/L, & 0 < z < L/2 \\ V_0(1 - z/L), & L/2 < z < L \end{cases}$$

find $V(\rho, z)$. Calculate the potential at $(\rho, z) = (0.8a, 0.3L)$.

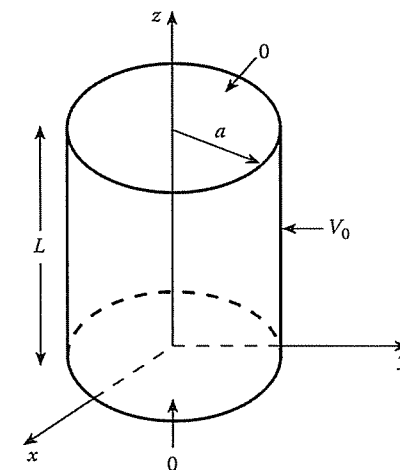


Figure 2.20
For Problem 2.9.

2.10 Determine the potential distribution in a hollow cylinder of radius a and length L with ends held at zero potential while the lateral surface is held at potential V_0 as in Figure 2.20. Calculate the potential along the axis of the cylinder when $L = 2a$.

2.11 The conductor whose cross section is shown in Figure 2.21 is maintained at $V = 0$ everywhere except on the curved electrode where it is held at $V = V_0$. Find the potential distribution $V(\rho, \phi)$.

2.12 Solve the PDE

$$\frac{\partial^2 \Phi}{\partial \rho^2} + \frac{1}{\rho} \frac{\partial \Phi}{\partial \rho} = \frac{\partial^2 \Phi}{\partial t^2}, \quad 0 \leq \rho \leq a, t \geq 0$$

under the conditions

$$\begin{aligned} \Phi(0, t) &\text{ is bounded,} & \Phi(a, t) &= 0, t \geq 0, \\ \Phi(\rho, 0) &= (1 - \rho^2/a^2), & \left. \frac{\partial \Phi}{\partial t} \right|_{t=0} &= 0, 0 \leq \rho \leq a \end{aligned}$$

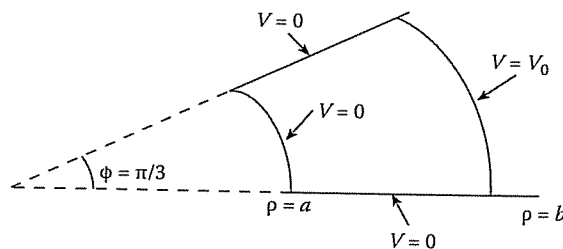


Figure 2.21
For Problem 2.11.

2.13 Find the solution of

$$\nabla^2 U = \frac{\partial U}{\partial t} \rightarrow U_{\rho\rho} + \frac{1}{\rho} U_\rho = U_t, \quad 0 < \rho < 1, t > 0$$

subject to

$$U(1, t) = 0, \quad U(\rho, 0) = T_o \text{ (constant)}$$

2.14 Determine the solution to

$$U_{\rho\rho} + \frac{1}{\rho} U_\rho + U_{zz} = U_t, \quad 0 < \rho < 1, 0 < z < 1, t > 0$$

subject to the boundary conditions

$$U(\rho, 0, t) = 0 = U(\rho, 1, t) = U(1, z, t)$$

and initial condition

$$U(\rho, z, 0) = T_o \text{ (constant)}$$

2.15 (a) Prove that

$$e^{\pm j\rho \sin \phi} = \sum_{n=-\infty}^{\infty} (\pm 1)^n J_n(\rho) e^{jn\phi}$$

(b) Derive the *Bessel's integral formula*

$$J_n(\rho) = \frac{1}{\pi} \int_0^\pi \cos(n\theta - \rho \sin \theta) d\theta$$

2.16 Show that

$$\cos x = J_0(x) + 2 \sum_{n=1}^{\infty} (-1)^n J_{2n}(x)$$

and

$$\sin x = 2 \sum_{n=1}^{\infty} (-1)^{n+1} J_{2n+1}(x)$$

which demonstrate the close tie between Bessel function and trigonometric functions.

2.17 Prove that

$$(a) J_{1/2}(x) = \sqrt{\frac{2}{\pi x}} \sin x,$$

$$(b) J_{-1/2}(x) = \sqrt{\frac{2}{\pi x}} \cos x,$$

$$(c) \frac{d}{dx} [x^{-n} J_n(x)] = -x^n J_{n+1}(x).$$

$$(d) \left. \frac{d^n}{dx^n} J_n(x) \right|_{x=0} = \frac{1}{2^n},$$

$$(e) \frac{d}{dx} [x z_n(x)] = -n z_n(x) + x z_{n-1}(x) = (n+1) z_n(x) + x z_{n+1}(x)$$

2.18 Reduce $\int x^2 J_2(x) dx$ to an integral involving only $J_0(x)$.

2.19 Write a computer program that will evaluate the first five roots λ_{nm} of Bessel function $J_n(x)$ for $n = 1, 2, \dots, 5$, i.e., $J_n(\lambda_{nm}) = 0$.

2.20 Evaluate

(a)

$$\int_{-1}^1 P_1(x) P_2(x) dx,$$

(b)

$$\int_{-1}^1 [P_4(x)]^2 dx,$$

(c)

$$\int_0^1 x^2 P_3(x) dx$$

2.21 In Legendre series of the form $\sum_{n=0}^{\infty} A_n P_n(x)$, expand

$$(a) f(x) = \begin{cases} 0, & -1 < x < 0, \\ 1, & 0 < x < 1 \end{cases}$$

$$(b) f(x) = x^3, \quad -1 < x < 1,$$

$$(c) f(x) = \begin{cases} 0, & -1 < x < 0, \\ x, & 0 < x < 1 \end{cases}$$

$$(d) f(x) = \begin{cases} 1+x, & -1 < x < 0, \\ 1-x, & 0 < x < 1 \end{cases}$$

2.22 Solve Laplace's equation:

$$(a) \nabla^2 U = 0, \quad 0 \leq r \leq a, \quad U(a, \theta) = \begin{cases} 1, & 0 < \theta < \pi/2, \\ 0, & \text{otherwise} \end{cases}$$

$$(b) \nabla^2 U = 0, \quad r > a, \quad \frac{\partial U}{\partial r} \Big|_{r=a} = \cos \theta + 3 \cos^3 \theta, \quad 0 < \theta < \pi,$$

$$(c) \nabla^2 U = 0, \quad r < a, \quad 0 < \theta < \pi, \quad 0 < \phi < 2\pi, \\ U(a, \theta, \phi) = \sin^2 \theta$$

2.23 A hollow conducting sphere of radius a has its upper half charged to potential V_o while its lower half is grounded. Find the potential distribution inside and outside the sphere.

2.24 A circular disk of radius a carries charge of surface charge density ρ_o . Show that the potential at point $(0, 0, z)$ on its axis $\theta = 0$ is

$$V = \frac{\rho_o}{2\epsilon} \left[(z^2 + a^2)^{1/2} - z \right]$$

From this deduce the potential at any point (r, θ, ϕ) .

2.25 (a) Verify the three-term recurrence relation

$$(2n+1)xP_n(x) = (n+1)P_{n+1}(x) + nP_{n-1}(x)$$

(b) Use the recurrence relation to find $P_6(x)$ and $P_7(x)$.

2.26 Establish the formula

$$P_n(-x) = (-1)^n P_n(x)$$

2.27 Verify the following identities:

$$(a) \int_{-1}^1 P_n(x)P_m(x)dx = \frac{2}{2n+1} \delta_{nm},$$

$$(b) \int_{-1}^1 P_n^m(x)P_k^m(x)dx = \frac{2}{2n+1} \frac{(n+m)!}{(n-m)!} \delta_{nk}$$

2.28 Rework the problem in Figure 2.8 if the boundary conditions are now

$$V(r=a) = V_o, \quad V(r \rightarrow \infty) = E_o r \cos \theta + V_o$$

Find V and E everywhere. Determine the maximum value of the field strength.

2.29 In a sphere of radius a , obtain the solution $V(r, \theta)$ of Laplace's equation

$$\nabla^2 V(r, \theta) = 0, \quad r \leq a$$

subject to

$$V(a, \theta) = 3 \cos^2 \theta + 3 \cos \theta + 1$$

2.30 Determine the solution to Laplace's equation

$$\nabla^2 V = 0$$

outside a sphere $r > a$ subject to the boundary condition

$$\frac{\partial}{\partial r} V(a, \theta) = \cos \theta + 3 \cos^3 \theta$$

2.31 Find the potential distribution inside and outside a dielectric sphere of radius a placed in a uniform electric field E_o .

Hint: The problem to be solved is $\nabla^2 V = 0$ subject to

$$\epsilon_r \frac{\partial V_1}{\partial r} = \frac{\partial V_2}{\partial r} \quad \text{on } r = a, \quad V_1 = V_2 \text{ on } r = a, \\ V_2 = -E_o r \cos \theta \quad \text{as } r \rightarrow \infty$$

2.32 (a) Derive the recurrence relation of the associated Legendre polynomials

$$P_n^{m+1}(x) = \frac{2mx}{(1-x^2)^{1/2}} P_n^m(x) - [n(n+1) - m(m-1)] P_n^{m-1}(x)$$

(b) Using the recurrence relation on the formula for P_n^m , find P_3^2 , P_3^3 , P_4^1 , and P_4^2 .

2.33 Expand $V = \cos 2\phi \sin^2 \phi$ in terms of the spherical harmonics $P_n^m(\cos \theta) \sin m\phi$ and $P_n^m(\cos \theta) \cos m\phi$.

2.34 In the prolate spheroidal coordinates (ξ, η, ϕ) , the equation

$$\nabla^2 \Phi + k^2 \Phi = 0$$

assumes the form

$$\frac{\partial}{\partial \xi} \left[(\xi^2 - 1) \frac{\partial \Phi}{\partial \xi} \right] + \frac{\partial}{\partial \eta} \left[(1 - \eta^2) \frac{\partial \Phi}{\partial \eta} \right] + \left[\frac{1}{\xi^2 - 1} \right. \\ \left. + \frac{1}{1 - \eta^2} \right] \frac{\partial^2 \Phi}{\partial \phi^2} + k^2 d^2 (\xi^2 - \eta^2) \Phi = 0$$

Show that the separated equations are

$$\begin{aligned} \frac{d}{d\xi} \left[(\xi^2 + 1) \frac{d\Psi_1}{d\xi} \right] + \left[k^2 d^2 \xi^2 - \frac{m^2}{\xi^2 - 1} - c \right] \Psi_1 &= 0 \\ \frac{d}{d\eta} \left[(1 - \eta^2) \frac{d\Psi_2}{d\eta} \right] - \left[k^2 d^2 \eta^2 + \frac{m^2}{1 - \eta^2} - c \right] \Psi_2 &= 0 \\ \frac{d^2 \Psi_3}{d\phi^2} + m^2 \Psi_3 &= 0 \end{aligned}$$

where m and c are separation constants.

- 2.35 Solve Equation (2.203) if $a = b = c = \pi$ and

(a) $f(x, y, z) = e^{-x}$, (b) $f(x, y, z) = \sin^2 x$.

- 2.36 Solve the inhomogeneous potential problem

$$U_{xx} + U_{yy} = -xy, \quad 0 < x < \pi, 0 < y < \pi$$

Subject to the following boundary conditions

$$U(0, y) = 0, \quad U(\pi, y) = 0$$

$$U(x, 0) = 0, \quad U(x, \pi) = U_o(\text{constant})$$

- 2.37 Solve the inhomogeneous PDE

$$\frac{\partial^2 \Phi}{\partial \rho^2} + \frac{1}{\rho} \frac{\partial \Phi}{\partial \rho} - \frac{\partial^2 \Phi}{\partial t^2} = -\Phi_o \sin \omega t, \quad 0 \leq \rho \leq a, t \geq 0$$

subject to the conditions $\Phi(a, t) = 0$, $\Phi(\rho, 0) = 0$, $\Phi_t(\rho, 0) = 0$, Φ is finite for all $0 \leq \rho \leq a$. Take Φ_o as a constant and $a\omega$ not being a zero of $J_0(x)$.

- 2.38 Infinitely long metal box has a rectangular cross section shown in Figure 2.22. If the box is filled with charge $\rho_v = \rho_o x/a$, find V inside the box.
- 2.39 In Section 2.7.2, find \mathbf{E}_g and \mathbf{E}_e , the electric field intensities in gas and liquid, respectively.
- 2.40 Consider the potential problem shown in Figure 2.23. The potentials at $x = 0$, $x = a$, and $y = 0$ sides are zero while the potential at $y = b$ side is V_o . Using the series expansion technique similar to that used in Section 2.7.2, find the potential distribution in the solution region.
- 2.41 Consider a grounded rectangular pipe with the cross section shown in Figure 2.24. Assuming that the pipe is partially filled with hydrocarbons with charge density ρ_o , apply the same series expansion technique used in Section 2.7.2 to find the potential distribution in the pipe.

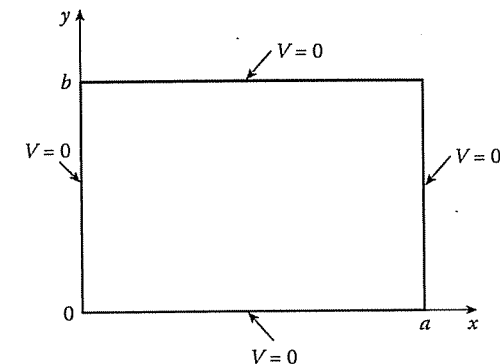


Figure 2.22
For Problem 2.38.

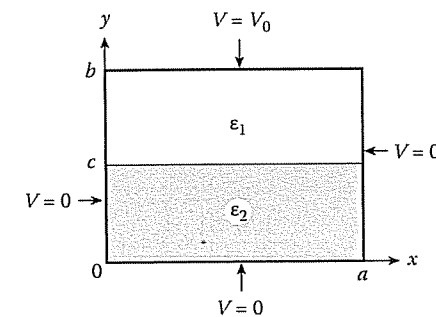


Figure 2.23
Potential system for Problem 2.40.

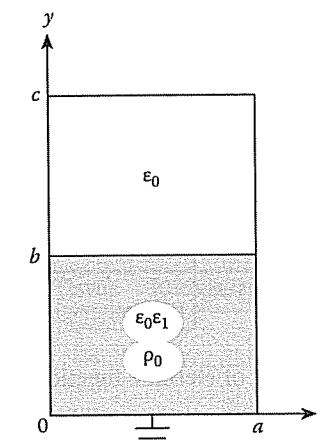


Figure 2.24
Earthed rectangular pipe partially filled with charged liquid—for Problem 2.36.

- 2.42 Write a program to generate associated Legendre polynomial, with $x = \cos\theta = 0.5$. You may use either series expansion or recurrence relations. Take $0 \leq n \leq 15, 0 \leq m \leq n$. Compare your results with those tabulated in standard tables.
- 2.43 Use the product generating function

$$G(x+y, t) = G(x, t)G(y, t)$$

to derive the *addition theorem*

$$J_n(x+y) = \sum_{m=-\infty}^{\infty} J_m(x)J_{n-m}(y)$$

Recall that

$$G(x, t) = \exp\left[\frac{x}{2}\left(t - \frac{1}{t}\right)\right] = \sum_{n=-\infty}^{\infty} t^n J_n(x)$$

- 2.44 Evaluate

- (a) $H_3(x)$ and $H_4(x)$
 (b) $L_3(x)$ and $L_4(x)$

- 2.45 Show that

$$\begin{aligned} \int T_0(x) dx &= T_1(x) \\ \int T_1(x) dx &= \frac{1}{4}T_2(x) + \frac{1}{4} \\ \int T_n(x) dx &= \frac{1}{2} \left(\frac{T_{n+1}(x)}{n+1} - \frac{T_{n-1}(x)}{n-1} \right), \quad n > 1 \end{aligned}$$

so that integration can be done directly in Chebyshev polynomials.

- 2.46 A function is defined by

$$f(x) = \begin{cases} 1, & -1 \leq x \leq 1 \\ 0, & \text{otherwise} \end{cases}$$

- (a) Expand $f(x)$ in a series of Hermite functions,
 (b) expand $f(x)$ in a series of Laguerre functions.

- 2.47 By expressing E_θ^i and E_ϕ^i in terms of the spherical wave functions, show that Equation (2.235) is valid.

- 2.48 By defining

$$\rho_n(x) = \frac{d}{dx} \ln [x h_n^{(2)}(x)], \quad \sigma_n(x) = \frac{d}{dx} \ln [x j_n(x)],$$

show that the scattering amplitude coefficients can be written as

$$\begin{aligned} a_n &= \frac{j_n(\alpha)}{h_n^{(2)}(\alpha)} \left[\frac{\sigma_n(\alpha) - m\sigma_n(m\alpha)}{\rho_n(\alpha) - m\rho_n(m\alpha)} \right] \\ b_n &= \frac{j_n(\alpha)}{h_n^{(2)}(\alpha)} \left[\frac{\sigma_n(m\alpha) - m\sigma_n(\alpha)}{\sigma_n(m\alpha) - m\rho_n(\alpha)} \right] \end{aligned}$$

- 2.49 For the problem in Figure 2.14, plot $|E_z^i|/|E_x^i|$ for $-a < z < a$ along the axis of the dielectric sphere of radius $a = 9$ cm in the $x-z$ plane. Take $E_o = 1$, $\omega = 2\pi \times 5 \times 10^9$ rad/s, $\epsilon_1 = 4\epsilon_o$, $\mu_1 = \mu_o$, $\sigma_1 = 0$. You may modify the program in Figure 2.15 or write your own.
- 2.50 In analytical treatment of the radio-frequency radiation effect on the human body, the human skull is frequently modeled as a lossy sphere. Of major concern is the calculation of the normalized heating potential

$$\Phi(r) = \frac{1}{2} \sigma \frac{|E'(r)|^2}{|E_o|^2} \quad (\Omega \cdot m)^{-1},$$

where E' is the internal electric field strength and E_o is the peak incident field strength. If the human skull can be represented by a homogeneous sphere of radius $a = 10$ cm, plot $\Phi(r)$ against the radial distance $-10 \leq r = z \leq 10$ cm. Assume an incident field as in Figure 2.14 with $f = 1$ GHz, $\mu_r = 1$, $\epsilon_r = 60$, $\sigma = 0.9$ mhos/m, $E_o = 1$.

- 2.51 Instead of the homogeneous spherical model assumed in the previous problem, consider the multilayered spherical model shown in Figure 2.25 with each region labeled by an integer p , such that $p = 1$ represents the central core region and $p = 4$ represents air. At $f = 2.45$ GHz, plot the heating potential along the x axis, y axis, and z axis. Assume the data given below.

Region p	Tissue	Radius (mm)	ϵ_r	σ (mho/m)
1	muscle	18.5	46	2.5
2	fat	19	6.95	0.29
3	skin	20	43	2.5
4	air		1	0
$\mu_r = 1$				

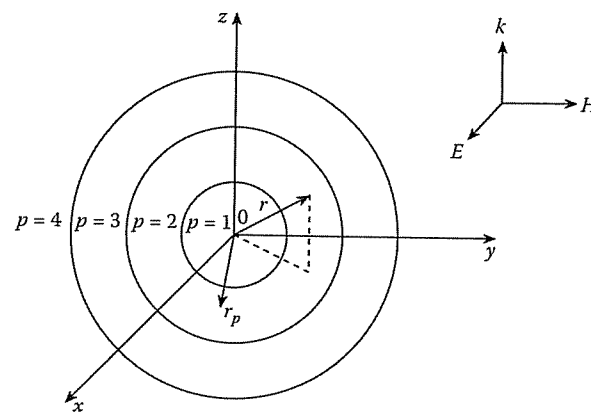


Figure 2.25

For problem 2.51, a multilayered spherical model of the human skull.

Note that for each region p , the resultant field consists of the transmitted and scattered fields and is in general given by

$$E_p(r, \theta, \phi) = E_o e^{j\omega t} \sum_{n=1}^{\infty} (-j)^n \frac{2n+1}{n(n+1)} [a_{np} M_{np}^{(4)}(k) + j b_{np} N_{np}^{(4)}(k) + c_{np} M_{np}^{(1)}(k_1) + j d_{np} N_{np}^{(1)}(k_1)]$$

- 2.52 The absorption characteristic of biological bodies is determined in terms of the specific absorption rate (SAR) defined as the total power absorbed divided as the power incident on the geometrical cross section. For an incident power density of 1 mW/cm^2 in a spherical model of the human head,

$$\text{SAR} = 2 \frac{Q_{\text{abs}}}{\pi a} \quad \text{mW/cm}^3$$

where a is in centimeters. Using the above relation, plot SAR against frequency for $0.1 < f < 3 \text{ GHz}$, $a = 10 \text{ cm}$ assuming frequency-dependent and dielectric properties of head as

$$\epsilon_r = 5 \left(\frac{12 + (f/f_o)^2}{1 + (f/f_o)^2} \right)$$

$$\sigma = 6 \left(\frac{1 + 62(f/f_o)^2}{1 + (f/f_o)^2} \right)$$

where f is in GHz and $f_o = 20 \text{ GHz}$.

- 2.53 For the previous problem, repeat the calculations of SAR assuming a six-layered spherical model of the human skull (similar to that of Figure 2.25) of outer radius $a = 10 \text{ cm}$. Plot P_a/P_i vs. frequency for $0.1 < f < 3 \text{ GHz}$ where

$$\frac{P_a}{P_i} = \frac{2}{\alpha^2} \sum (2n+1) [\text{Re}(a_n + b_n) - (|a_n|^2 + |b_n|^2)],$$

P_a = absorbed power, P_i = incident power, $\alpha = 2\pi a/\lambda$, λ is the wavelength in the external medium. Use the dimensions and electrical properties shown below.

Layer p	Tissue	Radius (mm)	ϵ_r	σ_o (mho/m)
1	brain	9	$5\nabla(f)$	$6\Delta(f)$
2	CSF	12	$7\nabla(f)$	$8\Delta(f)$
3	dura	13	$4\nabla(f)$	$8\Delta(f)$
4	bone	17.3	5	62
5	fat	18.5	6.95	0.29
6	skin	20	43	2.5

where $\mu_r = 1$,

$$\nabla(f) = \frac{1 + 12(f/f_o)^2}{1 + (f/f_o)^2},$$

$$\Delta(f) = \frac{1 + 62(f/f_o)^2}{1 + (f/f_o)^2},$$

f is in GHz, and $f_o = 20 \text{ GHz}$. Compare your result with that from the previous problem.

Chapter 3

Finite Difference Methods

What is time? The Swiss manufacture it. Italians want it. The Americans say it is money. Hindus say it does not exist. I say time is a crook. - Peter Lorre

3.1 Introduction

It is rare for real-life EM problems to fall neatly into a class that can be solved by the analytical methods presented in the preceding chapter. Classical approaches may fail if [1]

- the partial differential equation (PDE) is not linear and cannot be linearized without seriously affecting the result
- the solution region is complex
- the boundary conditions are of mixed types
- the boundary conditions are time-dependent
- the medium is inhomogeneous or anisotropic

Whenever a problem with such complexity arises, numerical solutions must be employed. Of the numerical methods available for solving PDEs, those employing finite differences are more easily understood, more frequently used, and more universally applicable than any other.

The finite difference method (FDM) was first developed by A. Thom [2] in the 1920s under the title “the method of squares” to solve nonlinear hydrodynamic equations. Since then, the method has found applications in solving different field problems. The finite difference techniques are based upon approximations which permit replacing differential equations by finite difference equations. These finite difference approximations are algebraic in form; they relate the value of the dependent variable at a

point in the solution region to the values at some neighboring points. Thus a finite difference solution basically involves three steps:

- (1) dividing the solution region into a grid of nodes
- (2) approximating the given differential equation by finite difference equivalent that relates the dependent variable at a point in the solution region to its values at the neighboring points
- (3) solving the difference equations subject to the prescribed boundary conditions and/or initial conditions

The course of action taken in three steps is dictated by the nature of the problem being solved, the solution region, and the boundary conditions. The most commonly used grid patterns for two-dimensional problems are shown in Figure 3.1. A three-dimensional grid pattern will be considered later in the chapter.

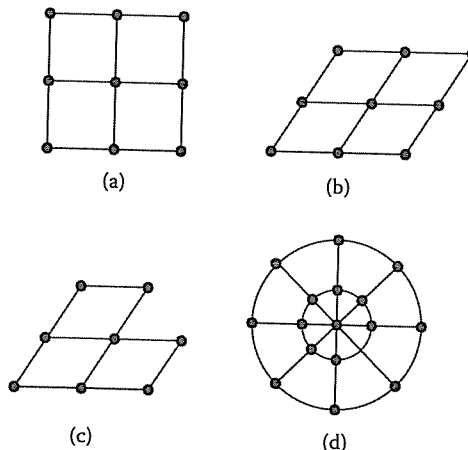


Figure 3.1

Common grid patterns: (a) rectangular grid, (b) skew grid, (c) triangular grid, (d) circular grid.

3.2 Finite Difference Schemes

Before finding the finite difference solutions to specific PDEs, we will look at how one constructs finite difference approximations from a given differential equation. This essentially involves estimating derivatives numerically.

Given a function $f(x)$ shown in Figure 3.2, we can approximate its derivative, slope or the tangent at P by the slope of the arc PB, giving the *forward-difference* formula

3.2. FINITE DIFFERENCE SCHEMES

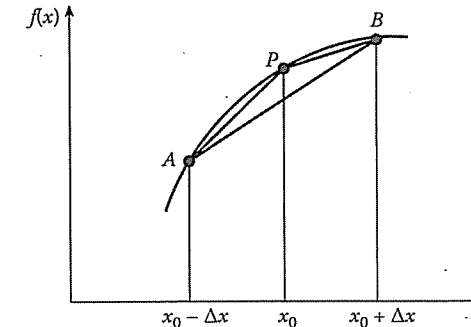


Figure 3.2

Estimates for the derivative of $f(x)$ at P using forward, backward, and central differences.

$$f'(x_o) \simeq \frac{f(x_o + \Delta x) - f(x_o)}{\Delta x} \quad (3.1)$$

or the slope of the arc AP, yielding the *backward-difference* formula

$$f'(x_o) \simeq \frac{f(x_o) - f(x_o - \Delta x)}{\Delta x} \quad (3.2)$$

or the slope of the arc AB, resulting in the *central-difference* formula

$$f'(x_o) \simeq \frac{f(x_o + \Delta x) - f(x_o - \Delta x)}{2\Delta x} \quad (3.3)$$

We can also estimate the second derivative of $f(x)$ at P by applying Equation (3.3) twice

$$\begin{aligned} f''(x_o) &\simeq \frac{f'(x_o + \Delta x/2) - f'(x_o - \Delta x/2)}{\Delta x} \\ &= \frac{1}{\Delta x} \left[\frac{f(x_o + \Delta x) - f(x_o)}{\Delta x} - \frac{f(x_o) - f(x_o - \Delta x)}{\Delta x} \right] \end{aligned}$$

or

$$f''(x_o) \simeq \frac{f(x_o + \Delta x) - 2f(x_o) + f(x_o - \Delta x)}{(\Delta x)^2} \quad (3.4)$$

Any approximation of a derivative in terms of values at a discrete set of points is called *finite difference* approximation.

The approach used above in obtaining finite difference approximations is rather intuitive. A more general approach is using Taylor's series. According to the well-known expansion,

$$f(x_o + \Delta x) = f(x_o) + \Delta x f'(x_o) + \frac{1}{2!} (\Delta x)^2 f''(x_o) + \frac{1}{3!} (\Delta x)^3 f'''(x_o) + \dots \quad (3.5)$$

and

$$f(x_o - \Delta x) = f(x_o) - \Delta x f'(x_o) + \frac{1}{2!} (\Delta x)^2 f''(x_o) - \frac{1}{3!} (\Delta x)^3 f'''(x_o) + \dots \quad (3.6)$$

Upon adding these expansions,

$$f(x_o + \Delta x) + f(x_o - \Delta x) = 2f(x_o) + (\Delta x)^2 f''(x_o) + O(\Delta x)^4 \quad (3.7)$$

where $O(\Delta x)^4$ is the error introduced by truncating the series. We say that this error is of the order $(\Delta x)^4$ or simply $O(\Delta x)^4$. Therefore, $O(\Delta x)^4$ represents terms that are not greater than $(\Delta x)^4$. Assuming that these terms are negligible,

$$f''(x_o) \simeq \frac{f(x_o + \Delta x) - 2f(x_o) + f(x_o - \Delta x)}{(\Delta x)^2}$$

which is Equation (3.4). Subtracting Equation (3.6) from Equation (3.5) and neglecting terms of the order $(\Delta x)^3$ yields

$$f'(x_o) \simeq \frac{f(x_o + \Delta x) - f(x_o - \Delta x)}{2\Delta x}$$

which is Equation (3.3). This shows that the leading errors in Equations (3.3) and (3.4) are of the order $(\Delta x)^2$. Similarly, the difference formula in Equations (3.1) and (3.2) have truncation errors of $O(\Delta x)$. Higher order finite difference approximations can be obtained by taking more terms in Taylor series expansion. If the infinite Taylor series were retained, an exact solution would be realized for the problem. However, for practical reasons, the infinite series is usually truncated after the second-order term. This imposes an error which exists in all finite difference solutions.

To apply the difference method to find the solution of a function $\Phi(x, t)$, we divide the solution region in the $x - t$ plane into equal rectangles or meshes of sides Δx and Δt as in Figure 3.3. We let the coordinates (x, t) of a typical grid point or node be

$$\begin{aligned} x &= i\Delta x, & i &= 0, 1, 2, \dots \\ t &= j\Delta t, & j &= 0, 1, 2, \dots \end{aligned} \quad (3.8a)$$

and the value of Φ at P be

$$\Phi_P = \Phi(i\Delta x, j\Delta t) = \Phi(i, j) \quad (3.8b)$$

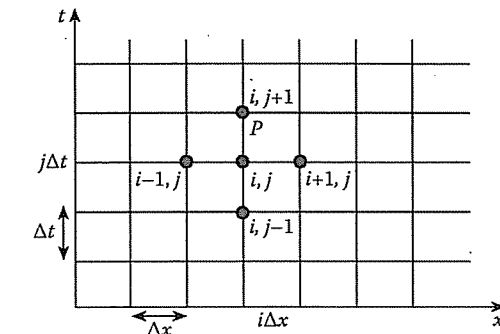


Figure 3.3

Finite difference mesh for two independent variables x and t .

With this notation, the central difference approximations of the derivatives of Φ at the (i, j) th node are

$$\Phi_x|_{i,j} \simeq \frac{\Phi(i+1, j) - \Phi(i-1, j)}{2\Delta x}, \quad (3.9a)$$

$$\Phi_t|_{i,j} \simeq \frac{\Phi(i, j+1) - \Phi(i, j-1)}{2\Delta t}, \quad (3.9b)$$

$$\Phi_{xx}|_{i,j} \simeq \frac{\Phi(i+1, j) - 2\Phi(i, j) + \Phi(i-1, j)}{(\Delta x)^2}, \quad (3.9c)$$

$$\Phi_{tt}|_{i,j} \simeq \frac{\Phi(i, j+1) - 2\Phi(i, j) + \Phi(i, j-1)}{(\Delta t)^2} \quad (3.9d)$$

Table 3.1 gives some useful finite difference approximations for Φ_x and Φ_{xx} .

3.3 Finite Differencing of Parabolic PDEs

Consider a simple example of a parabolic (or diffusion) partial differential equation with one spatial independent variable

$$k \frac{\partial \Phi}{\partial t} = \frac{\partial^2 \Phi}{\partial x^2} \quad (3.10)$$

where k is a constant. The equivalent finite difference approximation is

$$k \frac{\Phi(i, j+1) - \Phi(i, j)}{\Delta t} = \frac{\Phi(i+1, j) - 2\Phi(i, j) + \Phi(i-1, j)}{(\Delta x)^2} \quad (3.11)$$

where $x = i\Delta x, i = 0, 1, 2, \dots, n, t = j\Delta t, j = 0, 1, 2, \dots$. In Equation (3.11), we have used the forward difference formula for the derivative with respect to t and

Table 3.1 Finite Difference Approximations for Φ_x and Φ_{xx}

Derivative	Finite Difference Approximation	Type	Error
Φ_x	$\frac{\Phi_{i+1} - \Phi_i}{\Delta x}$	FD	$O(\Delta x)$
	$\frac{\Phi_i - \Phi_{i-1}}{\Delta x}$	BD	$O(\Delta x)$
	$\frac{\Phi_{i+1} - \Phi_{i-1}}{2\Delta x}$	CD	$O(\Delta x)^2$
	$\frac{-\Phi_{i+2} + 4\Phi_{i+1} - 3\Phi_i}{2\Delta x}$	FD	$O(\Delta x)^2$
	$\frac{3\Phi_i - 4\Phi_{i-1} + \Phi_{i-2}}{2\Delta x}$	BD	$O(\Delta x)^2$
	$\frac{-\Phi_{i+2} + 8\Phi_{i+1} - 8\Phi_{i-1} + \Phi_{i-2}}{12\Delta x}$	CD	$O(\Delta x)^4$
Φ_{xx}	$\frac{\Phi_{i+2} - 2\Phi_{i+1} + \Phi_i}{(\Delta x)^2}$	FD	$O(\Delta x)^2$
	$\frac{\Phi_i - 2\Phi_{i-1} + \Phi_{i-2}}{(\Delta x)^2}$	BD	$O(\Delta x)^2$
	$\frac{\Phi_{i+1} - 2\Phi_i + \Phi_{i-1}}{(\Delta x)^2}$	CD	$O(\Delta x)^2$
	$\frac{-\Phi_{i+2} + 16\Phi_{i+1} - 30\Phi_i + 16\Phi_{i-1} - \Phi_{i-2}}{12(\Delta x)^2}$	CD	$O(\Delta x)^4$

where FD = Forward Difference, BD = Backward Difference, and CD = Central Difference.

central difference formula for that with respect to x . If we let

$$r = \frac{\Delta t}{k(\Delta x)^2}, \quad (3.12)$$

Equation (3.11) can be written as

$$\Phi(i, j+1) = r\Phi(i+1, j) + (1-2r)\Phi(i, j) + r\Phi(i-1, j) \quad (3.13)$$

This *explicit formula* can be used to compute $\Phi(x, t + \Delta t)$ explicitly in terms of $\Phi(x, t)$. Thus the values of Φ along the first time row (see Figure 3.3), $t = \Delta t$, can be calculated in terms of the boundary and initial conditions, then the values of Φ along the second time row, $t = 2\Delta t$, are calculated in terms of the first time row, and so on.

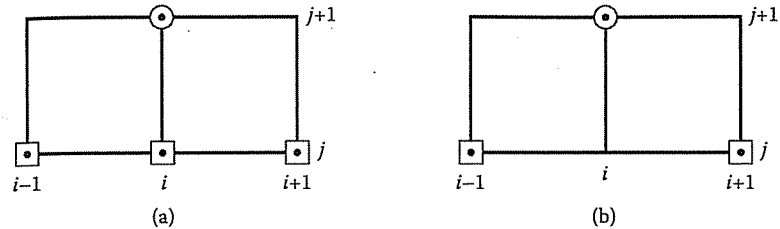
A graphic way of describing the difference formula of Equation (3.13) is through the *computational molecule* of Figure 3.4(a), where the square is used to represent the grid point where Φ is presumed known and a circle where Φ is unknown.

In order to ensure a stable solution or reduce errors, care must be exercised in selecting the value of r in Equations (3.12) and (3.13). It will be shown in Section 3.6 that Equation (3.13) is valid only if the coefficient $(1-2r)$ in Equation (3.13) is nonnegative or $0 < r \leq 1/2$. If we choose $r = 1/2$, Equation (3.13) becomes

$$\Phi(i, j+1) = \frac{1}{2}[\Phi(i+1, j) + \Phi(i-1, j)] \quad (3.14)$$

so that the computational molecule becomes that shown in Figure 3.4(b).

3.3. FINITE DIFFERENCING OF PARABOLIC PDES

**Figure 3.4**

Computational molecule for parabolic PDE: (a) for $0 < r \leq 1/2$, (b) for $r = 1/2$.

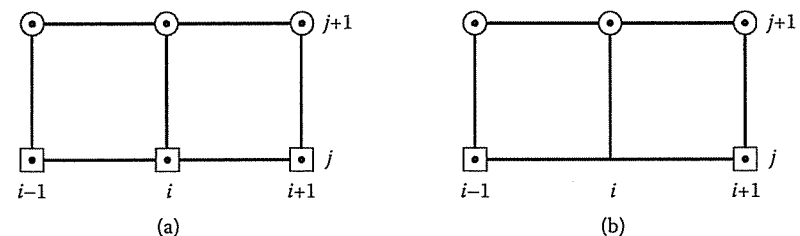
The fact that obtaining stable solutions depends on r or the size of the time step Δt renders the explicit formula of Equation (3.13) inefficient. Although the formula is simple to implement, its computation is slow. An *implicit formula*, proposed by Crank and Nicholson in 1974, is valid for all finite values of r . We replace $\partial^2\Phi/\partial x^2$ in Equation (3.10) by the average of the central difference formulas on the j th and $(j+1)$ th time rows so that

$$k \frac{\Phi(i, j+1) - \Phi(i, j)}{\Delta t} = \frac{1}{2} \left[\frac{\Phi(i+1, j) - 2\Phi(i, j) + \Phi(i-1, j)}{(\Delta x)^2} + \frac{\Phi(i+1, j+1) - 2\Phi(i, j+1) + \Phi(i-1, j+1)}{(\Delta x)^2} \right]$$

This can be rewritten as

$$\begin{aligned} -r\Phi(i-1, j+1) + 2(1+r)\Phi(i, j+1) - r\Phi(i+1, j+1) \\ = r\Phi(i-1, j) + 2(1-r)\Phi(i, j) + r\Phi(i+1, j) \end{aligned} \quad (3.15)$$

where r is given by Equation (3.12). The right side of Equation (3.15) consists of three known values, while the left side has the three unknown values of Φ . This is illustrated in the computational molecule of Figure 3.5(a). Thus if there are n free nodes along each time row, then for $j = 0$, applying Equation (3.15) to nodes $i = 1, 2, \dots, n$

**Figure 3.5**

Computational molecule for Crank–Nicholson method: (a) for finite values of r , (b) for $r = 1$.

results in n simultaneous equations with n unknown values of Φ and known initial and boundary values of Φ . Similarly, for $j = 1$, we obtain n simultaneous equations for n unknown values of Φ in terms of the known values $j = 0$, and so on. The combination of accuracy and unconditional stability allows the use of a much larger time step with the Crank–Nicholson method than is possible with the explicit formula. Although the method is valid for all finite values of r , a convenient choice of $r = 1$ reduces Equation (3.15) to

$$-\Phi(i-1, j+1) + 4\Phi(i, j+1) - \Phi(i+1, j+1) = \Phi(i-1, j) + \Phi(i+1, j) \quad (3.16)$$

with the computational molecule of Figure 3.5(b).

More complex finite difference schemes can be developed by applying the same principles discussed above. Two of such schemes are the Leapfrog method and the Dufort–Frankel method [3, 4]. These and those discussed earlier are summarized in Table 3.2. Notice that the last two methods are two-step finite difference schemes in that finding Φ at time $j+1$ requires knowing Φ at two previous time steps j and $j-1$, whereas the first two methods are one-step schemes. For further treatment on the finite difference solution of parabolic PDEs, see Smith [5] and Ferziger [6].

Example 3.1

Solve the diffusion equation

$$\frac{\partial^2 \Phi}{\partial x^2} = \frac{\partial \Phi}{\partial t}, \quad 0 \leq x \leq 1 \quad (3.17)$$

subject to the boundary conditions

$$\Phi(0, t) = 0 = \Phi(1, t) = 0, \quad t > 0 \quad (3.18a)$$

and initial condition

$$\Phi(x, 0) = 100 \quad (3.18b)$$

Solution

This problem may be regarded as a mathematical model of the temperature distribution in a rod of length $L = 1$ m with its end in contact with ice blocks (or held at 0°C) and the rod initially at 100°C . With that physical interpretation, our problem is finding the internal temperature Φ as a function of position and time. We will solve this problem using both explicit and implicit methods.

(a) Explicit Method

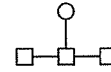
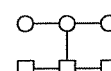
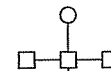
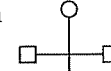
For easy hand calculations, let us choose $\Delta x = 0.1, r = 1/2$ so that

$$\Delta t = kr(\Delta x)^2 = 0.005$$

3.3. FINITE DIFFERENCING OF PARABOLIC PDES

Table 3.2 Finite Difference Approximation to the Parabolic Equation:

$$\frac{\partial \Phi}{\partial t} = \frac{1}{k} \frac{\partial^2 \Phi}{\partial x^2}, k > 0$$

Method	Algorithm	Molecule
1. First order (Euler)	$\frac{\Phi_i^{j+1} - \Phi_i^j}{\Delta t} = \frac{\Phi_{i+1}^j - 2\Phi_i^j + \Phi_{i-1}^j}{k(\Delta x)^2}$ explicit, stable for $r = \Delta t / k(\Delta x)^2 \leq 0.5$	
2. Crank–Nicholson	$\frac{\Phi_i^{j+1} - \Phi_i^j}{\Delta t} = \frac{\Phi_{i+1}^{j+1} - 2\Phi_i^{j+1} + \Phi_{i-1}^{j+1}}{2k(\Delta x)^2} + \frac{\Phi_{i+1}^j - 2\Phi_i^j + \Phi_{i-1}^j}{2k(\Delta x)^2}$ implicit, always stable	
3. Leapfrog	$\frac{\Phi_i^{j+1} - \Phi_i^{j-1}}{2\Delta t} = \frac{\Phi_{i+1}^j - 2\Phi_i^j + \Phi_{i-1}^j}{k(\Delta x)^2}$ explicit, always unstable	
4. Dufort–Frankel	$\frac{\Phi_i^{j+1} - \Phi_i^{j-1}}{2\Delta t} = \frac{\Phi_{i+1}^j - \Phi_i^{j+1} - \Phi_i^{j-1} + \Phi_{i-1}^j}{k(\Delta x)^2}$ explicit, unconditionally stable	

since $k = 1$. We need the solution for only $0 \leq x \leq 0.5$ because the problem is symmetric with respect to $x = 0.5$. First we calculate the initial and boundary values using Equation (3.18). These values of Φ at the fixed nodes are shown in Table 3.3 for $x = 0, x = 1$, and $t = 0$. Notice that the values of $\Phi(0, 0)$ and $\Phi(1, 0)$ are taken as the average of 0 and 100. We now calculate Φ at the free nodes using Equation (3.14) or the molecule of Figure 3.4(b). The result is shown in Table 3.3. The analytic solution to Equation (3.17) subject to Equation (3.18) is

$$\Phi(x, t) = \frac{400}{\pi} \sum_{k=0}^{\infty} \frac{1}{n} \sin n\pi x \exp(-n^2\pi^2 t), \quad n = 2k + 1$$

Comparison of the explicit finite difference solution with the analytic solution at $x = 0.4$ is shown in Table 3.4. The table shows that the finite difference solution is reasonably accurate. Greater accuracy can be achieved by choosing smaller values of Δx and Δt .

Table 3.3 Results for Example 3.1

<i>x</i>	0	0.1	0.2	0.3	0.4	0.5	0.6	...	1.0
<i>t</i>	0	50	100	100	100	100	100		50
0.005	0	75.0	100	100	100	100	100		0
0.01	0	50	87.5	100	100	100	100		0
0.015	0	43.75	75	93.75	100	100	100		0
0.02	0	37.5	68.75	87.5	96.87	100	96.87		0
0.025	0	34.37	62.5	82.81	93.75	96.87	93.75		0
0.03	0	31.25	58.59	78.21	89.84	93.75	89.84		0
:									
0.1	0	14.66	27.92	38.39	45.18	47.44	45.18		0

Table 3.4 Comparison of Explicit Finite Difference Solution with Analytic Solution; for Example 3.1

<i>t</i>	Finite Difference Solution at <i>x</i> = 0.4	Analytic Solution at <i>x</i> = 0.4	Percentage Error
0.005	100	99.99	0.01
0.01	100	99.53	0.47
0.015	100	97.85	2.2
0.02	96.87	95.18	1.8
0.025	93.75	91.91	2.0
0.03	89.84	88.32	1.7
0.035	85.94	84.61	1.6
0.04	82.03	80.88	1.4
:			
0.10	45.18	45.13	0.11

(b) Implicit Method

Let us choose $\Delta x = 0.2$, $r = 1$ so that $\Delta t = 0.04$. The values of Φ at the fixed nodes are calculated as in part (a) (see Table 3.3). For the free nodes, we apply Equation (3.16) or the molecule of Figure 3.5(b). If we denote $\Phi(i, j+1)$ by Φ_i ($i = 1, 2, 3, 4$), the values of Φ for the first time step (Figure 3.6) can be obtained by solving the following simultaneous equations:

$$\begin{aligned} -0 + 4\Phi_1 - \Phi_2 &= 50 + 100 \\ -\Phi_1 + 4\Phi_2 + \Phi_3 &= 100 + 100 \\ -\Phi_2 + 4\Phi_3 - \Phi_4 &= 100 + 100 \\ -\Phi_3 + 4\Phi_4 - 0 &= 100 + 50 \end{aligned}$$

3.4. FINITE DIFFERENCING OF HYPERBOLIC PDES

We obtain

$$\Phi_1 = 58.13, \quad \Phi_2 = 82.54, \quad \Phi_3 = 72, \quad \Phi_4 = 55.5$$

at $t = 0.04$. Using these values of Φ , we apply Equation (3.16) to obtain another set of simultaneous equations for $t = 0.08$ as

$$-0 + 4\Phi_1 - \Phi_2 = 0 + 82.54$$

$$-\Phi_1 + 4\Phi_2 - \Phi_3 = 58.13 + 72$$

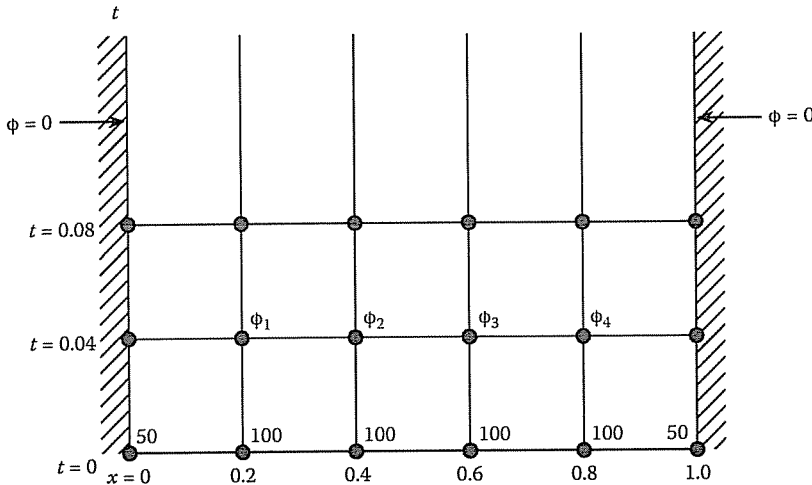
$$-\Phi_2 + 4\Phi_3 - \Phi_4 = 82.54 + 55.5$$

$$-\Phi_3 + 4\Phi_4 - 0 = 72 + 0$$

which results in

$$\Phi_1 = 34.44, \quad \Phi_2 = 55.23, \quad \Phi_3 = 56.33, \quad \Phi_4 = 32.08$$

This procedure can be programmed and accuracy can be increased by choosing more points for each time step.

**Figure 3.6**

For Example 3.1, part (b).

3.4 Finite Differencing of Hyperbolic PDEs

The simplest hyperbolic partial differential equation is the wave equation of the form

$$u^2 \frac{\partial^2 \Phi}{\partial x^2} = \frac{\partial^2 \Phi}{\partial t^2} \quad (3.19)$$

where u is the speed of the wave. An equivalent finite difference formula is

$$\frac{u^2 \Phi(i+1, j) - 2\Phi(i, j) + \Phi(i-1, j)}{(\Delta x)^2} = \frac{\Phi(i, j+1) - 2\Phi(i, j) + \Phi(i, j-1)}{(\Delta t)^2}$$

where $x = i\Delta x$, $t = j\Delta t$, $i, j = 0, 1, 2, \dots$. This equation can be written as

$$\boxed{\Phi(i, j+1) = 2(1-r)\Phi(i, j) + r[\Phi(i+1, j) + \Phi(i-1, j)] - \Phi(i, j-1)} \quad (3.20)$$

where $\Phi(i, j)$ is an approximation to $\Phi(x, t)$ and r is the “aspect ratio” given by

$$r = \left(\frac{u\Delta t}{\Delta x} \right)^2 \quad (3.21)$$

Equation (3.20) is an explicit formula for the wave equation. The corresponding computational molecule is shown in Figure 3.7(a). For the solution algorithm in

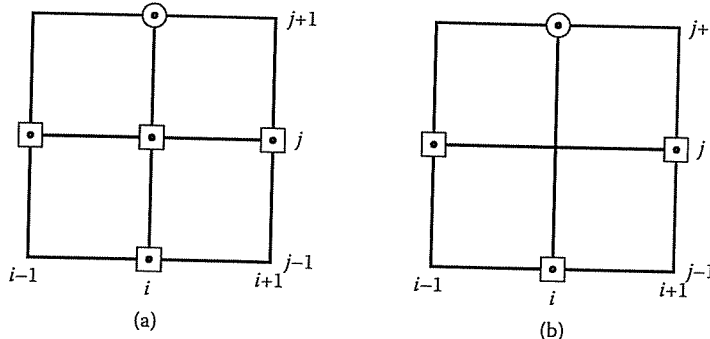


Figure 3.7

Computational molecule for wave equation: (a) for arbitrary $r \leq 1$, (b) for $r = 1$.

Equation (3.20) to be stable, the aspect ratio $r \leq 1$, as will be shown in Example 3.5. If we choose $r = 1$, Equation (3.20) becomes

$$\Phi(i, j+1) = \Phi(i+1, j) + \Phi(i-1, j) - \Phi(i, j-1) \quad (3.22)$$

with the computational molecule in Figure 3.7(b). Unlike the single-step schemes of Equations (3.13) and (3.15), the two-step schemes of Equations (3.20) and (3.22) require that the values of Φ at times j and $j-1$ be known to get Φ at time $j+1$. Thus, we must derive a separate algorithm to “start” the solution of Equation (3.20) or (3.22); that is, we must compute $\Phi(i, 1)$ and $\Phi(i, 2)$. To do this, we utilize the prescribed initial condition. For example, suppose the initial condition on the PDE in Equation (3.19) is

$$\left. \frac{\partial \Phi}{\partial t} \right|_{t=0} = 0$$

3.4. FINITE DIFFERENCING OF HYPERBOLIC PDES

We use the backward-difference formula

$$\frac{\partial \Phi(x, 0)}{\partial t} \sim \frac{\Phi(i, 1) - \Phi(i, -1)}{2\Delta t} = 0$$

or

$$\Phi(i, 1) = \Phi(i, -1) \quad (3.23)$$

Substituting Equation (3.23) into Equation (3.20) and taking $j = 0$ (i.e., at $t = 0$), we get

$$\Phi(i, 1) = 2(1-r)\Phi(i, 0) + r[\Phi(i-1, 0) + \Phi(i+1, 0)] - \Phi(i, 1)$$

or

$$\Phi(i, 1) = (1-r)\Phi(i, 0) + \frac{r}{2}[\Phi(i-1, 0) + \Phi(i+1, 0)] \quad (3.24)$$

Using the starting formula in Equation (3.24) together with the prescribed boundary and initial conditions, the value of Φ at any grid point (i, j) can be obtained directly from Equation (3.20).

There are implicit methods for solving hyperbolic PDEs just as we have implicit methods for parabolic PDEs. However, for hyperbolic PDEs, implicit methods result in an infinite number of simultaneous equations to be solved and therefore cannot be used without making some simplifying assumptions. Interested readers are referred to Smith [5] or Ferziger [6].

Example 3.2

Solve the wave equation

$$\Phi_{tt} = \Phi_{xx}, \quad 0 < x < 1, \quad t \geq 0$$

subject to the boundary conditions

$$\Phi(0, t) = 0 = \Phi(1, t), \quad t \geq 0$$

and the initial conditions

$$\begin{aligned} \Phi(x, 0) &= \sin \pi x, \quad 0 < x < 1, \\ \Phi_t(x, 0) &= 0, \quad 0 < x < 1 \end{aligned} \quad \square$$

Solution

The analytical solution is easily obtained as

$$\Phi(x, t) = \sin \pi x \cos \pi t \quad (3.25)$$

Using the explicit finite difference scheme of Equation (3.20) with $r = 1$, we obtain

$$\Phi(i, j+1) = \Phi(i-1, j) + \Phi(i+1, j) - \Phi(i, j-1), \quad j \geq 1 \quad (3.26)$$

For $j = 0$, substituting

$$\Phi_t = \frac{\Phi(i, 1) - \Phi(i, -1)}{2\Delta t} = 0$$

or

$$\Phi(i, 1) = \Phi(i, -1)$$

into Equation (3.26) gives the starting formula

$$\Phi(i, 1) = \frac{1}{2}[\Phi(i - 1, 0) + \Phi(i + 1, 0)] \quad (3.27)$$

Since $u = 1$, and $r = 1$, $\Delta t = \Delta x$. Also, since the problem is symmetric with respect to $x = 0.5$, we solve for Φ using Equations (3.26) and (3.27) within $0 < x < 0.5$, $t \geq 0$. We can either calculate the values by hand or write a simple computer program. With the MATLAB code in Figure 3.8, the result shown in Table 3.5 is obtained for $\Delta t = \Delta x = 0.1$. The finite difference solution agrees with the exact solution in Equation (3.25) to six decimal places. The accuracy of the FD solution can be increased by choosing a smaller spatial increment Δx and a smaller time increment Δt .

Table 3.5 Solution of the Wave Equation in Example 3.2

x	0	0.1	0.2	0.3	0.4	0.5	0.6	...
t								
0.0	0	0.3090	0.5879	0.8990	0.9511	1.0	0.9511	
0.1	0	0.2939	0.5590	0.7694	0.9045	0.9511	0.9045	
0.2	0	0.2500	0.4755	0.6545	0.7694	0.8090	0.7694	
0.3	0	0.1816	0.3455	0.4755	0.5590	0.5878	0.5590	
0.4	0	0.0955	0.1816	0.2500	0.2939	0.3090	0.2939	
0.5	0	0	0	0	0	0	0	
0.6	0	-0.0955	-0.1816	-0.2500	-0.2939	-0.3090	-0.2939	
0.7	0	-0.1816	-0.3455	-0.4755	-0.5590	-0.5878	-0.5590	
⋮	⋮	⋮	⋮	⋮	⋮	⋮	⋮	⋮

```
% ****
% MATLAB code for example 3.2 on one-dimensional wave equation solved
% using an explicit finite difference scheme
% *****

clear all; format compact; tic

%Explicit Method
delx = 0.1; % resolution size
r = 1; % 'aspect ratio'
u = 1; % Constant of given wave equation
delt = r^2*delx/u; % time step size
Tsteps = round(1/delt); % Number of time steps

% X1 is the potential grid of the simulation, due to symmetry only half
% of the field is calculated.
X1 = zeros(Tsteps,1/(2*delx)+2); % Initialize X1

%Initial conditions and reflection line defined
x = 0:delx:.5+delx;
X1(1,:) = sin(pi*x);
X1(2,2:end-1) = .5*(X1(1,1:end-2)+X1(1,3:end));
X1(2,end) = X1(2,end-2); %reflection line

for row = 3:size(X1,1)
    for col = 2:size(X1,2)-1
        X1(row,col) = X1(row-1,col-1)+X1(row-1,col+1)-X1(row-2,col); % eqn. (3.26)
    end
    X1(row,end) = X1(row,end-2); %reflected line
end

%Use symmetry condition to create entire field
X2 = [X1,fliplr(X1(:,1:end-3))];

figure(1), imagesc(0:delx:1,(0:delt:Tsteps*delt),X2), colorbar
ylabel('\leftarrow time (sec)')
xlabel('x')
title('Hyperbolic PDE')

if (delx==.1)
    dispmat = [X1(1:8,1:7)];
    disp(sprintf('\nCompare to Table 3.5, Solution of the Wave Equation in Exam-'
    ple 3.2'))
    disp(num2str(dispmat))
end
```

Figure 3.8
MATLAB code for Example 3.2.

We can use the central difference approximation for the partial derivatives of which the simplest forms are

$$\frac{\partial^2 \Phi}{\partial x^2} = \frac{\Phi(i+1, j) - 2\Phi(i, j) + \Phi(i-1, j)}{(\Delta x)^2} + O(\Delta x)^2 \quad (3.29a)$$

$$\frac{\partial^2 \Phi}{\partial y^2} = \frac{\Phi(i, j+1) - 2\Phi(i, j) + \Phi(i, j-1)}{(\Delta y)^2} + O(\Delta y)^2 \quad (3.29b)$$

3.5 Finite Differencing of Elliptic PDEs

A typical elliptic PDE is Poisson's equation, which in two dimensions is given by

$$\nabla^2 \Phi = \frac{\partial^2 \Phi}{\partial x^2} + \frac{\partial^2 \Phi}{\partial y^2} = g(x, y) \quad (3.28)$$

where $x = i\Delta x$, $y = j\Delta y$, and $i, j = 0, 1, 2, \dots$. If we assume that $\Delta x = \Delta y = h$, to simplify calculations, substituting Equation (3.29) into Equation (3.28) gives

$$[\Phi(i+1, j) + \Phi(i-1, j) + \Phi(i, j+1) + \Phi(i, j-1)] - 4\Phi(i, j) = h^2 g(i, j)$$

or

$$\Phi(i, j) = \frac{1}{4} [\Phi(i+1, j) + \Phi(i-1, j) + \Phi(i, j+1) + \Phi(i, j-1) - h^2 g(i, j)] \quad (3.30)$$

at every point (i, j) in the mesh for Poisson's equation. The spatial increment h is called the *mesh size*. A special case of Equation (3.28) is when the source term vanishes, i.e., $g(x, y) = 0$. This leads to Laplace's equation. Thus for Laplace's equation, Equation (3.30) becomes

$$\Phi(i, j) = \frac{1}{4} [\Phi(i+1, j) + \Phi(i-1, j) + \Phi(i, j+1) + \Phi(i, j-1)] \quad (3.31)$$

It is worth noting that Equation (3.31) states that the value of Φ for each point is the average of those at the four surrounding points. The five-point computational molecule for the difference scheme in Equation (3.31) is illustrated in Figure 3.9(a), where values of the coefficients are shown. This is a convenient way of displaying finite difference algorithms for elliptic PDEs. The molecule in Figure 3.9(a) is the second order approximation of Laplace's equation. This is obviously not the only way to approximate Laplace's equation, but it is the most popular choice. An alternative fourth order difference is

$$\begin{aligned} & -20\Phi(i, j) + 4[\Phi(i+1, j) + \Phi(i-1, j) + \Phi(i, j+1) + \Phi(i, j-1)] \\ & + \Phi(i+1, j-1) + \Phi(i-1, j-1) + \Phi(i-1, j+1) \\ & + \Phi(i+1, j+1) = 0 \end{aligned} \quad (3.32)$$

The corresponding computational molecule is shown in Figure 3.9(b).

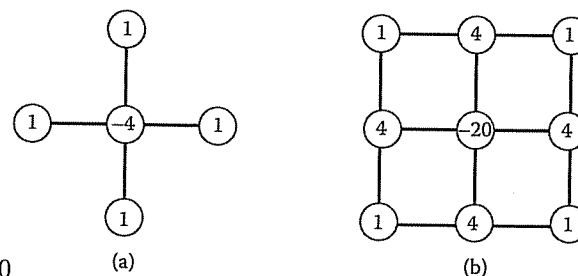


Figure 3.9

Computational molecules for Laplace's equation based on: (a) second order approximation, (b) fourth order approximation.

The application of the finite difference method to elliptic PDEs often leads to a large system of algebraic equations, and their solution is a major problem in itself. Two commonly used methods of solving the system of equations are band matrix and iterative methods.

3.5.1 Band Matrix Method

From Equations (3.30) to (3.32), we notice that only nearest neighboring nodes affect the value of Φ at each node. Hence application of any of Equations (3.30) to (3.32) to all free nodes in the solution region results in a set of simultaneous equations of the form

$$[A][X] = [B] \quad (3.33)$$

where $[A]$ is a *sparse* matrix (it has many zero elements), $[X]$ is a column matrix consisting of the unknown values of Φ at the free nodes, and $[B]$ is a column matrix containing the known values of Φ at fixed nodes. Matrix $[A]$ is also banded in that its nonzero terms appear clustered near the main diagonal. Matrix $[X]$, containing the unknown elements, can be obtained from

$$[X] = [A]^{-1}[B] \quad (3.34)$$

or by solving Equation (3.33) using the Gauss elimination discussed in Appendix C.1.

3.5.2 Iterative Methods

The iterative methods are generally used to solve a large system of simultaneous equations. An iterative method for solving equations is one in which a first approximation is used to calculate a second approximation, which in turn is used to calculate a third approximation, and so on. The three common iterative methods (Jacobi, Gauss-Seidel, and successive over-relaxation (SOR)) are discussed in Appendix C.2. We will apply only SOR here.

To apply the method of SOR to Equation (3.30), for example, we first define the *residual* $R(i, j)$ at node (i, j) as the amount by which the value of $\Phi(i, j)$ does not satisfy Equation (3.30), i.e.,

$$\begin{aligned} R(i, j) = & \Phi(i+1, j) + \Phi(i-1, j) + \Phi(i, j+1) \\ & + \Phi(i, j-1) - 4\Phi(i, j) - h^2 g(i, j) \end{aligned} \quad (3.35)$$

The value of the residual at k th iteration, denoted by $R^k(i, j)$, may be regarded as a correction which must be added to $\Phi(i, j)$ to make it nearer to the correct value. As convergence to the correct value is approached, $R^k(i, j)$ tends to zero. Hence to improve the rate of convergence, we multiply the residual by a number ω and add that to $\Phi(i, j)$ at the k th iteration to get $\Phi(i, j)$ at $(k+1)$ th iteration. Thus

$$\Phi^{k+1}(i, j) = \Phi^k(i, j) + \frac{\omega}{4} R^k(i, j)$$

or

$$\begin{aligned}\Phi^{k+1}(i, j) = & \Phi^k(i, j) + \frac{\omega}{4} [\Phi^k(i+1, j) + \Phi^k(i-1, j) + \Phi^k(i, j-1) \\ & + \Phi^k(i, j+1) - 4\Phi^k(i, j) - h^2 g(i, j)]\end{aligned}\quad (3.36)$$

The parameter ω is called the *relaxation factor* while the technique is known as the method of *successive over-relaxation*. The value of ω lies between 1 and 2. (When $\omega = 1$, the method is simply called successive relaxation.) Its optimum value ω_{opt} must be found by trial-and-error. In order to start Equation (3.36), an initial guess, $\Phi^0(i, j)$, is made at every free node. Typically, we may choose $\Phi^0(i, j) = 0$ or the average of Φ at the fixed nodes.

Example 3.3

Solve Laplace's equation

$$\nabla^2 V = 0, \quad 0 \leq x \leq 1, \quad 0 \leq y \leq 1$$

with $V(x, 1) = 45x(1-x)$, $V(x, 0) = 0 = V(0, y) = V(1, y)$. \square

Solution

Let $h = 1/3$ so that the solution region is as in Figure 3.10. Applying Equation (3.31) to each of the four points leads to

$$\begin{aligned}4V_1 - V_2 - V_3 - 0 &= 10 \\ -V_1 + 4V_2 - 0 - V_4 &= 10 \\ -V_1 - 0 + 4V_3 - V_4 &= 0 \\ -0 - V_2 - V_3 + 4V_4 &= 0\end{aligned}$$

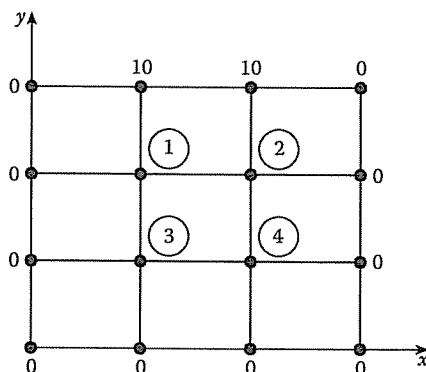


Figure 3.10

Finite difference grid for Example 3.3.

This can be written as

$$\begin{bmatrix} 4 & -1 & -1 & 0 \\ -1 & 4 & 0 & -1 \\ -1 & 0 & 4 & -1 \\ 0 & -1 & -1 & 4 \end{bmatrix} \begin{bmatrix} V_1 \\ V_2 \\ V_3 \\ V_4 \end{bmatrix} = \begin{bmatrix} 10 \\ 10 \\ 0 \\ 0 \end{bmatrix}$$

or

$$[A][V] = [B]$$

where $[A]$ is the band matrix, $[V]$ is the column matrix containing the unknown potentials at the free nodes, and $[B]$ is the column matrix of potentials at the fixed nodes. Solving the equations either by matrix inversion or by Gauss elimination, we obtain

$$V_1 = 3.75, \quad V_2 = 3.75, \quad V_3 = 1.25, \quad V_4 = 1.25 \quad \blacksquare$$

with MATLAB, $[V] = \text{inv}[A][B]$.

Example 3.4

Solve Poisson's equation

$$\nabla^2 V = -\frac{\rho_s}{\epsilon}, \quad 0 \leq x, y \leq 1$$

and obtain the potential at the grid points shown in Figure 3.11. Assume $\rho_s = x(y-1)$ nC/m³ and $\epsilon_r = 1.0$. Use the method of successive over-relaxation. \square

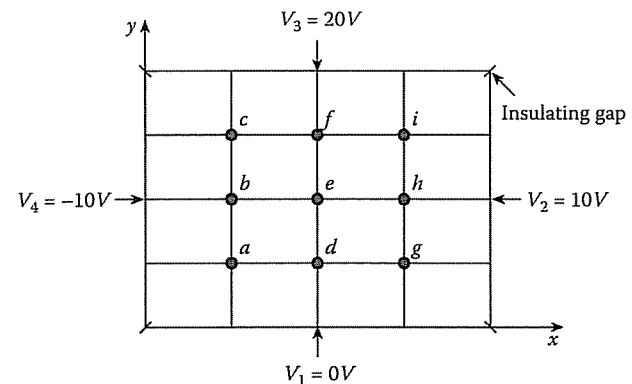


Figure 3.11
Solution region for the problem in Example 3.4.

Solution

This problem has an exact analytical solution and is deliberately chosen so that we can verify the numerical results with exact ones, and we can also see how a problem

with a complicated analytical solution is easily solved using finite difference method. For the exact solution, we use the superposition theorem and let

$$V = V_1 + V_2$$

where V_1 is the solution to Laplace's equation $\nabla^2 V_1 = 0$ with the inhomogeneous boundary conditions shown in Figure 3.11 and V_2 is the solution to Poisson's equation $\nabla^2 V_2 = g = -\rho_s/\epsilon$ subject to homogeneous boundary conditions. From Example 2.1, it is evident that

$$V = V_I + V_{II} + V_{III} + V_{IV}$$

where V_I to V_{IV} are defined by Equations (2.53) to (2.56). V_2 can be obtained by the series expansion method of Section 2.7. From Example 2.12,

$$V_2 = \sum_{m=1}^{\infty} \sum_{n=1}^{\infty} A_{mn} \sin \frac{m\pi x}{a} \sin \frac{n\pi y}{b}$$

where

$$\begin{aligned} A_{mn} &= \int_0^a \int_0^b g(x, y) \sin \frac{m\pi x}{a} \sin \frac{n\pi y}{b} dx dy \\ &= \frac{[1.0 - \frac{1}{b}[1 - (-1)^n]]}{[(m\pi/a)^2 + (n\pi/b)^2]} \cdot \frac{(-1)^{m+n} 144ab}{mn\pi}, \end{aligned}$$

$a = b = 1$, and $g(x, y) = -x(y-1) \cdot 10^{-9}/\epsilon_o$.

For the finite difference solution, it can be shown that in a rectangular region, the optimum over-relaxation factor is given by the smaller root of the quadratic equation [10]

$$t^2\omega^2 - 16\omega + 16 = 0$$

where $t = \cos(\pi/N_x) + \cos(\pi/N_y)$ and N_x and N_y are the number of intervals along x and y axes, respectively. Hence

$$\omega = \frac{8 - \sqrt{64 - 16t^2}}{t^2}$$

We try three cases of $N_x = N_y = 4, 12$, and 20 so that $\Delta x = \Delta y = h = 1/4, 1/12$, and $1/20$, respectively. Also we set

$$g(x, y) = -\frac{\rho_s}{\epsilon} = -\frac{x(y-1) \cdot 10^{-9}}{10^{-9}/36\pi} = -36\pi x(y-1)$$

Figure 3.12 presents the MATLAB code for the solution of this problem. The potentials at the free nodes for the different cases of h are shown in Table 3.6. Notice that as the mesh size h reduces, the solution becomes more accurate, but it takes more iterations for the same tolerance.

```

***** FINITE DIFFERENCE SOLUTION OF POISSON'S EQUATION:
***** VXX + VYY = G
***** USING THE METHOD OF SUCCESSIVE OVER-RELAXATION

NX : NO. OF INTERVALS ALONG X-AXIS
NY : NO. OF INTERVALS ALONG Y-AXIS
A X B : DIMENSION OF THE SOLUTION REGION
V(I,J) : POTENTIAL AT GRID POINT (X,Y) = H*(I,J)
WHERE I = 0,1,...,NX, J = 0,1,...,NY
H : MESH SIZE
*****
***** SPECIFY BOUNDARY VALUES AND NECESSARY PARAMETERS
A=1;B=1;
V1=0;V2=10;V3=20;V4=-10;
NX= 20; %4 12 20
NY= NX;
H = A/NX;
% SET INITIAL GUESS EQUAL TO ZEROS OR TO AVERAGE OF FIXED VALUES

for I=1:NX-1
    for J=1:NY-1
        V(I+1,J+1)=(V1 + V2 + V3 + V4)/4.0;
    end
end
% SET POTENTIALS AT FIXED NODES
for I = 1:NX-1
    V(I+1,1)=V1;
    V(I+1,NY+1)=V3;
end
for J=1:NY-1
    V(1,J+1)=V4;
    V(NX+1,J+1)=V2;
end
V(1,1)=(V1 + V4)/2.0;
V(NX+1,1)=(V1 + V2)/2.0;
V(1,NY+1)=(V3 + V4)/2.0;
V(NX+1,NY+1)=(V2 + V3)/2.0;
% FIND THE OPTIMUM OVER-RELAXATION FACTOR
T = cos(pi/NX) + cos(pi/NY);
W = ( 8 - sqrt(64 - 16*T^2))/(T^2);
disp(['SOR Factor Omega = ', num2str(W)])
W4 = W/4;
% ITERATION BEGINS
NCOUNT = 0;

loop = 1;
while loop == 1;
    RMIN = 0;
    for I = 1:NX-1
        X = H*I;
        for J = 1:NY-1
            Y = H*J;
            G = -36.0*pi*X*(Y - 1.0);
            R = W4*( V(I+2,J+1) + V(I,J+1) + V(I+1,J+2) + V(I+1,J) -
4.0*V(I+1,J+1) - G*H*H );
            if abs(R) < RMIN
                RMIN = abs(R);
            end
        end
    end
    if RMIN > 1e-06
        loop = 1;
    else
        loop = 0;
    end
end

```

Figure 3.12
MATLAB code for Example 3.4 (Continued).

```

RMIN = RMIN + abs(R);
V(I+1,J+1) = V(I+1,J+1) + R;
end

RMIN = RMIN/(NX*NY);
if(RMIN>=0.0001)
    NCOUNT = NCOUNT + 1;
    if(NCOUNT>100)
        loop = 0;
        disp('SOLUTION DOES NOT CONVERGE IN 100 ITERATIONS')
    end
else
    %Then RMIN is less than .0001 and then solution has converged
    loop = 0;
    disp(['Solution Converges in ',num2str(NCOUNT),' iterations'])
    disp(['h = ', num2str(H)])
end

Vnum = V;

%Grab original points a through i
abc = zeros(1,9);
a_tic = 1;
vec = [0:H:1];
for ii = .25:.25:.75
    for jj = .25:.25:.75
        xind = find(vec==ii);
        yind = find(vec==jj);
        %disp([xind,yind])
        abc(a_tic) = Vnum(xind,yind);
        a_tic = a_tic + 1;
    end
end

% OUTPUT THE FINITIE DIFFERENCE APPROX. RESULTS
-----  

% CALCULATE THE EXACT SOLUTION
%
% POISSON'S EQUATION WITH HOMOGENEOUS BOUNDARY CONDITIONS
% SOLVED BY SERIES EXPANSION
%
for I = 1:NX-1
    X = H*I;
    for J = 1:NY-1
        Y = H*J;
        SUM = 0;
        for M = 1:10 % TAKE ONLY 10 TERMS OF THE SERIES
            FM = M;
            for N = 1:10
                FN = N;
                FACTOR1 = (FM*pi/A)^2 + (FN*pi/B)^2;
                FACTOR2 = (-1)^(M+N)*144*A*B/(pi*FM*FN);
                FACTOR3 = 1 - (1 - (-1)^N)/B;
                FACTOR = FACTOR2*FACTOR3/FACTOR1;
                SUM = SUM + FACTOR*sin(FM*pi*X/A)*sin(FN*pi*Y/B);
            end
        end
        VH = SUM;
    end
end

```

Figure 3.12

(Cont.) MATLAB code for Example 3.4.

```

% LAPLACE'S EQUATION WITH INHOMOGENEOUS BOUNDARY CONDITIONS
% SOLVED USING THE METHOD OF SEPARATION OF VARIABLES

C1=4*pi;
C2=4*pi;
C3=4*pi;
C4=4*pi;
SUM=0;
for K = 1:10 % TAKE ONLY 10 TERMS OF THE SERIES
    N=2*K-1;
    AN=N;
    A1=sin(AN*pi*X/B);
    A2=sinh(AN*pi*(A-Y)/B);
    A3=AN*sinh(AN*pi*A/B);
    TERM1=C1*A1*A2/A3;
    B1=sinh(AN*pi*X/A);
    B2=sin(AN*pi*Y/A);
    B3=AN*sinh(AN*pi*B/A);
    TERM2=C2*B1*B2/B3;
    D1=sin(AN*pi*X/B);
    D2=sinh(AN*pi*Y/B);
    D3=AN*sinh(AN*pi*A/B);
    TERM3=C3*D1*D2/D3;
    E1=sinh(AN*pi*(B-X)/A);
    E2=sin(AN*pi*Y/A);
    E3=AN*sinh(AN*pi*B/A);
    TERM4=C4*E1*E2/E3;
    TERM = TERM1 + TERM2 + TERM3 + TERM4;
    SUM=SUM + TERM;
end
VI = SUM;
Vexact(I+1,J+1) = VH + VI;
end
end

%Grab original points a through i
abc2 = zeros(1,9);
a_tic = 1;
vec = [0:H:1];
for ii = .25:.25:.75
    for jj = .25:.25:.75
        xind = find(vec==ii);
        yind = find(vec==jj);
        %disp([xind,yind])
        abc2(a_tic) = Vexact(xind,yind);
        a_tic = a_tic + 1;
    end
end

figure(1),
imagesc(flipud(Vnum')),
colorbar
ylabel('y'), xlabel('x')
title('Example 3.4: Poisson PDE')

format short g
disp(' numerical exact')
disp([abc' abc2'])
```

Figure 3.12

(Cont.) MATLAB code for Example 3.4.

Table 3.6 Successive Over-Relaxation Solution of Example 3.4

Node	$h = 1/4$ $\omega_{opt} = 1.171$ 8 iterations	$h = 1/12$ $\omega_{opt} = 1.729$ 26 iterations	$h = 1/20$ $\omega_{opt} = 1.729$ 43 iterations	Exact Solution
a	-3.247	-3.409	-3.424	-3.429
b	-1.703	-1.982	-2.012	-2.029
c	4.305	4.279	4.277	4.277
d	-0.0393	-0.0961	-0.1087	-0.1182
e	3.012	2.928	2.921	2.913
f	9.368	9.556	9.578	9.593
g	3.044	2.921	2.909	2.902
h	6.111	6.072	6.069	6.065
i	11.04	11.12	11.23	11.13

3.6. ACCURACY AND STABILITY OF FD SOLUTIONS

Roundoff errors reflect the fact that computations can be done only with a finite precision on a computer. This unavoidable source of errors is due to the limited size of registers in the arithmetic unit of the computer. Roundoff errors can be minimized by the use of double-precision arithmetic. The only way to avoid roundoff errors completely is to code all operations using integer arithmetic. This is hardly possible in most practical situations.

Although it has been noted that reducing the mesh size h will increase accuracy, it is not possible to indefinitely reduce h . Decreasing the truncation error by using a finer mesh may result in increasing the roundoff error due to the increased number of arithmetic operations. A point is reached where the minimum total error occurs for any particular algorithm using any given word length [9]. This is illustrated in Figure 3.13. The concern about accuracy leads us to question whether the finite difference solution

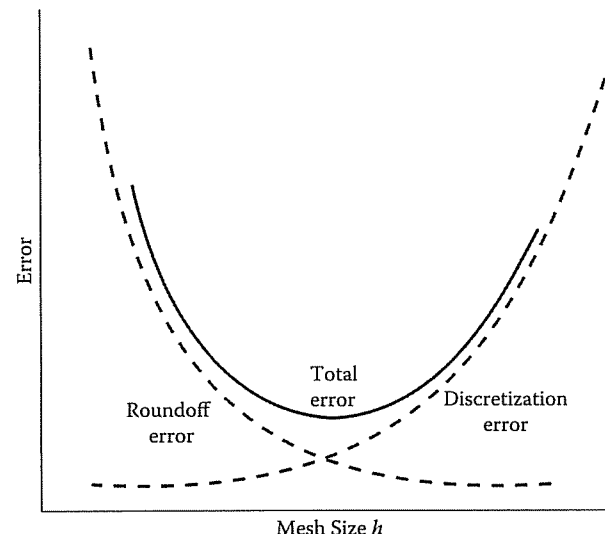


Figure 3.13
Error as a function of the mesh size.

can grow unbounded, a property termed the instability of the difference scheme. A numerical algorithm is said to be stable if a small error at any stage produces a smaller cumulative error. It is unstable otherwise. The consequence of instability (producing unbounded solution) is disastrous. To determine whether a finite difference scheme is stable, we define an error, ϵ^n , which occurs at time step n , assuming that there is one independent variable. We define the amplification of this error at time step $n+1$ as

$$\epsilon^{n+1} = g\epsilon^n \quad (3.37)$$

3.6 Accuracy and Stability of FD Solutions

The question of accuracy and stability of numerical methods is extremely important if our solution is to be reliable and useful. Accuracy has to do with the closeness of the approximate solution to exact solutions (assuming they exist). Stability is the requirement that the scheme does not increase the magnitude of the solution with increase in time.

There are three sources of errors that are nearly unavoidable in numerical solution of physical problems [8]:

1. modeling errors,
2. truncation (or discretization) errors, and
3. roundoff errors.

Each of these error types will affect accuracy and therefore degrade the solution.

The modeling errors are due to several assumptions made in arriving at the mathematical model. For example, a nonlinear system may be represented by a linear PDE. Truncation errors arise from the fact that in numerical analysis, we can deal only with a finite number of terms from processes which are usually described by infinite series. For example, in deriving finite difference schemes, some higher-order terms in the Taylor series expansion were neglected, thereby introducing truncation error. Truncation errors may be reduced by using finer meshes, that is, by reducing the mesh size h and time increment Δt . Alternatively, truncation errors may be reduced by using a large number of terms in the series expansion of derivatives, that is, by using higher-order approximations. However, care must be exercised in applying higher-order approximations. Instability may result if we apply a difference equation of an order higher than the PDE being examined. These higher-order difference equations may introduce "spurious solutions."

where g is known as the *amplification factor*. In more complex situations, we have two or more independent variables, and Equation (3.37) becomes

$$[\epsilon]^{n+1} = [G][\epsilon]^n \quad (3.38)$$

where $[G]$ is the amplification matrix. For the stability of the difference scheme, it is required that Equation (3.37) satisfy

$$|\epsilon^{n+1}| \leq |\epsilon^n|$$

or

$$|g| \leq 1 \quad (3.39a)$$

For the case in Equation (3.38),

$$\|G\| \leq 1 \quad (3.39b)$$

One useful and simple method of finding a stability criterion for a difference scheme is to construct a Fourier analysis of the difference equation and thereby derive the amplification factor. We illustrate this technique, known as *von Neumann's method* [4, 5, 7, 10], by considering the explicit scheme of Equation (3.13):

$$\Phi_i^{n+1} = (1 - 2r)\Phi_i^n + r(\Phi_{i+1}^n + \Phi_{i-1}^n) \quad (3.40)$$

where $r = \Delta t/k(\Delta x)^2$. We have changed our usual notation so that we can use $j = \sqrt{-1}$ in the Fourier series. Let the solution be

$$\Phi_i^n = \sum A^n(t)e^{jki.x}, \quad 0 \leq x \leq 1 \quad (3.41a)$$

where k is the wave number. Since the differential equation (3.10) approximated by Equation (3.13) is linear, we need consider only a Fourier mode, i.e.,

$$\Phi_i^n = A^n(t)e^{jki.x} \quad (3.41b)$$

Substituting Equation (3.41b) into Equation (3.40) gives

$$A^{n+1}e^{jki.x} = (1 - 2r)A^n e^{jki.x} + r(e^{jki.x} + e^{-jki.x})A^n e^{jki.x}$$

or

$$A^{n+1} = A^n[1 - 2r + 2r \cos kx] \quad (3.42)$$

Hence the amplification factor is

$$\begin{aligned} g &= \frac{A^{n+1}}{A^n} = 1 - 2r + 2r \cos kx \\ &= 1 - 4r \sin^2 \frac{kx}{2} \end{aligned} \quad (3.43)$$

In order to satisfy Equation (3.39a),

$$\left| 1 - 4r \sin^2 \frac{kx}{2} \right| \leq 1$$

Since this condition must hold for every wave number k , we take the maximum value of the sine function so that

$$1 - 4r \geq -1 \quad \text{and} \quad r \geq 0$$

or

$$r \geq \frac{1}{2} \quad \text{and} \quad r \geq 0$$

Of course, $r = 0$ implies $\Delta t = 0$, which is impractical. Thus

$$0 < r \leq \frac{1}{2} \quad (3.44)$$

Example 3.5

For the finite difference scheme of Equation (3.20), use the von Neumann approach to determine the stability condition. \square

Solution

We assume a trial solution of the form

$$\Phi_i^n = A^n e^{jki.x}$$

Substituting this into Equation (3.20) results in

$$A^{n+1}e^{jki.x} = 2(1 - r)A^n e^{jki.x} + r(e^{jki.x} + e^{-jki.x})A^n e^{jki.x} - A^{n-1}e^{jki.x}$$

or

$$A^{n+1} = A^n[2(1 - r) + 2r \cos kx] - A^{n-1} \quad (3.45)$$

In terms of $g = A^{n+1}/A^n$, Equation (3.45) becomes

$$g^2 - 2pg + 1 = 0 \quad (3.46)$$

where $p = 1 - 2r \sin^2 \frac{kx}{2}$. The quadratic equation (3.46) has solutions

$$g_1 = p + [p^2 - 1]^{1/2}, \quad g_2 = p - [p^2 - 1]^{1/2}$$

For $|g_i| \leq 1$, where $i = 1, 2$, p must lie between 1 and -1 , i.e., $-1 \leq p \leq 1$ or

$$-1 \leq 1 - 2r \sin^2 \frac{kx}{2} \leq 1$$

which implies that $r \leq 1$ or $u \Delta t \leq \Delta x$ for stability. This idea can be extended to show that the stability condition for two-dimensional wave equation is $u \Delta t / h < \frac{1}{\sqrt{2}}$, where $h = \Delta x = \Delta y$. \square

3.7 Practical Applications I — Guided Structures

The finite difference method has been applied successfully to solve many EM-related problems. Besides those simple examples we have considered earlier in this chapter, the method has been applied to diverse problems [11] including

- transmission-line problems [12]–[21],
- waveguides [21]–[26],
- microwave circuit [27]–[30],
- EM penetration and scattering problems [31, 32],
- EM pulse (EMP) problems [33],
- EM exploration of minerals [34], and
- EM energy deposition in human bodies [35, 36].

It is practically impossible to cover all those applications within the limited scope of this text. In this section, we consider the relatively easier problems of transmission lines and waveguides while the problems of penetration and scattering of EM waves will be treated in the next section. Other applications utilize basically similar techniques.

3.7.1 Transmission Lines

The finite difference techniques are suited for computing the characteristic impedance, phase velocity, and attenuation of several transmission lines—polygonal lines, shielded strip lines, coupled strip lines, microstrip lines, coaxial lines, and rectangular lines [12]–[19]. The knowledge of the basic parameters of these lines is of paramount importance in the design of microwave circuits.

For concreteness, consider the microstrip line shown in Figure 3.14(a). The geometry in Figure 3.14(a) is deliberately selected to be able to illustrate how one accounts for discrete inhomogeneities (i.e., homogeneous media separated by interfaces) and lines of symmetry using a finite difference technique. The techniques presented are equally applicable to other lines. Assuming that the mode is TEM, having components of neither **E** nor **H** fields in the direction of propagation, the fields obey Laplace's equation over the line cross section. The TEM mode assumption provides good approximations if the line dimensions are much smaller than half a wavelength, which means that the operating frequency is far below cutoff frequency for all higher order modes [16]. Also due to biaxial symmetry about the two axes only one quarter of the cross section needs to be considered as shown in Figure 3.14(b).

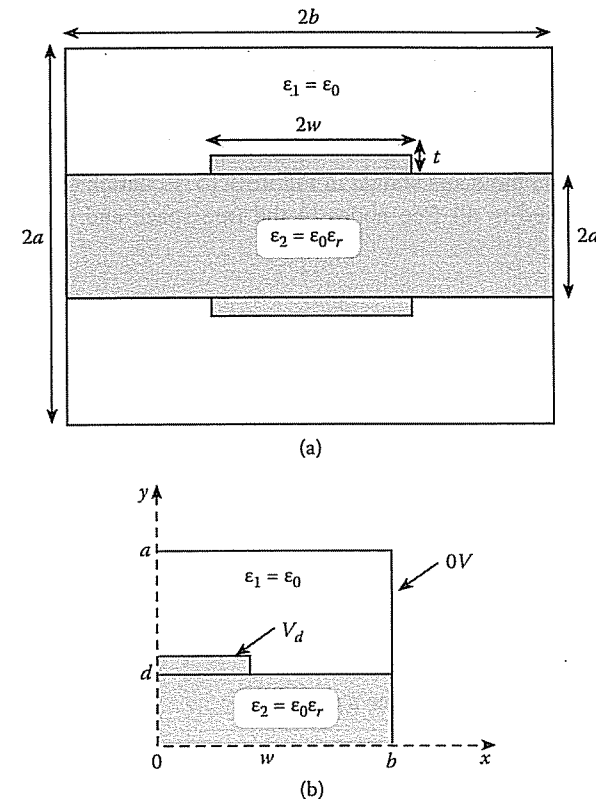


Figure 3.14

(a) Shielded double-strip line with partial dielectric support; (b) problem in (a) simplified by making full use of symmetry.

The finite difference approximation of Laplace's equation, $\nabla^2 V = 0$, was derived in Equation (3.31), namely,

$$V(i, j) = \frac{1}{4} [V(i+1, j) + V(i-1, j) + V(i, j+1) + V(i, j-1)] \quad (3.47)$$

For the sake of conciseness, let us denote

$$\begin{aligned} V_o &= V(i, j) \\ V_1 &= V(i, j+1) \\ V_2 &= V(i-1, j) \\ V_3 &= V(i, j-1) \\ V_4 &= V(i+1, j) \end{aligned} \quad (3.48)$$

so that Equation (3.47) becomes

$$V_o = \frac{1}{4} [V_1 + V_2 + V_3 + V_4] \quad (3.49)$$

with the computation molecule shown in Figure 3.15. Equation (3.49) is the general formula to be applied to all free nodes in the free space and dielectric region of Figure 3.14(b).

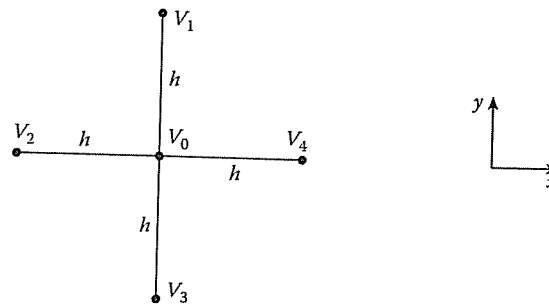


Figure 3.15
Computation molecule for Laplace's equation.

On the dielectric boundary, the boundary condition,

$$D_{1n} = D_{2n}, \quad (3.50)$$

must be imposed. We recall that this condition is based on Gauss's law for the electric field, i.e.,

$$\oint_{\ell} \mathbf{D} \cdot d\mathbf{l} = \oint_{\ell} \epsilon \mathbf{E} \cdot d\mathbf{l} = Q_{\text{enc}} = 0 \quad (3.51)$$

since no free charge is deliberately placed on the dielectric boundary. Substituting $\mathbf{E} = -\nabla V$ in Equation (3.51) gives

$$0 = \oint_{\ell} \epsilon \nabla V \cdot d\mathbf{l} = \oint_{\ell} \epsilon \frac{\partial V}{\partial n} dl \quad (3.52)$$

where $\partial V / \partial n$ denotes the derivative of V normal to the contour ℓ . Applying Equation (3.52) to the interface in Figure 3.16 yields

$$0 = \epsilon_1 \frac{(V_1 - V_0)}{h} h + \epsilon_1 \frac{(V_2 - V_0)}{h} \frac{h}{2} + \epsilon_2 \frac{(V_2 - V_0)}{h} \frac{h}{2} \\ + \epsilon_2 \frac{(V_3 - V_0)}{h} h + \epsilon_2 \frac{(V_4 - V_0)}{h} \frac{h}{2} + \epsilon_1 \frac{(V_4 - V_0)}{h} \frac{h}{2}$$

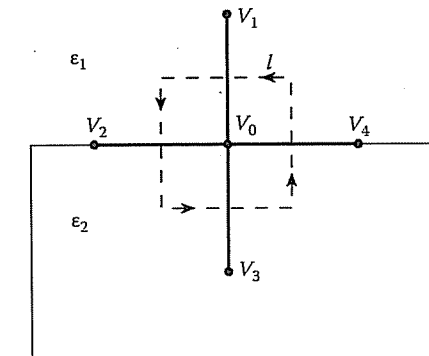


Figure 3.16
Interface between media of dielectric permittivities ϵ_1 and ϵ_2 .

Rearranging the terms,

$$2(\epsilon_1 + \epsilon_2) V_0 = \epsilon_1 V_1 + \epsilon_2 V_3 + \frac{(\epsilon_1 + \epsilon_2)}{2} (V_2 + V_4)$$

or

$$V_0 = \frac{\epsilon_1}{2(\epsilon_1 + \epsilon_2)} V_1 + \frac{\epsilon_2}{2(\epsilon_1 + \epsilon_2)} V_3 + \frac{1}{4} V_2 + \frac{1}{4} V_4 \quad (3.53)$$

This is the finite difference equivalent of the boundary condition in Equation (3.50). Notice that the discrete inhomogeneity does not affect points 2 and 4 on the boundary but affects points 1 and 3 in proportion to their corresponding permittivities. Also note that when $\epsilon_1 = \epsilon_2$, Equation (3.53) reduces to Equation (3.49).

On the line of symmetry, we impose the condition

$$\frac{\partial V}{\partial n} = 0 \quad (3.54)$$

This implies that on the line of symmetry along the y -axis, ($x = 0$ or $i = 0$) $\frac{\partial V}{\partial x} = (V_4 - V_2)/2h = 0$ or $V_2 = V_4$ so that Equation (3.49) becomes

$$V_o = \frac{1}{4} [V_1 + V_3 + 2V_4] \quad (3.55a)$$

or

$$V(0, j) = \frac{1}{4} [V(0, j+1) + V(0, j-1) + 2V(1, j)] \quad (3.55b)$$

On the line of symmetry along the x -axis ($y = 0$ or $j = 0$), $\frac{\partial V}{\partial y} = (V_1 - V_3)/2h = 0$ or $V_3 = V_1$ so that

$$V_o = \frac{1}{4}[2V_1 + V_2 + V_4] \quad (3.56a)$$

or

$$V(i, 0) = \frac{1}{4}[2V(i, 1) + V(i - 1, 0) + V(i + 1, 0)] \quad (3.56b)$$

The computation molecules for Equations (3.55) and (3.56) are displayed in Figure 3.17.

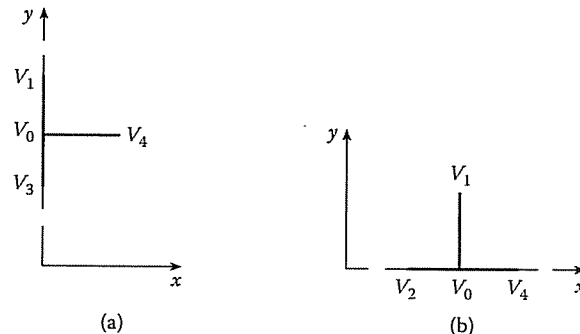


Figure 3.17

Computation molecule used for satisfying symmetry conditions: (a) $\partial V / \partial x = 0$, (b) $\partial V / \partial y = 0$.

By setting the potential at the fixed nodes equal to their prescribed values and applying Equations (3.49), (3.53), (3.55), and (3.56) to the free nodes according to the band matrix or iterative methods discussed in Section 3.5, the potential at the free nodes can be determined. Once this is accomplished, the quantities of interest can be calculated.

The characteristic impedance Z_o and phase velocity u of the line are defined as

$$Z_o = \sqrt{\frac{L}{C}} \quad (3.57a)$$

$$u = \frac{1}{\sqrt{LC}} \quad (3.57b)$$

where L and C are the inductance and capacitance per unit length, respectively. If the dielectric medium is nonmagnetic ($\mu = \mu_o$), the characteristic impedance Z_{oo} and

phase velocity u_o with the dielectric removed (i.e., the line is air-filled) are given by

$$Z_{oo} = \sqrt{\frac{L}{C_o}} \quad (3.58a)$$

$$u_o = \frac{1}{\sqrt{LC_o}} \quad (3.58b)$$

where C_o is the capacitance per unit length without the dielectric. Combining Equations (3.57) and (3.58) yields

$$Z_o = \frac{1}{u_o \sqrt{CC_o}} = \frac{1}{uC} \quad (3.59a)$$

$$u = u_o \sqrt{\frac{C_o}{C}} = \frac{u_o}{\sqrt{\epsilon_{eff}}} \quad (3.59b)$$

$$\epsilon_{eff} = \frac{C}{C_o} \quad (3.59c)$$

where $u_o = c = 3 \times 10^8$ m/s, the speed of light in free space, and ϵ_{eff} is the effective dielectric constant. Thus to find Z_o and u for an inhomogeneous medium requires calculating the capacitance per unit length of the structure, with and without the dielectric substrate.

If V_d is the potential difference between the inner and the outer conductors,

$$C = \frac{4Q}{V_d}, \quad (3.60)$$

so that the problem is reduced to finding the charge per unit length Q . (The factor 4 is needed since we are working on only one quarter of the cross section.) To find Q , we apply Gauss's law to a closed path ℓ enclosing the inner conductor. We may select ℓ as the rectangular path between two adjacent rectangles as shown in Figure 3.18.

$$\begin{aligned} Q &= \oint_{\ell} \mathbf{D} \cdot d\mathbf{l} = \oint_{\ell} \epsilon \frac{\partial V}{\partial n} d\ell \\ &= \epsilon \left(\frac{V_P - V_N}{\Delta x} \right) \Delta y + \epsilon \left(\frac{V_M - V_L}{\Delta x} \right) \Delta y + \epsilon \left(\frac{V_H - V_L}{\Delta y} \right) \Delta x \\ &\quad + \epsilon \left(\frac{V_G - V_K}{\Delta y} \right) \Delta x + \dots \end{aligned} \quad (3.61)$$

Since $\Delta x = \Delta y = h$,

$$Q = (\epsilon V_P + \epsilon V_M + \epsilon V_H + \epsilon V_G + \dots) - (\epsilon V_N + 2\epsilon V_L + \epsilon V_K + \dots)$$

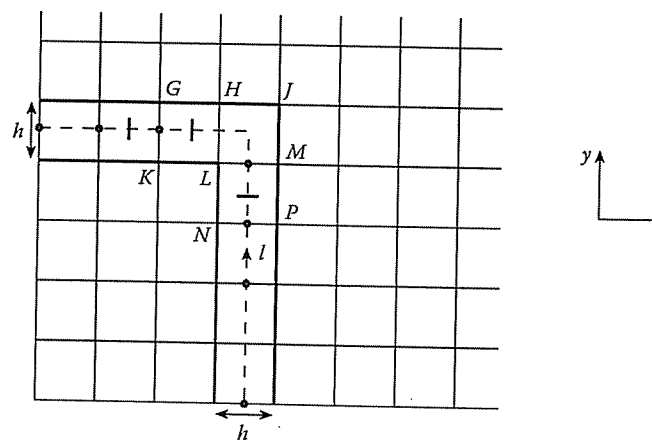


Figure 3.18

The rectangular path ℓ used in calculating charge enclosed.

or

$$\begin{aligned} Q = \epsilon_o \left[\sum \epsilon_{ri} V_i \quad \text{for nodes } i \text{ on outer rectangle GHJMP} \right. \\ \left. \text{with corners (such as J) not counted} \right] \\ - \epsilon_o \left[\sum \epsilon_{ri} V_i \quad \text{for nodes } i \text{ on inner rectangle KLN} \right. \\ \left. \text{with corners (such as L) counted twice} \right], \end{aligned} \quad (3.62)$$

where V_i and ϵ_{ri} are the potential and dielectric constant at the i th node. If i is on the dielectric interface, $\epsilon_{ri} = (\epsilon_{r1} + \epsilon_{r2})/2$. Also if i is on the line of symmetry, we use $V_i/2$ instead of V_i to avoid including V_i twice in Equation (3.60), where factor 4 is applied. We also find

$$C_o = 4Q_o/V_d \quad (3.63)$$

where Q_o is obtained by removing the dielectric, finding V_i at the free nodes and then using Equation (3.62) with $\epsilon_{ri} = 1$ at all nodes. Once Q and Q_o are calculated, we obtain C and C_o from Equations (3.60) and (3.63) and Z_o and u from Equation (3.59).

An outline of the procedure is given below.

- (1) Calculate V (with the dielectric space replaced by free space) using Equations (3.49), (3.53), (3.55), and (3.56).
- (2) Determine Q using Equation (3.62).

$$(3) \text{ Find } C_o = \frac{4Q_o}{V_d}.$$

$$(4) \text{ Repeat steps (1) and (2) (with the dielectric space) and find } C = \frac{4Q}{V_d}.$$

$$(5) \text{ Finally, calculate } Z_o = \frac{1}{c\sqrt{CC_o}}, c = 3 \times 10^8 \text{ m/s.}$$

The attenuation of the line can be calculated by following similar procedure outlined in [14, 20, 21]. The procedure for handling boundaries at infinity and that for boundary singularities in finite difference analysis are discussed in [37, 38].

3.7.2 Waveguides

The solution of waveguide problems is well suited for finite difference schemes because the solution region is closed. This amounts to solving the Helmholtz or wave equation

$$\nabla^2 \Phi + k^2 \Phi = 0 \quad (3.64)$$

where $\Phi = E_z$ for TM modes or $\Phi = H_z$ for TE modes, while k is the wave number given by

$$k^2 = \omega^2 \mu \epsilon - \beta^2 \quad (3.65)$$

The permittivity ϵ of the dielectric medium can be real for a lossless medium or complex for a lossy medium. We consider all fields to vary with time and axial distance as $\exp j(\omega t - \beta z)$. In the eigenvalue problem of Equation (3.64), both k and Φ are to be determined. The cutoff wavelength is $\lambda_c = 2\pi/k_c$. For each value of the cutoff wave number k_c , there is a solution for the eigenfunction Φ_i , which represents the field configuration of a propagating mode.

To apply the finite difference method, we discretize the cross section of the waveguide by a suitable square mesh. Applying Equation (3.29) to Equation (3.64) gives

$$\boxed{\Phi(i+1, j) + \Phi(i-1, j) + \Phi(i, j+1) + \Phi(i, j-1) - (4 - h^2 k^2) \Phi(i, j) = 0} \quad (3.66)$$

where $\Delta x = \Delta y = h$ is the mesh size. Equation (3.66) applies to all the free or interior nodes. At the boundary points, we apply Dirichlet condition ($\Phi = 0$) for the TM modes and Neumann condition ($\partial \Phi / \partial n = 0$) for the TE modes. This implies that at point A in Figure 3.19, for example,

$$\Phi_A = 0 \quad (3.67)$$

for TM modes. At point A, $\partial \Phi / \partial n = 0$ implies that $\Phi_D = \Phi_E$ so that Equation (3.64) becomes

$$\Phi_B + \Phi_C + 2\Phi_D - (4 - h^2 k^2) \Phi_A = 0 \quad (3.68)$$

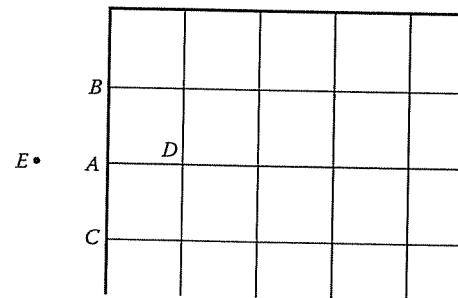


Figure 3.19

Finite difference mesh for a waveguide.

for TE modes. By applying Equation (3.66) and either Equation (3.67) or (3.68) to all mesh points in the waveguide cross section, we obtain m simultaneous equations involving the m unknowns ($\Phi_1, \Phi_2, \dots, \Phi_m$). These simultaneous equations may be conveniently cast into the matrix equation

$$(A - \lambda I)\Phi = 0 \quad (3.69a)$$

or

$$A\Phi = \lambda\Phi \quad (3.69b)$$

where A is an $m \times m$ band matrix of known integer elements, I is an identity matrix, $\Phi = (\Phi_1, \Phi_2, \dots, \Phi_m)$ is the eigenvector, and

$$\lambda = (kh)^2 = \left(\frac{2\pi h}{\lambda_c}\right)^2 \quad (3.70)$$

is the eigenvalue. There are several ways of determining λ and the corresponding Φ . We consider two of these options.

The first option is the *direct method*. Equation (3.69) can be satisfied only if the determinant of $(A - \lambda I)$ vanishes, i.e.,

$$|A - \lambda I| = 0 \quad (3.71)$$

This results in a polynomial in λ , which can be solved [39] for the various eigenvalues λ . For each λ , we obtain the corresponding Φ from Equation (3.66). This method requires storing the relevant matrix elements and does not take advantage of the fact that matrix A is sparse. In favor of the method is the fact that a computer subroutine usually exists (see [40] or Appendix C.4) that solves the eigenvalue problem in Equation (3.71) and that determines all the eigenvalues of the matrix. These eigenvalues give the dominant and higher modes of the waveguide, although accuracy deteriorates rapidly with mode number.

3.7. PRACTICAL APPLICATIONS I – GUIDED STRUCTURES

The second option is the *iterative method*. In this case, the matrix elements are usually generated rather than stored. We begin with $\Phi_1 = \Phi_2 = \dots = \Phi_m = 1$ and a guessed value for k . The field Φ_{ij}^{k+1} at the (i, j) th node in the $(k + 1)$ th iteration is obtained from its known value in the k th iteration using

$$\Phi_{ij}^{k+1} = \Phi_{ij}^k + \frac{\omega R_{ij}}{(4 - h^2 k^2)} \quad (3.72)$$

where ω is the acceleration factor, $1 < \omega < 2$, and R_{ij} is the residual at the (i, j) th node given by

$$R_{ij} = \Phi_{ij} + \Phi_{ij-1} + \Phi_{ij+1} + \Phi_{ij-2} - (4 - h^2 k^2) \Phi_{ij} \quad (3.73)$$

After three or four scans of the complete mesh using Equation (3.73), the value of $\lambda = h^2 k^2$ should be updated using Raleigh formula

$$k^2 = \frac{-\int_S \Phi \nabla^2 \Phi dS}{\int_S \Phi^2 dS} \quad (3.74)$$

The finite difference equivalent of Equation (3.74) is

$$k^2 = \frac{-\sum_{i=1}^m \sum_{j=1}^n \Phi_{ij} [\Phi_{ij+1} + \Phi_{ij-1} + \Phi_{ij+2} + \Phi_{ij-2} - 4\Phi_{ij}]}{h^2 \sum_{i=1}^m \sum_{j=1}^n \Phi_{ij}^2} \quad (3.75)$$

where Φ s are the latest field values after three or four scans of the mesh and the summation is carried out over all points in the mesh. The new value of k obtained from Equation (3.75) is now used in applying Equation (3.72) over the mesh for another three or four times to give more accurate field values, which are again substituted into Equation (3.75) to update k . This process is continued until the difference between consecutive values of k is within a specified acceptable tolerance.

If the first option is to be applied, matrix A must first be found. To obtain matrix A is not easy. Assuming TM modes, one way of calculating A is to number the free nodes from left to right, bottom to top, starting from the left-hand corner as shown typically in Figure 3.20. If there are n_x and n_y divisions along the x and y directions, the number of free nodes is

$$n_f = (n_x - 1)(n_y - 1) \quad (3.76)$$

Each free node must be assigned two sets of numbers, one to correspond to m in Φ_m and the other to correspond to (i, j) in Φ_{ij} . An array $NL(i, j) = m, i = 1, 2, \dots, n_x - 1, j = 1, 2, \dots, n_y - 1$ is easily developed to relate the two numbering schemes. To determine the value of element A_{mn} , we search $NL(i, j)$ to find (i_m, j_m) and (i_n, j_n) , which are the values of (i, j) corresponding to nodes m and n , respectively. With these

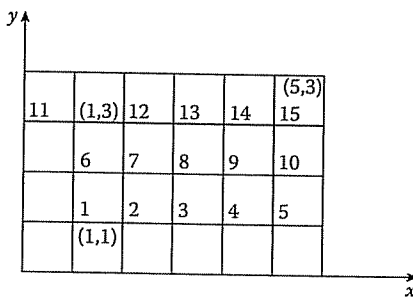


Figure 3.20
Relating node numbering schemes for $n_x = 6, n_y = 4$.

ideas, we obtain

$$A_{mn} = \begin{cases} 4, & m = n \\ -1, & i_m = i_n, \quad j_m = j_n + 1 \\ -1, & i_m = i_n, \quad j_m = j_n - 1 \\ -1, & i_m = i_n + 1, \quad j_m = j_n \\ -1, & i_m = i_n - 1, \quad j_m = j_n \\ 0, & \text{otherwise} \end{cases} \quad (3.77)$$

Example 3.6

Calculate Z_o for the microstrip transmission line in Figure 3.14 with

$$\begin{aligned} a = b &= 2.5 \text{ cm}, & d &= 0.5 \text{ cm}, & w &= 1 \text{ cm} \\ t &= 0.001 \text{ cm}, & \epsilon_1 = \epsilon_o, & \epsilon_2 = 2.35\epsilon_o & \square \end{aligned}$$

Solution

This problem is representative of the various types of problems that can be solved using the concepts developed in Section 3.7.1. The computer program in Figure 3.21 was developed based on the five-step procedure outlined above. By specifying the step size h and the number of iterations, the program first sets the potential at all nodes equal to zero. The potential on the outer conductor is set equal to zero, while that on the inner conductor is set to 100 volts so that $V_d = 100$. The program finds C_o when the dielectric slab is removed and C when the slab is in place and finally determines Z_o . For a selected h , the number of iterations must be large enough and greater than the number of divisions along x or y direction. Table 3.7 shows some typical results.

```

*****
* Using the finite difference method
* This program calculates the characteristic impedance of the transmission
* line shown in Figure 3.14.
*****

clear all; format compact;

% Output:
%   H      NT      zo
% -----
% 0.25    700    49.05
% 0.1     500    58.074
% 0.05    500    65.817
% 0.05    700    63.103
% 0.05    1000   61.53

H = 0.05;
NT = 1000;

A = 2.5; B = 2.5; D = 0.5; W = 1.0;
ER=2.35;
EO=8.81E-12;
U=3.0E+8;

NX = A/B;
NY = B/H;
ND = D/B;
NW = W/H;
VD = 100.0;

% CALCULATE CHARGE WITH AND WITHOUT DIELECTRIC
ERR = 1.0;
for L=1:2
    E1 = EO;
    E2 = EO*ERR;

    % INITIALIZATION
    V = zeros(NX+2,NY+2);

    % SET POTENTIAL ON INNER CONDUCTOR (FIXED NODES) EQUAL TO VD
    V(2:NW+2,ND+2) = VD;

    % CALCULATE POTENTIAL AT FREE NODES
    P1 = E1/(2*(E1 + E2));
    P2 = E2/(2*(E1 + E2));
    for K=1:NT
        for I=0:NX-1
            for J=0:NY-1
                if( (J==ND)&&(I<=NW) )
                    %do nothing
                elseif (J==ND)
                    % IMPOSE BOUNDARY CONDITION AT THE INTERFACE
                    V(I+2,J+2) = 0.25*(V(I+3,J+2) + V(I+1,J+2)) + ...
                    P1*V(I+2,J+3) + P2*V(I+2,J+1);
                end
            end
        end
    end
end

```

Figure 3.21
MATLAB code for Example 3.6 (Continued).

```

elseif(I==0)
    % IMPOSE SYMMETRY CONDITION ALONG Y-AXIS
    V(I+2,J+2) = (2*V(I+3,J+2) + V(I+2,J+3) + V(I+2,J+1))/4.0;
elseif(J==0)
    % IMPOSE SYMMETRY CONDITION ALONG X-AXIS
    V(I+2,J+2) = (V(I+3,J+2) + V(I+1,J+2) + 2*V(I+2,J+3))/4.0;
else
    V(I+2,J+2) = (V(I+3,J+2)+V(I+1,J+2)+V(I+2,J+3)+V(I+2,J+1))/4.0;
end
end
% Animation of calculation
% figure(1), imagesc(V), colorbar, title([num2str(K), '/', num2str(NT)])
% drawnow
end

% NOW, CALCULATE THE TOTAL CHARGE ENCLOSED IN A
% RECTANGULAR PATH SURROUNDING THE INNER CONDUCTOR
IOUT = round((NX + NW)/2);
JOUT = round((NY + ND)/2);
% SUM POTENTIAL ON INNER AND OUTER LOOPS
for K=1:2
    SUM = E1*sum(V(3:IOUT+1,JOUT+2)) ...
        + E1*V(2,JOUT+2)/2 + E2*V(IOUT+2,2)/2;
    for J=1:JOUT-1
        if(J<ND)
            SUM = SUM + E2*V(IOUT+2,J+2);
        elseif(J==ND)
            SUM = SUM + (E1+E2)*V(IOUT+2,J+2)/2;
        else
            SUM = SUM + E1*V(IOUT+2,J+2);
        end
    end
    if K==1
        SV(1) = SUM;
    end
    IOUT = IOUT - 1;
    JOUT = JOUT - 1;
end
SUM = SUM + 2.0*E1*V(IOUT+2,JOUT+2);
SV(2) = SUM;
Q(L) = abs( SV(1) - SV(2) );
ERR = ER;
end

% FINALLY, CALCULATE Z0
C0 = 4.0*Q(1)/VD;
C1 = 4.0*Q(2)/VD;
Z0 = 1.0/( U*sqrt(C0*C1) );
disp([H,NT,Z0])

```

Figure 3.21

(Cont.) MATLAB code for Example 3.6.

Table 3.7 Characteristic Impedance of a Microstrip Line for Example 3.6

h	Number of Iterations	Z_o
0.25	700	49.05
0.1	500	58.07
0.05	500	65.82
0.05	700	63.10
0.05	1000	61.53
Other method [41]: $Z_o = 62.50$		

3.8 Practical Applications II — Wave Scattering (FDTD)

The finite-difference time-domain (FDTD) formulation of EM field problems is a convenient tool for solving scattering problems. The FDTD method, first introduced by Yee [42] in 1966 and later developed by Taflove and others [31, 32, 35], [43]–[46], is a direct solution of Maxwell's time-dependent curl equations. The scheme treats the irradiation of the scatterer as an initial value problem. Our discussion on the FDTD method will cover

- Yee's finite difference algorithm,
- accuracy and stability,
- lattice truncation conditions,
- initial fields, and
- programming aspects.

Some model examples with MATLAB codes will be provided to illustrate the method.

3.8.1 Yee's Finite Difference Algorithm

In an isotropic medium, Maxwell's equations can be written as

$$\nabla \times \mathbf{E} = -\mu \frac{\partial \mathbf{H}}{\partial t} \quad (3.78a)$$

$$\nabla \times \mathbf{H} = \sigma \mathbf{E} + \epsilon \frac{\partial \mathbf{E}}{\partial t} \quad (3.78b)$$

The vector Equation (3.78) represents a system of six scalar equations, which can be expressed in rectangular coordinate system as

$$\frac{\partial H_x}{\partial t} = \frac{1}{\mu} \left(\frac{\partial E_y}{\partial z} - \frac{\partial E_z}{\partial y} \right), \quad (3.79a)$$

$$\frac{\partial H_y}{\partial t} = \frac{1}{\mu} \left(\frac{\partial E_z}{\partial x} - \frac{\partial E_x}{\partial z} \right), \quad (3.79b)$$

$$\frac{\partial H_z}{\partial t} = \frac{1}{\mu} \left(\frac{\partial E_x}{\partial y} - \frac{\partial E_y}{\partial x} \right), \quad (3.79c)$$

$$\frac{\partial E_x}{\partial t} = \frac{1}{\epsilon} \left(\frac{\partial H_z}{\partial y} - \frac{\partial H_y}{\partial z} - \sigma E_x \right), \quad (3.79d)$$

$$\frac{\partial E_y}{\partial t} = \frac{1}{\epsilon} \left(\frac{\partial H_x}{\partial z} - \frac{\partial H_z}{\partial x} - \sigma E_y \right), \quad (3.79e)$$

$$\frac{\partial E_z}{\partial t} = \frac{1}{\epsilon} \left(\frac{\partial H_y}{\partial x} - \frac{\partial H_x}{\partial y} - \sigma E_z \right) \quad (3.79f)$$

Following Yee's notation, we define a grid point in the solution region as

$$(i, j, k) \equiv (i \Delta x, j \Delta y, k \Delta z) \quad (3.80)$$

and any function of space and time as

$$F^n(i, j, k) \equiv F(i \delta, j \delta, k \delta, n \Delta t) \quad (3.81)$$

where $\delta = \Delta x = \Delta y = \Delta z$ is the space increment, and Δt is the time increment, while i, j, k , and n are integers. Using central finite difference approximation for space and time derivatives that are second-order accurate,

$$\frac{\partial F^n(i, j, k)}{\partial x} = \frac{F^n(i + 1/2, j, k) - F^n(i - 1/2, j, k)}{\delta} + O(\delta^2) \quad (3.82)$$

$$\frac{\partial F^n(i, j, k)}{\partial t} = \frac{F^{n+1/2}(i, j, k) - F^{n-1/2}(i, j, k)}{\Delta t} + O(\Delta t^2) \quad (3.83)$$

In applying Equation (3.82) to all the space derivatives in Equation (3.79), Yee positions the components of \mathbf{E} and \mathbf{H} about a unit cell of the lattice as shown in Figure 3.22. To incorporate Equation (3.83), the components of \mathbf{E} and \mathbf{H} are evaluated at alternate half-time steps. Thus we obtain the explicit finite difference approximation of Equation (3.79) as

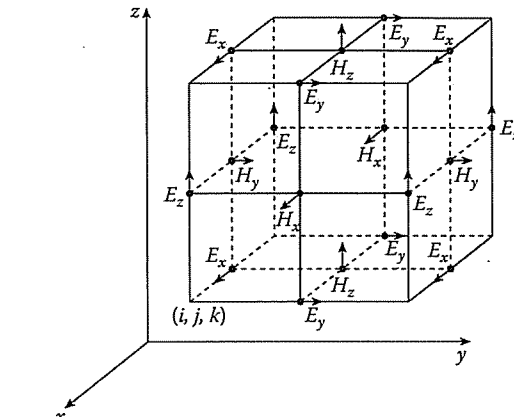


Figure 3.22
Positions of the field components in a unit cell of the Yee's lattice.

$$\begin{aligned} H_x^{n+1/2}(i, j + 1/2, k + 1/2) &= H_x^{n-1/2}(i, j + 1/2, k + 1/2) \\ &+ \frac{\delta t}{\mu(i, j + 1/2, k + 1/2)} [E_y^n(i, j + 1/2, k + 1) \\ &- E_y^n(i, j + 1/2, k) \\ &+ E_z^n(i, j, k + 1/2) - E_z^n(i, j + 1, k + 1/2)], \end{aligned} \quad (3.84a)$$

$$\begin{aligned} H_y^{n+1/2}(i + 1/2, j, k + 1/2) &= H_y^{n-1/2}(i + 1/2, j, k + 1/2) \\ &+ \frac{\delta t}{\mu(i + 1/2, j, k + 1/2)} [E_z^n(i + 1, j, k + 1/2) \\ &- E_z^n(i, j, k + 1/2) \\ &+ E_x^n(i + 1/2, j, k) - E_x^n(i + 1/2, j, k + 1)], \end{aligned} \quad (3.84b)$$

$$\begin{aligned} H_z^{n+1/2}(i + 1/2, j + 1/2, k) &= H_z^{n-1/2}(i + 1/2, j + 1/2, k) \\ &+ \frac{\delta t}{\mu(i + 1/2, j + 1/2, k)} [E_x^n(i + 1/2, j + 1, k) \\ &- E_x^n(i + 1/2, j, k) \\ &+ E_y^n(i, j + 1/2, k) - E_y^n(i + 1, j + 1/2, k)], \end{aligned} \quad (3.84c)$$

$$\begin{aligned}
 E_x^{n+1}(i+1/2, j, k) &= \left(1 - \frac{\sigma(i+1/2, j, k)\delta t}{\epsilon(i+1/2, j, k)} \right) \\
 &\quad + \frac{\delta t}{\epsilon(i+1/2, j, k)\delta} [H_z^{n+1/2}(i+1/2, j+1/2, k) \\
 &\quad - H_z^{n+1/2}(i+1/2, j-1/2, k) \\
 &\quad + H_y^{n+1/2}(i+1/2, j, k-1/2) \\
 &\quad - H_y^{n+1/2}(i+1/2, j, k+1/2)] ,
 \end{aligned} \tag{3.84d}$$

$$\begin{aligned}
 E_y^{n+1}(i, j+1/2, k) &= \left(1 - \frac{\sigma(i, j+1/2, k)\delta t}{\epsilon(i, j+1/2, k)} \right) \\
 &\quad + \frac{\delta t}{\epsilon(i, j+1/2, k)\delta} [H_x^{n+1/2}(i, j+1/2, k+1/2) \\
 &\quad - H_x^{n+1/2}(i, j+1/2, k-1/2) \\
 &\quad + H_z^{n+1/2}(i-1/2, j+1/2, k) \\
 &\quad - H_z^{n+1/2}(i+1/2, j+1/2, k)] ,
 \end{aligned} \tag{3.84e}$$

$$\begin{aligned}
 E_z^{n+1}(i, j, k+1/2) &= \left(1 - \frac{\sigma(i, j, k+1/2)\delta t}{\epsilon(i, j, k+1/2)} \right) \\
 &\quad + \frac{\delta t}{\epsilon(i, j, k+1/2)\delta} [H_y^{n+1/2}(i+1/2, j, k+1/2) \\
 &\quad - H_y^{n+1/2}(i-1/2, j, k+1/2) \\
 &\quad + H_x^{n+1/2}(i, j-1/2, k+1/2) \\
 &\quad - H_x^{n+1/2}(i, j+1/2, k+1/2)]
 \end{aligned} \tag{3.84f}$$

Notice from Equations (3.84a)–(3.84f) and Figure 3.22 that the components of \mathbf{E} and \mathbf{H} are interleaved within the unit cell and are evaluated at alternate half-time steps. All the field components are present in a quarter of a unit cell as shown typically in Figure 3.23(a). Figure 3.23(b) illustrates typical relations between field components on a plane; this is particularly useful when incorporating boundary conditions. The figure can be inferred from Equation (3.79d) or Equation (3.84d). In translating the hyperbolic system of Equations (3.84a)–(3.84f) into a computer code, one must make sure that, within the same time loop, one type of field component is calculated first and the results obtained are used in calculating another type.

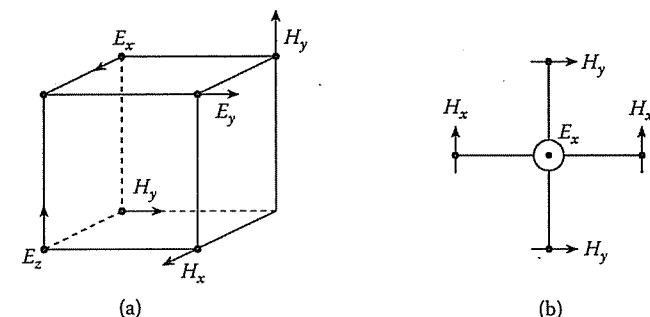


Figure 3.23

Typical relations between field components: (a) within a quarter of a unit cell, (b) in a plane.

3.8.2 Accuracy and Stability

To ensure the accuracy of the computed results, the spatial increment δ must be small compared to the wavelength (usually $\leq \lambda/10$) or minimum dimension of the scatterer. This amounts to having 10 or more cells per wavelength. To ensure the stability of the finite difference scheme of Equations (3.84a)–(3.84f), the time increment Δt must satisfy the following stability condition [43, 47]:

$$u_{\max} \Delta t \leq \left[\frac{1}{\Delta x^2} + \frac{1}{\Delta y^2} + \frac{1}{\Delta z^2} \right]^{-1/2} \tag{3.85}$$

where u_{\max} is the maximum wave phase velocity within the model. Since we are using a cubic cell with $\Delta x = \Delta y = \Delta z = \delta$, Equation (3.85) becomes

$$\frac{u_{\max} \Delta t}{\delta} \leq \frac{1}{\sqrt{n}} \tag{3.86}$$

where n is the number of space dimensions. [n here should not be confused with n in Equation (3.84). The former n refers to the number of dimensions, whereas the latter refers to time.] For practical reasons, it is best to choose the ratio of the time increment to spatial increment as large as possible yet satisfying Equation (3.86).

3.8.3 Lattice Truncation Conditions

A basic difficulty encountered in applying the FDTD method to scattering problems is that the domain in which the field is to be computed is open or unbounded (see Figure 1.3). Since no computer can store an unlimited amount of data, a finite difference scheme over the whole domain is impractical. We must limit the extent of our solution region. In other words, an artificial boundary must be enforced, as in Figure 3.24, to create the numerical illusion of an infinite space. The solution region must

be large enough to enclose the scatterer, and suitable boundary conditions on the artificial boundary must be used to simulate the extension of the solution region to infinity. Outer boundary conditions of this type have been called either *radiation conditions*, *absorbing boundary conditions*, or *lattice truncation conditions*. Although several types of boundary conditions have been proposed [48, 49], we will only consider those developed by Taflove et al. [43, 44].

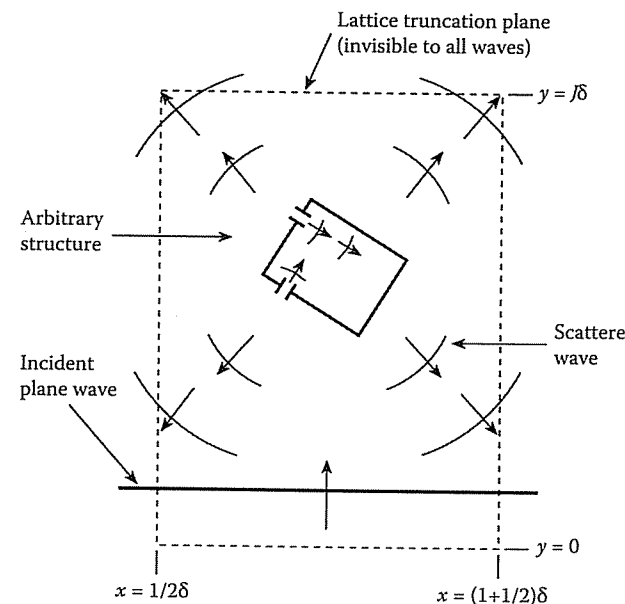


Figure 3.24
Solution region with lattice truncation.

The lattice truncation conditions developed by Taflove et al. allow excellent overall accuracy and numerical stability even when the lattice truncation planes are positioned no more than 5δ from the surface of the scatterer. The conditions relate in a simple way the values of the field components at the truncation planes to the field components at points one or more δ within the lattice (or solution region).

For simplicity, we first consider one-dimensional wave propagation. Assume waves have only E_z and H_x components and propagate in the $\pm y$ directions. Also assume a time step of $\delta t = \delta y/c$, the maximum allowed by the stability condition of Equation (3.86). If the lattice extends from $y = 0$ to $y = J\Delta y$, with E_z component at the end points, the truncation conditions are

$$E_z^n(0) = E_z^{n-1}(1) \quad (3.87a)$$

$$E_z^n(J) = E_z^{n-1}(J-1) \quad (3.87b)$$

3.8. PRACTICAL APPLICATIONS II — WAVE SCATTERING (FDTD)

With these lattice conditions, all possible $\pm y$ -directed waves are absorbed at $y = 0$ and $J\Delta y$ without reflection. Equation (3.87) assumes free-space propagation. If we wish to simulate the lattice truncation in a dielectric medium of refractive index m , Equation (3.87) is modified to

$$E_z^n(0) = E_z^{n-m}(1) \quad (3.88a)$$

$$E_z^n(J) = E_z^{n-m}(J-1) \quad (3.88b)$$

For the three-dimensional case, we consider scattered waves having all six field components and propagating in all possible directions. Assume a time step of $\delta t = \delta/2c$, a value which is about 13% lower than the maximum allowed ($\delta t = \delta/\sqrt{3}c$) by Equation (3.86). If the lattice occupies $\frac{1}{2}\delta < x < (I_{\max} + \frac{1}{2})\delta$, $0 < y < J_{\max}\delta$, $0 < z < K_{\max}\delta$, the truncation conditions are [36, 44]:

(a) plane $i = 1/2$

$$\begin{aligned} H_y^n(1/2, j, k + 1/2) = & \frac{1}{3} [H_y^{n-2}(3/2, j, k - 1/2) + H_y^{n-2}(3/2, j, k + 1/2) \\ & + H_y^{n-2}(3/2, j, k + 3/2)], \end{aligned} \quad (3.89a)$$

$$\begin{aligned} H_z^n(1/2, j + 1/2, k) = & \frac{1}{3} [H_z^{n-2}(3/2, j + 1/2, k - 1) + H_z^{n-2}(3/2, j + 1/2, k) \\ & + H_z^{n-2}(3/2, j + 1/2, k + 1)], \end{aligned} \quad (3.89b)$$

(b) plane $i = I_{\max} + 1/2$

$$\begin{aligned} H_y^n(I_{\max} + 1/2, j, k + 1/2) = & \frac{1}{3} [H_y^{n-2}(I_{\max} - 1/2, j, k - 1/2) \\ & + H_y^{n-2}(I_{\max} - 1/2, j, k + 1/2) \\ & + H_y^{n-2}(I_{\max} - 1/2, j, k + 3/2)], \end{aligned} \quad (3.89c)$$

$$\begin{aligned} H_z^n(I_{\max} + 1/2, j + 1/2, k) = & \frac{1}{3} [H_z^{n-2}(I_{\max} - 1/2, j + 1/2, k - 1) \\ & + H_z^{n-2}(I_{\max} - 1/2, j + 1/2, k) \\ & + H_z^{n-2}(I_{\max} - 1/2, j + 1/2, k + 1)], \end{aligned} \quad (3.89d)$$

(c) plane $j = 0$,

$$E_x^n(i + 1/2, 0, k) = E_x^{n-2}(i + 1/2, 1, k), \quad (3.89e)$$

$$E_z^n(i, 0, k + 1/2) = E_z^{n-2}(i, 1, k + 1/2), \quad (3.89f)$$

(d) plane $j = J_{\max}$

$$E_x^n(i + 1/2, J_{\max}, k) = E_x^{n-2}(i + 1/2, J_{\max} - 1, k) \quad (3.89g)$$

$$E_z^n(i, J_{\max}, k + 1/2) = E_z^{n-2}(i, J_{\max} - 1, k + 1/2), \quad (3.89h)$$

(e) plane $k = 0$,

$$\begin{aligned} E_x^n(i + 1/2, j, 0) &= \frac{1}{3} [E_x^{n-2}(i - 1/2, j, 1) \\ &\quad + E_x^{n-2}(i + 1/2, j, 1) \\ &\quad + E_x^{n-2}(i + 3/2, j, 1)], \end{aligned} \quad (3.89i)$$

$$\begin{aligned} E_y^n(i, j + 1/2, 0) &= \frac{1}{3} [E_y^{n-2}(i - 1, j + 1/2, 1) \\ &\quad + E_y^{n-2}(i, j + 1/2, 1) \\ &\quad + E_y^{n-2}(i + 1, j + 1/2, 1)], \end{aligned} \quad (3.89j)$$

(f) plane $k = K_{\max}$,

$$\begin{aligned} E_x^n(i + 1/2, j, K_{\max}) &= \frac{1}{3} [E_x^{n-2}(i - 1/2, j, K_{\max} - 1) \\ &\quad + E_x^{n-2}(i + 1/2, j, K_{\max} - 1) \\ &\quad + E_x^{n-2}(i + 3/2, j, K_{\max} - 1)], \end{aligned} \quad (3.89k)$$

$$\begin{aligned} E_y^n(i, j + 1/2, K_{\max}) &= \frac{1}{3} [E_y^{n-2}(i - 1, j + 1/2, K_{\max} - 1) \\ &\quad + E_y^{n-2}(i, j + 1/2, K_{\max} - 1) \\ &\quad + E_y^{n-2}(i + 1, j + 1/2, K_{\max} - 1)] \end{aligned} \quad (3.89l)$$

These boundary conditions minimize the reflection of any outgoing waves by simulating the propagation of the wave from the lattice plane adjacent to the lattice truncation plane in a number of time steps corresponding to the propagation delay. The averaging process is used to take into account all possible local angles of incidence of the outgoing wave at the lattice boundary and possible multiple incidences [43]. If the solution region is a dielectric medium of refractive index m rather than free space, we replace the superscript $n - 2$ in Equations (3.89a)–(3.89l) by $n - m$.

3.8.4 Initial Fields

The initial field components are obtained by simulating either an incident plane wave pulse or single-frequency plane wave. The simulation should not take excessive storage nor cause spurious wave reflections. A desirable plane wave source condition

3.8. PRACTICAL APPLICATIONS II – WAVE SCATTERING (FDTD)

takes into account the scattered fields at the source plane. For the three-dimensional case, a typical wave source condition at plane $y = j_s$ (near $y = 0$) is

$$E_z^n(i, j_s, k + 1/2) \leftarrow 1000 \sin(2\pi f n \delta t) + E_z^n(i, j_s, k + 1/2) \quad (3.90)$$

where f is the irradiation frequency. Equation (3.90) is a modification of the algorithm for all points on plane $y = j_s$; the value of the sinusoid is added to the value of E_z^n obtained from Equations (3.84a)–(3.84f).

At $t = 0$, the plane wave source of frequency f is assumed to be turned on. The propagation of waves from this source is simulated by time stepping, that is, repeatedly implementing Yee's finite difference algorithm on a lattice of points. The incident wave is tracked as it first propagates to the scatterer and then interacts with it via surface-current excitation, diffusion, penetration, and diffraction. Time stepping is continued until the sinusoidal steady state is achieved at each point. The field envelope, or maximum absolute value, during the final half-wave cycle of time stepping is taken as the magnitude of the phasor of the steady-state field [32, 43].

From experience, the number of time steps needed to reach the sinusoidal steady state can be greatly reduced by introducing a small isotropic conductivity σ_{ext} within the solution region exterior to the scatterer. This causes the fields to converge more rapidly to the expected steady-state condition.

3.8.5 Programming Aspects

Since most EM scattering problems involve nonmagnetic media ($\mu_r = 1$), the quantity $\delta t/\mu(i, j, k)\delta$ can be assumed constant for all (i, j, k) . The nine multiplications per unit cell per time required by Yee's algorithm of Equations (3.84a)–(3.84f) can be reduced to six multiplications, thereby reducing computer time. Following Taflove et al. [31, 35, 44], we define the following constants:

$$R = \delta t/2\epsilon_o, \quad (3.91a)$$

$$R_a = (c\delta t/\delta)^2, \quad (3.91b)$$

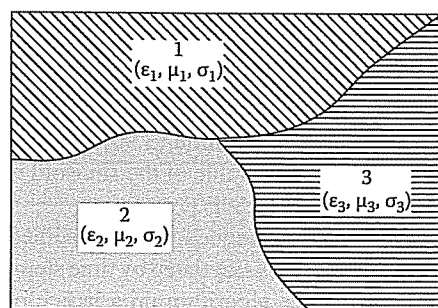
$$R_b = \delta t/\mu_o\delta, \quad (3.91c)$$

$$C_a = \frac{1 - R\sigma(m)/\epsilon_r(m)}{1 + R\sigma(m)/\epsilon_r(m)}, \quad (3.91d)$$

$$C_b = \frac{R_a}{\epsilon_r(m) + R\sigma(m)} \quad (3.91e)$$

where $m = \text{MEDIA}(i, j, k)$ is an integer referring to the dielectric or conducting medium type at location (i, j, k) . For example, for a solution region comprising three different homogeneous media shown in Figure 3.25, m is assumed to be 1 to 3. (This m should not be confused with the refractive index of the medium, mentioned earlier.) In addition to the constants in Equation (3.91), we define proportional electric field

$$\tilde{\mathbf{E}} = R_b \mathbf{E} \quad (3.92)$$

**Figure 3.25**

A typical inhomogeneous solution region with integer m assigned to each medium.

Thus Yee's algorithm is modified and simplified for easy programming as [50, 51]:

$$\begin{aligned} H_x^n(i, j, k) &= H_x^{n-1}(i, j, k) + \tilde{E}_y^{n-1}(i, j, k+1) \\ &\quad - \tilde{E}_y^{n-1}(i, j, k) - \tilde{E}_z^{n-1}(i, j+1, k) + \tilde{E}_z^{n-1}(i, j, k), \end{aligned} \quad (3.93a)$$

$$\begin{aligned} H_y^n(i, j, k) &= H_y^{n-1}(i, j, k) + \tilde{E}_z^{n-1}(i+1, j, k) - \tilde{E}_z^{n-1}(i, j, k) \\ &\quad - \tilde{E}_x^{n-1}(i, j, k+1) + \tilde{E}_x^{n-1}(i, j, k), \end{aligned} \quad (3.93b)$$

$$\begin{aligned} H_z^n(i, j, k) &= H_z^{n-1}(i, j, k) + \tilde{E}_x^{n-1}(i+1, j, k) - \tilde{E}_x^{n-1}(i, j, k) \\ &\quad - \tilde{E}_y^{n-1}(i+1, j, k) + \tilde{E}_y^{n-1}(i, j, k), \end{aligned} \quad (3.93c)$$

$$\begin{aligned} \tilde{E}_x^n(i, j, k) &= C_a(m) \tilde{E}_x^{n-1}(i, j, k) \\ &\quad + C_b(m) [H_z^{n-1}(i, j, k) - H_z^{n-1}(i, j-1, k) \\ &\quad - H_y^{n-1}(i, j, k) + H_y^{n-1}(i, j-1, k)], \end{aligned} \quad (3.93d)$$

$$\begin{aligned} \tilde{E}_y^n(i, j, k) &= C_a(m) \tilde{E}_y^{n-1}(i, j, k) \\ &\quad + C_b(m) [H_x^{n-1}(i, j, k) - H_x^{n-1}(i, j, k-1) \\ &\quad - H_z^{n-1}(i, j, k) + H_z^{n-1}(i-1, j, k)], \end{aligned} \quad (3.93e)$$

$$\begin{aligned} \tilde{E}_z^n(i, j, k) &= C_a(m) \tilde{E}_z^{n-1}(i, j, k) \\ &\quad + C_b(m) [H_y^{n-1}(i, j, k) - H_y^{n-1}(i-1, j, k) \\ &\quad - H_x^{n-1}(i, j, k) + H_x^{n-1}(i, j-1, k)] \end{aligned} \quad (3.93f)$$

The relationship between the original and modified algorithms is illustrated in Figure 3.26 and shown in Table 3.8. Needless to say, the truncation conditions in Equations (3.89a)–(3.89l) must be modified accordingly. This modification eliminates the need for computer storage of separate ϵ and σ arrays; only a MEDIA array which specifies the type-integer of the dielectric or conducting medium at the location of each electric field component in the lattice need be stored. Also the programming problem of handling half integral values of i, j, k has been eliminated.

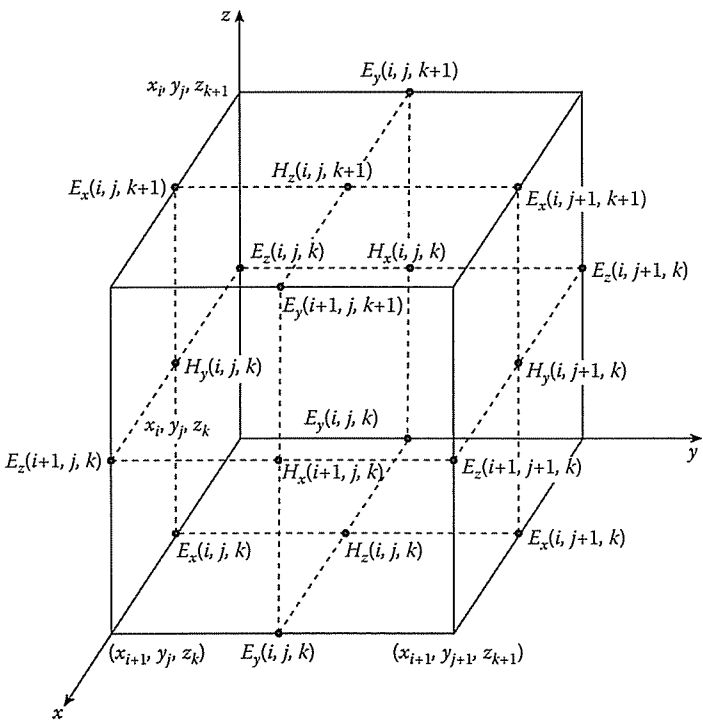


Figure 3.26
Modified node numbering.

With the modified algorithm, we determine the scattered fields as follows. Let the solution region, completely enclosing the scatterer, be defined by $0 < i < I_{\max}$, $0 < j < J_{\max}$, $0 < k < K_{\max}$. At $t \leq 0$, the program is started by setting all field components at the grip points equal to zero:

$$\tilde{E}_x^0(i, j, k) = \tilde{E}_y^0(i, j, k) = \tilde{E}_z^0(i, j, k) = 0 \quad (3.94a)$$

$$H_x^0(i, j, k) = H_y^0(i, j, k) = H_z^0(i, j, k) = 0 \quad (3.94b)$$

Table 3.8 Relationship Between Original and Modified Field Components (lattice size = $I_{\max}\delta \times J_{\max}\delta \times K_{\max}\delta$)

Original	Modified	Limits on Modified (i, j, k)
$H_x^{n+1/2}(x_i, y_{j+1/2}, z_{k+1/2})$	$H_x^n(i, j, k)$	$i = 0, \dots, I_{\max}$ $j = 0, \dots, J_{\max} - 1$ $k = 0, \dots, K_{\max} - 1$
$H_y^{n+1/2}(x_{i+1/2}, y_j, z_{k+1/2})$	$H_y^n(i, j, k)$	$i = 0, \dots, I_{\max} - 1$ $j = 0, \dots, J_{\max}$ $k = 0, \dots, K_{\max} - 1$
$H_z^{n+1/2}(x_{i+1/2}, y_{j+1/2}, z_k)$	$H_z^n(i, j, k)$	$i = 0, \dots, I_{\max} - 1$ $j = 0, \dots, J_{\max} - 1$ $k = 0, \dots, K_{\max}$
$E_x^n(x_{i+1/2}, y_j, z_k)$	$E_x^n(i, j, k)$	$i = 0, \dots, I_{\max} - 1$ $j = 0, \dots, J_{\max}$ $k = 0, \dots, K_{\max}$
$E_y^n(x_i, y_{j+1/2}, z_k)$	$E_y^n(i, j, k)$	$i = 0, \dots, I_{\max}$ $j = 0, \dots, J_{\max} - 1$ $k = 0, \dots, K_{\max}$
$E_z^n(x_i, y_j, z_{k+1/2})$	$E_z^n(i, j, k)$	$i = 0, \dots, I_{\max}$ $j = 0, \dots, J_{\max}$ $k = 0, \dots, K_{\max} - 1$

for $0 < i < I_{\max}$, $0 < j < J_{\max}$, $0 < k < K_{\max}$. If we know

$$H_x^{n-1}(i, j, k), E_z^{n-1}(i, j, k),$$

and

$$E_y^{n-1}(i, j, k)$$

at all grid points in the solution region, we can determine new $H_x^n(i, j, k)$ everywhere from Equation (3.93a). The same applies for finding other field components except that the lattice truncation conditions of Equations (3.89a)–(3.89l) must be applied when necessary. The plane wave source is activated at $t = \delta t$, the first time step, and left on during the entire run. The field components are advanced by Yee's finite difference formulas in Equations (3.93a)–(3.93f) and by the lattice truncation condition in Equations (3.89a)–(3.89l). The time stepping is continued for $t = N_{\max}\delta t$, where N_{\max} is chosen large enough that the sinusoidal steady state is achieved. In obtaining the steady state solutions, the program must not be left for too long (i.e., N_{\max} should not be too large), otherwise the imperfection of the boundary conditions causes the model to become unstable.

The FDTD method has the following inherent advantages over other modeling techniques, such as the moment method and transmission-line modeling:

- It is conceptually simple.

- The algorithm does not require the formulation of integral equations, and relatively complex scatterers can be treated without the inversion of large matrices.
- It is simple to implement for complicated, inhomogeneous conducting or dielectric structures because constitutive parameters (σ, μ, ϵ) can be assigned to each lattice point.
- Its computer memory requirement is not prohibitive for many complex structures of interest.
- The algorithm makes use of the memory in a simple sequential order.
- It is much easier to obtain frequency domain data from time domain results than the converse. Thus, it is more convenient to obtain frequency domain results via time domain when many frequencies are involved.

The method has the following disadvantages:

- Its implementation necessitates modeling an object as well as its surroundings. Thus, the required program execution time may be excessive.
- Its accuracy is at least one order of magnitude worse than that of the method of moments, for example.
- FDTD employs a low-order approximation in space that requires at least ten cells per wavelength to achieve acceptable accuracy.
- Since the computational meshes are rectangular in shape, they do not conform to scatterers with curved surfaces, as is the case of the cylindrical or spherical boundary.
- As in all finite difference algorithms, the field quantities are only known at grid nodes.

Time-domain modeling in three dimensions involves a number of issues which are yet to be resolved even for frequency-domain modeling. Among these are whether it is best to reduce Maxwell's equations to a second-order equation for the electric (or magnetic) field or to work directly with the coupled first-order equation. The former approach is used in [35], for example, for solving the problem of EM exploration for minerals. The latter approach has been used with great success in computing EM scattering from objects as demonstrated in this section. In spite of these unresolved issues, the FDTD algorithm has been applied to solve scattering and other problems including the following:

1. aperture penetration [44, 52, 53],
2. antenna/radiation problems [54]–[60],
3. microwave circuits [63]–[68],

4. eigenvalue problems [69],
5. EM absorption in human tissues (bioelectromagnetics) [35, 36], [70]–[74], and
6. other areas [75]–[79].

The following two examples are taken from the work of Taflove et al. [32, 43, 44]. The problems whose exact solutions are known will be used to illustrate the applications and accuracy of FDTD algorithm.

Example 3.7

Consider the scattering of $a + y$ -directed plane wave of frequency 2.5 GHz by a uniform, circular, dielectric cylinder of radius 6 cm. We assume that the cylinder is infinite in the z direction and that the incident fields do not vary along z . Thus $\partial/\partial z = 0$ and the problem is reduced to the two-dimensional scattering of the incident wave with only E_z , H_x , and H_y components. Our objective is to compute one of the components, say E_z , at points within the cylinder. \square

Solution

Assuming a lossless dielectric with

$$\epsilon_d = 4\epsilon_0, \quad \mu_d = \mu_0, \quad \sigma_d = 0, \quad (3.95)$$

the speed of the wave in the cylinder is

$$u_d = \frac{c}{\sqrt{\epsilon_r}} = 1.5 \times 10^8 \text{ m/s} \quad (3.96)$$

Hence $\lambda_d = u_d/f = 6$ cm. We may select $\delta = \Delta x = \Delta y = \Delta z = \lambda_d/20 = 0.3$ cm and $\delta t = \delta/2c = 5$ ps. Thus we use the two-dimensional grid of Figure 3.27 as the solution domain. Due to the symmetry of the scatterer, the domain can be reduced relative to Figure 3.27 to the 25×49 subdomain of Figure 3.28. Choosing the cylinder axis as passing through point $(i, j) = (25.5, 24.5)$ allows the *symmetry condition* to be imposed at line $i = 26$, i.e.,

$$\tilde{E}_z^n(26, j) = \tilde{E}_z^n(25, j) \quad (3.97)$$

Soft grid truncation conditions are applied at $j = 0, 49$ and $i = 1/2$, i.e.,

$$\tilde{E}_z^n(i, 0) = \frac{1}{3} [\tilde{E}_z^{n-2}(i-1, 1) + \tilde{E}_z^{n-2}(i, 1) + \tilde{E}_z^{n-2}(i+1, 1)], \quad (3.98)$$

$$\tilde{E}_z^n(i, 49) = \frac{1}{3} [\tilde{E}_z^{n-2}(i-1, 48) + \tilde{E}_z^{n-2}(i, 48) + \tilde{E}_z^{n-2}(i+1, 48)], \quad (3.99)$$

$$H_y^n(0.5, 49) = \frac{1}{3} [H_y^{n-2}(1.5, j) + H_y^{n-2}(1.5, j-1) + H_y^{n-2}(1.5, j+1)] \quad (3.100)$$

Assumptions:

$$E_x = E_y = 0; \quad H_z = 0$$

$$\frac{\partial}{\partial z} = 0$$

Maxwell's Equations:

$$\frac{\partial H_x}{\partial t} = -\frac{1}{\mu} \frac{\partial E_z}{\partial y}$$

$$\frac{\partial H_y}{\partial t} = \frac{1}{\mu} \frac{\partial E_z}{\partial x}$$

$$\frac{\partial E_z}{\partial t} =$$

$$\frac{1}{\epsilon} \left(\frac{\partial H_y}{\partial x} - \frac{\partial H_x}{\partial y} - \sigma E_x \right)$$

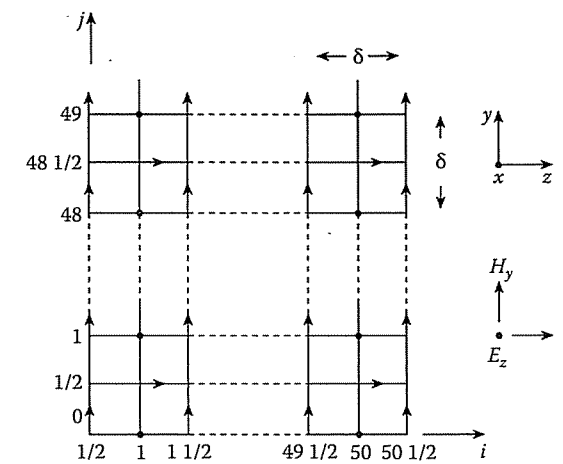


Figure 3.27
Two-dimensional lattice for Example 3.7.

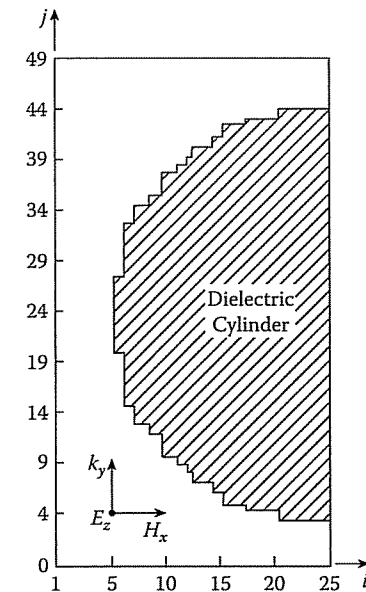


Figure 3.28
Finite difference model of cylindrical dielectric scatterer relative to the grid of Figure 3.27.

where $n - 2$ is due to the fact that $\delta = 2c\delta t$ is selected. Notice that the actual values of (i, j, k) are used here, while the modified values for easy programming are used in the program; the relationship between the two types of values is in Table 3.8.

Grid points (i, j) internal to the cylinder, determined by

$$[(i - 25.5)^2 + (j - 24.5)^2]^{1/2} \leq 20, \quad (3.101)$$

are assigned the constitutive parameters ϵ_d, μ_o , and ϵ_d , while grid points external to the cylinder are assigned parameters of free space ($\epsilon = \epsilon_o, \mu = \mu_o, \sigma = 0$).

A FORTRAN program has been developed by Bemmel [80] based on the ideas expounded above. A similar but more general code is THREDE developed by Holland [50]. The program starts by setting all field components at grid points equal to zero. A plane wave source

$$\tilde{E}_z^n(i, 2) \leftarrow 1000 \sin(2\pi f n \delta t) + \tilde{E}_z^n(i, 2) \quad (3.102)$$

is used to generate the incident wave at $j = 2$ and $n = 1$, the first time step, and left on during the entire run. The program is time stepped to $t = N_{\max} \delta t$, where N_{\max} is large enough that sinusoidal steady state is achieved. Since $f = 2.5$ GHz, the wave period $T = 1/f = 400$ ps = $80\delta t$. Hence $N_{\max} = 500 = 6.25T/\delta t$ is sufficient to reach steady state. Thus the process is terminated after 500 timesteps. Typical results are portrayed in Figure 3.29 for the envelope of $E_z^n(15, j)$ for $460 \leq n \leq 500$. Figure 3.29 also shows the exact solution using series expansion [81]. Bemmel's code has both the numerical and exact solutions. By simply changing the constitutive parameters of the media and specifying the boundary of the scatterer (through a look-up table for complex objects), the program can be applied to almost any two-dimensional scattering or penetration problem. ■

Example 3.8

Consider the penetration of $a + y$ -directed plane wave of frequency 2.5 GHz by a uniform, dielectric sphere of radius 4.5 cm. The problem is similar to the previous example except that it is three dimensional and more general. We assume that the incident wave has only E_z and H_x components. □

Solution

As in the previous example, we assume that internal to the lossless dielectric sphere,

$$\epsilon_d = 4\epsilon_o, \quad \mu_d = \mu_o, \quad \sigma_d = 0 \quad (3.103)$$

We select

$$\delta = \lambda_d/20 = 0.3 \text{ cm} \quad (3.104)$$

and

$$\delta t = \delta/2c = 5 \text{ ps} \quad (3.105)$$

This choice of the grid size implies that the radius of the sphere is $4.5/0.3 = 15$ units. The sphere model centered at grid point $(19.5, 20, 19)$ in a $19 \times 39 \times 19$ lattice is

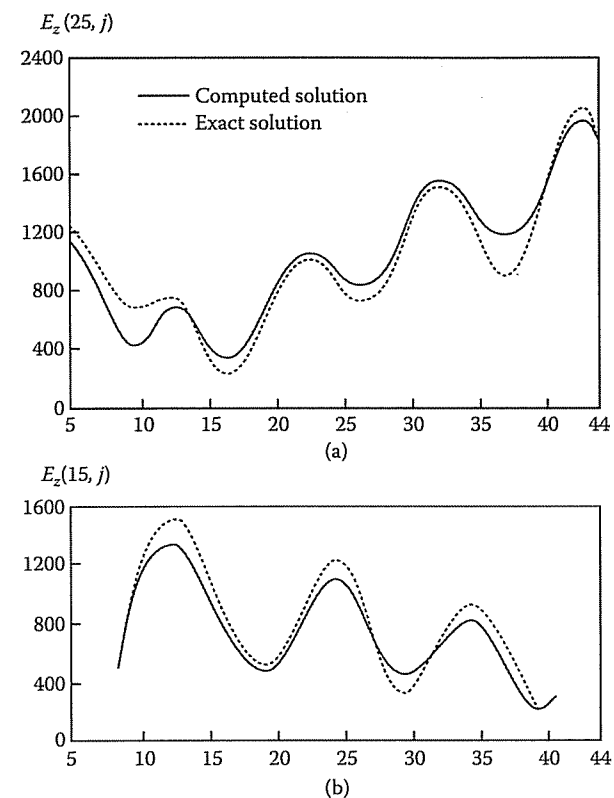


Figure 3.29

Computed internal E_z on line: (a) $i = 25$, (b) $i = 15$.

portrayed in Figure 3.30 at two lattice symmetry planes $k = 19$ and $i = 19.5$. Grid points (i, j, k) internal to the sphere are determined by

$$[(i - 19.5)^2 + (j - 20)^2 + (k - 19)^2]^{1/2} \leq 15 \quad (3.106)$$

Rather than assigning $\sigma = 0$ to points external to the sphere, a value $\sigma = 0.1$ mho/m is assumed to reduce spurious wave reflections. The MATLAB code shown in Figure 3.31, a modified version of Bemmel's [80], is used to generate field components E_y and E_z near the sphere irradiation axis. With the dimensions and constitutive parameters of the sphere specified as input data, the program is developed based on the following steps:

1. Compute the parameters of each medium using Equation (3.91) where $m = 1, 2$.
2. Initialize field components.
3. Use the FDTD algorithm in Equations (3.93a)–(3.93f) to generate field components. This is the heart of the program. It entails taking the following steps:

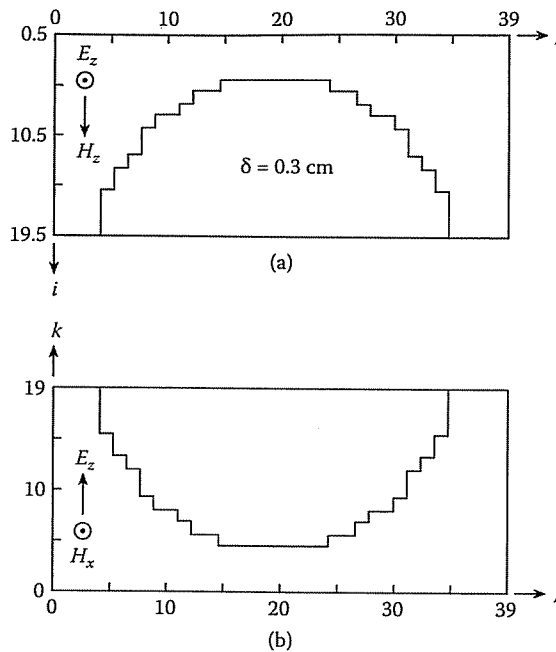


Figure 3.30
FDTD model of dielectric sphere.

- Calculate actual values of grid point (x, y, z) using the relationship in Table 3.8. This will be needed later to identify the constitutive parameters of the medium at that point using subroutine MEDIA.
- Apply soft lattice truncation conditions in Equations (3.89a)–(3.89l) at appropriate boundaries, i.e., at $x = \delta/2$, $y = 0$, y_{\max} , and $z = 0$. Notice that some of the conditions in Equations (3.89a)–(3.89l) are not necessary in this case because we restrict the solution to one fourth of the sphere due to geometrical symmetry. At other boundaries ($x = x_{\max}$ and $z = z_{\max}$), the symmetry conditions are imposed. For example, at $k = 19$,

$$\tilde{E}_x^n(i, j, 20) = \tilde{E}_x^n(i, j, 18)$$

- Apply FDTD algorithm in Equations (3.93a)–(3.93f).
- Activate the plane wave source, i.e.,

$$\tilde{E}_z^n(i, j, k) \leftarrow \sin(2\pi f n \delta t) + \tilde{E}_z^n(i, j_s, k)$$

where $j_s = 3$ or any plane near $y = 0$.

- Time step until steady state is reached.
- Obtain the maximum absolute values (envelopes) of field components in the last half-wave and output the results.

3.8. PRACTICAL APPLICATIONS II — WAVE SCATTERING (FDTD)

```

*****
* APPLICATION OF THE FINITE DIFFERENCE METHOD
* This program involves the penetration of a lossless dielectric SPHERE
* by a plane wave. The program provides in the maximum absolute value of
* Ez and Ez during the final half-wave of time-stepping
* Assumption:
* +y-directed incident wave with components Ez and Hx.
* I,J,K,NN correspond to X,Y,Z, and Time.
* IMAX,JMAX,KMAX are the maximum values of x,y,z
* NNMAX is the total number of timesteps.
* NHW represents one half-wave cycle.
* MED is the number of different uniform media sections.
* JS is the j-position of the plane wave front.

* THIS PROGRAM WAS DEVELOPED BY V. BEMMEL [80]
* AND LATER IMPROVED BY D. TERRY

clear all; format compact; tic

IMAX=19; JMAX=39; KMAX=19;
NMAX=2; NNMAX=500; NHW=40; MED=2; JS=3;
DELTA=3E-3; CL=3.0E8; F=2.5E9;

% Define scatterer dimensions
OI=19.5; OJ=20.0; OK=19.0; RADIUS=15.0;
ER=[1.0,4.0]; % CONSTITUTIVE PARAMETERS
SIG=[0.1,0.0];

% Statement function to compute position w.r.t. center of the sphere
E0=(1E-9)/(36*pi);
U0=(1E-7)*4*pi;
DT=DELTA/(2*CL);
R=DT/E0;
RA=(DT^2)/(U0*E0*(DELTA^2));
RB=DT/(U0*DELTA);
TPIFDT = 2.0*pi*F*DT;

*****
* STEP # 1 - COMPUTE MEDIA PARAMETERS
*****

CA = 1-R*SIG./ER;
CB = RA./ER;
CBMRB = CB/RB;

% (i) CALCULATE THE REAL/ACTUAL GRID POINTS

% Initialize the media arrays. Index (M) determines which
% medium each point is actually located in and is used to
% index into arrays which determine the constitutive
% parameters of the medium. There are separate M determining
% arrays for EX, EY, and EZ. These arrays correlate the
% integer values of I,J,K to the actual position within
% the lattice. Computing these values now and storing them in these
% arrays as opposed to computing them each time they are
% needed saves a large amount of computation time.

```

Figure 3.31
Computer program for FDTD three-dimensional scattering problem.
(Continued).

```

x = 0:(IMAX+1); y = 0:(JMAX+1); z = 0:(KMAX+1);
[Mx,My,Mz]=ndgrid(x,y,z);
IXMED = (sqrt((Mx-OI+.5).^2+(My-OJ).^2+(Mz-OK).^2)<=RADIUS)+1;
IYMED = (sqrt((Mx-OI).^2+(My-OJ+.5).^2+(Mz-OK).^2)<=RADIUS)+1;
IZMED = (sqrt((Mx-OI).^2+(My-OJ).^2+(Mz-OK+.5).^2)<=RADIUS)+1;

% ****
% STEP # 2 - INITIALIZE FIELD COMPONENTS
% ****
% components for output

EY1 = zeros(1,JMAX+2);
EZ1 = zeros(1,JMAX+2);

EX=zeros(IMAX+2,JMAX+2,KMAX+2,NMAX+1);
EY=zeros(IMAX+2,JMAX+2,KMAX+2,NMAX+1);
EZ=zeros(IMAX+2,JMAX+2,KMAX+2,NMAX+1);
HX=zeros(IMAX+2,JMAX+2,KMAX+2,NMAX+1);
HY=zeros(IMAX+2,JMAX+2,KMAX+2,NMAX+1);
HZ=zeros(IMAX+2,JMAX+2,KMAX+2,NMAX+1);

% ****
% STEP # 3 - USE FD/TD ALGORITHM TO GENERATE
% FIELD COMPONENTS
% ****
% SINCE ONLY FIELD COMPONENTS AT CURRENT TIME (t) AND PREVIOUS
% TWO TIME STEPS ( t-1 AND t-2) ARE REQUIRED FOR COMPUTATION,
% WE SAVE MEMORY SPACE BY USING THE FOLLOWING INDICES
% NCUR is index in for time t
% NPR1 is index in for t-1
% NPR2 is index in for t-2

% NOTES %%%%%%%%%%%%%%%%%%%%%%%%%%%%%%%%%%%%%%
% *ind03c.m I incremented the time so it goes 1 2 3, instead of 0 1 2
% %%%%%%%%%%%%%%%%%%%%%%%%%%%%%%%%%%%%%%

NCUR = 3;
NPR1 = 2;
NPR2 = 1;
for NN = 1:NNMAX % TIME LOOP
    if mod(NN,10)==0
        disp(['NN = ',num2str(NN)]) % DISPLAY PROGRESS
    end
    % Next time step - move indices up a notch.
    NPR2 = NPR1;
    NPR1 = NCUR;
    NCUR = mod( NCUR, 3)+1;
    for K=0:KMAX % Z LOOP
        for J=0:JMAX % Y LOOP
            for I=0:IMAX % X LOOP
                % (ii)-APPLY SOFT LATTICE TRUNCATION CONDITIONS
                %---x=delta/2
                if (I==0)
                    if ((K==KMAX)&&(K==0))
                        HY(0+1,J+1,K+1,NCUR) = (HY(1+1,J+1,K-
                        1+1,NPR2) + HY(1+1,J+1,K+1,NPR2)+ HY(1+1,J+1,K+1+1,NPR2))/3;
                end
            end
        end
    end
end

```

Figure 3.31

(Cont.) Computer program for FDTD three-dimensional scattering problem.

```

HZ(0+1,J+1,K+1,NCUR) = (HZ(1+1,J+1,K-
1+1,NPR2) + HZ(1+1,J+1,K+1,NPR2)+ HZ(1+1,J+1,K+1+1,NPR2))/3;

else
    if (K==KMAX)
        HY(0+1,J+1,KMAX+1,NCUR) = (HY(1+1,J+1,KMAX-
1+1,NPR2)+ HY(1+1,J+1,KMAX+1,NPR2))/2;
        HZ(0+1,J+1,K+1,NCUR)=( HZ(1+1,J+1,K-
1+1,NPR2)+ HZ(1+1,J+1,K+1,NPR2) )/2;
    else
        HY(0+1,J+1,K+1,NCUR) = ( HY(1+1,J+1,K+1,NPR2) +
        + HY(1+1,J+1,K+1+1,NPR2))/2;
        HZ(0+1,J+1,0+1,NPR2)=(HZ(1+1,J+1,0+1,NPR2) +
        HZ(1+1,J+1,1+1,NPR2))/2;
    end
end
% ---y=0
if (J==0)
    EX(I+1,0+1,K+1,NCUR)=EX(I+1,1+1,K+1,NPR2);
    EZ(I+1,0+1,K+1,NCUR)=EZ(I+1,1+1,K+1,NPR2);
else
    %---y=ymax
    if (J==JMAX)
        EX(I+1,JMAX+1,K+1,NCUR)=EX(I+1,JMAX-1+1,K+1,NPR2);
        EZ(I+1,JMAX+1,K+1,NCUR)=EZ(I+1,JMAX-1+1,K+1,NPR2);
    end
end
%---z=0
if(K==0)
    if ((I==0)&&(I==IMAX))
        EX(I+1,J+1,0+1,NCUR) = (EX(I-
        1+1,J+1,1+1,NPR2) + EX(I+1,J+1,1+1,NPR2)+EX(I+1,J+1,1+1,NPR2))/3;
        EY(I+1,J+1,0+1,NCUR) = (EY(I-
        1+1,J+1,1+1,NPR2) + EY(I+1,J+1,1+1,NPR2)+EY(I+1,J+1,1+1,NPR2))/3;
    else
        if (I==0)
            EX(0+1,J+1,0+1,NCUR)=(EX(0+1,J+1,1+1,NPR2) +
            EX(1+1,J+1,1+1,NPR2))/2;
            EY(I+1,J+1,0+1,NCUR)=(EY(I+1,J+1,1+1,NPR2) +
            EY(I+1+1,J+1,1+1,NPR2))/2;
        else
            EX(I+1,J+1,0+1,NCUR)=(EX(I-
            1+1,J+1,1+1,NPR2)+EX(I+1,J+1,1+1,NPR2))/2;
            EY(I+1,J+1,0+1,NCUR)=(EY(I-
            1+1,J+1,1+1,NPR2)+EY(I+1,J+1,1+1,NPR2))/2;
        end
    end
end
% (iii) APPLY FD/TD ALGORITHM
%----a. HX generation:
HX(I+1,J+1,K+1,NCUR)=HX(I+1,J+1,K+1,NPR1)+RB*(EY(I+1,J+1,K+1+1,NPR1)-
EY(I+1,J+1,K+1,NPR1)+EZ(I+1,J+1,K+1,NPR1)-EZ(I+1,J+1+1,K+1,NPR1));
%----b. HY generation:
HY(I+1,J+1,K+1,NCUR)=HY(I+1,J+1,K+1,NPR1)+RB*(EZ(I+1+1,J+1,K+1,NPR1)-
EZ(I+1,J+1,K+1,NPR1)+EX(I+1,J+1,K+1,NPR1)-EX(I+1,J+1,K+1+1,NPR1));

```

Figure 3.31

(Cont.) Computer program for FDTD three-dimensional scattering problem.

```

-----c. HZ generation:
HZ(I+1,J+1,K+1,NCUR)=HZ(I+1,J+1,K+1,NPR1)+RB*(EX(I+1,J+1+1,K+1,NPR1)-
EX(I+1,J+1,K+1,NPR1)+EY(I+1,J+1,K+1,NPR1)-EY(I+1+1,J+1,K+1,NPR1));
%---k=kmax ! SYMMETRY
if (K==KMAX)
    HX(I+1,J+1,KMAX+1,NCUR)=HX(I+1,J+1,KMAX-1+1,NCUR);
    HY(I+1,J+1,KMAX+1,NCUR)=HY(I+1,J+1,KMAX-1+1,NCUR);
end
% ----d. EX generation:
if ((J==0)&&(J==JMAX)&&(K==0))
    M = IXMED( I+1, J+1, K+1 );
EX(I+1,J+1,K+1,NCUR) = CA(M)*EX(I+1,J+1,K+1,NPR1) + CBMRB(M)*(HZ(I+1,J+1,K+1,NCUR)-
HZ(I+1,J-1+1,K+1,NCUR)+HY(I+1,J+1,K-1+1,NCUR)-HY(I+1,J+1,K+1,NCUR));
end
%----e. EY generation:
if(K==0)
    M = IYMED( I+1, J+1, K+1 );
    if I==0
EY(I+1,J+1,K+1,NCUR)=CA(M)*EY(I+1,J+1,K+1,NPR1) + CBMRB(M)*(HX(I+1,J+1,K+1,NCUR)-
HX(I+1,J+1,K-1+1,NCUR)+HZ(I-1+1,J+1,K+1,NCUR)-HZ(I+1,J+1,K+1,NCUR));
    else
EY(I+1,J+1,K+1,NCUR)=CA(M)*EY(I+1,J+1,K+1,NPR1) + CBMRB(M)*(HX(I+1,J+1,K+1,NCUR)-
HX(I+1,J+1,K-1+1,NCUR)+ 0 -HZ(I+1,J+1,K+1,NCUR));
    end
end
%----f. EZ generation:
if ((J==0)&&(J==JMAX))

    M = IZMED( I+1, J+1, K+1 );
    % sig(ext)=0 for Ez only from Taflove[32]
    if(M==1)
        CAM=1;
    else
        CAM=CA(M);
    end

    if I==0
EZ(I+1,J+1,K+1,NCUR)=CAM*EZ(I+1,J+1,K+1,NPR1)+CBMRB(M)*(HY(I+1,J+1,K+1,NCUR)-HY(I-
1+1,J+1,K+1,NCUR)+HX(I+1,J-1+1,K+1,NCUR)-HX(I+1,J+1,K+1,NCUR));
    else
EZ(I+1,J+1,K+1,NCUR)=CAM*EZ(I+1,J+1,K+1,NPR1)+CBMRB(M)*(HY(I+1,J+1,K+1,NCUR)-
0 +HX(I+1,J-1+1,K+1,NCUR)-HX(I+1,J+1,K+1,NCUR));
    end

    % (iv) APPLY THE PLANE-WAVE SOURCE
    if (J==JS)
        EZ(I+1,JS+1,K+1,NCUR) = EZ(I+1,JS+1,K+1,NCUR)+sin( TPIFDT*NN );
    end
end
%---i=imax+1/2 ! SYMMETRY
if(I==IMAX)
    EY(IMAX+1,J+1,K+1,NCUR)=EY(IMAX+1,J+1,K+1,NCUR);
    EZ(IMAX+1,J+1,K+1,NCUR)=EZ(IMAX+1,J+1,K+1,NCUR);
end
%---k=kmax
if(K==KMAX)
    EX(I+1,J+1,KMAX+1+1,NCUR)=EX(I+1,J+1,KMAX-1+1,NCUR);
    EY(I+1,J+1,KMAX+1+1,NCUR)=EY(I+1,J+1,KMAX-1+1,NCUR);
end
end % X LOOP

```

Figure 3.31

(Cont.) Computer program for FDTD three-dimensional scattering problem.

3.9. ABSORBING BOUNDARY CONDITIONS FOR FDTD

```

% **** STEP # 4 - RETAIN THE MAXIMUM ABSOLUTE VALUES DURING
% THE LAST HALF-WAVE
%
% ****
if ( (K==KMAX)&&(NN>(NNMAX-NHW)) )
    TEMP = abs( EY(IMAX+1,J+1,KMAX-1+1,NCUR) );
    if (TEMP > EY1(J+1) )
        EY1(J+1) = TEMP;
    end
    TEMP = abs( EZ(IMAX+1,J+1,KMAX+1,NCUR) );
    if (TEMP > EZ1(J+1) )
        EZ1(J+1) = TEMP;
    end
end
end % Y LOOP
end % Z LOOP
end % TIME LOOP
toc

figure(3),plot(6:34,EY1(6:34),'.-')
ylabel('Computed |E_y|/|E_i_n_c|')
xlabel('j')
grid on
figure(4),plot(5:34,EZ1(5:34),'.-')
ylabel('Computed |E_z|/|E_i_n_c|')
xlabel('j')
grid on

```

Figure 3.31

(Cont.) Computer program for FDTD three-dimensional scattering problem.

Figure 3.32 illustrates the results of the program. The values of $|E_y|$ and $|E_z|$ near the sphere axis are plotted against j for observation period $460 \leq n \leq 500$. The computed results are compared with Mie's exact solution [82] covered in Section 2.8. The code for calculating the exact solution is also found in Bemmel's work [80].

3.9 Absorbing Boundary Conditions for FDTD

The finite-difference time-domain (FDTD) method is a robust, flexible (adaptable to complex geometries), efficient, versatile, easy-to-understand, easy-to-implement, and user-friendly technique to solve Maxwell's equations in the time domain. Although the method did not receive as much attention as it deserved when it was suggested, it is now becoming the most popular method of choice in computational EM. It is finding widespread use for solving open-region scattering, radiation, penetration/absorption, electromagnetic interference (EMI), electromagnetic compatibility (EMC), diffusion, transient, bioelectromagnetics, and microwave circuit modeling problems. However, the method exhibits some problems such as slow convergence for solving resonant

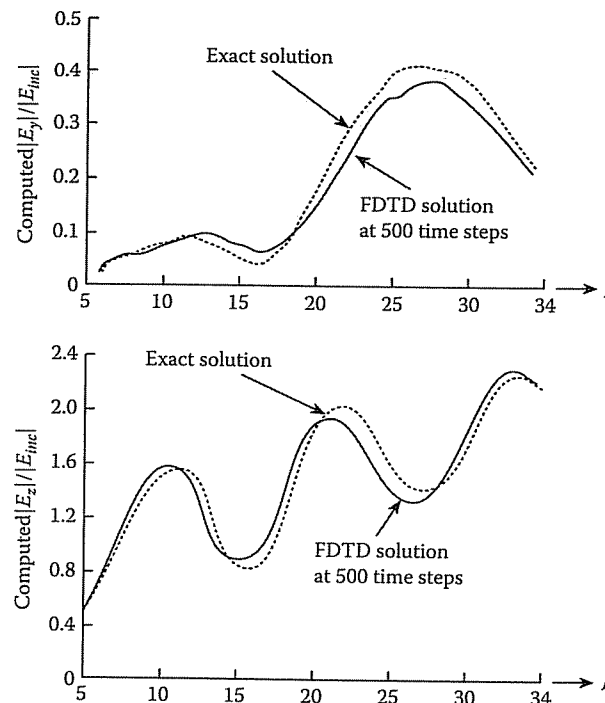


Figure 3.32

Computed $E_y(19.5, j, 18)$ and $E_z(19, j, 18.5)$ within the lossless dielectric sphere.

structures, requirement of large memory for inhomogeneous waveguide structures due to the necessity of a full-wave analysis, inability to properly handle curved boundaries due to its orthogonal nature, low stability, and low accuracy unless fine mesh is used, to mention a few. These problems prohibit the application of the standard FDTD technique and have led to various forms of its modifications [83]–[93] and hybrid FDTD methods [94]–[96]. Although these new FDTD methods have enhanced the standard FDTD (increase accuracy and stability, etc.), some researchers still prefer the standard FDTD.

One of the major problems inherent in the standard FDTD, however, is the requirement for artificial mesh truncation (boundary) condition. The artificial termination truncates the solution region electrically close to the radiating/scattering object but effectively simulates the solution to infinity. These artificial termination conditions are known as *absorbing boundary conditions* (ABCs) as they theoretically absorb incident and scattered fields. The accuracy of the ABC dictates the accuracy of the FDTD method. The need for accurate ABCs has resulted in various types of ABCs [97]–[107], which are fully discussed in [104]. Due to space limitation, we will consider only Berenger's *perfectly matched layer* (PML) type of ABC [100]–[104].

3.9. ABSORBING BOUNDARY CONDITIONS FOR FDTD

Since PML has been the most widely accepted and is set to revolutionize the FDTD method.

In the PML truncation technique, an artificial layer of absorbing material is placed around the outer boundary of the computational domain. The goal is to ensure that a plane wave that is incident from FDTD free space to the PML region at an arbitrary angle is completely absorbed there without reflection. This is the same as saying that there is complete transmission of the incident plane wave at the interface between free space and the PML region (see Figure 3.33). Thus the FDTD and the PML region are said to be *perfectly matched*.

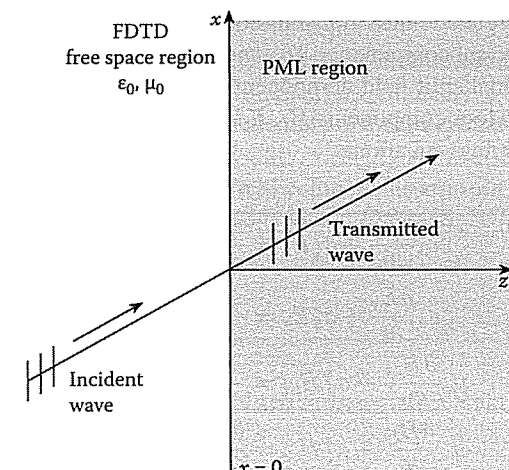


Figure 3.33

Reflectionless transmission of a plane wave at a PML/free-space interface.

To illustrate the PML technique, consider Maxwell's equation in two dimensions for transverse electric (TE) case with field components E_x , E_y and H_z and no variation with z . Expanding Equations (1.22c) and (1.22d) in Cartesian coordinates and setting $E_z = 0 = \frac{\partial}{\partial z}$, we obtain

$$\epsilon_0 \frac{\partial E_x}{\partial t} + \sigma E_x = \frac{\partial H_z}{\partial y} \quad (3.107a)$$

$$\epsilon_0 \frac{\partial E_y}{\partial t} + \sigma E_y = -\frac{\partial H_z}{\partial x} \quad (3.107b)$$

$$\mu_0 \frac{\partial H_z}{\partial t} + \sigma^* H_z = \frac{\partial E_x}{\partial y} - \frac{\partial E_y}{\partial x} \quad (3.107c)$$

where the PML, as a lossy medium, is characterized by an electrical conductivity σ and a magnetic conductivity σ^* . The conductivities are related as

$$\frac{\sigma}{\epsilon_0} = \frac{\sigma^*}{\mu_0} \quad (3.108)$$

This relationship ensures a required level of attenuation and forces the wave impedance of the PML to be equal to that of the free space. Thus a reflectionless transmission of a plane wave propagation across the interface is permitted. For oblique incident angles, the conductivity of the PML must have a certain anisotropy characteristic to ensure reflectionless transmission. To achieve this, the H_z component must be split into two subcomponents, H_{zx} and H_{zy} , with the possibility of assigning losses to the individual split field components. This is the cornerstone of the PML technique. It leads to four components E_x , E_y , H_{zx} , and H_{zy} and four (rather than the usual three) coupled field equations.

$$\epsilon_0 \frac{\partial E_x}{\partial t} + \sigma_y E_x = \frac{\partial (H_{zx} + H_{zy})}{\partial y} \quad (3.109a)$$

$$\epsilon_0 \frac{\partial E_y}{\partial t} + \sigma_x E_y = -\frac{\partial (H_{zx} + H_{zy})}{\partial x} \quad (3.109b)$$

$$\mu_0 \frac{\partial H_{zx}}{\partial t} + \sigma_x^* H_{zx} = -\frac{\partial E_y}{\partial x} \quad (3.109c)$$

$$\mu_0 \frac{\partial H_{zy}}{\partial t} + \sigma_y^* H_{zy} = \frac{\partial E_x}{\partial y} \quad (3.109d)$$

These equations can be discretized to provide the FDTD time-stepping equations for the PML region. The standard Yee time-stepping cannot be used because of the rapid attenuation to outgoing waves afforded by a PML medium. We use the exponentially differenced equations to preclude any possibility of diffusion instability. In the usual FDTD notations, the resulting four time-stepping equations for the PML region are [101]:

$$E_x^{n+1}(i+1/2, j) = e^{-\sigma_y(j)\delta t/\epsilon_0} E_x^n(i+1/2, j) \\ + \frac{(1 - e^{-\sigma_y(j)\delta t/\epsilon_0})}{\sigma_y(j)\delta} [H_{zx}^{n+1/2}(i+1/2, j+1/2) + H_{zy}^{n+1/2}(i+1/2, j+1/2) \\ - H_{zx}^{n+1/2}(i+1/2, j-1/2) - H_{zy}^{n+1/2}(i+1/2, j-1/2)] \quad (3.110a)$$

$$E_y^{n+1}(i, j+1/2) = e^{-\sigma_x(i)\delta t/\epsilon_0} E_y^n(i, j+1/2, k) \\ + \frac{(1 - e^{-\sigma_x(i)\delta t/\epsilon_0})}{\sigma_x(i)\delta} [H_{zx}^{n+1/2}(i-1/2, j+1/2) + H_{zy}^{n+1/2}(i-1/2, j+1/2) \\ - H_{zx}^{n+1/2}(i+1/2, j+1/2) - H_{zy}^{n+1/2}(i+1/2, j+1/2)] \quad (3.110b)$$

$$H_{zx}^{n+1/2}(i+1/2, j+1/2) = e^{-\sigma_x^*(i+1/2)\delta t/\mu_0} H_{zx}^{n-1/2}(i+1/2, j+1/2) \\ + \frac{(1 - e^{-\sigma_x^*(i+1/2)\delta t/\mu_0})}{\sigma_x^*(i+1/2)\delta} [E_y^n(i, j+1/2) - E_y^n(i+1, j+1/2)] \quad (3.110c)$$

$$H_{zy}^{n+1/2}(i+1/2, j+1/2) = e^{-\sigma_y^*(i+1/2)\delta t/\mu_0} H_{zy}^{n-1/2}(i+1/2, j+1/2) \\ + \frac{(1 - e^{-\sigma_y^*(i+1/2)\delta t/\mu_0})}{\sigma_y^*(i+1/2)\delta} [E_x^n(i+1/2, j+1) - E_x^n(i+1/2, j)] \quad (3.110d)$$

These equations can be directly implemented in an FDTD simulation to model PML medium. All that is required is to select the depth of the PML and its conductivity. In theory, the PML could be δ deep and have near-infinite conductivity. It has been shown, however, that increasing the conductivity gradually with depth minimizes reflections; hence the “layering” of the medium and the dependence of σ on i and j .

The TM case can be obtained by duality, with E_z split so that $E_z = E_{zx} + E_{zy}$. In three dimensions, all six Cartesian field components are split so that the resulting PML modification of Maxwell’s equations yields 12 equations [104].

3.10 Finite Differencing for Nonrectangular Systems

So far in this chapter, we have considered only rectangular solution regions within which a rectangular grid can be readily placed. Although we can always replace a nonrectangular solution region by an approximate rectangular one, our discussion in this chapter would be incomplete if we failed to apply the method to nonrectangular coordinates since it is sometimes preferable to use these coordinates. We will demonstrate the finite differencing technique in cylindrical coordinates (ρ, ϕ, z) and spherical coordinates (r, θ, ϕ) by solving Laplace’s equation $\nabla^2 V = 0$. The idea is readily extended to other PDEs.

3.10.1 Cylindrical Coordinates

Laplace’s equation in cylindrical coordinates can be written as

$$\nabla^2 V = \frac{\partial^2 V}{\partial \rho^2} + \frac{1}{\rho} \frac{\partial V}{\partial \rho} + \frac{1}{\rho^2} \frac{\partial^2 V}{\partial \phi^2} + \frac{\partial^2 V}{\partial z^2}, \quad (3.111)$$

Refer to the cylindrical system and finite difference molecule shown in Figure 3.34. At point $O(\rho_o, \phi_o, z_o)$, the equivalent finite difference approximation is

$$\frac{V_1 - 2V_o + V_2}{(\Delta\rho)^2} + \frac{1}{\rho_o} \frac{V_1 - V_2}{2\Delta\rho} + \frac{V_3 - 2V_o + V_4}{(\rho_o \Delta\phi)^2} + \frac{V_5 - 2V_o + V_6}{(\Delta z)^2} = 0 \quad (3.112)$$

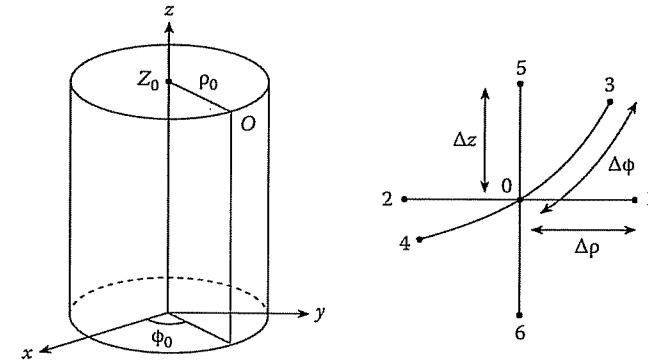


Figure 3.34
Typical node in cylindrical coordinate.

where $\Delta\rho$, $\Delta\phi$, and Δz are the step sizes along ρ , ϕ , and z , respectively, and

$$\begin{aligned} V_o &= V(\rho_o, \phi_o, z_o), \quad V_1 = V(\rho_o + \Delta\rho, \phi_o, z_o), \quad V_2 = V(\rho_o - \Delta\rho, \phi_o, z_o), \\ V_3 &= V(\rho_o, \phi_o + \rho_o \Delta\phi, z_o), \quad V_4 = V(\rho_o, \phi_o - \rho_o \Delta\phi, z_o), \\ V_5 &= V(\rho_o, \phi_o, z_o + \Delta z), \quad V_6 = V(\rho_o, \phi_o, z_o - \Delta z) \end{aligned} \quad (3.113)$$

We now consider a special case of Equation (3.112) for an axisymmetric system [108]. In this case, there is no dependence on ϕ so that $V = V(\rho, z)$. If we assume square nets so that $\Delta\rho = \Delta z = h$, the solution region is discretized as in Figure 3.35 and Equation (3.112) becomes

$$\left(1 + \frac{h}{2\rho_o}\right)V_1 + \left(1 - \frac{h}{2\rho_o}\right)V_2 + V_5 + V_6 - 4V_o = 0 \quad (3.114)$$

If point O is at $(\rho_o, z_o) = (ih, jh)$, then

$$1 + \frac{h}{2\rho_o} = \frac{2i+1}{2i}, \quad 1 - \frac{h}{2\rho_o} = \frac{2i-1}{2i}$$

so that Equation (3.114) becomes

$$V(i, j) = \frac{1}{4} \left[V(i, j-1) + V(i, j+1) + \left(\frac{2i-1}{2i}\right) V(i-1, j) + \left(\frac{2i+1}{2i}\right) V(i+1, j) \right] \quad (3.115)$$

Notice that in Equation (3.114), it appears we have a singularity for $\rho_o = 0$. However, by symmetry, all odd order derivatives must be zero. Hence

$$\left. \frac{\partial V}{\partial \rho} \right|_{\rho=0} = 0 \quad (3.116)$$

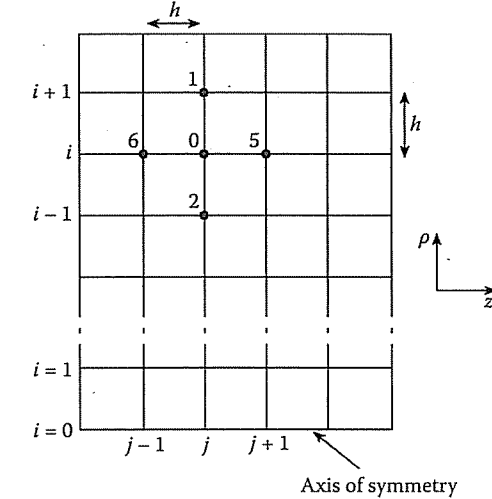


Figure 3.35
Finite difference grid for an axisymmetric system.

since

$$V(\Delta\rho, z_o) = V(-\Delta\rho, z_o) \quad (3.117)$$

Therefore by L'Hopital's rule,

$$\lim_{\rho_o \rightarrow 0} \frac{1}{\rho_o} \frac{\partial V}{\partial \rho} \Big|_{\rho_o} = \frac{\partial^2 V}{\partial \rho^2} \Big|_{\rho_o} \quad (3.118)$$

Thus, at $\rho = 0$, Laplace's equation becomes

$$2 \frac{\partial^2 V}{\partial \rho^2} + \frac{\partial^2 V}{\partial z^2} = 0 \quad (3.119)$$

The finite difference equivalent to Equation (3.119) is

$$V_o = \frac{1}{6}(4V_1 + V_5 + V_6)$$

or

$$V(0, j) = \frac{1}{6} [V(0, j-1) + V(0, j+1) + 4V(1, j)] \quad (3.120)$$

which is used at $\rho = 0$.

To solve Poisson's equation $\nabla^2 V = -\rho_v/\epsilon$ in cylindrical coordinates, we obtain the finite difference form by replacing zero on the right-hand side of Equation (3.112) with $g = -\rho_v/\epsilon$. We obtain

$$V(i, j) = \frac{1}{4} \left[V(i, j+1) + V(i, j-1) + \frac{2i-1}{2i} V(i-1, j) + \frac{2i+1}{2i} V(i+1, j) + gh^2 g \right] \quad (3.121)$$

where h is the step size.

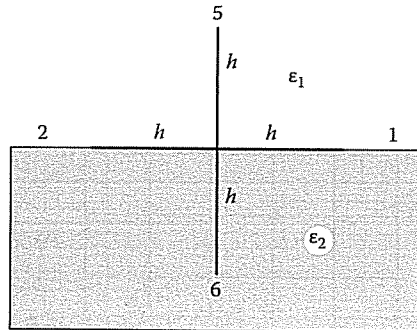


Figure 3.36
Interface between two dielectric media.

As in Section 3.7.1, the boundary condition $D_{1n} = D_{2n}$ must be imposed at the interface between two media. As an alternative to applying Gauss's law as in Section 3.7.1, we will apply Taylor series expansion [109]. Applying the series expansion to point 1, 2, 5 in medium 1 in Figure 3.36, we obtain

$$\begin{aligned} V_1 &= V_o + \frac{\partial V_o^{(1)}}{\partial \rho} h + \frac{\partial^2 V_o^{(1)}}{\partial \rho^2} \frac{h^2}{2} + \dots \\ V_2 &= V_o - \frac{\partial V_o^{(1)}}{\partial \rho} h + \frac{\partial^2 V_o^{(1)}}{\partial \rho^2} \frac{h^2}{2} - \dots \\ V_5 &= V_o + \frac{\partial V_o^{(1)}}{\partial z} h + \frac{\partial^2 V_o^{(1)}}{\partial z^2} \frac{h^2}{2} + \dots \end{aligned} \quad (3.122)$$

where superscript (1) denotes medium 1. Combining Equations (3.111) and (3.122) results in

$$h^2 \nabla^2 V = V_1 + V_2 + 2V_5 - 4V_o - 2h \frac{\partial V_o^{(1)}}{\partial z} + \frac{h(V_1 - V_2)}{2\rho_o} = 0$$

or

$$\frac{\partial V_o^{(1)}}{\partial z} = \frac{V_1 + V_2 + 2V_5 - 4V_o + \frac{h(V_1 - V_2)}{2\rho_o}}{2h} \quad (3.123)$$

Similarly, applying Taylor series to points 1, 2, and 6 in medium 2, we get

$$\begin{aligned} V_1 &= V_o + \frac{\partial V_o^{(1)}}{\partial \rho} h + \frac{\partial^2 V_o^{(1)}}{\partial \rho^2} \frac{h^2}{2} + \dots \\ V_2 &= V_o - \frac{\partial V_o^{(1)}}{\partial \rho} h + \frac{\partial^2 V_o^{(1)}}{\partial \rho^2} \frac{h^2}{2} - \dots \\ V_6 &= V_o - \frac{\partial V_o^{(2)}}{\partial z} h + \frac{\partial^2 V_o^{(2)}}{\partial z^2} \frac{h^2}{2} - \dots \end{aligned} \quad (3.124)$$

3.10. FINITE DIFFERENCING FOR NONRECTANGULAR SYSTEMS

Combining Equations (3.111) and (3.124) leads to

$$h^2 \nabla^2 V = V_1 + V_2 + 2V_6 - 4V_o - 2h \frac{\partial V_o^{(2)}}{\partial z} + \frac{h(V_1 - V_2)}{2\rho_o} = 0$$

or

$$-\frac{\partial V_o^{(2)}}{\partial z} = \frac{V_1 + V_2 + 2V_6 - 4V_o + \frac{h(V_1 - V_2)}{2\rho_o}}{2h} \quad (3.125)$$

But $D_{1n} = D_{2n}$ or

$$\epsilon_1 \frac{\partial V_o^{(1)}}{\partial z} = \epsilon_2 \frac{\partial V_o^{(2)}}{\partial z} \quad (3.126)$$

Substituting Equations (3.123) and (3.125) into Equation (3.126) and solving for V_o yields

$$V_o = \frac{1}{4} \left(1 + \frac{h}{2\rho_o} \right) V_1 + \frac{1}{4} \left(1 - \frac{h}{2\rho_o} \right) V_2 + \frac{\epsilon_1}{2(\epsilon_1 + \epsilon_2)} V_5 + \frac{\epsilon_2}{2(\epsilon_1 + \epsilon_2)} V_6 \quad (3.127)$$

Equation (3.127) is only applicable to interface points. Notice that Equation (3.127) becomes Equation (3.114) if $\epsilon_1 = \epsilon_2$.

Typical examples of finite difference approximations for boundary points, written for square nets in rectangular and cylindrical systems, are tabulated in Table 3.9. For more examples, see [12, 110]. The FDTD has also been applied in solving time-varying axisymmetric problems [93, 111].

3.10.2 Spherical Coordinates

In spherical coordinates, Laplace's equation can be written as

$$\nabla^2 V = \frac{\partial^2 V}{\partial r^2} + \frac{2}{r} \frac{\partial V}{\partial r} + \frac{1}{r^2} \frac{\partial^2 V}{\partial \theta^2} + \frac{\cot \theta}{r^2} \frac{\partial V}{\partial \theta} + \frac{1}{r^2 \sin^2 \theta} \frac{\partial^2 V}{\partial \phi^2} = 0 \quad (3.128)$$

At a grid point $O(r_o, \theta_o, \phi_o)$ shown in Figure 3.37, the finite difference approximation to Equation (3.128) is

$$\begin{aligned} &\frac{V_1 - 2V_o + V_2}{(\Delta r)^2} + \frac{2}{r_o} \left(\frac{V_1 - V_2}{2\Delta r} \right) + \frac{V_6 - 2V_o + V_5}{(r_o \Delta \theta)^2} \\ &+ \frac{\cot \theta_o}{r_o^2} \left(\frac{V_5 - V_6}{2\Delta \theta} \right) + \frac{V_3 - 2V_o + V_4}{(r_o \Delta \phi \sin \theta_o)^2} = 0 \end{aligned} \quad (3.129)$$

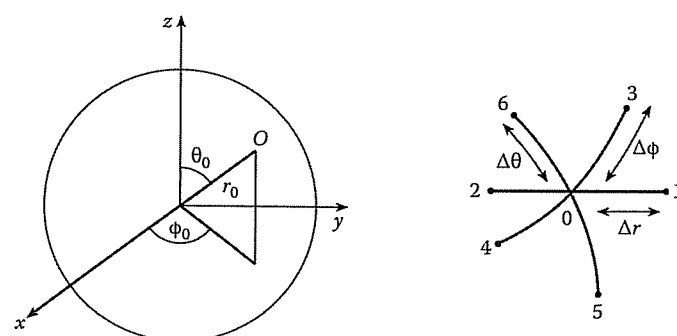
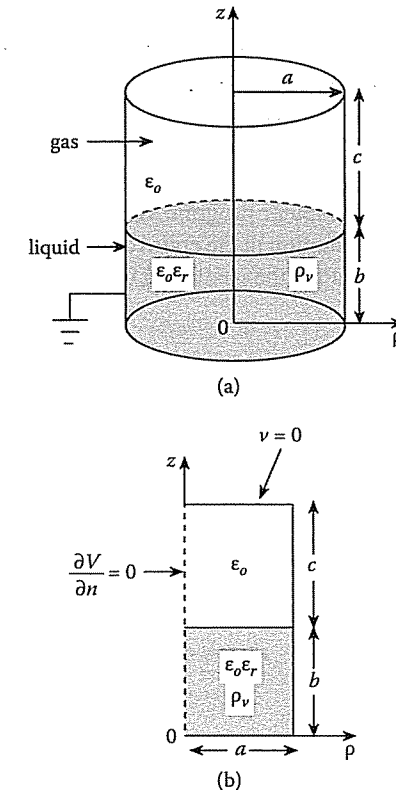
Note that θ increases from node 6 to 5, and hence we have $V_5 - V_6$ and not $V_6 - V_5$ in Equation (3.129).

Example 3.9

Consider an earthed metal cylindrical tank partly filled with a charge liquid, such as hydrocarbons, as illustrated in Figure 3.38 (a). Using the finite difference method,

Table 3.9 Finite Difference Approximations at Boundary Points

Description	Figure	Cartesian Equation	Cylindrical Equation
1. Bottom edge		$4V_0 = V_1 + V_2 + 2V_3$	$4V_0 = V_1 + V_2 + 4V_3$
2. Top edge		$4V_0 = V_1 + V_2 + 2V_4$	$4V_0 = V_1 + V_2 + 2V_3$
3. Left edge		$4V_0 = 2V_2 + V_3 + V_4$	$8V_0 = 4V_2 + \left(\frac{2i+1}{i}\right)V_3 + \left(\frac{2i-1}{i}\right)V_4$
4. Right edge		$4V_0 = 2V_2 + V_3 + V_4$	$8V_0 = 4V_2 + \left(\frac{2i+1}{i}\right)V_3 + \left(\frac{2i-1}{i}\right)V_4$
5. Bottom left corner point		$2V_0 = V_1 + V_3$	$3V_0 = V_1 + 2V_3$
6. Bottom right corner point		$2V_0 = V_2 + V_3$	$3V_0 = V_2 + 2V_3$
7. Top left corner point		$2V_0 = V_1 + V_4$	$3V_0 = V_1 + 2V_4$
8. Top right corner point		$2V_0 = V_2 + V_4$	$3V_0 = V_2 + 2V_4$

**Figure 3.37**
Typical node in spherical coordinates.**Figure 3.38**
For Example 3.9: (a) earthed cylindrical tank, (b) solution region.

determine the potential distribution in the entire domain. Plot the potential along $\rho = 0.5$, $0 < z < 2$ m and on the surface of the liquid. Take

$$\begin{aligned} a &= b = c = 1.0 \text{ m}, \\ \epsilon_r &= 2.0 \text{ (hydrocarbons)}, \\ \rho_v &= 10^{-5} \text{ C/m}^3 \quad \square \end{aligned}$$

Solution

The exact analytic solution to this problem was given in Section 2.7.2. ■

It is apparent from Figure 3.38 (a) and from the fact that ρ_v is uniform that $V = V(\rho, z)$ (i.e., the problem is two-dimensional) and the domain of the problem is symmetrical about the z -axis. Therefore, it is only necessary to investigate the solution region in Figure 3.38 (b) and impose the condition that the z -axis is a flux line, i.e., $\partial V / \partial n = \partial V / \partial \rho = 0$.

The finite difference grid of Figure 3.35 is used with $0 \leq i \leq I_{\max}$ and $0 \leq j \leq J_{\max}$. Choosing $\Delta\rho = \Delta z = h = 0.05$ m makes $I_{\max} = 20$ and $J_{\max} = 40$. Equation (3.115) is applied for gas space, and Equation (3.121) for liquid space. Along the z -axis, i.e., $i = 0$, we impose the Neumann condition in Equation (3.120). To account for the fact that the gas has dielectric constant $\epsilon_r 1$ while the liquid has $\epsilon_r 2$, we impose the boundary condition in Equation (3.127) on the liquid-gas interface.

Based on these ideas, the computer program shown in Figure 3.39 was developed to determine the potential distribution in the entire domain. The values of the potential along $\rho = 0.5$, $0 < z < 2$ and along the gas-liquid interface are plotted in Figure 3.40.

```
%%%%%%
% MATLAB CODE FOR EXAMPLE 3.9:
% AN AXISYMMETRIC PROBLEM OF AN EARTHED CYLINDER PARTIALLY FILLED WITH
% CHARGED LIQUID SOLVED USING FINITE DIFFERENCE SCHEME
%%%%%

A=1; % Radius of cylindrical tank (meters)
B=1; % Height of liquid in tank
C=1; % Height of gas in tank

ER1=1;ER2=2;EO=8.854E-12; %dielectric parameters

H = 0.05; %spacial step size
NA = A/H; %number of points along A
NB = B/H; %number of points along B
NC = C/H; %number of points along C
NBC = NB + NC; %%number of points along B & C
NMAX = 500; %number of iterations
RHOV = 1E-5;
G = -RHOV/(ER2*EO);
GH2 = G*H^2;

%INITIALIZE - THIS ALSO TAKES CARE OF DIRICHLET CONDITIONS
V = zeros(NA+1,NBC+1); %V(radius, height)

%NOW, APPLY FINITE DIFFERENCE SCHEME

for N = 1:NMAX
    for I = 2:NA %step through radius
        FM = (2*(I-1) - 1)/(2*(I-1)); %note that indicie starts at 1 instead of 0
        FP = (2*(I-1) + 1)/(2*(I-1));

```

Figure 3.39
MATLAB code for Example 3.9 (*Continued*).

```
%step through liquid (z+ direction)
for J = 2:NB
    V(I,J) = 0.25*( V(I,J-1) + V(I,J+1)...
        + FM*V(I-1,J) + FP*V(I+1,J) - GH2 );
end

%step through gas (z+ direction)
for J = NB+2:NBC
    V(I,J) = 0.25*( V(I,J-1) + V(I,J+1)...
        + FM*V(I-1,J) + FP*V(I+1,J) );
end

%ALONG THE GASS-LIQUID INTERFACE
V(I,NB+1) = 0.5*( V(I,NB+2)*ER1/(ER1+ER2)+...
    V(I,NB)*ER2/(ER1+ER2) )...
    + 0.25*(FM*V(I-1,NB+1)+FP*V(I+1,NB+1) );
end

%IMPOSE NEUMANN CONDITION ALONG THE Z-AXIS
for J = 2:NBC
    V(1,J) = ( 4.0*V(2,J) + V(1,J-1)+V(1,J+1))/6.0;
end

% OUTPUT THE POTENTIAL ALONG RHO = 0.5, 0 < Z < 1.0
NR5 = 0.5/H;

radius = 0:H:A;
height = 0:H:(B+C);

figure(1),
    subplot(211),
        plot(height,V(NR5+1,(0:NBC)+1)/1000.0)
        ylabel('V(kV)')
        title('Potential distribution in the tank of Figure 3.38 along \rho=0.5m')
    subplot(212)
        plot(radius ,V((0:NA)+1,NB+1)/1000.0)
        title('Potential distribution in the tank of Figure 3.38 along gas-liquid interface')
        ylabel('V(kV)')

figure(2),surf(height,radius,V/1000)
ylabel('radius in tank')
xlabel('height in tank')
zlabel('Potential (kV)')
```

Figure 3.39
(*Cont.*) MATLAB code for Example 3.9.

It is evident from the figure that the finite difference solution compares well with the exact solution in Section 2.7.2. It is the simplicity in concept and ease of programming finite difference schemes that make them very attractive for solving problems such as this.

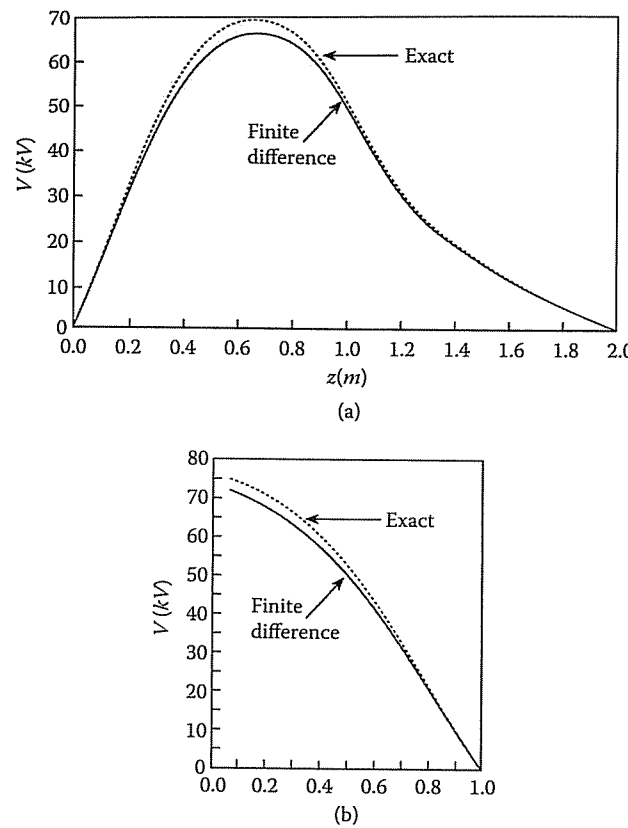


Figure 3.40

Potential distribution in the tank of Figure 3.38: (a) along $\rho = 0.5$ m, $0 \leq z \leq 2$ m; (b) along the gas-liquid interface.

3.11 Numerical Integration

Numerical integration (also called *numerical quadrature*) is used in science and engineering whenever a function cannot easily be integrated in closed form or when the function is described in the form of discrete data. Integration is a more stable and reliable process than differentiation. The term *quadrature* or *integration rule* will be used to indicate any formula that yields an integral approximation. Several integration rules have been developed over the years. The common ones include

1. Euler's rule,
2. Trapezoidal rule,

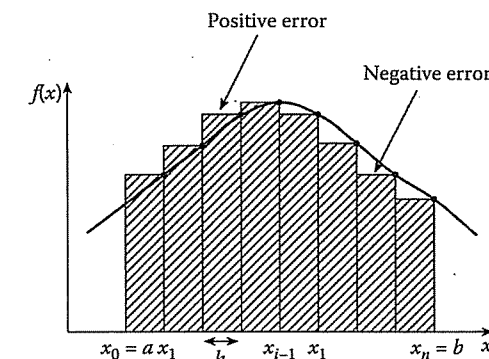


Figure 3.41
Integration using Euler's rule.

3. Simpson's rule,
4. Newton-Cotes rules, and
5. Gaussian (quadrature) rules.

The first three are simple and will be considered first to help build up background for other rules which are more general and accurate. A discussion on the subject of numerical integration with diverse FORTRAN codes can be found in Davis and Rabinowitz [112]. A program package called QUADPACK for automatic integration covering a wide variety of problems and various degrees of difficulty is presented in Piessens et al. [113]. Our discussion will be brief but sufficient for the purpose of this text.

3.11.1 Euler's Rule

To apply the Euler or rectangular rule in evaluating the integral

$$I = \int_a^b f(x) dx, \quad (3.130)$$

where $f(x)$ is shown in Figure 3.41, we seek an approximation for the area under the curve. We divide the curve into n equal intervals as shown in Figure 3.41. The subarea under the curve within $x_{i-1} < x < x_i$ is

$$A_i = \int_{x_{i-1}}^{x_i} f(x) dx \simeq h f_i \quad (3.131)$$

where $f_i = f(x_i)$. The total area under the curve is

$$\begin{aligned} I &= \int_a^b f(x) dx \simeq \sum_{i=1}^n A_i \\ &= h [f_1 + f_2 + \cdots + f_n] \end{aligned}$$

or

$$I = h \sum_{i=1}^n f_i \quad (3.132)$$

It is clear from Figure 3.41 that this quadrature method gives an inaccurate result since each A_i is less or greater than the true area introducing negative or positive error, respectively.

3.11.2 Trapezoidal Rule

To evaluate the same integral in Equation (3.130) using the trapezoidal rule, the subareas are chosen as shown in Figure 3.42. For the interval $x_{i-1} < x < x_i$,

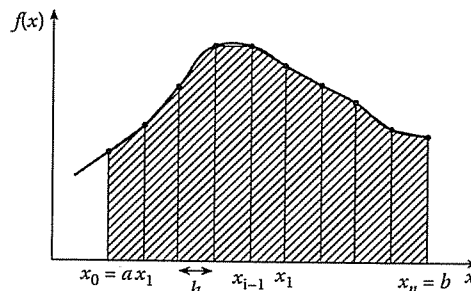


Figure 3.42
Integration using the trapezoidal rule.

$$A_i = \int_{x_{i-1}}^{x_i} f(x) dx \simeq \left(\frac{f_{i-1} + f_i}{2} \right) h \quad (3.133)$$

Hence

$$\begin{aligned} I &= \int_a^b f(x) dx \simeq \sum_{i=1}^n A_i \\ &= h \left[\frac{f_0 + f_1}{2} + \frac{f_1 + f_2}{2} + \dots + \frac{f_{n-2} + f_{n-1}}{2} + \frac{f_{n-1} + f_n}{2} \right] \\ &= \frac{h}{2} [f_0 + 2f_1 + 2f_2 + \dots + 2f_{n-1} + f_n] \end{aligned}$$

or

$$I = h \sum_{i=1}^{n-1} f_i + \frac{h}{2} (f_0 + f_n) \quad (3.134)$$

3.11. NUMERICAL INTEGRATION

3.11.3 Simpson's Rule

Simpson's rule gives a still more accurate result than the trapezoidal rule. While the trapezoidal rule approximates the curve by connecting successive points on the curve by straight lines, Simpson's rule connects successive groups of three points on the curve by a second-degree polynomial (i.e., a parabola). Thus

$$A_i = \int_{x_{i-1}}^{x_i} f(x) dx \simeq \frac{h}{3} (f_{i-1} + 4f_i + f_{i+1}) \quad (3.135)$$

Therefore

$$\begin{aligned} I &= \int_a^b f(x) dx \simeq \sum_{i=1}^n A_i \\ &= \frac{h}{3} [f_0 + 4f_1 + 2f_2 + 4f_3 + \dots + 2f_{n-2} + 4f_{n-1} + f_n] \end{aligned} \quad (3.136)$$

where n is even.

The computational molecules for Euler's, trapezoidal, and Simpson's rules are shown in Figure 3.43. Now that we have considered simple quadrature rules to help build up background, we now consider more general, accurate methods.

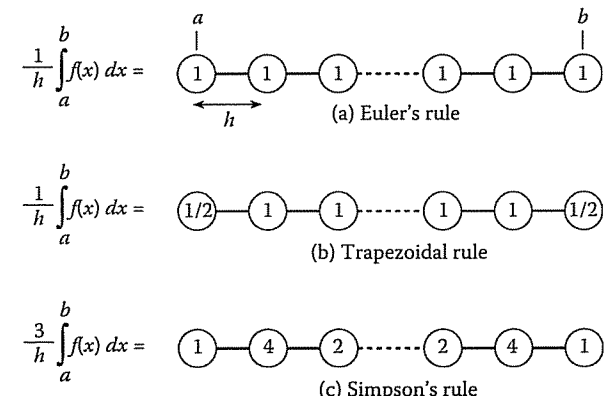


Figure 3.43
Computational molecules for integration.

3.11.4 Newton-Cotes Rules

To apply a Newton-Cotes rule to evaluate the integral in Equation (3.130), we divide the interval $a < x < b$ into m equal intervals so that

$$h = \frac{b-a}{m} \quad (3.137)$$

where m is a multiple of n , and n is the number of intervals covered at a time or the order of the approximating polynomial. The subarea in the interval $x_{n(i-1)} < x < x_{ni}$

is

$$A_i = \int_{x_{n(i-1)}}^{x_n} f(x) dx \simeq \frac{nh}{N} \sum_{k=0}^n C_k^n f(x_{n(i-1)+k}) \quad (3.138)$$

The coefficients C_k^n , $0 \leq k \leq n$, are called Newton–Cotes numbers and tabulated in Table 3.10. The numbers are obtained from

$$C_k^n = \frac{1}{n} \int_0^N L_k(s) ds \quad (3.139)$$

where

$$L_k(s) = \prod_{j=0, j \neq k}^n \frac{s - j}{k - j} \quad (3.140)$$

It is easily shown that the coefficients are symmetric, i.e.,

$$C_k^n = C_{n-k}^n \quad (3.141a)$$

and they sum up to unity, i.e.,

$$\sum_{k=0}^n C_k^n = 1 \quad (3.141b)$$

Table 3.10 Newton–Cotes Numbers

n	N	NC_o^n	NC_1^n	NC_2^n	NC_3^n	NC_4^n	NC_5^n	NC_6^n	NC_7^n	NC_8^n
1	2	1	1							
2	6	1	4	1						
3	8	1	3	3	1					
4	90	7	32	12	32	7				
5	288	19	75	50	50	75	19			
6	840	41	216	27	272	27	216	41		
7	17280	751	3577	1323	2989	2989	1323	3577	751	
8	24350	989	5888	-928	10946	-4540	10946	-928	5888	989

For example, for $n = 2$,

$$\begin{aligned} C_0^2 &= \frac{1}{2} \int_0^6 \frac{(s-1)(s-2)}{(-1)(-2)} ds = \frac{1}{6}, \\ C_1^2 &= \frac{1}{2} \int_0^6 \frac{s(s-2)}{1(-1)} ds = \frac{4}{6}, \\ C_2^2 &= \frac{1}{2} \int_0^6 \frac{s(s-1)}{2(1)} ds = \frac{1}{6} \end{aligned}$$

Once the subareas are found using Equation (3.138), then

$$I = \int_a^b f(x) dx \simeq \sum_{i=1}^{m/n} A_i \quad (3.142)$$

3.11. NUMERICAL INTEGRATION

The most widely known Newton–Cotes formulas are

$n = 1$ (2-point; trapezoidal rule)

$$A_i \simeq \frac{h}{2} (f_{i+1} + f_i), \quad (3.143)$$

$n = 2$ (3-point; Simpson's 1/3 rule)

$$A_i \simeq \frac{h}{3} (f_{i-1} + 4f_i + f_{i+1}), \quad (3.144)$$

$n = 3$ (4-point; Newton's rule)

$$A_i \simeq \frac{3h}{8} (f_i + 3f_{i+1} + 3f_{i+2} + f_{i+3}) \quad (3.145)$$

3.11.5 Gaussian Rules

The integration rules considered so far involve the use of equally spaced abscissa points. The idea of integration rules using unequally spaced abscissa points stems from Gauss. The Gaussian rules are more complicated but more accurate than the Newton–Cotes rules. A Gaussian rule has the general form

$$\boxed{\int_a^b f(x) dx \simeq \sum_{i=1}^n w_i f(x_i)} \quad (3.146)$$

where (a, b) is the interval for which a sequence of orthogonal polynomials $\{w_i(x)\}$ exists, x_i are the zeros of $w_i(x)$, and the weights w_i are such that Equation (3.146) is of degree of precision $2n - 1$. Any of the orthogonal polynomials discussed in Chapter 2 can be used to give a particular Gaussian rule. Commonly used rules are Gauss–Legendre, Gauss–Chebyshev, etc., since the sample points x_i are the roots of the Legendre, Chebyshev, etc., of degree n . For the Legendre ($n = 1$ to 16) and Laguerre ($n = 1$ to 16) polynomials, the zeros x_i and weights w_i have been tabulated in [114].

Using Gauss–Legendre rule,

$$\int_a^b f(x) dx \simeq \frac{b-a}{2} \sum_{i=1}^n w_i f(u_i) \quad (3.147)$$

where $u_i = \frac{b-a}{2} x_i + \frac{b+a}{2}$ are the transformation of the roots x_i of Legendre polynomials from limits $(-1, 1)$ to finite limits (a, b) . The values of the abscissas x_i and weights w_i for n up to 7 are presented in Table 3.11; for higher values of n , the interested reader is referred to [114, 115]. Note that $-1 < x_i < 1$ and $\sum_{i=1}^n w_i = 2$.

The Gauss–Chebyshev rule is similar to the Gauss–Legendre rule. We use Equation (3.147) except that the sample points x_i , the roots of Chebyshev polynomial $T_n(x)$, are

$$x_i = \cos \frac{(2i-1)}{2n}, \quad i = 1, 2, \dots, n \quad (3.148)$$

Table 3.11 Abscissas (Roots of Legendre Polynomials) and Weights for Gauss-Legendre Integration

$\pm x_i$	w_i
0.57735 02691 89626	$n = 2$ 1.00000 00000 00000
0.00000 00000 00000	$n = 3$ 0.88888 88888 88889
0.77459 66692 41483	0.55555 55555 55556
0.33998 10435 84856	$n = 4$ 0.65214 51548 62546
0.86113 63115 94053	0.34785 48451 37454
0.00000 00000 00000	$n = 5$ 0.56888 88888 88889
0.53846 93101 05683	0.47862 86704 99366
0.90617 98459 38664	0.23692 68850 56189
0.23861 91860 83197	$n = 6$ 0.46791 39345 72691
0.66120 93864 66265	0.36076 15730 48139
0.93246 95142 03152	0.17132 44923 79170
0.00000 00000 00000	$n = 7$ 0.41795 91836 73469
0.40584 51513 77397	0.38183 00505 05119
0.74153 11855 99394	0.27970 53914 89277
0.94910 79123 42759	0.12948 49661 68870

and the weights are all equal [116], i.e.,

$$w_i = \frac{\pi}{n} \quad (3.149)$$

When either of the limits of integration a or b or both are $\pm\infty$, we use Gauss-Laguerre or Gauss-Hermite rule. For the Gauss-Laguerre rule,

$$\int_0^\infty f(x) dx \approx \sum_{i=1}^n w_i f(x_i) \quad (3.150)$$

where the appropriate abscissas x_i , the roots of Laguerre polynomials, and weights w_i are listed for n up to 7 in Table 3.12. For the Gauss-Hermite rule,

$$\int_{-\infty}^\infty f(x) dx \approx \sum_{i=1}^n w_i f(x_i) \quad (3.151)$$

where the abscissas x_i , the roots of the Hermite polynomials, and weights w_i are listed for n up to 7 in Table 3.13. An integral over (a, ∞) is taken care of by a change

3.11. NUMERICAL INTEGRATION

Table 3.12 Abscissas (Roots of Laguerre Polynomials) and Weights for Gauss-Laguerre Integration

$\pm x_i$	w_i
0.58578 64376 27	$n = 2$ 1.53332 603312
3.41421 35623 73	4.45095 733505
0.41577 45567 83	$n = 3$ 1.07769 285927
2.29428 03602 79	2.76214 296190
6.28994 50829 37	5.60109 462543
0.32254 76896 19	$n = 4$ 0.83273 912383
1.74576 11011 58	2.04810 243845
4.53662 02969 21	3.63114 630582
9.39507 09123 01	6.48714 508441
0.26356 03197 18	$n = 5$ 0.67909 404220
1.41340 30591 07	1.63848 787360
3.59642 57710 41	2.76944 324237
12.64080 08442 76	7.21918 635435
0.22284 66041 79	$n = 6$ 0.57353 550742
1.18893 21016 73	1.36925 259071
2.99273 63260 59	2.26068 459338
5.77514 35691 05	3.35052 458236
9.83746 74183 83	4.88682 680021
15.98287 39806 02	7.84901 594560
0.19304 36765 60	$n = 7$ 0.49647 759754
1.02666 48953 39	1.17764 306086
2.56787 67449 51	1.91824 978166
4.90035 30845 26	2.77184 863623
8.18215 34445 63	3.84124 912249
12.73418 02917 98	5.38067 820792
19.39572 78622 63	8.40543 248683

of variable so that

$$\int_a^\infty f(x) dx = \int_0^\infty f(y+a) dy \quad (3.152)$$

We apply Equation (3.146) with $f(x)$ evaluated at points $x_i + a$, $i = 1, 2, \dots, n$ and x_i s are tabulated in Table 3.12.

Table 3.13 Abscissas (Roots of Hermite Polynomials) and Weights for Gauss–Hermite Integration

$\pm x_i$	w_i
0.70710 67811 86548	1.46114 11826 611
0.00000 00000 00000	1.18163 59006 037
1.22474 48713 91589	1.32393 11752 136
n = 2	
0.52464 76232 75290	1.05996 44828 950
1.65068 01238 85785	1.24022 58176 958
n = 3	
0.00000 00000 00000	0.94530 87204 829
0.95857 24646 13819	0.98658 09967 514
2.02018 28704 56086	1.18148 86255 360
n = 4	
0.43607 74119 27617	0.87640 13344 362
1.33584 90740 13697	0.93558 05576 312
2.35060 49736 74492	1.13690 83326 745
n = 5	
0.00000 00000 00000	0.81026 46175 568
0.81628 78828 58965	0.82868 73032 836
1.67355 16287 67471	0.89718 46002 252
2.65196 13568 35233	1.10133 07296 103
n = 6	
0.43607 74119 27617	0.87640 13344 362
1.33584 90740 13697	0.93558 05576 312
2.35060 49736 74492	1.13690 83326 745
n = 7	
0.00000 00000 00000	0.81026 46175 568
0.81628 78828 58965	0.82868 73032 836
1.67355 16287 67471	0.89718 46002 252
2.65196 13568 35233	1.10133 07296 103

A major drawback with Gaussian rules is that if one wishes to improve the accuracy, one must increase n which means that the values of w_i and x_i must be included in the program for each value of n . Another disadvantage is that the function $f(x)$ must be explicit since the sample points x_i are unassigned.

3.11.6 Multiple Integration

This is an extension of one-dimensional (1D) integration discussed so far. A double integral is evaluated by means of two successive applications of the rules presented above for single integral [117]. To evaluate the integral using the Newton–Cotes or Simpson's 1/3 rule ($n = 2$), for example,

$$I = \int_a^b \int_c^d f(x, y) dx dy \quad (3.153)$$

3.11. NUMERICAL INTEGRATION

over a rectangular region $a < x < b$, $c < y < d$, we divide the region into $m \cdot l$ smaller rectangles with sides

$$h_x = \frac{b-a}{m} \quad (3.154a)$$

$$h_y = \frac{d-c}{l} \quad (3.154b)$$

where m and l are multiples of $n = 2$. The subarea

$$A_{ij} = \int_{y_{n(j-1)}}^{y_{n(j+1)}} dy \int_{x_{(i-1)}}^{x_{(i+1)}} f(x, y) dy \quad (3.155)$$

is evaluated by integrating along x and then along y according to Equation (3.144):

$$A_{ij} \approx \frac{h_x}{3} (g_{j-1} + 4g_j + g_{j+1}) \quad (3.156)$$

where

$$g_j \approx \frac{h_y}{3} (f_{i-1,j} + 4f_{i,j} + f_{i+1,j}) \quad (3.157)$$

Substitution of Equation (3.157) into Equation (3.156) yields

$$A_{ij} = \frac{h_x h_y}{9} [(f_{i+1,j+1} + f_{i+1,j-1} + f_{i-1,j+1} + f_{i-1,j-1}) + 4(f_{i,j+1} + f_{i,j-1} + f_{i+1,j} + f_{i-1,j}) + 16f_{i,j}] \quad (3.158)$$

The corresponding schematic or integration molecule is shown in Figure 3.44. Summing the value of A_{ij} for all subareas yields

$$I = \sum_{i=1}^{m/n} \sum_{j=1}^{l/n} A_{ij} \quad (3.159)$$

The procedure applied in the 2D integral can be extended to a 3D integral. To evaluate

$$I = \int_a^b \int_c^d \int_e^f f(x, y, z) dx dy dz \quad (3.160)$$

using the $n = 2$ rule, the cuboid $a < x < b$, $c < y < d$, $e < z < f$ is divided into $m \cdot l \cdot p$ smaller cuboids of sides

$$h_x = \frac{b-a}{m} \quad (3.161)$$

$$h_y = \frac{d-c}{l} \quad (3.161)$$

$$h_z = \frac{f-e}{p} \quad (3.161)$$

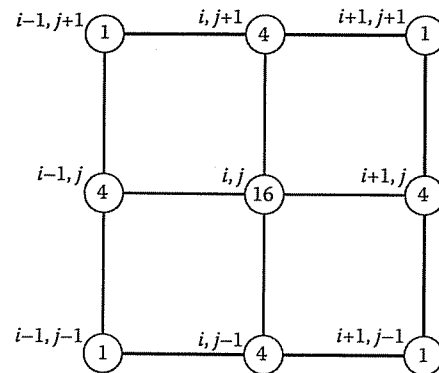


Figure 3.44
Double integration molecule for Simpson's 1/3 rule.

where m , l , and p are multiples of $n = 2$. The subvolume A_{ijk} is evaluated by integrating along x according to Equation (3.144) to obtain

$$g_{j,k} = \frac{h_x}{3} (f_{i+1,j,k} + 4f_{i,j,k} + f_{i-1,j,k}), \quad (3.162)$$

then along y to obtain

$$g_k = \frac{h_y}{3} (g_{j+1,k} + 4g_{j,k} + g_{j-1,k}), \quad (3.163)$$

and finally along z to obtain

$$A_{ijk} = \frac{h_z}{3} (g_{k+1} + 4g_k + g_{k-1}) \quad (3.164)$$

Substituting Equations (3.162) and (3.163) into Equation (3.164) results in [117]

$$\begin{aligned} A_{ijk} = & \frac{h_x h_y h_z}{27} [(f_{i-1,j-1,k+1} + 4f_{i-1,j,k+1} + f_{i-1,j+1,k+1}) \\ & + (4f_{i,j-1,k+1} + 16f_{i,j,k+1} + 4f_{i,j+1,k+1}) \\ & + (f_{i+1,j-1,k+1} + 4f_{i+1,j,k+1} + f_{i+1,j+1,k+1}) \\ & + (4f_{i-1,j-1,k} + 16f_{i-1,j,k} + 4f_{i-1,j+1,k}) \\ & + (16f_{i,j-1,k} + 64f_{i,j,k} + 16f_{i,j+1,k}) \\ & + (4f_{i+1,j-1,k} + 16f_{i+1,j,k} + 4f_{i+1,j+1,k}) \\ & + (f_{i-1,j-1,k-1} + 4f_{i-1,j,k-1} + f_{i-1,j+1,k-1}) \\ & + (4f_{i,j-1,k-1} + 16f_{i,j,k-1} + 4f_{i,j+1,k-1}) \\ & + (f_{i+1,j-1,k-1} + 4f_{i+1,j,k-1} + f_{i+1,j+1,k-1})] \end{aligned} \quad (3.165)$$

The integration molecule is portrayed in Figure 3.45. Observe that the molecule is symmetric with respect to all planes that cut the molecule in half.

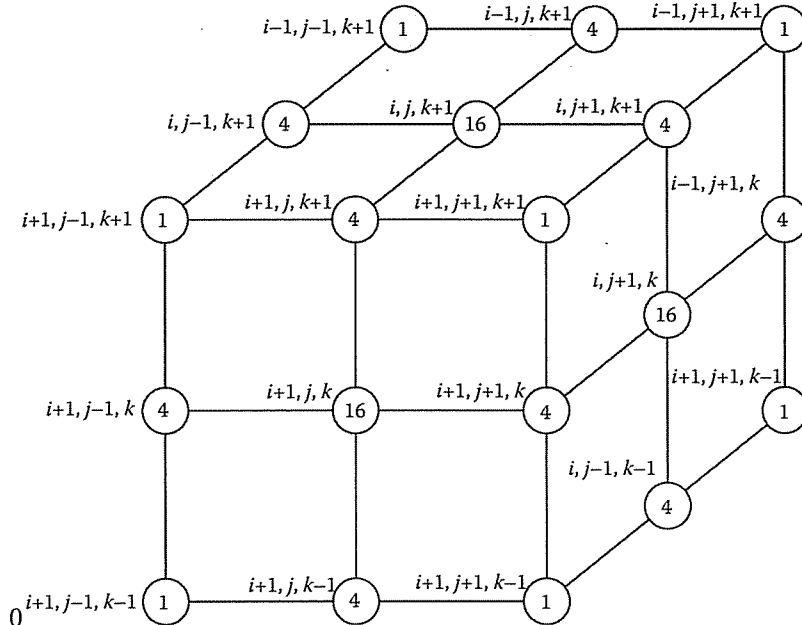


Figure 3.45
Triple integration molecule for Simpson's 1/3 rule.

Example 3.10

Write a program that uses the Newton–Cotes rule ($n = 6$) to evaluate Bessel function of order m , i.e.,

$$J_m(x) = \frac{1}{\pi} \int_0^\pi \cos(x \sin \theta - m\theta) d\theta$$

Run the program for $m = 0$ and $x = 0.1, 0.2, \dots, 2.0$. \square

Solution

The computer program is shown in Figure 3.46. The program is based on Equations (3.138) and (3.142). It evaluates the integral within a subinterval $\theta_{n(i-1)} < \theta < \theta_{ni}$. The summation over all the subintervals gives the required integral. The result for $m = 0$ and $0.1 < x < 2.0$ is shown in Table 3.14; the values agree up to six significant figures with those in standard tables [115, p. 390]. The program is intentionally made general so that n , the corresponding Newton–Cotes numbers, and the integrand can be changed easily. Although the integrand in Figure 3.46 is real, the program can be modified for complex integrand by simply declaring complex the affected variables. \blacksquare

```
% Create custom Bessel function
lwr = 0; %lower limit of integration
uppr= pi; %upper limit of integration
theta = linspace(0,pi,N+1);

for ii = 1:length(x)
    % Create function to be integrated
    A = cos(x(ii))*sin(theta)-m*theta)/pi;

    %Integrate with Newton-Cotes method
    J_m(ii) = nc_method(A,lwr,uppr,n);
end

% Difference between MATLAB and custom Bessel
compare = J-J_m;

% eps is the Spacing of floating point numbers in MATLAB.
% Any number smaller than in magnitude than eps is essentially zero
% Try 1 + eps, this is equal to 1.
v_eps = [eps, eps];
x_eps = [x(1),x(end)];

figure(1),
    subplot(211),plot(x,J,x,J_m,:')
    title('Comparison between MATLAB and Custom Bessel function')
    legend('MATLAB','Custom')
    subplot(212),plot(x,compare,'-o',x_eps,v_eps,x_eps,-v_eps)
    title('Difference between MATLAB and Custom Bessel')
    legend('difference','+eps','-eps')

%figure(2),plot(theta,A)

(a)
```

Figure 3.46

(a) Main program for Example 3.10.

```
function I = nc_method(f,a,b,n)
    % I = nc_method_fun(f,a,b,n)
    %
    % Calculates Newton-Cotes Method Quadrature
    %
    % Inputs:
    % f : data vector from function to be integrated
    % a : lower integration limit
    % b : upper integration limit
    % n : order of approximating polynomial
    %
    % Output:
    % I : Value of Integral
    %
    % NOTE that m (the number of sections) must be a multiple of the order of
    % the approximation polynomial

    m = length(f)-1; %Divide the data into m sections

    %Below checks if the requirement that m is a multiple of n
    if rem(m,n) ~= 0
        disp('Error: length(f)-1 must be a multiple of n')
        I = NaN; return
    end

    h = (b-a)/m; %step size.
    C = nc_weight(n); %Get Newton-Cotes Number.
    I = 0; %intialize I
    for ii = 1:n:m,
        ind2 = (ii:ii+n); %select indicies of function
        Ai = n*h*f(ind2)*C; %Equation (3.138)
        I = I+Ai; %Equation (3.142)
    end

    function q = nc_weight(n)
        % returns in q the weights for the N-point Newton-Cotes quadrature rule.
        % N must be between 1 and 8.

        if (n<1)
            disp('error: newton-cotes order must be at least 1!')
        elseif (n==1) % Trapezoidal rule:
            q = [1 1]/2;
        elseif (n==2) % Simpson's rule:
            q = [1 4 1]/6;
        elseif (n==3) % Simpson's 3/8 rule:
            q = [1 3 3 1]/8;
        elseif (n==4)% Boole's rule:
            q = [7 32 12 32 7]/90;
```

Figure 3.46

(b) Function for the main program in (a); for Example 3.10.

```

elseif (n==5)
    q = [19 75 50 50 75 19]'/288;
elseif (n==6)
    q = [41 216 27 272 27 216 41]'/840;
elseif (n==7)
    q = [751 3577 1323 2989 2989 1323 3577 751]'/17280;
elseif (n==8)
    q = [989 5888 -928 10496 -4540 10496 -928 5888 989]'/28350;
else
    disp('error: N must be no more than 8!')
end
(b)

```

Figure 3.46

(b) Function for the main program in (a); for Example 3.10. (Continued.)

Table 3.14 Result of the Program in Figure 3.46 for $m = 0$

x	$J_0(x)$
0.1	0.9975015
0.2	0.9900251
0.3	0.9776263
0.4	0.9603984
0.5	0.9384694
:	:
1.5	0.5118274
1.6	0.4554018
1.7	0.3979859
1.8	0.3399859
1.9	0.2818182
2.0	0.2238902

3.12 Concluding Remarks

Only a brief treatment of the finite difference analysis of PDEs is given here. There are many valuable references on the subject which answer many of the questions left unanswered here [3]–[8], [10, 104, 105]. The book by Smith [5] gives an excellent exposition with numerous examples. The problems of stability and convergence of finite difference solutions are further discussed in [118, 119], while the error estimates are discussed in [120].

As noted in Section 3.8, the finite difference method has some inherent advantages and disadvantages. It is conceptually simple and easy to program. The finite difference

3.12. CONCLUDING REMARKS

approximation to a given PDE is by no means unique; more accurate expressions can be obtained by employing more elaborate and complicated formulas. However, the relatively simple approximations may be employed to yield solutions of any specified accuracy simply by reducing the mesh size provided that the criteria for stability and convergence are met.

A very important difficulty in finite differencing of PDEs, especially parabolic and hyperbolic types, is that if one value of Φ is not calculated and therefore is set equal to zero by mistake, the solution may become unstable. For example, in finding the difference between $\Phi_i = 1000$ and $\Phi_{i+1} = 1002$, if Φ_{i+1} is set equal to zero by mistake, the difference of 1000 instead of 2 may cause instability. To guard against such error, care must be taken to ensure that Φ is calculated at every point, particularly at boundary points.

A serious limitation of the finite difference method is that interpolation of some kind must be used to determine solutions at points not on the grid. Suppose we want to find Φ at a point P which is not on the grid, as in Figure 3.47. Assuming Φ is known at the four grid points surrounding P , at a distance x_o along the bottom edge of the rectangle in Figure 3.47,

$$\Phi_b = \frac{x_o}{\Delta x} [\Phi(i+1, j) - \Phi(i, j)] + \Phi(i, j) \quad (3.166)$$

At a distance x_o along the top edge,

$$\Phi_t = \frac{x_o}{\Delta x} [\Phi(i+1, j+1) - \Phi(i, j+1)] + \Phi(i, j+1) \quad (3.167)$$

The value of Φ at P is estimated by combining Equations (3.166) and (3.167), i.e.,

$$\Phi_P = \frac{y_o}{\Delta y} (\Phi_t - \Phi_b) + \Phi_b \quad (3.168)$$

One obvious way to avoid interpolation is to use a finer grid if possible.

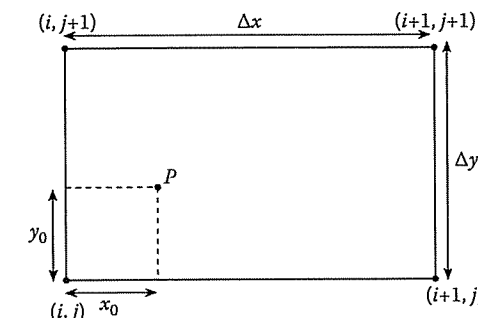


Figure 3.47
Evaluating Φ at a point P not on the grid.

References

- [1] L.D. Kovach, *Boundary-Value Problems*. Reading, MA: Addison-Wesley, 1984, pp. 355–379.
- [2] A. Thom and C.J. Apelt, *Field Computations in Engineering and Physics*. London: D. Van Nostrand, 1961, p. v.
- [3] R.D. Richtmyer and K.W. Morton, *Difference Methods for Initial-Value Problems*, 2nd ed. New York: Interscience Publ., 1976, pp. 185–193.
- [4] D. Potter, *Computational Physics*. London: John Wiley, 1973, pp. 40–79.
- [5] G.D. Smith, *Numerical Solution of Partial Differential Equations: Finite Difference Methods*, 3rd ed., Oxford Univ. Press, New York, 1985.
- [6] J.H. Ferziger, *Numerical Methods for Engineering Application*. New York: John Wiley, 1981.
- [7] L. Lapidus and G.F. Pinder, *Numerical Solution of Partial Differential Equations in Science and Engineering*. New York: John Wiley, 1982, pp. 166–185.
- [8] V. Vernuri and W.J. Karplus, *Digital Computer Treatment of Partial Differential Equations*. Englewood Cliffs, NJ: Prentice-Hall, 1981, pp. 88–92.
- [9] A. Wexler, “Computation of electromagnetic fields,” *IEEE Trans. Micro. Theo. Tech.*, vol. MTT-17, no. 8, Aug. 1969, pp. 416–439.
- [10] G. de Vahl Davis, *Numerical Methods in Engineering and Science*. London: Allen & Unwin, 1986.
- [11] Special issue of *IEEE Transactions on Microwave Theory and Techniques*, vol. MTT-17, no. 8, Aug. 1969 on “Computer-oriented microwave practices” covers various applications of finite difference methods to EM problems.
- [12] H.E. Green, “The numerical solution of some important transmission-line problems,” *IEEE Trans. Micro. Theo. Tech.*, vol. MTT-13, no. 5, Sept. 1965, pp. 676–692.
- [13] M.N.O. Sadiku, “Finite difference solution of electrodynamic problems,” *Int. Elect. Engr. Educ.*, vol. 28, April 1991, pp. 107–122.
- [14] M.F. Iskander, “A new course on computational methods in electromagnetics,” *IEEE Trans. Educ.*, vol. 31, no. 2, May 1988, pp. 101–115.
- [15] W.S. Metcalf, “Characteristic impedance of rectangular transmission lines,” *Proc. IEE*, vol. 112, no. 11, Nov. 1965, pp. 2033–2039.

REFERENCES

- [16] M.V. Schneider, “Computation of impedance and attenuation of TEM-lines by finite difference methods,” *IEEE Micro. Theo. Tech.*, vol. MTT-13, no. 6, Nov. 1965, pp. 793–800.
- [17] M. Sendaula, M. Sadiku, and R. Heiman, “Crosstalk computation in coupled transmission lines,” *Proc. IEEE Southeastcon*, April 1991, pp. 790–795.
- [18] A.R. Djordjevic et al., “Time-domain response of multiconductor transmission lines,” *Proc. IEEE*, vol. 75, no. 6, June 1987, pp. 743–764.
- [19] R.R. Gupta, “Accurate impedance determination of coupled TEM conductors,” *IEEE Trans. Micro. Theo. Tech.*, vol. MTT-17, no. 12, Aug. 1969, pp. 479–489.
- [20] E. Yamashita et al., “Characterization method and simple design formulas of MDS lines proposed for MMIC’s,” *IEEE Trans. Micro. Theo. Tech.*, vol. MTT-35, no. 12, Dec. 1987, pp. 1355–1362.
- [21] J.R. Molberg and D.K. Reynolds, “Iterative solutions of the scalar Helmholtz equations in lossy regions,” *IEEE Trans. Micro. Theo. Tech.*, vol. MTT-17, no. 8, Aug. 1969, pp. 460–477.
- [22] J.B. Davies and C.A. Muilwyk, “Numerical solution of uniform hollow waveguides with boundaries of arbitrary shape,” *Proc. IEEE*, vol. 113, no. 2, Feb. 1966, pp. 277–284.
- [23] J.S. Hornsby and A. Gopinath, “Numerical analysis of a dielectric-loaded waveguide with a microstrip line—finite-difference methods,” *IEEE Trans. Micro. Theo. Tech.*, vol. MTT-17, no. 9, Sept. 1969, pp. 684–690.
- [24] M.J. Beubien and A. Wexler, “An accurate finite-difference method for higher-order waveguide modes,” *IEEE Trans. Micro. Theo. Tech.*, vol. MTT-16, no. 12, Dec. 1968, pp. 1007–1017.
- [25] C.A. Muilwyk and J.B. Davies, “The numerical solution of rectangular waveguide junctions and discontinuities of arbitrary cross section,” *IEEE Trans. Micro. Theo. Tech.*, vol. MTT-15, no. 8, Aug. 1967, pp. 450–455.
- [26] J.H. Collins and P. Daly, “Calculations for guided electromagnetic waves using finite-difference methods,” *J. Electronics & Control*, vol. 14, 1963, pp. 361–380.
- [27] T. Itoh (ed.), *Numerical Techniques for Microwaves and Millimeterwave Passive Structures*. New York: John Wiley, 1989.
- [28] D.H. Sinnott et al., “The finite difference solution of microwave circuit problems,” *IEEE Trans. Micro. Theo. Tech.*, vol. MTT-17, no. 8, Aug. 1969, pp. 464–478.

- [29] W.K. Gwarek, "Analysis of an arbitrarily-shaped planar circuit—a time-domain approach," *IEEE Trans. Micro. Theo. Tech.*, vol. MTT-33, no. 10, Oct. 1985, pp. 1067–1072.
- [30] M. De Pourceq, "Field and power-density calculations in closed microwave systems by three-dimensional finite differences," *IEEE Proc.*, vol. 132, Pt. H, no. 6, Oct. 1985, pp. 360–368.
- [31] A. Taflove and K.R. Umashankar, "Solution of complex electromagnetic penetration and scattering problems in unbounded regions," in A.J. Kalinowski (ed.), *Computational Methods for Infinite Domain Media-Structure Interaction*. Washington, DC: ASME, vol. 46, 1981, pp. 83–113.
- [32] A. Taflove, "Application of the finite-difference time-domain method to sinusoidal steady-state electromagnetic-penetration problems," *IEEE Trans. EM Comp.*, vol. EMC-22, no. 3, Aug. 1980, pp. 191–202.
- [33] K.S. Kunz and K.M. Lee, "A three-dimensional finite-difference solution of the external response of an aircraft to a complex transient EM environment" (2 parts), *IEEE Trans. EM Comp.*, vol. EMC-20, no. 2, May 1978, pp. 328–341.
- [34] M.L. Oristaglio and G.W. Hohman, "Diffusion of electromagnetic fields into a two-dimensional earth: A finite-difference approach," *Geophysics*, vol. 49, no. 7, July 1984, pp. 870–894.
- [35] K. Umashankar and A. Taflove, "A novel method to analyze electromagnetic scattering of complex objects," *IEEE Trans. EM Comp.*, vol. EMC-24, no. 4, Nov. 1982, pp. 397–405.
- [36] R.W.M. Lau and R.J. Sheppard, "The modelling of biological systems in three dimensions using the time domain finite-difference method" (2 parts), *Phys. Med. Biol.*, vol. 31, no. 11, 1986, pp. 1247–1266.
- [37] F. Sandy and J. Sage, "Use of finite difference approximations to partial differential equations for problems having boundaries at infinity," *IEEE Trans. Micro. Theo. Tech.*, May 1971, pp. 484–486.
- [38] K.B. Whiting, "A treatment for boundary singularities in finite difference solutions of Laplace's equation," *IEEE Trans. Micro. Theo. Tech.*, vol. MTT-16, no. 10, Oct. 1968, pp. 889–891.
- [39] G.E. Forsythe and W.R. Wasow, *Finite Difference Methods for Partial Differential Equations*. New York: John Wiley, 1960.
- [40] M.L. James et al., *Applied Numerical Methods for Digital Computation*, 3rd ed. New York: Harper & Row, 1985, pp. 203–274.
- [41] Y. Naiheng and R.F. Harrington, "Characteristic impedance of transmission lines with arbitrary dielectrics under the TEM approximation," *IEEE Trans. Micro. Theo. Tech.*, vol. MTT-34, no. 4, April 1986, pp. 472–475.

- [42] K.S. Yee, "Numerical solution of initial boundary-value problems involving Maxwell's equations in isotropic media," *IEEE Trans. Ant. Prop.*, vol. AP-14, May 1966, pp. 302–307.
- [43] A. Taflove and M.E. Brodwin, "Numerical solution of steady-state electromagnetic scattering problems using the time-dependent Maxwell's equations," *IEEE Micro. Theo. Tech.*, vol. MTT-23, no. 8, Aug. 1975, pp. 623–630.
- [44] A. Taflove and K. Umashankar, "A hybrid moment method/finite-difference time-domain approach to electromagnetic coupling and aperture penetration into complex geometries," *IEEE Trans. Ant. Prop.*, vol. AP-30, no. 4, July 1982, pp. 617–627. Also in B. J. Strait (ed.), *Applications of the Method of Moments to Electromagnetic Fields*. Orlando, FL: SCEE Press, Feb. 1980, pp. 361–426.
- [45] M. Okoniewski, "Vector wave equation 2D-FDTD method for guided wave equation," *IEEE Micro. Guided Wave Lett.*, vol. 3, no. 9, Sept. 1993, pp. 307–309.
- [46] A. Taflove and K.R. Umashankar, "The finite-difference time-domain method for numerical modeling of electromagnetic wave interactions," *Electromagnetics*, vol. 10, 1990, pp. 105–126.
- [47] M.N.O. Sadiku, V. Bemmel, and S. Agbo, "Stability criteria for finite-difference time-domain algorithm," *Proc. IEEE Southeastcon*, April 1990, pp. 48–50.
- [48] J.G. Blaschak and G.A. Kriegsmann, "A comparative study of absorbing boundary conditions," *J. Comp. Phys.*, vol. 77, 1988, pp. 109–139.
- [49] G. Mux, "Absorbing boundary conditions for the finite-difference approximation of the time-domain electromagnetic-field equations," *IEEE Trans. EM Comp.*, vol. EMC-23, no. 4, Nov. 1981, pp. 377–382.
- [50] R. Holland, "THREDE: A free-field EMP coupling and scattering code," *IEEE Trans. Nucl. Sci.*, vol. NS-24, no. 6, Dec. 1977, pp. 2416–2421.
- [51] R.W. Ziolkowski et al., "Three-dimensional computer modeling of electromagnetic fields: A global lookback lattice truncation scheme," *J. Comp. Phy.*, vol. 50, 1983, pp. 360–408.
- [52] E.R. Demarest, "A finite difference—time domain technique for modeling narrow apertures in conducting scatterers," *IEEE Trans. Ant. Prop.*, vol. AP-35, no. 7, July 1987, pp. 826–831.
- [53] A. Taflove et al., "Detailed FDTD analysis of electromagnetic fields penetrating narrow slots and lapped joints in thick conducting screens," *IEEE Trans. Ant. Prop.*, vol. 36, no. 2, Feb. 1988, pp. 24–257.
- [54] H. Meskanen and O. Pekonen, "FDTD analysis of field distribution in an elevator car by using various antenna positions and orientations," *Elect. Lett.*, vol. 34, no. 6, March 1998, pp. 534–535.

- [55] J.G. Maloney, G.S. Smith, and W.R. Scott, "Accurate computation of the radiation from simple antennas using the finite-difference time-domain method," *IEEE Trans. Ant. Prog.*, vol. 38, no. 7, July 1990, pp. 1059–1068.
- [56] J.G. Maloney and Smith, "The efficient modeling of thin material sheets in the finite-difference time-domain (FDTD) method," *IEEE Trans. Ant. Prog.*, vol. 40, no. 3, March 1992, pp. 323–330.
- [57] P.A. Tirkas and C.A. Balanis, "Finite-difference time-domain method for antenna radiation," *IEEE Trans. Ant. Prog.*, vol. 40, no. 4, March 1992, pp. 334–340.
- [58] E. Thiele and A. Taflove, "FDTD analysis of vivaldi flared horn antennas and arrays," *IEEE Trans. Ant. Prog.*, vol. 42, no. 5, May 1994, pp. 633–641.
- [59] J.S. Colburn and Y. Rahmat-Samii, "Human proximity effects on circular polarized handset antennas in personal satellite communications," *IEEE Trans. Ant. Prog.*, vol. 46, no. 6, June 1998, pp. 813–820.
- [60] K. Uehara and K. Kagoshima, "Rigorous analysis of microstrip phased array antennas using a new FDTD method," *Elect. Lett.*, vol. 30, no. 2, Jan. 1994, pp. 100–101.
- [61] H. Klingbell, K. Beilenhoff, and H.L. Hartnagel, "FDTD full-wave analysis and modeling of dielectric and metallic losses of CPW short circuits," *IEEE Trans. Micro. Theo. Tech.*, vol. 44, no. 3, March 1996, pp. 485–487.
- [62] C. Zhao and I. Awai, "Applications of the finite difference techniques to the compensated VIP 3 dB directional coupler," *IEEE Trans. Micro. Theo. Tech.*, vol. 44, no. 11, Nov. 1996, pp. 2045–2052.
- [63] T. Shibata et al., "Analysis of microstrip circuits using three-dimensional full-wave electromagnetic field analysis in the time-domain," *IEEE Trans. Micro. Theo. Tech.*, vol. 36, no. 6, June 1988, pp. 1064–1070.
- [64] W.K. Gwarek, "Analysis of arbitrarily shaped two-dimensional microwave circuits by finite-difference time-domain method," *IEEE Trans. Micro. Theo. Tech.*, vol. 36, no. 4, April 1988, pp. 738–744.
- [65] X. Zhang, et al., "Calculation of the dispersive characteristics of microstrips by the time-domain finite-difference method," *IEEE Trans. Micro. Theo. Tech.*, vol. 36, no. 2, Feb. 1988, pp. 263–267.
- [66] X. Zhang and K.K. Mei, "Time-domain finite-difference approach to the calculation of the frequency-dependent characteristics of microstrip discontinuities," *IEEE Trans. Micro. Theo. Tech.*, vol. 36, no. 12, Dec. 1988, pp. 1775–1787.
- [67] R.W. Larson, "Special purpose computers for the time domain advance of Maxwell's equations," *IEEE Trans. Magnetics*, vol. 25, no. 4, July 1989, pp. 2913–2915.

- [68] K.K. Mei et al., "Conformal time domain finite difference method," *Radio Sci.*, vol. 19, no. 5, Sept./Oct. 1984, pp. 1145–1147.
- [69] D.H. Choi and W.J.R. Hoefer, "The finite-difference time-domain method and its application to eigenvalue problems," *IEEE Trans. Micro. Theo. Tech.*, vol. MTT-36, no. 12, Dec. 1986, pp. 1464–1470.
- [70] D.M. Sullivan et al., "Use of the finite-difference time-domain method in calculating EM absorption in human tissues," *IEEE Trans. Biomed. Engr.*, vol. BME-34, no. 2, Feb. 1987, pp. 148–157.
- [71] A.D. Tinniswood, C.M. Furse, and O.P. Gandhi, "Computations of SAR distributions for two anatomically based models of the human head using CAD files of commercial telephone and the parallelized FDTD code," *IEEE Trans. Ant. Prog.*, vol. 46, no. 6, June 1998, pp. 829–833.
- [72] D. Dunn, C.M. Rappaport and A.J. Terzuoli, "FDTD verification of deep-set brain tumor hyperthermia using a spherical microwave source distribution," *IEEE Trans. Micro. Theo. Tech.*, vol. 44, no. 10, Oct. 1996, pp. 1769–1777.
- [73] V. Hombach et al., "The dependence of EM energy absorption upon human head modeling at 900 MHz," *IEEE Trans. Micro. Theo. Tech.*, vol. 44, no. 10, Oct. 1996, pp. 1865–1873.
- [74] O. Fujiwara and A. Kato, "Computation of SAR inside eyeball for 1.5-GHz microwave exposure using finite-difference time-domain technique," *IEICE Trans. Comm.*, vol. E77-B, no. 6, June 1994, pp. 732–737.
- [75] A. Christ and H.L. Hartnagel, "Three-dimensional finite-difference method for the analysis of microwave-device embedding," *IEEE Trans. Micro. Theo. Tech.*, vol. MTT-35, no. 8, Aug. 1987, pp. 688–696.
- [76] J.H. Wheaton, "A 3D analysis of Maxwell's equations for cavities of arbitrary shape," *J. Comp. Phys.*, vol. 75, 1988, pp. 168–189.
- [77] R. Luebers et al., "A frequency-dependence finite-difference time-domain formulation for dispersive materials," *IEEE Trans. EMC*, vol. 32, no. 3, Aug. 1990, pp. 222–227.
- [78] R. Holland, "Finite-difference time-domain (FDTD) analysis of magnetic diffusion," *IEEE Trans. EMC*, vol. 36, no. 1, Feb. 1994, pp. 32–39.
- [79] A. Taflove and K.R. Umashankar, "Review of FDTD numerical modeling of electromagnetic wave scattering and radar cross section," *Proc. IEEE*, vol. 77, no. 5, May 1989, pp. 682–699.
- [80] V. Bemmel, "Time-domain finite-difference analysis of electromagnetic scattering and penetration problems," *M. Sc. Thesis*, Dept. of Electrical and Computer Engr., Florida Atlantic University, Boca Raton, Dec. 1987.
- [81] D.S. Jones, *The Theory of Electromagnetism*. New York: Macmillan, 1964, pp. 450–452.

- [82] J.A. Stratton, *Electromagnetic Theory*. New York: McGraw-Hill, 1941, pp. 563–573.
- [83] G.A. Kriegsmann, A. Taflove, and K.R. Umashankar, “A new formulation of electromagnetic wave scattering using an on-surface radiation boundary condition approach,” *IEEE Trans. Ant. Prop.*, vol. 35, no. 2, Feb. 1987, pp. 153–161.
- [84] B. Zhiqiang et al., “A new finite-difference time-domain algorithm for solving Maxwell’s equation,” *IEEE Micro. Guided Wave Lett.*, vol. 1, no. 12, Dec. 1991, pp. 382–384.
- [85] S.X.R. Vahldieck and H. Jin, “Full-wave analysis of guided wave structures using a novel 2-D FDTD,” *IEEE Micro. Guided Wave Lett.*, vol. 2, no. 5, May 1992, pp. 165–167.
- [86] R. Mittra and P.H. Harms, “A new finite-difference time-domain (FDTD) algorithm for efficient field computation in resonator narrow-band structures,” *IEEE Micro. Guided Wave Lett.*, vol. 3, no. 9, Sept. 1993, pp. 336–318.
- [87] J.B. Cole, “A high accuracy realization of the Yee algorithm using non-standard finite differences,” *IEEE Trans. Micro. Theo. Tech.*, vol. 45, no. 6, June 1997, pp. 991–996.
- [88] J.B. Cole, “A high accuracy FDTD algorithm to solve microwave propagation and scattering problems on a coarse grid,” *IEEE Trans. Micro. Theo. Tech.*, vol. 43, no. 9, Sept. 1995, pp. 2053–2058.
- [89] U. Oguz, L. Gurel, and O. Arkan, “An efficient and accurate technique for the incident-wave excitations in the FDTD method,” *IEEE Trans. Micro. Theo. Tech.*, vol. 46, no. 6, June 1998, pp. 869–882.
- [90] I.J. Craddock and C.J. Railton, “A new technique for the stable incorporation of static field solutions in the FDTD method for the analysis of thin wires and narrow strips,” *IEEE Trans. Micro. Theo. Tech.*, vol. 46, no. 8, Aug. 1998, pp. 1091–1096.
- [91] J.B. Cole et al., “Finite-difference time-domain simulations of wave propagation and scattering as a research and educational tool,” *Computer in Physics*, vol. 9, no. 2, March/April 1995, pp. 235–239.
- [92] P.H. Harms, J.F. Lee, and R. Mittra, “A study of the nonorthogonal FDTD method versus the conventional FDTD technique for computing resonant frequency of cylindrical cavities,” *IEEE Trans. Micro. Theo. Tech.*, vol. 40, no. 4, April 1992, pp. 741–746.
- [93] Y. Chen, R. Mittra, and P. Harms, “Finite-difference time-domain algorithm for solving Maxwell’s equations in rotationally symmetric geometries,” *IEEE Trans. Micro. Theo. Tech.*, vol. 44, no. 6, June 1996, pp. 832–839.

- [94] C. Wang, B.Q. Gao, and C.P. Deng, “Q factor of a resonator by the finite difference time-domain method incorporating perturbation techniques,” *Electr. Lett.*, vol. 29, no. 21, Oct. 1993, pp. 1866–1867.
- [95] G. Cerri et al., “MoM-FDTD hybrid technique for analysing scattering problems,” *Electr. Lett.*, vol. 34, no. 5, March 1998, pp. 438–440.
- [96] A.R. Bretones, R. Mittra, and R.G. Martin, “A hybrid technique combining the method of moments in the time domain and FDTD,” *IEEE Micro. Guided Wave Lett.*, vol. 8, no. 8, Aug. 1998, pp. 281–283.
- [97] C.J. Railton, E.M. Daniel, and J.P. McGeehan, “Use of second order absorbing boundary conditions for the termination of planar waveguides in the FDTD method,” *Electr. Lett.*, vol. 29, no. 10, May 1993, pp. 900–902.
- [98] P.Y. Wang et al., “Higher order formulation of absorbing boundary conditions for finite-difference time-domain method,” *Electr. Lett.*, vol. 29, no. 23, Nov. 1993, pp. 2018–2019.
- [99] J.C. Olivier, “On the synthesis of exact free space absorbing boundary conditions for the finite-difference time-domain method,” *IEEE Trans. Ant. Prop.*, vol. 40, no. 4, April 1992, pp. 456–460.
- [100] D.S. Katz, E.T. Thiele, and A. Taflove, “Validation and extension to three dimensions of the Berenger PML absorbing boundary conditions for FDTD meshes,” *IEEE Micro. Guided Wave Lett.*, vol. 4, no. 6, Aug. 1994, pp. 268–270.
- [101] J.P. Berenger, “A perfectly matched layer for the absorption of electromagnetic waves,” *J. Comp. Phys.*, vol. 114, Aug. 1994, pp. 185–200.
- [102] J.P. Berenger, “Perfectly matched layer for the FDTD solution of wave-structure interaction problems,” *IEEE Trans. Ant. Prop.*, vol. 44, no. 1, Jan. 1996, pp. 110–117.
- [103] D.T. Prescott and N.V. Shuley, “Reflection analysis of FDTD boundary conditions – Part I: Time-space absorbing boundaries,” *IEEE Trans. Micro. Theo. Tech.*, vol. 45, no. 8, Aug. 1997, pp. 1162–1170. Part II, pp. 1171–1178.
- [104] A. Taflove, *Computational Electrodynamics: The Finite-Difference Time-Domain Method*. Boston, MA: Artech House, 1995, pp. 145–202.
- [105] K.S. Kunz and R.J. Luebbers, *The Finite-Difference Time-Domain Method for Electromagnetic*. Boca Raton, FL: CRC Press, 1993, pp. 347–358.
- [106] A. Taflove and K.R. Umashankar, “The finite-difference time-domain method for numerical modeling of electromagnetic wave interactions with arbitrary structures,” in M.A. Morgan (ed.), *Finite Element and Difference Methods in Electromagnetic Scattering*. New York: Elsevier, 1990, pp. 287–373.

- [107] K.K. Mei and J. Fang, "Superabsorption — a method to improve absorbing boundary conditions," *IEEE Trans. Ant. Prop.*, vol. 40, no. 9, Sept. 1992, pp. 1001–1010.
- [108] M. DiStasio and W.C. McHarris, "Electrostatic problems? Relax!" *Am. J. Phys.*, vol. 47, no. 5, May 1979, pp. 440–444.
- [109] M.N.O. Sadiku, "Finite difference solution of axisymmetric potential problems," *Int. J. Appl. Engr. Educ.*, vol. 6, no. 4, 1990, pp. 479–485.
- [110] H.E. Green, "The numerical solution of transmission line problems," in L. Young (ed.), *Advances in Microwaves*, vol. 2. New York: Academic Press, 1967, pp. 327–393.
- [111] C.D. Taylor et al., "Electromagnetic pulse scattering in time varying inhomogeneous media," *IEEE Trans. Ant. Prop.*, vol. AP-17, no. 5, Sept. 1969, pp. 585–589.
- [112] P.J. Davis and P. Rabinowitz, *Methods of Numerical Integration*. New York: Academic Press, 1975.
- [113] R. Piessens et al., *QUADPACK: A Subroutine Package for Automatic Integration*. Berlin: Springer-Verlag, 1980.
- [114] *Tables of Functions and Zeros of Functions*. Washington, DC: National Bureau of Standards, Applied Mathematical Series, no. 37, 1954.
- [115] M. Abramowitz and I.A. Stegun (eds.), *Handbook of Mathematical Functions*. Washington, DC: National Bureau of Standards, Applied Mathematical Series, no. 55, 1964.
- [116] L.G. Kelly, *Handbook of Numerical Methods and Applications*. Reading, MA: Addison-Wesley, 1967, pp. 57–61.
- [117] M.N.O. Sadiku and R. Jongakiem, "Newton–Cotes rules for triple integrals," *Proc. IEEE Southeastcon*, April 1990, pp. 471–475.
- [118] B.P. Rynne, "Instabilities in time marching methods for scattering problems," *Electromagnetics*, vol. 6, no. 2, 1986, pp. 129–144.
- [119] J.I. Steger and R.F. Warming, "On the convergence of certain finite-difference schemes by an inverse-matrix method," *J. Comp. Phys.*, vol. 17, 1975, pp. 103–121.
- [120] D.W. Kelly, et al., "A posteriori error estimates in finite difference techniques," *J. Comp. Phys.*, vol. 74, 1988, pp. 214–232.

Problems

3.1 Show that the following finite difference approximations for Φ_x are valid:

(a) forward difference,

$$\frac{-\Phi_{i+2} + 4\Phi_{i+1} - 3\Phi_i}{2\Delta x}$$

(b) backward difference,

$$\frac{3\Phi_i - 4\Phi_{i-1} + \Phi_{i-2}}{2\Delta x}$$

(c) central difference

$$\frac{-\Phi_{i+2} + 8\Phi_{i+1} - 8\Phi_{i-1} + \Phi_{i-2}}{12\Delta x}$$

3.2 Solve $y'' - y = -1$, $0 < x < 1$ with $y'(0) = 0$, $y(1) = 2$. You should use finite difference method and take $\Delta x = 0.25$.

3.3 Solve the equation $\Phi_t = \Phi_{xx}$, $0 \leq x \leq 1$, subject to initial and boundary conditions

$$\begin{aligned}\Phi(x, 0) &= \sin \pi x, \quad 0 \leq x \leq 1, \\ \Phi(0, t) &= 0 = \Phi(1, t) \quad t > 0\end{aligned}$$

Obtain the solution by hand calculation and use $\Delta x = 0.25$ and $r = 0.5$.

3.4 Derive the Crank–Nicholson implicit algorithm for the hyperbolic equation $\Phi_{xx} = a^2 \Phi_{yy}$, $a^2 = \text{constant}$. Let $\Delta x = \Delta y = \Delta$.

3.5 Given a boundary-value problem defined by

$$\frac{d^2\Phi}{dx^2} = x + 1, \quad 0 < x < 1$$

subject to $\Phi(0) = 0$ and $\Phi(1) = 1$, use the finite difference method to find $\Phi(0.5)$. You may take $\Delta = 0.25$ and perform 5 iterations. Compare your result with the exact solution.

3.6 Prove that the fourth-order approximation of Laplace's equation $\Phi_{xx} + \Phi_{yy} = 0$ is

$$\begin{aligned}60\Phi(i, j) - 16[\Phi(i+1, j) + \Phi(i-1, j) + \Phi(i, j+1) + \Phi(i, j-1)] \\ + \Phi(i+2, j) + \Phi(i-2, j) + \Phi(i, j+2) + \Phi(i, j-2) = 0\end{aligned}$$

Draw the computational molecule for the finite difference scheme.

- 3.7 (a) If $\Delta x \neq \Delta y$, show that for the computational molecule in Figure 3.48 (a), Equation (3.49) becomes

$$V_o = \frac{V_1}{2(1+\alpha)} + \frac{V_2}{2(1+\alpha)} + \frac{V_3}{2(1+1/\alpha)} + \frac{V_4}{2(1+1/\alpha)}$$

where $\alpha = (\Delta x/\Delta y)^2$.

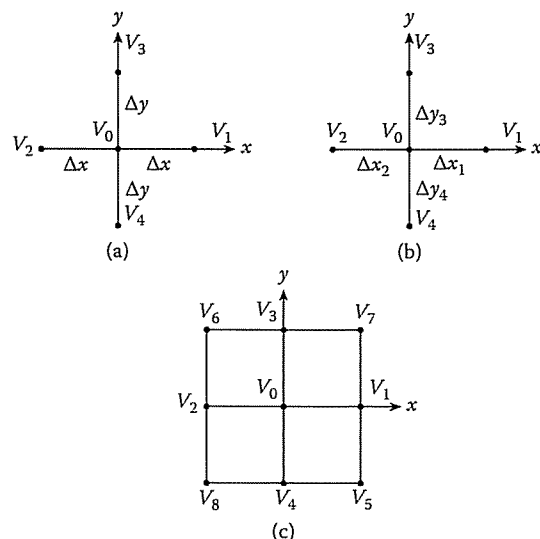


Figure 3.48
For Problem 3.7.

- (b) Show that for the molecule in Figure 3.48 (b), Equation (3.49) becomes

$$\begin{aligned} V_o &= \frac{V_1}{(1+\Delta x_1/\Delta x_2)(1+\Delta x_1\Delta x_2/\Delta y_3\Delta y_4)} \\ &+ \frac{V_2}{(1+\Delta x_2/\Delta x_1)(1+\Delta x_1\Delta x_2/\Delta y_3\Delta y_4)} \\ &+ \frac{V_3}{(1+\Delta y_3/\Delta y_4)(1+\Delta y_3\Delta y_4/\Delta x_1\Delta x_2)} \\ &+ \frac{V_4}{(1+\Delta y_4/\Delta y_3)(1+\Delta y_3\Delta y_4/\Delta x_1\Delta x_2)} \end{aligned}$$

The molecule in Figure 3.48 (b) is useful in treating irregular boundaries.

- (c) For the nine-point molecule in Figure 3.48 (c), show that

$$V_o = \frac{1}{8} \sum_{i=1}^8 V_i$$

This is a more accurate difference equation than Equation (3.49).

PROBLEMS

- 3.8 A Dirichlet problem is characterized by

$$U_{xx} + U_{yy} = 0, \quad 0 < x < 1, 0 < y < 1$$

$$U(0, y) = 0, \quad U(x, 0) = 0$$

$$U(1, y) = 100y, \quad U(x, 1) = 100x$$

By selecting $\Delta x = \Delta y = 0.25$, we have the square grid shown in Figure 3.49. Determine the potential at the nine free nodes.

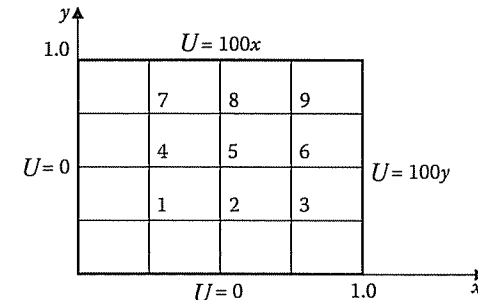


Figure 3.49
For Problem 3.8.

- 3.9 For a long hollow conductor with a uniform U-shape cross section shown in Figure 3.50, find the potential at points A, B, C, D, and E.

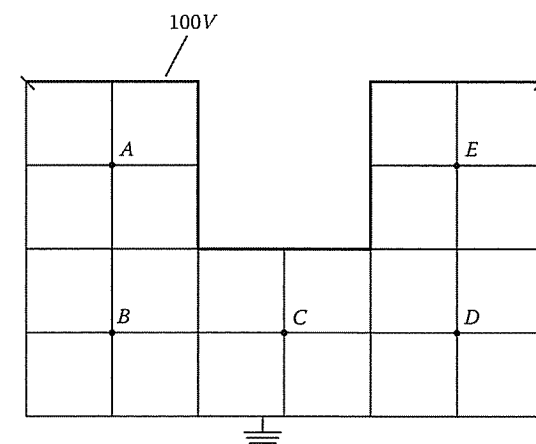


Figure 3.50
For Problem 3.9.

- 3.10 It is desired to solve

$$\frac{\partial^2 \Phi}{\partial x^2} + \frac{\partial^2 \Phi}{\partial y^2} + 50 = 0$$

in the square region $0 \leq x \leq 1, 0 \leq y \leq 1$ subject to the boundary conditions $\Phi = 10$ at $x = 0, 1$, $\Phi_y = 40$ at $y = 0$, $\Phi_y = -20$ at $y = 1$.

- (a) Set up a system of finite difference equations which will allow the solution to be found at $x = y = 0.25$ using $\Delta x = \Delta y = h = 0.25$. Perform three iterations.
- (b) Develop a program to solve the same problem using $h = 0.05, 0.1$, and 0.2 .
- 3.11 A potential problem is characterized by Poisson's equation

$$U_{xx} + U_{yy} = -2, \quad 0 < x < 6, 0 < y < 8$$

with zero potential $U = 0$ on the boundaries. By selecting $\Delta x = \Delta y = h = 2$, we realize that there are six free nodes as shown in Figure 3.51. Use finite difference to determine the potential at the free nodes.

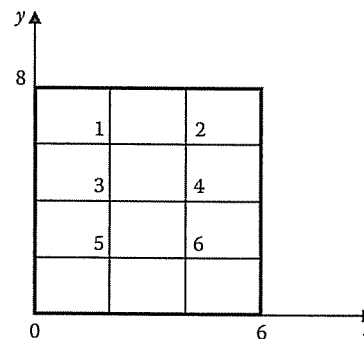


Figure 3.51
For Problem 3.11.

- 3.12 Modify the code of Figure 3.12 to solve the following three-dimensional problem:

$$\nabla^2 V = -\rho_v/\epsilon, \quad 0 \leq x \leq 1, \quad 0 \leq y \leq 1, \quad 0 \leq z \leq 1 \text{ meter},$$

where $\rho_v = xyz^2 nC/m^2$ and $\epsilon = 2\epsilon_0$ subject to the boundary conditions

$$V(0, y, z) = 0 = V(1, y, z)$$

$$V(x, 0, z) = 0 = V(x, 1, z)$$

$$V(x, y, 0) = 0, \quad V(x, y, 1) = V_o$$

Find the potential at the center of the cube and compare your result with the analytic solution. Take $V_o = 100$ volts.

- 3.13 Show that the leapfrog method applied to the parabolic equation (3.10) is unstable, whereas applying the DuFort-Frankel scheme yields an unconditionally stable solution.

PROBLEMS

3.14 The advective equation

$$\frac{\partial \Phi}{\partial t} + u \frac{\partial \Phi}{\partial x} = 0, \quad u > 0$$

can be discretized as

$$\Phi_i^{n+1} = \Phi_i^n - r(\Phi_{i+1}^n - \Phi_{i-1}^n),$$

where $r = u \Delta t / 2 \Delta x$. Show that the difference scheme is unstable. An alternative scheme is

$$\Phi_{i+1} = \frac{1}{2}(\Phi_{i+1}^n + \Phi_{i-1}^n) - r(\Phi_{i+1}^n - \Phi_{i-1}^n)$$

Find the condition on r for which this scheme is stable.

3.15 The two-dimensional parabolic equation

$$\frac{\partial U}{\partial t} = \frac{\partial^2 U}{\partial x^2} + \frac{\partial^2 U}{\partial y^2}, \quad 0 \leq x \leq 1, 0 \leq y \leq 1, \quad t > 0$$

is approximated by the finite difference methods:

$$(i) U_{i,j}^{n+1} = [1 + r(\delta_x^2 + \delta_y^2)]U_{i,j}^n$$

$$(ii) U_{i,j}^{n+1} = (1 + r\delta_x^2)(1 + r\delta_y^2)U_{i,j}^n \quad \text{where } r = \Delta t / h^2, h = \Delta x = \Delta y \text{ and}$$

$$\delta_x^2 U_{i,j}^n = U_{i-1,j}^n - 2U_{i,j}^n + U_{i+1,j}^n$$

$$\delta_y^2 U_{i,j}^n = U_{i,j-1}^n - 2U_{i,j}^n + U_{i,j+1}^n$$

Show that (i) is stable for $r \leq 1/4$ and (ii) is stable for $r \leq 1/2$

- 3.16 (a) The constitutive parameters of the earth allow the displacement currents to be negligibly small. In this type of medium, show that Maxwell's equations for two-dimensional TM mode, where

$$\mathbf{E}(x, y, t) = E_z \mathbf{a}_z$$

and

$$\mathbf{H}(x, y, t) = H_x \mathbf{a}_x + H_y \mathbf{a}_y,$$

reduce to the diffusion equation

$$\frac{\partial^2 E}{\partial x^2} + \frac{\partial^2 E}{\partial y^2} - \mu\sigma \frac{\partial E}{\partial t} = \mu \frac{\partial J_s}{\partial t}$$

where $E = E_z$ and J_s is the source current density in the z direction.

- (b) Taking $J_s = 0$, $\Delta x = \Delta y = \Delta$, and

$$\sum E_{i,j} = E_{i+1,j}^n + E_{i-1,j}^n + E_{i,j+1}^n + E_{i,j-1}^n,$$

show that applying Euler, leapfrog, and DuFort–Frankel difference methods to the diffusion equation gives:

Euler:

$$E_{i,j}^{n+1} = (1 - 4r)E_{i,j}^n + r \sum E_{i,j}^n,$$

Leapfrog:

$$E_{i,j}^{n+1} = E_{i,j}^{n-1} + 2r \left(\sum E_{i,j}^n - 4E_{i,j}^n \right),$$

DuFort–Frankel:

$$E_{i,j}^{n+1} = \frac{1 - 4r}{1 + 4r} E_{i,j}^{n-1} + \frac{2r}{1 + 4r} \sum E_{i,j}^n$$

where $r = \Delta t / (\sigma \mu \Delta^2)$.

- (c) Analyze the stability of these finite difference schemes by substituting for $E_{i,j}^n$ a Fourier mode of the form

$$E_{i,j}^n = E(x = i\Delta, y = j\Delta, t = n\Delta t) = A_n \cos(k_x i \Delta) \cos(k_y j \Delta)$$

- 3.17 Yee's FDTD algorithm for one-dimensional wave problems is given by

$$H_y^{n+1/2}(k + 1/2) = H_y^{n-1/2}(k + 1/2) + \frac{\delta t}{\mu \delta} [E_x^n(k) - E_x^n(k + 1)]$$

Determine the stability criterion for the scheme by letting

$$E_x^n(k) = A^n e^{j\beta k \delta}, \quad H_y^n(k) = \frac{A^n}{\eta} e^{j\beta k \delta},$$

where $\eta = (\mu/\epsilon)^{1/2}$ is the intrinsic impedance of the medium.

- 3.18 (a) The potential system in Figure 3.52 (a) is symmetric about the y -axis. Set the initial values at free nodes equal to zero and calculate (by hand) the potential at nodes 1 to 5 for 5 or more iterations.
 (b) Consider the square mesh in Figure 3.52(b). By setting initial values at the free nodes equal to zero, find (by hand calculation) the potential at nodes 1 to 4 for 5 or more iterations.
- 3.19 The potential system shown in Figure 3.53 is a quarter section of a transmission line. Using hand calculation, find the potential at nodes 1, 2, 3, 4, and 5 after 5 iterations.
- 3.20 Modify the program in Figure 3.21 or write your own program to calculate Z_o for the microstrip line shown in Figure 3.54. Take $a = 2.02$, $b = 7.0$, $h = 1.0 = w$, $t = 0.01$, $\epsilon_1 = \epsilon_0$, $\epsilon_2 = 9.6\epsilon_0$.

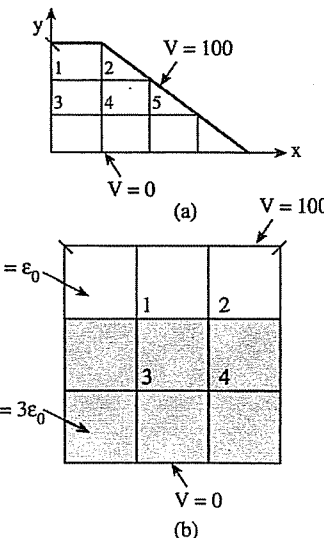


Figure 3.52
For Problem 3.18.

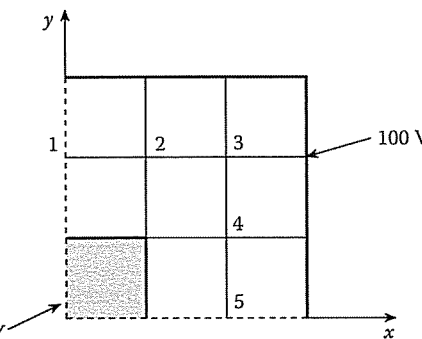


Figure 3.53
For Problem 3.19.

- 3.21 Use the FDM to calculate the characteristic impedance of the high-frequency, air-filled rectangular transmission line shown in Figure 3.55. Take advantage of the symmetry of the problem and consider cases for which
 (a) $B/A = 1.0$, $a/A = 1/2$, $b/B = 1/2$, $a = 1$,
 (b) $B/A = 1/2$, $a/A = 1/3$, $b/B = 1/3$, $a = 1$.
- 3.22 Figure 3.56 shows a shield microstrip line. Write a program to calculate the potential distribution within the cross section of the line. Take $\epsilon_1 = \epsilon_0$, $\epsilon_2 = 3.5\epsilon_0$ and $h = 0.5$ mm. Find the potential at the middle of the conducting plates.

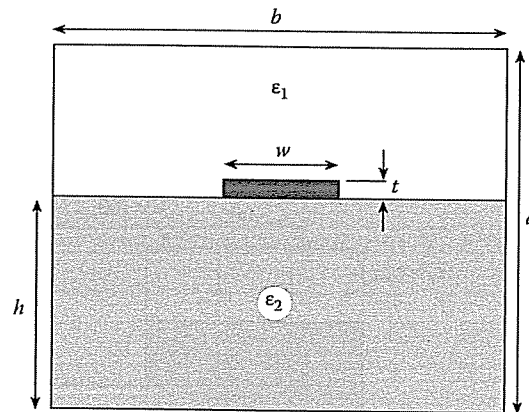


Figure 3.54
For Problem 3.20.

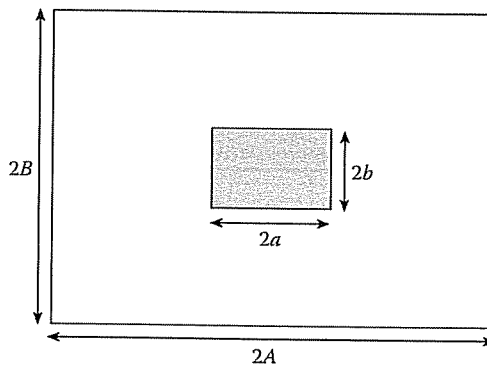


Figure 3.55
For Problem 3.21.

- 3.23 Use the FDM to determine the lowest (or dominant) cut-off wave-number k_c of the TM_{11} mode in waveguides with square ($a \times a$) and rectangular ($a \times b$, $b = 2a$) cross sections. Compare your results with the exact solution

$$k_c = \sqrt{(m\pi/a)^2 + (n\pi/b)^2}$$

where $m = n = 1$. Take $a = 1$.

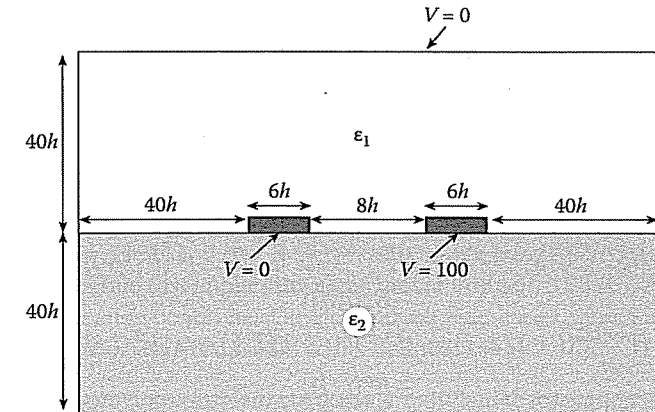


Figure 3.56
For Problem 3.22.

- 3.24 Instead of the 5-point scheme of Equation (3.121), use a more accurate 5-point formula

$$\begin{aligned} 2i(8i^2 - 5)V(i, j) &= (4i^3 + 2i^2 - 4i + 1)V(i+1, j) \\ &\quad + (4i^3 - 2i^2 - 4i - 1)V(i-1, j) \\ &\quad + i(4i^2 - 1)V(i, j+1) + i(4i^2 - 1)V(i, j-1) \end{aligned}$$

in Example 3.9 while other things remain the same.

- 3.25 For two-dimensional problems in which the field components do not vary with z coordinate ($\partial/\partial z = 0$), show that Yee's algorithm of Equations (3.84a)–(3.84f) becomes

- (a) for TE waves ($E_z = 0$)

$$\begin{aligned} H_z^{n+1/2}(i+1/2, j+1/2) &= H_z^{n-1/2}(i+1/2, j+1/2) \\ &\quad - \alpha [E_y^n(i+1, j+1/2) - E_y^n(i, j+1/2)] \\ &\quad + \alpha [E_y^n(i+1/2, j+1) - E_y^n(i+1/2, j)], \end{aligned}$$

$$E_x^{n+1}(i+1/2, j) = E_x^n(i+1/2, j) + \beta [H_z^{n+1/2}(i+1/2, j+1/2) \\ - H_z^{n+1/2}(i+1/2, j-1/2)],$$

$$E_z^{n+1}(i, j+1/2) = \gamma E_y^n(i, j+1/2) - \beta [H_z^{n+1/2}(i+1/2, j+1/2) \\ - H_z^{n+1/2}(i-1/2, j+1/2)];$$

(b) for TM waves ($H_z = 0$)

$$\begin{aligned} E_z^{n+1}(i, j) &= \gamma E_z^n(i, j) + \beta [H_y^{n+1/2}(i + 1/2, j) \\ &\quad - H_y^{n+1/2}(i - 1/2, j)] \\ &\quad - \beta [H_x^{n+1/2}(i, j + 1/2) - H_x^{n+1/2}(i, j - 1/2)], \end{aligned}$$

$$\begin{aligned} H_x^{n+1/2}(i, j + 1/2) &= H_x^{n-1/2}(i, j + 1/2) - \alpha [E_z^n(i, j + 1) \\ &\quad - E_z^n(i, j)], \end{aligned}$$

$$\begin{aligned} H_y^{n+1/2}(i + 1/2, j) &= H_y^{n-1/2}(i + 1/2, j) + \alpha [E_z^n(i + 1, j) \\ &\quad - E_z^n(i, j)], \end{aligned}$$

where

$$\alpha = \frac{\delta t}{\mu \delta}, \quad \beta = \frac{\delta t}{\epsilon \delta}, \quad \gamma = 1 - \frac{\sigma \delta t}{\epsilon},$$

and $\delta = \Delta x = \Delta y$.

- 3.26 Consider the diffraction/scattering of an incident TM wave by a perfectly conducting square of side $4a$. The conducting obstacle occupies $17 < i < 49$, $33 < j < 65$, while artificial boundaries are placed at $i = 1, 81$, $j = 0.5, 97.5$ as shown in Figure 3.57. Assume an incident wave with only E_z and H_y components

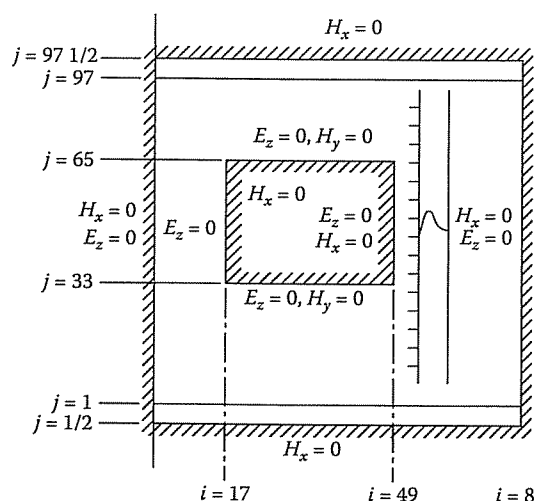


Figure 3.57
For Problem 3.26.

given by

$$\begin{aligned} E_z &= \begin{cases} \sin \pi \theta, & 0 < \theta < 1 \\ 0, & \text{otherwise} \end{cases} \\ H_y &= \frac{1}{\eta_o} E_z \end{aligned}$$

where $\eta_o = 120\pi\Omega$, $\theta = \frac{(x-50a+ct)}{8a}$, $\Delta x = \Delta y = a/8$, $\Delta t = c\Delta x = a/16$. Write a program that applies the algorithm in Problem 3.25 (b). Assume “hard lattice truncation conditions” at the artificial boundaries shown in Figure 3.57 and reproduce Yee’s result [42] in his figure 3.

- 3.27 Repeat the previous problem but assume “soft lattice truncation conditions” of Equations (3.87) to (3.89a)–(3.89l) at the artificial boundaries.
- 3.28 For axisymmetric problems (no variation with respect to ϕ), show that Yee’s algorithm for TM waves can be written as

$$\begin{aligned} H_\phi^{n+1}(i, j) &= H_\phi^n(i, j) + \alpha [E_z^{n+1/2}(i, j + 1/2) - E_z^{n+1/2}(i, j - 1/2)] \\ &\quad - \alpha [E_\rho^{n+1/2}(i + 1/2, j) - E_\rho^{n+1/2}(i - 1/2, j)] \end{aligned}$$

$$\begin{aligned} E_z^{n+3/2}(i, j + 1/2) &= \gamma E_z^{n+1/2}(i, j + 1/2) \\ &\quad + \beta \left[\frac{1}{j} H_\phi^{n+1}(i, j + 1/2) + H_\phi^{n+1}(i, j + 1) - H_\phi^{n+1}(i, j) \right], \end{aligned}$$

$$E_\rho^{n+3/2}(i + 1/2, j) = \gamma E_\rho^{n+1/2}(i + 1/2, j) - \beta [H_\phi^{n+1}(i + 1, j) - H_\phi^{n+1}(i, j)],$$

where

$$\alpha = \frac{\delta t}{\mu \delta}, \quad \beta = \frac{\delta t}{\epsilon \delta}, \quad \gamma = 1 - \frac{\sigma \delta t}{\epsilon}, \quad \delta = \Delta \rho = \Delta z,$$

and $H_\phi(z, \rho, t) = H_\phi(z = i\Delta z, \rho = (j - 1/2)\Delta \rho, t = n\delta t) = H_\phi^n(i, j)$.

- 3.29 (a) Show that the finite difference discretization of Mur’s ABC for two-dimensional problem

$$\frac{\partial E_z}{\partial x} - \frac{1}{c_o} \frac{\partial E_z}{\partial t} - \frac{c_o \mu_o}{2} \frac{\partial H_x}{\partial y} = 0$$

at the boundary $x = 0$ is

$$\begin{aligned} E_z^{n+1}(0, j) &= E_z^n(0, j) + \frac{c_o \delta t - \delta}{c_o \delta t + \delta} [E_z^{n+1}(0, j) - E_z^n(0, j)] \\ &\quad - \frac{\mu_o c_o}{2(c_o \delta t + \delta)} [H_x^{n+1/2}(0, j + 1/2) - H_x^{n+1/2}(0, j - 1/2) \\ &\quad + H_x^{n+1/2}(1, j + 1/2) - H_x^{n+1/2}(1, j - 1/2)] \end{aligned}$$

where c_o is the velocity of wave propagation.

(b) Discretize the first-order boundary condition

$$\frac{\partial E_z}{\partial x} - \frac{1}{c_o} \frac{\partial E_z}{\partial t} = 0$$

at $x = 0$.

- 3.30 For a three-dimensional problem, the PML modification of Maxwell's equations yields 12 equations because all six Cartesian field components split. Obtain the 12 resulting equations.
- 3.31 In a PML region, E_z is split into E_{zx} and E_{zy} for the TM case. Show that Maxwell's equation becomes

$$\begin{aligned}\epsilon_o \frac{\partial E_{zx}}{\partial t} + \sigma_x E_{zx} &= \frac{\partial H_y}{\partial x} \\ \epsilon_o \frac{\partial E_{zy}}{\partial t} + \sigma_y E_{zy} &= -\frac{\partial H_x}{\partial y} \\ \mu_o \frac{\partial H_x}{\partial t} + \sigma_y^* H_x &= -\frac{\partial}{\partial y}(E_{zx} + E_{zy}) \\ \mu_o \frac{\partial H_y}{\partial t} + \sigma_x^* H_y &= \frac{\partial}{\partial x}(E_{zx} + E_{zy})\end{aligned}$$

- 3.32 An FDTD equation for a PML region is given by

$$\begin{aligned}H_z^{n+1/2}(i+1/2, k) &= H_z^{n-1/2}(i+1/2, k) \\ -\frac{\delta t}{\mu\delta} [E_{yx}^n(i+1, k) + E_{yz}^n(i+1, k) - E_{yx}^n(i, k) - E_{yz}^n(i, k)]\end{aligned}$$

where δ , δt , n , i , and k have their usual FDTD meanings. By substituting the harmonic dependence $e^{j\omega t} e^{-jk_z z}$, show that the impedance of the PML region is

$$Z_z = \frac{E_y}{H_z} = \frac{\mu_o \delta}{\delta t} \frac{\sin(\omega \delta t / 2)}{\sin(k_o \delta / 2)}$$

- 3.33 Consider the finite cylindrical conductor held at $V = 100$ volts and enclosed in a larger grounded cylinder as in Figure 3.59. Such a deceptively simple looking problem is beyond closed form solution, but by employing finite difference techniques, the problem can be solved without much effort. Using the finite difference method, write a program that determines the potential distribution in the axisymmetric solution region. Output the potential at $(\rho, z) = (2, 10), (5, 10), (8, 10), (5, 2)$, and $(5, 18)$.
- 3.34 The problem in Figure 3.60 is a prototype of an electrostatic particle focusing system which is employed in a recoil-mass time-of-flight spectrometer. Write a program to determine the potential distribution in the system. The problem is similar to the previous problem except that the outer conductor abruptly expands radius by a factor of 2. Output the potential at $(\rho, z) = (5, 18), (5, 10), (5, 2), (10, 2)$, and $(15, 2)$.

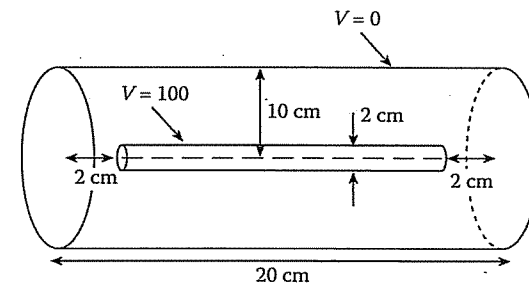


Figure 3.58
For Problem 3.33.

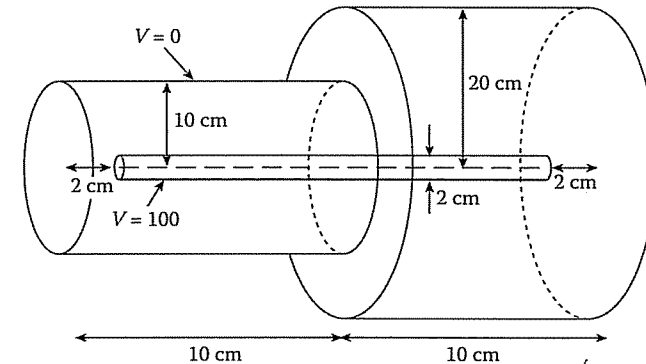


Figure 3.59
For Problem 3.34.

- 3.35 The conventional 3-D FDTD lattice in cylindrical coordinates is shown in Figure 3.60 (a) while its projection on the $\rho - z$ plane is in Figure 3.60 (b). Show that by discretizing Maxwell's equation,

$$\begin{aligned}E_\rho^{n+1}(i, j) &= \frac{(1 - \frac{\sigma\delta}{2\epsilon})}{(1 + \frac{\sigma\delta}{2\epsilon})} E_\rho^n(i, j) - \frac{\delta t}{\epsilon\delta} \frac{1}{(1 + \frac{\sigma\delta}{2\epsilon})} \\ &\quad [H_\phi^{n+1/2}(i, j) - H_\phi^{n+1/2}(i, j-1)]\end{aligned}$$

where $\delta = \Delta z = \Delta \rho$. Obtain the FDTD equations for H_ρ and H_ϕ .

- 3.36 Consider the one-dimensional parabolic equation in cylindrical coordinates

$$\nabla^2 U = \frac{\partial U}{\partial t}$$

or

$$U_{\rho\rho} + \frac{1}{\rho} U_\rho = U_t, \quad 0 < \rho < 1, t > 0$$

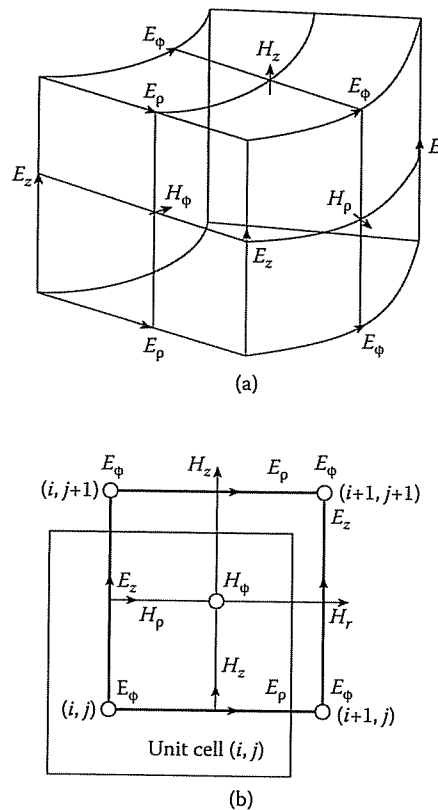


Figure 3.60

For Problem 3.35: (a) A conventional 3-D FDTD lattice in cylindrical coordinates, (b) projection of 3-D FDTD cell at $\rho - z$ plane.

subject to $U(1, t) = 0, t > 0$

$$U(\rho, 0) = T_o \text{ (constant)}$$

By selecting $\Delta\rho = h = 0.1$, and $T_o = 10$, calculate U at $\rho = 0.5, t = 0.1, 0.2, 0.3, 0.4, 0.5, 1.0$ using finite difference. Compare your results with the exact solution

$$U(\rho, t) = 2T_o \sum_{n=1}^{\infty} \frac{J_0(\lambda_n \rho)}{\lambda_n J_1(\lambda_n)} \exp(-\lambda_n^2 t)$$

where J_0 and J_1 are Bessel functions of orders 0 and 1 respectively and λ_n are the positive roots of J_0 .

- 3.37 For a two-dimensional heat equation in cylindrical system, consider

$$\nabla^2 U = \frac{\partial U}{\partial t}$$

or

$$U_{\rho\rho} + \frac{1}{\rho} U_\rho + U_{zz} = U_t, \quad 0 < \rho < 1, 0 < z < 1, t > 0$$

with the boundary conditions

$$\begin{aligned} U(\rho, 0, t) &= 0 = U(\rho, 1, t), \quad 0 < \rho < 1, t > 0 \\ U(1, z, t) &= 0, \quad 0 < z < 1, t > 0 \end{aligned}$$

and initial condition

$$U(\rho, z, 0) = T_o, \quad 0 < \rho < 1, 0 < z < 1$$

By selecting $\Delta z = \Delta\rho = h = 0.1$, and $T_o = 10$, use the finite difference method to determine U at $\rho = 0.5, z = 0.5, t = 0.05, 0.1, 0.15, 0.2, 0.25, 0.3$.

- 3.38 Given the tabulated values of $y = \sin x$ for $x = 0.4$ to 0.52 radians in intervals of $\Delta x = 0.02$, find (a) $\frac{dy}{dx}$ at $x = 0.44$, (b) $\int_{0.4}^{0.52} y dx$ using Simpson's rule.

x	$\sin x$
0.40	0.38942
0.42	0.40776
0.44	0.42594
0.46	0.44395
0.48	0.46178
0.50	0.47943
0.52	0.49688

- 3.39 (a) Use a pocket calculator to determine the approximate area under the curve $f(x) = 4 - x^2$, $0 < x < 1$ by the trapezoidal rule with $h = 0.2$.
 (b) Repeat part (a) using the Newton-Cotes rule with $n = 3$.

- 3.40 For a half-wave dipole, evaluating the integral

$$\int_0^{1/2} \frac{\cos^2(\frac{\pi}{2} \cos \theta)}{\sin \theta} d\theta$$

is usually required. Evaluate this integral numerically using any quadrature rule of your choice.

- 3.41 Compute

$$\int_0^1 e^{-x} dx$$

using the Newton-Cotes rule for cases $n = 2, 4$, and 6 . Compare your results with exact values.

3.42 Evaluate

$$\int_0^{2\pi} x \cos 10x \sin 20x \, dx$$

- (a) using the trapezoidal rule with $\Delta x = \pi/10$
- (b) using Simpson's 1/3-rule with $\Delta x = \pi/10$
- (c) using Gaussian quadrature.

3.43 The criterion for accuracy of the numerical approximation of an integral

$$I = \int_a^b f(x) \, dx \simeq \sum_{i=0}^{\infty} a_i f(x_i)$$

is that the formula is exact for all polynomials of degree less than or equal to n . If $a = 0$, $b = 4$, and the values of $f(x)$ are available at points $x_0 = 0$, $x_1 = 1$, $x_2 = 3$, $x_3 = 4$, find the values of the coefficients a_i for which the above requirement of accuracy is met.

3.44 The elliptic integral of the first type

$$F(k, \phi) = \int_0^\phi (1 - k^2 \sin^2 \theta)^{-1/2} \, d\theta$$

cannot be evaluated in a closed form. Write a program using Simpson's rule to determine $F(k, \phi)$ for $k = 0.5$ and $\phi = \pi/2$.

3.45 The following integral represents radiation from a circular aperture antenna with a constant current amplitude and phase distribution

$$I = \int_0^1 \int_0^{2\pi} e^{j\alpha\rho \cos \phi} \rho d\phi d\rho$$

Find I numerically for $\alpha = 5$ and compare your result with the exact result

$$I(\alpha) = \frac{2\pi J_1(\alpha)}{\alpha}$$

3.46 Evaluate the following double integral using the trapezoidal rule:

- (a) $\int_0^{\pi/2} \int_0^{\pi/2} \sin(\sqrt{2xy}) \, dx \, dy$,
- (b) $\int_1^5 \int_1^5 [x^2 + y^2]^{-1/2} \, dx \, dy$,
- (c) $\int_2^4 \left[\int_4^6 \ln(xy^2) \, dx \right] \, dy$

Chapter 4

Variational Methods

Injustice anywhere is a threat to justice everywhere. - Martin Luther King, Jr.

4.1 Introduction

In solving problems arising from mathematical physics and engineering, we find that it is often possible to replace the problem of integrating a differential equation by the equivalent problem of seeking a function that gives a minimum value of some integral. Problems of this type are called *variational problems*. The methods that allow us to reduce the problem of integrating a differential equation to the equivalent variational problem are usually called *variational methods* [1]. The variational methods form a common base for both the method of moments (MOM) and the finite element method (FEM). Therefore, it is appropriate that we study the variational methods before MOM and FEM. Besides, it is relatively easy to formulate the solution of certain differential and integral equations in variational terms. Also, variational methods give accurate results without making excessive demands on computer storage and time.

Variational methods can be classified into two groups: direct and indirect methods. The direct method is the classical Rayleigh–Ritz method, while the indirect methods are collectively referred to as the method of weighted residuals: collocation (or point-matching), subdomain, Galerkin, and least square methods. The variational solution of a given PDE using an indirect method usually involves two basic steps [2]:

- casting the PDE into variational form, and
- determining the approximate solution using one of the methods.

The literature on the theory and applications of variational methods to EM problems is quite extensive, and no attempt will be made to provide an exhaustive list of references. Numerous additional references may be found in those cited in this chapter. Owing to a lack of space, we can only hint at some of the topics usually covered in an introduction to this subject.

4.2 Operators in Linear Spaces

In this section, we will review some principles of operators in linear spaces and establish notation [2]–[5]. We define the *inner (dot or scalar) product* of functions u and v as

$$\langle u, v \rangle = \int_{\Omega} uv^* d\Omega \quad (4.1)$$

where $*$ denotes the complex conjugate and the integration is performed over Ω , which may be one-, two-, or three-dimensional physical space depending on the problem. In a sense, the inner product $\langle u, v \rangle$ gives the component or projection of function u in the direction of v . If \mathbf{u} and \mathbf{v} are vector fields, we modify Equation (4.1) slightly to include a dot between them, i.e.,

$$\langle \mathbf{u}, \mathbf{v} \rangle = \int_{\Omega} \mathbf{u} \cdot \mathbf{v}^* d\Omega \quad (4.2)$$

However, we shall consider u and v to be complex-valued scalar functions. For each pair of u and v belonging to the linear space, a number $\langle u, v \rangle$ is obtained that satisfies

$$(1) \quad \langle u, v \rangle = \langle v, u \rangle^*, \quad (4.3a)$$

$$(2) \quad \langle \alpha u_1 + \beta u_2, v \rangle = \alpha \langle u_1, v \rangle + \beta \langle u_2, v \rangle, \quad (4.3b)$$

$$(3) \quad \langle u, u \rangle > 0 \quad \text{if } u \neq 0, \quad (4.3c)$$

$$(4) \quad \langle u, u \rangle = 0 \quad \text{if } u = 0 \quad (4.3d)$$

If $\langle u, v \rangle = 0$, u and v are said to be *orthogonal*. Notice that these properties mimic familiar properties of the dot product in three-dimensional space. Equation (4.3) is easily derived from Equation (4.1). Note that from Equations (4.3a) and (4.3b),

$$\langle u, \alpha v \rangle = \alpha^* \langle v, u \rangle^* = \alpha^* \langle u, v \rangle$$

where α is a complex scalar.

Equation (4.1) is called an *unweighted or standard inner product*. A *weighted inner product* is given by

$$\langle u, v \rangle = \int_{\Omega} uv^* w d\Omega \quad (4.4)$$

where w is a suitable weight function.

4.2. OPERATORS IN LINEAR SPACES

We define the norm of the function u as

$$\|u\| = \sqrt{\langle u, u \rangle} \quad (4.5)$$

The norm is a measure of the “length” or “magnitude” of the function. (As far as a field is concerned, the norm is its rms value.) A vector is said to be *normal* if its norm is 1. Since the *Schwarz inequality*

$$|\langle u, v \rangle| \leq \|u\| \|v\| \quad (4.6)$$

holds for any inner product space, the angle θ between two nonzero vectors \mathbf{u} and \mathbf{v} can be obtained as

$$\theta = \cos^{-1} \frac{\langle \mathbf{u}, \mathbf{v} \rangle}{\|\mathbf{u}\| \|\mathbf{v}\|} \quad (4.7)$$

We now consider the operator equation

$$L\Phi = g \quad (4.8)$$

where L is any linear operator, Φ is the unknown function, and g is the source function. The space spanned by all functions resulting from the operator L is

$$\langle L\Phi, g \rangle = \langle \Phi, L^a g \rangle \quad (4.9)$$

The operator L is said to be

(1) self-adjoint if $L = L^a$, i.e., $\langle L\Phi, g \rangle = \langle \Phi, Lg \rangle$,

(2) positive definite if $\langle L\Phi, \Phi \rangle > 0$ for any $\Phi \neq 0$ in the domain of L ,

(3) negative definite if $\langle L\Phi, \Phi \rangle < 0$ for any $\Phi \neq 0$ in the domain of L .

The properties of the solution of Equation (4.8) depend strongly on the properties of the operator L . If, for example, L is positive definite, we can easily show that the solution of Φ in Equation (4.8) is unique, i.e., Equation (4.8) cannot have more than one solution. To do this, suppose that Φ and Ψ are two solutions to Equation (4.8) such that $L\Phi = g$ and $L\Psi = g$. Then, by virtue of linearity of L , $f = \Phi - \Psi$ is also a solution. Therefore, $Lf = 0$. Since L is positive definite, $f = 0$ implies that $\Phi = \Psi$ and confirms the uniqueness of the solution Φ .

Example 4.1

Find the inner product of $u(x) = 1 - x$ and $v(x) = 2x$ in the interval $(0, 1)$. □

Solution

In this case, both u and v are real functions. Hence

$$\begin{aligned}\langle u, v \rangle &= \langle v, u \rangle = \int_0^1 (1-x)2x \, dx \\ &= 2 \left(\frac{x^2}{2} - \frac{x^3}{3} \right) \Big|_0^1 = 0.333\end{aligned}$$

Example 4.2

Show that the operator

$$L = -\nabla^2 = -\frac{\partial^2}{\partial x^2} - \frac{\partial^2}{\partial y^2}$$

is self-adjoint. \square

Solution

$$\langle Lu, v \rangle = - \int_S v \nabla^2 u \, dS$$

Taking u and v to be real functions (for convenience) and applying the Green's identity

$$\oint_{\ell} v \frac{\partial u}{\partial n} \, dl = \int_S \nabla u \cdot \nabla v \, dS + \int_S v \nabla^2 u \, dS$$

yields

$$\langle Lu, v \rangle = \int_S \nabla u \cdot \nabla v \, dS - \oint_{\ell} v \frac{\partial u}{\partial n} \, dl \quad (4.10)$$

where S is bounded by ℓ and \mathbf{n} is the outward normal. Similarly

$$\langle u, Lv \rangle = \int_S \nabla u \cdot \nabla v \, dS - \oint_{\ell} u \frac{\partial v}{\partial n} \, dl \quad (4.11)$$

The line integrals in Equations (4.10) and (4.11) vanish under either the homogeneous Dirichlet or Neumann boundary conditions. Under the homogeneous mixed boundary conditions, they become equal. Thus, L is self-adjoint under any one of these boundary conditions. L is also positive definite. \blacksquare

4.3 Calculus of Variations

The calculus of variations, an extension of ordinary calculus, is a discipline that is concerned primarily with the theory of maxima and minima. Here we are concerned with seeking the extrema (minima or maxima) of an integral expression involving

4.3. CALCULUS OF VARIATIONS

a function of functions or *functionals*. Whereas a function produces a number as a result of giving values to one or more independent variables, a functional produces a number that depends on the entire form of one or more functions between prescribed limits. In a sense, a functional is a measure of the function. A simple example is the inner product $\langle u, v \rangle$.

In the calculus of variation, we are interested in the necessary condition for a functional to achieve a stationary value. This necessary condition on the functional is generally in the form of a differential equation with boundary conditions on the required function.

Consider the problem of finding a function $y(x)$ such that the function

$$I(y) = \int_a^b F(x, y, y') \, dx, \quad (4.12a)$$

subject to the boundary conditions

$$y(a) = A, \quad y(b) = B, \quad (4.12b)$$

is rendered stationary. The integrand $F(x, y, y')$ is a given function of x , y , and $y' = dy/dx$. In Equation (4.12a), $I(y)$ is called a *functional* or *variational* (or *stationary*) principle. The problem here is finding an extremizing function $y(x)$ for which the functional $I(y)$ has an extremum. Before attacking this problem, it is necessary that we introduce the operator δ , called the *variational symbol*.

The variation δy of a function $y(x)$ is an infinitesimal change in y for a fixed value of the independent variable x , i.e., for $\delta x = 0$. The variation δy of y vanishes at points where y is prescribed (since the prescribed value cannot be varied) and it is arbitrary elsewhere (see Figure 4.1). Due to the change in y (i.e., $y \rightarrow y + \delta y$), there

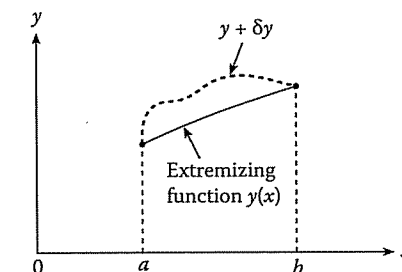


Figure 4.1
Variation of extremizing function with fixed ends.

is a corresponding change in F . The first variation of F at y is defined by

$$\delta F = \frac{\partial F}{\partial y} \delta y + \frac{\partial F}{\partial y'} \delta y' \quad (4.13)$$

This is analogous to the total differential of F ,

$$dF = \frac{\partial F}{\partial x} dx + \frac{\partial F}{\partial y} dy + \frac{\partial F}{\partial y'} dy' \quad (4.14)$$

where $\delta x = 0$ since x does not change as y changes to $y + \delta y$. Thus, we note that the operator δ is similar to the differential operator. Therefore, if $F_1 = F_1(y)$ and $F_2 = F_2(y)$, then

$$(i) \quad \delta(F_1 \pm F_2) = \delta F_1 \pm \delta F_2, \quad (4.15a)$$

$$(ii) \quad \delta(F_1 F_2) = F_2 \delta F_1 + F_1 \delta F_2, \quad (4.15b)$$

$$(iii) \quad \delta\left(\frac{F_1}{F_2}\right) = \frac{F_2 \delta F_1 - F_1 \delta F_2}{F_2^2}, \quad (4.15c)$$

$$(iv) \quad \delta(F_1)^n = n(F_1)^{n-1} \delta F_1, \quad (4.15d)$$

$$(v) \quad \frac{d}{dx}(\delta y) = \delta\left(\frac{dy}{dx}\right), \quad (4.15e)$$

$$(vi) \quad \delta \int_a^b y(x) dx = \int_a^b \delta y(x) dx \quad (4.15f)$$

A necessary condition for the function $I(y)$ in Equation (4.12a) to have an extremum is that the variation vanishes, i.e.,

$$\boxed{\delta I = 0} \quad (4.16)$$

To apply this condition, we must be able to find the variation δI of I in Equation (4.12a). To this end, let $h(x)$ be an increment in $y(x)$. For Equation (4.12b) to be satisfied by $y(x) + h(x)$,

$$h(a) = h(b) = 0 \quad (4.17)$$

The corresponding increment in I in Equation (4.12a) is

$$\begin{aligned} \Delta I &= I(y+h) - I(y) \\ &= \int_a^b [F(x, y+h, y'+h') - F(x, y, y')] dx \end{aligned}$$

On applying Taylor's expansion,

$$\begin{aligned} \Delta I &= \int_a^b [F_y(x, y, y')h - F_{y'}(x, y, y')h'] dx \\ &\quad + \text{higher order terms} \\ &= \delta I + O(h^2) \end{aligned}$$

where

$$\delta I = \int_a^b [F_y(x, y, y')h - F_{y'}(x, y, y')h'] dx$$

4.3. CALCULUS OF VARIATIONS

Integration by parts leads to

$$\delta I = \int_a^b \left[\frac{\partial F}{\partial y} - \frac{d}{dx} \left(\frac{\partial F}{\partial y'} \right) \right] h dx + \frac{\partial F}{\partial y'} h \Big|_{x=0}^{x=b}$$

The last term vanishes since $h(b) = h(a) = 0$ according to Equation (4.17). In order that $\delta I = 0$, the integrand must vanish, i.e.,

$$\frac{\partial F}{\partial y} - \frac{d}{dx} \left(\frac{\partial F}{\partial y'} \right) = 0$$

or

$$\boxed{F_y - \frac{d}{dx} F_{y'} = 0} \quad (4.18)$$

This is called *Euler's* (or *Euler-Lagrange*) equation. Thus a necessary condition for $I(y)$ to have an extremum for a given function $y(x)$ is that $y(x)$ satisfies Euler's equation.

This idea can be extended to more general cases. In the case considered so far, we have one dependent variable y and one independent variable x , i.e., $y = y(x)$. If we have one dependent variable u and two independent variables x and y , i.e., $u = u(x, y)$, then

$$I(u) = \int S F(x, y, u, u_x, u_y) dS \quad (4.19)$$

where $u_x = \partial u / \partial x$, $u_y = \partial u / \partial y$, and $dS = dx dy$. The functional in Equation (4.19) is stationary when $\delta I = 0$, and it is easily shown that the corresponding Euler's equation is [6]

$$\boxed{\frac{\partial F}{\partial u} - \frac{\partial}{\partial x} \left(\frac{\partial F}{\partial u_x} \right) - \frac{\partial}{\partial y} \left(\frac{\partial F}{\partial u_y} \right) = 0} \quad (4.20)$$

Next we consider the case of two independent variables x and y and two dependent variables $u(x, y)$ and $v(x, y)$. The functional to be minimized is

$$I(u, v) = \int S F(x, y, u, v, u_x, u_y, v_x, v_y) dS \quad (4.21)$$

The corresponding Euler's equation is

$$\boxed{\frac{\partial F}{\partial u} - \frac{\partial}{\partial x} \left(\frac{\partial F}{\partial u_x} \right) - \frac{\partial}{\partial y} \left(\frac{\partial F}{\partial u_y} \right) = 0} \quad (4.22a)$$

$$\boxed{\frac{\partial F}{\partial v} - \frac{\partial}{\partial x} \left(\frac{\partial F}{\partial v_x} \right) - \frac{\partial}{\partial y} \left(\frac{\partial F}{\partial v_y} \right) = 0} \quad (4.22b)$$

Another case is when the functional depends on second- or higher-order derivatives. For example,

$$I(y) = \int_a^b F(x, y, y', y'', \dots, y^{(n)}) dx \quad (4.23)$$

In this case, the corresponding Euler's equation is

$$F_y - \frac{d}{dx} F_{y'} + \frac{d^2}{dx^2} F_{y''} - \frac{d^3}{dx^3} F_{y'''} + \cdots + (-1)^n \frac{d^n}{dx^n} F_{y^{(n)}} = 0 \quad (4.24)$$

Note that each of Euler's equations (4.18), (4.20), (4.22), and (4.24) is a differential equation.

Example 4.3

Given the functional

$$I(\Phi) = \int_S \left[\frac{1}{2} (\Phi_x^2 + \Phi_y^2) - f(x, y)\Phi \right] dx dy,$$

obtain the relevant Euler's equation. \square

Solution

Let

$$F(x, y, \Phi, \Phi_x, \Phi_y) = \frac{1}{2} (\Phi_x^2 + \Phi_y^2) - f(x, y)\Phi$$

showing that we have two independent variables x and y and one dependent variable Φ . Hence, Euler's equation (4.20) becomes

$$-f(x, y) - \frac{\partial}{\partial x} \Phi_x - \frac{\partial}{\partial y} \Phi_y = 0$$

or

$$\Phi_{xx} + \Phi_{yy} = -f(x, y),$$

i.e.,

$$\nabla^2 \Phi = -f(x, y)$$

which is Poisson's equation. Thus, solving Poisson's equation is equivalent to finding Φ that extremizes the given functional $I(\Phi)$. \blacksquare

4.4 Construction of Functionals from PDEs

In the previous section, we noticed that Euler's equation produces the governing differential equation corresponding to a given functional or variational principle. Here we seek the inverse procedure of constructing a variational principle for a given differential equation. The procedure for finding the functional associated with the differential equation involves four basic steps [2, 7]:

4.4. CONSTRUCTION OF FUNCTIONALS FROM PDES

- Multiply the operator equation $L\Phi = g$ (Euler's equation) with the variational $\delta\Phi$ of the dependent variable Φ and integrate over the domain of the problem.
- Use the divergence theorem or integration by parts to transfer the derivatives to variation $\delta\Phi$.
- Express the boundary integrals in terms of the specified boundary conditions.
- Bring the variational operator δ outside the integrals.

The procedure is best illustrated with an example. Suppose we are interested in finding the variational principle associated with the Poisson's equation

$$\nabla^2 \Phi = -f(x, y) \quad (4.25)$$

which is the converse of what we did in Example 4.3. After taking step 1, we have

$$\begin{aligned} \delta I &= \iint [-\nabla^2 \Phi - f] \delta\Phi dx dy = 0 \\ &= - \iint \nabla^2 \Phi \delta\Phi dx dy - \iint f \delta\Phi dx dy \end{aligned}$$

This can be evaluated by applying divergence theorem or integrating by parts. To integrate by parts, let $u = \delta\Phi$, $dv = \frac{\partial}{\partial x} \left(\frac{\partial \Phi}{\partial x} \right) dx$ so that $du = \frac{\partial}{\partial x} \delta\Phi dx$, $v = \frac{\partial \Phi}{\partial x}$ and

$$-\int \left[\int \frac{\partial}{\partial x} \left(\frac{\partial \Phi}{\partial x} \right) \delta\Phi dx \right] dy = -\int \left[\delta\Phi \frac{\partial \Phi}{\partial x} - \int \frac{\partial \Phi}{\partial x} \frac{\partial}{\partial x} \delta\Phi dx \right] dy$$

Thus

$$\begin{aligned} \delta I &= \iint \left[\frac{\partial \Phi}{\partial x} \frac{\partial}{\partial x} \delta\Phi + \frac{\partial \Phi}{\partial y} \frac{\partial}{\partial y} \delta\Phi - \delta f \Phi \right] dx dy \\ &\quad - \int \delta\Phi \frac{\partial \Phi}{\partial x} dy - \int \delta\Phi \frac{\partial \Phi}{\partial y} dx \\ \delta I &= \frac{\delta}{2} \iint \left[\left(\frac{\partial \Phi}{\partial x} \right)^2 + \left(\frac{\partial \Phi}{\partial y} \right)^2 - 2f\Phi \right] dx dy \\ &\quad - \delta \int \Phi \frac{\partial \Phi}{\partial x} dy - \delta \int \Phi \frac{\partial \Phi}{\partial y} dx \end{aligned} \quad (4.26)$$

The last two terms vanish if we assume either the homogeneous Dirichlet or Neumann conditions at the boundaries. Hence

$$\delta I = \delta \iint \frac{1}{2} [\Phi_x^2 + \Phi_y^2 - 2\Phi f] dx dy,$$

i.e.,

$$I(\Phi) = \frac{1}{2} \iint [\Phi_x^2 + \Phi_y^2 - 2\Phi f] dx dy \quad (4.27)$$

as expected.

Rather than following the four steps listed above to find the function $I(\Phi)$ corresponding to the operator equation (4.8), an alternative approach is provided by Mikhlin [1, pp. 74–78]. According to Mikhlin, if L in Equation (4.8) is real, self-adjoint, and positive definite, the solution of Equation (4.8) minimizes the functional

$$I(\Phi) = \langle L\Phi, \Phi \rangle - 2\langle \Phi, g \rangle \quad (4.28)$$

(See Problem 4.6 for a proof.) Thus Equation (4.27), for example, can be obtained from Equation (4.25) by applying Equation (4.28). This approach has been applied to derive variational solutions of integral equations [8].

Other systematic approaches for the derivation of variational principles for EM problems include Hamilton's principle or the principle of least action [9, 10], Lagrange multipliers [10]–[14], and a technique described as variational electromagnetics [15, 16]. The method of Lagrange undetermined multipliers is particularly useful for deriving a functional for a PDE whose arguments are constrained. Table 4.1 provides the variational principles for some differential equations commonly found in EM-related problems.

Table 4.1 Variational Principle Associated with Common PDEs in EM¹

Name of Equation	Partial Differential Equation (PDE)	Variational Principle
Inhomogeneous		
wave equation	$\nabla^2\Phi + k^2\Phi = g$	$I(\Phi) = \frac{1}{2} \int_v [\nabla\Phi ^2 - k^2\Phi^2 + 2g\Phi] dv$
Homogeneous		
wave equation	$\nabla^2\Phi + k^2\Phi = 0$	$I(\Phi) = \frac{1}{2} \int_v [\nabla\Phi ^2 - k^2\Phi^2] dv$ or $\nabla^2\Phi - \frac{1}{u^2}\Phi_{tt} = 0$ $I(\Phi) = \frac{1}{2} \int^{t_0} \int_v [\nabla\Phi ^2 - \frac{1}{u^2}\Phi_t^2] dv dt$
Diffusion equation	$\nabla^2\Phi - k\Phi_t = 0$	$I(\Phi) = \frac{1}{2} \int^{t_0} \int_v [\nabla\Phi ^2 - k\Phi\Phi_t] dv dt$
Poisson's equation	$\nabla^2\Phi = g$	$I(\Phi) = \frac{1}{2} \int_v [\nabla\Phi ^2 + 2g\Phi] dv$
Laplace's equation	$\nabla^2\Phi = 0$	$I(\Phi) = \frac{1}{2} \int_v [\nabla\Phi ^2] dv$

¹ Note that $|\nabla\Phi|^2 = \nabla\Phi \cdot \nabla\Phi = \Phi_x^2 + \Phi_y^2 + \Phi_z^2$.

Example 4.4

Find the functional for the ordinary differential equation

$$y'' + y + x = 0, \quad 0 < x < 1$$

subject to $y(0) = y(1) = 0$. \square **Solution**

Given that

$$\frac{d^2y}{dx^2} + y + x = 0, \quad 0 < x < 1,$$

we obtain

$$\begin{aligned} \delta I &= \int_0^1 \left(\frac{d^2y}{dx^2} + y + x \right) \delta y dx = 0 \\ &= \int_0^1 \frac{d^2y}{dx^2} \delta y dx + \int_0^1 y \delta y dx + \int_0^1 x \delta y dx \end{aligned}$$

Integrating the first term by parts,

$$\delta I = \delta y \left. \frac{dy}{dx} \right|_{x=0}^{x=1} - \int_0^1 \frac{dy}{dx} \frac{d}{dx} \delta y + \int_0^1 \frac{1}{2} \delta(y^2) dx + \delta \int_0^1 xy dx$$

Since y is fixed at $x = 0, 1$, $\delta y(1) = \delta y(0) = 0$. Hence

$$\begin{aligned} \delta I &= - \int_0^1 \frac{1}{2} \left(\frac{dy}{dx} \right)^2 dx + \frac{1}{2} \delta \int_0^1 y^2 dx + \delta \int_0^1 xy dx \\ &= \frac{\delta}{2} \int_0^1 [-y'^2 + y^2 + 2xy] dx \end{aligned}$$

or

$$I(y) = \frac{1}{2} \int_0^1 [-y'^2 + y^2 + 2xy] dx$$

Check: Taking $F(x, y, y') = y'^2 - y^2 - 2xy$, Euler's equation $F_y - \frac{d}{dx}F_{y'} = 0$ gives the differential equation

$$y'' + y + x = 0 \quad \square$$

4.5 Rayleigh-Ritz Method

The Rayleigh-Ritz method is the direct variational method for minimizing a given functional. It is direct in that it yields a solution to the variational problem without recourse to the associated differential equation [17]. In other words, it is the direct

application of variational principles discussed in the previous sections. The method was first presented by Rayleigh in 1877 and extended by Ritz in 1909. Without loss of generality, let the associated variational principle be

$$I(\Phi) = \int_S F(x, y, \Phi, \Phi_x, \Phi_y) dS \quad (4.29)$$

Our objective is to minimize this integral. In the Rayleigh–Ritz method, we select a linearly independent set of functions called *expansion functions* (or *basis functions*) u_n and construct an approximate solution to Equation (4.29), satisfying some prescribed boundary conditions. The solution is in the form of a finite series

$$\tilde{\Phi} \simeq \sum_{n=1}^N a_n u_n + u_o \quad (4.30)$$

where u_o meets the nonhomogeneous boundary conditions, and u_n satisfies homogeneous boundary conditions. a_n are expansion coefficients to be determined and $\tilde{\Phi}$ is an approximate solution to Φ (the exact solution). We substitute Equation (4.30) into Equation (4.29) and convert the integral $I(\Phi)$ into a function of N coefficients a_1, a_2, \dots, a_N , i.e.,

$$I(\Phi) = I(a_1, a_2, \dots, a_N)$$

The minimum of this function is obtained when its partial derivatives with respect to each coefficient are zero:

$$\frac{\partial I}{\partial a_1} = 0, \quad \frac{\partial I}{\partial a_2} = 0, \dots, \frac{\partial I}{\partial a_N} = 0$$

or

$$\boxed{\frac{\partial I}{\partial a_n} = 0, \quad n = 1, 2, \dots, N} \quad (4.31)$$

Thus we obtain a set of N simultaneous equations. The system of linear algebraic equations obtained is solved to get a_n , which are finally substituted into the approximate solution of Equation (4.30). In the approximate solution of Equation (4.30), if $\tilde{\Phi} \rightarrow \Phi$ as $N \rightarrow \infty$ in some sense, then the procedure is said to *converge* to the exact solution.

An alternative, perhaps easier, procedure to determine the expansion coefficients a_n is by solving a system of simultaneous equations obtained as follows [4, 18]. Substituting Equation (4.30) (ignoring u_o since it can be lumped with the right-hand side of the equation) into Equation (4.28) yields

$$\begin{aligned} I &= \left\langle \sum_{m=1}^N a_m L u_m, \sum_{n=1}^N a_n u_n \right\rangle - 2 \left\langle \sum_{m=1}^N a_m u_m, g \right\rangle \\ &= \sum_{m=1}^N \sum_{n=1}^N \langle L u_m, u_n \rangle a_n a_m - 2 \sum_{m=1}^N \langle u_m, g \rangle a_m \end{aligned}$$

4.5. RAYLEIGH–RITZ METHOD

Expanding this into powers of a_m results in

$$\begin{aligned} I &= \langle L u_m, u_m \rangle a_m^2 + \sum_{n \neq m}^N \langle L u_m, u_n \rangle a_m a_n + \sum_{k \neq m}^N \langle L u_k, u_m \rangle a_k a_m \\ &\quad - 2 \langle g, u_m \rangle a_m + \text{terms not containing } a_m \end{aligned} \quad (4.32)$$

Assuming L is self-adjoint and replacing k with n in the second summation,

$$I = \langle L u_m, u_m \rangle a_m^2 + 2 \sum_{n \neq m}^N \langle L u_m, u_n \rangle a_n a_m - 2 \langle g, u_m \rangle a_m + \dots \quad (4.33)$$

Since we are interested in selecting a_m such that I is minimized, Equation (4.33) must satisfy Equation (4.31). Thus differentiating Equation (4.33) with respect to a_m and setting the result equal to zero leads to

$$\sum_{n=1}^N \langle L u_m, u_n \rangle a_n = \langle g, u_m \rangle, \quad m = 1, 2, \dots, N \quad (4.34)$$

which can be put in matrix form as

$$\begin{bmatrix} \langle L u_1, u_1 \rangle & \langle L u_1, u_2 \rangle & \cdots & \langle L u_1, u_N \rangle \\ \vdots & & & \vdots \\ \langle L u_N, u_1 \rangle & \langle L u_N, u_2 \rangle & \cdots & \langle L u_N, u_N \rangle \end{bmatrix} \begin{bmatrix} a_1 \\ \vdots \\ a_N \end{bmatrix} = \begin{bmatrix} \langle g, u_1 \rangle \\ \vdots \\ \langle g, u_N \rangle \end{bmatrix} \quad (4.35a)$$

or

$$[A][X] = [B] \quad (4.35b)$$

where $A_{mn} = \langle L u_m, u_n \rangle$, $B_m = \langle g, u_m \rangle$, $X_n = a_n$. Solving for $[X]$ in Equation (4.35) and substituting a_m in Equation (4.30) gives the approximate solution $\tilde{\Phi}$. Equation (4.35) is called the *Rayleigh–Ritz system*.

We are yet to know how the expansion functions are selected. They are selected to satisfy the prescribed boundary conditions of the problem. u_o is chosen to satisfy the inhomogeneous boundary conditions, while $u_n (n = 1, 2, \dots, N)$ are selected to satisfy the homogeneous boundary conditions. If the prescribed boundary conditions are all homogeneous (Dirichlet conditions), $u_o = 0$. The next section will discuss more on the selection of the expansion functions.

The Rayleigh–Ritz method has two major limitations. First, the variational principle in Equation (4.29) may not exist in some problems such as in nonself-adjoint equations (odd order derivatives). Second, it is difficult, if not impossible, to find the functions u_o satisfying the global boundary conditions for the domains with complicated geometries [19].

Example 4.5

Use the Rayleigh-Ritz method to solve the ordinary differential equation:

$$\Phi'' + 4\Phi - x^2 = 0, \quad 0 < x < 1$$

subject to $\Phi(0) = 0 = \Phi(1)$. \square

Solution

The exact solution is

$$\Phi(x) = \frac{\sin 2(1-x) - \sin 2x}{8 \sin 2} + \frac{x^2}{4} - \frac{1}{8}$$

The variational principle associated with $\Phi'' + 4\Phi - x^2 = 0$ is

$$I(\Phi) = \int_0^1 [(\Phi')^2 - 4\Phi^2 + 2x^2\Phi] dx \quad (4.36)$$

This is readily verified using Euler's equation. We let the approximate solution be

$$\tilde{\Phi} = u_o + \sum_{n=1}^N a_n u_n \quad (4.37)$$

where $u_o = 0$, $u_n = x^n(1-x)$ since $\Phi(0) = 0 = \Phi(1)$ must be satisfied. [This choice of u_n is not unique. Other possible choices are $u_n = x(1-x^n)$ and $u_n = \sin n\pi x$. Note that each choice satisfies the prescribed boundary conditions.] Let us try different values of N , the number of expansion coefficients. We can find the expansion coefficients a_n in two ways: using the functional directly as in Equation (4.31) or using the Rayleigh-Ritz system of Equation (4.35).

Method 1

For $N = 1$, $\tilde{\Phi} = a_1 u_1 = a_1 x(1-x)$. Substituting this into Equation (4.36) gives

$$\begin{aligned} I(a_1) &= \int_0^1 \left[a_1^2 (1-2x)^2 - 4a_1^2 (x-x^2)^2 + 2a_1 x^3 (1-x) \right] dx \\ &= \frac{1}{5} a_1^2 + \frac{1}{10} a_1 \end{aligned}$$

$I(a_1)$ is minimum when

$$\frac{\partial I}{\partial a_1} = 0 \rightarrow \frac{2}{5} a_1 + \frac{1}{10} = 0 \quad \text{or} \quad a_1 = -\frac{1}{4}$$

Hence the quadratic approximate solution is

$$\tilde{\Phi} = -\frac{1}{4} x(1-x) \quad (4.38)$$

4.5. RAYLEIGH-RITZ METHOD

For $N = 2$, $\tilde{\Phi} = a_1 u_1 + a_2 u_2 = a_1 x(1-x) + a_2 x^2(1-x)$. Substituting $\tilde{\Phi}$ into Equation (4.36),

$$\begin{aligned} I(a_1, a_2) &= \int_0^1 \left[[a_1(1-2x) + a_2(2x-3x^2)]^2 - 4[a_1(x-x^2) + a_2(x^2-x^3)]^2 \right. \\ &\quad \left. + 2a_1 x^2(x-x^2) + 2a_1 x^2(x^2-x^3) \right] dx \\ &= \frac{1}{5} a_1^2 + \frac{2}{21} a_2^2 + \frac{1}{5} a_1 a_2 + \frac{1}{10} a_1 + \frac{1}{15} a_2 \\ \frac{\partial I}{\partial a_1} &= 0 \rightarrow \frac{2}{5} a_1 + \frac{1}{5} a_2 + \frac{1}{10} = 0 \end{aligned}$$

or

$$4a_1 + 2a_2 = -1 \quad (4.39a)$$

$$\frac{\partial I}{\partial a_2} = 0 \rightarrow \frac{4}{21} a_2 + \frac{1}{5} a_1 + \frac{1}{15} = 0$$

or

$$21a_1 + 20a_2 = -7 \quad (4.39b)$$

Solving Equation (4.39) gives

$$a_1 = -\frac{6}{38}, \quad a_2 = -\frac{7}{38}$$

and hence the cubic approximate solution is

$$\tilde{\Phi} = -\frac{6}{38} x(1-x) - \frac{7}{38} x^2(1-x)$$

or

$$\tilde{\Phi} = \frac{x}{38} (7x^2 - x - 6)$$

Method 2

We now determine a_m using Equation (4.35). From the given differential equation,

$$L = \frac{d^2}{dx^2} + 4, \quad g = x^2$$

Hence

$$\begin{aligned} A_{mn} &= \langle Lu_m, u_n \rangle = \langle u_m, Lu_n \rangle \\ &= \int_0^1 x^m (1-x) \left[\left(\frac{d^2}{dx^2} + 4 \right) x^n (1-x) \right] dx, \\ A_{mn} &= \frac{n(n-1)}{m+n-1} - \frac{2n^2}{m+n} + \frac{n(n+1)+4}{m+n+1} - \frac{8}{m+n+2} + \frac{4}{m+n+3}, \\ B_n &= \langle g, u_n \rangle = \int_0^1 x^2 n^n (1-x) dx = \frac{1}{n+3} - \frac{1}{n+4} \end{aligned}$$

When $N = 1$, $A_{11} = -\frac{1}{5}$, $B_1 = \frac{1}{20}$, i.e.,

$$-\frac{1}{5}a_1 = \frac{1}{20} \rightarrow a_1 = -\frac{1}{4}$$

as before. When $N = 2$,

$$A_{11} = -\frac{1}{5}, A_{12} = A_{21} = -\frac{1}{10}, A_{22} = -\frac{2}{21}, B_1 = \frac{1}{20}, B_2 = \frac{1}{30}$$

Hence

$$\begin{bmatrix} -\frac{1}{5} & -\frac{1}{10} \\ -\frac{1}{10} & -\frac{2}{21} \end{bmatrix} \begin{bmatrix} a_1 \\ a_2 \end{bmatrix} = \begin{bmatrix} \frac{1}{20} \\ \frac{1}{30} \end{bmatrix}$$

which gives $a_1 = -\frac{6}{38}$, $a_2 = -\frac{7}{38}$ as obtained previously. When $N = 3$,

$$A_{13} = A_{31} = -\frac{13}{210}, A_{23} = A_{32} = -\frac{28}{105}, A_{33} = -\frac{22}{315}, B_3 = \frac{1}{42},$$

i.e.,

$$\begin{bmatrix} -\frac{1}{5} & -\frac{1}{10} & -\frac{13}{210} \\ -\frac{1}{10} & -\frac{2}{21} & -\frac{28}{105} \\ -\frac{13}{210} & -\frac{28}{105} & -\frac{22}{315} \end{bmatrix} \begin{bmatrix} a_1 \\ a_2 \\ a_3 \end{bmatrix} = \begin{bmatrix} \frac{1}{20} \\ \frac{1}{30} \\ \frac{1}{42} \end{bmatrix}$$

from which we obtain

$$a_1 = -\frac{6}{38}, \quad a_2 = -\frac{7}{38}, \quad a_3 = 0$$

showing that we obtain the same solution as for the case $N = 2$. For different values of x , $0 < x < 1$, the Rayleigh–Ritz solution is compared with the exact solution in Table 4.2. ■

Table 4.2 Comparison of Exact Solution with the Rayleigh–Ritz Solution of

$$\Phi'' + 4\Phi - x^2 = 0, \Phi(0) = 0 = \Phi(1)$$

x	Exact Solution	Rayleigh–Ritz		Solution $N = 2$
		$N = 1$	$N = 2$	
0.0	0.0	0.0	0.0	0.0
0.2	-0.0301	-0.0400	-0.0312	
0.4	-0.0555	-0.0600	-0.0556	
0.6	-0.0625	-0.0625	-0.0644	
0.8	-0.0489	-0.0400	-0.0488	
1.0	0.0	0.0	0.0	

4.5. RAYLEIGH–RITZ METHOD

Example 4.6

Using the Rayleigh–Ritz method, solve Poisson's equation:

$$\nabla^2 V = -\rho_o, \quad \rho_o = \text{constant}$$

in a square $-1 \leq x \leq 1$, $-1 \leq y \leq 1$, subject to the homogeneous boundary conditions $V(x, \pm 1) = 0 = V(\pm 1, y)$. ■

Solution

Due to the symmetry of the problem, we choose the basis functions as

$$u_{mn} = (1-x^2)(1-y^2)(x^{2m}y^{2n} + x^{2n}y^{2m}), \quad m, n = 0, 1, 2, \dots$$

Hence

$$\tilde{\Phi} = (1-x^2)(1-y^2)[a_1 + a_2(x^2+y^2) + a_3x^2y^2 + a_4(x^4+y^4) + \dots]$$

Case 1: When $m = n = 0$, we obtain the first approximation ($N = 1$) as

$$\tilde{\Phi} = a_1 u_1$$

where $u_1 = (1-x^2)(1-y^2)$.

$$\begin{aligned} A_{11} &= \langle Lu_1, u_1 \rangle = \int_{-1}^1 \int_{-1}^1 \left(\frac{\partial^2 u_1}{\partial x^2} + \frac{\partial^2 u_1}{\partial y^2} \right) u_1 dx dy \\ &= -8 \int_0^1 \int_0^1 (2-x^2-y^2)(1-x^2)(1-y^2) dx dy \\ &= -\frac{256}{45}, \end{aligned}$$

$$B_1 = \langle g, u_1 \rangle = - \int_{-1}^1 \int_{-1}^1 (1-x^2)(1-y^2) \rho_o dx dy = -\frac{16\rho_o}{9}$$

Hence

$$-\frac{256}{45}a_1 = -\frac{16}{9}\rho_o \rightarrow a_1 = \frac{5}{16}\rho_o$$

and

$$\tilde{\Phi} = \frac{5}{16}\rho_o(1-x^2)(1-y^2)$$

Case 2: When $m = n = 1$, we obtain the second order approximation ($N = 2$) as

$$\tilde{\Phi} = a_1 u_1 + a_2 u_2$$

where $u_1 = (1 - x^2)(1 - y^2)$, $u_2 = (1 - x^2)(1 - y^2)(x^2 + y^2)$. A_{11} and B_1 are the same as in case 1.

$$A_{12} = A_{21} = \langle Lu_1, u_2 \rangle = -\frac{1024}{525},$$

$$A_{22} = \langle Lu_2, u_2 \rangle = -\frac{11264}{4725},$$

$$B_2 = \langle g, u_2 \rangle = -\frac{32}{45}\rho_o$$

Hence

$$\begin{bmatrix} -\frac{256}{45} & -\frac{1024}{525} \\ -\frac{1024}{525} & -\frac{11264}{4725} \end{bmatrix} \begin{bmatrix} a_1 \\ a_2 \end{bmatrix} = \begin{bmatrix} -\frac{16}{9}\rho_o \\ -\frac{32}{45}\rho_o \end{bmatrix}$$

Solving this yields

$$a_1 = \frac{1295}{4432}\rho_o = 0.2922\rho_o, \quad a_2 = \frac{525}{8864}\rho_o = 0.0592\rho_o$$

and

$$\tilde{\Phi} = (1 - x^2)(1 - y^2)(0.2922 + 0.0592(x^2 + y^2))\rho_o$$

4.6 Weighted Residual Method

As noted earlier, the Rayleigh–Ritz method is applicable when a suitable functional exists. In cases where such a functional cannot be found, we apply one of the techniques collectively referred to as the *method of weighted residuals*. The method is more general and has wider application than the Rayleigh–Ritz method because it is not limited to a class of variational problems.

Consider the operator equation

$$L\Phi = g \quad (4.40)$$

In the weighted residual method, the solution to Equation (4.40) is approximated, in the same manner as in the Rayleigh–Ritz method, using the expansion functions, u_n , i.e.,

$$\tilde{\Phi} = \sum_{n=1}^N a_n u_n \quad (4.41a)$$

where a_n are the expansion coefficients. We seek to make

$$L\tilde{\Phi} \approx g \quad (4.41b)$$

4.6. WEIGHTED RESIDUAL METHOD

Substitution of the approximate solution in the operator equation results in a *residual* R (an error in the equation), i.e.,

$$R = L(\tilde{\Phi} - \Phi) = L\tilde{\Phi} - g \quad (4.42)$$

In the weighted residual method, the weighting functions w_m (which, in general, are not the same as the expansion functions u_n) are chosen such that the integral of a weighted residual of the approximation is zero, i.e.,

$$\int w_m R dv = 0$$

or

$$\langle w_m, R \rangle = 0 \quad (4.43)$$

If a set of *weighting functions* $\{w_m\}$ (also known as *testing functions*) are chosen and the inner product of Equation (4.41b) is taken for each w_m , we obtain

$$\sum_{n=1}^N a_n \langle w_m, Lu_n \rangle = \langle w_m, g \rangle, \quad m = 1, 2, \dots, N \quad (4.44)$$

The system of linear equations (4.44) can be cast into matrix form as

$$[A][X] = [B] \quad (4.45)$$

where $A_{mn} = \langle w_m, Lu_n \rangle$, $B_m = \langle w_m, g \rangle$, $X_n = a_n$. Solving for $[X]$ in Equation (4.45) and substituting for a_n in Equation (4.41a) gives the approximate solution to Equation (4.40). However, there are different ways of choosing the weighting functions w_m leading to

- collocation (or point-matching) method,
- subdomain method,
- Galerkin method,
- least squares method.

4.6.1 Collocation Method

We select the Dirac delta function as the weighting function, i.e.,

$$w_m(\mathbf{r}) = \delta(\mathbf{r} - \mathbf{r}_m) = \begin{cases} 1, & \mathbf{r} = \mathbf{r}_m \\ 0, & \mathbf{r} \neq \mathbf{r}_m \end{cases} \quad (4.46)$$

Substituting Equation (4.46) into Equation (4.43) results in

$$R(\mathbf{r}) = 0 \quad (4.47)$$

Thus we select as many collocation (or matching) points in the interval as there are unknown coefficients a_n and make the residual zero at those points. This is equivalent to enforcing

$$\sum_{n=1}^N La_n u_n = g \quad (4.48)$$

at discrete points in the region of interest, generally where boundary conditions must be met. Although the point-matching method is the simplest specialization for computation, it is not possible to determine in advance for a particular operator equation what collocation points would be suitable. An accurate result is ensured only if judicious choice of the match points is taken. (This will be illustrated in Example 4.7.) It is important to note that the finite difference method is a particular case of collocation with locally defined expansion functions [20]. The validity and legitimacy of the point-matching technique are discussed in [21, 22].

4.6.2 Subdomain Method

We select weighting functions w_m , each of which exists only over subdomains of the domain of Φ . Typical examples of such functions for one-dimensional problems are illustrated in Figure 4.2 and defined as follows:

(1) Piecewise uniform (or pulse) function:

$$w_m(x) = \begin{cases} 1, & x_{m-1} < x < x_{m+1} \\ 0, & \text{otherwise} \end{cases} \quad (4.49a)$$

(2) Piecewise linear (or triangular) function:

$$w_m(x) = \begin{cases} \frac{\Delta - |x - x_m|}{\Delta}, & x_{m-1} < x < x_{m+1} \\ 0, & \text{otherwise} \end{cases} \quad (4.49b)$$

(3) Piecewise sinusoidal function:

$$w_m(x) = \begin{cases} \frac{\sin k(x - |x - x_m|)}{\Delta}, & x_{m-1} < x < x_{m+1} \\ 0, & \text{otherwise} \end{cases} \quad (4.49c)$$

Using the unit pulse function, for example, is equivalent to dividing the domain of Φ into as many subdomains as there are unknown terms and letting the average value of R over such subdomains vanish.

4.6.3 Galerkin Method

We select basis functions as the weighting function, i.e., $w_m = u_m$. When the operator is a linear differential operator of even order, the Galerkin method¹ reduces

¹The Galerkin method was developed by the Russian engineer B.G. Galerkin in 1915.

4.6. WEIGHTED RESIDUAL METHOD

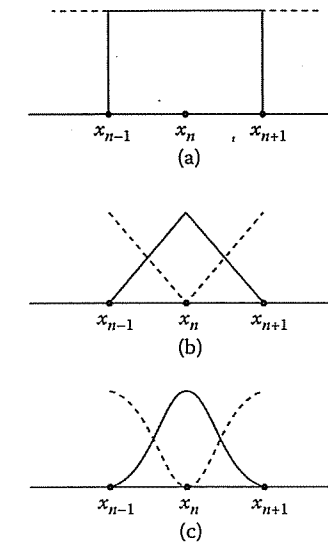


Figure 4.2

Typical subdomain weighting functions: (a) piecewise uniform function, (b) piecewise linear function, (c) piecewise sinusoidal function.

to the Rayleigh–Ritz method. This is due to the fact that the differentiation can be transferred to the weighting functions and the resulting coefficient matrix $[A]$ will be symmetric [7]. In order for the Galerkin method to be applicable, the operator must be of a certain type. Also, the expansion function u_n must span both the domain and the range of the operator.

4.6.4 Least Squares Method

This involves minimizing the integral of the square of the residual, i.e.,

$$\frac{\partial}{\partial a_m} \int R^2 dv = 0$$

or

$$\int \frac{\partial R}{\partial a_m} R dv = 0 \quad (4.50)$$

Comparing Equation (4.50) with Equation (4.43) shows that we must choose

$$w_m = \frac{\partial R}{\partial a_m} = Lu_m \quad (4.51)$$

This may be viewed as requiring that

$$\frac{1}{2} \int R^2 dv$$

be minimum. In other words, the choice of w_m corresponds to minimizing the mean square residual. It should be noted that the least squares method involves higher order derivatives which will, in general, lead to a better convergence than the Rayleigh-Ritz method or Galerkin method, but it has the disadvantage of requiring higher order weighting functions [19].

The concept of convergence discussed in the previous section applies here as well. That is, if the approximate solution $\tilde{\Phi}$ were to converge to the exact solution Φ as $N \rightarrow \infty$, the residual must approach zero as $N \rightarrow \infty$. Otherwise, the sequence of approximate solutions may not converge to any meaningful result.

The inner product involved in applying a weighted residual method can sometimes be evaluated analytically, but in most practical situations it is evaluated numerically. Due to a careless evaluation of the inner product, one may think that the least squares technique is being used when the resulting solution is identical to a point-matching solution. To avoid such erroneous results or conclusions, one must be certain that the overall number of points involved in the numerical integration is not smaller than the number of unknowns, N , involved in the weighted residual method [23].

The accuracy and efficiency of a weighted residual method are largely dependent on the selection of expansion functions. The solution may be exact or approximate depending on how we select the expansion and weighting functions [17]. The criteria for selecting expansion and weighting functions in a weighted residual method are provided in the work of Sarkar and others [24]–[27]. We summarize their results here. The expansion functions u_n are selected to satisfy the following requirements [27]:

- (1) The expansion functions should be in the domain of the operator L in some sense, i.e., they should satisfy the differentiability criterion and they must satisfy the boundary conditions for the operator. It is not necessary for each expansion function to satisfy exactly the boundary conditions. What is required is that the total solution must satisfy the boundary conditions at least in some distributional sense. The same holds for the differentiability conditions.
- (2) The expansion functions must be such that $L u_n$ form a complete set for the range of the operator. It really does not matter whether the expansion functions are complete in the domain of the operator. What is important is that u_n must be chosen in such a way that $L u_n$ is complete. This will be illustrated in Example 4.8.

From a mathematical point of view, the choice of expansion functions does not depend on the choice of weighting functions. It is required that the weighting functions w_n must make the difference $\Phi - \tilde{\Phi}$ small. For the Galerkin method to be applicable, the expansion functions u_n must span both the domain and the range of the operator. For the least squares method, the weighting functions are already presented and defined by $L u_n$. It is necessary that $L u_n$ form a complete set. The least squares technique mathematically and numerically is one of the safest techniques to utilize when very little is known about the nature of the operator and the exact solution.

4.6. WEIGHTED RESIDUAL METHOD

Example 4.7

Find an approximate solution to

$$\Phi'' + 4\Phi - x^2 = 0, \quad 0 < x < 1,$$

with $\Phi(0) = 0$, $\Phi'(1) = 1$, using the method of weighted residuals. \square

Solution

The exact solution is

$$\Phi(x) = \frac{\cos 2(x-1) + 2 \sin 2x}{8 \cos 2} - \frac{x^2}{4} - \frac{1}{8} \quad (4.52)$$

Let the approximate solution be

$$\tilde{\Phi} = u_0 + \sum_{n=1}^N a_n u_n \quad (4.53)$$

The boundary conditions can be decomposed into two parts:

- (1) homogeneous part $\rightarrow \Phi(0) = 0, \Phi'(0) = 0$,
- (2) inhomogeneous part $\rightarrow \Phi'(1) = 1$.

We choose u_0 to satisfy the inhomogeneous boundary condition. A reasonable choice is

$$u_0 = x \quad (4.54a)$$

We choose $u_n (n = 1, 2, \dots, N)$ to satisfy the homogeneous boundary condition. Suppose we select

$$u_n(x) = x^n \left(x - \frac{n+1}{n} \right) \quad (4.54b)$$

Thus, if we take $N = 2$, the approximate solution is

$$\begin{aligned} \tilde{\Phi} &= u_0 + a_1 u_1 + a_2 u_2 \\ &= x + a_1 x(x-2) + a_2 x^2(x-3/2) \end{aligned} \quad (4.55)$$

where the expansion coefficients, a_1 and a_2 , are to be determined. We find the residual R using Equation (4.42), namely,

$$\begin{aligned} R &= L \tilde{\Phi} - g \\ &= \left(\frac{d^2}{dx^2} + 4 \right) \tilde{\Phi} - x^2 \\ &= a_1 (4x^2 - 8x + 2) + a_2 (4x^3 - 6x^2 + 6x - 3) - x^2 + 4x \end{aligned} \quad (4.56)$$

We now apply each of the four techniques discussed and compare the solutions.

Method 1: (collocation or point-matching method)

Since we have two unknowns a_1 and a_2 , we select two match points, at $x = \frac{1}{3}$ and $x = \frac{2}{3}$, and set the residual equal to zero at those points, i.e.,

$$R\left(\frac{1}{3}\right) = 0 \rightarrow 6a_1 + 41a_2 = 33$$

$$R\left(\frac{2}{3}\right) = 0 \rightarrow 42a_1 + 13a_2 = 60$$

Solving these equations,

$$a_1 = \frac{677}{548}, \quad a_2 = \frac{342}{548}$$

Substituting a_1 and a_2 into Equation (4.55) gives

$$\tilde{\Phi}(x) = -1.471x + 0.2993x^2 + 0.6241x^3 \quad (4.57)$$

To illustrate the dependence of the solution on the match points, suppose we select $x = \frac{1}{4}$ and $x = \frac{3}{4}$ as the match points. Then

$$R\left(\frac{1}{4}\right) = 0 \rightarrow -4a_1 + 29a_2 = 15$$

$$R\left(\frac{3}{4}\right) = 0 \rightarrow 28a_1 + 3a_2 = 39$$

Solving for a_1 and a_2 , we obtain

$$a_1 = \frac{543}{412}, \quad a_2 = \frac{288}{412}$$

with the approximate solution

$$\tilde{\Phi}(x) = -1.636x + 0.2694x^2 + 0.699x^3 \quad (4.58)$$

We will refer to the solutions in Equations (4.57) and (4.58) as collocation 1 and collocation 2, respectively. It is evident from Table 4.3 that collocation 2 is more accurate than collocation 1.

Method 2: (subdomain method)

Divide the interval $0 < x < 1$ into two segments since we have two unknowns a_1 and a_2 . We select pulse functions as weighting functions:

$$w_1 = 1, \quad 0 < x < \frac{1}{2},$$

$$w_2 = 1, \quad \frac{1}{2} < x < 1$$

4.6. WEIGHTED RESIDUAL METHOD

so that

$$\int_0^{1/2} w_1 R dx = 0 \rightarrow -8a_1 + 45a_2 = 22$$

$$\int_{1/2}^1 w_2 R dx = 0 \rightarrow 40a_1 + 3a_2 = 58$$

Solving the two equations gives

$$a_1 = \frac{53}{38}, \quad a_2 = \frac{28}{38}$$

and hence Equation (4.55) becomes

$$\tilde{\Phi}(x) = -1.789x + 0.2895x^2 + 0.7368x^3 \quad (4.59)$$

Method 3: (Galerkin method)

In this case, we select $w_m = u_m$, i.e.,

$$w_1 = x(x-2), \quad w_2 = x^2(x-3/2)$$

We now apply Equation (4.43), namely, $\int w_m R dx = 0$. We obtain

$$\int_0^1 (x^2 - 2x) R dx = 0 \rightarrow 24a_1 + 11a_2 = 41$$

$$\int_0^1 \left(x^3 - \frac{3}{2}x^2\right) R dx = 0 \rightarrow 77a_1 + 15a_2 = 119$$

Solving these leads to

$$a_1 = \frac{694}{487}, \quad a_2 = \frac{301}{487}$$

Substituting a_1 and a_2 into Equation (4.55) gives

$$\tilde{\Phi}(x) = -1.85x + 0.4979x^2 + 0.6181x^3 \quad (4.60)$$

Method 4: (least squares method)

For this method, we select $w_m = \frac{\partial R}{\partial a_m}$, i.e.,

$$w_1 = 4x^2 - 8x + 2, \quad w_2 = 4x^3 - 6x^2 + 6x - 3$$

Applying Equation (4.43)

$$\int_0^1 w_1 R dx = 0 \rightarrow 7a_1 - 2a_2 = 8$$

$$\int_0^1 w_2 R dx = 0 \rightarrow -112a_1 + 438a_2 = 161$$

Thus

$$a_1 = \frac{3826}{2842}, \quad a_2 = \frac{2023}{2842}$$

and Equation (4.55) becomes

$$\tilde{\Phi}(x) = -1.6925x + 0.2785x^2 + 0.7118x^3 \quad (4.61)$$

Notice that the approximate solutions in Equations (4.57) to (4.61) all satisfy the boundary conditions $\Phi(0) = 0$ and $\Phi'(1) = 1$. The five approximate solutions are compared in Table 4.3.

Table 4.3 Comparison of the Weighted Residual Solutions of the Problem in Example 4.7 with the Exact Solution in Equation (4.52)

x	Exact Solution	Collocation 1	Collocation 2	Subdomain	Galerkin	Least Squares
0.0	0.0000	0.0000	0.0000	0.0000	0.0000	0.0000
0.1	-0.1736	-0.1435	-0.1602	-0.1753	-0.1794	-0.1657
0.2	-0.3402	-0.2772	-0.3108	-0.3403	-0.3451	-0.3217
0.3	-0.4928	-0.3975	-0.4477	-0.4907	-0.4935	-0.4635
0.4	-0.6248	-0.5006	-0.5666	-0.6221	-0.6208	-0.5869
0.5	-0.7303	-0.5827	-0.6633	-0.7300	-0.7233	-0.6877
0.6	-0.8042	-0.6400	-0.7336	-0.8100	-0.7972	-0.7615
0.7	-0.8424	-0.6690	-0.7734	-0.8577	-0.8390	-0.8041
0.8	-0.8422	-0.6657	-0.7785	-0.8687	-0.8449	-0.8113
0.9	-0.8019	-0.6264	-0.7446	-0.8385	-0.8111	-0.7788
1.0	-0.7216	-0.5476	-0.6676	-0.7627	-0.7340	-0.7022

Example 4.8

This example illustrates the fact that expansion functions u_n must be selected such that $L u_n$ form a complete set for the range of the operator L . Consider the differential equation

$$-\Phi'' = 2 + \sin x, \quad 0 \leq x \leq 2\pi \quad (4.62)$$

subject to

$$\Phi(0) = \Phi(2\pi) = 0 \quad (4.63)$$

Suppose we carelessly select

$$u_n = \sin nx, \quad n = 1, 2, \dots \quad (4.64)$$

as the expansion functions, the approximate solution is

$$\tilde{\Phi} = \sum_{n=1}^N a_n \sin nx \quad (4.65)$$

4.7. EIGENVALUE PROBLEMS

If we apply the Galerkin method, we obtain

$$\tilde{\Phi} = \sin x \quad (4.66)$$

Although u_n satisfy both the differentiability and boundary conditions, Equation (4.66) does not satisfy Equation (4.62). Hence Equation (4.66) is an incorrect solution. The problem is that the set $\{\sin nx\}$ does not form a complete set. If we add constant and cosine terms to the expansion functions in Equation (4.65), then

$$\tilde{\Phi} = a_0 + \sum_{n=1}^N [a_n \sin nx + b_n \cos nx] \quad (4.67)$$

As $N \rightarrow \infty$, Equation (4.67) is the classical Fourier series solution. Applying the Galerkin method leads to

$$\tilde{\Phi} = \sin nx \quad (4.68)$$

which is again an incorrect solution. The problem is that even though u_n form a complete set, $L u_n$ do not. For example, nonzero constants cannot be approximated by $L u_n$. In order for $L u_n$ to form a complete set, $\tilde{\Phi}$ must be of the form

$$\tilde{\Phi} = \sum_{n=1}^N [a_n \sin nx + b_n \cos nx] + a_0 + cx + dx^2 \quad (4.69)$$

Notice that the expansion functions $\{1, x, x^2, \sin nx, \cos nx\}$ in the interval $[0, 2\pi]$ form a linearly dependent set. This is because any function such as x or x^2 can be represented in the interval $[0, 2\pi]$ by the set $\{\sin nx, \cos nx\}$. Applying the Galerkin method, Equation (4.69) leads to

$$\tilde{\Phi} = \sin x + x(2\pi - x) \quad (4.70)$$

which is the exact solution Φ . \square

4.7 Eigenvalue Problems

As mentioned in Section 1.3.2, eigenvalue (nondeterministic) problems are described by equations of the type

$$L\Phi = \lambda M\Phi \quad (4.71)$$

where L and M are differential or integral, scalar or vector operators. The problem here is the determination of the eigenvalues λ and the corresponding eigenfunctions Φ .

It can be shown [11] that the variational principle for λ takes the form

$$\lambda = \min \frac{\langle \Phi, L\Phi \rangle}{\langle \Phi, M\Phi \rangle} = \min \frac{\int \Phi L\Phi dv}{\int \Phi M\Phi dv} \quad (4.72)$$

We may apply Equation (4.72) to the Helmholtz equation for scalar waves, for example,

$$\nabla^2 \Phi + k^2 \Phi = 0 \quad (4.73)$$

Comparing Equation (4.73) with Equation (4.71), we obtain $L = -\nabla^2$, $M = 1$ (the identity operator), $\lambda = k^2$ so that

$$k^2 = \min \frac{\int \Phi \nabla^2 \Phi dv}{\int \Phi^2 dv} \quad (4.74)$$

Applying Green's identity (see Example 1.1),

$$\int_v (U \nabla^2 V + \nabla U \cdot \nabla V) dv = \oint U \frac{\partial V}{\partial n} dS,$$

to Equation (4.74) yields

$$k^2 = \min \frac{\int_v |\nabla \Phi|^2 dv - \oint \Phi \frac{\partial \Phi}{\partial n} dS}{\int_v \Phi^2 dv} \quad (4.75)$$

Consider the following special cases.

- (a) For homogeneous boundary conditions of the Dirichlet type ($\Phi = 0$) or Neumann type ($\frac{\partial \Phi}{\partial n} = 0$). Equation (4.75) reduces to

$$k^2 = \min \frac{\int_v |\nabla \Phi|^2 dv}{\int_v \Phi^2 dv} \quad (4.76)$$

- (b) For mixed boundary conditions ($\frac{\partial \Phi}{\partial n} + h\Phi = 0$), Equation (4.75) becomes

$$k^2 = \min \frac{\int_v |\nabla \Phi|^2 dv + \oint h\Phi^2 dS}{\int_v \Phi^2 dv} \quad (4.77)$$

It is usually possible to solve Equation (4.71) in a different way. We choose the basis functions u_1, u_2, \dots, u_N which satisfy the boundary conditions and assume the approximate solution

$$\tilde{\Phi} = a_1 u_1 + a_2 u_2 + \dots + a_N u_N$$

4.7. EIGENVALUE PROBLEMS

or

$$\tilde{\Phi} = \sum_{n=1}^N a_n u_n \quad (4.78)$$

Substituting this into Equation (4.71) gives

$$\sum_{n=1}^N a_n L u_n = \lambda \sum_{n=1}^N a_n M u_n \quad (4.79)$$

Choosing the weighting functions w_m and taking the inner product of Equation (4.79) with each w_m , we obtain

$$\sum_{n=1}^N [\langle w_m, L u_n \rangle - \lambda \langle w_m, M u_n \rangle] a_n = 0, \quad m = 1, 2, \dots, N \quad (4.80)$$

This can be cast into matrix form as

$$\sum_{n=1}^N (A_{mn} - \lambda B_{mn}) X_n = 0 \quad (4.81)$$

where $A_{mn} = \langle w_m, L u_n \rangle$, $B_{mn} = \langle w_m, M u_n \rangle$, $X_n = a_n$. Thus we have a set of homogeneous equations. In order for $\tilde{\Phi}$ in Equation (4.78) not to vanish, it is necessary that the expansion coefficients a_n not all be equal to zero. This implies that the determinant of simultaneous equations (4.81) vanish, i.e.,

$$\begin{vmatrix} A_{11} - \lambda B_{11} & A_{12} - \lambda B_{12} & \cdots & A_{1N} - \lambda B_{1N} \\ \vdots & & & \vdots \\ A_{N1} - \lambda B_{N1} & A_{N2} - \lambda B_{N2} & \cdots & A_{NN} - \lambda B_{NN} \end{vmatrix} = 0$$

or

$$|[A] - \lambda [B]| = 0 \quad (4.82)$$

Solving this gives N approximate eigenvalues $\lambda_1, \dots, \lambda_N$. The various ways of choosing w_m leads to different weighted residual techniques as discussed in the previous section.

Examples of eigenvalue problems for which variational methods have been applied include [28]–[37]:

- the cutoff frequency of a waveguide,
- the propagation constant of a waveguide, and
- the resonant frequency of a resonator.

Example 4.9

Solve the eigenvalue problem

$$\Phi'' + \lambda\Phi = 0, \quad 0 < x < 1$$

with boundary conditions $\Phi(0) = 0 = \Phi(1)$. \square

Solution

The exact eigenvalues are

$$\lambda_n = (n\pi)^2, \quad n = 1, 2, 3, \dots \quad (4.83)$$

and the corresponding (normalized) eigenfunctions are

$$\Phi_n = \sqrt{2} \sin(n\pi x) \quad (4.84)$$

where Φ_n has been normalized to unity, i.e., $\langle \Phi_n, \Phi_n \rangle = 1$.

The approximate eigenvalues and eigenfunctions can be obtained by using either Equation (4.72) or Equation (4.82). Let the approximate solution be

$$\tilde{\Phi}(x) = \sum_{k=0}^N a_k u_k, \quad u_k = x(1-x^k) \quad (4.85)$$

From the given problem, $L = -\frac{d^2}{dx^2}$, $M = 1$ (identity operator). Using the Galerkin method, $w_m = u_m$.

$$\begin{aligned} A_{mn} &= \langle u_m, Lu_n \rangle = \int_0^1 (x - x^{m+1}) \left[-\frac{d^2}{dx^2} (x - x^{n+1}) \right] dx \\ &= \frac{mn}{m+n+1}, \end{aligned} \quad (4.86)$$

$$\begin{aligned} B_{mn} &= \langle u_m, Mu_n \rangle = \int_0^1 (x - x^{m+1})(x - x^{n+1}) dx \\ &= \frac{mn(m+n+6)}{3(m+3)(n+3)(m+n+3)} \end{aligned} \quad (4.87)$$

The eigenvalues are obtained from

$$| [A] - \lambda [B] | = 0 \quad (4.88)$$

For $N = 1$,

$$A_{11} = \frac{1}{3}, \quad B_{11} = \frac{1}{30},$$

4.7. EIGENVALUE PROBLEMS

giving

$$\frac{1}{3} - \lambda \frac{1}{30} = 0 \quad \rightarrow \quad \lambda = 10$$

The first approximate eigenvalue is $\lambda = 10$, a good approximation to the exact value of $\pi^2 = 9.8696$. The corresponding eigenfunction $\tilde{\Phi} = a_1(x - x^2)$ can be normalized to unity so that

$$\tilde{\Phi} = \sqrt{30}(x - x^2)$$

For $N = 2$, evaluating Equations (4.86) and (4.87), we obtain

$$\begin{bmatrix} \frac{1}{3} & \frac{1}{2} \\ \frac{1}{2} & \frac{4}{5} \end{bmatrix} \begin{bmatrix} a_1 \\ a_2 \end{bmatrix} = \lambda \begin{bmatrix} \frac{1}{30} & \frac{1}{20} \\ \frac{1}{20} & \frac{8}{105} \end{bmatrix} \begin{bmatrix} a_1 \\ a_2 \end{bmatrix}$$

or

$$\begin{vmatrix} 10 - \lambda & 0 \\ 0 & 42 - \lambda \end{vmatrix} = 0$$

giving eigenvalues $\lambda_1 = 10, \lambda_2 = 42$, compared with the exact values $\lambda_1 = \pi^2 = 9.8696, \lambda_2 = 4\pi^2 = 39.4784$, and the corresponding normalized eigenfunctions are

$$\tilde{\Phi}_1 = \sqrt{30}(x - x^2)$$

$$\tilde{\Phi}_2 = 2\sqrt{210}(x - x^2) - 2\sqrt{210}(x - x^3)$$

Continuing this way for higher N , the approximate eigenvalues shown in Table 4.4 are obtained. Unfortunately, the labor of computation increases as more u_k are included in $\tilde{\Phi}$. Notice from Table 4.4 that the approximate eigenvalues are always greater than the exact values. This is always true for a self-adjoint, positive definite operator [17]. Figure 4.3 shows the comparison between the approximate and exact eigenfunctions. \square

Table 4.4 Comparison Between Approximate and Exact Eigenvalues for Example 4.9

Exact	Approximate			
	$N = 1$	$N = 2$	$N = 3$	$N = 4$
9.870	10.0	10.0	9.8697	9.8697
39.478		42.0	39.497	39.478
88.826			102.133	102.133
157.914				200.583

Example 4.10

Calculate the cutoff frequency of the inhomogeneous rectangular waveguide shown in Figure 4.4. Take $\epsilon = 4\epsilon_o$ and $s = a/3$. \square

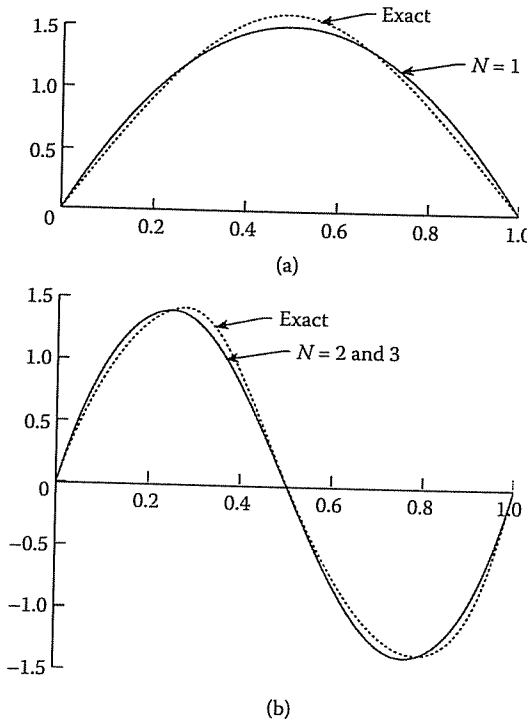


Figure 4.3

Comparison of approximate eigenfunctions with the exact solutions: (a) first eigenfunction, (b) second eigenfunction. (After Harrington [17]; with permission of Krieger Publishing Co.)

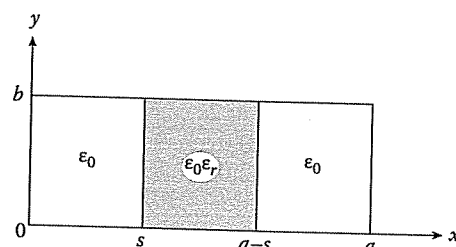


Figure 4.4
A symmetrically loaded rectangular waveguide.

Solution

We will find the lowest mode having $\frac{\partial}{\partial y} \equiv 0$. It is this dominant mode that is of most practical value. Since the dielectric constant varies from one region to another, it is

reasonable to choose Φ to be an electric field, i.e., $\Phi = E_y$. Also, since $k^2 = \frac{\omega^2}{u^2} = \omega^2 \mu_o \epsilon_o$, Equation (4.74) becomes

$$\begin{aligned} \omega^2 \mu_o \epsilon_o \int_0^s E_y^2 dx + \omega^2 \mu_o \epsilon_o \epsilon_r \int_s^{a-s} E_y^2 dx + \omega^2 \mu_o \epsilon_o \int_{a-s}^a E_y^2 dx \\ = - \int_0^a E_y \frac{d^2 E_y}{dx^2} dx \end{aligned} \quad (4.89)$$

Notice that in this implementation of Equation (4.74), there are no coefficients so that there is nothing to minimize. We simply take k^2 as a ratio. Equation (4.89) can be written as

$$\omega^2 \mu_o \epsilon_o \int_0^a E_y^2 dx + \omega^2 \mu_o \epsilon_o (\epsilon_r - 1) \int_s^{a-s} E_y^2 dx = - \int_0^a E_y \frac{d^2 E_y}{dx^2} dx \quad (4.90)$$

We now choose the trial function for E_y . It must be chosen to satisfy the boundary conditions, namely, $E_y = 0$ at $x = 0, a$. Since $E_y \sim \sin \frac{n\pi x}{a}$ for the empty waveguide, it makes sense to choose the trial function of the form

$$E_y = \sum_{n=1,3,5}^{\infty} c_n \sin \frac{n\pi x}{a} \quad (4.91)$$

We choose the odd values of n because the dielectric is symmetrically placed; otherwise we would have both odd and even terms.

Let us consider the trial function

$$E_y = \sin \frac{\pi x}{a} \quad (4.92)$$

Substituting Equation (4.92) into Equation (4.90) yields

$$\begin{aligned} \omega^2 \mu_o \epsilon_o \int_0^a \sin^2 \frac{\pi x}{a} dx + \omega^2 \mu_o \epsilon_o (\epsilon_r - 1) \int_s^{a-s} \sin^2 \frac{\pi x}{a} dx \\ = \frac{\pi^2}{a^2} \int_0^a \sin^2 \frac{\pi x}{a} dx \end{aligned} \quad (4.93)$$

which leads to

$$\omega^2 \mu_o \epsilon_o \left\{ 1 + (\epsilon_r - 1) \left[\left(1 - \frac{2s}{a} \right) + \frac{1}{\pi} \sin \frac{2\pi s}{a} \right] \right\} = \frac{\pi^2}{a^2}$$

But $k_o^2 = \omega^2 \mu_o \epsilon_o = \frac{4\pi^2}{\lambda_c^2}$, where λ_c is the cutoff wavelength of the waveguide filled with vacuum. Hence

$$\frac{4\pi^2}{\lambda_c^2} = \frac{(\pi/a)^2}{1 + (\epsilon_r - 1) \left[\left(1 - \frac{2s}{a} \right) + \frac{1}{\pi} \sin \frac{2\pi s}{a} \right]}$$

Taking $\epsilon_r = 4$ and $s = a/3$ gives

$$\frac{4\pi^2}{\lambda_c^2} = \frac{(\pi/a)^2}{2 + \frac{3\sqrt{3}}{2\pi}}$$

or

$$\frac{a}{\lambda_c} = 0.2974$$

This is a considerable reduction in a/λ_c compared with the value of $a/\lambda_c = 0.5$ for the empty guide. The accuracy of the result may be improved by choosing more terms in Equation (4.91). ■

4.8 Practical Applications

The various techniques discussed in this chapter have been applied to solve a considerable number of EM problems. We select a simple example for illustration [38, 39]. This example illustrates the conventional use of the least squares method.

Consider a strip transmission line enclosed in a box containing a homogeneous medium as shown in Figure 4.5. If a TEM mode of propagation is assumed, Laplace's

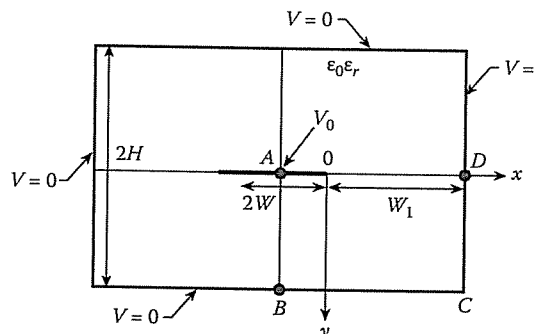


Figure 4.5
The strip line enclosed in a shielded box.

equation

$$\nabla^2 V = 0 \quad (4.94)$$

is obeyed. Due to symmetry, we will consider only one quarter section of the line as in Figure 4.6 and adopt a boundary condition $\frac{\partial V}{\partial x} = 0$ at $x = -W$. We allow for the singularity at the edge of the strip. The variation of the potential in the vicinity of

4.8. PRACTICAL APPLICATIONS

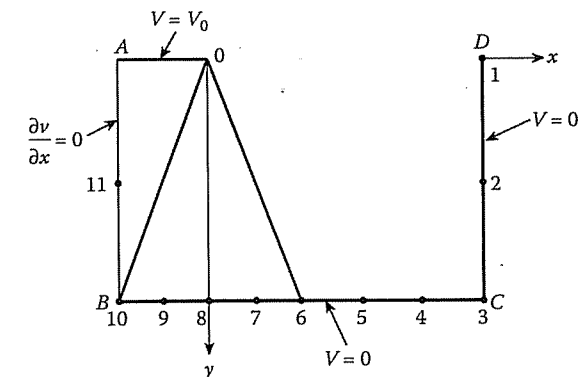


Figure 4.6
A quarter-section of the strip line.

such a singularity is approximated, in terms of trigonometric basis functions, as

$$V = V_0 + \sum_{k=1,3,5}^{\infty} c_k \rho^{k/2} \cos \frac{k\phi}{2}, \quad (4.95)$$

where V_0 is the potential on the trip conductor and the expansion coefficients c_k are to be determined. If we truncate the infinite series in Equation (4.95) so that we have N unknown coefficients, we determine the coefficients by requiring that Equation (4.95) be satisfied at $M (\geq N)$ points on the boundary. If $M = N$, we are applying the collocation method. If $M > N$, we obtain an overdetermined system of equations which can be solved by the method of least squares. Enforcing Equation (4.95) at M boundary points, we obtain M simultaneous equations

$$\begin{bmatrix} V_1 \\ V_2 \\ \vdots \\ V_M \end{bmatrix} = \begin{bmatrix} A_{11} & A_{12} & \dots & A_{1N} \\ A_{21} & A_{22} & \dots & A_{2N} \\ \vdots & \vdots & \ddots & \vdots \\ A_{M1} & A_{M2} & \dots & A_{MN} \end{bmatrix} \begin{bmatrix} c_1 \\ c_2 \\ \vdots \\ c_M \end{bmatrix}$$

i.e.,

$$[V] = [A][X] \quad (4.96)$$

where $[X]$ is an $N \times 1$ matrix containing the unknown expansion coefficients, $[V]$ is an $M \times 1$ column matrix containing the boundary conditions, and $[A]$ is the $M \times N$ coefficient matrix. Due to redundancy, $[X]$ cannot be uniquely determined from Equation (4.96) if $M > N$. To solve this redundant system of equations by the method of least squares, we define the residual matrix $[R]$ as

$$[R] = [A][X] - [V] \quad (4.97)$$

We seek for $[X]$, which minimizes $[R]^2$. Consider

$$[I] = [R]^t [R] = [[A][X] - [V]]^t [[A][X] - [V]] \\ \frac{\partial [I]}{\partial [X]} = 0 \rightarrow [A]^t [A][X] - [A]^t [V] = 0$$

or

$$[X] = [[A]^t [A]]^{-1} [A]^t [V] \quad (4.98)$$

where the superscript t denotes the transposition of the relevant matrix. Thus we have reduced the original redundant system of equations to a determinate set of N simultaneous equations in N unknown coefficients c_1, c_2, \dots, c_N .

Once $[X] = [c_1, c_2, \dots, c_N]$ is determined from Equation (4.98), the approximate solution in Equation (4.95) is completely determined. We can now determine the capacitance and consequently the characteristic impedance of the line for a given value of width-to-height ratio. The capacitance is determined from

$$C = \frac{Q}{V_o} = Q \quad (4.99)$$

if we let $V_o = 1$ V. The characteristic impedance is found from [40]

$$Z_o = \frac{\sqrt{\epsilon_r}}{cC} \quad (4.100)$$

where $c = 3 \times 10^8$ m/s, the speed of light in vacuum. The major problem here is finding Q in Equation (4.99). If we divide the boundary BCD into segments,

$$Q = \int \rho_L dl = 4 \sum_{BCD} \rho_L \Delta l$$

where the charge density $\rho_L = \mathbf{D} \cdot \mathbf{a}_n = \epsilon \mathbf{E} \cdot \mathbf{a}_n$, $\mathbf{E} = -\nabla V$, and the factor 4 is due to the fact that we consider only one quarter section of the line. But

$$\nabla V = \frac{\partial V}{\partial \rho} \mathbf{a}_\rho + \frac{1}{\rho} \frac{\partial V}{\partial \phi} \mathbf{a}_\phi, \\ \mathbf{E} = - \sum_{k=\text{odd}} \frac{k}{2} c_k \rho^{k/2-1} \left(\cos \frac{k\phi}{2} \mathbf{a}_\rho - \sin \frac{k\phi}{2} \mathbf{a}_\phi \right)$$

Since $\mathbf{a}_x = \cos \phi \mathbf{a}_\rho - \sin \phi \mathbf{a}_\phi$ and $\mathbf{a}_y = \sin \phi \mathbf{a}_\rho + \cos \phi \mathbf{a}_\phi$,

$$\rho_L|_{CD} = \epsilon \mathbf{E} \cdot \mathbf{a}_x \\ = -\epsilon \sum_{k=\text{odd}} \frac{k}{2} c_k \rho^{k/2-1} \left(\cos \frac{k\phi}{2} \cos \phi + \sin \frac{k\phi}{2} \sin \phi \right) \quad (4.101a)$$

and

$$\rho_L|_{BC} = \epsilon \mathbf{E} \cdot \mathbf{a}_y \\ = -\epsilon \sum_{k=\text{odd}} \frac{k}{2} c_k \rho^{k/2-1} \left(\cos \frac{k\phi}{2} \sin \phi - \sin \frac{k\phi}{2} \cos \phi \right) \quad (4.101b)$$

4.8. PRACTICAL APPLICATIONS

Example 4.11

Using the collocation (or point matching) method, write a computer program to calculate the characteristics impedance of the line shown in Figure 4.5. Take

$$(a) W = H = 1.0 \text{ m}, W_1 = 5.0 \text{ m}, \epsilon_r = 1, V_0 = 1 \text{ V},$$

$$(b) W = H = 0.5 \text{ m}, W_1 = 5.0 \text{ m}, \epsilon_r = 1, V_0 = 1 \text{ V}. \quad \square$$

Solution

The computer program is presented in Figure 4.7. For the first run, we take the number of matching points $N = 11$; the points are selected as illustrated in Figure 4.6. The selection of the points is based on our prior knowledge of the fact that the flux lines are concentrated on the side of the strip line numbered 6 to 10; hence more points are chosen on that side.

The first step is to determine the potential distribution within the strip line using Equation (4.95). In order to determine the expansion coefficients c_k in Equation (4.95), we let Equation (4.95) be satisfied at the matching points. On points 1 to 10 in Figure 4.6, $V = 0$ so that Equation (4.95) can be written as

$$-V_o = \sum_{k=1,3,5}^{\infty} c_k \rho^{k/2} \cos \frac{k\phi}{2} \quad (4.102)$$

The infinite series is terminated at $k = 19$ so that 10 points are selected on the sides of the strip line. The 11th point is selected such that $\frac{\partial V}{\partial x} = 0$ is satisfied at the point. Hence at point 11,

$$0 = \frac{\partial V}{\partial x} = \cos \phi \frac{\partial V}{\partial \rho} - \frac{\sin \phi}{\rho} \frac{\partial V}{\partial \phi}$$

or

$$0 = \sum_{k=1,3,5} \frac{k}{2} c_k \rho^{k/2-1} \left(\cos \frac{k\phi}{2} \cos \phi + \sin \frac{k\phi}{2} \sin \phi \right) \quad (4.103)$$

With Equations (4.102) and (4.103), we set up a matrix equation of the form

$$[B] = [F][A] \quad (4.104)$$

where

$$B_k = \begin{cases} -V_o, & k \neq N \\ 0, & k = N, \end{cases} \\ F_{ki} = \begin{cases} \rho_i^{k/2} \cos k\phi_i/2, & i = 1, \dots, N-1, \\ \frac{k}{2} \rho_i^{k/2-1} (\cos(k\phi_i/2) \cos \phi_i + \sin(k\phi_i/2) \sin \phi_i), & i = N, k = 1, \dots, N \end{cases}$$

```
clear all; format compact; tic
```

```
% Output of this program
% W = H      N      Nx      Ny      Zo
% 1          7      5      2      67.735
% 1          11     8      3      64.963
% 0.5        7      5      2      96.758
% 0.5        11     8      3      99.098

% ****
% THIS PROGRAM CALCULATES THE CHARACTERISTIC IMPEDANCE
% Zo OF A BOXED MICROSTRIP LINE USING COLLOCATION
% POINT-MATCHING METHOD
% ****

X=[5 5 5, 4.0, 2.0, 1.0, 0.5, 0.0, -0.5, -1.0 -1]; Y=[0.0,
0.5, 1 1 1 1 1 1 ,0.5];
EO=8.8541E-12; VL=3.0E+8;

% INPUT DATA
% W : Width of conductor
% H : Vertical separation of conductor and ground planes
% V0 : Potential at the conductor
% W1 : Horizontal separation of conductor and ground plane
% NMAX : Number of matching points
% NBC : NO. OF POINTS ON BC OR X-AXIS
% ER : Dielectric parameter

for qq = 1:4
    switch qq
        case 1
            W = 1; NMAX = 7; NBC = 5;
            str = sprintf('\n\nW=%d %d %d %d %d', W, N, Nx, Ny, Zo);
            disp(str)
        case 2
            W = 1; NMAX = 11; NBC = 8;
        case 3
            W = .5; NMAX = 7; NBC = 5;
        case 4
            W = .5; NMAX = 11; NBC = 8;
    end

    H = W;
    W1 = 5.0;
    ER = 1.0;
    V0 = 1.0;
    NCD = NMAX - NBC; % NO. OF POINTS ON DC OR Y-AXIS
    DX = (W + W1)/NBC;
    DY = H/NCD;
    EPS = EO*ER;
```

Figure 4.7

Computer program for Example 4.11 (*Continued*).

4.8. PRACTICAL APPLICATIONS

```
% CALCULATE R & PHI FOR EACH POINT (X,Y)

for N = 1:NMAX
    R(N) = sqrt( X(N)^2 + Y(N)^2 );
    if (X(N))<0
        PHI(N) = pi - atan( Y(N)/abs(X(N)) );
    elseif X(N)==0
        PHI(N) = pi/2;
    elseif X(N)>0
        PHI(N) = atan( Y(N)/X(N) );
    end
end

% CALCULATE MATRICES F(I,J) AND B(I)

for I = 1:NMAX
    B(I) = -V0;
    M = 0;
    for J = 1:NMAX
        M = 2*J - 1;
        FM = (M)/2.0;
        if (I==NMAX)
            CC = cos(PHI(I))*cos(PHI(I)*FM);
            SS = sin(PHI(I))*sin(PHI(I)*FM);
            F(I,J) = ( R(I)^(FM-1.) )*(CC + SS)*FM;
            B(I) = 0.0;
        else
            F(I,J) = ( R(I)^(FM) )*cos(FM*PHI(I));
        end
    end
end

% DETERMINE THE EXPANSION COEFFICIENTS A(I)

IDM = 30;
F = inv(F);
for I = 1:NMAX
    A(I) = 0.0;
    for J = 1:NMAX
        A(I) = A(I) + F(I,J)*B(J);
    end
end

% NOW, CALCULATE CHARGE ON THE X-SIDE, i.e. BC

RHO = 0.0;
YC = H;
XC = -W - DX/2.0;
for I = 1:NBC
    XC = XC + DX;
    RC = sqrt(XC^2 + YC^2);
```

Figure 4.7

(*Cont.*) Computer program for Example 4.11.

```

if(XC)<=0
    PC = pi - atan(YC/abs(XC));
else
    PC = atan(YC/XC);
end

for K = 1:NMAX
    FK = (2*K - 1)/2.0;
    RRO = sin(PC)*cos(FK*PC) - cos(PC)*sin(FK*PC);
    RHO = RHO - A(K)*FK*(RC^(FK-1))*RRO*DX*EPS;
end

% NEXT, CALCULATE THE CHARGE ON THE Y-SIDE, i.e. DC

XC = W1;
YC = -DY/2;
for I = 1:NCD
    YC = YC + DY;
    RC = sqrt(XC^2 + YC^2);
    PC = atan(YC/XC);
    for K = 1:NMAX
        FK = (2*K - 1)/2;
        RRO = cos(PC)*cos(FK*PC) + sin(PC)*sin(FK*PC);
        RHO = RHO - A(K)*FK*(RC^(FK-1))*RRO*DY*EPS;
    end
end

% CALCULATE THE CHARACTERISTIC IMPEDANCE Z0

Q = 4.0*RHO;
C = abs(Q)/V0;
Z0 = sqrt(ER)/( C*VL );
%disp([C,Z0])
%disp([W N NBC NCD C Z0])
str = sprintf(' %3g  %3g  %3g  %3g  %g ',W, N, NBC, NCD, Z0);
disp(str)
end

```

Figure 4.7*(Cont.) Computer program for Example 4.11.*

where (ρ_i, ϕ_i) are the cylindrical coordinates of the i th point. Matrix $[A]$ consists of the unknown expansion coefficients c_k . By matrix inversion, we obtain $[A]$ as

$$[A] = [F]^{-1} [B] \quad (4.105)$$

Once the expansion coefficients are determined, we now calculate the total charge on the sides of the strip line using Equation (4.101) and

$$Q = 4 \sum_{BDC} \rho_L \Delta l$$

4.9. CONCLUDING REMARKS

Finally, we obtain Z_o from Equations (4.99) and (4.100). Table 4.5 shows the results obtained using the program in Figure 4.7 for different cases. In Table 4.5, $N = N_x + N_y$, where N_x and N_y are the number of matching points selected along the x and y axes, respectively. By comparing Figure 4.5 with Figure 2.13, one may be tempted to apply Equation (2.223) to obtain the exact solution of part (a) as 61.1Ω . But we must recall that Equation (2.223) was derived based on the assumption that $w \gg b$ in Figure 2.12 or $W \gg H$ in Figure 4.5. The assumption is not valid in this case, the exact solution given in [39] is more appropriate.

Table 4.5 Characteristic Impedance of the Strip Transmission Line of Figure 4.5; for Example 4.11 with $W_1 = 5.0$

$W = H$	N	N_x	N_y	c_1	Calculated $Z_o(\Omega)$	Exact [39] $Z_o(\Omega)$
1.0	7	5	2	-1.1549	67.735	65.16
	11	8	3	-1.1266	64.963	
0.5	7	5	2	-1.1549	96.758	100.57
	11	8	3	-1.1266	99.098	

4.9 Concluding Remarks

This chapter has provided an elementary introduction to the basic idea of variational techniques. The variational methods provide simple but powerful solutions to physical problems provided we can find approximate basis functions. A prominent feature of the variational method lies in the ability to achieve high accuracy with few terms in the approximate solution. A major drawback is the difficulty encountered in selecting the basis functions. In spite of the drawback, the variational methods have been very useful and provide basis for both the method of moments and the finite element method to be discussed in the forthcoming chapters.

Needless to say, our discussion on variational techniques in this chapter has been only introductory. An exhaustive treatment of the subject can be found in [1, 6, 10, 11], [41]–[43]. Various applications of variational methods to EM-related problems include

- waveguides and resonators [28]–[37]
- transmission lines [38, 39], [44]–[47]
- acoustic radiation [48]
- wave propagation [49]–[51]
- transient problems [52]
- scattering problems [53]–[59].

The problem of variational principles for EM waves in inhomogeneous media is discussed in [60].

References

- [1] S.G. Mikhlin, *Variational Methods in Mathematical Physics*. New York: Macmillan, 1964, pp. xv, 4–78.
- [2] J.N. Reddy, *An Introduction to the Finite Element Method*. New York: McGraw-Hill, 2nd ed., 1993, pp. 18–64.
- [3] R.B. Guenther and J.W. Lee, *Partial Differential Equations of Mathematical Physics and Integral Equations*. Englewood Cliffs, NJ: Prentice-Hall, 1988, pp. 434–485.
- [4] A. Wexler, “Computation of electromagnetic fields,” *IEEE Trans. Micro. Theo. Tech.*, vol. MTT-17, no. 8, Aug. 1969, pp. 416–439.
- [5] M.M. Ney, “Method of moments as applied to electromagnetic problems,” *IEEE Trans. Micro. Theo. Tech.*, vol. MTT-33, no. 10, Oct. 1985, pp. 972–980.
- [6] I.M. Gelfand and S.V. Fomin, *Calculus of Variations* (translated from Russian by R.A. Silverman). Englewood Cliffs, NJ: Prentice-Hall, 1963.
- [7] J.N. Reddy and M.L. Rasmussen, *Advanced Engineering Analysis*. New York: John Wiley, 1982, pp. 377–386.
- [8] B.H. McDonald et al., “Variational solution of integral equations,” *IEEE Trans. Micro. Theo. Tech.*, vol. MTT-22, no. 3, Mar. 1974, pp. 237–248. See also vol. MTT-23, no. 2, Feb. 1975, pp. 265–266 for correction to the paper.
- [9] K. Morishita and N. Kumagai, “Unified approach to the derivation of variational expression for electromagnetic fields,” *IEEE Trans. Micro. Theo. Tech.*, vol. MTT-25, no. 1, Jan. 1977, pp. 34–39.
- [10] B.L. Moiseiwitsch, *Variational Principles*. London: Interscience Pub., 1966.
- [11] L. Cairo and T. Kahan, *Variational Technique in Electromagnetics*. New York: Gordon & Breach, 1965, pp. 48–65.
- [12] K. Kalikstein, “Formulation of variational principles via Lagrange multipliers,” *J. Math. Phys.*, vol. 22, no. 7, July 1981, pp. 1433–1437.
- [13] K. Kalikstein and A. Sepulveda, “Variational principles and variational functions in electromagnetic scattering,” *IEEE Trans. Ant. Prog.*, vol. AP-29, no. 5, Sept. 1981, pp. 811–815.

REFERENCES

- [14] P. Hammond, “Equilibrium and duality in electromagnetic field problems,” *J. Frank. Inst.*, vol. 306, no. 1, July 1978, pp. 133–157.
- [15] S.K. Jeng and C.H. Chen, “On variational electromagnetics,” *IEEE Trans. Ant. Prog.*, vol. AP-32, no. 9, Sept. 1984, pp. 902–907.
- [16] S.J. Chung and C.H. Chen, “Partial variational principle for electromagnetic field problems: Theory and applications,” *IEEE Trans. Micro. Theo. Tech.*, vol. 36, no. 3, Mar. 1988, pp. 473–479.
- [17] R.F. Harrington, *Field Computation by Moment Methods*. Malabar, FL: R.E. Krieger, 1968, pp. 19, 126–131.
- [18] S.G. Mikhlin and K.I. Smolitskiy, *Approximate Methods for Solution of Differential and Integral Equations*. New York: Elsevier, 1967, pp. 147–270.
- [19] T.J. Chung, *Finite Element Analysis in Fluid Dynamics*. New York: McGraw-Hill, 1978, pp. 36–43.
- [20] O.C. Zienkiewicz and R.L. Taylor, *The Finite Element Method*. London: MacGraw-Hill, 1989, vol. 1, 4th ed., pp. 206–259.
- [21] L. Lewin, “On the restricted validity of point-matching techniques,” *IEEE Trans. Micro. Theo. Tech.*, vol. MTT-18, no. 12, Dec. 1970, pp. 1041–1047.
- [22] R.F. Muller, “On the legitimacy of an assumption underlying the point-matching method,” *IEEE Trans. Micro. Theo. Tech.*, vol. MTT-18, June 1970, pp. 325–327.
- [23] A.R. Djordjevic and T.K. Sarkar, “A theorem on the moment methods,” *IEEE Trans. Ant. Prog.*, vol. AP-35, no. 3, Mar. 1987, pp. 353–355.
- [24] T.K. Sarkar, “A study of the various methods for computing electromagnetic field utilizing thin wire integral equations,” *Radio Sci.*, vol. 18, no. 1, Jan./Feb., pp. 29–38.
- [25] T.K. Sarkar, “A note on the variational method (Rayleigh–Ritz), Galerkin’s method, and the method of least squares,” *Radio Sci.*, vol. 18, no. 6, Nov./Dec. 1983, pp. 1207–1224.
- [26] T.K. Sarkar, “A note on the choice of weighting functions in the method of moments,” *IEEE Trans. Ant. Prog.*, vol. AP-33, no. 4, April 1985, pp. 436–441.
- [27] T.K. Sarkar et al., “On the choice of expansion and weighting functions in the numerical solution of operator equations,” *IEEE Trans. Ant. Prog.*, vol. AP-33, no. 9, Sept. 1985, pp. 988–996.
- [28] A.D. Berk, “Variational principles for electromagnetic resonators and waveguides,” *IRE Trans. Ant. Prog.*, vol. AP-4, April 1956, pp. 104–111.
- [29] G.J. Gabriel and M.E. Brodwin, “The solution of guided waves in inhomogeneous anisotropic media by perturbation and variation methods,” *IEEE Trans. Micro. Theo. Tech.*, vol. MTT-13, May 1965, pp. 364–370.

- [30] W. English and F. Young, "An E vector variational formulation of the Maxwell equations for cylindrical waveguide problems," *IEEE Trans. Micro. Theo. Tech.*, vol. MTT-19, Jan. 1971, pp. 40–46.
- [31] H.Y. Yee and N.F. Audeh, "Uniform waveguides with arbitrary cross-section considered by the point-matching method," *IEEE Trans. Micro. Theo. Tech.*, vol. MTT-13, Nov. 1965, pp. 847–851.
- [32] J.A. Fuller and N.F. Audeh, "The point-matching solution of uniform nonsymmetric waveguides," *IEEE Trans. Micro. Theo. Tech.*, vol. MTT-17, no. 2, Feb. 1969, pp. 114–115.
- [33] R.B. Wu and C.H. Chen, "On the variational reaction theory for dielectric waveguides," *IEEE Trans. Micro. Theo. Tech.*, vol. M-33, no. 6, June 1985, pp. 477–483.
- [34] T.E. Rozzi, "The variational treatment of thick interacting inductive irises," *IEEE Trans. Micro. Theo. Tech.*, vol. MTT-21, no. 2, Feb. 1973, pp. 82–88.
- [35] A.D. McAulay, "Variational finite-element solution of dissipative waveguide and transportation application," *IEEE Trans. Micro. Theo. Tech.*, vol. MTT-25, no. 5, May 1977, pp. 382–392.
- [36] L.V. Lindell, "A variational method for nonstandard eigenvalue problems in waveguides and resonator analysis," *IEEE Trans. Micro. Theo. Tech.*, vol. MTT-30, no. 8, Aug. 1982, pp. 1194–1204. See comment on this paper in vol. MTT-31, no. 9, Sept. 1983, pp. 786–789.
- [37] K. Chang, "Variational solutions on two opposite narrow resonant strips in waveguide," *IEEE Trans. Micro. Theo. Tech.*, vol. MTT-35, no. 2, Feb. 1987, pp. 151–158.
- [38] T.K. Seshadri et al., "Application of 'corner function approach' to strip line problems," *Int. J. Electron.*, vol. 44, no. 5, May 1978, pp. 525–528.
- [39] T.K. Seshadri et al., "Least squares collocation as applied to the analysis of strip transmission lines," *Proc. IEEE*, vol. 67, no. 2, Feb. 1979, pp. 314–315.
- [40] M.N.O. Sadiku, *Elements of Electromagnetics*, 4th ed. New York: Oxford Univ. Press, 2007, Chap. 11.
- [41] P.M. Morse and H. Feshback, *Methods of Theoretical Physics*. New York: McGraw-Hill, 2 volumes, 1953.
- [42] R.E. Collin, *Field Theory of Guided Waves*. New York: McGraw-Hill, 1960, pp. 148–164, 314–367.
- [43] D.G. Bodner and D.T. Paris, "New variational principle in electromagnetics," *IEEE Trans. Ant. Prog.*, vol. AP-18, no. 2, March 1970, pp. 216–223.
- [44] T.D. Tsiboukis, "Estimation of the characteristic impedance of a transmission line by variational methods," *IEEE Proc.*, vol. 132, Pt. H, no. 3, June 1985, pp. 171–175.

REFERENCES

- [45] E. Yamashita and R. Mittra, "Variational method for the analysis of microstrip lines," *IEEE Trans. Micro. Theo. Tech.*, vol. MTT-16, no. 4, Apr. 1968, pp. 251–256.
- [46] E. Yamashita, "Variational method for the analysis of microstrip-like transmission lines," *IEEE Trans. Micro. Theo. Tech.*, vol. MTT-16, no. 8, Aug. 1968, pp. 529–535.
- [47] F. Medina and M. Horno, "Capacitance and inductance matrices for multistrip structures in multilayered anisotropic dielectrics," *IEEE Trans. Micro. Theo. Tech.*, vol. MTT-35, no. 11, Nov. 1987, pp. 1002–1008.
- [48] F.H. Fenlon, "Calculation of the acoustic radiation of field at the surface of a finite cylinder by the method of weighted residuals," *Proc. IEEE*, vol. 57, no. 3, March 1969, pp. 291–306.
- [49] C.H. Chen and Y.W. Kiang, "A variational theory for wave propagation in a one-dimensional inhomogeneous medium," *IEEE Trans. Ant. Prog.*, vol. AP-28, no. 6, Nov. 1980, pp. 762–769.
- [50] S.K. Jeng and C.H. Chen, "Variational finite element solution of electromagnetic wave propagation in a one-dimensional inhomogeneous anisotropic medium," *J. Appl. Phys.*, vol. 55, no. 3, Feb. 1984, pp. 630–636.
- [51] J.A. Bennett, "On the application of variation techniques to the ray theory of radio propagation," *Radio Sci.*, vol. 4, no. 8, Aug. 1969, pp. 667–678.
- [52] J.T. Kuo and D.H. Cho, "Transient time-domain electromagnetics," *Geophys.*, vol. 45, no. 2, Feb. 1980, pp. 271–291.
- [53] R.D. Kodis, "An introduction to variational methods in electromagnetic scattering," *J. Soc. Industr. Appl. Math.*, vol. 2, no. 2, June 1954, pp. 89–112.
- [54] D.S. Jones, "A critique of the variational method in scattering problems," *IRE Trans.*, vol. AP-4, no. 3, 1965, pp. 297–301.
- [55] R.J. Wagner, "Variational principles for electromagnetic potential scattering," *Phys. Rev.*, vol. 131, no. 1, July 1963, pp. 423–434.
- [56] J.A. Krill and R.A. Farrell, "Comparison between variational, perturbational, and exact solutions for scattering from a random rough-surface model," *J. Opt. Soc. Am.*, vol. 68, June 1978, pp. 768–774.
- [57] R.B. Wu and C.H. Chen, "Variational reaction formulation of scattering problem for anisotropic dielectric cylinders," *IEEE Trans. Ant. Prog.*, vol. 34, no. 5, May 1986, pp. 640–645.
- [58] J.A. Krill and R.H. Andreo, "Vector stochastic variational principles for electromagnetic wave scattering," *IEEE Trans. Ant. Prog.*, vol. AP-28, no. 6, Nov. 1980, pp. 770–776.

- [59] R.W. Hart and R.A. Farrell, "A variational principle for scattering from rough surfaces," *IEEE Trans. Ant. Prog.*, vol. AP-25, no. 5, Sept. 1977, pp. 708-713.
 [60] J.R. Willis, "Variational principles and operator equations for electromagnetic waves in inhomogeneous media," *Wave Motion*, vol. 6, no. 2, 1984, pp. 127-139.

Problems

4.1 Find $\langle u, v \rangle$ if

- $u = x^2, v = 2 - x$ in the interval $-1 < x < 1$,
- $u = 1, v = x^2 - 2y^2$ in the rectangular region $0 < x < 1, 1 < y < 2$,
- $u = x + y, v = xz$ in the cylindrical region $x^2 + y^2 \leq 4, 0 < z < 5$.

4.2 Show that

- $\langle h(x), f(x) \rangle = \langle h(x), f(-x) \rangle$,
- $\langle h(ax), f(x) \rangle = \left\langle h(x), \frac{1}{a} f\left(\frac{x}{a}\right) \right\rangle$,
- $\left\langle \frac{df}{dx}, h(x) \right\rangle = - \left\langle f(x), \frac{dh}{dx} \right\rangle$,
- $\left\langle \frac{d^n f}{dx^n}, h(x) \right\rangle = (-1)^n - \left\langle f(x), \frac{d^n h}{dx^n} \right\rangle$

Note from (d) that $L = \frac{d}{dx}, \frac{d^3}{dx^3}$, etc., are not self-adjoint, whereas $L = \frac{d^2}{dx^2}, \frac{d^4}{dx^4}$, etc., are.

4.3 Find the Euler partial differential equation for each of the following functionals:

- $\int_a^b \sqrt{1+y'} dx$
- $\int_a^b y \sqrt{1+y'^2} dx$
- $\int_a^b \cos(xy') dx$

4.4 Repeat Problem 4.3 for the following functionals:

- $\int_a^b (y'^2 - y^2) dx$

PROBLEMS

(b) $\int_a^b [5y^2 - (y'')^2 + 10x] dx$

(c) $\int_a^b (3uv - u^2 + u'^2 - v'^2) dx$

4.5 Determine the extremal $y(x)$ for each of the following variational problems:

(a) $\int_0^1 (2y'^2 + yy' + y' + y) dx, y(0) = 0, y(1) = 1$

(b) $\int (y'^2 - y^2) dx, y(0) = 1, y(\pi/2) = 0$

4.6 If L is a positive definite, self-adjoint operator and $L\Phi = g$ has a solution Φ_o , show that the function

$$I = \langle L\Phi, \Phi \rangle - 2\langle \Phi, g \rangle,$$

where Φ and g are real functions, is minimized by the solution Φ_o .

4.7 Show that a function that minimizes the functional

$$I(\Phi) = \frac{1}{2} \int_S [|\nabla \Phi|^2 - k^2 \Phi^2 + 2g\Phi] dS$$

is the solution to the inhomogeneous Helmholtz equation

$$\nabla^2 \Phi + k^2 \Phi = g$$

4.8 Using Euler's equation, obtain the differential equation corresponding to the electrostatic field functional

$$I = \int_v \left[\frac{1}{2} \epsilon E^2 - \rho_v V \right] dv$$

where $E = |\mathbf{E}|$ and ρ_v is the volume charge density.

4.9 Repeat Problem 4.8 for the energy function for steady state currents

$$I = \int_v \frac{1}{2} \mathbf{J} \cdot \mathbf{E} dv$$

where $\mathbf{J} = \sigma \mathbf{E}$.

4.10 Poisson's equation in an anisotropic medium is

$$\frac{\partial}{\partial x} \left(\epsilon_x \frac{\partial V}{\partial x} \right) + \frac{\partial}{\partial y} \left(\epsilon_y \frac{\partial V}{\partial y} \right) + \frac{\partial}{\partial z} \left(\epsilon_z \frac{\partial V}{\partial z} \right) = -\rho_v$$

in three dimensions. Derive the functional for the boundary value problem. Assume ϵ_x, ϵ_y , and ϵ_z are constants.

- 4.11 Show that the variational principle for the boundary value problem

$$\nabla^2 \Phi = f(x, y, z)$$

subject to the mixed boundary condition

$$\frac{\partial \Phi}{\partial n} + g\Phi = h \text{ on } S$$

is

$$I(\Phi) = \int_v [|\nabla \Phi|^2 - 2fg] dv + \oint [g\Phi^2 - 2h\Phi] dS$$

- 4.12 Obtain the variational principle for the differential equation

$$-\frac{d^2y}{dx^2} + y = \sin \pi x, \quad 0 < x < 1$$

subject to $y(0) = 0 = y(1)$.

- 4.13 Determine the variational principle for

$$\Phi'' = \Phi - 4xe^x, \quad 0 < x < 1$$

subject to $\Phi'(0) = \Phi(0) + 1$, $\Phi'(1) = \Phi(1) - e$.

- 4.14 For the boundary value problem

$$-\Phi'' = x, \quad 0 < x < 1$$

$$\Phi(0) = 0, \quad \Phi(1) = 2$$

determine the approximate solution using the Rayleigh–Ritz method with basis functions

$$u_k = x^k(x-1), \quad k = 0, 1, 2, \dots, M$$

Try cases when $M = 1, 2$, and 3 .

- 4.15 Rework Example 4.5 using

(a) $u_m = x(1-x^m)$,

(b) $u_m = \sin m\pi x$, $m = 1, 2, 3, \dots, M$. Try cases when $M = 1, 2$, and 3 .

- 4.16 Solve the differential equation

$$-\Phi''(x) + 0.1\Phi(x) = 1, \quad 0 \leq x \leq 10$$

subject to the boundary conditions $\Phi'(0) = 0 = \Phi(0)$ using the trial function

$$\tilde{\Phi}(x) = a_1 \cos \frac{\pi x}{20} + a_2 \cos \frac{3\pi x}{20} + a_3 \cos \frac{5\pi x}{20}$$

Determine the expansion coefficients using (a) collocation method, (b) subdomain method, (c) Galerkin method, (d) least squares method.

- 4.17 For the boundary value problem

$$\Phi'' + \Phi + x = 0, \quad 0 < x < 1$$

with homogeneous boundary conditions $\Phi = 0$ at $x = 0$ and $x = 1$, determine the coefficients of the approximate solution function

$$\tilde{\Phi}(x) = x(1-x)(a_1 + a_2x)$$

using (a) collocation method (choose $x = 1/4$, $x = 1/2$ as collocation points), (b) Galerkin method, (c) least squares method.

- 4.18 Use the Ritz method to solve the ordinary differential equation

$$\frac{d^2y}{dx^2} + 100x^2 = 0, \quad 0 \leq x \leq 1$$

subject to $y(0) = 0 = y(1)$. Use the trial function $u_1 = x(1-x^2)$.

- 4.19 Rework Problem 4.18 using the trial function $u_1 = x(1-x^3)$.

- 4.20 Given the boundary value problem

$$y'' + (1+x^2)y + 1 = 0, \quad -1 < x < 1 \quad y(-1) = 0 = y(1),$$

solve for y assuming the approximate solution

$$\tilde{y} = a_1(1-x^2)(1-4x^2) + a_2x^2(1-x^2)$$

Use the Galerkin and the least squares methods to determine a_1 and a_2 .

- 4.21 Consider the problem

$$\Phi'' + x\Phi' + \Phi = 2x, \quad 0 < x < 1$$

subject to $\Phi(0) = 1$, $\Phi(1) = 0$. Find the approximate solution using the Galerkin method. Use $u_k = x^k(1-x)$, $k = 0, 1, \dots, N$. Try $N = 3$.

- 4.22 Solve the differential equation

$$\frac{d^2\Phi}{dx^2} - \Phi + 100x = 0, \quad 0 \leq x \leq 10$$

subject to $\Phi(0) = 0 = \Phi(10)$. Assume the two trial functions

$$u_1(x) = x(1-x^2), \quad u_2(x) = x(1-x^4)$$

Take the two collocation points at $x = 1/3$ and $x = 2/3$.

- 4.23 Determine the first three eigenvalues of the equation

$$y'' + \lambda y = 0, \quad 0 < x < 1,$$

$y(0) = 0 = y(1)$ using collocation at $x = 1/4, 1/2, 3/4$.

- 4.24 The differential equation governing the vibration of a string is given by

$$\frac{d^2\Phi}{dx^2} + \lambda\Phi = 0, \quad 0 \leq x \leq 1$$

with the boundary conditions

$$\Phi(0) = 0 = \Phi(1)$$

where λ is the eigenvalue. Using the trial solution

$$\Phi(x) = a_1x(1-x) + a_2x^2(1-x)$$

where a_1 and a_2 are constants, use Galerkin's method to determine the eigenvalues of the string.

- 4.25 Determine the fundamental eigenvalue of the problem

$$-\Phi''(x) + 0.1\Phi(x) = \lambda\Phi(x), \quad 0 < x < 10$$

subject to $\Phi(0) = 0 = \Phi(10)$. Use the trial function

$$\tilde{\Phi}(x) = x(x-10)$$

- 4.26 Obtain the lowest eigenvalue of the problem

$$\nabla^2\Phi + \lambda\Phi = 0, \quad 0 < \rho < 1$$

with $\Phi = 0$ at $\rho = 1$.

- 4.27 Rework Example 4.10 using the trial function

$$E_y = \sin \frac{\pi x}{a} + c_1 \sin \frac{3\pi x}{a}$$

where c_1 is a coefficient to be chosen such that $\omega^2\epsilon_o\mu_o$ is minimized.

- 4.28 Consider the waveguide in Figure 4.4 as homogeneous. To determine the cutoff frequency, we may use the polynomial trial function

$$H_z = Ax^3 + Bx^2 + Cx + D$$

By applying the conditions

$$\begin{aligned} H_z &= 1 \quad \text{at } x = 0, \quad H_z = -1 \quad \text{at } x = a, \\ \frac{\partial H_z}{\partial x} &= 0 \quad \text{at } x = 0, a, \end{aligned}$$

determine A , B , C , and D . Using the trial function, calculate the cutoff frequency.

Chapter 5

Moment Methods

Life is too short to do anything for oneself that one can pay others to do for one.

- Somerset Maugham

5.1 Introduction

In Section 1.3.2, it was mentioned that most EM problems can be stated in terms of an inhomogeneous equation

$$L\Phi = g \quad (5.1)$$

where L is an operator which may be differential, integral, or integro-differential, g is the known excitation or source function, and Φ is the unknown function to be determined. So far, we have limited our discussion to cases for which L is differential. In this chapter, we will treat L as an integral or integro-differential operator.

The *method of moments* (MOM) is a general procedure for solving Equation (5.1). The method owes its name to the process of taking moments by multiplying with appropriate weighing functions and integrating, as discussed in Section 4.6. The name "method of moments" has its origin in Russian literature [1, 2]. In western literature, the first use of the name is usually attributed to Harrington [3]. The origin and development of the moment method are fully documented by Harrington [4, 5].

The method of moments is essentially the method of weighted residuals discussed in Section 4.6. Therefore, the method is applicable for solving both differential and integral equations.

The use of MOM in EM has become popular since the work of Richmond [6] in 1965 and Harrington [7] in 1967. The method has been successfully applied to a wide variety of EM problems of practical interest such as radiation due to thin-wire elements and arrays, scattering problems, analysis of microstrips and lossy structures, propagation over an inhomogeneous earth, and antenna beam pattern, to mention a few. An updated review of the method is found in a paper by Ney [8]. The literature on MOM is already so large as to prohibit a comprehensive bibliography. A partial bibliography is provided by Adams [9].

- 4.24 The differential equation governing the vibration of a string is given by

$$\frac{d^2\Phi}{dx^2} + \lambda\Phi = 0, \quad 0 \leq x \leq 1$$

with the boundary conditions

$$\Phi(0) = 0 = \Phi(1)$$

where λ is the eigenvalue. Using the trial solution

$$\Phi(x) = a_1x(1-x) + a_2x^2(1-x)$$

where a_1 and a_2 are constants, use Galerkin's method to determine the eigenvalues of the string.

- 4.25 Determine the fundamental eigenvalue of the problem

$$-\Phi''(x) + 0.1\Phi(x) = \lambda\Phi(x), \quad 0 < x < 10$$

subject to $\Phi(0) = 0 = \Phi(10)$. Use the trial function

$$\tilde{\Phi}(x) = x(x-10)$$

- 4.26 Obtain the lowest eigenvalue of the problem

$$\nabla^2\Phi + \lambda\Phi = 0, \quad 0 < \rho < 1$$

with $\Phi = 0$ at $\rho = 1$.

- 4.27 Rework Example 4.10 using the trial function

$$E_y = \sin \frac{\pi x}{a} + c_1 \sin \frac{3\pi x}{a}$$

where c_1 is a coefficient to be chosen such that $\omega^2\epsilon_o\mu_o$ is minimized.

- 4.28 Consider the waveguide in Figure 4.4 as homogeneous. To determine the cutoff frequency, we may use the polynomial trial function

$$H_z = Ax^3 + Bx^2 + Cx + D$$

By applying the conditions

$$\begin{aligned} H_z &= 1 \quad \text{at } x = 0, \quad H_z = -1 \quad \text{at } x = a, \\ \frac{\partial H_z}{\partial x} &= 0 \quad \text{at } x = 0, a, \end{aligned}$$

determine A , B , C , and D . Using the trial function, calculate the cutoff frequency.

Chapter 5

Moment Methods

Life is too short to do anything for oneself that one can pay others to do for one.

- Somerset Maugham

5.1 Introduction

In Section 1.3.2, it was mentioned that most EM problems can be stated in terms of an inhomogeneous equation

$$L\Phi = g \quad (5.1)$$

where L is an operator which may be differential, integral, or integro-differential, g is the known excitation or source function, and Φ is the unknown function to be determined. So far, we have limited our discussion to cases for which L is differential. In this chapter, we will treat L as an integral or integro-differential operator.

The *method of moments* (MOM) is a general procedure for solving Equation (5.1). The method owes its name to the process of taking moments by multiplying with appropriate weighing functions and integrating, as discussed in Section 4.6. The name "method of moments" has its origin in Russian literature [1, 2]. In western literature, the first use of the name is usually attributed to Harrington [3]. The origin and development of the moment method are fully documented by Harrington [4, 5].

The method of moments is essentially the method of weighted residuals discussed in Section 4.6. Therefore, the method is applicable for solving both differential and integral equations.

The use of MOM in EM has become popular since the work of Richmond [6] in 1965 and Harrington [7] in 1967. The method has been successfully applied to a wide variety of EM problems of practical interest such as radiation due to thin-wire elements and arrays, scattering problems, analysis of microstrips and lossy structures, propagation over an inhomogeneous earth, and antenna beam pattern, to mention a few. An updated review of the method is found in a paper by Ney [8]. The literature on MOM is already so large as to prohibit a comprehensive bibliography. A partial bibliography is provided by Adams [9].

The procedure for applying MOM to solve Equation (5.1) usually involves four steps:

- (1) derivation of the appropriate integral equation (IE),
- (2) conversion (discretization) of the IE into a matrix equation using basis (or expansions) functions and weighting (or testing) functions,
- (3) evaluation of the matrix elements, and
- (4) solving the matrix equation and obtaining the parameters of interest.

The basic tools for step (2) have already been mastered in Section 4.6; in this chapter we will apply them to IEs rather than PDEs. Just as we studied PDEs themselves in Section 1.3.2, we will first study IEs.

5.2 Integral Equations

An integral equation is any equation involving unknown function Φ under the integral sign. Simple examples of integral equations are Fourier, Laplace, and Hankel transforms.

5.2.1 Classification of Integral Equations

Linear integral equations that are most frequently studied fall into two categories named after Fredholm and Volterra. One class is the Fredholm equations of the first, second, and third kind, namely,

$$f(x) = \int_a^b K(x, t)\Phi(t)dt, \quad (5.2)$$

$$f(x) = \Phi(x) - \lambda \int_a^b K(x, t)\Phi(t)dt, \quad (5.3)$$

$$f(x) = a(x)\Phi(x) - \lambda \int_a^b K(x, t)\Phi(t)dt, \quad (5.4)$$

where λ is a scalar (or possibly complex) parameter. Functions $K(x, t)$ and $f(x)$ and the limits a and b are known, while $\Phi(x)$ is unknown. The function $K(x, t)$ is known as the *kernel* of the integral equation. The parameter λ is sometimes equal to unity.

The second class of integral equations are the Volterra equations of the first, second, and third kind, namely,

5.2. INTEGRAL EQUATIONS

$$f(x) = \int_a^x K(x, t)\Phi(t)dt, \quad (5.5)$$

$$f(x) = \Phi(x) - \lambda \int_a^x K(x, t)\Phi(t)dt, \quad (5.6)$$

$$f(x) = a(x)\Phi(x) - \lambda \int_a^x K(x, t)\Phi(t)dt, \quad (5.7)$$

with a variable upper limit of integration. If $f(x) = 0$, the integral equations (5.2) to (5.7) become homogeneous. Note that Equations (5.2) to (5.7) are all linear equations in that Φ enters the equations in a linear manner. An integral equation is nonlinear if Φ appears in the power of $n > 1$ under the integral sign. For example, the integral equation

$$f(x) = \Phi(x) - \int_a^b K(x, t)\Phi^2(t)dt \quad (5.8)$$

is nonlinear. Also, if limit a or b or the kernel $K(x, t)$ becomes infinite, an integral equation is said to be singular. Finally, a kernel $K(x, t)$ is said to be symmetric if $K(x, t) = K(t, x)$.

5.2.2 Connection Between Differential and Integral Equations

The above classification of one-dimensional integral equations arises naturally from the theory of differential equations, thereby showing a close connection between the integral and differential formulation of a given problem. Most ordinary differential equations can be expressed as integral equations, but the reverse is not true. While boundary conditions are imposed externally in differential equations, they are incorporated within an integral equation.

For example, consider the first order ordinary differential equation

$$\frac{d\Phi}{dx} = F(x, \Phi), \quad a \leq x \leq b \quad (5.9)$$

subject to $\Phi(a) = \text{constant}$. This can be written as the Volterra integral of the second kind. Integrating Equation (5.9) gives

$$\Phi(x) = \int_a^x F(t, \Phi(t))dt + c_1$$

where $c_1 = \Phi(a)$. Hence Equation (5.9) is the same as

$$\Phi(x) = \Phi(a) + \int_a^x F(t, \Phi(t))dt \quad (5.10)$$

Any solution of Equation (5.10) satisfies both Equation (5.9) and the boundary conditions. Thus an integral equation formulation incorporates both the differential equation and the boundary conditions.

Similarly, consider the second-order ordinary differential equation

$$\frac{d^2\Phi}{dx^2} = F(x, \Phi), \quad a \leq x \leq b \quad (5.11)$$

Integrating once yields

$$\frac{d\Phi}{dx} = \int_a^x F(x, \Phi(t)) dt + c_1 \quad (5.12)$$

where $c_1 = \Phi'(a)$. Integrating Equation (5.12) by parts,

$$\Phi(x) = c_2 + c_1 x + \int_a^x (x-t) F(x, \Phi(t)) dt$$

where $c_2 = \Phi(a) - \Phi'(a)a$. Hence

$$\Phi(x) = \Phi(a) + (x-a)\Phi'(a) + \int_a^x (x-t) F(x, \Phi(t)) dt \quad (5.13)$$

Again, we notice that the integral equation (5.13) represents both the differential equation (5.11) and the boundary conditions. We have considered only one-dimensional integral equations involving unknown functions in two or more space dimensions will be discussed later.

Example 5.1

Solve the Volterra integral equation

$$\Phi(x) = 1 + \int_0^x \Phi(t) dt \quad \square$$

Solution

This can be solved directly or indirectly by finding the solution of the corresponding differential equation. To solve it directly, we differentiate both sides of the given integral equation. In general, given an integral

$$g(x) = \int_{\alpha(x)}^{\beta(x)} f(x, t) dt \quad (5.14)$$

with variable limits, we differentiate this using the Leibnitz rule, namely,

$$g'(x) = \int_{\alpha(x)}^{\beta(x)} \frac{\partial f(x, t)}{\partial x} dt + f(x, \beta) \beta' - f(x, \alpha) \alpha' \quad (5.15)$$

Differentiating the given integral equation, we obtain

$$\frac{d\Phi}{dx} = \Phi(x) \quad (5.16a)$$

5.2. INTEGRAL EQUATIONS

or

$$\frac{d\Phi}{\Phi} = dx \quad (5.16b)$$

Integrating gives

$$\ln \Phi = x + \ln c_o$$

or

$$\Phi = c_o e^x$$

where $\ln c_o$ is the integration constant. From the given integral equation

$$\Phi(0) = 1 = c_o$$

Hence

$$\Phi(x) = e^x \quad (5.17)$$

is the required solution. This can be checked by substituting it into the given integral equation.

An indirect way of solving the integral equation is by comparing it with Equation (5.10) and noting that

$$a = 0, \Phi(a) = \Phi(0) = 1$$

and that $F(x, \Phi) = \Phi(x)$. Hence the corresponding first order differential equation is

$$\frac{d\Phi}{dx} = \Phi, \quad \Phi(0) = 1$$

which is the same as Equation (5.16), and the solution in Equation (5.17) follows. ■

Example 5.2

Find the integral equation corresponding to the differential equation

$$\Phi''' - 3\Phi'' - 6\Phi' + 8\Phi = 0$$

subject to $\Phi''(0) = \Phi'(0) = \Phi(0) = 1$. □

Solution

Let $\Phi''' = F(\Phi, \Phi', \Phi'', x) = 3\Phi'' + 6\Phi' - 8\Phi$. Integrating both sides,

$$\Phi'' = 3\Phi' + 6\Phi - 8 \int_0^x \Phi(t) dt + c_1 \quad (5.18)$$

where c_1 is determined from the initial values, i.e.,

$$1 = 3 + 6 + c_1 \rightarrow c_1 = -8$$

Integrating both sides of Equation (5.18) gives

$$\Phi' = 3\Phi + 6 \int_0^x \Phi(t) dt - 8 \int_0^x (x-t)\Phi(t) dt - 8x + c_2 \quad (5.19)$$

where

$$1 = 3 + c_2 \rightarrow c_2 = -2$$

Finally, we integrate both sides of Equation (5.19) to get

$$\Phi = 3 \int_0^x \Phi(t) dt + 6 \int_0^x (x-t)\Phi(t) dt - 4 \int_0^x (x-t)^2 \Phi(t) dt - 4x^2 - 2x + c_3$$

where $1 = c_3$. Thus the integral equation equivalent to the given differential equation is

$$\Phi(x) = 1 - 2x - 4x^2 + \int_0^x [3 + 6(x-t) - 4(x-t)^2] \Phi(t) dt \quad \blacksquare$$

5.3 Green's Functions

A more systematic means of obtaining an IE from a PDE is by constructing an auxiliary function known as the *Green's function*¹ for that problem [10]–[13]. The Green's function, also known as the *source function* or *influence function*, is the kernel function obtained from a linear boundary value problem and forms the essential link between the differential and integral formulations. Green's function also provides a method of dealing with the source term (g in $L\Phi = g$) in a PDE. In other words, it provides an alternative approach to the series expansion method of Section 2.7 for solving inhomogeneous boundary-value problems by reducing the inhomogeneous problem to a homogeneous one.

To obtain the field caused by a distributed source by the Green's function technique, we find the effects of each elementary portion of source and sum them. If $G(\mathbf{r}, \mathbf{r}')$ is the field at the observation point (or field point) \mathbf{r} caused by a unit point source at the source point \mathbf{r}' , then the field at \mathbf{r} by a source distribution $g(\mathbf{r}')$ is the integral of $g(\mathbf{r}')G(\mathbf{r}, \mathbf{r}')$ over the range of \mathbf{r}' occupied by the source. The function G is the Green's function. Thus, physically, the Green's function $G(\mathbf{r}, \mathbf{r}')$ represents the potential at \mathbf{r} due to a unit point charge at \mathbf{r}' . For example, the solution to the Dirichlet problem

$$\begin{aligned} \nabla^2 \Phi &= g && \text{in } R \\ \Phi &= f && \text{on } B \end{aligned} \quad (5.20)$$

is given by

$$\Phi = \int_R g(\mathbf{r}') G(\mathbf{r}, \mathbf{r}') d\mathbf{v}' + \oint_B f \frac{\partial G}{\partial n} dS \quad (5.21)$$

¹Named after George Green (1793–1841), an English mathematician.

where n denotes the outward normal to the boundary B of the solution region R . It is obvious from Equation (5.21) that the solution Φ can be determined provided the Green's function G is known. So the real problem is not that of finding the solution but that of constructing the Green's function for the problem.

Consider the linear second order PDE

$$L\Phi = g \quad (5.22)$$

We define the Green's function corresponding to the differential operator L as a solution of the point source inhomogeneous equation

$$LG(\mathbf{r}, \mathbf{r}') = \delta(\mathbf{r}, \mathbf{r}') \quad (5.23)$$

where \mathbf{r} and \mathbf{r}' are the position vectors of the field point (x, y, z) and source point (x', y', z') , respectively, and $\delta(\mathbf{r}, \mathbf{r}')$ is the Dirac delta function, which vanishes for $\mathbf{r} \neq \mathbf{r}'$ and satisfies

$$\int \delta(\mathbf{r}, \mathbf{r}') g(\mathbf{r}') d\mathbf{v}' = g(\mathbf{r}) \quad (5.24)$$

From Equation (5.23), we notice that the Green function $G(\mathbf{r}, \mathbf{r}')$ can be interpreted as the solution to the given boundary value problem with the source term g replaced by the unit impulse function. Thus $G(\mathbf{r}, \mathbf{r}')$ physically represents the response of the linear system to a unit impulse applied at the point $\mathbf{r} = \mathbf{r}'$.

The Green's function has the following properties [13]:

(a) G satisfies the equation $LG = 0$ except at the source point \mathbf{r}' , i.e.,

$$LG(\mathbf{r}, \mathbf{r}') = \delta(\mathbf{r}, \mathbf{r}') \quad (5.23)$$

(b) G is symmetric in the sense that

$$G(\mathbf{r}, \mathbf{r}') = G(\mathbf{r}', \mathbf{r}) \quad (5.25)$$

(c) G satisfies that prescribed boundary value f on B , i.e.,

$$G = f \quad \text{on } B \quad (5.26)$$

(d) The directional derivative $\partial G / \partial n$ has a discontinuity at \mathbf{r}' which is specified by the equation

$$\lim_{\epsilon \rightarrow 0} \oint_S \frac{\partial G}{\partial n} dS = 1 \quad (5.27)$$

where n is the outward normal to the sphere of radius ϵ as shown in Figure 5.1, i.e.,

$$|\mathbf{r} - \mathbf{r}'| = \epsilon^2$$

Property (b) expresses the *principle of reciprocity*; it implies that an exchange of source and observer does not affect G . The property is proved by Myint-U [13] by applying Green's second identity in conjunction with Equation (5.23) while property (d) is proved by applying divergence theorem along with Equation (5.23).

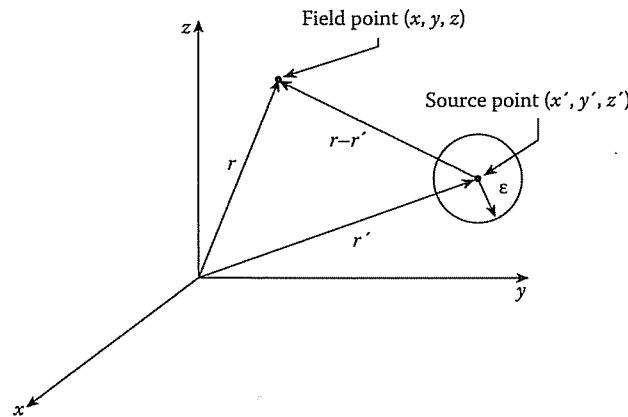


Figure 5.1

Illustration of the field point (x, y, z) and source point (x', y', z') .

5.3.1 For Free Space

We now illustrate how to construct the free space Green's function G corresponding to a PDE. It is usually convenient to let G be the sum of a particular integral of the inhomogeneous equation $LG = g$ and the solution of the associated homogeneous equation $LG = 0$. In other words, we let

$$G(\mathbf{r}, \mathbf{r}') = F(\mathbf{r}, \mathbf{r}') + U(\mathbf{r}, \mathbf{r}')$$
 (5.28)

where F , known as the free-space Green's function or fundamental solution, satisfies

$$LF = \delta(\mathbf{r}, \mathbf{r}') \quad \text{in } R$$
 (5.29)

and U satisfies

$$LU = 0 \quad \text{in } R$$
 (5.30)

so that by superposition $G = F + U$ satisfies Equation (5.23). Also $G = f$ on the boundary B requires that

$$U = -F + f \quad \text{on } B$$
 (5.31)

Notice that F need not satisfy the boundary condition.

We apply this to two specific examples. First, consider the two-dimensional problem for which

$$L = \frac{\partial^2}{\partial x^2} + \frac{\partial^2}{\partial y^2} = \nabla^2$$
 (5.32)

The corresponding Green's function $G(x, y; x', y')$ satisfies

$$\nabla^2 G(x, y; x', y') = \delta(x - x') \delta(y - y')$$
 (5.33)

5.3. GREEN'S FUNCTIONS

Hence, F must satisfy

$$\nabla^2 F = \delta(x - x') \delta(y - y')$$

For $\rho = [(x - x')^2 + (y - y')^2]^{1/2} > 0$, i.e., for $x \neq x'$, $y \neq y'$,

$$\nabla^2 F = \frac{1}{\rho} \frac{\partial}{\partial \rho} \left(\rho \frac{\partial F}{\partial \rho} \right) = 0$$
 (5.34)

which is integrated twice to give

$$F = A \ln \rho + B$$
 (5.35)

Applying the property in Equation (5.27)

$$\lim_{\epsilon \rightarrow 0} \oint \frac{dF}{d\rho} dl = \lim_{\epsilon \rightarrow 0} \int_0^{2\pi} \frac{A}{\rho} \rho d\phi = 2\pi A = 1$$

or $A = \frac{1}{2\pi}$. Since B is arbitrary, we may choose $B = 0$. Thus

$$F = \frac{1}{2\pi} \ln \rho$$

and

$$G = F + U = \frac{1}{2\pi} \ln \rho + U$$
 (5.36)

We choose U so that G satisfies prescribed boundary conditions.

For the three-dimensional problem,

$$L = \nabla^2 = \frac{\partial^2}{\partial x^2} + \frac{\partial^2}{\partial y^2} + \frac{\partial^2}{\partial z^2}$$
 (5.37)

and the corresponding Green's function $G(x, y, z; x', y', z')$ satisfies

$$LG(x, y, z; x', y', z') = \delta(x - x') \delta(y - y') \delta(z - z')$$
 (5.38)

Hence, F must satisfy

$$\begin{aligned} \nabla^2 F &= \delta(x - x') \delta(y - y') \delta(z - z') \\ &= \delta(\mathbf{r} - \mathbf{r}') \end{aligned}$$

For $\mathbf{r} \neq \mathbf{r}'$,

$$\nabla^2 F = \frac{1}{r^2} \frac{d}{dr} \left(r^2 \frac{dF}{dr} \right) = 0$$
 (5.39)

which is integrated twice to yield

$$F = -\frac{A}{r} + B$$
 (5.40)

Applying Equation (5.27),

$$1 = \lim_{\epsilon \rightarrow 0} \oint \frac{dF}{dr} dS = \lim_{\epsilon \rightarrow 0} \int_0^{2\pi} \int_0^\pi \frac{A}{r^2} r^2 \sin \phi d\theta d\phi = 4\pi A$$

or $A = \frac{1}{4\pi}$. Choosing $B = 0$ leads to

$$F = -\frac{1}{4\pi r}$$

and

$$G = F + U = -\frac{1}{4\pi r} + U \quad (5.41)$$

where U is chosen so that G satisfies prescribed boundary conditions.

Table 5.1 lists some Green functions that are commonly used in the solution of EM-related problems. It should be observed from Table 5.1 that the form of the three-dimensional Green's function for the steady-state wave equation tends to the Green's function for Laplace's equation as the wave number k approaches zero. It is also worthy of remark that each of the Green's functions in closed form as in Table 5.1 can be expressed in series form. For example, the Green's function

$$\begin{aligned} F &= -\frac{j}{4} H_0^{(1)}(k|\rho - \rho'|) \\ &= -\frac{j}{4} H_0^{(1)}\left(k[\rho^2 + \rho'^2 - 2\rho\rho' \cos(\phi - \phi')]\right)^{1/2} \end{aligned} \quad (5.42)$$

Table 5.1 Free-Space Green's Functions

Operator Equation	Laplace's Equation	Steady-State Helmholtz's (or wave) Equation ¹	Modified Steady-State Helmholtz's (or wave) Equation
Solution Region	$\nabla^2 G = \delta(\mathbf{r}, \mathbf{r}')$	$\nabla^2 G + k^2 G = \delta(\mathbf{r}, \mathbf{r}')$	$\nabla^2 G - k^2 G = \delta(\mathbf{r}, \mathbf{r}')$
1-dimensional	no solution for $(-\infty, \infty)$	$-\frac{j}{2k} \exp(jk x - x')$	$-\frac{1}{2k} \exp(-k x - x')$
2-dimensional	$\frac{1}{2\pi} \ln \rho - \rho' $	$-\frac{j}{4} H_0^{(1)}(k \rho - \rho')$	$-\frac{1}{2\pi} K_0(k \rho - \rho')$
3-dimensional	$-\frac{1}{4\pi(r - r')}$	$-\frac{\exp(jk r - r')}{4\pi r - r' }$	$-\frac{\exp(-k r - r')}{4\pi r - r' }$

¹ The wave equation has the time factor $e^{j\omega t}$ so that $k = \omega\sqrt{\mu\epsilon}$.

5.3. GREEN'S FUNCTIONS

can be written in series form as

$$F = \begin{cases} -\frac{j}{4} \sum_{n=-\infty}^{\infty} H_n^{(1)}(k\rho') J_n(k\rho) e^{-jn(\phi - \phi')}, & \rho < \rho' \\ -\frac{j}{4} \sum_{n=-\infty}^{\infty} H_n^{(1)}(k\rho) J_n(k\rho') e^{-jn(\phi - \phi')}, & \rho > \rho' \end{cases} \quad (5.43)$$

This is obtained from addition theorem for Hankel functions [14]. It should be noted that Green's functions are very difficult to construct in an explicit form except for the simplest shapes of domain.

With the aid of the Green's function, we can construct the integral equation corresponding to Poisson's equation in three dimensions

$$\nabla^2 V = -\frac{\rho_v}{\epsilon} \quad (5.44)$$

as

$$V = \int \frac{\rho_v}{\epsilon} G(\mathbf{r}, \mathbf{r}') dv'$$

or

$$V = \int \frac{\rho_v dv'}{4\pi\epsilon r} \quad (5.45)$$

Similarly, the integral equation corresponding to Helmholtz's equation in three dimensions

$$\nabla^2 \Phi + k^2 \Phi = g \quad (5.46)$$

as

$$\Phi = \int g G(\mathbf{r}, \mathbf{r}') dv'$$

or

$$\Phi = \int \frac{g e^{jkr}}{4\pi r} dv' \quad (5.47)$$

where an outgoing wave is assumed.

5.3.2 For Domain with Conducting Boundaries

The Green's functions derived so far are useful if the domain is free space. When the domain is bounded by one or more grounded planes, there are two ways to obtain Green's function:

- (a) the method of images [12], [15]–[22] and
- (b) the eigenfunction expansion [12, 16, 17], [22]–[30].

(a) Method of Images

The method of images is a powerful technique for obtaining the field due to one or more sources with conducting boundary planes. If a point charge q is at some distance h from a grounded conducting plane, the boundary condition imposed by the plane on the resulting potential field may be satisfied by replacing the plane with an “image charge” $-q$ located at a position which is the mirror location of q . Using this idea to obtain the Green’s function is perhaps best illustrated with an example.

Consider the region between the ground planes at $y = 0$ and $y = h$ as shown in Figure 5.2. The Green’s function $G(x, y; x', y')$ is the potential at the point (x, y) , which results when a unit line charge of 1 C/m is placed at the point (x', y') . If no ground planes were present, the potential at distance ρ from a unit line charge would be

$$V(\rho) = \frac{1}{4\pi\epsilon} \ln \rho^2 \quad (5.48)$$

In order to satisfy the boundary conditions on the ground planes, an infinite set of images is derived as shown in Figure 5.2. The potential due to such a sequence of line charges (including the original) within the strip is the superposition of an infinite series of images:

$$\begin{aligned} G(x, y; x', y') &= \frac{1}{4\pi\epsilon} \left(\ln \left[(x - x')^2 + (y + y')^2 \right] - \ln \left[(x - x')^2 + (y + y')^2 \right] \right. \\ &\quad + \sum_{n=1}^{\infty} (-1)^n \left\{ \ln \left[(x - x')^2 + (y + y' - 2nh)^2 \right] \right. \\ &\quad - \ln \left[(x - x')^2 + (y - y' - 2nh)^2 \right] \\ &\quad + \ln \left[(x - x')^2 + (y + y' - 2nh)^2 \right] \\ &\quad \left. - \ln \left[(x - x')^2 + (y - y' - 2nh)^2 \right] \right\} \\ &= \frac{1}{4\pi\epsilon} \sum_{n=-\infty}^{\infty} \ln \left[\frac{(x - x')^2 + (y + y' - 2nh)^2}{(x - x')^2 + (y - y' - 2nh)^2} \right] \end{aligned} \quad (5.49)$$

This series converges slowly and is awkward for numerical computation. It can be summed to give [15]

$$G(x, y; x', y') = \frac{1}{4\pi\epsilon} \ln \left[\frac{\sinh^2 \left(\frac{\pi(x-x')}{2h} \right) + \sin^2 \left(\frac{\pi(y+y')}{2h} \right)}{\sinh^2 \left(\frac{\pi(x-x')}{2h} \right) + \sin^2 \left(\frac{\pi(y-y')}{2h} \right)} \right] \quad (5.50)$$

This expression can be shown to satisfy the appropriate boundary conditions along the ground plane, i.e., $G(x, y; x', y') = 0$ at $y = 0$ or $y = h$. Note that G has exactly one singularity at $x = x'$, $y = y'$ in the region $0 \leq y \leq h$.

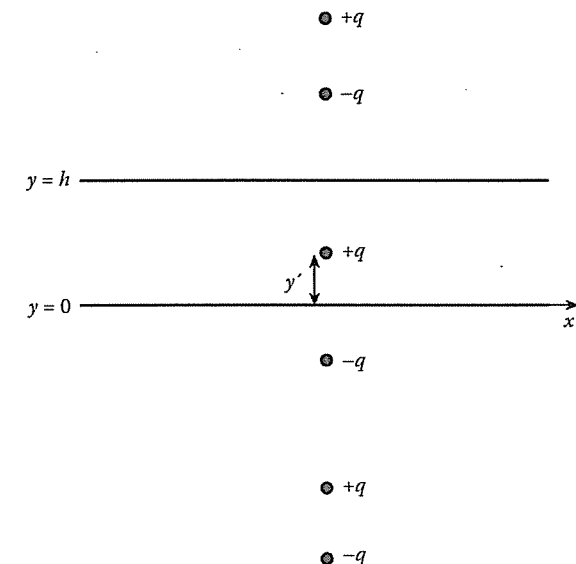


Figure 5.2

A single charge placed between two conducting planes produces the same potential as does the system of image charges when no conducting planes are present.

In order to evaluate an integral involving $G(x, y; x', y')$ in Equation (5.50), it is convenient to take out the singular portion of the unit source function. We rewrite Equation (5.50) as

$$G(x, y; x', y') = -\frac{1}{4\pi\epsilon} \ln \left[(x - x')^2 + (y + y')^2 \right] + g(x, y; x', y') \quad (5.51)$$

where

$$\begin{aligned} g(x, y; x', y') &= \\ \frac{1}{4\pi\epsilon} \ln \left[\frac{\left[(x - x')^2 (y - y')^2 \right] \left[\sinh^2 \left(\frac{\pi(x-x')}{2h} \right) + \sin^2 \left(\frac{\pi(y+y')}{2h} \right) \right]}{\sinh^2 \left(\frac{\pi(x-x')}{2h} \right) + \sin^2 \left(\frac{\pi(y-y')}{2h} \right)} \right] \end{aligned} \quad (5.52)$$

Note that $g(x, y; x', y')$ is finite everywhere in $0 \leq y \leq h$. The integral involving g is evaluated numerically, while the one involving the singular logarithmic term is evaluated analytically with the aid of integral tables.

The method of images has been applied in derivating the Green's functions for multiconductor transmission lines [18]–[20] and planar microwave circuits [16, 17, 21]. The method is restricted to the shapes enclosed by boundaries that are straight conductors.

(b) Eigenfunction Expansion

This method is suitable for deriving the Green's function for differential equations whose homogeneous solution is known. The Green's function is represented in terms of a series of orthonormal functions that satisfy the boundary conditions associated with the differential equation. To illustrate the eigenfunction expansion procedure, suppose we are interested in the Green's function for the wave equation

$$\frac{\partial^2 \Psi}{\partial x^2} + \frac{\partial^2 \Psi}{\partial y^2} + k^2 \Psi = 0 \quad (5.53)$$

subject to

$$\frac{\partial \Psi}{\partial n} = 0 \quad \text{or} \quad \Psi = 0 \quad (5.54)$$

Let the eigenfunctions and eigenvalues of Equation (5.53) that satisfy Equation (5.54) be Ψ_j and k_j , respectively, i.e.,

$$\nabla^2 \Psi_j + k_j^2 \Psi_j = 0 \quad (5.55)$$

Assuming that Ψ_j form a complete set of orthonormal functions,

$$\int_S \Psi_j^* \Psi_i dxdy = \begin{cases} 1, & j = i \\ 0, & j \neq i \end{cases} \quad (5.56)$$

where the asterisk (*) denotes complex conjugation. $G(x, y; x', y')$ can be expanded in terms of Ψ_j , i.e.,

$$G(x, y; x', y') = \sum_{j=1}^{\infty} a_j \Psi_j(x, y) \quad (5.57)$$

Since the Green's function must satisfy

$$(\nabla^2 + k^2) G(x, y; x', y') = \delta(x - x') \delta(y - y'), \quad (5.58)$$

substituting Equations (5.55) and (5.57) into Equation (5.58), we obtain

$$\sum_{j=1}^{\infty} a_j (k^2 - k_j^2) \Psi_j = \delta(x - x') \delta(y - y') \quad (5.59)$$

5.3. GREEN'S FUNCTIONS

Multiplying both sides by Ψ_i^* and integrating over the region S gives

$$\sum_{j=1}^{\infty} a_j (k^2 - k_j^2) \int_S \Psi_j \Psi_i^* dxdy = \Psi_i^*(x', y') \quad (5.60)$$

Imposing the orthonormal property in Equation (5.56) leads to

$$a_i (k^2 - k_i^2) = \Psi_i^*(x', y')$$

or

$$a_i = \frac{\Psi_i^*(x', y')}{(k^2 - k_i^2)} \quad (5.61)$$

Thus

$$G(x, y; x', y') = \sum_{j=1}^{\infty} \frac{\Psi_j(x, y) \Psi_j^*(x', y')}{(k^2 - k_j^2)} \quad (5.62)$$

The eigenfunction expansion approach has been applied to derive the Green's functions for plane conducting boundaries such as rectangular box and prism [22], planar microwave circuits [16, 17, 25], multilayered dielectric structures [23, 24], waveguides [28], and surfaces of revolution [27]. The approach is limited to separable coordinate systems since the requisite eigenfunctions can be determined for only these cases.

Example 5.3

Construct a Green's function for

$$\nabla^2 V = 0$$

subject to $V(a, \phi) = f(\phi)$ within a circular disk $\rho \leq a$. \square

Solution

Since $g = 0$, the solution is obtained from Equation (5.21) as

$$V = \oint_C f \frac{\partial G}{\partial n} dl \quad (5.63)$$

where the circle C is the boundary of the disk as shown in Figure 5.3. Let

$$G = F + U,$$

where F is already found to be

$$F = \frac{1}{2\pi} \ln |\rho - \rho'|,$$

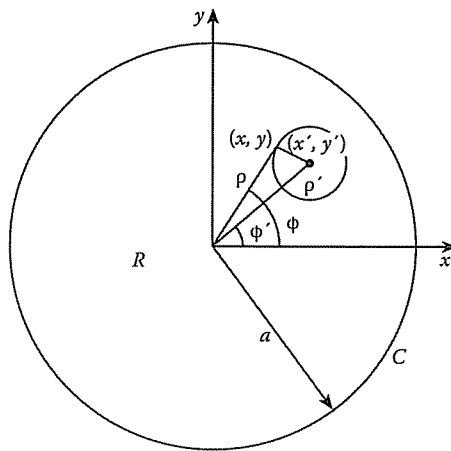


Figure 5.3
A disk of radius a .

i.e.,

$$F(\rho, \phi; \rho', \phi') = \frac{1}{4\pi} \ln [\rho'^2 + \rho'^2 - 2\rho\rho' \cos(\phi - \phi')] \quad (5.64)$$

The major problem is finding U . But

$$\nabla^2 U = 0 \quad \text{in } R \quad (5.65a)$$

with

$$U = -F \quad \text{on } C$$

or

$$U(a, \phi; \rho', \phi') = -\frac{1}{4\pi} \ln [a^2 + \rho'^2 - 2a\rho' \cos(\phi - \phi')] \quad (5.65b)$$

Thus U can be found by solving the PDE in Equation (5.65a) subject to the condition in Equation (5.65b). Applying the separation of variables method,

$$U = \frac{A_0}{2} + \sum_{n=1}^{\infty} \rho^n [A_n \cos n\phi + B_n \sin n\phi] \quad (5.66)$$

The term ρ^{-n} is not included since U must be bounded at $\rho = 0$. To impose the boundary condition in Equation (5.65b) on the solution in Equation (5.66), we first express Equation (5.65b) in Fourier series using the identity

$$\sum_{n=1}^{\infty} \frac{z^n}{n} \cos n\theta = \int_0^z \frac{\cos \theta - \lambda}{1 + \lambda^2 - 2\lambda \cos \theta} d\lambda = -\frac{1}{2} \ln [1 + z^2 - 2z \cos \theta] \quad (5.67)$$

5.3. GREEN'S FUNCTIONS

Hence Equation (5.65b) becomes

$$\begin{aligned} U(a, \phi; \rho', \phi') &= -\frac{1}{4\pi} \ln a^2 \left[1 + (\rho'/a)^2 - \frac{2\rho'}{a} \cos(\phi - \phi') \right] \\ &= -\frac{1}{2\pi} \ln a + \frac{1}{2\pi} \sum_{n=1}^{\infty} \left[\frac{\rho'}{a} \right]^n \frac{\cos n(\phi - \phi')}{n} \\ &= -\frac{1}{2\pi} \ln a + \frac{1}{2\pi} \sum_{n=1}^{\infty} \left[\frac{\rho'}{a} \right]^n \frac{(\cos n\phi \cos n\phi' + \sin n\phi \sin n\phi')}{n}. \end{aligned} \quad (5.68)$$

Comparing Equation (5.66) with Equation (5.68) at $\rho = a$, we obtain the coefficients A_n and B_n as

$$\begin{aligned} \frac{A_0}{2} &= -\frac{1}{2\pi} \ln a \\ a^n A_n &= \frac{1}{2\pi n} \left[\frac{\rho'}{a} \right]^n \cos n\phi' \\ a^n B_n &= \frac{1}{2\pi n} \left[\frac{\rho'}{a} \right]^n \sin n\phi' \end{aligned}$$

Thus Equation (5.66) becomes

$$\begin{aligned} U(\rho, \phi; \rho', \phi') &= -\frac{1}{2\pi} \ln a + \frac{1}{2\pi} \sum_{n=1}^{\infty} \left[\frac{\rho'}{a} \right]^n \left[\frac{\rho}{a} \right]^n \frac{\cos n(\phi - \phi')}{n} \\ &= -\frac{1}{2\pi} \ln a - \frac{1}{4\pi} \ln \left[1 + \left[\frac{\rho\rho'}{a^2} \right]^2 - \frac{2\rho\rho'}{a^2} \cos(\phi - \phi') \right] \end{aligned} \quad (5.69)$$

From Equations (5.64) and Equation (5.69), we obtain the Green's function as

$$\begin{aligned} G &= \frac{1}{4\pi} \ln [\rho^2 + \rho'^2 - 2\rho\rho' \cos(\phi - \phi')] \\ &\quad - \frac{1}{4\pi} \ln \left[a^2 + \frac{\rho'^2 \rho^2}{a^2} - 2\rho\rho' \cos(\phi - \phi') \right] \end{aligned} \quad (5.70)$$

An alternative means of constructing the Green's function is the method of images. Let us obtain Equation (5.70) using the method of images. Let

$$G(P, P') = \frac{1}{2\pi} \ln r + U$$

The problem reduces to finding the induced field U , which is harmonic within the disk and is equal to $-\frac{1}{2\pi} \ln r$ on C . Let P' be the singular point of Green's function

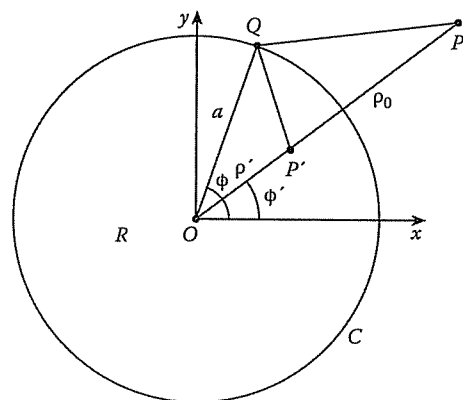


Figure 5.4

The image point P_o of P' with respect to circle C so that $OP' \times OP_o = OQ = a^2$ and OQP' and OQP_o are similar triangles.

and let P_o be the image of P' with respect to the circle C as shown in Figure 5.4. The triangles OQP' and OQP_o are similar because the angle at O is common and the sides adjacent to it are proportional. Thus

$$\frac{\rho'}{a} = \frac{a}{\rho_o} \rightarrow \rho' \rho_o = a^2 \quad (5.71)$$

That is, the product of OP' and OP_o is equal to the square of the radius OQ . At a point Q on C , it is evident from Figure 5.4 that

$$r_{QP'} = \frac{\rho'}{a} r_{QP_o}$$

Therefore,

$$U = -\frac{1}{2\pi} \ln \frac{\rho' r_{PP_o}}{a} \quad (5.72)$$

and

$$G = \frac{1}{2\pi} \ln r_{PP'} - \frac{1}{2\pi} \ln \frac{\rho'}{a} r_{PP_o} \quad (5.73)$$

Since $r_{PP'}$ is the distance between $P(\rho, \phi)$ and $P'(\rho', \phi')$ while r_{PP_o} is the distance between $P(\rho, \phi)$ and $P_o(\rho'_o, \phi) = P_o(a^2/\rho', \phi)$,

$$r_{PP'}^2 = \rho^2 + \rho'^2 - 2\rho\rho' \cos(\phi - \phi'),$$

$$r_{PP_o}^2 = \rho^2 + \frac{a^4}{\rho'^2} - 2\rho \frac{a^2}{\rho'} \cos(\phi - \phi')$$

5.3. GREEN'S FUNCTIONS

Substituting these in Equation (5.73), we obtain

$$G = \frac{1}{4\pi} \ln [\rho^2 + \rho'^2 - 2\rho\rho' \cos(\phi - \phi')] - \frac{1}{4\pi} \ln \left[a^2 + \frac{\rho'^2 \rho^2}{a^2} - 2\rho\rho' \cos(\phi - \phi') \right] \quad (5.74)$$

which is the same as Equation (5.70). From Equation (5.70) or (5.74), the directional derivative $\partial G / \partial n = (\nabla G \cdot \mathbf{a}_n)$ on C is given by

$$\begin{aligned} \frac{\partial G}{\partial \rho'} \Big|_{\rho'=a} &= \frac{2a - 2\rho \cos(\phi - \phi')}{4\pi [a^2 + \rho^2 - 2a\rho \cos(\phi - \phi')]} \\ &\quad - \frac{\frac{2\rho^2}{a} - 2\rho \cos(\phi - \phi')}{4\pi [a^2 + \rho^2 - 2a\rho \cos(\phi - \phi')]} \\ &= \frac{a^2 - \rho^2}{2\pi a [a^2 + \rho^2 - 2a\rho \cos(\phi - \phi')]} \end{aligned}$$

Hence the solution in Equation (5.63) becomes (with $dl = ad\phi'$)

$$V(\rho, \phi) = \frac{1}{2\pi} \int_0^{2\pi} \frac{(a^2 - \rho^2) f(\phi') d\phi'}{[a^2 + \rho^2 - 2a\rho \cos(\phi - \phi')]} \quad (5.75)$$

which is known as *Poisson's integral formula*. □

Example 5.4

Obtain the solution for the Laplace operator on unbounded half-space, $z \leq 0$, with the condition $V(z=0) = f$. □

Solution

Again the solution is

$$V = \oint_S f \frac{\partial G}{\partial n} dS$$

where S is the plane $z = 0$. We let

$$G = \frac{1}{4\pi |\mathbf{r} - \mathbf{r}'|} + U,$$

so that the major problem is reduced to finding U . Using the method of images, it is easy to see that the image point of $P'(x', y', z')$ is $P_o(x', y', -z')$ as shown in Figure 5.5. Hence

$$U = -\frac{1}{4\pi |\mathbf{r} - \mathbf{r}_o|}$$

and

$$G = \frac{1}{4\pi |\mathbf{r} - \mathbf{r}'|} - \frac{1}{4\pi |\mathbf{r} - \mathbf{r}_o|},$$

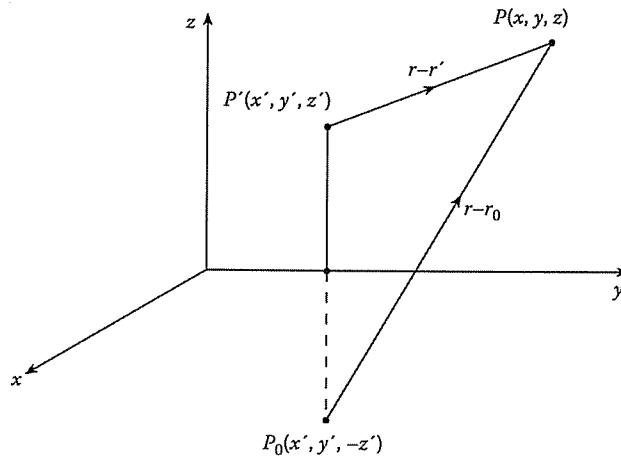


Figure 5.5
Half-space problem of Example 5.4.

where

$$\begin{aligned} |\mathbf{r} - \mathbf{r}'| &= \left[(x - x')^2 + (y - y')^2 + (z - z')^2 \right]^{1/2} \\ |\mathbf{r} - \mathbf{r}_0| &= \left[(x - x')^2 + (y - y')^2 + (z + z')^2 \right]^{1/2} \end{aligned}$$

Notice that G reduces to zero at $z = 0$ and has the required singularity at $P'(x', y', z')$. The directional derivative $\partial G / \partial n$ on plane $z = 0$ is

$$\begin{aligned} \frac{\partial G}{\partial z'} \Big|_{z'=0} &= \frac{1}{4\pi} \left[\frac{(z - z')}{|\mathbf{r} - \mathbf{r}'|^3} + \frac{(z + z')}{|\mathbf{r} - \mathbf{r}_0|^3} \right] \Big|_{z'=0} \\ &= \frac{z}{2\pi [(x - x')^2 + (y - y')^2 + z^2]^{3/2}} \end{aligned}$$

Hence

$$V(x, y, z) = \frac{1}{2\pi} \int_{-\infty}^{\infty} \int_{-\infty}^{\infty} \frac{zf(x', y') dx' dy'}{[(x - x')^2 + (y - y')^2 + z^2]^{3/2}}$$

Example 5.5

Using Green's function, construct the solution for Poisson's equation

$$\frac{\partial^2 V}{\partial x^2} + \frac{\partial^2 V}{\partial y^2} = f(x, y)$$

subject to the boundary conditions

$$V(0, y) = V(a, y) = V(x, 0) = V(x, b) = 0 \quad \square$$

Solution

According to Equation (5.21), the solution is

$$V(x, y) = \int_0^b \int_0^a f(x', y') G(x, y; x', y') dx' dy' \quad (5.76)$$

so that our problem is essentially that of obtaining the Green's function $G(x, y; x', y')$. The Green's function satisfies

$$\frac{\partial^2 G}{\partial x^2} + \frac{\partial^2 G}{\partial y^2} = \delta(x - x') \delta(y - y') \quad (5.77)$$

To apply the series expansion method of finding G , we must first determine eigenfunctions $\Psi(x, y)$ of Laplace's equation, i.e.,

$$\nabla^2 \Psi = \lambda \Psi$$

where Ψ satisfies the boundary conditions. It is evident that the normalized eigenfunctions are

$$\Psi_{mn} = \frac{2}{\sqrt{ab}} \sin \frac{m\pi x}{a} \sin \frac{n\pi y}{b}$$

with the corresponding eigenvalues

$$\lambda_{mn} = -\left(\frac{m^2\pi^2}{a^2} + \frac{n^2\pi^2}{b^2}\right)$$

Thus,

$$G(x, y; x', y') = \frac{2}{\sqrt{ab}} \sum_{m=1}^{\infty} \sum_{n=1}^{\infty} A_{mn}(x', y') \sin \frac{m\pi x}{a} \sin \frac{n\pi y}{b} \quad (5.78)$$

The expansion coefficients, A_{mn} , are determined by substituting Equation (5.78) into Equation (5.77), multiplying both sides by $\sin \frac{m\pi x}{a} \sin \frac{n\pi y}{b}$, and integrating over $0 < x < a$, $0 < y < b$. Using the orthonormality property of the eigenfunctions and the shifting property of the delta function results in

$$-\left(\frac{m^2\pi^2}{a^2} + \frac{n^2\pi^2}{b^2}\right) A_{mn} = \frac{2}{\sqrt{ab}} \sin \frac{m\pi x'}{a} \sin \frac{n\pi y'}{b}$$

Obtaining A_{mn} from this and substituting in Equation (5.78) gives

$$G(x, y; x', y') = -\frac{4}{ab} \sum_{m=1}^{\infty} \sum_{n=1}^{\infty} \frac{\sin \frac{m\pi x}{a} \sin \frac{m\pi x'}{a} \sin \frac{n\pi y}{b} \sin \frac{n\pi y'}{b}}{m^2\pi^2/a^2 + n^2\pi^2/b^2} \quad (5.79)$$

Another way of obtaining Green's function is by means of a single series rather than a double summation in Equation (5.79). It can be shown that [28, 29]

$$G(x, y; x', y') = \begin{cases} -\frac{2}{\pi} \sum_{n=1}^{\infty} \frac{\sin \frac{n\pi x}{b} \sinh \frac{n\pi(a-x')}{b} \sin \frac{n\pi y}{b} \sinh \frac{n\pi y'}{b}}{n \sinh \frac{n\pi a}{b}}, & x < x' \\ -\frac{2}{\pi} \sum_{n=1}^{\infty} \frac{\sinh \frac{n\pi x'}{b} \sin \frac{n\pi(a-x)}{b} \sin \frac{n\pi y}{b} \sinh \frac{n\pi y'}{b}}{n \sinh \frac{n\pi a}{b}}, & x > x' \end{cases} \quad (5.80)$$

By Fourier series expansion, it can be verified that the expressions in Equations (5.79) and (5.80) are identical. Besides the factor $\frac{1}{\epsilon}$, the Green's function in Equation (5.79) or Equation (5.80) gives the potential V due to a unit line source at (x', y') in the region $0 < x < a$, $0 < y < b$ as shown in Figure 5.6. ■

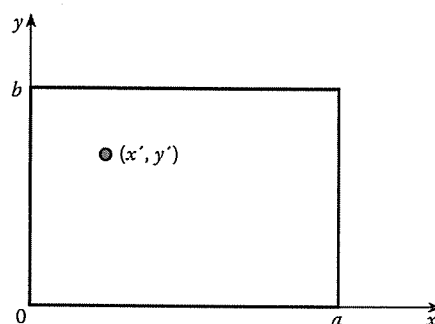


Figure 5.6
Line source in a rectangular region.

Example 5.6

An infinite line source I_z is located at (ρ', ϕ') in a wedge waveguide shown in Figure 5.7. Derive the electric field due to the line. ■

Solution

Assuming the time factor $e^{j\omega t}$, the z -component of \mathbf{E} for the TE mode satisfies the wave equation

$$\nabla^2 E_z + k^2 E_z = j\omega\mu I_z \quad (5.81)$$

with

$$\frac{\partial E_z}{\partial n} = 0$$

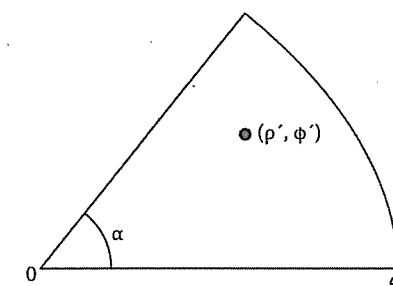


Figure 5.7
Line source in a waveguide.

where $k = \omega\sqrt{\mu\epsilon}$ and n is the outward unit normal at any point on the periphery of the cross section. The Green's function for this problem satisfies

$$\nabla^2 G + k^2 G = j\omega\mu\delta(\rho - \rho') \quad (5.82)$$

with

$$\frac{\partial G}{\partial n} = 0$$

so that the solution to Equation (5.81) is

$$E_z = j\omega\mu \int_S I_z(\rho', \phi') G(\rho, \phi; \rho', \phi') dS \quad (5.83)$$

To determine the Green's function $G(\rho, \phi; \rho', \phi')$, we find Ψ_i so that Equation (5.62) can be applied. The boundary condition $\frac{\partial G}{\partial n} = 0$ implies that

$$\frac{1}{\rho} \frac{\partial G}{\partial \phi} \Big|_{\phi=0} = 0 = \frac{1}{\rho} \frac{\partial G}{\partial \phi} \Big|_{\phi=\alpha} = \frac{\partial G}{\partial \rho} \Big|_{\rho=a} \quad (5.84)$$

The set of functions which satisfy the boundary conditions are

$$\Psi_{mv}(\rho, \phi) = J_v(k_{mv}\rho) \cos v\phi \quad (5.85)$$

where

$$v = n\pi/\alpha, \quad n = 0, 1, 2, \dots, \quad (5.86a)$$

k_{mv} are chosen to satisfy

$$\frac{\partial}{\partial \rho} J_v(k_{mv}\rho) \Big|_{\rho=a} = 0, \quad (5.86b)$$

and the subscript m is used to denote the m th root of Equation (5.86b); m can take the value zero for $n = 0$. The functions Ψ_{mv} are orthogonal if and only if v is an integer

which implies that v is an integral multiple of α . Let $\alpha = \pi/\ell$, where ℓ is a positive integer, so that Φ_{mv} are mutually orthogonal. To obtain the Green's function using Equation (5.62), these eigenfunctions must be normalized over the region, i.e.,

$$\int_0^a J_v^2(k_{mv}\rho) d\rho = \begin{cases} a^2/2, & m = v \\ \frac{1}{2} [a^2 - (v^2/k_{mv}^2)] J_v^2(k_{mv}a), & \text{otherwise} \end{cases} \quad (5.87a)$$

$$\int_0^\alpha \cos^2 v\phi d\phi = \begin{cases} \frac{\pi}{\ell}, & v = 0 \\ \frac{\pi}{2\ell}, & \text{otherwise} \end{cases} \quad (5.87b)$$

where $v = n\ell$. Using the normalized eigenfunctions, we obtain

$$G(\rho, \phi; \rho', \phi') = \frac{j2\ell}{\omega\epsilon\pi a^2} - 4j\ell\omega\mu \sum_{n=1}^{\infty} \sum_{m=1}^{\infty} \frac{J_v(k_{mv}\rho) J_v(k_{mv}\rho') \cos v\phi \cos v\phi'}{\epsilon_v \pi \left(a^2 - \frac{v^2}{k_{mv}^2}\right) J_v^2(k_{mv}a) (k^2 - k_{mv}^2)} \quad (5.88)$$

where

$$\epsilon_v = \begin{cases} 2, & v = 0 \\ 1, & v \neq 0 \end{cases} \quad (5.89)$$

We have employed the fact that $\omega\mu/k^2 = \frac{1}{\omega\epsilon}$ to obtain the first term on the right-hand side of Equation (5.88). ■

5.4 Applications I — Quasi-Static Problems

The method of moments has been applied to so many EM problems that covering all of them is practically impossible. We will consider only the relatively easy ones to illustrate the techniques involved. Once the basic approach has been mastered, it will be easy for the reader to extend the idea to attack more complicated problems.

We will apply MOM to a static problem in this section; more involved application will be considered in the sections to follow. We will consider the problem of determining the characteristic impedance Z_o of a strip transmission line [31].

Consider the strip transmission of Figure 5.8(a). If the line is assumed to be infinitely long, the problem is reduced to a two-dimensional TEM problem of line sources in a plane as in Figure 5.8(b). Let the potential difference of the strips be $V_d = 2V$ so that strip 1 is maintained at $+1V$ while strip 2 is at $-1V$. Our objective is to find the

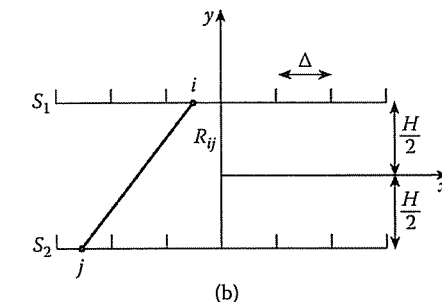
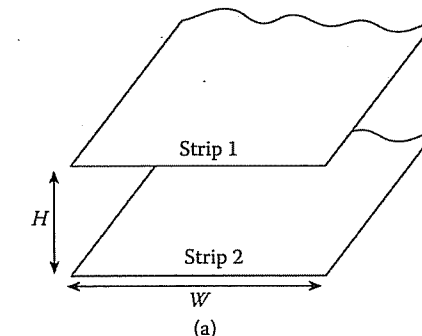


Figure 5.8

(a) The strip transmission line. (b) The two-dimensional view.

surface charge density $\rho(x, y)$ on the strips so that the total charge per unit length on one strip can be found as

$$Q_\ell = \int \rho dl \quad (5.90)$$

(Q_ℓ is charge per unit length as distinct from the total charge on the strip because we are treating a three-dimensional problem as a two-dimensional one.) Once Q is known, the capacitance per unit length C_ℓ can be found from

$$C_\ell = \frac{Q_\ell}{V_d} \quad (5.91)$$

Finally, the line characteristic impedance is obtained:

$$Z_o = \frac{(\mu\epsilon)^{1/2}}{C_\ell} = \frac{1}{u C_\ell} \quad (5.92)$$

where $u = 1/\sqrt{\mu\epsilon}$ is the speed of the wave in the (lossless) dielectric medium between the strips. Everything is straightforward once the charge density $\rho(x, y)$ in Equation (5.90) is known. To find ρ using MOM, we divide each strip into n subareas

of equal width Δ so that subareas in strip 1 are numbered $1, 2, \dots, n$, while those in strip 2 are numbered $n+1, n+2, n+3, \dots, 2n$. The potential at an arbitrary field point is

$$V(x, y) = \frac{1}{2\pi\epsilon} \int \rho(x', y') \ln \frac{R}{r_o} dx' dy' \quad (5.93)$$

where R is the distance between source and field points, i.e.,

$$R = [(x - x')^2 + (y - y')^2]^{1/2} \quad (5.94)$$

Since the integral in Equation (5.93) may be regarded as rectangular subareas in a numerical sense, the potential at the center of a typical subarea S_i is

$$V_i = \frac{1}{2\pi\epsilon} \sum_{j=1}^{2n} \rho_j \int_{S_i} \ln \frac{R_{ij}}{r_o} dx'$$

or

$$V_i = \sum_{j=1}^{2n} A_{ij} \rho_j \quad (5.95)$$

where

$$A_{ij} = \frac{1}{2\pi\epsilon} \int_{S_i} \ln \frac{R_{ij}}{r_o} dx', \quad (5.96)$$

R_{ij} is the distance between i th and j th subareas, and $A_{ij} \rho_j$ represents the potential at point i due to subarea j . In Equation (5.95), we have assumed that the charge density ρ is constant within each subarea. For all the subareas $S_i, i = 1, 2, \dots, 2n$ we have

$$V_1 = \sum_{j=1}^{2n} \rho_j A_{1j} = 1$$

$$V_2 = \sum_{j=1}^{2n} \rho_j A_{2j} = 1$$

⋮

$$V_n = \sum_{j=1}^{2n} \rho_j A_{nj} = 1$$

$$V_{n+1} = \sum_{j=1}^{2n} \rho_j A_{n+1,j} = -1$$

⋮

$$V_{2n} = \sum_{j=1}^{2n} \rho_j A_{2n,j} = -1$$

Thus we obtain a set of $2n$ simultaneous equations with $2n$ unknown charge densities ρ_i . In matrix form,

$$\begin{bmatrix} A_{11} & A_{12} & \cdots & A_{1,2n} \\ A_{21} & A_{22} & \cdots & A_{2,2n} \\ \vdots & & & \\ A_{2n,1} & A_{2n,2} & \cdots & A_{2n,2n} \end{bmatrix} \begin{bmatrix} \rho_1 \\ \rho_2 \\ \vdots \\ \rho_{2n} \end{bmatrix} = \begin{bmatrix} 1 \\ 1 \\ \vdots \\ -1 \\ -1 \end{bmatrix}$$

or simply

$$[A][\rho] = [B] \quad (5.97)$$

It can be shown that [32] the elements of matrix $[A]$ expressed in Equation (5.96) can be reduced to

$$A_{ij} = \begin{cases} \frac{\Delta}{2\pi\epsilon} \ln \frac{R_{ij}}{r_o}, & i \neq j \\ \frac{\Delta}{2\pi\epsilon} \left[\ln \frac{\Delta}{r_o} - 1.5 \right], & i = j \end{cases} \quad (5.98)$$

where r_o is a constant scale factor (commonly taken as unity). From Equation (5.97), we obtain $[\rho]$ either by solving the simultaneous equation or by matrix inversion, i.e.,

$$[\rho] = [A]^{-1}[B] \quad (5.99)$$

Once $[\rho]$ is known, we determine C_ℓ from Equations (5.90) and (5.91) as

$$C_\ell = \sum_{j=1}^n \rho_j \Delta / V_d \quad (5.100)$$

where $V_d = 2V$. Obtaining Z_o follows from Equations (5.92) and (5.100).

Example 5.7

Write a program to find the characteristic impedance Z_o of a strip line with $H = 2\text{m}$, $W = 5\text{m}$, $\epsilon = \epsilon_o$, $\mu_o = \mu_o$, and $V_d = 2V$. \square

Solution

The MATLAB program is shown in Figure 5.9. With the given data, the program calculates the elements of matrices $[A]$ and $[B]$ and determines $[\rho]$ by matrix inversion. With the computed charge densities the capacitance per unit length is calculated using Equation (5.100) and the characteristic impedance from Equation (5.92). Table 5.2 presents the computed values of Z_o for a different number of segments per strip, n . The results agree well with $Z_o = 50 \Omega$ from Wheeler's curve [33]. \blacksquare

```

% ****
% USING MOMENTS METHOD,
% THIS PROGRAM DETERMINES THE CHARACTERISTIC IMPEDANCE
% OF A STRIP TRANSMISSION LINE
% WITH CROSS-SECTION W X H
% THE STRIPS MAITAINED AT 1 VOLT AND -1 VOLT.
%
% ONE STRIP IS LOCATED ON THE Y = H/2 PLANE WHILE THE OTHER
% IS LOCATED ON THE Y = -H/2 PLANE.
%
% ALL DIMENSIONS ARE IS S.I. UNITS
%
% N IS THE NUMBER OF SUBSECTIONS INTO WHICH EACH STRIP IS DIVIDED
% ****
%
% FIRST, SPECIFY THE PARAMETERS

NN = [3 7 11 18 39 59];

disp(' ')
disp('n      zo')

for N = NN
    CL=3.0e8; % SPEED OF LIGHT IN FREE SPACE
    ER=1.0;
    EO=8.8541878176E-12;
    H=2.0;
    W=5.0;

    NT=2*N;
    DELTA = W/(N);

    % SECOND, CALCULATE THE MATCH POINTS
    % AND THE COEFFICIENT MATRIX [A]

    for K=1:N
        X(K) = DELTA*(K - .5);
        Y(K) = -H/2.0;
        X(K+N) = X(K);
        Y(K+N) = H/2.0;
    end

    FACTOR = DELTA/(2.0*pi*EO);

    for I=1:NT
        for J=1:NT
            if(I==J)      %eqn (5.98)
                A(I,J) = -(log(DELTA) - 1.5)*FACTOR;
            else
                R = sqrt( (X(I) - X(J))^2 + (Y(I) - Y(J))^2 );
                A(I,J) = -log(R)*FACTOR;
            end
        end
    end
end

```

Figure 5.9

MATLAB program for Example 5.7 (*Continued*).

```

% NOW DETERMINE THE MATRIX OF CONSTANT VECTOR [B]
%
for K=1:N
    B(K)=1.0;
    %The line below was commented!
    B(K+N) = -1.0;      %rja -this line needed to be un-commented
end

%
% INVERT MATRIX A(I,J) AND CALCULATE MATRIX RO(N)
% CONSISTING OF THE UNKNOWN ELEMENTS
% ALSO CALCULATE THE TOTAL CHARGE Q,
% THE CAPACITANCE C, AND THE CHARACTERISTIC IMPEDANCE ZO.

NIV=NT;
NMAX=100;
A = inv(A);
for I=1:NT
    RO(I)=0.0;
    %The line below had an error N instead of NT
    for M=1:NT
        RO(I)=RO(I) + A(I,M)*B(M);
    end
end
SUM=0.0;
for I=1:N
    SUM = SUM + RO(I);
end
Q=SUM*DELTA;
VD=2.0;
C=abs(Q)/VD;
ZO = sqrt(ER)/(CL*C);

disp(num2str([N ZO ]))

end

```

Figure 5.9

(Cont.) MATLAB program for Example 5.7.

Table 5.2 Characteristic Impedance of a Strip Transmission Line

<i>n</i>	Z_o (in Ω)
3	53.02
7	51.07
11	50.49
18	50.39
39	49.71
59	49.61

5.5 Applications II — Scattering Problems

The purpose of this section is to illustrate, with two examples, how the method of moments can be applied to solve electromagnetic scattering problems. The first example is on scattering of a plane wave by a perfectly conducting cylinder [3], while the second is on scattering of a plane wave by an arbitrary array of parallel wires [34].

5.5.1 Scattering by Conducting Cylinder

Consider an infinitely long, perfectly conducting cylinder located at a far distance from a radiating source. Assuming a time-harmonic field with time factor $e^{j\omega t}$, Maxwell's equations can be written in phasor form as

$$\nabla \cdot \mathbf{E}_s = 0 \quad (5.101a)$$

$$\nabla \cdot \mathbf{H}_s = 0 \quad (5.101b)$$

$$\nabla \times \mathbf{E}_s = -j\omega\mu\mathbf{H}_s \quad (5.101c)$$

$$\nabla \times \mathbf{H}_s = \mathbf{J}_s + j\omega\epsilon\mathbf{E}_s \quad (5.101d)$$

where the subscript s denotes phasor or complex quantities. Henceforth, we will drop subscript s for simplicity and use the same symbols for the frequency-domain quantities and time-domain quantities. It is assumed that the reader can differentiate between the two quantities. Taking the curl of Equation (5.101c) and applying Equation (5.101d), we obtain

$$\nabla \times \nabla \times \mathbf{E} = -j\omega\mu\nabla \times \mathbf{H} = -j\omega\mu(\mathbf{J} + j\omega\epsilon\mathbf{E}) \quad (5.102)$$

Introducing the vector identity

$$\nabla \times \nabla \times \mathbf{A} = \nabla(\nabla \cdot \mathbf{A}) - \nabla^2 \mathbf{A}$$

into Equation (5.102) gives

$$\nabla(\nabla \cdot \mathbf{E}) - \nabla^2 \mathbf{E} = -j\omega\mu(\mathbf{J} + j\omega\epsilon\mathbf{E})$$

In view of Equation (5.101a), $\nabla(\nabla \cdot \mathbf{E}) = 0$ so that

$$\nabla^2 \mathbf{E} + k^2 \mathbf{E} = j\omega\mu\mathbf{J} \quad (5.103)$$

where $k = \omega(\mu\epsilon)^{1/2} = 2\pi/\lambda$ is the wave number and λ is the wavelength. Equation (5.103) is the vector form of the Helmholtz wave equation. If we assume a TM wave ($H_z = 0$) with $\mathbf{E} = E_z(x, y)\mathbf{a}_z$, the vector equation (5.103) becomes a scalar equation, namely,

$$\nabla^2 E_z + k^2 E_z = j\omega\mu J_z \quad (5.104)$$

where $\mathbf{J} = J_z\mathbf{a}_z$ is the source current density. The integral solution to Equation (5.104) is

$$E_z(x, y) = E_z(\rho) = -\frac{k\eta_o}{4} \int_S J_z(\rho') H_0^{(2)}(k|\rho - \rho'|) dS' \quad (5.105)$$

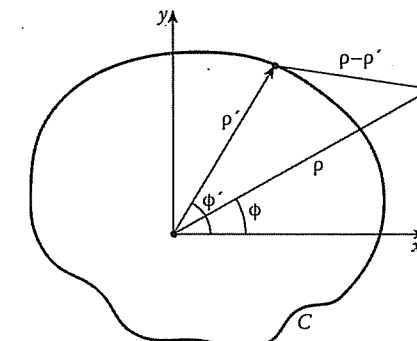


Figure 5.10

Cross section of the cylinder.

where $\rho = x\mathbf{a}_x + y\mathbf{a}_y$ is the field point, $\rho' = x'\mathbf{a}_x + y'\mathbf{a}_y$ is the source point, $\eta_o = (\mu_o/\epsilon_o)^{1/2} \simeq 377 \Omega$ is the intrinsic impedance of free space, and $H_0^{(2)}$ = Hankel function of the second kind of zero order since an outward-traveling wave is assumed. The integration in Equation (5.105) is over the cross section of the cylinder shown in Figure 5.10.

If field E_z^i is incident on a perfectly conducting cylinder, it induces surface current J_z on the conducting cylinder, which in turn produces a scattered field E_z^s . The scattered field E_z^s due to J_z is expressed by Equation (5.105). On the boundary C , the tangential component of the total field must vanish. Thus

$$E_z^i + E_z^s = 0 \text{ on } C \quad (5.106)$$

Substitution of Equation (5.105) into Equation (5.106) yields

$$E_z^i(\rho) = \frac{k\eta_o}{4} \int_C J_z(\rho') H_0^{(2)}(k|\rho - \rho'|) dL' \quad (5.107)$$

In the integral equation (5.107), the induced surface current density J_z is the only unknown. We determine J_z using the moment method.

We divide the boundary C into N segments and apply the point matching technique. On a segment ΔC_n , Equation (5.107) becomes

$$E_z^i(\rho_n) = \frac{k\eta_o}{4} \sum_{m=1}^N J_z(\rho_m) H_0^{(2)}(k|\rho_n - \rho_m|) \Delta C_m \quad (5.108)$$

where the integration in Equation (5.107) has been replaced by summation. On applying Equation (5.108) to all segments, a system of simultaneous equations results. The system of equations can be cast in matrix form as

$$\begin{bmatrix} E_z^i(\rho_1) \\ E_z^i(\rho_2) \\ \vdots \\ E_z^i(\rho_N) \end{bmatrix} = \begin{bmatrix} A_{11} & A_{12} & \dots & A_{1N} \\ A_{21} & A_{22} & \dots & A_{2N} \\ \vdots & \vdots & & \vdots \\ A_{N1} & A_{N2} & \dots & A_{NN} \end{bmatrix} \begin{bmatrix} J_z(\rho_1) \\ J_z(\rho_2) \\ \vdots \\ J_z(\rho_N) \end{bmatrix} \quad (5.109a)$$

or

$$[E] = [A][J] \quad (5.109b)$$

Hence

$$[J] = [A]^{-1}[E] \quad (5.110)$$

To determine the exact values of elements of matrix $[A]$ may be difficult. Approximately [6],

$$A_{mn} \simeq \begin{cases} \frac{\eta_o k}{4} \Delta C_n H_0^{(2)} \left\{ k(x_n - x_m)^2 + (y_n - y_m)^2 \right\}^{(1/2)}, & m \neq n \\ \frac{\eta_o k}{4} \left[1 - j \frac{2}{\pi} \log_{10} \left(\frac{\gamma k \Delta C_n}{4e} \right) \right], & m = n \end{cases} \quad (5.111)$$

where (x_n, y_n) is the midpoint of ΔC_n , $e = 2.718\dots$, and $\gamma = 1.781\dots$. Thus for a given cross section and specified incident field E_z^i , the induced surface current density J_z can be found from Equation (5.110). To be specific, assume the propagation vector \mathbf{k} is directed as shown in Figure 5.11 so that

$$E_z^i = E_o e^{j\mathbf{k} \cdot \mathbf{r}}$$

where $\mathbf{r} = x\mathbf{a}_x + y\mathbf{a}_y$, $\mathbf{k} = k(\cos\phi_i \mathbf{a}_x + \sin\phi_i \mathbf{a}_y)$, $k = 2\pi/\lambda$, and ϕ_i is the incidence angle. Taking $E_o = 1$ so that $|E_z^i| = 1$,

$$E_z^i = e^{jk(x \cos\phi_i + y \sin\phi_i)} \quad (5.112)$$

Given any C (dictated by the cross section of the cylinder), we can substitute Equations (5.111) and (5.112) into Equation (5.109) and determine $[J]$ from Equation (5.110). Once J_z , the induced current density, is known, we calculate the *scattering cross section* σ defined by

$$\begin{aligned} \sigma(\phi, \phi_i) &= 2\pi\rho \left| \frac{E_z^s(\phi)}{E_z^s(\phi_i)} \right|^2 \\ &= \frac{k\eta_o^2}{4} \left| \int_C J_z(x', y') e^{jk(x' \cos\phi + y' \sin\phi)} dl' \right|^2 \end{aligned} \quad (5.113)$$

where ϕ is the angle at the observation point, the point at which σ is evaluated. In matrix form,

$$\sigma(\phi_i, \phi) = \frac{k\eta_o^2}{4} \left| [V_n^s] [Z_{nm}]^{-1} [V_m^i] \right|^2 \quad (5.114)$$

where

$$V_m^i = \Delta C_m e^{jk(x_m \cos\phi_i + y_m \cos\phi_i)}, \quad (5.115a)$$

$$V_n^s = \Delta C_n e^{jk(x_n \cos\phi + y_n \cos\phi)}, \quad (5.115b)$$

and

$$Z_{mn} = \Delta C_m A_{mn} \quad (5.115c)$$

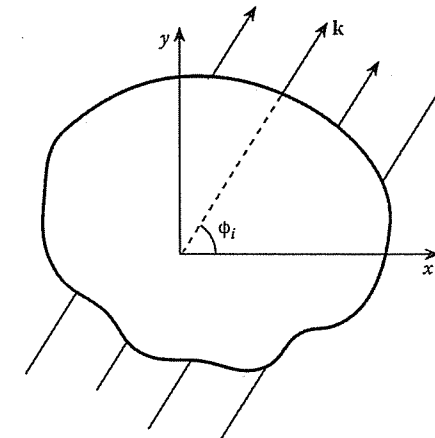


Figure 5.11
Typical propagation of vector \mathbf{k} .

5.5.2 Scattering by an Arbitrary Array of Parallel Wires

This problem is of more general nature than the one just described. As a matter of fact, any infinitely long, perfectly conducting, thin metal can be modeled as an array of parallel wires. It will be shown that the scattering pattern due to an arbitrary array of line sources approaches that of a solid conducting cylinder of the same cross-sectional geometry if a sufficiently large number of wires are present and they are arrayed on a closed curve. Hence the problem of scattering by a conducting cylinder presented above can also be modeled with the techniques to be described here.

Consider an arbitrary array of N parallel, infinitely long wires placed parallel to the z -axis [34]. Three of such wires are illustrated in Figure 5.12. Let a harmonic TM wave be incident on the wires. Assuming a time factor $e^{j\omega t}$, the incident wave in

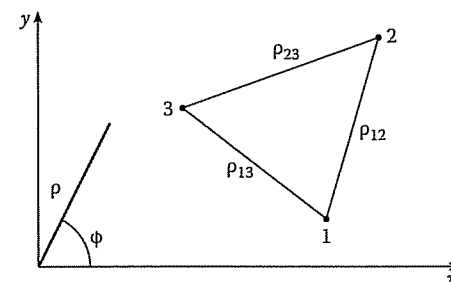


Figure 5.12
An array of three wires parallel to the z -axis.

phasor form is given by

$$E_z^i = E_i(x, y)e^{-jhz} \quad (5.116)$$

where

$$E_i(x, y) = E_o e^{-jk(x \sin \theta_i \cos \phi_i + y \sin \theta_i \sin \phi_i)} \quad (5.117a)$$

$$h = k \cos \theta_i, \quad (5.117b)$$

$$k = \frac{2\pi}{\lambda} = \omega(\mu\epsilon)^{1/2}, \quad (5.117c)$$

and θ_i and ϕ_i define the axis of propagation as illustrated in Figure 5.13. The incident wave induces current on the surface of wire n . The induced current density has only z component.

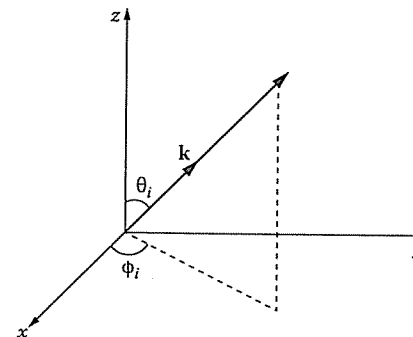


Figure 5.13
Propagation vector k .

It can be shown that the field due to a harmonic current I_n uniformly distributed on a circular cylinder of radius a_n has a z component given by

$$E_n = -I'_n H_0^{(2)}(g\rho_n) e^{-jhz}, \quad \rho_n > a_n \quad (5.118)$$

where

$$I'_n = \frac{\omega \mu g^2}{4k^2} I_n J_0(ga_n), \quad (5.119)$$

$$g^2 + h^2 = k^2, \quad (5.120)$$

J_0 is Bessel function of order zero, and H_0 is Hankel function of the second kind of order zero. By induction theorem, if I_n is regarded as the induced current, Equation (5.118) may be considered as the scattered field, i.e.,

$$E_z^s = -\sum_{n=1}^N I'_n H_0^{(2)}(g\rho_n) e^{-jhz} \quad (5.121)$$

where the summation is taken over all the N wires. On the surface of each wire (assumed perfectly conducting),

$$E_z^i + E_z^s = 0$$

or

$$E_z^i = -E_z^s, \quad \rho = \rho_n \quad (5.122)$$

Substitution of Equations (5.116) and (5.121) into Equation (5.122) leads to

$$\sum_{n=1}^N I'_n H_0^{(2)}(g\rho_{mn}) = E_i(x_m, y_m) \quad (5.123)$$

where

$$\rho_{mn} = \begin{cases} \sqrt{(x_m - x_n)^2 + (y_m - y_n)^2} & , m \neq n \\ a_m & , m = n \end{cases} \quad (5.124)$$

and a_m is the radius of the m th wire. In matrix form, Equation (5.123) can be written as

$$[A][I] = [B]$$

or

$$[I] = [A]^{-1}[B] \quad (5.125)$$

where

$$I_n = I'_n, \quad (5.126a)$$

$$A_{mn} = H_0^{(2)}(g\rho_{mn}), \quad (5.126b)$$

$$B_m = E_o e^{-jk(x_m \sin \theta_i \cos \phi_i + y_m \sin \theta_i \sin \phi_i)} \quad (5.126c)$$

Once I'_n is calculated from Equation (5.125), the scattered field can be obtained as

$$E_z^s = -\sum_{n=1}^N I'_n H_0^{(2)}(g\rho_n) e^{-jhz} \quad (5.127)$$

Finally, we may calculate the “distant scattering pattern,” defined as

$$E(\phi) = \sum_{n=1}^N I'_n e^{jg(x_n \cos \phi + y_n \sin \phi)} \quad (5.128)$$

The following example, taken from Richmond’s work [34], will be used to illustrate the techniques discussed in the latter half of this section.

Example 5.8

Consider the two arrays shown in Figure 5.14. For Figure 5.14(a), take

no. of wires, $N = 15$

wire radius, $ka = 0.05$

wire spacing, $ks = 1.0$

$\theta_o = 90^\circ$, $\phi_o = 40^\circ$, $270^\circ < \phi < 90^\circ$

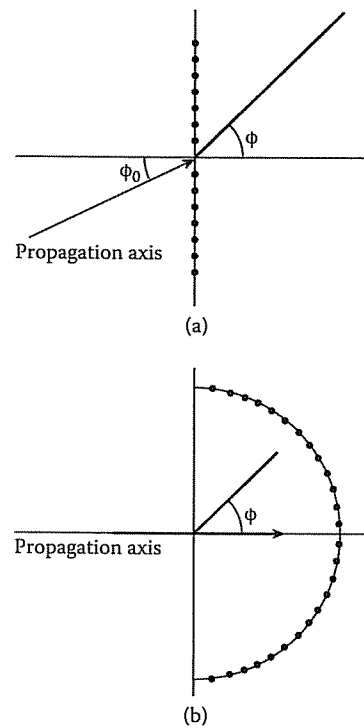


Figure 5.14

For Example 5.8: (a) A plane array of 15 parallel wires, (b) a semicircular array of 30 parallel wires.

and for Figure 5.14(b), take

$$\text{no. of wires, } N = 30$$

$$\text{wire radius, } ka = 0.05$$

$$\text{cylinder radius, } R = 1.12 \lambda$$

$$\theta_0 = 90^\circ, \phi_0 = 0, 0 < \phi < 180^\circ$$

For the two arrays, calculate and plot the scattering pattern as a function of ϕ . \square

Solution

The MATLAB code for calculating the scattering pattern $E(\phi)$ based on Equation (5.128) is shown in Figure 5.15. The same program can be used for the two arrays in Figure 5.14, except that the input data on N, ka, ks and the locations $(x_n, y_n), n = 1, 2, \dots, N$ of the wires are different. The program essentially calculates I_n required in Equation (5.128) using Equations (5.125) and (5.126). The plots of $E(\phi)$ against ϕ are portrayed in Figures 5.16 and 5.17 for the arrays in Figure 5.14(a) and 5.14(b), respectively. \blacksquare

```
%=====
% THIS PROGRAM CALCULATES THE SCATTERING PATTERN
% OF AN ARRAY OF PARALLEL WIRES
% =====

clear; format compact;

thearray = 1; % thearray equals 1 for a plane array and 2 for a semicircular array

%PHIO and THETAO define the axis of propagation
THETAO = pi/2.0; %elevation angle pi/2
LAMBDA=1.0; %wavelength
EO = 1.0; %E field
R = 1.125*LAMBDA; %Radius of semicircle array
K = 2.0*pi/LAMBDA; %Propagation constant
AA = 0.05/K; %wire radius
S = 1.0/K; %wire spacing
H = K*cos(THETAO); %H & G are part of the incident wave definition
G = sqrt( K^2 - H^2 );

% DEFINE WIRE LOCATIONS
if thearray ==1
    NN = 15; %Number of wires
    PHIO = 40;
    X = zeros(1,NN);
    Y = linspace(-1,1,NN);
elseif thearray ==2
    NN = 30;
    PHIO = 0.0;
    PHI2 = linspace(-pi/2,pi/2,NN);
    X = R*cos(PHI2);
    Y = R*sin(PHI2);
end
% CALCULATE RHO
[Mx,My]=meshgrid(X,Y);
RHO = sqrt((Mx-Mx').^2+(My-My').^2)+diag(AA*ones(1,NN));

% CONSTRUCT MATRIX [A]
A = besselh(0,2,G*RHO);

% CONSTRUCT MATRIX [B]
ALPHA = X*sin(THETAO)*cos(PHIO)+ Y*sin(THETAO)*sin(PHIO);
B = EO*exp( -i*K*ALPHA).';

% SOLVE FOR MATRIX[I] CONSISTING OF "MODIFIED CURRENT" OR CURRENT COEFFICIENTS
I = inv(A);
I = A*B;

% FINALLY, CALCULATE THE SCATTERING PATTERN E(PHI)
PHI = linspace(0,pi,128);
ALP = cos(PHI.')*X + sin(PHI.')*Y;
E = abs(exp( i*G*ALP)*I);
```

Figure 5.15
Computer program for Example 5.8 (Continued).

```
% Plot E(PHI)
if thearray ==2
    figure(1),plot(PHI*180/pi,E)
    title('Scattering Pattern')
    xlabel('phi (Degrees)')
    ylabel('E(phi)')
    grid on
elseif thearray ==1
    % ang = PHI*180/pi-90;
    % field = fftshift(E);

    figure(2),plot(PHI*180/pi,E)
    title('Example 5.8 compare to Figure 5.16')
    xlabel('phi (Degrees)')
    ylabel('E(phi)')
    grid on
end
```

Figure 5.15
(Cont.) Computer program for Example 5.8.

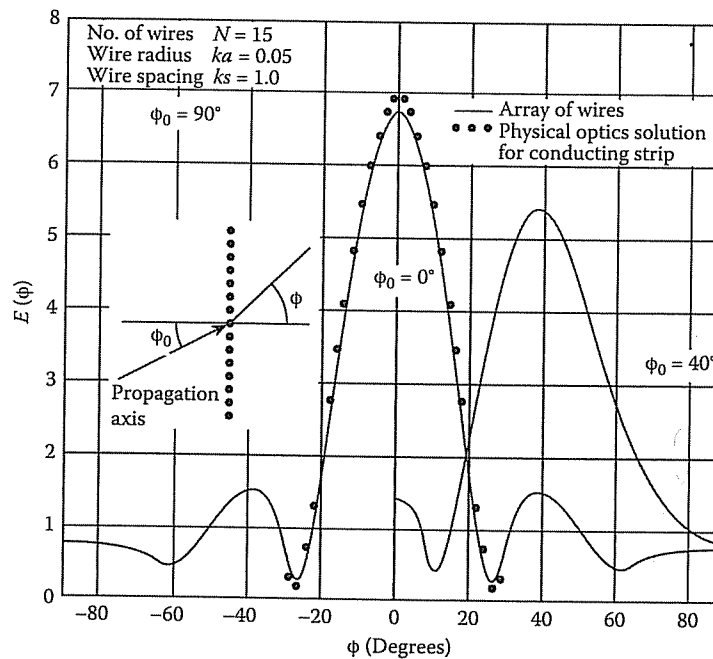


Figure 5.16
Scattering pattern for the plane array of Figure 5.14(a).

5.6. APPLICATIONS III – RADIATION PROBLEMS

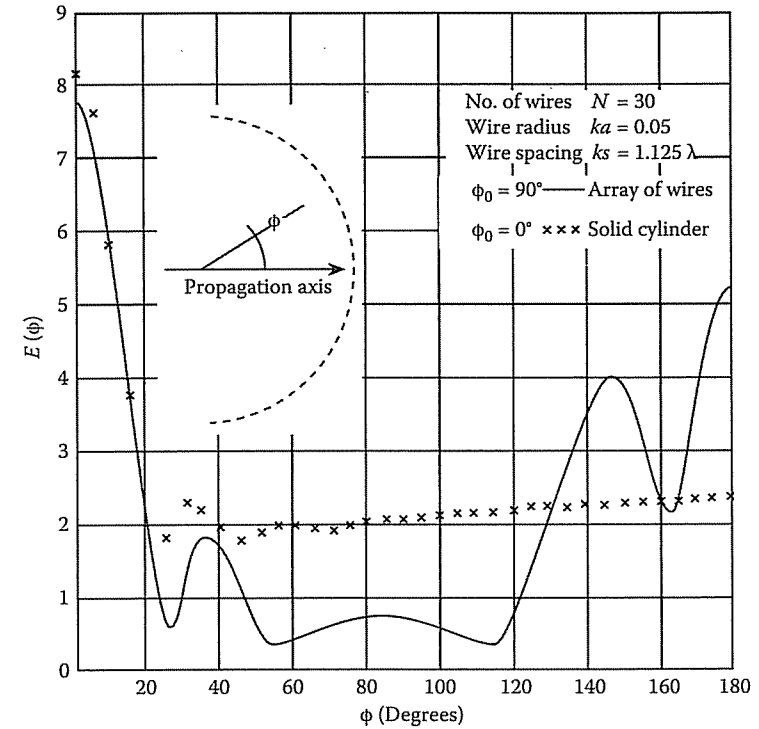


Figure 5.17
Scattering pattern for the semicircular array of Figure 5.14(b).

5.6 Applications III – Radiation Problems

In this section, we consider the application of MOM to wires or cylindrical antennas. The distinction between scatterers considered in the previous section and antennas to be treated here is primarily that of the location of the source. An object acts as a scatterer if it is far from the source; it acts as an antenna if the source is on it [3].

Consider a perfectly conducting cylindrical antenna of radius a , extending from $z = -\ell/2$ to $z = \ell/2$ as shown in Figure 5.18. Let the antenna be situated in a lossless homogeneous dielectric medium ($\sigma = 0$). Assuming a z -directed current on the cylinder ($\mathbf{J} = J_z a_z$), only axial electric field E_z is produced due to axial symmetry. The electric field can be expressed in terms of the retarded potentials of Equation (1.38)

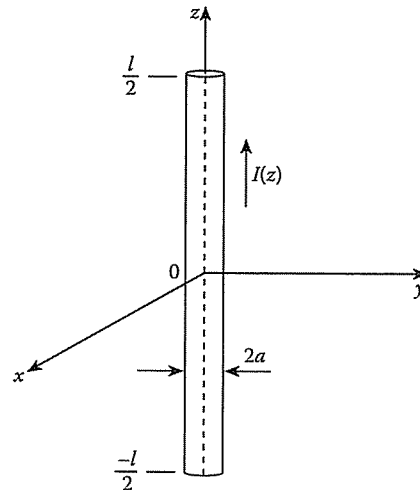


Figure 5.18
Cylindrical antenna of length l and radius a .

as

$$E_z = -j\omega A_z - \frac{\partial V}{\partial z} \quad (5.129)$$

Applying the Lorentz condition of Equation (1.41), namely,

$$\frac{\partial A_z}{\partial z} = -j\omega\mu\epsilon V, \quad (5.130)$$

Equation (5.129) becomes

$$E_z = -j\omega \left(1 + \frac{1}{k^2} \frac{\partial^2}{\partial z^2} \right) A_z \quad (5.131)$$

where $k = \omega(\mu\epsilon)^{1/2} = 2\pi/\lambda$, ω is the angular frequency of the suppressed harmonic time variation $e^{j\omega t}$. From Equation (1.44)

$$A_z = \mu \int_{-\ell/2}^{\ell/2} I(z') G(x, y, z; x', y', z') dz' \quad (5.132)$$

where $G(x, y, z; x', y', z')$ is the free space Greens' function, i.e.,

$$G(x, y, z; x', y', z') = \frac{e^{-jkR}}{4\pi R} \quad (5.133)$$

and R is the distance between observation point (x, y, z) and source point (x', y', z') or

$$R = \left[(x - x')^2 + (y - y')^2 + (z - z')^2 \right]^{1/2} \quad (5.134)$$

Combining Equations (5.131) and (5.132) gives

$$E_z = -j\omega\mu \left(1 + \frac{1}{k^2} \frac{d^2}{dz^2} \right) \int_{-\ell/2}^{\ell/2} I(z') G(x, y, z; x', y', z') dz' \quad (5.135)$$

This integro-differential equation is not convenient for numerical analysis because it requires evaluation of the second derivative with respect to z of the integral. We will now consider two types of modification of Equation (5.135) leading to Hallen's (magnetic vector potential) and Pocklington's (electric field) integral equations. Either of these integral equations can be used to determine the current distribution on a cylindrical antenna or scatterer and subsequently calculate all other quantities of interest.

5.6.1 Hallen's Integral Equation

We can rewrite Equation (5.135) in a compact form as

$$\left(\frac{d^2}{dz^2} + k^2 \right) F(z) = k^2 S(z), \quad -\ell/2 < z < \ell/2 \quad (5.136)$$

where

$$F(z) = \int_{-\ell/2}^{\ell/2} I(z') G(z, z') dz', \quad (5.137a)$$

$$S(z) = -\frac{E_z}{j\omega\mu} \quad (5.137b)$$

Equation (5.136) is a second-order linear ordinary differential equation. The general solution to the homogeneous equation

$$\left(\frac{d^2}{dz^2} + k^2 \right) F(z) = 0,$$

which is consistent with the boundary condition that the current must be zero at the wire ends ($z = \pm\ell/2$), is

$$F_h(z) = c_1 \cos kz + c_2 \sin kz \quad (5.138)$$

where c_1 and c_2 are integration constants. The particular solution of Equation (5.136) can be obtained, for example, by the Lagrange method of varying constants [35] as

$$F_p(z) = k \int_{-\ell/2}^{\ell/2} S(z') \sin k|z - z'| dz' \quad (5.139)$$

Thus from Equations (5.137) to (5.139), the solution to Equation (5.136) is

$$\begin{aligned} \int_{-\ell/2}^{\ell/2} I(z') G(z, z') dz' &= c_1 \cos kz + c_2 \sin kz \\ &\quad - \frac{j}{\eta} \int_{-\ell/2}^{\ell/2} E_z(z') \sin k|z - z'| dz' \end{aligned} \quad (5.140)$$

where $\eta = \sqrt{\mu/\epsilon}$ is the intrinsic impedance of the surrounding medium. Equation (5.140) is referred to as *Hallen's integral equation* [36] for a perfectly conducting cylindrical antenna or scatterer. The equation has been generalized by Mei [37] to perfectly conducting wires of arbitrary shape. Hallen's IE is computationally convenient since its kernel contains only ℓ/r terms. Its major advantage is the ease with which a converged solution may be obtained, while its major drawback lies in the additional work required in finding the integration constants c_1 and c_2 [35, 38].

5.6.2 Pocklington's Integral Equation

We can also rewrite Equation (5.135) by introducing the operator in parentheses under the integral sign so that

$$\int_{-\ell/2}^{\ell/2} I(z') \left(\frac{\partial^2}{\partial z^2} + k^2 \right) G(z, z') dz' = j\omega\epsilon E_z \quad (5.141)$$

This is known as *Pocklington's integral equation* [39]. Note that Pocklington's IE has E_z , which represents the field from the source on the right-hand side. Both Pocklington's and Hallen's IEs can be used to treat wire antennas. The third type of IE derivable from Equation (5.135) is the Schelkunoff's IE, found in [35].

5.6.3 Expansion and Weighting Functions

Having derived suitable integral equations, we can now find solutions for a variety of wire antennas or scatterers. This usually entails reducing the integral equations to a set of simultaneous linear equations using the method of moments. The unknown current $I(z)$ along the wire is approximated by a finite set $u_n(z)$ of basis (or expansion) functions with unknown amplitudes as discussed in the last chapter. That is, we let

$$I(z) = \sum_{n=1}^N I_n u_n(z), \quad (5.142)$$

where N is the number of basis functions needed to cover the wire and the expansion coefficients I_n are to be determined. The functions u_n are chosen to be linearly independent. The basis functions commonly used in solving antenna or scattering problems are of two types: entire domain functions and subdomain functions. The entire domain basis functions exist over the full domain $-\ell/2 < z < \ell/2$. Typical examples are [8, 40]

(1) Fourier:

$$u_n(z) = \cos(n-1)\nu/2, \quad (5.143a)$$

(2) Chebychev:

$$u_n(z) = T_{2n-2}(\nu), \quad (5.143b)$$

(3) Maclaurin:

$$u_n(z) = \nu^{2n-2}, \quad (5.143c)$$

(4) Legendre:

$$u_n(z) = P_{2n-2}(\nu), \quad (5.143d)$$

(5) Hermite:

$$u_n(z) = H_{2n-2}(\nu), \quad (5.143e)$$

where $\nu = 2z/\ell$ and $n = 1, 2, \dots, N$. The subdomain basis functions exist only on one of the N nonoverlapping segments into which the domain is divided. Typical examples are [41, 42]

(1) piecewise constant (pulse) function:

$$u_n(z) = \begin{cases} 1, & z_{n-1/2} < z < z_{n+1/2} \\ 0, & \text{otherwise,} \end{cases} \quad (5.144a)$$

(2) piecewise linear (triangular) function:

$$u_n(z) = \begin{cases} \frac{\Delta - |z - z_n|}{\Delta}, & z_{n-1} < z < z_{n+1} \\ 0, & \text{otherwise,} \end{cases} \quad (5.144b)$$

(3) piecewise sinusoidal function:

$$u_n(z) = \begin{cases} \frac{\sin k(z - |z - z_n|)}{\sin k\Delta}, & z_{n-1} < z < z_{n+1} \\ 0, & \text{otherwise,} \end{cases} \quad (5.144c)$$

where $\Delta = \ell/N$, assuming equal subintervals although this is unnecessary. Figure 5.19 illustrates these subdomain functions. The entire domain basis functions are of limited applications since they require a prior knowledge of the nature of the function to be represented. The subdomain functions are the most commonly used, particularly in developing general-purpose user-oriented computer codes for treating wire problems. For this reason, we will focus on using subdomain functions as basis functions.

Substitution of the approximate representation of current $I(z)$ in Equation (5.142) into Pocklington's IE of Equation (5.141) gives

$$\int_{-\ell/2}^{\ell/2} \sum_{n=1}^N I_n u_n(z') K(z_m, z') dz' \simeq E_z(z_m) \quad (5.145)$$

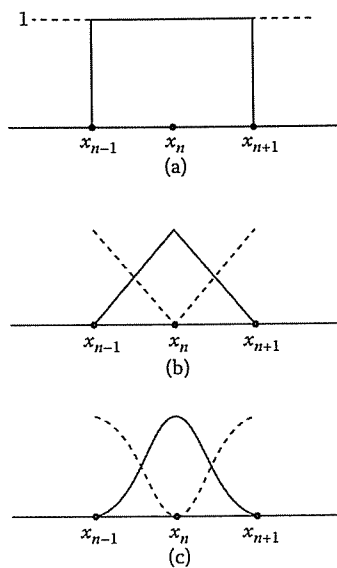


Figure 5.19

Typical subdomain weighting functions: (a) piecewise uniform function, (b) piecewise linear function, (c) piecewise sinusoidal function.

where

$$K(z_m, z') = \frac{1}{j\omega\epsilon} \left(\frac{\partial^2}{\partial z^2} + k^2 \right) G(z_m, z')$$

is the kernel, \$z = z_m\$ on segment \$m\$ is the point on the wire at which the IE is being enforced. Equation (5.145) may be written as

$$\sum_{n=1}^N I_n \int_{\Delta z_n} K(z_m, z') u_n(z') dz' \simeq E_z(z_m)$$

or

$$\sum_{n=1}^N I_n g_m = E_z(z_m) \quad (5.146)$$

where

$$g_m = \int_{\Delta z'_n} K(z_m, z') u_n(z') dz' \quad (5.147)$$

In order to solve for the unknown current amplitudes \$I_n\$ (\$n = 1, 2, \dots, N\$), \$N\$ equations need to be derived from Equation (5.146). We achieve this by multiplying Equation (5.146) by weighting (or testing) functions \$w_n\$ (\$n = 1, 2, \dots, n\$) and integrating

over the wire length. In other words, we let Equation (5.146) be satisfied in an average sense over the entire domain. This leads to forming the inner product between each of the weighting functions and \$g_m\$ so that Equation (5.146) is reduced to

$$\sum_{n=1}^N I_n \langle w_n, g_m \rangle = \langle w_m, E_z \rangle, \quad m = 1, 2, \dots, N \quad (5.148)$$

Thus we have a set of \$N\$ simultaneous equations which can be written in matrix form as

$$\begin{bmatrix} \langle w_1, g_1 \rangle & \dots & \langle w_1, g_N \rangle \\ \langle w_2, g_1 \rangle & \dots & \langle w_2, g_N \rangle \\ \vdots & & \vdots \\ \langle w_N, g_1 \rangle & \dots & \langle w_N, g_N \rangle \end{bmatrix} \begin{bmatrix} I_1 \\ I_2 \\ \vdots \\ I_N \end{bmatrix} = \begin{bmatrix} \langle w_1, E_z \rangle \\ \langle w_2, E_z \rangle \\ \vdots \\ \langle w_N, E_z \rangle \end{bmatrix}$$

or

$$[Z][I] = [V] \quad (5.149)$$

where \$z_{mn} = \langle w_n, g_m \rangle\$ and \$V_m = \langle w_m, E_z \rangle\$. The desired solution for the current is then obtained by solving the simultaneous equations (5.149) or by matrix inversion, i.e.,

$$[I] = [Z]^{-1}[V] \quad (5.150)$$

Because of the similarity of Equation (5.149) to the network equations, the matrices \$[Z]\$, \$[V]\$, and \$[I]\$ are referred to as *generalized impedance*, *voltage*, and *current* matrices, respectively [6]. Once the current distribution \$I(z')\$ is determined from Equation (5.149) or (5.150), parameters of practical interest such as input impedance and radiation patterns are readily obtained.

The weighting functions \$\{w_n\}\$ must be chosen so that each Equation (5.148) is linearly independent and computation of the necessary numerical integration is minimized. Evaluation of the integrals in Equation (5.149) is often the most time-consuming portion of scattering or radiation problems. Sometimes we select similar types of functions for both weighting and expansion. As discussed in the previous chapter, choosing \$w_n = u_n\$ leads to Galerkin's method, while choosing \$w_n = \delta(z - z_n)\$ results in point matching (or colocation) method. The point matching method is simpler than Galerkin's method and is sufficiently adequate for many EM problems. However, it tends to be a slower converging method. The general rules that should be followed in selecting the weighting functions are addressed in [43]. The following examples are taken from [41], [44]–[46].

Example 5.9

Solve the Hallen's integral equation

$$\int_{-\ell/2}^{\ell/2} I(z') G(z, z') dz' = -\frac{j}{\eta_o} (A \cos kz + B \sin k|z|)$$

where $k = 2\pi/\lambda$ is the phase constant and $\eta_o = 377 \Omega$ is the intrinsic impedance of free space. Consider a straight wire dipole with length $L = 0.5 \lambda$ and radius $a = 0.005\lambda$. \square

Solution

The integral equation has the form

$$\int_{-\ell/2}^{\ell/2} I(z') K(z, z') dz' = D(z) \quad (5.151)$$

which is a Fredholm integral equation of the first kind. In Equation (5.151),

$$K(z, z') = G(z, z') = \frac{e^{-jkR}}{4\pi R}, \quad (5.152a)$$

$$R = \sqrt{a^2 + (z - z')^2}, \quad (5.152b)$$

and

$$D(z) = -\frac{j}{\eta_o} [A \cos(kz) + B \sin(k|z|)] \quad (5.152c)$$

If the terminal voltage of the wire antenna is V_T , the constant $B = V_T/2$. The absolute value in $\sin k|z|$ expresses the assumption of antenna symmetry, i.e., $I(-z') = I(z')$. Thus

$$\int_{-\ell/2}^{\ell/2} I(z') \frac{e^{-jkR}}{4\pi R} dz' = -\frac{j}{\eta_o} \left[A \cos kz + \frac{V_T}{2} \sin kz \right] \quad (5.153)$$

If we let

$$I(z) = \sum_{n=1}^N I_n u_n(z), \quad (5.154)$$

Equation (5.153) will contain N unknown variables I_n and the unknown constant A . To determine the $N+1$ unknowns, we divide the wire into N segments. For the sake of simplicity, we choose segments of equal lengths $\Delta z = \ell/N$ and select $N+1$ matching points such as

$$z = -\ell/2, -\ell/2 + \Delta z, \dots, 0, \dots, \ell/2 - \Delta z, \ell/2$$

At each match point $z = z_m$,

$$\int_{-\ell/2}^{\ell/2} \sum_{n=1}^N I_n u_n(z') K(z_m, z') dz' = D(z_m) \quad (5.155)$$

Taking the inner products (moments) by multiplying either side with a weighting function $w_m(z)$ and integrating both sides,

$$\begin{aligned} & \int_{-\ell/2}^{\ell/2} \int_{-\ell/2}^{\ell/2} \sum_{n=1}^N I_n u_n(z') K(z_m, z') dz' w_m(z) dz \\ &= \int_{-\ell/2}^{\ell/2} D(z_m) w_m(z) dz \end{aligned} \quad (5.156)$$

By reversing the order of the summation and integration,

$$\begin{aligned} & \sum_{n=1}^N I_n \int_{-\ell/2}^{\ell/2} u_n(z') \int_{-\ell/2}^{\ell/2} K(z_m, z') w_m(z) dz dz' \\ &= \int_{-\ell/2}^{\ell/2} D(z_m) w_m(z) dz \end{aligned} \quad (5.157)$$

The integration on either side of Equation (5.157) can be carried out numerically or analytically if possible. If we use the point matching method by selecting the weighting function as delta function, then

$$w_m(z) = \delta(z - z_m)$$

Since the integral of any function multiplied by $\delta(z - z_m)$ gives the value of the function at $z = z_m$, Equation (5.157) becomes

$$\sum_{n=1}^N I_n \int_{-\ell/2}^{\ell/2} u_n(z') K(z_m, z') dz' = D(z_m), \quad (5.158)$$

where $m = 1, 2, \dots, N+1$. Also, if we choose pulse function as the basis or expansion function,

$$u_n(z) = \begin{cases} 1, & z_n - \Delta z/2 < z < z_n + \Delta z/2 \\ 0, & \text{elsewhere,} \end{cases}$$

and Equation (5.158) yields

$$\sum_{n=1}^N I_n \int_{z_n - \Delta z/2}^{z_n + \Delta z/2} K(z_m, z') dz' = D(z_m) \quad (5.159)$$

Substitution of Equation (5.152) into Equation (5.159) gives

$$\sum_{n=1}^N I_n \int_{z_n - \Delta z/2}^{z_n + \Delta z/2} \frac{e^{jkR_m}}{4\pi R_m} dz' = -\frac{j}{\eta_o} \left[A \cos kz_m + \frac{V_T}{2} \sin k|z_m| \right] \quad (5.160)$$

where $m = 1, 2, \dots, N+1$ and $R_m = [a^2 + (z_m - z')^2]^{1/2}$. Thus we have a set of $N+1$ simultaneous equations, which can be cast in matrix form as

$$\begin{bmatrix} F_{11} & F_{12} & \dots & F_{1,N} & \frac{j}{\eta} \cos(kz_1) \\ F_{21} & F_{22} & \dots & F_{2,N} & \frac{j}{\eta} \cos(kz_2) \\ \vdots & & & & \vdots \\ F_{N+1,1} & F_{N+1,2} & \dots & F_{N+1,N} & \frac{j}{\eta} \cos(kz_{N+1}) \end{bmatrix} \begin{bmatrix} I_1 \\ I_2 \\ \vdots \\ A \end{bmatrix} = \begin{bmatrix} -\frac{j}{2\eta} V_T \sin k|z_1| \\ -\frac{j}{2\eta} V_T \sin k|z_2| \\ \vdots \\ -\frac{j}{2\eta} V_T \sin k|z_{N+1}| \end{bmatrix} \quad (5.161a)$$

or

$$[F][X] = [Q] \quad (5.161b)$$

where

$$F_{mn} = \int_{z_n-\Delta z/2}^{z_n+\Delta z/2} \frac{e^{-jkR_m}}{4\pi R_m} dz' \quad (5.162)$$

The $N+1$ unknowns are determined by solving Equation (5.161) in the usual manner. To evaluate F_{mn} analytically rather than numerically, let the integrand in Equation (5.162) be separated into its real (RE) and imaginary (IM) parts,

$$\begin{aligned} \frac{e^{-jkR_m}}{R_m} &= \text{RE} + j\text{IM} \\ &= \frac{\cos kR_m}{R_m} - j \frac{\sin kR_m}{R_m} \end{aligned} \quad (5.163)$$

IM as a function of z' is a smooth curve so that

$$\begin{aligned} \int_{z_n-\Delta z/2}^{z_n+\Delta z/2} \text{IM}(z') dz' &= - \int_{z_n-\Delta z/2}^{z_n+\Delta z/2} \frac{\sin k[a^2 + (z_m - z')^2]^{1/2}}{[a^2 + (z_m - z')^2]^{1/2}} dz' \\ &\approx - \frac{\Delta z \sin k[a^2 + (z_m - z_n)^2]^{1/2}}{[a^2 + (z_m - z_n)^2]^{1/2}} \end{aligned} \quad (5.164)$$

The approximation is accurate as long as $\Delta z < 0.05 \lambda$. On the other hand, RE changes rapidly as $z' \rightarrow z_m$ due to R_m . Hence

$$\begin{aligned} \int_{z_n-\Delta z/2}^{z_n+\Delta z/2} \text{RE}(z') dz' &= - \int_{z_n-\Delta z/2}^{z_n+\Delta z/2} \frac{\cos k[a^2 + (z_m - z')^2]^{1/2}}{[a^2 + (z_m - z')^2]^{1/2}} dz' \\ &\simeq \cos k[a^2 + (z_m - z_n)^2]^{1/2} \int_{z_n-\Delta z/2}^{z_n+\Delta z/2} \frac{dz'}{[a^2 + (z_m - z')^2]^{1/2}} \\ &= \cos k[a^2 + (z_m - z_n)^2]^{1/2} \\ &\ln \left[\frac{z_m + \Delta z/2 - z_n + [a^2 + (z_m - z_n + \Delta z/2)^2]^{1/2}}{z_m - \Delta z/2 - z_n + [a^2 + (z_m - z_n - \Delta z/2)^2]^{1/2}} \right] \end{aligned} \quad (5.165)$$

Thus

$$\begin{aligned} F_{mn} &\simeq \frac{1}{4\pi} \cos k[a^2 + (z_m - z_n)^2]^{1/2} \\ &\times \ln \left[\frac{z_m + \Delta z/2 - z_n + [a^2 + (z_m - z_n + \Delta z/2)^2]^{1/2}}{z_m - \Delta z/2 - z_n + [a^2 + (z_m - z_n - \Delta z/2)^2]^{1/2}} \right] \\ &- \frac{j \Delta z \sin k[a^2 + (z_m - z_n)^2]^{1/2}}{4\pi [a^2 + (z_m - z_n)^2]^{1/2}} \end{aligned} \quad (5.166)$$

A typical example of the current distribution obtained for $\ell = \lambda$, $a = 0.01 \lambda$ is shown in Figure 5.20, where the sinusoidal distribution commonly assumed for wire antennas is also shown for comparison. Notice the remarkable difference between the two near the dipole center.

Example 5.10

Consider a perfectly conducting scatterer or antenna of a cylindrical nature shown in Figure 5.21. Determine the axial current $I(z)$ on the structure by solving the electric field integral equation (EFIE)

$$\frac{j\eta}{4k\pi} \left(\frac{d^2}{dz^2} + k^2 \right) \int_{-h}^h I(z') G(z, z') dz' = E_z^i(z) \quad (5.167)$$

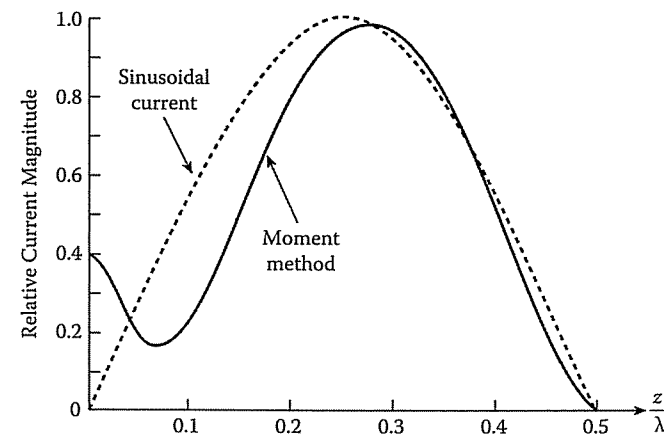


Figure 5.20

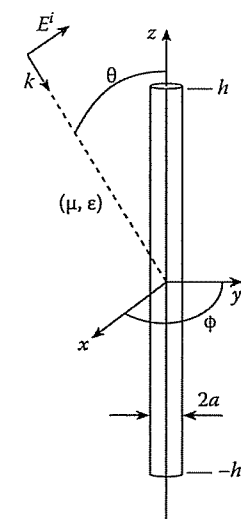
Current distribution of straight center-fed dipole.

where

$$G(z, z') = \frac{1}{2\pi} \int_0^{2\pi} \frac{e^{-jkR}}{R} d\phi',$$

$$R = \left[(z - z')^2 + 4a^2 \sin^2 \frac{\phi'}{2} \right]^{1/2},$$

$$\eta = \sqrt{\frac{\mu}{\epsilon}}, \quad \text{and} \quad k = \frac{2\pi}{\lambda}$$

Figure 5.21
Cylindrical scatterer or antenna.**Solution**

If the radius $a \ll \lambda$ (the wavelength) and $a \ll 2h$ (the length of the wire), the structure can be regarded as a “thin-wire” antenna or scatterer. As a scatterer, we may consider a plane wave excitation

$$E_z^i(z) = E_o \sin \theta e^{jkz \cos \theta} \quad (5.168a)$$

where θ is the angle of incidence. As an antenna, we may assume a delta-gap generator

$$E_z^i = V \delta(z - z_g) \quad (5.168b)$$

where V is the generator voltage and $z = z_g$ is the location of the generator.

In order to apply the method of moments to the given integral Equation (5.167), we expand the currents in terms of pulse basis function as

$$I(z) = \sum_{n=1}^N I_n u_n(z) \quad (5.169)$$

where

$$u_n(z) = \begin{cases} 1, & z_{n-1/2} < z < z_{n+1/2} \\ 0, & \text{elsewhere} \end{cases}$$

Substituting Equation (5.169) into Equation (5.167) and weighting the result with triangular functions

$$w_m(z) = \begin{cases} \frac{z - z_{m-1}}{\Delta}, & z_{m-1} < z < z_m \\ -\frac{z - z_{m+1}}{\Delta}, & z_{m-1} < z < z_{m+1} \\ 0, & \text{elsewhere,} \end{cases} \quad (5.170)$$

where $\Delta = 2h/N$, leads to

$$\sum_{n=1}^N Z_{mn} I_n = V_m, \quad m = 1, 2, \dots, N \quad (5.171)$$

Figure 5.22 illustrates $u_n(z)$ and $w_m(z)$. Equation (5.171) can be cast in matrix form as

$$[Z][I] = [V] \quad (5.172)$$

where $[I]$ can be solved using any standard method. For the impedance matrix $[Z]$, the elements are given by

$$Z_{mn} = \frac{j\eta}{4\pi k} \frac{2}{\Delta} \left[\frac{1}{2} G_{m-1,n} - \left(1 - \frac{k^2 \Delta^2}{2} \right) G_{m,n} + \frac{1}{2} G_{m+1,n} \right] \quad (5.173)$$

where

$$G_{m,n} = \int_{z_n - \Delta/2}^{z_n + \Delta/2} G(z_m, z') dz' \quad (5.174)$$

To obtain Equation (5.173), we have used the approximation

$$\int_{z_{m-1}}^{z_{m+1}} w_m(z) f(z) dz = \Delta f(z_m)$$

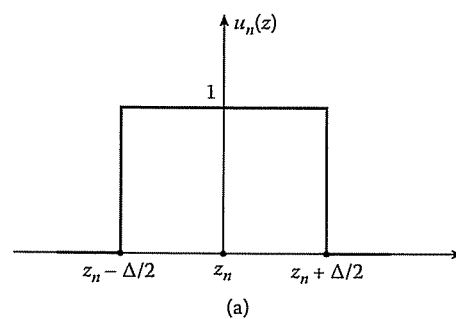
For the plane wave excitation, the elements of the forcing vector [V] are

$$V_m = \Delta E_0 e^{j k z_m \cos \theta} \quad (5.175a)$$

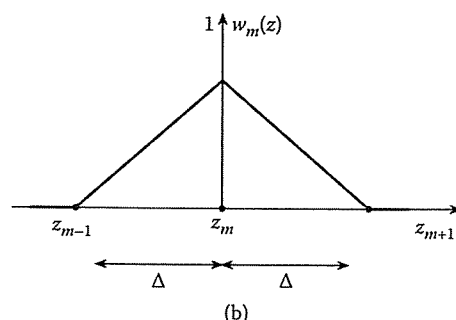
For delta-gap generator,

$$V_m = V \delta_{mg} \quad (5.175b)$$

where g is the index of the feed zone pulse.



(a)



(b)

Figure 5.22

For Example 5.10: (a) Pulse basis function, (b) triangular weighting function.

Solving Equation (5.172) requires that we incorporate a method to perform numerically the double integration in Equation (5.174). The kernel $G(z, z')$ exhibits a logarithmic singularity as $|z - z'| \rightarrow 0$, and therefore care must be exercised. To circumvent the difficulty, we let

$$G(z, z') = \frac{1}{2\pi} \int_0^{2\pi} \frac{e^{-jkR}}{R} d\phi' = G_o(z, z') + G_1(z, z') \quad (5.176)$$

where

$$G_o(z, z') = \frac{1}{2\pi} \int_0^{2\pi} \frac{d\phi'}{R} \quad (5.177)$$

and

$$G_1(z, z') = \frac{1}{2\pi} \int_0^{2\pi} \frac{e^{-jkR} - 1}{R} d\phi' \quad (5.178)$$

We note that

$$G_o(z, z') \xrightarrow{\left(\frac{z-z'}{2a}\right) \rightarrow 0} -\frac{1}{\pi a} \ln \frac{|z - z'|}{8a}$$

and hence we replace $G_o(z, z')$ by

$$\left[G_o(z, z') + \frac{1}{\pi a} \ln \frac{|z - z'|}{8a} \right] - \frac{1}{\pi a} \ln \frac{|z - z'|}{8a} \quad (5.179)$$

The term $G_1(z, z')$ is nonsingular, while the singularity of $G_o(z, z')$ can be avoided by using Equation (5.179). Thus the double integral involved in evaluating Z_{mn} is easily done numerically. It is interesting to note that Z_{mn} would remain the same if we had chosen the triangular basis function and pulse weighting function [46]. ■

5.7 Applications IV – EM Absorption in the Human Body

The interest in hyperthermia (or electromagnetic heating of deep-seated tumors) and in the assessment of possible health hazards due to EM radiation have prompted the development of analytical and numerical techniques for evaluating EM power deposition in the interior of the human body or a biological system [47]. The overall need is to provide a scientific basis for the establishment of an EM radiation safety standard. Since human experimentation is not possible, irradiation experiments must be performed on animals. Theoretical models are required to interpret and confirm the experiment, develop an extrapolation process, and thereby develop a radiation safety standard for humans [48].

The mathematical complexity of the problem has led researchers to investigate simple models of tissue structures such as plane slab, dielectric cylinder homogeneous and layered spheres, and prolate spheroid. A review of these earlier efforts is given in [49, 50]. Although spherical models are still being used to study the power deposition characteristics of the head of humans and animals, realistic block model composed of cubical cells is being used to simulate the whole body.

The key issue in this bioelectromagnetic effort is how much EM energy is absorbed by a biological body and where is it deposited. This is usually quantified in terms of the specific absorption rate (SAR), which is the mass normalized rate of energy absorbed by the body. At a specific location, SAR may be defined by

$$\text{SAR} = \frac{\sigma}{\rho} |E|^2 \quad (5.180)$$

where σ = tissue conductivity, ρ = tissue mass density, E = rms value of the internal field strength. Thus the localized SAR is directly related to the internal electric field and the major effort involves the determination of the electric field distribution within the biological body. The method of moments has been extensively utilized to calculate localized SARs in block model representation of humans and animals.

As mentioned in Section 5.1, an application of MOM to EM problems usually involves four steps:

- deriving the appropriate IE,
- transforming the IE into a matrix equation (discretization),
- evaluating the matrix elements, and
- solving the resulting set of simultaneous equations.

We will apply these steps for calculating the electric field induced in an arbitrary human body or a biological system illuminated by an incident EM wave.

5.7.1 Derivation of Integral Equations

In general, the induced electric field inside a biological body was found to be quite complicated even for the simple case of assuming the plane wave as the incident field. The complexity is due to the irregularity of the body geometry, and the fact that the body is finitely conducting. To handle the complexity, the so-called *tensor integral-equation* (TIE) was developed by Livesay and Chen [51]. Only the essential steps will be provided here; the interested reader is referred to [51]–[53].

Consider a biological body of an arbitrary shape, with constitutive parameters ϵ, μ, σ illuminated by an incident (or impressed) plane EM wave as shown in Figure 5.23. The induced current in the body gives rise to a scattered field \mathbf{E}^s , which may be accounted for by replacing the body with an equivalent free-space current density \mathbf{J}_{eq} given by

$$\mathbf{J}_{eq}(\mathbf{r}) = (\sigma(\mathbf{r}) + j\omega[\epsilon(\mathbf{r}) - \epsilon_0])\mathbf{E}(\mathbf{r}) = \tau(\mathbf{r})\mathbf{E}(\mathbf{r}) \quad (5.181)$$

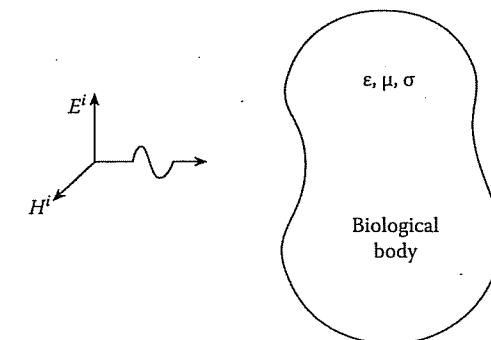


Figure 5.23
A biological body illuminated by a plane EM wave.

where a time factor $e^{j\omega t}$ is assumed. The first term in Equation (5.181) is the conduction current density, while the second term is the polarization current density. With the equivalent current density \mathbf{J}_{eq} , we can obtain the scattered fields \mathbf{E}^s and \mathbf{H}^s by solving Maxwell's equations

$$\nabla \times \mathbf{E}^s = -\mathbf{J}_{eq} - j\omega \mathbf{H}^s \quad (5.182a)$$

$$\nabla \times \mathbf{H}^s = j\omega \mathbf{E}^s \quad (5.182b)$$

where \mathbf{E}^s , \mathbf{H}^s , and \mathbf{J}_{eq} are all in phasor (complex) form. Elimination of \mathbf{E}^s or \mathbf{H}^s in Equation (5.182) leads to

$$\nabla \times \nabla \times \mathbf{E}^s - k_o^2 \mathbf{E}^s = -j\omega \mu_o \mathbf{J}_{eq} \quad (5.183a)$$

$$\nabla \times \nabla \times \mathbf{H}^s - k_o^2 \mathbf{H}^s = \nabla \times \mathbf{J}_{eq} \quad (5.183b)$$

where $k_o^2 = \omega^2 \mu_o \epsilon_o$. The solutions to Equation (5.183) are

$$\mathbf{E}^s = -j\omega \left[1 + \frac{1}{k_o^2} \nabla \nabla \cdot \right] \mathbf{A} \quad (5.184a)$$

$$\mathbf{H}^s = \frac{1}{\mu_o} \nabla \times \mathbf{A} \quad (5.184b)$$

where

$$\mathbf{A} = \mu_o \int_v G_o(\mathbf{r}, \mathbf{r}') \mathbf{J}_{eq}(\mathbf{r}') dv' \quad (5.185)$$

and

$$G_o(\mathbf{r}, \mathbf{r}') = \frac{e^{-jk_o(\mathbf{r}-\mathbf{r}')}}{4\pi |\mathbf{r} - \mathbf{r}'|} \quad (5.186)$$

is the free-space scalar Green's function. By the operator $\nabla \nabla \cdot$, we mean that $\nabla \nabla \cdot \mathbf{A} = \nabla(\nabla \cdot \mathbf{A})$. It is evident from Equations (5.184) to (5.186) that \mathbf{E}^s and \mathbf{H}^s depend on \mathbf{J}_{eq} .

Suppose \mathbf{J}_{eq} is an infinitesimal, elementary source at \mathbf{r}' pointed in the x direction so that

$$\mathbf{J}_{eq} = \delta(\mathbf{r} - \mathbf{r}') \mathbf{a}_x, \quad (5.187)$$

the corresponding vector potential is obtained from Equation (5.185) as

$$\mathbf{A} = \mu_0 G_o(\mathbf{r}, \mathbf{r}') \mathbf{a}_x \quad (5.188)$$

If $\mathbf{G}_{ox}(\mathbf{r}, \mathbf{r}')$ is the electric field produced by the elementary source, then $\mathbf{G}_{ox}(\mathbf{r}, \mathbf{r}')$ must satisfy

$$\nabla \times \nabla \times \mathbf{G}_{ox}(\mathbf{r}, \mathbf{r}') - k_o^2 \mathbf{G}_{ox}(\mathbf{r}, \mathbf{r}') = -j\omega \mu_0 \delta(\mathbf{r}, \mathbf{r}') \quad (5.189)$$

with solution

$$\mathbf{G}_{ox}(\mathbf{r}, \mathbf{r}') = -j\omega \mu_0 \left(1 + \frac{1}{k^2} \nabla \nabla \cdot \right) G_o(\mathbf{r}, \mathbf{r}') \quad (5.190)$$

$\mathbf{G}_{ox}(\mathbf{r}, \mathbf{r}')$ is referred to as a free-space vector Green's function with a source pointed in the x direction. We could also have $\mathbf{G}_{oy}(\mathbf{r}, \mathbf{r}')$ and $\mathbf{G}_{oz}(\mathbf{r}, \mathbf{r}')$ corresponding to infinitesimal, elementary sources pointed in the y and z direction, respectively. We now introduce a dyadic function² which can store the three vector Green functions $\mathbf{G}_{ox}(\mathbf{r}, \mathbf{r}')$, $\mathbf{G}_{oy}(\mathbf{r}, \mathbf{r}')$, and $\mathbf{G}_{oz}(\mathbf{r}, \mathbf{r}')$, i.e.,

$$\mathbf{G}_o(\mathbf{r}, \mathbf{r}') = \mathbf{G}_{ox}(\mathbf{r}, \mathbf{r}') \mathbf{a}_x + \mathbf{G}_{oy}(\mathbf{r}, \mathbf{r}') \mathbf{a}_y + \mathbf{G}_{oz}(\mathbf{r}, \mathbf{r}') \mathbf{a}_z \quad (5.191)$$

This is called free-space dyadic Green's function [53]. It is a solution to the dyadic differential equation

$$\nabla \times \nabla \times \mathbf{G}_o(\mathbf{r}, \mathbf{r}') - k_o^2 \mathbf{G}_o(\mathbf{r}, \mathbf{r}') = \tilde{I} \delta(\mathbf{r} - \mathbf{r}') \quad (5.192)$$

where \tilde{I} denotes the unit dyad (or idem factor) defined by

$$\tilde{I} = \mathbf{a}_x \mathbf{a}_x + \mathbf{a}_y \mathbf{a}_y + \mathbf{a}_z \mathbf{a}_z \quad (5.193)$$

The physical meaning of $\mathbf{G}_o(\mathbf{r}, \mathbf{r}')$ is rather obvious. $\mathbf{G}_o(\mathbf{r}, \mathbf{r}')$ is the electric field at a field point \mathbf{r} due to an infinitesimal source at \mathbf{r}' .

From Equations (5.184a) and (5.192), the solution of \mathbf{E} is

$$\mathbf{E}^s(\mathbf{r}) = -j\omega \mu_0 \int \mathbf{G}_o(\mathbf{r}, \mathbf{r}') \cdot \mathbf{J}_{eq}(\mathbf{r}') d\mathbf{v}' \quad (5.194)$$

Since $\mathbf{G}_o(\mathbf{r}, \mathbf{r}')$ has a singularity of the order $|\mathbf{r} - \mathbf{r}'|^3$, the integral in Equation (5.194) diverges if the field point \mathbf{r} is inside the volume v of the body (or source region).

²A dyad is a group of two or a pair of quantities. A dyadic function, denoted by \tilde{D} , is formed by two functions, i.e., $\tilde{D} = AB$. See Tai [53] or Balanis [28] for an exposition on dyadic functions.

This difficulty is overcome by excluding a small volume surrounding the field point first and then letting the small volume approach zero. The process entails defining the principal value (PV) and adding a correction term needed to yield the correct solution. Thus

$$\mathbf{E}^s(\mathbf{r}) = PV \int_v \mathbf{J}_{eq}(\mathbf{r}) \cdot \mathbf{G}(\mathbf{r}, \mathbf{r}') d\mathbf{v}' + [\mathbf{E}^s(\mathbf{r})]_{\text{correction}} \quad (5.195)$$

The correction term has been evaluated [51, 52] to be $-\mathbf{J}_{eq}/j3\omega\epsilon_0$ so that

$$\mathbf{E}^s(\mathbf{r}) = PV \int_v \mathbf{J}_{eq}(\mathbf{r}) \cdot \mathbf{G}(\mathbf{r}, \mathbf{r}') d\mathbf{v}' - \frac{\mathbf{J}_{eq}(\mathbf{r})}{j3\omega\epsilon_0} \quad (5.196)$$

The total electric field inside the body is the sum of the incident field \mathbf{E}^i and scattered field \mathbf{E}^s , i.e.,

$$\mathbf{E}(\mathbf{r}) = \mathbf{E}^i(\mathbf{r}) + \mathbf{E}^s(\mathbf{r}) \quad (5.197)$$

Combining Equations (5.181), (5.196), and (5.197) gives the desired tensor integral equation for $\mathbf{E}(\mathbf{r})$:

$$\left[1 + \frac{\tau(\mathbf{r})}{3j\omega\epsilon_0} \right] \mathbf{E}(\mathbf{r}) - PV \int_v \tau(\mathbf{r}') \mathbf{E}(\mathbf{r}) \cdot \mathbf{G}(\mathbf{r}, \mathbf{r}') d\mathbf{v}' = \mathbf{E}^i(\mathbf{r}) \quad (5.198)$$

In Equation (5.198), $\tau(\mathbf{r}) = \sigma(\mathbf{r}) + j\omega[\epsilon(\mathbf{r}) - \epsilon_0]$ and the incident electric field \mathbf{E}^i are known quantities; the total electric field \mathbf{E} inside the body is unknown and is to be determined by MOM.

5.7.2 Transformation to Matrix Equation (Discretization)

The inner product $\mathbf{E}(\mathbf{r}) \cdot \mathbf{G}(\mathbf{r}, \mathbf{r}')$ in Equation (5.198) may be represented as

$$\mathbf{E}(\mathbf{r}) \cdot \mathbf{G}(\mathbf{r}, \mathbf{r}') = \begin{bmatrix} \mathbf{G}_{xx}(\mathbf{r}, \mathbf{r}') & \mathbf{G}_{xy}(\mathbf{r}, \mathbf{r}') & \mathbf{G}_{xz}(\mathbf{r}, \mathbf{r}') \\ \mathbf{G}_{yx}(\mathbf{r}, \mathbf{r}') & \mathbf{G}_{yy}(\mathbf{r}, \mathbf{r}') & \mathbf{G}_{yz}(\mathbf{r}, \mathbf{r}') \\ \mathbf{G}_{zx}(\mathbf{r}, \mathbf{r}') & \mathbf{G}_{zy}(\mathbf{r}, \mathbf{r}') & \mathbf{G}_{zz}(\mathbf{r}, \mathbf{r}') \end{bmatrix} \begin{bmatrix} E_x(\mathbf{r}') \\ E_y(\mathbf{r}') \\ E_z(\mathbf{r}') \end{bmatrix} \quad (5.199)$$

showing that $\mathbf{G}(\mathbf{r}, \mathbf{r}')$ is a symmetric dyad. If we let

$$x_1 = x, \quad x_2 = y, \quad x_3 = z,$$

then $G_{x_p x_q}(\mathbf{r}, \mathbf{r}')$ can be written as

$$G_{x_p x_q}(\mathbf{r}, \mathbf{r}') = -j\omega \mu_0 \left[\delta_{pq} + \frac{1}{k_o^2} \frac{\partial^2}{\partial x_q \partial x_p} \right] G_o(\mathbf{r}, \mathbf{r}'), \quad p, q = 1, 2, 3 \quad (5.200)$$

We now apply MOM to transform Equation (5.198) into a matrix equation. We partition the body into N subvolumes or cells, each denoted by v_m ($m = 1, 2, \dots, N$), and

assume that $\mathbf{E}(\mathbf{r})$ and $\tau(\mathbf{r})$ are constant within each cell. If \mathbf{r}_m is the center of the m th cell, requiring that each scalar component of Equation (5.198) be satisfied at \mathbf{r}_m this leads to

$$\left[1 + \frac{\tau(\mathbf{r})}{3j\omega\epsilon_0}\right] E_{x_p}(\mathbf{r}_m) - \sum_{q=1}^3 \left[\sum_{q=1}^3 \tau(\mathbf{r}_n) PV \int_{v_n} G_{x_p x_q}(\mathbf{r}_m, \mathbf{r}') dv' \right] E_{x_q}(\mathbf{r}_n) = E_{x_p}^i(\mathbf{r}_m) \quad (5.201)$$

If we let $[G_{x_p x_q}]$ be an $N \times N$ matrix with elements

$$G_{x_p x_q}^{mn} = \tau(\mathbf{r}_n) PV \int_{v_n} G_{x_p x_q}(\mathbf{r}_m, \mathbf{r}') dv' - \delta_{pq} \delta_{mn} \left[1 + \frac{\tau(\mathbf{r})}{3j\omega\epsilon_0}\right], \quad (5.202)$$

where $m, n = 1, 2, \dots, N$, $p, q = 1, 2, 3$, and let $[E_{x_p}]$ and $[E_{x_p}^i]$ be column matrices with elements

$$E_{x_p} = \begin{bmatrix} E_{x_p}(\mathbf{r}_1) \\ \vdots \\ E_{x_p}(\mathbf{r}_N) \end{bmatrix}, \quad E_{x_p}^i = \begin{bmatrix} E_{x_p}^i(\mathbf{r}_1) \\ \vdots \\ E_{x_p}^i(\mathbf{r}_N) \end{bmatrix}, \quad (5.203)$$

then from Equations (5.198) and (5.201), we obtain $3N$ simultaneous equations for E_x , E_y and E_z at the centers of N cells by the point matching technique. These simultaneous equations can be written in matrix form as

$$\begin{bmatrix} [G_{xx}] & [G_{xy}] & [G_{xz}] \\ \hline [G_{yx}] & [G_{yy}] & [G_{yz}] \\ \hline [G_{zx}] & [G_{zy}] & [G_{zz}] \end{bmatrix} \begin{bmatrix} [E_x] \\ \hline [E_y] \\ \hline [E_z] \end{bmatrix} = - \begin{bmatrix} [E_x^i] \\ \hline [E_y^i] \\ \hline [E_z^i] \end{bmatrix} \quad (5.204a)$$

or simply

$$[G][E] = -[E^i] \quad (5.204b)$$

where $[G]$ is $3N \times 3N$ matrix and $[E]$ and $[E^i]$ are $3N$ column matrices.

5.7.3 Evaluation of Matrix Elements

Although the matrix $[E^i]$ in Equation (5.204) is known, while the matrix $[E]$ is to be determined, the elements of the matrix $[G]$, defined in Equation (5.202), are yet to be calculated. For the off-diagonal elements of $[G_{x_p x_q}]$, \mathbf{r}_m is not in the n th cell (\mathbf{r}_m is not in v_n) so that $G_{x_p x_q}(\mathbf{r}_m, \mathbf{r}')$ is continuous in v_n and the principal value operation can be dropped. Equation (5.202) becomes

$$G_{x_p x_q}^{mn} = \tau(\mathbf{r}_n) \int_{v_n} G_{x_p x_q}(\mathbf{r}_m, \mathbf{r}') dv', \quad m \neq n \quad (5.205)$$

As a first approximation,

$$G_{x_p x_q}^{mn} = \tau(\mathbf{r}_n) G_{x_p x_q}(\mathbf{r}_m, \mathbf{r}') \Delta v_n, \quad m \neq n \quad (5.206)$$

where Δv_n is the volume of cell v_n . Incorporating Equations (5.190) and (5.200) into Equation (5.206) yields

$$\begin{aligned} G_{x_p x_q}^{mn} = & \frac{-j\omega\mu k_o \Delta v_n \tau(\mathbf{r}_n) \exp(-j\alpha_{mn})}{4\pi\alpha_{mn}^3} \left[(\alpha_{mn}^2 - 1 - j\alpha_{mn}) \delta_{pq} \right. \\ & \left. + \cos\theta_{x_p}^{mn} \cos\theta_{x_q}^{mn} (3 - \alpha_{mn}^2 + 3j\alpha_{mn}) \right], \quad m \neq n \end{aligned} \quad (5.207)$$

where

$$\begin{aligned} \alpha_{mn} &= k_o R_{mn}, \quad R_{mn} = |\mathbf{r}_m - \mathbf{r}_n|, \\ \cos\theta_{x_p}^{mn} &= \frac{x_p^m - x_p^n}{R_{mn}}, \quad \cos\theta_{x_q}^{mn} = \frac{x_q^m - x_q^n}{R_{mn}}, \\ \mathbf{r}_m &= (x_1^m, x_2^m, x_3^m), \quad \mathbf{r}_n = (x_1^n, x_2^n, x_3^n) \end{aligned}$$

The approximation in Equation (5.207) yields adequate results provided N is large. If greater accuracy is desired, the integral in Equation (5.205) must be evaluated numerically.

For the diagonal terms ($m = n$), Equation (5.202) becomes

$$G_{x_p x_q}^{nn} = \tau(\mathbf{r}_n) PV \int_{v_n} G_{x_p x_q}(\mathbf{r}_n, \mathbf{r}') dv' - \delta_{pq} \left[1 + \frac{\tau(\mathbf{r})}{3j\omega\epsilon_0}\right] \quad (5.208)$$

To evaluate this integral, we approximate cell v_n by an equivolumic sphere of radius a_n centered at \mathbf{r}_n , i.e.,

$$\Delta v = \frac{4}{3}\pi a_n^3$$

or

$$a_n = \left(\frac{3\Delta v}{4\pi} \right)^{1/3} \quad (5.209)$$

After a lengthy calculation, we obtain [51]

$$\begin{aligned} G_{x_p x_q}^{nn} = \delta_{pq} & \left[\frac{-2j\omega\mu\tau(r_n)}{3k_o^2} (\exp[-jk_o a_n](1 + jk_o a_n) - 1) \right. \\ & \left. - \left(1 + \frac{\tau(r_n)}{3j\omega\epsilon_0}\right) \right], \quad m = n \end{aligned} \quad (5.210)$$

In case the shape of cell v_n differs considerably from that of a sphere, the approximation in Equation (5.210) may yield poor results. To have a greater accuracy, a small cube, cylinder, or sphere is created around \mathbf{r}_n to evaluate the correction term, and the integration through the remainder of v_n is performed numerically.

5.7.4 Solution of the Matrix Equation

Once the elements of matrix $[G]$ are evaluated, we are ready to solve Equation (5.204), namely,

$$[G][E] = -[E^i] \quad (5.204)$$

With the known incident electric field represented by $[E^i]$, the total induced electric field represented by $[E]$ can be obtained from Equation (5.204) by inverting $[G]$ or by employing a Gauss-Jordan elimination method. If matrix inversion is used, the total induced electric field inside the biological body is obtained from

$$[E] = -[G]^{-1}[E^i] \quad (5.211)$$

Guru and Chen [55] have developed computer programs that yield accurate results on the induced electric field and the absorption power density in various biological bodies irradiated by various EM waves. The validity and accuracy of their numerical results were verified by experiments.

In the following examples, we illustrate the accuracy of the numerical procedure with one simple elementary shape and one advanced shape of biological bodies. The examples are taken from the works of Chen and others [52], [56]–[58].

Example 5.11

Determine the distribution of the energy absorption rate or EM heating induced by plane EM waves of 918 MHz in spherical models of animal brain having radius 3 cm. Assume the \mathbf{E}^i field expressed as

$$\mathbf{E}^i = E_o e^{-jk_o z} \mathbf{a}_x = \mathbf{a}_x E_o (\cos k_o z - j \sin k_o z) \text{ V/m} \quad (5.212)$$

where $k_o = 2\pi/\lambda = 2\pi f/c$, $E_o = \sqrt{2\eta_o P_i}$, P_i is the incident power in mW/cm^2 and $\eta_o = 377 \Omega$ is the intrinsic impedance of free space. Take $P_i = 1 \text{ mW/cm}^2$ ($E_o = 86.83 \text{ V/m}$), $\epsilon_r = 35$, $\sigma = 0.7 \text{ s/m}$. \square

Solution

In order to apply MOM, we first approximate the spherical model by a “cubic sphere.” Figure 5.24 portrays an example in which one eighth of a sphere is approximated by 40 or 73 cubic cells. The center of each cell, for the case of 40 cells, is determined from Figure 5.25. \mathbf{E}^i at the center of each cell can be calculated using Equation (5.212). With the computed \mathbf{E}^i and the elements of the matrix $[G_{x_p x_q}]$ calculated using Equations (5.207) and (5.210), the induced electric field \mathbf{E} in each cell is computed from Equation (5.211). Once \mathbf{E} is obtained, the absorption rate of the EM energy is determined using

$$P = \frac{\sigma}{2} |\mathbf{E}|^2 \quad (5.213)$$

The average heating is obtained by averaging P in the brain. The curve showing relative heating as a function of location is obtained by normalizing the distribution of P with respect to the maximum value of P at a certain location in the brain.

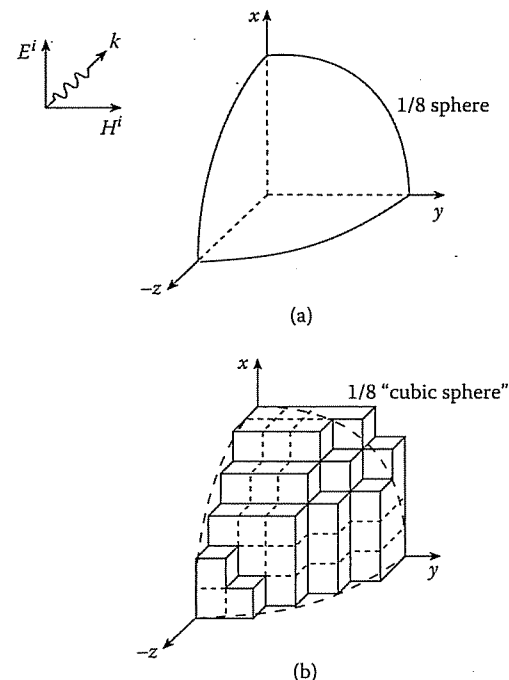


Figure 5.24

For Example 5.11: (a) One eighth of a sphere, (b) a “cubic sphere” constructed from 73 cubic cells.

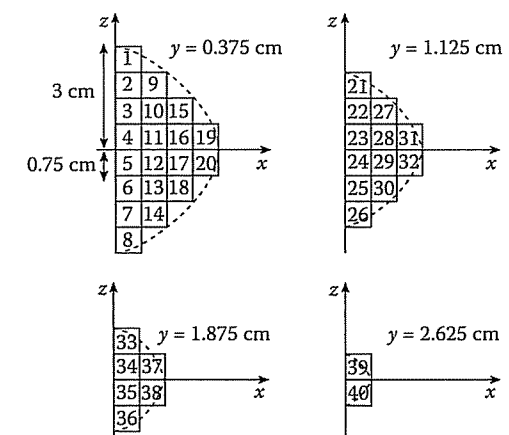


Figure 5.25

Geometry and dimensions of one half of the spherical model of the brain constructed from 40 cells. The cell numbering is used in the program of Figure 5.26.

The computer program for the computation is shown in Figure 5.26. It is a modified version of the one developed by Jongakiem [58]. The numerical results are shown in Figure 5.27(a), where relative heating along the x -, y -, and z -axes in the brain is plotted. The three curves identified by X , Y , and Z correspond with the distributions of the relative heating along x -, y -, and z -axes, respectively. Observe the strong standing wave patterns with peak heating located somewhere near the center of the brain. The average and maximum heating are found to be 0.3202 and 0.885 in mW/cm^3 . The exact solution obtained from Mie theory (see Section 2.8) is shown in Figure 5.27(b). The average and maximum heating from exact solution are 0.295 and 0.814 mW/cm^3 , respectively. A comparison of Figures 5.27(a) and (b) confirms the accuracy of the numerical procedure. ■

```
% This program determines the power absorption of biological bodies.
% bodies are assumed to have the permeability of freespace
% eo = permittivity of free space
% er = relative permittivity of the body
% f = frequency in Hz, w in rad/s
% sig = conductivity
% xd, yd and zd have the x, y z coordinates of the cells
% N is the number of cells
% Ei = incident electric field
% Rmn = distance between cell m and n.
% cxpmn and cxqmn = cos(theta_xp_mn) and cos(theta_xq_mn)
% We compute the 9 block matrices separately although one might have a
% function to that and combine them into the G matrix.
% For the diagonal blocks we compute the diagonal elements.
% for the off-diagonal blocks they are zeros.

clear all; close all
R=3e-2; H = R/4; an = H*(0.75/pi)^(1/3);
eo = 8.854e-12; muo = pi*4e-7;
f = 918e6; er = 35; sig=0.7;
w = 2*pi*f; ko = w*sqrt(muo*eo);
N=40; %

xd = [0.5*H*ones(1,8) 1.5*H*ones(1,6) 2.5*H*ones(1,4) 3.5*H 3.5*H ...
       0.5*H*ones(1,6) 1.5*H*ones(1,4) 2.5*H*ones(1,2) ...
       0.5*H*ones(1,4) 1.5*H*ones(1,2) ...
       0.5*H*ones(1,2)];
yd= [0.5*H*ones(1,20) 1.5*H*ones(1,12) 2.5*H*ones(1,6) 3.5*H*ones(1,2)];
```

Figure 5.26

Computer program for Example 5.11 (Continued).

```
zd=[(3.5*H:-H:-3.5*H) (2.5*H:-H:-2.5*H) (1.5*H:-H:-1.5*H) 0.5*H -
0.5*H ...
(2.5*H:-H:-2.5*H) (1.5*H:-H:-1.5*H) 0.5*H -0.5*H ...
(1.5*H:-H:-1.5*H) 0.5*H -0.5*H ...
0.5*H -0.5*H];
r=[xd(:) yd(:) zd(:)];

tow=[(sig+j*w*eo*(er-1))*ones(N,1)];

A=-j*w*muo*ko*H^3/4/pi;
C=-2*j*w*muo/3/ko^2*(exp(-j*ko*an)*(1+j*ko*an)-1)-1/3/j/w/eo;
Ei = [86.83*exp(-j*ko*zd(:));0*exp(-j*ko*zd(:));0*exp(-j*ko*zd(:))];

%Gxx
for m=1:N
    for n=1:N
        if m==n
            Gxx(m,n) = C*tow(n)-1;
        else
            Rmn=norm(r(m,:)-r(n,:));
            almn = ko*Rmn;
            cxpmn =(r(m,1)-r(n,1))/Rmn;
            cxqmn =(r(m,1)-r(n,1))/Rmn;
            B = (almn^2-1-j*almn)+cxpmn*cxqmn*(3-almn^2+3*j*almn);
            Gxx(m,n)= A* tow(n)*exp(-j*almn)/almn^3*B;
        end
    end
end

%Gyy
for m=1:N
    for n=1:N
        if m==n
            Gyy(m,n) = C*tow(n)-1;
        else
            Rmn=norm(r(m,:)-r(n,:));
            almn = ko*Rmn;
            cxpmn =(r(m,2)-r(n,2))/Rmn;
            cxqmn =(r(m,2)-r(n,2))/Rmn;
            B = (almn^2-1-j*almn)+cxpmn*cxqmn*(3-almn^2+3*j*almn);
            Gyy(m,n)= A* tow(n)*exp(-j*almn)/almn^3*B;
        end
    end
end
```

Figure 5.26

(Cont.) Computer program for Example 5.11.

```

%Gzz
for m=1:N
    for n=1:N
        if m==n
            Gzz(m,n) = C*tow(n)-1;
        else
            Rmn=norm(r(m,:)-r(n,:));
            almn = ko*Rmn;
            cxpmn =(r(m,3)-r(n,3))/Rmn;
            cxqmn =(r(m,3)-r(n,3))/Rmn;

            B = (almn^2-1-j*almn)+cxpmn*cxqmn*(3-almn^2+3*j*almn);
            Gzz(m,n)= A* tow(n)*exp(-j*almn)/almn^3*B;
        end
    end
end

%Gxy
for m=1:N
    for n=1:N
        if m==n
            Rmn=norm(r(m,:)-r(n,:));
            almn = ko*Rmn;
            cxpmn =(r(m,1)-r(n,1))/Rmn;
            cxqmn =(r(m,2)-r(n,2))/Rmn;
            B = cxpmn*cxqmn*(3-almn^2+3*j*almn);
            Gxy(m,n)= A* tow(n)*exp(-j*almn)/almn^3*B;
        end
    end
end

%Gxz
for m=1:N
    for n=1:N
        if m==n
            Rmn=norm(r(m,:)-r(n,:));
            almn = ko*Rmn;
            cxpmn =(r(m,1)-r(n,1))/Rmn;
            cxqmn =(r(m,3)-r(n,3))/Rmn;

            B = cxpmn*cxqmn*(3-almn^2+3*j*almn);
            Gxz(m,n)= A* tow(n)*exp(-j*almn)/almn^3*B;
        end
    end
end

```

Figure 5.26

(Cont.) Computer program for Example 5.11.

```

%Gyx
for m=1:N
    for n=1:N
        if m==n
            Rmn=norm(r(m,:)-r(n,:));
            almn = ko*Rmn;
            cxpmn =(r(m,2)-r(n,2))/Rmn;
            cxqmn =(r(m,1)-r(n,1))/Rmn;

            B = cxpmn*cxqmn*(3-almn^2+3*j*almn);
            Gyx(m,n)= A* tow(n)*exp(-j*almn)/almn^3*B;
        end
    end
end

%Gyz
for m=1:N
    for n=1:N
        if m==n
            Rmn=norm(r(m,:)-r(n,:));
            almn = ko*Rmn;
            cxpmn =(r(m,2)-r(n,2))/Rmn;
            cxqmn =(r(m,3)-r(n,3))/Rmn;

            B = cxpmn*cxqmn*(3-almn^2+3*j*almn);
            Gyz(m,n)= A* tow(n)*exp(-j*almn)/almn^3*B;
        end
    end
end

%Gzx
for m=1:N
    for n=1:N
        if m==n
            Rmn=norm(r(m,:)-r(n,:));
            almn = ko*Rmn;
            cxpmn =(r(m,3)-r(n,3))/Rmn;
            cxqmn =(r(m,1)-r(n,1))/Rmn;

            B = cxpmn*cxqmn*(3-almn^2+3*j*almn);
            Gzx(m,n)= A* tow(n)*exp(-j*almn)/almn^3*B;
        end
    end
end

%Gzy
for m=1:N
    for n=1:N

```

Figure 5.26

(Cont.) Computer program for Example 5.11.

```

if m==n
Rmn=norm(r(m,:)-r(n,:));
almn = ko*Rmn;
cxpmn =(r(m,3)-r(n,3))/Rmn;
cxqmn =(r(m,2)-r(n,2))/Rmn;

B = cxpmn*cxqmn*(3-almn^2+3*j*almn);
Gzy(m,n)= A* tow(n)*exp(-j*almn)/almn^3*B;
end
end
G = [Gxx Gxy Gxz;Gyx Gyy Gyz;Gzx Gzy Gzz];
E = -G\Em;
Nx=[4 11 16 19];
Ny=[4 23 34 39];
Nz= 8:-1:1;

Exaxis = (abs(E(Nx)).^2+abs(E(N+Nx)).^2+abs(E(2*N+Nx)).^2);
Exaxis = [Exaxis(4:-1:1);Exaxis];
Eyaxis = (abs(E(Ny)).^2+abs(E(N+Ny)).^2+abs(E(2*N+Ny)).^2);
Eyaxis = [Eyaxis(4:-1:1);Eyaxis];
Ezaxis = 2*(abs(E(Nz)).^2+abs(E(N+Nz)).^2+abs(E(2*N+Nz)).^2);

EMAX=max([Exaxis;Eyaxis;Ezaxis]);
Exaxis=Exaxis/EMAX;
Eyaxis=Eyaxis/EMAX;
Ezaxis=Ezaxis/EMAX;
pd=(-2.625:.75:2.625);
plot(pd,Exaxis,'ok');hold on
plot(pd,Eyaxis,'ok','MarkerFaceColor','k');
plot(pd,Ezaxis,'sk');
pdi=(-2.625:5.25/199:2.625);
Exaxisi=interp1(pd,Exaxis,pdi,'spline');
Eyaxisi=interp1(pd,Eyaxis,pdi,'spline');
Ezaxisi=interp1(pd,Ezaxis,pdi,'spline');
plot(pdi,Exaxisi,'k','LineWidth',2);
plot(pdi,Eyaxisi,'-k','LineWidth',2);
plot(pdi,Ezaxisi,:k,'LineWidth',2);
xlabel('cm','FontSize',12)
axis([-3 3 0 1.1]);grid
text(-1.5,.28,'y')
text(-1.5,.45,'z')
text(-1.5,.92,'x')

```

Figure 5.26

(Cont.) Computer program for Example 5.11.

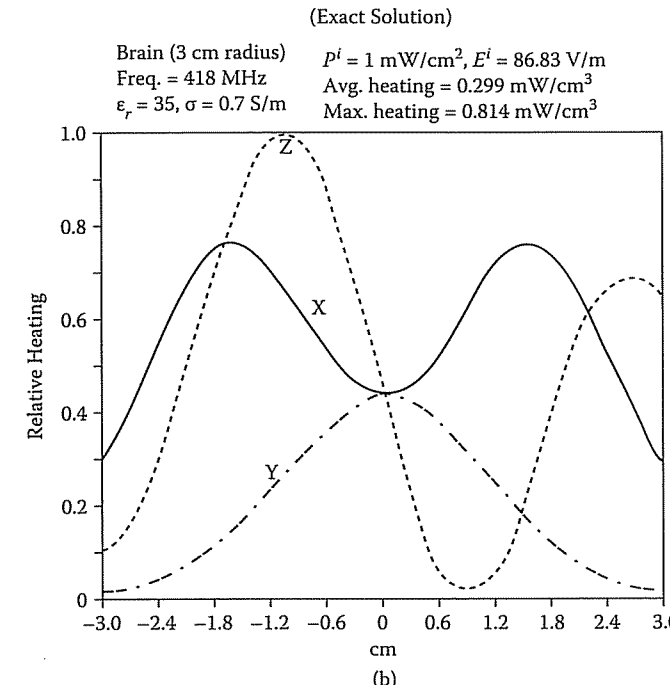
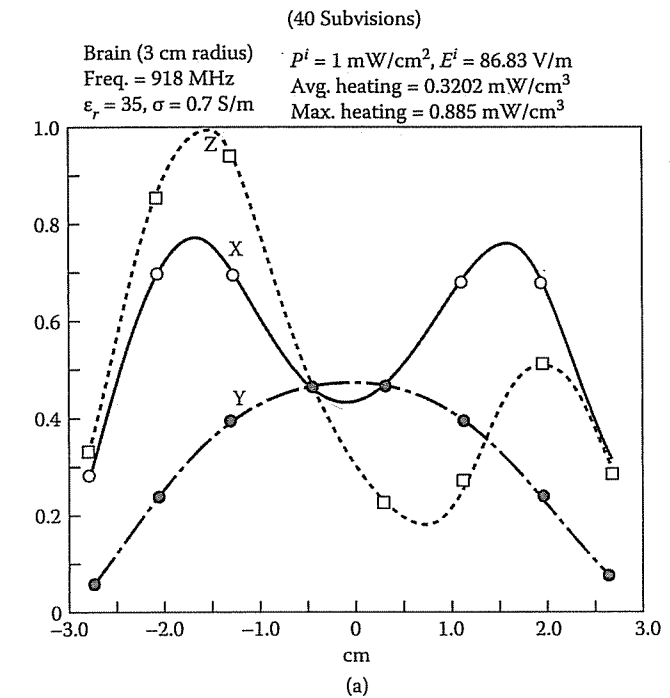


Figure 5.27

Distributions of heating along the x -, y -, and z -axis of a spherical model of an animal brain [57]: (a) MOM solution, (b) exact solution.

Example 5.12

Having validated the accuracy of the tensor-integral-equation (TIE) method, determine the induced electric field and specific absorption rate (SAR) of EM energy inside a model of typical human body irradiation (Figure 5.28), by EM wave at 80 MHz with vertical polarization, i.e.,

$$\mathbf{E} = \mathbf{a}_x \quad \text{V/m}$$

at normal incidence. Assume the body at 80 MHz is that of a high-water content tissue with $\epsilon = 80\epsilon_0$, $\mu = \mu_0$, $\sigma = 0.84 \text{ S/m}$. \square

Solution

The body is partitioned into 108 cubic cells of various sizes ranging from 5 cm^3 to 12 cm^3 . To ensure accurate results, the cell size is kept smaller than a quarter-wavelength (of the medium). With the coordinates of the center of each cell figured out from Figure 5.28, the program in Figure 5.26 can be used to find induced electric field components E_x , E_y , and E_z at the centers of the cells due to an incident electric field 1 V/m (maximum value) at normal incidence. The SAR is calculated from $(\sigma/2)(E_x^2 + E_y^2 + E_z^2)$. Figures 5.29 to 5.31 illustrate E_x , E_y , and E_z at the center of each cell. Observe that E_y and E_z are much smaller than E_x at this frequency due to the polarization of the incident wave.

As mentioned earlier, the model of the human body shown in Figure 5.28 is due to Chen and Guru [56]. An improved, more realistic model due to Gandhi et al. [59]–[61] is shown in Figure 5.32. \blacksquare

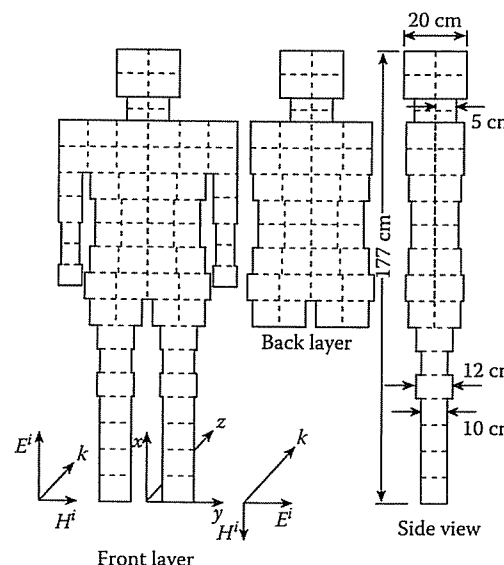


Figure 5.28

Geometry and dimensions of a model of typical human body of height 1.77 m [52].

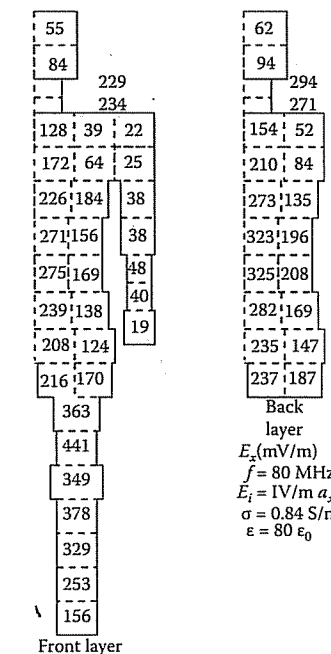


Figure 5.29

Induced E_x (in mV/m) at the center of each cell due to E_x^i of 1 V/m [52].

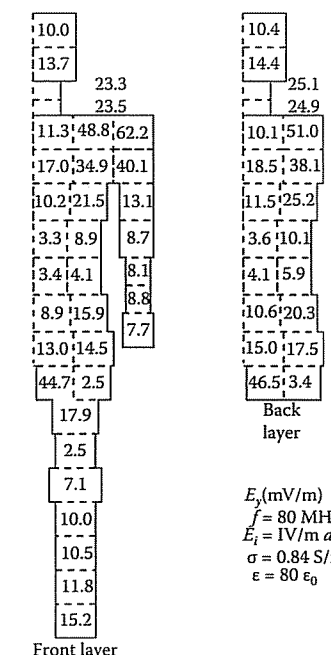
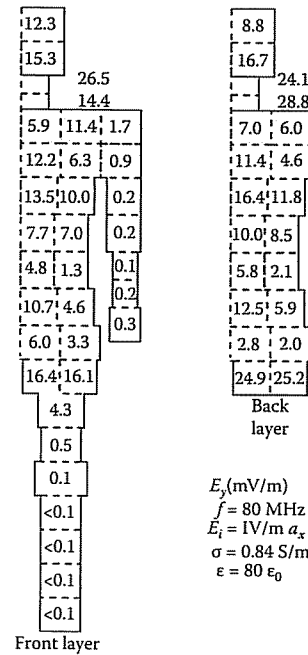
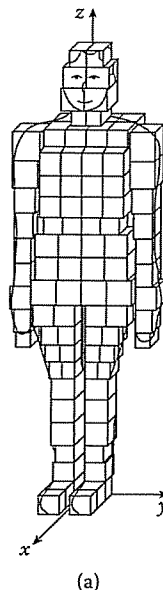


Figure 5.30

Induced E_y (in mV/m) at the center of each cell due to E_x^i of 1 V/m [52].

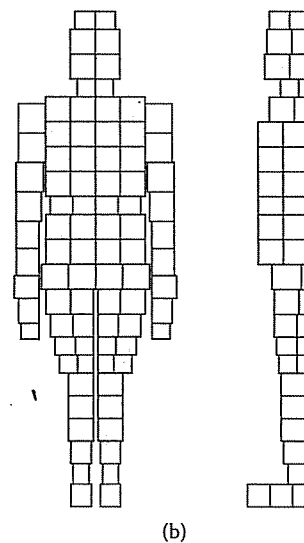
**Figure 5.31**

Induced E_z (in mV/m) at the center of each cell due to E_x^i of 1 V/m [52].

**Figure 5.32**

A more realistic block model of the human body [59]: (a) In three dimensions, (b) Front and side views. (*Continued*).

5.8. CONCLUDING REMARKS

**Figure 5.32**

(*Cont.*) A more realistic block model of the human body [59]: (a) In three dimensions, (b) Front and side views.

5.8 Concluding Remarks

The method of moments is a powerful numerical method capable of applying weighted residual techniques to reduce an integral equation to a matrix equation. The solution of the matrix equation is usually carried out via inversion, elimination, or iterative techniques. Although MOM is commonly applied to open problems such as those involving radiation and scattering, it has been successfully applied to closed problems such as waveguides and cavities.

Needless to say, the issues on MOM covered in this chapter have been carefully selected. We have only attempted to cover the background and reference material upon which the reader can easily build. The interested reader is referred to the literature for more in-depth treatment of each subject. General concepts on MOM are covered in [3] and [62]. Clear and elementary discussions on IEs and Green's functions may be found in [10]–[12], [28]–[30], [62]–[65]. For further study on the theory of the method of moments, one should see [6, 9, 10, 28, 40].

The number of problems that can be treated by MOM is endless, and the examples given in this chapter just scratch the surface. The following problems represent typical EM-related application areas:

- electrostatic problems [31], [66]–[69]
- wire antennas and scatterers [34, 37, 42, 44, 70, 78]
- scattering and radiation from bodies of revolution [79, 80]

- scattering and radiation from bodies of arbitrary shapes [38, 81, 82]
- transmission lines [18]–[20], [23, 24], [83]–[86]
- aperture problems [87]–[89]
- biomagnetic problems [47]–[52], [90]–[92].

A number of user-oriented computer programs have evolved over the years to solve electromagnetic integral equations by the method of moments. These codes can handle radiation and scattering problems in both the frequency and time domains. Reviews of the codes may be found in [38, 93]. The most popular of these codes is the Numerical Electromagnetic Code (NEC) developed at the Lawrence Livermore National Laboratory [7, 94]. NEC is a frequency domain antenna modeling FORTRAN code applying the MOM to IEs for wire and surface structures. Its most notable features are probably that it is user oriented, includes documentation, and is available; for these reasons, it is being used in public and private institutions. A compact version of NEC is the mini-numerical electromagnetic code (MININEC) [95], which is intended to be used in personal computers.

It is important that we recognize the fact that MOM is limited in application to radiation and scattering from bodies that are electrically large. The size of the scatterer or radiator must be of the order λ^3 . This is because the cost of storing, inverting, and computing matrix elements becomes prohibitively large. At high frequencies, asymptotic techniques such as the geometrical theory of diffraction (GTD) are usually employed to derive approximate but accurate solutions [46, 96, 97].

References

- [1] L.V. Kantorovich and V.I. Krylov, *Approximate Methods of Higher Analysis* (translated from Russian by C.D. Benster). New York: John Wiley, 1964.
- [2] Y.U. Vorobev, *Method of Moments in Applied Mathematics* (translated from Russian by Seckler). New York: Gordon & Breach, 1965.
- [3] R.F. Harrington, *Field Computation by Moment Methods*. Malabar, FL: Krieger, 1968.
- [4] B.J. Strait, *Applications of the Method of Moments to Electromagnetics*. St. Cloud, FL: SCEEE Press, 1980.
- [5] R.F. Harrington, “Origin and development of the method moments for field computation,” in E.K. Miller et al. (eds.), *Computational Electromagnetics*. New York: IEEE Press, 1992, pp. 43–47.
- [6] J.H. Richmond, “Digital computer solutions of the rigorous equations for scattering problems,” *Proc. IEEE*, vol. 53, Aug. 1965, pp. 796–804.

- [7] R.F. Harrington, “Matrix methods for field problems,” *Proc. IEEE*, vol. 55, no. 2, Feb. 1967, pp. 136–149.
- [8] M.M. Ney, “Method of moments as applied to electromagnetics problems,” *IEEE Trans. Micro. Theo. Tech.*, vol. MTT-33, no. 10, Oct. 1985, pp. 972–980.
- [9] A.T. Adams, “An introduction to the method of moments,” Syracuse Univ., *Report RADC TR-73-217*, vol. 1, Aug. 1974.
- [10] M.D. Greenberg, *Application of Green Functions in Science and Engineering*. Englewood Cliffs, NJ: Prentice-Hall, 1971.
- [11] A. Ishimaru, *Electromagnetic Wave Propagation, Radiation, and Scattering*. Englewood Cliffs, NJ: Prentice-Hall, 1991, pp. 121–148.
- [12] P.M. Morse and H. Feshbach, *Methods of Theoretical Physics*. New York: McGraw-Hill, 1953, Part I, Chap. 7, pp. 791–895.
- [13] T. Myint-U, *Partial Differential Equations of Mathematical Physics*, 2nd ed. New York: North-Holland, 1980, Chap. 10, pp. 282–305.
- [14] R.F. Harrington, *Time-Harmonic Electromagnetic Fields*. New York: McGraw-Hill, 1961, p. 232.
- [15] I.V. Bewley, *Two-dimensional Fields in Electrical Engineering*. New York: Dover Publ., 1963, pp. 151–166.
- [16] K.C. Gupta et al., *Computer-aided Design of Microwave Circuits*. Dedham, MA: Artech House, 1981, pp. 237–261.
- [17] T. Itoh (ed.), *Numerical Techniques for Microwaves and Millimeterwave Passive Structures*. New York: John Wiley & Sons, 1989, pp. 221–250.
- [18] D.W. Kammler, “Calculation of characteristic admittance and coupling coefficients for strip transmission lines,” *IEEE Trans. Micro. Tech.*, vol. MTT-16, no. 11, Nov. 1968, pp. 925–937.
- [19] Y.M. Hill et al., “A general method for obtaining impedance and coupling characteristics of practical microstrip and triplate transmission line configurations,” *IBM J. Res. Dev.*, vol. 13, May 1969, pp. 314–322.
- [20] W.T. Weeks, “Calculation of coefficients of capacitance of multiconductor transmission lines in the presence of a dielectric interface,” *IEEE Trans. Micro. Theo. Tech.*, vol. MTT-18, no. 1, Jan. 1970, pp. 35–43.
- [21] R. Chadha and K.C. Gupta, “Green’s functions for triangular segments in planar microwave circuits,” *IEEE Trans. Micro. Theo. Tech.*, vol. MTT-28, no. 10, Oct. 1980, pp. 1139–1143.
- [22] R. Terras and R. Swanson, “Image methods for constructing Green’s functions and eigenfunctions for domains with plane boundaries,” *J. Math. Phys.*, vol. 21, no. 8, Aug. 1980, pp. 2140–2153.

- [23] E. Yamashita and K. Atsuki, "Stripline with rectangular outer conductor and three dielectric layers," *IEEE Trans. Micro. Theo. Tech.*, vol. MTT-18, no. 5, May 1970, pp. 238-244.
- [24] R. Crampagne et al., "A simple method for determining the Green's function for a large class of MIC lines having multilayered dielectric structures," *IEEE Trans. Micro. Theo. Tech.*, vol. MTT-26, no. 2, Feb. 1978, pp. 82-87.
- [25] R. Chadha and K.C. Gupta, "Green's functions for circular sectors, annular rings, and annular sectors in planar microwave circuits," *IEEE Trans. Micro. Theo. Tech.*, vol. MTT-29, no. 1, Jan. 1981, pp. 68-71.
- [26] P.H. Pathak, "On the eigenfunction expansion of electromagnetic dyadic Green's functions," *IEEE Trans. Ant. Prog.*, vol. AP-31, no. 6, Nov. 1983, pp. 837-846.
- [27] R.F. Harrington and J.R. Mautz, "Green's functions for surfaces of revolution," *Radio Sci.*, vol. 7, no. 5, May 1972, pp. 603-611.
- [28] C.A. Balanis, *Advanced Engineering Electromagnetics*. New York: John Wiley, 1989, pp. 670-742, 851-916.
- [29] E. Butkov, *Mathematical Physics*. New York: Addison-Wesley, 1968, pp. 503-552.
- [30] J.D. Jackson, *Classical Electrodynamics*, 2nd ed. New York: John Wiley, 1975, pp. 119-135.
- [31] L.L. Tsai and C.E. Smith, "Moment methods in electromagnetics undergraduates," *IEEE Trans. Educ.*, vol. E-21, no. 1, Feb. 1978, pp. 14-22.
- [32] P.P. Sylvester and R.L. Ferrari, *Finite Elements for Electrical Engineers*. Cambridge, UK: Cambridge University Press, 1983, pp. 103-105.
- [33] H.A. Wheeler, "Transmission-line properties of parallel strips separated by a dielectric sheet," *IEEE Trans. Micro. Theo. Tech.*, vol. MTT-13, Mar. 1965, pp. 172-185.
- [34] J.H. Richmond, "Scattering by an arbitrary array of parallel wires," *IEEE Trans. Micro. Theo. Tech.*, vol. MTT-13, no. 4, July 1965, pp. 408-412.
- [35] B.D. Popovic et al., *Analysis and Synthesis of Wire Antennas*. Chichester, UK: Research Studies Press, 1982, pp. 3-21.
- [36] E. Hallen, "Theoretical investigations into the transmitting and receiving qualities of antennae," *Nova Acta Regiae Soc. Sci. Upsaliensis*, Ser. IV, no. 11, 1938, pp. 1-44.
- [37] K.K. Mei, "On the integral equations of thin wire antennas," *IEEE Trans. Ant. Prog.*, vol. AP-13, 1965, pp. 374-378.
- [38] J. Moore and P. Pizer (eds.), *Moment Methods in Electromagnetics: Techniques and Applications*. Letchworth, UK: Research Studies Press, 1984.

- [39] H.C. Pocklington, "Electrical oscillations in wire," *Cambridge Phil. Soc. Proc.*, vol. 9, 1897, pp. 324-332.
- [40] R. Mittra (ed.), *Computer Techniques for Electromagnetics*. Oxford: Pergamon Press, 1973, pp. 7-95.
- [41] C.A. Balanis, *Antenna Theory: Analysis and Design*. New York: Harper & Row, 1982, pp. 283-321.
- [42] C.M. Butler and D.R. Wilton, "Analysis of various numerical techniques applied to thin-wire scatterers," *IEEE Trans. Ant. Prog.*, vol. AP-23, no. 4, July 1975, pp. 524-540. Also in [46, pp. 46-52].
- [43] T.K. Sarkar, "A note on the choice of weighting functions in the method of moments," *IEEE Trans. Ant. Prog.*, vol. AP-33, no. 4, April 1985, pp. 436-441.
- [44] F.M. Landstorfer and R.F. Sacher, *Optimisation of Wire Antenna*. Letchworth, UK: Research Studies Press, 1985, pp. 18-33.
- [45] K.A. Michalski and C.M. Butler, "An efficient technique for solving the wire integral equation with non-uniform sampling," *Conf. Proc. IEEE Southeastcon.*, April 1983, pp. 507-510.
- [46] R.F. Harrington et al. (eds.), *Lectures on Computational Methods in Electromagnetics*. St. Cloud, FL: SCEEE Press, 1981.
- [47] R. Kastner and R. Mittra, "A new stacked two-dimensional spectral iterative technique (SIT) for analyzing microwave power deposition in biological media," *IEEE Trans. Micro. Theo. Tech.*, vol. MTT-31, no. 1, Nov. 1983, pp. 898-904.
- [48] P.W. Barber, "Electromagnetic power deposition in prolate spheroidal models of man and animals at resonance," *IEEE Trans. Biomed. Engr.*, vol. BME-24, no. 6, Nov. 1977, pp. 513-521.
- [49] J.M. Osepchuk (ed.), *Biological Effects of Electromagnetic Radiation*. New York: IEEE Press, 1983.
- [50] R.J. Spiegel, "A review of numerical models for predicting the energy deposition and resultant thermal response of humans exposed to electromagnetic fields," *IEEE Trans. Micro. Theo. Tech.*, vol. MTT-32, no. 8, Aug. 1984, pp. 730-746.
- [51] D.E. Livesey and K.M. Chen, "Electromagnetic fields induced inside arbitrary shaped biological bodies," *IEEE Trans. Micro. Theo. Tech.*, vol. MTT-22, no. 12, Dec. 1974, pp. 1273-1280.
- [52] J.A. Kong (ed.), *Research Topics in Electromagnetic Theory*. New York: John Wiley, 1981, pp. 290-355.
- [53] C.T. Tai, *Dyadic Green's Functions in Electromagnetic Theory*. Scranton, PA: Intex Educational Pub., 1971, pp. 46-54.

- [54] J. Van Bladel, "Some remarks on Green's dyadic infinite space," *IRE Trans. Ant. Prog.*, vol. AP-9, Nov. 1961, pp. 563-566.
- [55] B.S. Guru and K.M. Chen, "A computer program for calculating the induced EM field inside an irradiated body," Dept. of Electrical Engineering and System Science, Michigan State Univ., East Lansing, MI 48824, 1976.
- [56] K.M. Chen and B.S. Guru, "Internal EM field and absorbed power density in human torsos induced by 1-500 MHz EM waves," *IEEE Micro. Theo. Tech.*, vol. MTT-25, no. 9, Sept. 1977, pp. 746-756.
- [57] R. Ruksopollmuang and K.M. Chen, "Heating of spherical versus realistic models of human and infrahuman heads by electromagnetic waves," *Radio Sci.*, vol. 14, no. 6S, Nov.-Dec., 1979, pp. 51-62.
- [58] R. Jongakiem, "Electromagnetic absorption in biological bodies," *M.Sc. Thesis*, Dept. of Electrical and Computer Engineering, Florida Atlantic Univ., Boca Raton, Aug. 1988.
- [59] O.P. Gandhi, "Electromagnetic absorption in an inhomogeneous model of man for realistic exposure conditions," *Bioelectromagnetics*, vol. 3, 1982, pp. 81-90.
- [60] O.P. Gandhi et al., "Part-body and multibody effects on absorption of radio-frequency electromagnetic energy by animals and by models of man," *Radio Sci.*, vol. 14, no. 6S, Nov.-Dec., 1979, pp. 15-21.
- [61] M.J. Hagmann, O.P. Gandhi, and C.H. Durney, "Numerical calculation of electromagnetic energy deposition for a realistic model of man," *IEEE Trans. Micro. Theo. Tech.*, vol. MTT-27, no. 9, Sept. 1979, pp. 804-809.
- [62] J.J. Wang, "Generalized moment methods in electromagnetics," *IEEE Proc.*, vol. 137, Pt. H, no. 2, April 1990, pp. 127-132.
- [63] G. Goertzel and N. Tralli, *Some Mathematical Methods of Physics*. New York: McGraw-Hill, 1960.
- [64] W.V. Lovitt, *Linear Integral Equations*. New York: Dover Publ., 1950.
- [65] C.D. Green, *Integral Equation Methods*. New York: Barnes & Noble, 1969.
- [66] R.F. Harrington et al., "Computation of Laplacian potentials by an equivalent source method," *Proc. IEEE*, vol. 116, no. 10, Oct. 1969, pp. 1715-1720.
- [67] J.R. Mautz and R.F. Harrington, "Computation of rotationally symmetric Laplacian," *Proc. IEEE*, vol. 117, no. 4, April 1970, pp. 850-852.
- [68] S.M. Rao et al., "A simple numerical solution procedure for static problems involving arbitrary-shaped surfaces," *IEEE Trans. Ant. Prog.*, vol. AP-27, no. 5, Sept. 1979, pp. 604-608.
- [69] K. Adamiak, "Application of integral equations for solving inverse problems in stationary electromagnetic fields," *Int. J. Num. Meth. Engr.*, vol. 21, 1985, pp. 1447-1485.

- [70] A.W. Glisson, "An integral equation for electromagnetic scattering from homogeneous dielectric bodies," *IEEE Trans. Ant. Prog.*, vol. AP-33, no. 2, Sept. 1984, pp. 172-175.
- [71] E. Max, "Integral equation for scattering by a dielectric," *IEEE Trans. Ant. Prog.*, vol. AP-32, no. 2, Feb. 1984, pp. 166-172.
- [72] A.T. Adams et al., "Near fields of wire antennas by matrix methods," *IEEE Trans. Ant. Prog.*, vol. AP-21, no. 5, Sept. 1973, pp. 602-610.
- [73] R.F. Harrington and J.R. Mautz, "Electromagnetic behavior of circular wire loops with arbitrary excitation and loading," *Proc. IEEE*, vol. 115, Jan. 1969, pp. 68-77.
- [74] S.A. Adekola and O.U. Okereke, "Analysis of a circular loop antenna using moment methods," *Int. J. Elect.*, vol. 66, no. 5, 1989, pp. 821-834.
- [75] E.K. Miller et al., "Computer evaluation of large low-frequency antennas," *IEEE Trans. Ant. Prog.*, vol. AP-21, no. 3, May 1973, pp. 386-389.
- [76] K.S.H. Lee et al., "Limitations of wire-grid modeling of a closed surface," *IEEE Trans. Elect. Comp.*, vol. EMC-18, no. 3, Aug. 1976, pp. 123-129.
- [77] E.H. Newman and D.M. Pozar, "Considerations for efficient wire/surface modeling," *IEEE Trans. Ant. Prog.*, vol. AP-28, no. 1, Jan. 1980, pp. 121-125.
- [78] J. Perini and D.J. Buchanan, "Assessment of MOM techniques for shipboard applications," *IEEE Trans. Elect. Comp.*, vol. EMC-24, no. 1, Feb. 1982, pp. 32-39.
- [79] J.R. Mautz and R.F. Harrington, "Radiation and scattering from bodies of revolution," *Appl. Sci. Res.*, vol. 20, June 1969, pp. 405-435.
- [80] A.W. Glisson and C.M. Butler, "Analysis of a wire antenna in the presence of a body of revolution," *IEEE Trans. Ant. Prog.*, vol. AP-28, Sept. 1980, pp. 604-609.
- [81] J.H. Richmond, "A wire-grid model for scattering by conducting bodies," *IEEE Trans. Ant. Prog.*, vol. AP-14, Nov. 1966, pp. 782-786.
- [82] S.M. Rao et al., "Electromagnetic scattering by surfaces of arbitrary shape," *IEEE Trans. Ant. Prog.*, vol. AP-30, May 1966, pp. 409-418.
- [83] A. Farrar and A.T. Adams, "Matrix methods for microstrip three-dimensional problems," *IEEE Trans. Micro. Theo. Tech.*, vol. MTT-20, no. 8, Aug. 1972, pp. 497-505.
- [84] A. Farrar and A.T. Adams, "Computation of propagation constants for the fundamental and higher-order modes in microstrip," *IEEE Trans. Micro. Theo. Tech.*, vol. MTT-24, no. 7, July 1972, pp. 456-460.

- [85] A. Farrar and A.T. Adams, "Characteristic impedance of microstrip by the method of moments," *IEEE Trans. Micro. Theo. Tech.*, vol. MTT-18, no. 1, Jan 1970, pp. 68, 69.
- [86] A. Farrar and A.T. Adams, "Computation of lumped microstrip capacitance by matrix methods—rectangular sections and end effects," *IEEE Trans. Micro. Theo. Tech.*, vol. MTT-19, no. 5, May 1971, pp. 495, 496.
- [87] R.F. Harrington and J.R. Mautz, "A generalized network formulation for aperture problems," *IEEE Trans. Ant. Prog.*, vol. AP-24, Nov. 1976, pp. 870–873.
- [88] R.H. Harrington and D.T. Auckland, "Electromagnetic transmission through narrow slots in thick conducting screens," *IEEE Trans. Ant. Prog.*, vol. AP-28, Sept. 1980, pp. 616–622.
- [89] C.M. Butler and K.R. Umashankar, "Electromagnetic excitation of a scatterer coupled to an aperture in a conducting screen," *Proc. IEEE*, vol. 127, Pt. H, June 1980, pp. 161–169.
- [90] Special issue on electromagnetic wave interactions with biological systems, *IEEE Trans. Micro. Theo. Tech.*, vol. MTT-32, no. 8, Aug. 1984.
- [91] Special issue on effects of electromagnetic radiation, *IEEE Engr. Med. Biol. Mag.*, March 1987.
- [92] Helsinki symposium on biological effects of electromagnetic radiation, *Radio Sci.*, vol. 17, no. 5S, Sept.-Oct. 1982.
- [93] R.M. Bevensee, "Computer codes for EMP interaction and coupling," *IEEE Trans. Ant. Prog.*, vol. AP-26, no. 1, Jan. 1978, pp. 156–165.
- [94] G.J. Burke and A.J. Poggio, *Numerical Electromagnetic Code (NEC)—Method of Moments*. Lawrence Livermore National Lab., Livermore, CA, Jan. 1981.
- [95] J.W. Rockway et al., *The MININEC System: Microcomputer Analysis of Wire Antennas*. Norwood, MA: Artech House, 1988.
- [96] R. Mittra (ed.), *Numerical and Asymptotic Techniques in Electromagnetics*. New York: Springer-Verlag, 1975.
- [97] G.L. James, *Geometrical Theory of Diffraction for Electromagnetic Waves*, 3rd ed. London: Peregrinus, 1986.

PROBLEMS

$$(a) \Phi(x) = \frac{5x}{6} + \frac{1}{2} \int_0^1 xt\Phi(t)dt \quad [\text{solution } \Phi(x) = x],$$

$$(b) \Phi(x) = \cos x - \sin x + 2 \int_0^x \sin(x-t)\Phi(t)dt \quad [\text{solution } \Phi(x) = e^{-x}],$$

$$(c) \Phi(x) = -\cosh x + \lambda \int_{-1}^1 \cosh(x+t)\Phi(t)dt$$

$$\left[\frac{\cosh x}{\frac{\lambda}{2} \sinh 2 + \lambda - 1} \right]$$

solution $\Phi(x) =$

5.2 Classify the following integral equations:

$$(a) u(x) = \int_{-\infty}^{\infty} e^{ix\lambda} u(\lambda)d\lambda$$

$$(b) u(x) = e^x - \lambda \int_0^1 G(x,y)u(y)dy$$

$$(c) u(x) = \int_x^1 \frac{f(\lambda)d\lambda}{(\lambda^2 - x^2)^{1/2}}$$

$$(d) u(x) = \sin x + 2 \int_0^x \cos(x-y)u(y)dy$$

5.3 Solve the following Volterra integral equations:

$$(a) \Phi(x) = 5 + 2 \int_0^x t\Phi(t)dt,$$

$$(b) \Phi(x) = x + \int_0^x (t-x)\Phi(t)dt$$

5.4 Find the integral equation corresponding to each of the following differential equations:

$$(a) y'' = -y, \quad y(0) = 0, \quad y'(1) = 1,$$

$$(b) y'' + y = \cos x, \quad y(0) = 0, \quad y'(0) = 1$$

5.5 Construct the Green's function for the differential equation

$$G_{xx} + k^2 G = -\delta(x-x'), \quad 0 < x < a$$

subject to $G(0) = G(a) = 0$

5.6 Show that

$$G(x, z; x', z') = \frac{j}{a} \sum_{n=1}^{\infty} \frac{\sin(n\pi x/a) \sin(n\pi x'/a)}{k_n} e^{jk_n(z-z')},$$

where $k_n^2 = k^2 - (n\pi/a)^2$ is the Green's function for Helmholtz's equation.

Problems

- 5.1 Classify the following integral equations and show that they have the stated solutions:

- 5.7 Derive the Green's function for

$$\nabla^2 \Phi = f, \quad 0 < x, y < 1$$

subject to zero boundary conditions.

- 5.8 Find the Green's function satisfying

$$G_{xx} + G_{yy} + 2G_x = \delta(x - x')\delta(y - y'), \quad 0 < x < a, 0 < y < b$$

and

$$G(0, y) = G(a, y) = G(x, 0) = G(x, b) = 0$$

- 5.9 (a) Verify by Fourier expansion that Equations (5.79) and (5.80) in Example 5.5 are equivalent.
 (b) Show that another form of expressing Equation (5.79) is

$$G(x, y; x', y') = \begin{cases} -\frac{2}{\pi} \sum_{m=1}^{\infty} \sinh \frac{m\pi(b-y')}{a} \sin \frac{m\pi y}{a} \frac{m\pi x}{a} \frac{m\pi x'}{a}, & y < y' \\ -\frac{2}{\pi} \sum_{m=1}^{\infty} \sinh \frac{m\pi y'}{a} \sin \frac{m\pi(b-y)}{a} \frac{m\pi x}{a} \frac{m\pi x'}{a}, & y > y' \end{cases}$$

- 5.10 The two-dimensional delta function expressed in cylindrical coordinates reads

$$\delta(\rho - \rho') = \frac{1}{\rho} \delta(\rho - \rho') \delta(\phi - \phi')$$

Obtain the Green's function for the potential problem

$$\nabla^2 G = \frac{1}{\rho} \delta(\rho - \rho') \delta(\phi - \phi')$$

with the region defined in Figure 5.33. Assume homogeneous Dirichlet boundary conditions.

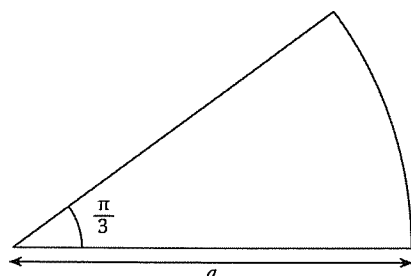


Figure 5.33
For Problem 5.10.

- 5.11 Consider the transmission line with cross section as shown in Figure 5.34. In a TEM wave approximation, the potential distribution satisfies Poisson's equation

$$\nabla^2 V = -\frac{\rho_s}{\epsilon}$$

subject to the following continuity and boundary conditions:

$$\begin{aligned} \frac{\partial}{\partial x} V(x, h_1 - 0) &= \frac{\partial}{\partial x} V(x, h_1 + 0) \\ \frac{\partial}{\partial x} V(x, h_1 + h_2 - 0) &= \frac{\partial}{\partial x} V(x, h_1 + h_2 + 0) \\ \epsilon_1 \frac{\partial}{\partial y} V(x, h_1 - 0) &= \epsilon_2 \frac{\partial}{\partial y} V(x, h_1 + 0) \\ \epsilon_2 \frac{\partial}{\partial y} V(x, h_1 + h_2 - 0) &= \epsilon_3 \frac{\partial}{\partial y} V(x, h_1 + h_2 + 0) - \rho_s(x, h_1 + h_2) \\ V(0, y) = V(a, y) = V(x, 0) = V(x, b) &= 0 \end{aligned}$$

Using series expansion method, evaluate the Green's function at $y = h_1 + h_2$, i.e., $G(x, y; x', h_1 + h_2)$.

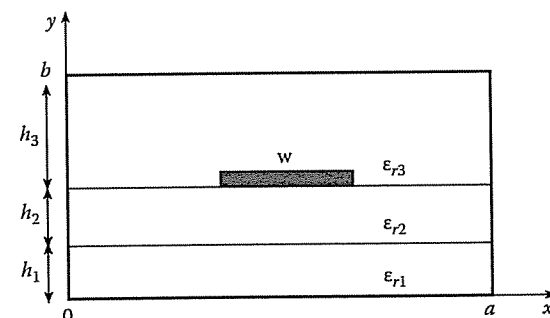


Figure 5.34
For Problem 5.11.

- 5.12 Show that the free-space Green's function for $L = \nabla^2 + k^2$ in two-dimensional space is $-\frac{i}{4} H_0^{(1)}(k\rho)$.

- 5.13 The spherical Green's function $h_0^{(2)}(|\mathbf{r} - \mathbf{r}'|)$ can be expanded in terms of spherical Bessel functions and Legendre polynomials. Show that

$$h_0^{(2)}(|\mathbf{r} - \mathbf{r}'|) = \begin{cases} \sum_{n=0}^{\infty} (2n+1) h_n^2(r') j_n(r) P_n(\cos\alpha), & r < r' \\ \sum_{n=0}^{\infty} (2n+1) h_n^2(r) j_n(r') P_n(\cos\alpha), & r > r' \end{cases}$$

where $\cos\alpha = \cos\theta \cos\theta' + \sin\theta \sin\theta' \cos(\phi - \phi')$. From this, derive the plane wave expansion

$$e^{-j\mathbf{k}\cdot\mathbf{r}} = \sum_{n=0}^{\infty} (-j)^n (2n+1) j_n(kr) P_n(\cos\alpha)$$

- 5.14 Given the kernel

$$K(x, y) = \begin{cases} (1-x)y, & 0 \leq y \leq x \leq 1 \\ (1-y)x, & 0 \leq x \leq y \leq 1 \end{cases}$$

Show that

$$K(x, y) = 2 \sum_{n=1}^{\infty} \frac{\sin n\pi x \sin n\pi y}{n^2 \pi^2}$$

and that

$$\frac{\pi^2}{4} = \sum_{n=1}^{\infty} \frac{1}{n^2}$$

- 5.15 Derive the closed form solution for Poisson's equation

$$\nabla^2 V = g$$

in the quarter-plane shown in Figure 5.35 with

$$V = f(x), \quad y = 0, \quad \frac{\partial V}{\partial x} = h(y), \quad x = 0$$

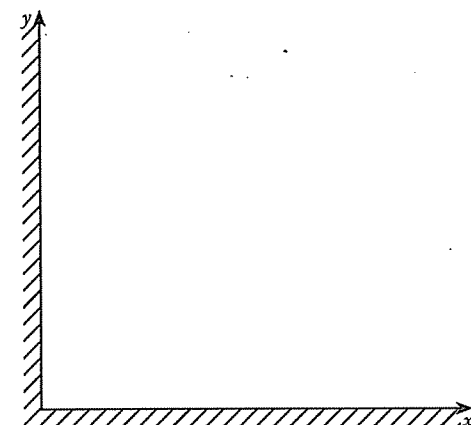


Figure 5.35
For Problem 5.15.

- 5.16 Consider the cross section of a microstrip transmission line shown in Figure 5.36. Let $G_{ij}\rho_j$ be the potential at the field point i on the center conductor due to the charge on subsection j . (It is assumed that the charge is concentrated in the filament along the center of the subsection.) G_{ij} is the Green's function for this problem and is given by

$$G_{ij} = \frac{1}{4\pi\epsilon_r} \sum_{n=1}^{\infty} \left[k^{2(n-1)} \ln \frac{A_{ij}^2 + (4n-2)^2}{A_{ij}^2 + (4n-4)^2} + k^{2n-1} \ln \frac{A_{ij}^2 + (4n-2)^2}{A_{ij}^2 + (4n)^2} \right]$$

where

$$A_{ij} = \frac{\Delta}{H} |2(i-1) - 2(j-1) - 1|, \quad k = \frac{\epsilon_r - 1}{\epsilon_r + 1},$$

$\Delta = W/N$, and N is the number of equal subsections into which the center conductor is divided. By setting the potential equal to unity on the center conductor, one can find

$$C = \sum_{j=1}^{\infty} \rho_j \quad (\text{farads/m})$$

and

$$Z_o = \frac{1}{c\sqrt{C_o C}}$$

where $c = 3 \times 10^8$ m/s and C_o is the capacitance per unit length for an air-filled transmission line (i.e., set $k = 1$ in G_{ij}). Find Z_o for $N = 30$ and

- (a) $\epsilon_r = 6.0$, $W = 4 \text{ cm}$, $H = 4 \text{ cm}$
 (b) $\epsilon_r = 16.0$, $W = 8 \text{ cm}$, $H = 4 \text{ cm}$.

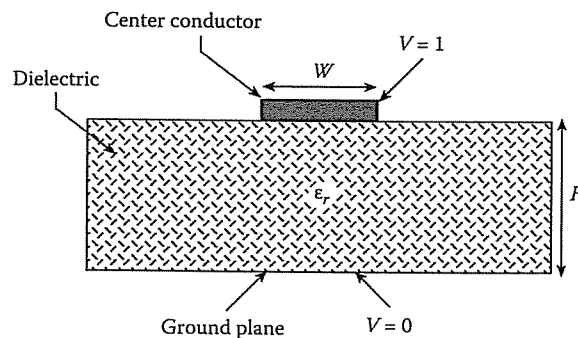


Figure 5.36
For Problem 5.16.

- 5.17 Consider the three-charge model shown in Figure 5.37. The radius of each charged sphere is a and the separation distances are equal; i.e. $d_1 = d_2 = d$. The potential system results in

$$\begin{bmatrix} +V \\ 0 \\ -V \end{bmatrix} = \frac{1}{4\pi\epsilon_0} \begin{bmatrix} \frac{1}{a} & \frac{1}{d} & \frac{1}{2d} \\ \frac{1}{d} & \frac{1}{a} & \frac{1}{d} \\ \frac{1}{2d} & \frac{1}{d} & \frac{1}{a} \end{bmatrix} \begin{bmatrix} Q_1 \\ Q_2 \\ Q_3 \end{bmatrix}$$

Let $V = 1$, $a/d = 1/10$. Use MATLAB to compute Q_1 , Q_2 , and Q_3 in terms of $4\pi\epsilon_0 d$.

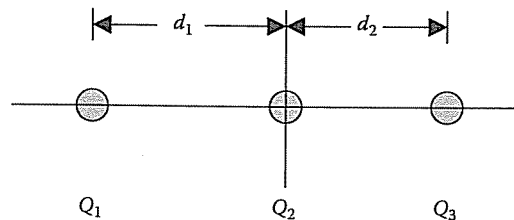


Figure 5.37
For Problem 5.17.

PROBLEMS

- 5.18 Consider the sheet model for representing the p-n junction as shown in Figure 5.38. In matrix form,

$$\begin{bmatrix} V(-2d) \\ V(-d) \\ V(0) \\ V(+d) \\ V(+2d) \end{bmatrix} = \frac{-d}{2\epsilon} \begin{bmatrix} 0 & 1 & 2 & 3 & 2 \\ 1/2 & 0 & 1 & 2 & 3/2 \\ 1 & 1 & 0 & 1 & 1 \\ 3/2 & 2 & 1 & 0 & 1/2 \\ 2 & 3 & 2 & 1 & 0 \end{bmatrix} \begin{bmatrix} \sigma_1 \\ \sigma_2 \\ \sigma_3 \\ \sigma_4 \\ \sigma_5 \end{bmatrix}$$

Let $V(-2d) = -2$, $V(-d) = -1.5$, $V(0) = 0$, $V(+d) = 1.5$, $V(+2d) = 2$. Using MATLAB, obtain the charges $\sigma_1, \sigma_2, \sigma_3, \sigma_4$, and σ_5 .

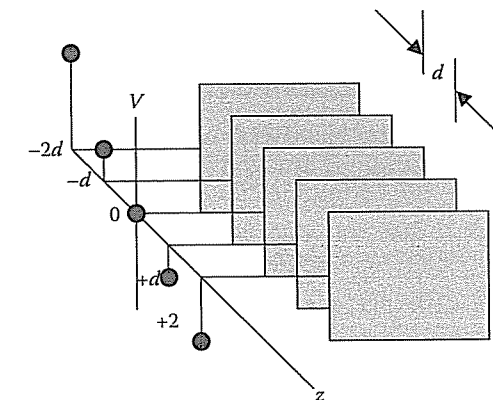


Figure 5.38
For Problem 5.18.

- 5.19 A rectangular section of microstrip transmission line of length L , width W , and height H above the ground plane is shown in Figure 5.39. The section is subdivided into N subsections. A typical subsection ΔS_j , of sides Δx_j and Δy_j , is assumed to bear a uniform surface charge density ρ_j . The potential V_i at ΔS_i due to a uniform charge density ρ_j on ΔS_j ($j = 1, 2, \dots, N$) is

$$V_i = \sum_{j=1}^N G_{ij} \rho_j$$

where

$$\begin{aligned}
 G_{ij} = & \sum_{n=1}^{\infty} \frac{k^{n-1}(-1)^{n+1}}{2\pi\epsilon_0(\epsilon_r + 1)} \\
 & \left[(x_j - x_i) \ln \frac{(y_j - y_i) + \sqrt{(x_j - x_i)^2 + (y_j - y_i)^2 + (2n-2)^2 H^2}}{(y_j + \Delta y_j - y_i) + \sqrt{(x_j - x_i)^2 + (y_j + \Delta y_j - y_i)^2 + (2n-2)^2 H^2}} \right. \\
 & + (x_j + \Delta x_j - x_i) \\
 & \ln \frac{(y_j + \Delta y_j - y_i) + \sqrt{(x_j + \Delta x_j - x_i)^2 + (y_j + \Delta y_j - y_i)^2 + (2n-2)^2 H^2}}{(y_j - y_i) + \sqrt{(x_j + \Delta x_j - x_i)^2 + (y_j - y_i)^2 + (2n-2)^2 H^2}} \\
 & + (y_j - y_i) \ln \frac{(x_j - x_i) + \sqrt{(x_j - x_i)^2 + (y_j - y_i)^2 + (2n-2)^2 H^2}}{(x_j + \Delta x_j - x_i) + \sqrt{(x_j + \Delta x_j - x_i)^2 + (y_j - y_i)^2 + (2n-2)^2 H^2}} \\
 & + (y_j + \Delta y_j - y_i) \\
 & \ln \frac{(x_j + \Delta x_j - x_i) + \sqrt{(x_j + \Delta x_j - x_i)^2 + (y_j + \Delta y_j - y_i)^2 + (2n-2)^2 H^2}}{(x_j - x_i) + \sqrt{(x_j - x_i)^2 + (y_j + \Delta y_j - y_i)^2 + (2n-2)^2 H^2}} \\
 & - (2n-2)H \tan^{-1} \frac{(x_j - x_i)(y_j - y_i)}{(2n-2)H \sqrt{(x_j - x_i)^2 + (y_j - y_i)^2 + (2n-2)^2 H^2}} \\
 & - (2n-2) \\
 & H \tan^{-1} \frac{(x_j + \Delta x_j - x_i)(y_j + \Delta y_j - y_i)}{(2n-2)H \sqrt{(x_j + \Delta x_j - x_i)^2 + (y_j + \Delta y_j - y_i)^2 + (2n-2)^2 H^2}} \\
 & + (2n-2)H \tan^{-1} \frac{(x_j - x_i)(y_j + \Delta y_j - y_i)}{(2n-2)H \sqrt{(x_j - x_i)^2 + (y_j + \Delta y_j - y_i)^2 + (2n-2)^2 H^2}} \\
 & \left. + (2n-2)H \tan^{-1} \frac{(x_j + \Delta x_j - x_i)(y_j - y_i)}{(2n-2)H \sqrt{(x_j + \Delta x_j - x_i)^2 + (y_j - y_i)^2 + (2n-2)^2 H^2}} \right]
 \end{aligned}$$

and $k = \frac{\epsilon_r - 1}{\epsilon_r + 1}$. If the ground plane is assumed to be at zero potential while the conducting strip at 1 V potential, we can find

$$C = \sum_{j=1}^N \rho_j$$

Find C for

- (a) $\epsilon_r = 9.6$, $W = L = H = 2$ cm,
- (b) $\epsilon_r = 9.6$, $W = H = 2$ cm, $L = 1$ cm.

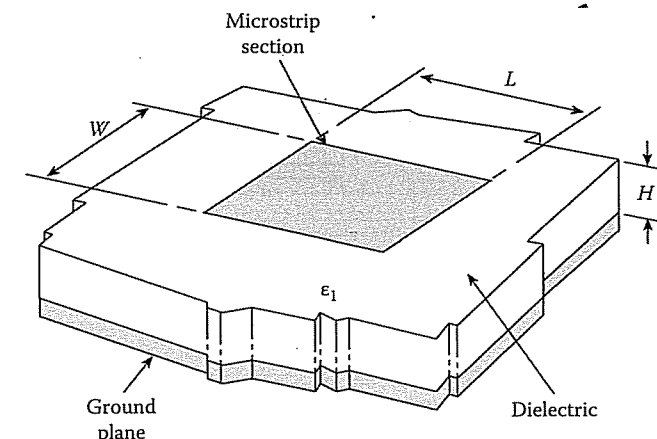


Figure 5.39

For Problem 5.19.

- 5.20 For a conducting elliptic cylinder with cross section in Figure 5.40(a), write a program to determine the scattering cross section $\sigma(\phi_i, \phi)$ due to a plane TM wave. Consider $\phi = 0^\circ, 10^\circ, \dots, 180^\circ$ and cases $\phi_i = 0^\circ, 30^\circ$, and 90° . Plot $\sigma(\phi_i, \phi)$ against ϕ for each ϕ_i . Take $\lambda = 1$ m, $2a = \lambda/2$, $2b = \lambda$, $N = 18$.

Hint: Due to symmetry, consider only one half of the cross section as in Figure 5.40(b). An ellipse is described by

$$\frac{x^2}{a^2} + \frac{y^2}{b^2} = 1$$

With $x = r \cos \phi$, $y = r \sin \phi$, it is readily shown that

$$r = \frac{a}{\sqrt{\cos^2 \phi + v^2 \sin^2 \phi}}, \quad v = a/b, \quad dl = rd\phi.$$

- 5.21 Use the program in Figure 5.15 (or develop your own program) to calculate the scattering pattern for each array of parallel wires shown in Figure 5.41.
- 5.22 Repeat Problem 5.20 using the techniques of Section 5.5.2. That is, consider the cylinder in Figure 5.41(a) as an array of parallel wires.
- 5.23 Consider the scattering problem of a dielectric cylinder with cross section shown in Figure 5.42. It is illuminated by a TM wave. To obtain the field $[E]$ inside the dielectric cylinder, MOM formulation leads to the matrix equation

$$[A][E] = [E^i]$$

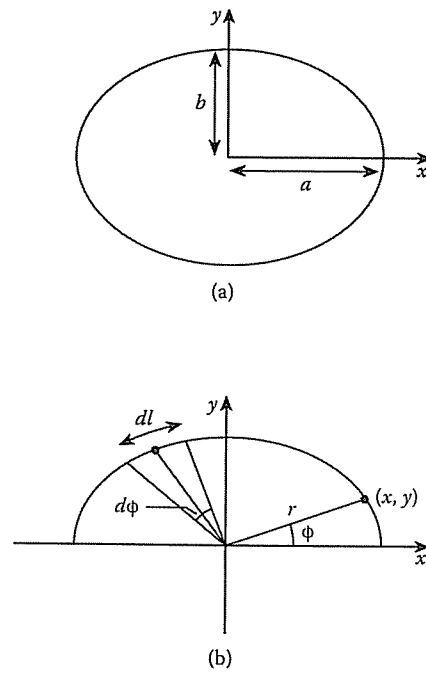


Figure 5.40
For Problem 5.20.

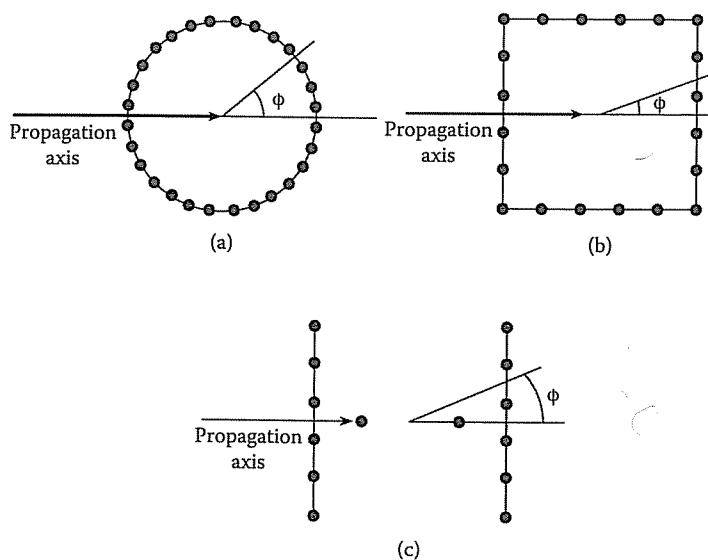


Figure 5.41
Arrays of parallel wires: (a) cylinder, (b) square, (c) I-beam, for Problem 5.21.

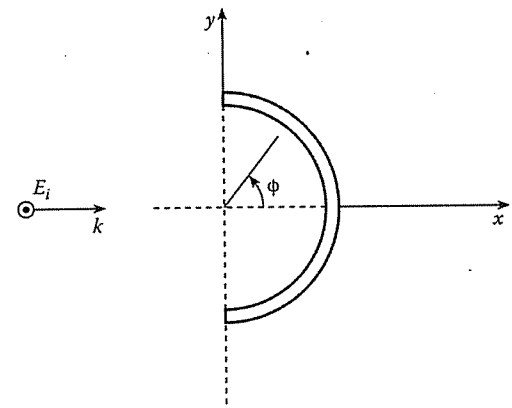


Figure 5.42
For Problem 5.23.

where

$$A_{mn} = \begin{cases} \epsilon_m + j\frac{\pi}{2}(\epsilon_m - 1)ka_n H_1^{(2)}(ka_m), & m = n \\ j\frac{\pi}{2}(\epsilon_m - 1)ka_n J_1(ka_n)H_0^{(2)}(k\rho_{mn}), & m \neq n \end{cases}$$

$$E_m^i = e^{jk(x_m \cos \phi_i + y_m \sin \phi_i)}$$

$$\rho_{mn} = \sqrt{(x_m - x_n)^2 + (y_m - y_n)^2}, \quad m, n = 1, 2, \dots, N$$

N is the number of cells the cylinder is divided into, ϵ_m is the average dielectric constant of cell m , a_m is the radius of the equivalent circular cell which has the same cross section as cell m . Solve the above matrix equation and obtain E_n , $n = 1, 2, \dots, N$. Use E_n to obtain the echo width of the dielectric cylinder, i.e.,

$$W(\phi) = \frac{\pi^2 k}{|E^i|^2} \left| \sum_{n=1}^N (\epsilon_n - 1) E_n a_n J_1(ka_n) e^{jk(x_n \cos \phi + y_n \sin \phi)} \right|^2$$

for $\phi = 0^\circ, 5^\circ, 10^\circ, \dots, 180^\circ$. Plot $W(\phi)$ versus ϕ . For the dielectric cylinder, take $\mu = \mu_o$, $\epsilon = 4\epsilon_o$, inner radius is 0.25λ , outer radius is 0.4λ , and $\lambda = 1\text{m}$.

5.24 The integral equation

$$-\frac{1}{2\pi} \int_{-w}^w I(z') \ln |z - z'| dz' = f(z), \quad -w < z < w$$

can be cast into matrix equation

$$[S][I] = [F]$$

using pulse basis function and delta expansion function (point matching).

(a) Show that

$$S_{mn} = \frac{\Delta}{2\pi} \left[1 - \ln \Delta - \frac{1}{2} \ln \left| (m-n)^2 - \frac{1}{4} \right| - (m-n) \ln \frac{|m-n+1/2|}{|m-n-1/2|} \right]$$

$$F_n = f(z_n)$$

where $z_n = -w + \Delta(n - 1/2)$, $n = 1, 2, \dots, N$, $\Delta = 2w/N$. Note that $[S]$ is a Toeplitz matrix having only N distinct elements.

(b) Determine the unknowns $\{I_m\}$ with $f(z) = 1$, $N = 10$, $2w = 1$.

(c) Repeat part (b) with $f(z) = z$, $N = 10$, $2w = 1$.

- 5.25 For a dipole antenna $[Z] [I] = [V]$ or

$$\begin{bmatrix} 0.9869 - j3324 & 0.4935 + j1753 \\ 0.9869 + j3506 & 2.576 - j1849 \end{bmatrix} \begin{bmatrix} I_1 \\ I_2 \end{bmatrix} = \begin{bmatrix} 0.02505 \\ 0.02505 \end{bmatrix}$$

Obtain the current vector.

- 5.26 Derive Equation (5.141) from Equation (5.135).

- 5.27 A two-term representation of the current distribution on a thin, center-fed half-wavelength dipole antenna is given by

$$I(z) = \sum_{n=1}^2 B_n \sin \left(\frac{2\pi n}{\lambda} (\lambda/4 - |z|) \right)$$

Substituting this into Hallen's integral equation gives

$$\sum_{n=1}^2 B_n \int_{-\lambda/4}^{\lambda/4} \sin \left[\frac{2\pi n}{\lambda} (\lambda/4 - |z'|) \right] G(z, z') dz' + \frac{jC_1}{\eta_o} \cos k_o z$$

$$= -\frac{j}{\eta_o} V_T \sin k_o |z|$$

where $\eta_o = 120\pi$, $k_o = \frac{2\pi}{\lambda} = \frac{2\pi f}{c}$, and $G(z, z')$ is given by Equation (5.152).

Taking $V_T = 1$ volt, $\lambda = 1$ m, $a/\lambda = 7.022 \times 10^{-3}$, and match points at $z = 0, \lambda/8, \lambda/4$, determine the constants B_1, B_2 , and C_1 . Plot the real and imaginary parts of $I(z)$ against z .

- 5.28 Using Hallen's IE, determine the current distribution $I(z)$ on a straight dipole of length ℓ . Plot $|I| = |I_r + jI_i|$ against z . Assume excitation by a unit voltage, $N = 51$, $\Omega = 2 \ln \frac{\ell}{a} = 12.5$, and consider cases (a) $\ell = \lambda/2$, (b) $\ell = 1.5\lambda$.

- 5.29 (a) Show that Pocklington integral equation (5.141) can be written as

$$-E_z^i = \frac{\lambda \sqrt{\mu/\epsilon}}{8j\pi a^2} \int_{-\ell/2}^{\ell/2} \frac{I(z') e^{-jkR}}{R^5} [(1 + jkR)(2R^2 - 3a^2) + k^2 a^2 R^2] dz'$$

(b) By changing variables, $z' - z = a \tan \theta$, show that

$$-E_z^i = \frac{\lambda \sqrt{\mu/\epsilon}}{8j\pi^2 a^2} \int_{\theta_1}^{\theta_2} I(\theta') e^{-jka/\cos \theta'} \cdot [(jka + \cos \theta') (2 - 2 \cos^2 \theta') + k^2 a^2 \cos \theta'] d\theta'$$

where $\theta_1 = -\tan^{-1} \frac{\ell/2 + z}{a}$, $\theta_2 = \tan^{-1} \frac{\ell/2 - z}{a}$.

- 5.30 Using the program in Figure 5.26 (or your own self-developed program), calculate the electric field inside a thin conducting layer ($\mu = \mu_o$, $\epsilon = 70\epsilon_o$, $\sigma = 1$ mho/m) shown in Figure 5.43. Assume plane wave with electric field perpendicular to the plane of the layer, i.e.,

$$\mathbf{E}^i = e^{-jk_o z} \mathbf{a}_x \quad \text{V/m}$$

where $k_o = 2\pi f/c$. Consider only one half of the layer. Calculate $|E_x|/|E^i|$ and neglect E_y and E_z at the center of the cells since they are very small compared with E_x . Take $a = 0.5$ cm, $b = 4$ cm, $c = 6$ cm.

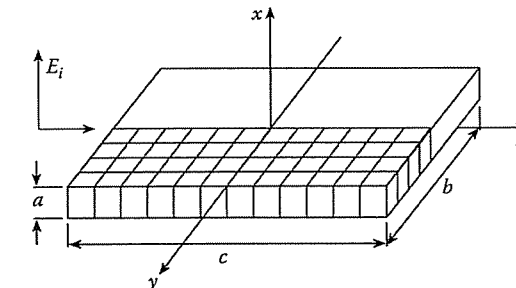


Figure 5.43
For Problem 5.30.

- 5.31 Consider an adult torso with a height 1.7 m and a shape shown in Figure 5.44. If the torso is illuminated by a vertically polarized EM wave of 80 MHz with an incident electric field of 1 V/m, calculate the absorbed power density given by

$$\frac{\sigma}{2} (E_x^2 + E_y^2 + E_z^2)$$

at the center of each cell. Take $\mu = \mu_o$, $\epsilon = 80\epsilon_o$, $\sigma = 0.84$ mhos/m.

- 5.32 Suppose the dielectric cylinder in Problem 5.23 is a biological body modeled by a cylinder of cross-section 75×50 cm 2 , shown in Figure 5.45. A TM wave of frequency $f = 300$ MHz is normally incident on the body. Compute the

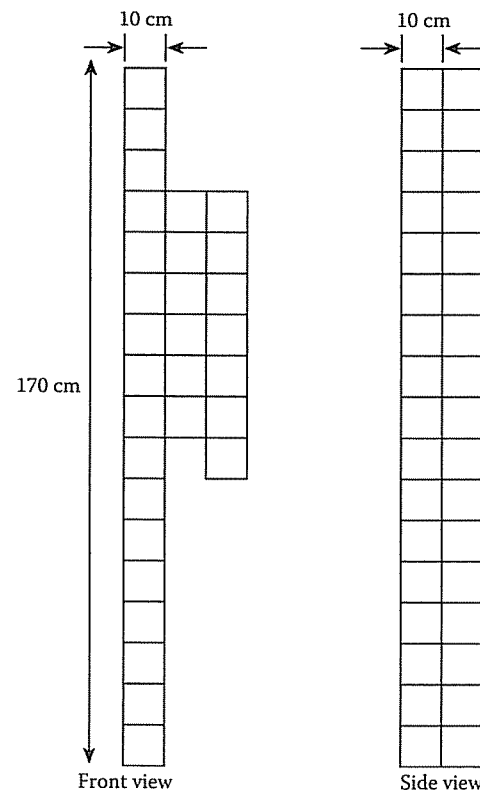


Figure 5.44
An adult torso: for Problem 5.31.

fields inside the body using the MOM formulation of Problem 5.23. In this case, take ϵ_m as complex permittivity of cell m , i.e.,

$$\epsilon_m = \epsilon_{rm} - j(\sigma_m/\omega\epsilon_0), \quad m = 1, 2, \dots, N = 150$$

To make the body inhomogeneous, take $\epsilon_{rm} = 8$ and $\sigma_m = 0.03$ for cells 65, 66, 75, 85, and 86; take $\epsilon_{rm} = 7$ and $\sigma_m = 0.04$ for cells 64, 67, 74, 77, 84, and 87; and take $\epsilon_{rm} = 5$ and $\sigma_m = 0.02$ for all the other cells. Compute E_n .

E_i
④ k

141	142	143	144	145	146	147	148	149	150
131									140
121									130
111									120
101									110
91									100
81			84	85	86	87			90
71			74	75	76	77			80
61			64	65	66	67			70
51									60
41									50
31									40
21									30
11									20
1	2	3	4	5	6	7	8	9	10

Figure 5.45
For Problem 5.32.

Chapter 6

Finite Element Method

The ultimate measure of a man is not where he stands in moments of comfort and convenience, but where he stands at times of challenge and controversy.

- Martin Luther King, Jr.

6.1 Introduction

The finite element method (FEM) has its origin in the field of structural analysis. Although the earlier mathematical treatment of the method was provided by Courant [1] in 1943, the method was not applied to electromagnetic (EM) problems until 1968. Since then the method has been employed in diverse areas such as waveguide problems, electric machines, semiconductor devices, microstrips, and absorption of EM radiation by biological bodies.

Although the finite difference method (FDM) and the method of moments (MOM) are conceptually simpler and easier to program than the FEM, FEM is a more powerful and versatile numerical technique for handling problems involving complex geometries and inhomogeneous media. The systematic generality of the method makes it possible to construct general-purpose computer programs for solving a wide range of problems. Consequently, programs developed for a particular discipline have been applied successfully to solve problems in a different field with little or no modification [2].

The finite element analysis of any problem involves basically four steps [3]:

- discretizing the solution region into a finite number of *subregions* or *elements*,
- deriving governing equations for a typical element,
- assembling of all elements in the solution region, and
- solving the system of equations obtained.

Discretization of the continuum involves dividing up the solution region into sub-domains, called *finite elements*. Figure 6.1 shows some typical elements for one-, two-, and three-dimensional problems. The problem of discretization will be fully treated in Sections 6.5 and 6.6. The other three steps will be described in detail in the subsequent sections.

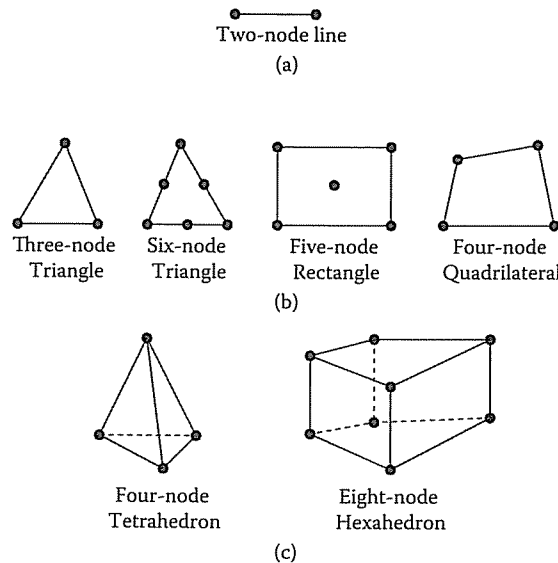


Figure 6.1
Typical finite elements: (a) One-dimensional, (b) two-dimensional, (c) three-dimensional.

6.2 Solution of Laplace's Equation

As an application of FEM to electrostatic problems, let us apply the four steps mentioned above to solve Laplace's equation, $\nabla^2 V = 0$. For the purpose of illustration, we will strictly follow the four steps mentioned above.

6.2.1 Finite Element Discretization

To find the potential distribution $V(x, y)$ for the two-dimensional solution region shown in Figure 6.2(a), we divide the region into a number of finite elements as illustrated in Figure 6.2(b). In Figure 6.2(b), the solution region is subdivided into nine nonoverlapping *finite elements*; elements 6, 8, and 9 are four-node quadrilaterals,

6.2. SOLUTION OF LAPLACE'S EQUATION

while other elements are three-node triangles. In practical situations, however, it is preferred, for ease of computation, to have elements of the same type throughout the region. That is, in Figure 6.2(b), we could have split each quadrilateral into two triangles so that we would have 12 triangular elements altogether. The subdivision of the solution region into elements is usually done by hand, but in situations where a large number of elements is required, automatic schemes to be discussed in Sections 6.5 and 6.6 are used.

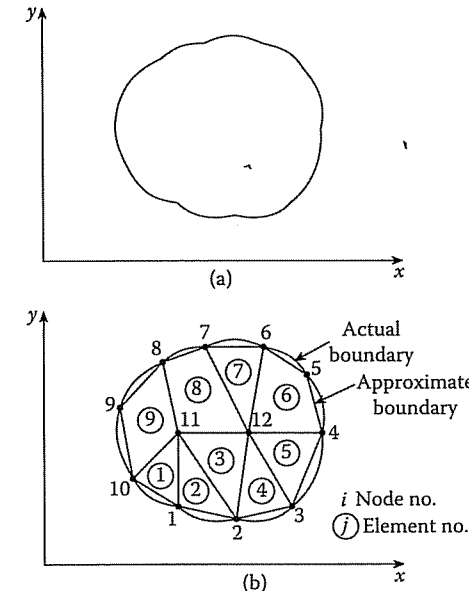


Figure 6.2
(a) The solution region; (b) its finite element discretization.

We seek an approximation for the potential V_e within an element e and then interrelate the potential distribution in various elements such that the potential is continuous across interelement boundaries. The approximate solution for the whole region is

$$V(x, y) \approx \sum_{e=1}^N V_e(x, y), \quad (6.1)$$

where N is the number of triangular elements into which the solution region is divided. The most common form of approximation for V_e within an element is polynomial approximation, namely,

$$V_e(x, y) = a + bx + cy \quad (6.2)$$

for a triangular element and

$$V_e(x, y) = a + bx + cy + dxy \quad (6.3)$$

for a quadrilateral element. The constants a, b, c , and d are to be determined. The potential V_e in general is nonzero within element e but zero outside e . In view of the fact that quadrilateral elements do not conform to curved boundary as easily as triangular elements, we prefer to use triangular elements throughout our analysis in this chapter. Notice that our assumption of linear variation of potential within the triangular element as in Equation (6.2) is the same as assuming that the electric field is uniform within the element, i.e.,

$$\mathbf{E}_e = -\nabla V_e = -(ba_x + ca_y) \quad (6.4)$$

6.2.2 Element Governing Equations

Consider a typical triangular element shown in Figure 6.3. The potential V_{e1} , V_{e2} , and V_{e3} at nodes 1, 2, and 3, respectively, are obtained using Equation (6.2), i.e.,

$$\begin{bmatrix} V_{e1} \\ V_{e2} \\ V_{e3} \end{bmatrix} = \begin{bmatrix} 1 & x_1 & y_1 \\ 1 & x_2 & y_2 \\ 1 & x_3 & y_3 \end{bmatrix} \begin{bmatrix} a \\ b \\ c \end{bmatrix} \quad (6.5)$$

The coefficients a, b , and c are determined from Equation (6.5) as

$$\begin{bmatrix} a \\ b \\ c \end{bmatrix} = \begin{bmatrix} 1 & x_1 & y_1 \\ 1 & x_2 & y_2 \\ 1 & x_3 & y_3 \end{bmatrix}^{-1} \begin{bmatrix} V_{e1} \\ V_{e2} \\ V_{e3} \end{bmatrix} \quad (6.6)$$

Substituting this into Equation (6.2) gives

$$V_e = [1 \ x \ y] \frac{1}{2A} \begin{bmatrix} (x_2y_3 - x_3y_2) & (x_3y_1 - x_1y_3) & (x_1y_2 - x_2y_1) \\ (y_2 - y_3) & (y_3 - y_1) & (y_1 - y_2) \\ (x_3 - x_2) & (x_1 - x_3) & (x_2 - x_1) \end{bmatrix} \begin{bmatrix} V_{e1} \\ V_{e2} \\ V_{e3} \end{bmatrix}$$

or

$$V_e = \sum_{i=1}^3 \alpha_i(x, y) V_{ei} \quad (6.7)$$

where

$$\alpha_1 = \frac{1}{2A} [(x_2y_3 - x_3y_2) + (y_2 - y_3)x + (x_3 - x_2)y], \quad (6.8a)$$

$$\alpha_2 = \frac{1}{2A} [(x_3y_1 - x_1y_3) + (y_3 - y_1)x + (x_1 - x_3)y], \quad (6.8b)$$

$$\alpha_3 = \frac{1}{2A} [(x_1y_2 - x_2y_1) + (y_1 - y_2)x + (x_2 - x_1)y], \quad (6.8c)$$

and A is the area of the element e , i.e.,

$$\begin{aligned} 2A &= \begin{vmatrix} 1 & x_1 & y_1 \\ 1 & x_2 & y_2 \\ 1 & x_3 & y_3 \end{vmatrix} \\ &= (x_1y_2 - x_2y_1) + (x_3y_1 - x_1y_3) + (x_2y_3 - x_3y_2) \end{aligned}$$

6.2. SOLUTION OF LAPLACE'S EQUATION

or

$$A = \frac{1}{2} [(x_2 - x_1)(y_3 - y_1) - (x_3 - x_1)(y_2 - y_1)] \quad (6.9)$$

The value of A is positive if the nodes are numbered counterclockwise (starting from any node) as shown by the arrow in Figure 6.3. Note that Equation (6.7) gives

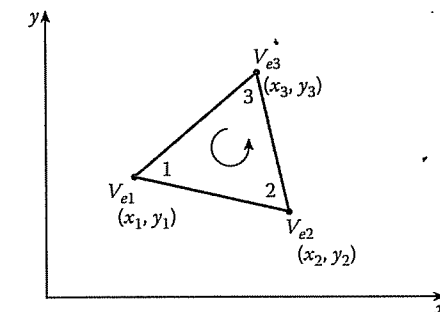


Figure 6.3

Typical triangular element; local node numbering 1-2-3 must proceed counterclockwise as indicated by the arrow.

the potential at any point (x, y) within the element provided that the potentials at the vertices are known. This is unlike finite difference analysis, where the potential is known at the grid points only. Also note that α_i are linear interpolation functions. They are called the *element shape functions* and they have the following properties [4]:

$$\alpha_i = \begin{cases} 1, & i = j \\ 0, & i \neq j \end{cases} \quad (6.10a)$$

$$\sum_{i=1}^3 \alpha_i(x, y) = 1 \quad (6.10b)$$

The shape functions α_1, α_2 , and α_3 are illustrated in Figure 6.4.

The functional corresponding to Laplace's equation, $\nabla^2 V = 0$, is given by

$$W_e = \frac{1}{2} \int \epsilon |\mathbf{E}_e|^2 dS = \frac{1}{2} \int \epsilon |\nabla V_e|^2 dS \quad (6.11)$$

(Physically, the functional W_e is the energy per unit length associated with the element e .) From Equation (6.7),

$$\nabla V_e = \sum_{i=1}^3 V_{ei} \nabla \alpha_i \quad (6.12)$$

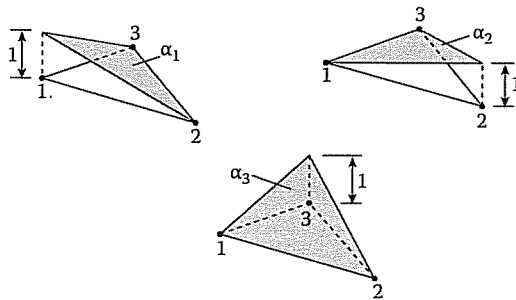


Figure 6.4

Shape functions α_1 , α_2 , and α_3 for a triangular element.

Substituting Equation (6.12) into Equation (6.11) gives

$$W_e = \frac{1}{2} \sum_{i=1}^3 \sum_{j=1}^3 \epsilon V_{ei} \left[\int \nabla \alpha_i \cdot \nabla \alpha_j dS \right] V_{ej} \quad (6.13)$$

If we define the term in brackets as

$$C_{ij}^{(e)} = \int \nabla \alpha_i \cdot \nabla \alpha_j dS, \quad (6.14)$$

we may write Equation (6.13) in matrix form as

$$W_e = \frac{1}{2} \epsilon [V_e]^t [C^{(e)}] [V_e] \quad (6.15)$$

where the superscript t denotes the transpose of the matrix,

$$[V_e] = \begin{bmatrix} V_{e1} \\ V_{e2} \\ V_{e3} \end{bmatrix} \quad (6.16a)$$

and

$$[C^{(e)}] = \begin{bmatrix} C_{11}^{(e)} & C_{12}^{(e)} & C_{13}^{(e)} \\ C_{21}^{(e)} & C_{22}^{(e)} & C_{23}^{(e)} \\ C_{31}^{(e)} & C_{32}^{(e)} & C_{33}^{(e)} \end{bmatrix} \quad (6.16b)$$

The matrix $[C^{(e)}]$ is usually called the *element coefficient matrix* (or "stiffness matrix" in structural analysis). The element $C_{ij}^{(e)}$ of the coefficient matrix may be regarded as the coupling between nodes i and j ; its value is obtained from Equations (6.8)

6.2. SOLUTION OF LAPLACE'S EQUATION

and (6.14). For example,

$$\begin{aligned} C_{12}^{(e)} &= \int \nabla \alpha_1 \cdot \nabla \alpha_2 dS \\ &= \frac{1}{4A^2} [(y_2 - y_3)(y_3 - y_1) + (x_3 - x_2)(x_1 - x_3)] \int dS \\ &= \frac{1}{4A} [(y_2 - y_3)(y_3 - y_1) + (x_3 - x_2)(x_1 - x_3)] \end{aligned} \quad (6.17a)$$

Similarly,

$$C_{13}^{(e)} = \frac{1}{4A} [(y_2 - y_3)(y_1 - y_2) + (x_3 - x_2)(x_2 - x_1)], \quad (6.17b)$$

$$C_{23}^{(e)} = \frac{1}{4A} [(y_3 - y_1)(y_1 - y_2) + (x_1 - x_3)(x_2 - x_1)], \quad (6.17c)$$

$$C_{11}^{(e)} = \frac{1}{4A} [(y_2 - y_3)^2 + (x_3 - x_2)^2], \quad (6.17d)$$

$$C_{22}^{(e)} = \frac{1}{4A} [(y_3 - y_1)^2 + (x_1 - x_3)^2], \quad (6.17e)$$

$$C_{33}^{(e)} = \frac{1}{4A} [(y_1 - y_2)^2 + (x_2 - x_1)^2] \quad (6.17f)$$

Also

$$C_{21}^{(e)} = C_{12}^{(e)}, \quad C_{31}^{(e)} = C_{13}^{(e)}, \quad C_{32}^{(e)} = C_{23}^{(e)} \quad (6.18)$$

6.2.3 Assembling of All Elements

Having considered a typical element, the next step is to assemble all such elements in the solution region. The energy associated with the assemblage of elements is

$$W = \sum_{e=1}^N W_e = \frac{1}{2} \epsilon [V]^t [C] [V] \quad (6.19)$$

where

$$[V] = \begin{bmatrix} V_1 \\ V_2 \\ V_3 \\ \vdots \\ V_n \end{bmatrix}, \quad (6.20)$$

n is the number of nodes, N is the number of elements, and $[C]$ is called the overall or *global coefficient matrix*, which is the assemblage of individual element coefficient

matrices. Notice that to obtain Equation (6.19), we have assumed that the whole solution region is homogeneous so that ϵ is constant. For an inhomogeneous solution region such as shown in Figure 6.5, for example, the region is discretized such that each finite element is homogeneous. In this case, Equation (6.11) still holds, but Equation (6.19) does not apply since $\epsilon (= \epsilon_r \epsilon_o)$ or simply ϵ_r varies from element to element. To apply Equation (6.19), we may replace ϵ by ϵ_o and multiply the integrand in Equation (6.14) by ϵ_r .

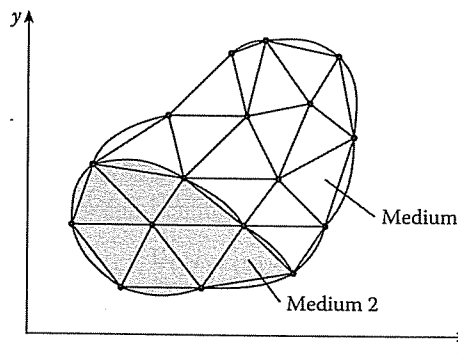


Figure 6.5
Discretization of an inhomogeneous solution region.

The process by which individual element coefficient matrices are assembled to obtain the global coefficient matrix is best illustrated with an example. Consider the finite element mesh consisting of three finite elements as shown in Figure 6.6. Observe

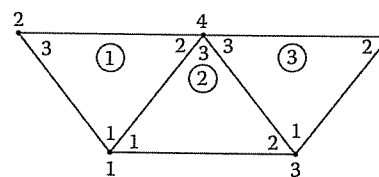


Figure 6.6
Assembly of three elements; $i-j-k$ corresponds to local numbering (1-2-3) of the element in Figure 6.3.

the numberings of the mesh. The numbering of nodes 1, 2, 3, 4, and 5 is called *global* numbering. The numbering $i-j-k$ is called *local* numbering, and it corresponds with 1-2-3 of the element in Figure 6.3. For example, for element 3 in Figure 6.6, the global numbering 3-5-4 corresponds with local numbering 1-2-3 of the element in Figure 6.3. (Note that the local numbering must be in counterclockwise sequence starting from any node of the element.) For element 3, we could choose 4-3-5 instead of 3-5-4 to correspond with 1-2-3 of the element in Figure 6.3. Thus the numbering

6.2. SOLUTION OF LAPLACE'S EQUATION

in Figure 6.6 is not unique. But whichever numbering is used, the global coefficient matrix remains the same. Assuming the particular numbering in Figure 6.6, the global coefficient matrix is expected to have the form

$$[C] = \begin{bmatrix} C_{11} & C_{12} & C_{13} & C_{14} & C_{15} \\ C_{21} & C_{22} & C_{23} & C_{24} & C_{25} \\ C_{31} & C_{32} & C_{33} & C_{34} & C_{35} \\ C_{41} & C_{42} & C_{43} & C_{44} & C_{45} \\ C_{51} & C_{52} & C_{53} & C_{54} & C_{55} \end{bmatrix} \quad (6.21)$$

which is a 5×5 matrix since five nodes ($n = 5$) are involved. Again, C_{ij} is the coupling between nodes i and j . We obtain C_{ij} by using the fact that the potential distribution must be continuous across interelement boundaries. The contribution to the i, j position in $[C]$ comes from all elements containing nodes i and j . For example, in Figure 6.6, elements 1 and 2 have global node 1 in common; hence

$$C_{11} = C_{11}^{(1)} + C_{11}^{(2)} \quad (6.22a)$$

Node 2 belongs to element 1 only; hence

$$C_{22} = C_{33}^{(1)} \quad (6.22b)$$

Node 4 belongs to elements 1, 2, and 3; consequently

$$C_{44} = C_{22}^{(1)} + C_{33}^{(2)} + C_{33}^{(3)} \quad (6.22c)$$

Nodes 1 and 4 belong simultaneously to elements 1 and 2; hence

$$C_{14} = C_{41} = C_{12}^{(1)} + C_{13}^{(2)} \quad (6.22d)$$

Since there is no coupling (or direct link) between nodes 2 and 3,

$$C_{23} = C_{32} = 0 \quad (6.22e)$$

Continuing in this manner, we obtain all the terms in the global coefficient matrix by inspection of Figure 6.6 as

$$\begin{bmatrix} C_{11}^{(1)} + C_{11}^{(2)} & C_{13}^{(1)} & C_{12}^{(2)} & C_{12}^{(1)} + C_{13}^{(2)} & 0 \\ C_{31}^{(1)} & C_{33}^{(1)} & 0 & C_{32}^{(1)} & 0 \\ C_{21}^{(2)} & 0 & C_{22}^{(2)} + C_{11}^{(3)} & C_{23}^{(2)} + C_{13}^{(3)} & C_{12}^{(3)} \\ C_{21}^{(1)} + C_{31}^{(2)} & C_{23}^{(1)} & C_{32}^{(2)} + C_{31}^{(3)} & C_{22}^{(1)} + C_{33}^{(2)} + C_{33}^{(3)} & C_{32}^{(3)} \\ 0 & 0 & C_{21}^{(3)} & C_{23}^{(3)} & C_{22}^{(3)} \end{bmatrix} \quad (6.23)$$

Note that element coefficient matrices overlap at nodes shared by elements and that there are 27 terms (9 for each of the 3 elements) in the global coefficient matrix $[C]$. Also note the following properties of the matrix $[C]$:

- (1) It is symmetric ($C_{ij} = C_{ji}$) just as the element coefficient matrix.
- (2) Since $C_{ij} = 0$ if no coupling exists between nodes i and j , it is expected that for a large number of elements $[C]$ becomes sparse. Matrix $[C]$ is also banded if the nodes are carefully numbered. It can be shown using Equation (6.17) that

$$\sum_{i=1}^3 C_{ij}^{(e)} = 0 = \sum_{j=1}^3 C_{ij}^{(e)}$$

- (3) It is singular. Although this is not so obvious, it can be shown using the element coefficient matrix of Equation (6.16b).

6.2.4 Solving the Resulting Equations

Using the concepts developed in Chapter 4, it can be shown that Laplace's equation is satisfied when the total energy in the solution region is minimum. Thus we require that the partial derivatives of W with respect to each nodal value of the potential be zero, i.e.,

$$\frac{\partial W}{\partial V_1} = \frac{\partial W}{\partial V_2} = \cdots = \frac{\partial W}{\partial V_n} = 0$$

or

$$\frac{\partial W}{\partial V_k} = 0, \quad k = 1, 2, \dots, n \quad (6.24)$$

For example, to get $\frac{\partial W}{\partial V_1} = 0$ for the finite element mesh of Figure 6.6, we substitute Equation (6.21) into Equation (6.19) and take the partial derivative of W with respect to V_1 . We obtain

$$0 = \frac{\partial W}{\partial V_1} = 2V_1C_{11} + V_2C_{12} + V_3C_{13} + V_4C_{14} + V_5C_{15} + V_2C_{21} + V_3C_{31} + V_4C_{41} + V_5C_{51}$$

or

$$0 = V_1C_{11} + V_2C_{12} + V_3C_{13} + V_4C_{14} + V_5C_{15} \quad (6.25)$$

In general, $\frac{\partial W}{\partial V_k} = 0$ leads to

$$0 = \sum_{i=1}^n V_i C_{ik} \quad (6.26)$$

6.2. SOLUTION OF LAPLACE'S EQUATION

where n is the number of nodes in the mesh. By writing Equation (6.26) for all nodes $k = 1, 2, \dots, n$, we obtain a set of simultaneous equations from which the solution of $[V]^t = [V_1, V_2, \dots, V_n]$ can be found. This can be done in two ways similar to those used in solving finite difference equations obtained from Laplace's equation in Section 3.5.

- (1) **Iteration Method:** Suppose node 1 in Figure 6.6, for example, is a free node. A free node is when the potential is unknown, whereas a fixed node is when the potential is prescribed. From Equation (6.25),

$$V_1 = -\frac{1}{C_{11}} \sum_{i=2}^5 V_i C_{1i} \quad (6.27)$$

Thus, in general, at node k in a mesh with n nodes

$$V_k = -\frac{1}{C_{kk}} \sum_{i=1, i \neq k}^n V_i C_{ki} \quad (6.28)$$

where node k is a free node. Since $C_{ki} = 0$ if node k is not directly connected to node i , only nodes that are directly linked to node k contribute to V_k in Equation (6.28). Equation (6.28) can be applied iteratively to all the free nodes. The iteration process begins by setting the potentials of fixed nodes (where the potentials are prescribed or known) to their prescribed values and the potentials at the free nodes (where the potentials are unknown) equal to zero or to the average potential [5]

$$V_{\text{ave}} = \frac{1}{2} (V_{\min} + V_{\max}) \quad (6.29)$$

where V_{\min} and V_{\max} are the minimum and maximum values of V at the fixed nodes. With these initial values, the potentials at the free nodes are calculated using Equation (6.28). At the end of the first iteration, when the new values have been calculated for all the free nodes, they become the old values for the second iteration. The procedure is repeated until the change between subsequent iterations is negligible enough.

- (2) **Band Matrix Method:** If all free nodes are numbered first and the fixed nodes last, Equation (6.19) can be written such that [4]

$$W = \frac{1}{2} \epsilon [V_f \ V_p] \begin{bmatrix} C_{ff} & C_{fp} \\ C_{pf} & C_{pp} \end{bmatrix} \begin{bmatrix} V_f \\ V_p \end{bmatrix} \quad (6.30)$$

where subscripts f and p , respectively, refer to nodes with free and fixed (or prescribed) potentials. Since V_p is constant (it consists of known, fixed values), we differentiate only with respect to V_f so that applying Equations (6.24) to (6.30) yields

$$[C_{ff} \ C_{fp}] \begin{bmatrix} V_f \\ V_p \end{bmatrix} = 0$$

or

$$[C_{ff}] [V_f] = -[C_{fp}] [V_p] \quad (6.31)$$

This equation can be written as

$$[A][V] = [B] \quad (6.32a)$$

or

$$[V] = [A]^{-1}[B] \quad (6.32b)$$

where $[V] = [V_f]$, $[A] = [C_{ff}]$, $[B] = -[C_{fp}][V_p]$. Since $[A]$ is, in general, nonsingular, the potential at the free nodes can be found using Equation (6.32). We can solve for $[V]$ in Equation (6.32a) using Gaussian elimination technique. We can also solve for $[V]$ in Equation (6.32b) using matrix inversion if the size of the matrix to be inverted is not large.

It is sometimes necessary to impose Neumann condition ($\frac{\partial V}{\partial n} = 0$) as a boundary condition or at the line of symmetry when we take advantage of the symmetry of the problem. Suppose, for concreteness, that a solution region is symmetric along the y -axis as in Figure 6.7. We impose condition ($\frac{\partial V}{\partial x} = 0$) along the y -axis by making

$$V_1 = V_2, \quad V_4 = V_5, \quad V_7 = V_8 \quad (6.33)$$

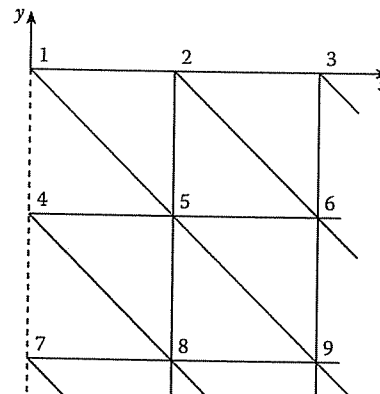


Figure 6.7

A solution region that is symmetric along the y -axis.

Notice that as from Equation (6.11) onward, the solution has been restricted to a two-dimensional problem involving Laplace's equation, $\nabla^2 V = 0$. The basic concepts developed in this section will be extended to finite element analysis of problems involving Poisson's equation ($\nabla^2 V = -\rho_v/\epsilon$, $\nabla^2 A = -\mu J$) or wave equation ($\nabla^2 \Phi - \gamma^2 \Phi = 0$) in the next sections.

6.2. SOLUTION OF LAPLACE'S EQUATION

The following two examples were solved in [3] using the band matrix method; here they are solved using the iterative method. \square

Example 6.1

Consider the two-element mesh shown in Figure 6.8(a). Using the finite element method, determine the potentials within the mesh. \square

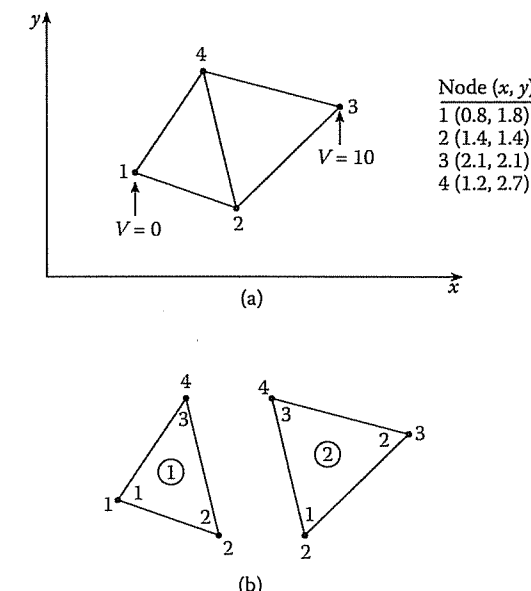


Figure 6.8

For Example 6.1: (a) Two-element mesh, (b) local and global numbering at the elements.

Solution

The element coefficient matrices can be calculated using Equations (6.17) and (6.18). However, our calculations will be easier if we define

$$P_1 = (y_2 - y_3), \quad P_2 = (y_3 - y_1), \quad P_3 = (y_1 - y_2), \quad (6.34)$$

$$Q_1 = (x_3 - x_2), \quad Q_2 = (x_1 - x_3), \quad Q_3 = (x_2 - x_1)$$

With P_i and Q_i ($i = 1, 2, 3$ are the local node numbers), each term in the element coefficient matrix is found as

$$C_{ij}^{(e)} = \frac{1}{4A} (P_i P_j + Q_i Q_j) \quad (6.35)$$

where $A = \frac{1}{2}(P_2Q_3 - P_3Q_2)$. It is evident that Equation (6.35) is more convenient to use than Equations (6.17) and (6.18). For element 1 consisting of global nodes 1-2-4 corresponding to the local numbering 1-2-3 as in Figure 6.8(b),

$$\begin{aligned} P_1 &= -1.3, & P_2 &= 0.9, & P_3 &= 0.4, \\ Q_1 &= -0.2, & Q_2 &= -0.4, & Q_3 &= 0.6, \\ A &= \frac{1}{2}(0.54 + 0.16) = 0.35 \end{aligned}$$

Substituting all of these into Equation (6.35) gives

$$[C^{(1)}] = \begin{bmatrix} 1.2357 & -0.7786 & -0.4571 \\ -0.7786 & 0.6929 & 0.0857 \\ -0.4571 & 0.0857 & 0.3714 \end{bmatrix} \quad (6.36)$$

Similarly, for element 2 consisting of nodes global 2-3-4 corresponding to local numbering 1-2-3 as in Figure 6.8(b),

$$\begin{aligned} P_1 &= -0.6, & P_2 &= 1.3, & P_3 &= -0.7, \\ Q_1 &= -0.9, & Q_2 &= 0.2, & Q_3 &= 0.7, \\ A &= \frac{1}{2}(0.91 + 0.14) = 0.525 \end{aligned}$$

Hence

$$[C^{(2)}] = \begin{bmatrix} 0.5571 & -0.4571 & -0.1 \\ -0.4571 & 0.8238 & -0.3667 \\ -0.1 & -0.3667 & 0.4667 \end{bmatrix} \quad (6.37)$$

The terms of the global coefficient matrix are obtained as follows:

$$\begin{aligned} C_{22} &= C_{22}^{(1)} + C_{11}^{(2)} = 0.6929 + 0.5571 = 1.25 \\ C_{24} &= C_{23}^{(1)} + C_{13}^{(2)} = 0.0857 - 0.1 = -0.0143 \\ C_{44} &= C_{33}^{(1)} + C_{33}^{(2)} = 0.3714 + 0.4667 = 0.8381 \\ C_{21} &= C_{21}^{(1)} = -0.7786 \\ C_{23} &= C_{12}^{(2)} = -0.4571 \\ C_{41} &= C_{31}^{(1)} = -0.4571 \\ C_{43} &= C_{32}^{(2)} = -0.3667 \end{aligned}$$

6.2. SOLUTION OF LAPLACE'S EQUATION

Note that we follow local numbering for the element coefficient matrix and global numbering for the global coefficient matrix. Thus

$$\begin{aligned} [C] &= \begin{bmatrix} C_{11}^{(1)} & C_{12}^{(1)} & 0 & C_{13}^{(1)} \\ C_{21}^{(1)} & C_{22}^{(1)} + C_{11}^{(2)} & C_{12}^{(2)} & C_{23}^{(1)} + C_{12}^{(2)} \\ 0 & C_{21}^{(2)} & C_{22}^{(2)} & C_{23}^{(2)} \\ C_{31}^{(1)} & C_{32}^{(1)} + C_{31}^{(2)} & C_{32}^{(2)} & C_{33}^{(1)} + C_{32}^{(2)} \end{bmatrix} \\ &= \begin{bmatrix} 1.2357 & -0.7786 & 0 & -0.4571 \\ -0.7786 & 1.25 & -0.4571 & -0.0143 \\ 0 & -0.4571 & 0.8238 & -0.3667 \\ -0.4571 & -0.0143 & -0.3667 & 0.8381 \end{bmatrix} \end{aligned} \quad (6.38)$$

Note that $\sum_{i=1}^4 C_{ij} = 0 = \sum_{j=1}^4 C_{ij}$. This may be used to check if C is properly obtained.

We now apply Equation (6.28) to the free nodes 2 and 4, i.e.,

$$V_2 = -\frac{1}{C_{22}} (V_1 C_{12} + V_3 C_{32} + V_4 C_{42})$$

$$V_4 = -\frac{1}{C_{44}} (V_1 C_{14} + V_2 C_{24} + V_3 C_{34})$$

or

$$V_2 = -\frac{1}{1.25} (-4.571 - 0.0143 V_4) \quad (6.39a)$$

$$V_4 = -\frac{1}{0.8381} (-0.143 V_2 - 3.667) \quad (6.39b)$$

By initially setting $V_2 = V_4 = 0$, we apply Equations (6.39a), (6.39b) iteratively. The first iteration gives $V_2 = 3.6568$, $V_4 = 4.4378$ and at the second iteration $V_2 = 3.7075$, $V_4 = 4.4386$. Just after two iterations, we obtain the same results as those from the band matrix method [3]. Thus the iterative technique is faster and is usually preferred for a large number of nodes. Once the values of the potentials at the nodes are known, the potential at any point within the mesh can be determined using Equation (6.7).

Example 6.2

Write a MATLAB program to solve Laplace's equation using the finite element method. Apply the program to the two-dimensional problem shown in Figure 6.9(a). \square

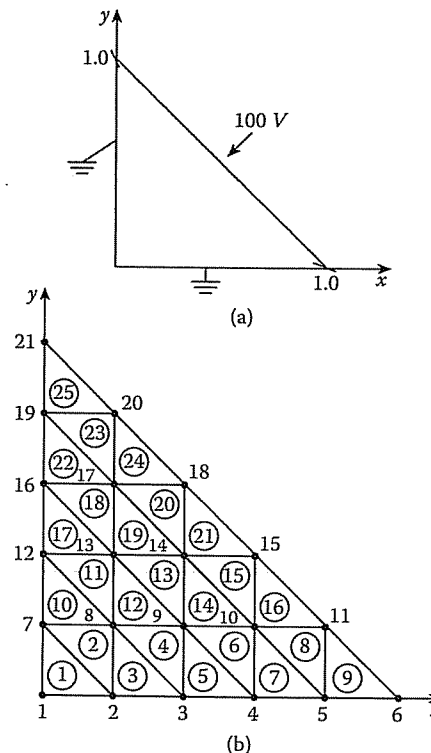


Figure 6.9

For Example 6.2: (a) Two-dimensional electrostatic problem, (b) solution region divided into 25 triangular elements.

Solution

The solution region is divided into 25 three-node triangular elements with total number of nodes being 21 as shown in Figure 6.9(b). This is a necessary step in order to have input data defining the geometry of the problem. Based on the discussions in Section 6.2, a general program for solving problems involving Laplace's equation using three-node triangular elements is developed as shown in Figure 6.10. The development of the program basically involves four steps indicated in the program and explained as follows.

Step 1: This involves inputting the necessary data defining the problem. This is the only step that depends on the geometry of the problem at hand. We input the number of elements, the number of nodes, the number of fixed nodes, the prescribed values of the potentials at the free nodes, the x and y coordinates of all nodes, and a list identifying the nodes belonging to each element in the order of the local numbering 1-2-3. For the problem in Figure 6.9, the three sets of data for coordinates, element-node relationship, and prescribed potentials at fixed nodes are shown in Tables 6.1, 6.2, and 6.3, respectively.

6.2. SOLUTION OF LAPLACE'S EQUATION

```
% FINITE ELEMENT SOLUTION OF LAPLACE'S EQUATION FOR
% TWO-DIMENSIONAL PROBLEMS
% TRIANGULAR ELEMENTS ARE USED

% THE UNKNOWN POTENTIALS ARE OBTAINED USING
% ITERATION METHOD

% ND = NO. OF NODES
% NE = NO. OF ELEMENTS
% NP = NO. OF FIXED NODES (WHERE POTENTIAL IS PRESCRIBED)
% NDP(I) = NODE NO. OF PRESCRIBED POTENTIAL, I = 1,2,...NP
% VAL(I) = VALUE OF PRESCRIBED POTENTIAL AT NODE NDP(I)
% NL(I,J) = LIST OF NODES FOR EACH ELEMENT I, WHERE
% LF(I) = LIST OF FREE NODES I = 1,2,...,NE=ND-NP
% J = 1, 2, 3 IS THE LOCAL NODE NUMBER
% CE(I,J) = ELEMENT COEFFICIENT MATRIX
% ER(I) = VALUE OF THE RELATIVE PERMITTIVITY FOR ELEMENT I
% C(I,J) = GLOBAL COEFFICIENT MATRIX
% X(I), Y(I) = GLOBAL COORDINATES OF NODE I
% XL(J), YL(J) = LOCAL COORDINATES OF NODE J = 1,2,3
% V(I) = POTENTIAL AT NODE I
% MATRICES P(I) AND Q(I) ARE DEFINED IN EQUATION(6.1.1)

***** FIRST STEP - INPUT DATA DEFINING GEOMETRY AND
***** BOUNDARY CONDITIONS
*****
clear;
NI = 50; %! NO. OF ITERATIONS
NE=25; %Number of Elements
ND=21;
NP=15;

X = [ 0 0.2 0.4 0.6 0.8 1.0 0 0.2 0.4 0.6 0.8 0 0.2 0.4 0.6 0 0.2 0.4 0 0.2 0 ];
Y = [ 0 0 0 0 0 0.2 0.2 0.2 0.2 0.4 0.4 0.4 0.4 0.4 0.6 0.6 0.6 0.6 0.8 0.8 1.0 ];

NDP = [ 1 2 3 4 5 6 7 11 12 15 16 18 19 20 21 ];
VAL = [ 0 0 0 0 0 50 0 100 0 100 0 100 0 100 0 100 50 ];

NL = [ 1 2 7 ; 2 8 7 ; 2 3 8 ; 3 9 8 ; 3 4 9 ; 4 10 9 ; 4 5 10 ; 5 11 10 ; 5 6 11 ; ...
        7 8 12 ; 8 13 12 ; 8 9 13 ; 9 14 13 ; 9 10 14 ; 10 15 14 ; 10 11 15 ; ...
        12 13 16 ; 13 17 16 ; 13 14 17 ; 14 18 17 ; 14 15 18 ; 16 17 19 ; 17 20 19 ; 17 18 20 ; 19 20 21 ];

EO = 1.0E-9/(36.0*pi);
ER = ones(1,NE);
% **** SECOND STEP - EVALUATE COEFFICIENT MATRIX FOR EACH
% ELEMENT AND ASSEMBLE GLOBALLY
%
C = zeros(ND,ND);
for I = 1: NE
    % FIND LOCAL COORDINATES XL, YL FOR ELEMENT I
    XL = X(NL(I,:));
    YL = Y(NL(I,:));

    P = [YL(2) - YL(3), YL(3) - YL(1), YL(1) - YL(2)];
    Q = [XL(3) - XL(2), XL(1) - XL(3), XL(2) - XL(1)];
    AREA = 0.5*abs( P(2)*Q(3) - Q(2)*P(3) );

```

Figure 6.10

Computer program for Example 6.2 (Continued).

```
% DETERMINE COEFFICIENT MATRIX FOR ELEMENT I
CE = ER(I)*(P'*P+Q'*Q)/(4*AREA);
% ASSEMBLE GLOBALLY - FIND C(I,J)
J=1:3;
L=1:3;
IR = NL(I,J);
IC = NL(I,L);
C(IR,IC) = C(IR,IC) + CE(J,L);
end

*****
THIRD STEP - SOLVE THE RESULTING SYSTEM
ITERATIVELY
*****

% DETERMINE LF - LIST OF FREE NODES
LF = setdiff(1:ND, NDP);
V = zeros(1,ND);
V(NDP) = VAL;
NF = length(LF);

for N = 1:N1
    for ii = 1:NF
        rowC = C(LF(ii),:);
        rowC(LF(ii)) = 0;
        V(LF(ii)) = -1/(C(LF(ii),LF(ii)))*rowC*V';
    end
    figure(1), stem(V), drawnow
end

disp({{'Node','X','Y','Potential'};num2cell([(1:ND)',X',Y',V'])});
```

Figure 6.10

(Cont.) Computer program for Example 6.2.

Step 2: This step entails finding the element coefficient matrix $[C^{(e)}]$ for each element and using the terms to form the global matrix $[C]$.

Step 3: At this stage, we first find the list of free nodes using the given list of prescribed nodes. We now apply Equation (6.28) iteratively to all the free nodes. The solution converges at 50 iterations or less since only 6 nodes are involved in this case. The solution obtained is exactly the same as those obtained using the band matrix method [3].

Step 4: This involves outputting the result of the computation. The output data for the problem in Figure 6.9 is presented in Table 6.4. The validity of the result in Table 6.4 is checked using the finite difference method. From the finite difference analysis, the potentials at the free nodes are obtained as

$$\begin{aligned} V_8 &= 15.41, \quad V_9 = 26.74, \quad V_{10} = 56.69, \\ V_{13} &= 34.88, \quad V_{14} = 65.41, \quad V_{17} = 58.72 \end{aligned}$$

Although the result obtained using finite difference is considered more accurate in this problem, increased accuracy of finite element analysis can be obtained by dividing

6.2. SOLUTION OF LAPLACE'S EQUATION

Table 6.1 Nodal Coordinates of the Finite Element Mesh in Figure 6.9

Node	x	y	Node	x	y
1	0.0	0.0	12	0.0	0.4
2	0.2	0.0	13	0.2	0.4
3	0.4	0.0	14	0.4	0.4
4	0.6	0.0	15	0.6	0.4
5	0.8	0.0	16	0.0	0.6
6	1.0	0.0	17	0.2	0.6
7	0.0	0.2	18	0.4	0.6
8	0.2	0.2	19	0.0	0.8
9	0.4	0.2	20	0.2	0.8
10	0.6	0.2	21	0.0	1.0
11	0.8	0.2			

Table 6.2 Element–Node Identification

Element	Local	Node	No.	Element	Local	Node	No.
	1	2	3		1	2	3
1	1	2	7	14	9	10	14
2	2	8	7	15	10	15	14
3	2	3	8	16	10	11	15
4	3	9	8	17	12	13	16
5	3	4	9	18	13	17	16
6	4	10	9	19	13	14	17
7	4	5	10	20	14	18	17
8	5	11	10	21	14	15	18
9	5	6	11	22	16	17	19
10	7	8	12	23	17	20	19
11	8	13	12	24	17	18	20
12	8	9	13	25	19	20	21
13	9	14	13				

Table 6.3 Prescribed Potentials at Fixed Nodes

Node	Prescribed Potential	Node	Prescribed Potential
1	0.0	18	100.0
2	0.0	20	100.0
3	0.0	21	50.0
4	0.0	19	0.0
5	0.0	16	0.0
6	50.0	12	0.0
11	100.0	7	0.0
15	100.0		

Table 6.4 Output Data of the Program in Figure 6.10.

No. of Nodes = 21, No. of Elements = 25, No. of Fixed Nodes = 15

Node	X	Y	Potential
1	0.00	0.00	0.000
2	0.20	0.00	0.000
3	0.40	0.00	0.000
4	0.60	0.00	0.000
5	0.80	0.00	0.000
6	1.00	0.00	50.000
7	0.00	0.20	0.000
8	0.20	0.20	18.182
9	0.40	0.20	36.364
10	0.60	0.20	59.091
11	0.80	0.20	100.000
12	0.00	0.40	0.000
13	0.20	0.40	36.364
14	0.40	0.40	68.182
15	0.60	0.40	100.000
16	0.00	0.60	0.000
17	0.20	0.60	59.091
18	0.40	0.60	100.000
19	0.00	0.80	0.000
20	0.20	0.80	100.000
21	0.00	1.00	50.00

the solution region into a greater number of triangular elements, or using higher-order elements to be discussed in Section 6.8. As alluded to earlier, the finite element method has two major advantages over the finite difference method. Field quantities are obtained only at discrete positions in the solution region using FDM; they can be obtained at any point in the solution region in FEM. Also, it is easier to handle complex geometries using FEM than using FDM. ■

6.3 Solution of Poisson's Equation

To solve the two-dimensional Poisson's equation,

$$\nabla^2 V = -\frac{\rho_v}{\epsilon} \quad (6.40)$$

using FEM, we take the same steps as in Section 6.2. Since the steps are essentially the same as in Section 6.2 except that we must include the source term, only the major differences will be highlighted here.

6.3. SOLUTION OF POISSON'S EQUATION

6.3.1 Deriving Element-Governing Equations

After the solution region is divided into triangular elements, we approximate the potential distribution $V_e(x, y)$ and the source term ρ_{ve} (for two-dimensional problems) over each triangular element by linear combinations of the local interpolation polynomial α_i , i.e.,

$$V_e = \sum_{i=1}^3 V_{ei} \alpha_i(x, y) \quad (6.41)$$

$$\rho_{ve} = \sum_{i=1}^3 \rho_{ei} \alpha_i(x, y) \quad (6.42)$$

The coefficients V_{ei} and ρ_{ei} , respectively, represent the values of V and ρ_v at node i of element e as in Figure 6.3. The values of ρ_{ei} are known since $\rho_v(x, y)$ is prescribed, while the values of V_{ei} are to be determined.

From Table 4.1, an energy functional whose associated Euler equation is Equation (6.40) is

$$F(V_e) = \frac{1}{2} \int_S [\epsilon |\nabla V_e|^2 - 2\rho_{ve} V_e] dS \quad (6.43)$$

$F(V_e)$ represents the total energy per length within element e . The first term under the integral sign, $\frac{1}{2} \mathbf{D} \cdot \mathbf{E} = \frac{1}{2} \epsilon |\nabla V_e|^2$, is the energy density in the electrostatic system, while the second term, $\rho_{se} V_e dS$, is the work done in moving the charge $\rho_{se} dS$ to its location at potential V_e . Substitution of Equations (6.41) and (6.42) into Equation (6.43) yields

$$F(V_e) = \frac{1}{2} \sum_{i=1}^3 \sum_{j=1}^3 \epsilon V_{ei} \left[\int \nabla \alpha_i \cdot \nabla \alpha_j dS \right] V_{ej} - \sum_{i=1}^3 \sum_{j=1}^3 V_{ei} \left[\int \alpha_i \alpha_j dS \right] \rho_{ej}$$

This can be written in matrix form as

$$F(V_e) = \frac{1}{2} \epsilon [V_e]^T [C^{(e)}] [V_e] - [V_e]^T [T^{(e)}] [\rho_e] \quad (6.44)$$

where

$$C_{ij}^{(e)} = \int \nabla \alpha_i \cdot \nabla \alpha_j dS \quad (6.45)$$

which is already defined in Equation (6.17) and

$$T_{ij}^{(e)} = \int \alpha_i \alpha_j dS \quad (6.46)$$

It will be shown in Section 6.8 that

$$T_{ij}^{(e)} = \begin{cases} A/12, & i \neq j \\ A/6 & i = j \end{cases} \quad (6.47)$$

where A is the area of the triangular element.

Equation (6.44) can be applied to every element in the solution region. We obtain the discretized functional for the whole solution region (with N elements and n nodes) as the sum of the functionals for the individual elements, i.e., from Equation (6.44),

$$F(V) = \sum_{e=1}^N F(V_e) = \frac{1}{2} \epsilon [V]^t [C] [V] - [V]^t [T] [\rho] \quad (6.48)$$

where t denotes transposition. In Equation (6.48), the column matrix $[V]$ consists of the values of V_{ei} , while the column matrix $[\rho]$ contains n values of the source function ρ_v at the nodes. The functional in Equation (6.48) is now minimized by differentiating with respect to V_{ei} and setting the result equal to zero.

6.3.2 Solving the Resulting Equations

The resulting equations can be solved by either the iteration method or the band matrix method as discussed in Section 6.2.4.

Iteration Method: Consider a solution region in Figure 6.6 having five nodes so that $n = 5$. From Equation (6.48),

$$\begin{aligned} F = \frac{1}{2} \epsilon [V_1 \ V_2 \ \dots \ V_5] & \begin{bmatrix} C_{11} & C_{12} & \dots & C_{15} \\ C_{21} & C_{22} & \dots & C_{25} \\ \vdots & & & \vdots \\ C_{51} & C_{52} & \dots & C_{55} \end{bmatrix} \begin{bmatrix} V_1 \\ V_2 \\ \vdots \\ V_5 \end{bmatrix} \\ & - [V_1 \ V_2 \ \dots \ V_5] \begin{bmatrix} T_{11} & T_{12} & \dots & T_{15} \\ T_{21} & T_{22} & \dots & T_{25} \\ \vdots & & & \vdots \\ T_{51} & T_{52} & \dots & T_{55} \end{bmatrix} \begin{bmatrix} \rho_1 \\ \rho_2 \\ \vdots \\ \rho_5 \end{bmatrix} \end{aligned} \quad (6.49)$$

We minimize the energy by applying

$$\frac{\partial F}{\partial V_k} = 0, \quad k = 1, 2, \dots, n \quad (6.50)$$

From Equation (6.49), we get $\frac{\partial F}{\partial V_1} = 0$, for example, as

$$\frac{\partial F}{\partial V_1} = \epsilon [V_1 C_{11} + V_2 C_{21} + \dots + V_5 C_{51}] - [T_{11} \rho_1 + T_{21} \rho_2 + \dots + T_{51} \rho_5] = 0$$

6.3. SOLUTION OF POISSON'S EQUATION

or

$$V_1 = -\frac{1}{C_{11}} \sum_{i=2}^5 V_i C_{i1} + \frac{1}{\epsilon C_{11}} \sum_{i=1}^5 T_{i1} \rho_i \quad (6.51)$$

Thus, in general, for a mesh with n nodes

$$V_k = -\frac{1}{C_{kk}} \sum_{i=1, i \neq k}^n V_i C_{ki} + \frac{1}{\epsilon C_{kk}} \sum_{i=1}^n T_{ki} \rho_i \quad (6.52)$$

where node k is assumed to be a free node.

By fixing the potential at the prescribed nodes and setting the potential at the free nodes initially equal to zero, we apply Equation (6.52) iteratively to all free nodes until convergence is reached.

Band Matrix Method: If we choose to solve the problem using the band matrix method, we let the free nodes be numbered first and the prescribed nodes last. By doing so, Equation (6.48) can be written as

$$F(V) = \frac{1}{2} \epsilon [V_f \ V_p] \begin{bmatrix} C_{ff} & C_{fp} \\ C_{pf} & C_{pp} \end{bmatrix} \begin{bmatrix} V_f \\ V_p \end{bmatrix} - [V_f \ V_p] \begin{bmatrix} T_{ff} & T_{fp} \\ T_{pf} & T_{pp} \end{bmatrix} \begin{bmatrix} \rho_f \\ \rho_p \end{bmatrix} \quad (6.53)$$

Minimizing $F(V)$ with respect to V_f , i.e.,

$$\frac{\partial F}{\partial V_f} = 0$$

gives

$$0 = \epsilon(C_{ff} V_f + C_{pf} V_p) - (T_{ff} \rho_f + T_{fp} \rho_p)$$

or

$$[C_{ff}] [V_f] = -[C_{fp}] [V_p] + \frac{1}{\epsilon} [T_{ff}] [\rho_f] + \frac{1}{\epsilon} [T_{fp}] [\rho_p] \quad (6.54)$$

This can be written as

$$[A][V] = [B] \quad (6.55)$$

where $[A] = [C_{ff}]$, $[V] = [V_f]$, and $[B]$ is the right-hand side of Equation (6.54). Equation (6.55) can be solved to determine $[V]$ either by matrix inversion or Gaussian elimination technique discussed in Appendix C. There is little point in giving examples on applying FEM to Poisson's problems, especially when it is noted that the difference between Equations (6.28) and (6.52) or Equations (6.54) and (6.31) is slight. See [19] for an example.

6.4 Solution of the Wave Equation

A typical wave equation is the inhomogeneous scalar Helmholtz's equation

$$\nabla^2 \Phi + k^2 \Phi = g \quad (6.56)$$

where Φ is the field quantity (for waveguide problem, $\Phi = H_z$ for TE mode or E_z for TM mode) to be determined, g is the source function, and $k = \omega\sqrt{\mu\epsilon}$ is the wave number of the medium. The following three distinct special cases of Equation (6.56) should be noted:

- (i) $k = 0 = g$: Laplace's equation;
- (ii) $k = 0$: Poisson's equation; and
- (iii) k is an unknown, $g = 0$: homogeneous, scalar Helmholtz's equation.

We know from Chapter 4 that the variational solution to the operator equation

$$L\Phi = g \quad (6.57)$$

is obtained by extremizing the functional

$$I(\Phi) = \langle L, \Phi \rangle - 2 \langle \Phi, g \rangle \quad (6.58)$$

Hence the solution of Equation (6.56) is equivalent to satisfying the boundary conditions and minimizing the functional

$$I(\Phi) = \frac{1}{2} \iint [|\nabla \Phi|^2 - k^2 \Phi^2 + 2\Phi g] dS \quad (6.59)$$

If other than the natural boundary conditions (i.e., Dirichlet or homogeneous Neumann conditions) must be satisfied, appropriate terms must be added to the functional as discussed in Chapter 4.

We now express potential Φ and source function g in terms of the shape functions α_i over a triangular element as

$$\boxed{\Phi_e(x, y) = \sum_{i=1}^3 \alpha_i \Phi_{ei}} \quad (6.60)$$

$$\boxed{g_e(x, y) = \sum_{i=1}^3 \alpha_i g_{ei}} \quad (6.61)$$

where Φ_{ei} and g_{ei} are, respectively, the values of Φ and g at nodal point i of element e .

6.4. SOLUTION OF THE WAVE EQUATION

Substituting Equations (6.60) and (6.61) into Equation (6.59) gives

$$\begin{aligned} I(\Phi_e) &= \frac{1}{2} \sum_{i=1}^3 \sum_{j=1}^3 \Phi_{ei} \Phi_{ej} \iint \nabla \alpha_i \cdot \nabla \alpha_j dS \\ &\quad - \frac{k^2}{2} \sum_{i=1}^3 \sum_{j=1}^3 \Phi_{ei} \Phi_{ej} \iint \alpha_i \alpha_j dS \\ &\quad + \sum_{i=1}^3 \sum_{j=1}^3 \Phi_{ei} g_{ej} \iint \alpha_i \alpha_j dS \\ &= \frac{1}{2} [\Phi_e]^t [C^{(e)}] [\Phi_e] \\ &\quad - \frac{k^2}{2} [\Phi_e]^t [T^{(e)}] [\Phi_e] + [\Phi_e]^t [T^{(e)}] [G_e] \end{aligned} \quad (6.62)$$

where $[\Phi_e] = [\Phi_{e1}, \Phi_{e2}, \Phi_{e3}]^t$, $[G_e] = [g_{e1}, g_{e2}, g_{e3}]^t$, and $[C^{(e)}]$ and $[T^{(e)}]$ are defined in Equations (6.17) and (6.47), respectively.

Equation (6.62), derived for a single element, can be applied for all N elements in the solution region. Thus,

$$I(\Phi) = \sum_{e=1}^N I(\Phi_e) \quad (6.63)$$

From Equations (6.62) and (6.63), $I(\Phi)$ can be expressed in matrix form as

$$I(\Phi) = \frac{1}{2} [\Phi]^t [C][\Phi] - \frac{k^2}{2} [\Phi]^t [T][\Phi] + [\Phi]^t [T][G] \quad (6.64)$$

where

$$[\Phi] = [\Phi_1, \Phi_2, \dots, \Phi_N]^t, \quad (6.65a)$$

$$[G] = [g_1, g_2, \dots, g_N]^t, \quad (6.65b)$$

and $[C]$ and $[T]$ are global matrices consisting of local matrices $[C^{(e)}]$ and $[T^{(e)}$, respectively.

Consider the special case in which the source function $g = 0$. Again, if free nodes are numbered first and the prescribed nodes last, we may write Equation (6.64) as

$$\begin{aligned} I &= \frac{1}{2} [\Phi_f \Phi_p] \begin{bmatrix} C_{ff} & C_{fp} \\ C_{pf} & C_{pp} \end{bmatrix} \begin{bmatrix} \Phi_f \\ \Phi_p \end{bmatrix} \\ &\quad - \frac{k^2}{2} [\Phi_f \Phi_p] \begin{bmatrix} T_{ff} & T_{fp} \\ T_{pf} & T_{pp} \end{bmatrix} \begin{bmatrix} \Phi_f \\ \Phi_p \end{bmatrix} \end{aligned} \quad (6.66)$$

Setting $\frac{\partial I}{\partial \Phi_f}$ equal to zero gives

$$[C_{ff} \ C_{fp}] \begin{bmatrix} \Phi_f \\ \Phi_p \end{bmatrix} - k^2 [T_{ff} \ T_{fp}] \begin{bmatrix} \Phi_f \\ \Phi_p \end{bmatrix} = 0 \quad (6.67)$$

For TM modes, $\Phi_p = 0$ and hence

$$[C_{ff} - k^2 T_{ff}] \Phi_f = 0 \quad (6.68)$$

Premultiplying by T_{ff}^{-1} gives

$$[T_{ff}^{-1} C_{ff} - k^2 I] \Phi_f = 0 \quad (6.69)$$

Letting

$$A = T_{ff}^{-1} C_{ff}, \quad k^2 = \lambda, \quad X = \Phi_f \quad (6.70a)$$

we obtain the standard eigenproblem

$$(A - \lambda I)X = 0 \quad (6.70b)$$

where I is a unit matrix. Any standard procedure [7] may be used to obtain some or all of the eigenvalues $\lambda_1, \lambda_2, \dots, \lambda_{n_f}$ and eigenvectors X_1, X_2, \dots, X_{n_f} , where n_f is the number of free nodes. The eigenvalues are always real since C and T are symmetric.

Solution of the algebraic eigenvalue problems in Equation (6.70) furnishes eigenvalues and eigenvectors, which form good approximations to the eigenvalues and eigenfunctions of the Helmholtz problem, i.e., the cutoff wavelengths and field distribution patterns of the various modes possible in a given waveguide.

The solution of the problem presented in this section, as summarized in Equation (6.69), can be viewed as the finite element solution of homogeneous waveguides. The idea can be extended to handle inhomogeneous waveguide problems [8]–[11]. However, in applying FEM to inhomogeneous problems, a serious difficulty is the appearance of spurious, nonphysical solutions. Several techniques have been proposed to overcome the difficulty [12]–[18].

Example 6.3

To apply the ideas presented in this section, we use the finite element analysis to determine the lowest (or dominant) cutoff wavenumber k_c of the TM_{11} mode in waveguides with square ($a \times a$) and rectangular ($a \times b$) cross sections for which the exact results are already known as

$$k_c = \sqrt{(m\pi/a)^2 + (n\pi/b)^2}$$

where $m = n = 1$.

It may be instructive to try with hand calculation the case of a square waveguide with 2 divisions in the x and y directions. In this case, there are 9 nodes, 8 triangular elements, and 1 free node ($n_f = 1$). Equation (6.68) becomes

$$C_{11} - k^2 T_{11} = 0$$

6.4. SOLUTION OF THE WAVE EQUATION

where C_{11} and T_{11} are obtained from Equations (6.34), (6.35), and (6.47) as

$$C_{11} = \frac{a^2}{2A}, \quad T_{11} = \frac{A}{12}, \quad A = \frac{a^2}{8}$$

Hence

$$k^2 = \frac{a^2}{2A^2} = \frac{32}{a^2}$$

or

$$ka = 5.656$$

which is about 27% off the exact solution. To improve the accuracy, we must use more elements.

The computer program in Figure 6.11 applies the ideas in this section to find k_c . The main program calls function GRID (to be discussed in Section 6.5) to generate the necessary input data from a given geometry. If n_x and n_y are the number of divisions in the x and y directions, the total number of elements $n_e = 2n_x n_y$. By simply specifying the values of a , b , n_x , and n_y , the program determines k_c . The results for the square ($a = b$) and rectangular ($b = 2a$) waveguides are presented in Tables 6.5a and 6.5b, respectively. □

Table 6.5 (a) Lowest Wavenumber for a Square Waveguide ($b = a$)

n_x	n_e	$k_c a$	% Error
2	8	5.656	27.3
3	18	5.030	13.2
5	50	4.657	4.82
7	98	4.553	2.47
10	200	4.497	1.22
Exact: $k_c a = 4.4429$, $n_y = n_x$			

Table 6.5 (b) Lowest Wavenumber for a Rectangular Waveguide ($b = 2a$)

n_x	n_e	$k_c a$	% Error
2	16	4.092	16.5
4	64	3.659	4.17
6	144	3.578	1.87
8	256	3.549	1.04
Exact: $k_c a = 3.5124$, $n_y = 2n_x$			

```

% FINITE ELEMENT SOLUTION OF LAPLACE'S EQUATION FOR
% TWO-DIMENSIONAL PROBLEMS
% TRIANGULAR ELEMENTS ARE USED

% THE UNKNOWN POTENTIALS ARE OBTAINED USING
% ITERATION METHOD

% ND = NO. OF NODES
% NE = NO. OF ELEMENTS
% NP = NO. OF FIXED NODES (WHERE POTENTIAL IS PRESCRIBED)
% NDP(I) = NODE NO. OF PRESCRIBED POTENTIAL, I = 1,2,...NP
% VAL(I) = VALUE OF PRESCRIBED POTENTIAL AT NODE NDP(I)
% NL(I,J) = LIST OF NODES FOR EACH ELEMENT I, WHERE
% LF(I) = LIST OF FREE NODES I = 1,2,...,NF=ND-NP
% J = 1, 2, 3 IS THE LOCAL NODE NUMBER
% CE(I,J) = ELEMENT COEFFICIENT MATRIX
% ER(I) = VALUE OF THE RELATIVE PERMITTIVITY FOR ELEMENT I
% C(I,J) = GLOBAL COEFFICIENT MATRIX
% X(I), Y(I) = GLOBAL COORDINATES OF NODE I
% XL(J), YL(J) = LOCAL COORDINATES OF NODE J = 1,2,3
% V(I) = POTENTIAL AT NODE I
% MATRICES P(I) AND Q(I) ARE DEFINED IN EQUATION(6.1.1)

***** FIRST STEP - INPUT DATA DEFINING GEOMETRY AND
***** BOUNDARY CONDITIONS
*****
clear;
NI = 50; %! NO. OF ITERATIONS
NE=25; %Number of Elements
ND=21;
NP=15;

X = [0 0.2 0.4 0.6 0.8 1.0 0 0.2 0.4 0.6 0.8 0 0.2 0.4 0.6 0 0.2 0.4 0 0.2 0];
Y = [0 0 0 0 0 0.2 0.2 0.2 0.2 0.4 0.4 0.4 0.4 0.6 0.6 0.6 0.8 0.8 1.0];

NDP = [1 2 3 4 5 6 7 11 12 15 16 18 19 20 21];
VAL = [0 0 0 0 50 0 100 0 100 0 100 0 100 50];

NL = [ 1 2 7 ; 2 8 7; 2 3 8; 3 9 8; 3 4 9; 4 10 9; 4 5 10; 5 11 10; 5 6 11;...
       7 8 12; 8 13 12; 8 9 13; 9 14 13; 9 10 14; 10 15 14; 10 11 15;...
       12 13 16; 13 17 16; 13 14 17; 14 18 17; 14 15 18; 16 17 19; 17 20 19; 17 18 20; 19 20 21];

EO = 1.0E-9/(36.0*pi);
ER = ones(1,NE);

***** SECOND STEP - EVALUATE COEFFICIENT MATRIX FOR EACH
***** ELEMENT AND ASSEMBLE GLOBALLY
*****
C = zeros(ND,ND);
for I = 1: NE
    FIND LOCAL COORDINATES XL, YL FOR ELEMENT I
    XL = X(NL(I,:));
    YL = Y(NL(I,:));

    P = [YL(2) - YL(3), YL(3) - YL(1), YL(1) - YL(2)];
    Q = [XL(3) - XL(2), XL(1) - XL(3), XL(2) - XL(1)];
    AREA = 0.5*abs( P(2)*Q(3) - Q(2)*P(3) );

```

Figure 6.11

Computer program for Example 6.3 (Continued).

```

% DETERMINE COEFFICIENT MATRIX FOR ELEMENT I
% CE = ER(I)*(P'*P+Q'*Q)/(4*AREA);
% ASSEMBLE GLOBALLY - FIND C(I,J)
% J=1:3;
% L=1:3;
% IR = NL(I,J);
% IC = NL(I,L);
% C(IR,IC) = C(IR,IC) + CE(J,L);
% end

***** THIRD STEP - SOLVE THE RESULTING SYSTEM
***** ITERATIVELY
***** DETERMINE LF - LIST OF FREE NODES
LF = setdiff(1:ND, NDP);
V = zeros(1,ND);
V(NDP) = VAL;
NF = length(LF);

for N = 1:NI
    for ii = 1:NF
        rowC = C(LF(ii),:);
        rowC(LF(ii)) = 0;
        V(LF(ii)) = -1/(C(LF(ii),LF(ii)))*rowC*V.';
    end
    figure(1), stem(V), drawnow
end

disp([{ 'Node' , 'X' , 'Y' , 'Potential' } ; num2cell([(1:ND)', X', Y', V'])]);

```

Figure 6.11

(Cont.) Computer program for Example 6.3.

6.5 Automatic Mesh Generation I — Rectangular Domains

One of the major difficulties encountered in the finite element analysis of continuum problems is the tedious and time-consuming effort required in data preparation. Efficient finite element programs must have node and element generating schemes, referred to collectively as *mesh generators*. Automatic mesh generation minimizes the input data required to specify a problem. It not only reduces the time involved in data preparation, it eliminates human errors introduced when data preparation is performed manually. Combining the automatic mesh generation program with computer graphics is particularly valuable since the output can be monitored visually. Since some applications of the FEM to EM problems involve simple rectangular domains, we consider the generation of simple meshes [19] here; automatic mesh generator for arbitrary domains will be discussed in Section 6.6.

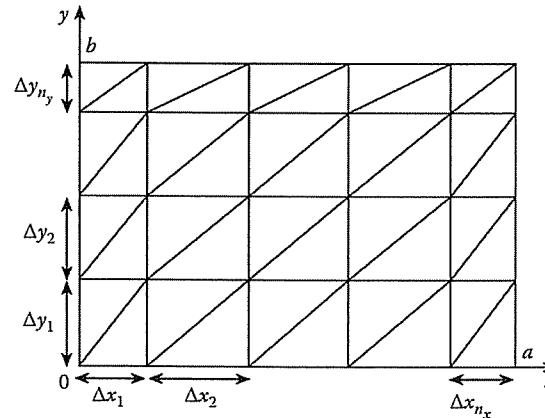


Figure 6.12
Discretization of a rectangular region into a nonuniform mesh.

Consider a rectangular solution region of size $a \times b$ as in Figure 6.12. Our goal is to divide the region into rectangular elements, each of which is later divided into two triangular elements. Suppose n_x and n_y are the number of divisions in x and y directions, the total number of elements and nodes are, respectively, given by

$$\begin{aligned} n_e &= 2n_x n_y \\ n_d &= (n_x + 1)(n_y + 1) \end{aligned} \quad (6.71)$$

Thus it is easy to figure out from Figure 6.12 a systematic way of numbering the elements and nodes. To obtain the global coordinates (x, y) for each node, we need an array containing $\Delta x_i, i = 1, 2, \dots, n_x$ and $\Delta y_j, j = 1, 2, \dots, n_y$, which are the distances between nodes in the x and y directions, respectively. If the order of node numbering is from left to right along horizontal rows and from bottom to top along the vertical rows, then the first node is the origin $(0,0)$. The next node is obtained as $x \rightarrow x + \Delta x_1$ while $y = 0$ remains unchanged. The following node has $x \rightarrow x + \Delta x_2, y = 0$, and so on until Δx_i are exhausted. We start the second horizontal row by starting with $x = 0, y \rightarrow y + \Delta y_1$ and increasing x until Δx_i are exhausted. We repeat the process until the last node $(n_x + 1)(n_y + 1)$ is reached, i.e., when Δx_i and Δy_i are exhausted simultaneously.

The procedure presented here allows for generating uniform and nonuniform meshes. A mesh is uniform if all Δx_i are equal and all Δy_i are equal; it is nonuniform otherwise. A nonuniform mesh is preferred if it is known in advance that the parameter of interest varies rapidly in some parts of the solution domain. This allows a concentration of relatively small elements in the regions where the parameter changes rapidly, particularly since these regions are often of greatest interest in the solution. Without the preknowledge of the rapid change in the unknown parameter, a uniform

6.6. AUTOMATIC MESH GENERATION II – ARBITRARY DOMAINS

mesh can be used. In that case, we set

$$\begin{aligned} \Delta x_1 &= \Delta x_2 = \dots = h_x \\ \Delta y_1 &= \Delta y_2 = \dots = h_y \end{aligned} \quad (6.72)$$

where $h_x = a/n_x$ and $h_y = b/n_y$.

In some cases, we also need a list of prescribed nodes. If we assume that all boundary points have prescribed potentials, the number n_p of prescribed node is given by

$$n_p = 2(n_x + n_y) \quad (6.73)$$

A simple way to obtain the list of boundary points is to enumerate points on the bottom, right, top, and left sides of the rectangular region in that order.

The ideas presented here are implemented in the function GRID in Figure 6.13. The subroutine can be used for generating a uniform or nonuniform mesh out of a given rectangular region. If a uniform mesh is desired, the required input parameters are a, b, n_x , and n_y . If, on the other hand, a nonuniform mesh is required, we need to supply $n_x, n_y, \Delta x_i, i = 1, 2, \dots, n_x$, and $\Delta y_j, j = 1, 2, \dots, n_y$. The output parameters are n_e, n_d, n_p , connectivity list, the global coordinates (x, y) of each node, and the list of prescribed nodes. It is needless to say that the subroutine GRID is not useful for a nonrectangular solution region. See the program in Figure 6.11 as an example on how to use subroutine GRID. A more general program for discretizing a solution region of any shape will be presented in the next section.

6.6 Automatic Mesh Generation II – Arbitrary Domains

As the solution regions become more complex than the ones considered in Section 6.5, the task of developing mesh generators becomes more tedious. A number of mesh generation algorithms (e.g., [21]–[33]) of varying degrees of automation have been proposed for arbitrary solution domains. Reviews of various mesh generation techniques can be found in [34].

The basic steps involved in a mesh generation are as follows [35, 36]:

- subdivide solution region into a few quadrilateral blocks,
- separately subdivide each block into elements,
- connect individual blocks.

Each step is explained as follows.

6.6.1 Definition of Blocks

The solution region is subdivided into quadrilateral blocks. Subdomains with different constitutive parameters (σ, μ, ϵ) must be represented by separate blocks. As

```

function [NE,ND,NP,NL,X,Y,NDP]=gridmesh(NX,NY,DX,DY)
% function [NE,ND,NP,NL,X,Y,NDP]=gridmesh(NX,NY,DX,DY)
% ****
% THIS PROGRAM DIVIDES A RECTANGULAR DOMAIN INTO
% TRIANGULAR ELEMENTS (NY BY NY NONUNIFORM
% MESH IN GENERAL)
% NX & NY ARE THE NUMBER OF SUBDIVISIONS ALONG X & Y AXES
% NE = NO. OF ELEMENTS IN THE MESH
% ND = NO. OF NODES IN THE MESH
% NP = NO. OF BOUNDARY (PRESCRIBED) NODES
% X(I) & Y(I) ARE GLOBAL COORDINATES OF NODE I
% DX(I) & DY(I) ARE DISTANCES BETWEEN NODES ALONG X & Y AXES
% NL(I,J) IS THE LIST OF NODES FOR ELEMENT I, J = 1, 2, 3 ARE
% LOCAL NUMBERS
% NDP(I) = LIST OF PRESCRIBED NODES I
%
% REF: J. N. REDDY, "AN INTRODUCTION TO THE FINITE ELEMENT
% METHOD." NEW YORK: MCGRAW-HILL, 1984, P. 436
%
% CALCULATE NE, ND, AND NP
NE = 2*NX*NY; %Number of elements
NP = 2*(NX + NY); %Number of prescribed nodes (edges)
NX1 = NX+1; %Number of nodes in the X direction
NY1 = NY +1; %Number of nodes in the Y direction
ND = NX1 * NY1; %Number of nodes in mesh
%
% Determine Node List which follows a regular pattern utilized below.
NL1 = 1:(NX1*NY);
NL1(NX1:NX1:end) = [];
NL3 = (NX+2):(NX+NX1*NY+1);
NL3(NX1:NX1:end) = [];
NL = zeros(NE,3);
NL(1:2:end,1) = NL1;
NL(2:2:end,1) = NL1;
NL(1:2:end,2) = NL3+1;
NL(2:2:end,2) = NL1+1;
NL(1:2:end,3) = NL3;
NL(2:2:end,3) = NL3+1;
%
% DETERMINE X AND Y (look saw tooth waves)
x1 = [0 cumsum(DX)']*ones(1,NY1);
X = reshape(x1,1,numel(x1));
y1 = ones(NX1,1)*[0 cumsum(DY)];
Y = reshape(y1,1,numel(y1));
%
% DETERMINE NDP, [bottom, right, top, left]
NDP = [1:(NX1), 2*(NX1):(NX1):ND, (ND-1):-1:(ND-NX), ((ND-2*NX-1)):-1:(NX1):(NX+2)];

```

Figure 6.13
Program GRID.

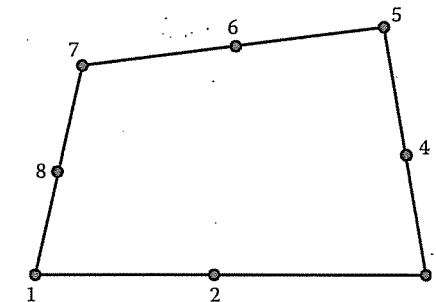


Figure 6.14
Typical quadrilateral block.

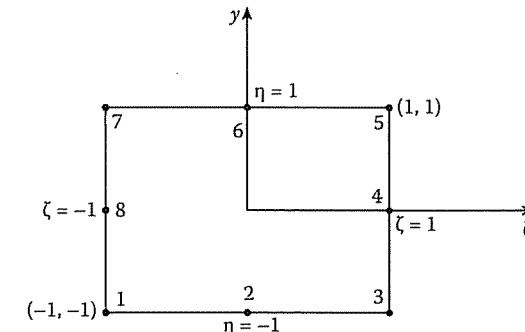


Figure 6.15
Eight-node serendipity element.

input data, we specify block topologies and the coordinates at eight points describing each block. Each block is represented by an eight-node quadratic isoparametric element. With natural coordinate system (ζ, η) , the x and y coordinates are represented as

$$x(\zeta, \eta) = \sum_{i=1}^8 \alpha_i(\zeta, \eta) x_i \quad (6.74)$$

$$y(\zeta, \eta) = \sum_{i=1}^8 \alpha_i(\zeta, \eta) y_i \quad (6.75)$$

where $\alpha_i(\zeta, \eta)$ is a shape function associated with node i , and (x_i, y_i) are the coordinates of node i defining the boundary of the quadrilateral block as shown in Figure 6.14. The shape functions are expressed in terms of the quadratic or parabolic isoparametric elements shown in Figure 6.15. They are given by

$$\alpha_i = \frac{1}{4} (1 + \zeta \zeta_i)(1 + \eta \eta_i)(\zeta \zeta_i + \eta \eta_i + 1), \quad i = 1, 3, 5, 7 \quad (6.76)$$

for corner nodes,

$$\begin{aligned}\alpha_i = & \frac{1}{2} \zeta_i^2 (1 + \zeta \zeta_i) (1 - \eta^2) \\ & + \frac{1}{2} \eta_i^2 (1 + \eta \eta_i + 1) (1 - \zeta^2), \quad i = 2, 4, 6, 8\end{aligned}\quad (6.77)$$

for midside nodes. Note the following properties of the shape functions:

- (1) They satisfy the conditions

$$\sum_{i=1}^n \alpha_i(\zeta, \eta) = 1 \quad (6.78a)$$

$$\alpha_i(\zeta_j, \eta_j) = \begin{cases} 1, & i = j \\ 0, & i \neq j \end{cases} \quad (6.78b)$$

- (2) They become quadratic along element edges ($\zeta = \pm 1, \eta = \pm 1$).

6.6.2 Subdivision of Each Block

For each block, we specify $N DIV X$ and $N DIV Y$, the number of element subdivisions to be made in the ζ and η directions, respectively. Also, we specify the weighting factors $(W_\zeta)_i$ and $(W_\eta)_i$ allowing for graded mesh within a block. In specifying $N DIV X$, $N DIV Y$, W_ζ , and W_η care must be taken to ensure that the subdivision along block interfaces (for adjacent blocks) are compatible. We initialize ζ and η to a value of -1 so that the natural coordinates are incremented according to

$$\zeta_i = \zeta_i + \frac{2(W_\zeta)_i}{W_\zeta^T \cdot F} \quad (6.79)$$

$$\eta_i = \eta_i + \frac{2(W_\eta)_i}{W_\eta^T \cdot F} \quad (6.80)$$

where

$$W_\zeta^T = \sum_{j=1}^{N DIV X} (W_\zeta)_j \quad (6.81a)$$

$$W_\eta^T = \sum_{j=1}^{N DIV X} (W_\eta)_j \quad (6.81b)$$

and

$$F = \begin{cases} 1, & \text{for linear elements} \\ 2, & \text{for quadratic elements} \end{cases}$$

Three element types are permitted: (a) linear four-node quadrilateral elements, (b) linear three-node triangular elements, and (c) quadratic eight-node isoparametric elements.

6.7 BANDWIDTH REDUCTION

6.6.3 Connection of Individual Blocks

After subdividing each block and numbering its nodal points separately, it is necessary to connect the blocks and have each node numbered uniquely. This is accomplished by comparing the coordinates of all nodal points and assigning the same number to all nodes having identical coordinates. That is, we compare the coordinates of node 1 with all other nodes, and then node 2 with other nodes, etc., until all repeated nodes are eliminated. The listing of the MATLAB code for automatic mesh generation is shown in Figure 6.16. The following example taken from [36] illustrates the application of the code.

Example 6.4

Utilize the `distmesh2d` function by Persson and Strang [36] in Figure 6.16 to discretize the geometry shown in Figure 6.17. This geometry is composed of the union of two rectangles whose bottom left and top right coordinates (x_1, y_1) , (x_2, y_2) are $(0, 0)$, $(5, 10)$ and $(5, 5)$, $(8, 10)$, and a circle void centered at $(2.5, 7.5)$ with radius of 1.5. \square

Solution

The code in Figure 6.16 describes the basic geometry of the structure with a signed distance function ‘`fd`’ which is a MATLAB inline function composed of the union of two rectangles and a circular void. The parameter “`box`” defines the limit of the solution space of the mesh and the parameter “`fix`” contains the pre-determined nodes in the mesh. `Distmesh2d` uses an iterative mesh generation technique based on the physical analogy between a simplex mesh and a truss structure. Meshpoints are the nodes of the truss. The main program in Figure 6.16(a) needs the subroutines `ddiff.m`, `dunion.m`, `dcirc.m`, and `drectangle.m` all provided in Figure 6.16(b). The completed mesh is shown in Figure 6.18. \blacksquare

6.7 Bandwidth Reduction

Since most of the matrices involved in FEM are symmetric, sparse, and banded, we can minimize the storage requirements and the solution time by storing only the elements involved in half bandwidth instead of storing the whole matrix. To take the fullest advantage of the benefits from using a banded matrix solution technique, we must make sure that the matrix bandwidth is as narrow as possible.

If we let d be the maximum difference between the lowest and the highest node numbers of any single element in the mesh, we define the semi-bandwidth B (which includes the diagonal term) of the coefficient matrix $[C]$ as

$$B = (d + 1)f \quad (6.82)$$

```

function ch6 FIG6_16
fd=inline('ddiff(dunion(drectangle(p,0,5,0,10),drectangle(p,5,8,5,10)),
dcircle(p,2.5,7.5,1.5) )','p');

box=[-1 -1; 8.1 10.1];
fix=[0 0; 0 5; 0 10; 5 0; 5 5; 5 10; 8 5; 8 10];
[p,t]=distmesh2d(fd,@uniform,0.7,box,fix);
disp('Mesh Complete')

function [p,t]=distmesh2d(fd,fh,h0,bbox,pfix,varargin)
%DISTMESH2D 2-D Mesh Generator using Distance Functions.
% [P,T]=DISTMESH2D(FD,FH,H0,BBOX,PFIX,FPARAMS)
%
% P: Node positions (Nx2)
% T: Triangle indices (NTx3)
% FD: Distance function d(x,y)
% FH: Scaled edge length function h(x,y)
% H0: Initial edge length
% BBOX: Bounding box [xmin,ymin; xmax,ymax]
% PFIX: Fixed node positions (NFIx2)
% FPARAMS: Additional parameters passed to FD and FH

Example: (Uniform Mesh on Unit Circle)
fd=inline('sqrt(sum(p.^2,2))-1','p');
[p,t]=distmesh2d(fd,@uniform,0.2,[-1,-1;1,1],[]);

Example: (Rectangle with circular hole, refined at circle boundary)
fd=inline('ddiff(drectangle(p,-1,1,-1,1),dcircle(p,0,0,0.5))','p');
fh=inline('min(4*sqrt(sum(p.^2,2))-1,2)','p');
[p,t]=distmesh2d(fd,fh,0.05,[-1,-1;1,1],[-1,-1;-1,1;-1,1,1]);

See also: MESHDEMO2D, DISTMESHND, DELAUNAYN, TRIMESH.

Copyright (C) 2004-2006 Per-Olof Persson.

dptol=.001; ttol=.1; Fscale=1.2; deltat=.2; geps=.001*h0; deps=sqrt(eps)*h0;

% 1. Create initial distribution in bounding box (equilateral triangles)
[x,y]=meshgrid(bbox(1,1):h0:bbox(2,1),bbox(1,2):h0*sqrt(3)/2:bbox(2,2));
x(2:2:end,:)=x(2:2:end,:)+h0/2; % Shift even rows
p=[x(:,y:)];
%
% 2. Remove points outside the region, apply the rejection method
p=p(feval(fd,p,varargin{1})<geps,:); % Keep only d<0 points
r0=1./feval(fh,p,varargin{1}).^2;
p=[pfix; p(rand(size(p,1),1)<r0./max(r0),:)]; % Rejection method
N=size(p,1); % Number of points N
pold=inf; % For first iteration
while 1
  % 3. Retriangulation by the Delaunay algorithm
  if max(sqrt(sum((p-pold).^2,2))/h0)>ttol % Any large movement?
    pold=p; % Save current positions
    t=delaunayn(p); % List of triangles
  end
end

```

Figure 6.16

MATLAB code for automatic mesh generation: (a) main program, (b) functions that the main function will need. (*Continued*).

```

pmid=(p(:,1,:)+p(:,2,:)+p(:,3,:))/3; % Compute centroids
t=t(feval(fd,pmid,varargin{:})<-geps,:); % Keep interior triangles
%
% 4. Describe each bar by a unique pair of nodes
bars=[t(:,[1,2]);t(:,[1,3]);t(:,[2,3])]; % Interior bars duplicated
bars=unique(sort(bars,2),'rows'); % Bars as node pairs
%
% 5. Graphical output of the current mesh
trimesh(t,p(:,1),p(:,2),zeros(N,1))
view(2),axis equal,axis off,drawnow
end

%
% 6. Move mesh points based on bar lengths L and forces F
barvec=p(bars(:,1,:)-p(bars(:,2,:)); % List of bar vectors
L=sqrt(sum(barvec.^2,2)); % L = Bar lengths
hbars=feval(fh,(p(bars(:,1,:))+p(bars(:,2,:))/2),varargin{:});
L0=hbars*Fscale*sqrt(sum(L.^2)/sum(hbars.^2)); % L0 = Desired lengths
F=max(L0-L,0); % Bar forces (scalars)
Fvec=F./L*[1,1].*barvec; % Bar forces (x,y components)
Ftot=full(sparse(bars(:,1,2,2)),ones(size(F))*[1,2,1,2],[Fvec,-Fvec],N,2));
Ftot(1:size(pfix,1),:)=0; % Force = 0 at fixed points
p=p+deltat*Ftot; % Update node positions

%
% 7. Bring outside points back to the boundary
d=feval(fd,p,varargin{:}); ix=d>0; % Find points outside (d>0)
dgradx=(feval(fd,[p(ix,1)+deps,p(ix,2)],varargin{:})-d(ix))/deps; % Numerical
dgrady=(feval(fd,[p(ix,1),p(ix,2)+deps],varargin{:})-
d(ix))/deps; % gradient
p(ix,:)=p(ix,:)-[d(ix).*dgradx,d(ix).*dgrady]; % Project back to boundary
%
% 8. Termination criterion: All interior nodes move less than dptol (scaled)
if max(sqrt(sum(deltat*Ftot(d<-geps,:).^2,2))/h0)<dptol, break; end
end

function h=huniform(p,varargin)
h=ones(size(p,1),1);

(a)

function d=drectangle(p,x1,x2,y1,y2)
d=-min(min(-y1+p(:,2),y2-p(:,2)),-x1+p(:,1)),x2-p(:,1));

function d=dcirc(p,xc,yc,r)
d=sqrt((p(:,1)-xc).^2+(p(:,2)-yc).^2)-r;

function d=dunion(d1,d2), d=min(d1,d2);

function d=ddiff(d1,d2), d=max(d1,-d2);

(b)

```

Figure 6.16

(*Cont.*) MATLAB code for automatic mesh generation: (a) main program, (b) functions that the main function will need.

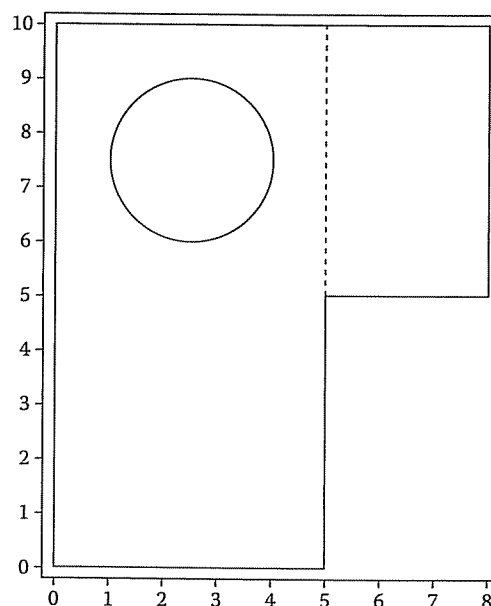


Figure 6.17
Solution region of Example 6.4.

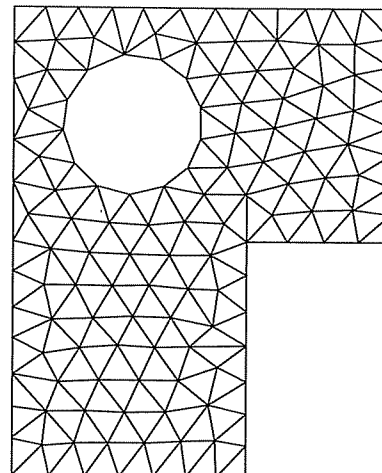


Figure 6.18
The generated mesh for Example 6.4.

6.7. BANDWIDTH REDUCTION

where f is the number of degrees of freedom (or number of parameters) at each node. If, for example, we are interested in calculating the electric field intensity \mathbf{E} for a three-dimensional problem, then we need E_x , E_y , and E_z at each node, and $f = 3$ in this case. Assuming that there is only one parameter per node,

$$B = d + 1 \quad (6.83)$$

The semi-bandwidth, which does not include the diagonal term, is obtained from Equation (6.82) or (6.83) by subtracting one from the right-hand side, i.e., for $f = 1$,

$$B = d \quad (6.84)$$

Throughout our discussion in this section, we will stick to the definition of semi-bandwidth in Equation (6.84). The total bandwidth may be obtained from Equation (6.84) as $2B + 1$.

The bandwidth of the global coefficient matrix depends on the node numbering. Hence, to minimize the bandwidth, the node numbering should be selected to minimize d . Good node numbering is usually such that nodes with widely different numbers are widely separated. To minimize d , we must number nodes across the narrowest part of the region.

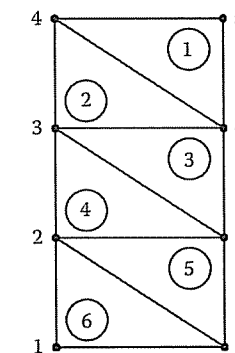


Figure 6.19
Original mesh with $B = 7$.

Consider, for the purpose of illustration, the mesh shown in Figure 6.19. If the mesh is numbered originally as in Figure 6.19, we obtain d_e for each element e as

$$d_1 = 2, d_2 = 3, d_3 = 4, d_4 = 5, d_5 = 6, d_6 = 7 \quad (6.85)$$

From this, we obtain

$$d = \text{maximum } d_e = 7$$

or

$$B = 7 \quad (6.86)$$

Alternatively, the semi-bandwidth may be determined from the coefficient matrix, which is obtained by mere inspection of Figure 6.19 as

$$[C] = \begin{array}{c|ccccccccc} & & & & & B=7 & & & \\ \hline & 1 & 2 & 3 & 4 & 5 & 6 & 7 & 8 \\ \hline 1 & x & x & & & & & & x \\ 2 & x & x & x & & & & x & x \\ 3 & & x & x & x & & x & & \\ 4 & & & x & x & x & x & & \\ 5 & & & & x & x & x & & \\ 6 & & & & x & x & x & x & x \\ 7 & & x & & & x & x & x & \\ 8 & x & x & & & & & & x \end{array} \quad (6.87)$$

where x indicates a possible nonzero term and blanks are zeros (i.e., $C_{ij} = 0$, indicating no coupling between nodes i and j). If the mesh is renumbered as in Figure 6.20(a),

$$d_1 = 4 = d_2 = d_3 = d_4 = d_5 = d_6 \quad (6.88')$$

and hence

$d = \text{maximum } d_e = 4$

or

$$B = 4 \quad (6.89)$$

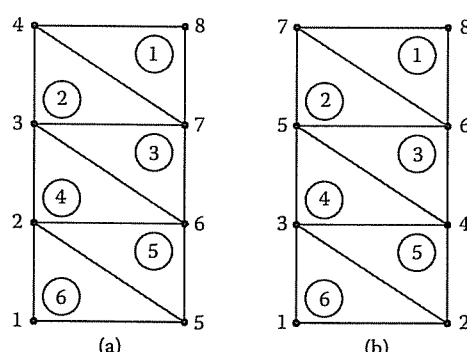


Figure 6.20

Renumbered nodes: (a) $B = 4$, (b) $B = 2$.

Finally, we may renumber the mesh as in Figure 6.20(b). In this case

$$d_1 = 2 = d_2 = d_3 = d_4 = d_5 = d_6 \quad (6.90)$$

and

$$d = \text{maximum } d_e = 2 \quad . \quad (6.91)$$

or

$$B = 2 \quad (6.92)$$

The value $B = 2$ may also be obtained from the coefficient matrix for the mesh in Figure 6.20(b), namely,

From Equation (6.93), one immediately notices that $[C]$ is symmetric and that terms are clustered in a band about the diagonal. Hence $[C]$ is sparse and banded so that only the data within the area **PQRS** of the matrix need to be stored—a total of 33 terms out of 64. This illustrates the savings in storage by a careful nodal numbering.

For a simple mesh, hand-labeling coupled with a careful inspection of the mesh (as we have done so far) can lead to a minimum bandwidth. However, for a large mesh, a hand-labeling technique becomes a tedious, time-consuming task, which in most cases may not be successful. It is particularly desirable that an automatic relabeling scheme is implemented within a mesh generation program. A number of algorithms have been proposed for bandwidth reduction by automatic mesh renumbering [37]–[40]. A simple, efficient algorithm is found in Collins [37].

6.8 Higher Order Elements

The finite elements we have used so far have been the linear type in that the shape function is of the order one. A higher order element is one in which the shape function or interpolation polynomial is of the order two or more.

The accuracy of a finite element solution can be improved by using finer mesh or using higher order elements or both. A discussion on mesh refinement versus higher order elements is given by Desai and Abel [2]; a motivation for using higher order

elements is given by Csendes in [41]. In general, fewer higher order elements are needed to achieve the same degree of accuracy in the final results. The higher order elements are particularly useful when the gradient of the field variable is expected to vary rapidly. They have been applied with great success in solving EM-related problems [4], [41]–[46].

6.8.1 Pascal Triangle

Higher-order triangular elements can be systematically developed with the aid of the so-called Pascal triangle given in Figure 6.21. The family of finite elements generated in this manner with the distribution of nodes illustrated in Figure 6.22. Note that in higher order elements, some secondary (side and/or interior) nodes are introduced in addition to the primary (corner) nodes so as to produce exactly the right number of nodes required to define the shape function of that order. The Pascal triangle contains terms of the basis functions of various degrees in variables x and y . An arbitrary function $\Phi_i(x, y)$ can be approximated in an element in terms of a complete n th order polynomial as

$$\Phi(x, y) = \sum_{i=1}^m \alpha_i \Phi_i \quad (6.94)$$

where

$$m = \frac{1}{2}(n+1)(n+2) \quad (6.95)$$

is the number of terms in complete polynomials (also the number of nodes in the triangle). For example, for second order ($n = 2$) or quadratic (six-node) triangular elements,

$$\Phi_e(x, y) = a_1 + a_2x + a_3y + a_4xy + a_5x^2 + a_6y^2 \quad (6.96)$$

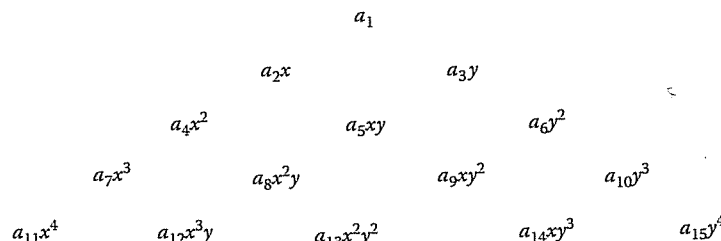


Figure 6.21

The Pascal triangle. The first row is (constant, $n = 0$), the second (linear, $n = 1$), the third (quadratic, $n = 2$), the fourth (cubic, $n = 3$), the fifth (quartic, $n = 4$).

6.8. HIGHER ORDER ELEMENTS

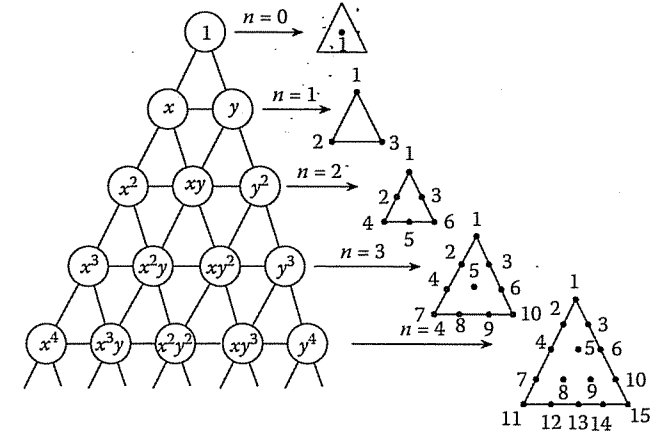


Figure 6.22

The Pascal triangle and the associated polynomial basis function for degree $n = 1$ to 4.

This equation has six coefficients, and hence the element must have six nodes. It is also complete through the second order terms. A systematic derivation of the interpolation function α for the higher order elements involves the use of the local coordinates.

6.8.2 Local Coordinates

The triangular local coordinates (ξ_1, ξ_2, ξ_3) are related to Cartesian coordinates (x, y) as

$$x = \xi_1 x_1 + \xi_2 x_2 + \xi_3 x_3 \quad (6.97)$$

$$y = \xi_1 y_1 + \xi_2 y_2 + \xi_3 y_3 \quad (6.98)$$

The local coordinates are dimensionless with values ranging from 0 to 1. By definition, ξ_i at any point within the triangle is the ratio of the perpendicular distance from the point to the side opposite to vertex i to the length of the altitude drawn from vertex i . Thus, from Figure 6.23 the value of ξ_1 at P, for example, is given by the ratio of the perpendicular distance d from the side opposite vertex 1 to the altitude h of that side, i.e.,

$$\xi_1 = \frac{d}{h} \quad (6.99)$$

Alternatively, from Figure 6.23, ξ_i at P can be defined as

$$\xi_i = \frac{A_i}{A} \quad (6.100)$$

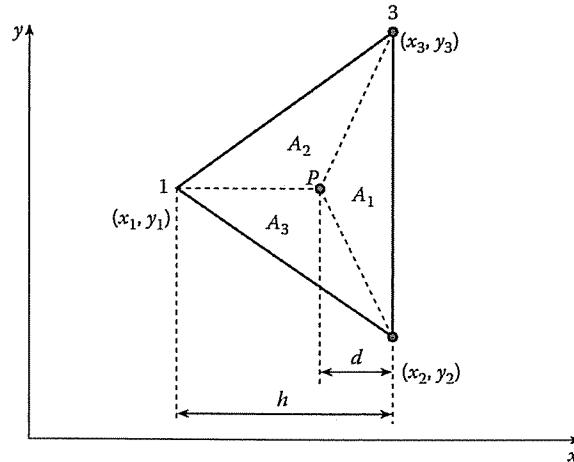


Figure 6.23

Definition of local coordinates.

so that

$$\xi_1 + \xi_2 + \xi_3 = 1 \quad (6.101)$$

since $A_1 + A_2 + A_3 = A$. In view of Equation (6.100), the local coordinates ξ_i are also called *area coordinates*. The variation of (ξ_1, ξ_2, ξ_3) inside an element is shown in Figure 6.24. Although the coordinates ξ_1 , ξ_2 , and ξ_3 are used to define a point P, only two are independent since they must satisfy Equation (6.101). The inverted form of Equations (6.97) and (6.98) is

$$\xi_i = \frac{1}{2A} [c_i + b_i x + a_i y] \quad (6.102)$$

where

$$\begin{aligned} a_i &= x_k - x_j, \\ b_i &= y_j - y_k, \\ c_i &= x_j y_k - x_k y_j \end{aligned}$$

$$A = \text{area of the triangle} = \frac{1}{2} (b_1 a_2 - b_2 a_1), \quad (6.103)$$

and (i, j, k) is an even permutation of $(1, 2, 3)$. (Notice that a_i and b_i are the same as Q_i and P_i in Equation (6.34).) The differentiation and integration in local coordinates

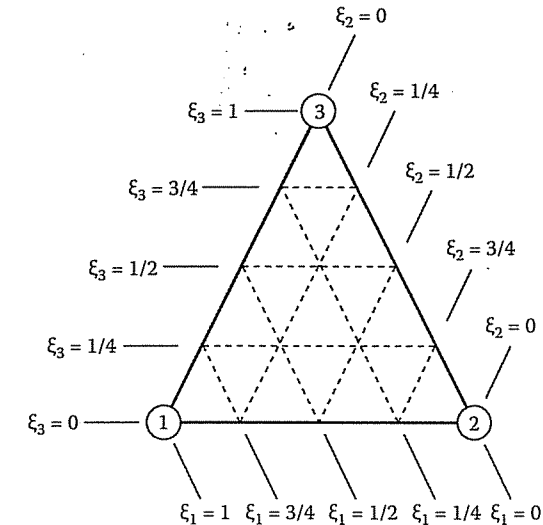


Figure 6.24

Variation of local coordinates.

are carried out using [47]:

$$\frac{\partial f}{\partial \xi_1} = a_2 \frac{\partial f}{\partial x} - b_2 \frac{\partial f}{\partial y} \quad (6.104a)$$

$$\frac{\partial f}{\partial \xi_2} = -a_1 \frac{\partial f}{\partial x} + b_1 \frac{\partial f}{\partial y} \quad (6.104b)$$

$$\frac{\partial f}{\partial x} = \frac{1}{2A} \left(b_1 \frac{\partial f}{\partial \xi_1} + b_2 \frac{\partial f}{\partial \xi_2} \right) \quad (6.104c)$$

$$\frac{\partial f}{\partial y} = \frac{1}{2A} \left(a_1 \frac{\partial f}{\partial \xi_1} + a_2 \frac{\partial f}{\partial \xi_2} \right) \quad (6.104d)$$

$$\iint f \, dS = 2A \int_0^1 \left[\int_0^{1-\xi_2} f(\xi_1, \xi_2) \, d\xi_1 \right] d\xi_2 \quad (6.104e)$$

$$\iint \xi_1^i \xi_2^j \xi_3^k \, dS = \frac{i! j! k!}{(i+j+k+2)!} 2A \quad (6.104f)$$

$$dS = 2A \, d\xi_1 \, d\xi_2 \quad (6.104g)$$

6.8.3 Shape Functions

We may now express the shape function for higher order elements in terms of local coordinates. Sometimes, it is convenient to label each point in the finite elements in Figure 6.22 with three integers i , j , and k from which its local coordinates (ξ_1, ξ_2, ξ_3)

can be found or vice versa. At each point P_{ijk}

$$(\xi_1, \xi_2, \xi_3) = \left(\frac{i}{n}, \frac{j}{n}, \frac{k}{n} \right) \quad (6.105)$$

Hence if a value of Φ , say Φ_{ijk} , is prescribed at each point P_{ijk} , Equation (6.94) can be written as

$$\Phi(\xi_1, \xi_2, \xi_3) = \sum_{i=1}^m \sum_{j=1}^{m-i} \alpha_{ijk}(\xi_1, \xi_2, \xi_3) \Phi_{ijk} \quad (6.106)$$

where

$$\alpha_\ell = \alpha_{ijk} = p_i(\xi_1) p_j(\xi_2) p_k(\xi_3), \quad \ell = 1, 2, \dots \quad (6.107)$$

$$p_r(\xi) = \begin{cases} \frac{1}{r!} \prod_{t=0}^{r-1} (n\xi - t), & r > 0 \\ 1, & r = 0 \end{cases} \quad (6.108)$$

and $r \in (i, j, k)$. $p_r(\xi)$ may also be written as

$$p_r(\xi) = \frac{(n\xi - r + 1)}{r} p_{r-1}(\xi), \quad r > 0 \quad (6.109)$$

where $p_0(\xi) = 1$.

The relationships between the subscripts $q \in \{1, 2, 3\}$ on ξ_q , $\ell \in \{1, 2, \dots, m\}$ on α_ℓ , and $r \in (i, j, k)$ on p_r and P_{ijk} in Equations (6.107) to (6.109) are illustrated in Figure 6.25 for n ranging from 1 to 4. Henceforth point P_{ijk} will be written as P_n for conciseness.

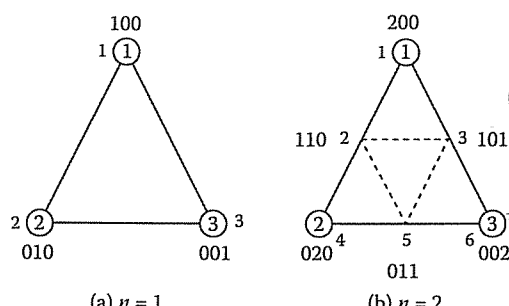


Figure 6.25

Distribution of nodes over triangles for $n = 1$ to 4. The triangles are in standard position (Continued).

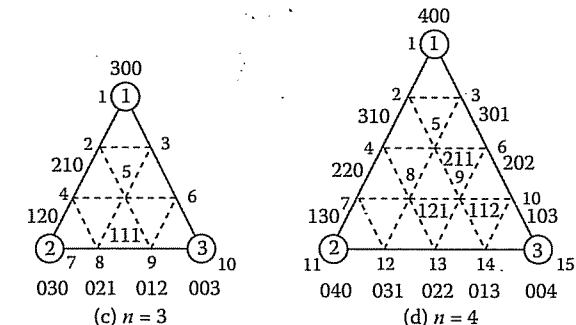


Figure 6.25

(Cont.) Distribution of nodes over triangles for $n = 1$ to 4. The triangles are in standard position.

Notice from Equation (6.108) or Equation (6.109) that

$$\begin{aligned} p_0(\xi) &= 1 \\ p_1(\xi) &= n\xi \\ p_2(\xi) &= \frac{1}{2}(n\xi - 1)n\xi \\ p_3(\xi) &= \frac{1}{6}(n\xi - 2)(n\xi - 1)n\xi \\ p_4(\xi) &= \frac{1}{24}(n\xi - 3)(n\xi - 2)(n\xi - 1)n\xi, \text{ etc} \end{aligned} \quad (6.110)$$

Substituting Equation (6.110) into Equation (6.107) gives the shape functions α_ℓ for nodes $\ell = 1, 2, \dots, m$, as shown in Table 6.6 for $n = 1$ to 4. Observe that each α_ℓ takes the value of 1 at node ℓ and value of 0 at all other nodes in the triangle. This is easily verified using Equation (6.105) in conjunction with Figure 6.25.

6.8.4 Fundamental Matrices

The fundamental matrices $[T]$ and $[Q]$ for triangular elements can be derived using the shape functions in Table 6.6. (For simplicity, the brackets $[]$ denoting a matrix quantity will be dropped in the remaining part of this section.) In Equation (6.46), the T matrix is defined as

$$T_{ij} = \iint \alpha_i \alpha_j dS \quad (6.46)$$

From Table 6.6, we substitute α_ℓ in Equation (6.46) and apply Equations (6.104e) and (6.104f) to obtain elements of T . For example, for $n = 1$,

$$T_{ij} = 2A \int_0^1 \int_0^{1-\xi_2} \xi_i \xi_j d\xi_1 d\xi_2$$

Table 6.6 Polynomial Basis Function $\alpha_\ell(\xi_1, \xi_2, \xi_3, \xi_4)$ for First-, Second-, Third-, and Fourth-Order

$n = 1$	$n = 2$	$n = 3$	$n = 4$
$\alpha_1 = \xi_1$	$\alpha_1 = \xi_1(2\xi_1 - 1)$	$\alpha_1 = \frac{1}{2}\xi_1(3\xi_1 - 2)(3\xi_1 - 1)$	$\alpha_1 = \frac{1}{6}\xi_1(4\xi_1 - 3)(4\xi_1 - 2)(4\xi_1 - 1)$
$\alpha_2 = \xi_2$	$\alpha_2 = 4\xi_1\xi_2$	$\alpha_2 = \frac{9}{2}\xi_1(3\xi_1 - 1)\xi_2$	$\alpha_2 = \frac{8}{3}\xi_1(4\xi_1 - 2)(4\xi_1 - 1)\xi_2$
$\alpha_3 = \xi_3$	$\alpha_3 = 4\xi_1\xi_3$	$\alpha_3 = \frac{9}{2}\xi_1(3\xi_1 - 1)\xi_3$	$\alpha_3 = \frac{8}{3}\xi_1(4\xi_1 - 2)(4\xi_1 - 1)\xi_3$
$\alpha_4 = \xi_2(2\xi_2 - 1)$	$\alpha_4 = \frac{1}{2}\xi_1(3\xi_2 - 1)\xi_2$	$\alpha_4 = 4\xi_1(4\xi_1 - 1)(4\xi_2 - 1)\xi_2$	
$\alpha_5 = 4\xi_2\xi_3$	$\alpha_5 = 27\xi_1\xi_2\xi_3$		$\alpha_5 = 32\xi_1(4\xi_1 - 1)\xi_2\xi_3$
$\alpha_6 = \xi_3(2\xi_3 - 1)$	$\alpha_6 = \frac{9}{2}\xi_1(3\xi_3 - 1)\xi_3$	$\alpha_6 = 4\xi_1(4\xi_1 - 1)(4\xi_3 - 1)\xi_3$	
	$\alpha_7 = \frac{1}{2}\xi_2(3\xi_2 - 2)(3\xi_2 - 1)$	$\alpha_7 = \frac{8}{3}\xi_1(4\xi_2 - 2)(4\xi_2 - 1)\xi_2$	
	$\alpha_8 = \frac{9}{2}\xi_2(3\xi_2 - 1)\xi_3$	$\alpha_8 = 32\xi_1(4\xi_2 - 1)\xi_2\xi_3$	
	$\alpha_9 = \frac{9}{2}\xi_2(3\xi_3 - 1)\xi_3$	$\alpha_9 = 32\xi_1\xi_2(4\xi_3 - 1)\xi_3$	
	$\alpha_{10} = \frac{1}{2}\xi_3(3\xi_3 - 2)(3\xi_3 - 1)$	$\alpha_{10} = \frac{8}{3}\xi_1(4\xi_3 - 2)(4\xi_3 - 1)\xi_3$	
		$\alpha_{11} = \frac{1}{6}\xi_2(4\xi_2 - 3)(4\xi_2 - 2)(4\xi_2 - 1)$	
		$\alpha_{12} = \frac{8}{3}\xi_2(4\xi_2 - 2)(4\xi_2 - 1)\xi_3$	
		$\alpha_{13} = 4\xi_2(4\xi_2 - 1)(4\xi_3 - 1)\xi_3$	
		$\alpha_{14} = \frac{8}{3}\xi_2(4\xi_3 - 2)(4\xi_3 - 1)\xi_3$	
		$\alpha_{15} = \frac{1}{6}\xi_3(4\xi_3 - 3)(4\xi_3 - 2)(4\xi_3 - 1)$	

When $i \neq j$,

$$T_{ij} = \frac{2A(1!)(1!)(0!)}{4!} = \frac{A}{12}, \quad (6.111a)$$

when $i = j$,

$$T_{ij} = \frac{2A(2!)}{4!} = \frac{A}{6} \quad (6.111b)$$

Hence

$$T = \frac{A}{12} \begin{bmatrix} 2 & 1 & 1 \\ 1 & 2 & 1 \\ 1 & 1 & 2 \end{bmatrix} \quad (6.112)$$

6.8. HIGHER ORDER ELEMENTS

By following the same procedure, higher order T matrices can be obtained. The T matrices for orders up to $n = 4$ are tabulated in Table 6.7, where the factor A , the area of the element, has been suppressed. The actual matrix elements are obtained from Table 6.7 by multiplying the tabulated numbers by A and dividing by the indicated common denominator. The following properties of the T matrix are noteworthy:

(a) T is symmetric with positive elements;

(b) elements of T all add up to the area of the triangle, i.e., $\sum_i^m \sum_j^m T_{ij} = A$, since

by definition $\sum_{\ell=1}^m \alpha_\ell = 1$ at any point within the element;

(c) elements for which the two triple subscripts form similar permutations are equal, i.e., $T_{ijk,prq} = T_{ikj,prq} = T_{kij,rpq} = T_{kji,rqp} = T_{jki,qrp} = T_{jik,qpr}$; this should be obvious from Equations (6.46) and (6.107).

These properties are not only useful in checking the matrix, they have proved useful in saving computer time and storage. It is interesting to know that the properties are independent of coordinate system [46].

In Equation (6.14) or Equation (6.45), elements of $[C]$ matrix are defined by

$$C_{ij} = \iint \left(\frac{\partial \alpha_i}{\partial x} \frac{\partial \alpha_j}{\partial x} + \frac{\partial \alpha_i}{\partial y} \frac{\partial \alpha_j}{\partial y} \right) dS \quad (6.113)$$

By applying Equations (6.104a) to (6.104d) to Equation (6.113), it can be shown that [4, 43]

$$C_{ij} = \frac{1}{2A} \sum_{q=1}^3 \cot \theta_q \iint \left(\frac{\partial \alpha_i}{\partial \xi_{q+1}} - \frac{\partial \alpha_i}{\partial \xi_{q-1}} \right) \left(\frac{\partial \alpha_j}{\partial \xi_{q+1}} - \frac{\partial \alpha_j}{\partial \xi_{q-1}} \right) d\xi_1 d\xi_2$$

or

$$C_{ij} = \sum_{q=1}^3 Q_{ij}^{(q)} \cot \theta_q \quad (6.114)$$

where θ_q is the included angle of vertex $q \in \{1, 2, 3\}$ of the triangle and

$$Q_{ij}^{(q)} = \iint \left(\frac{\partial \alpha_i}{\partial \xi_{q+1}} - \frac{\partial \alpha_i}{\partial \xi_{q-1}} \right) \left(\frac{\partial \alpha_j}{\partial \xi_{q+1}} - \frac{\partial \alpha_j}{\partial \xi_{q-1}} \right) d\xi_1 d\xi_2 \quad (6.115)$$

Table 6.7 Table of T Matrix for $n = 1$ to 4 (Continued)

$n = 1$	Common denominator: 12	2	1	1
$n = 2$	Common denominator: 180	1	2	1
$n = 3$	Common denominator: 6720	1	1	2
76	18	18	0	36
18	540	270	-189	162
18	270	540	-135	162
0	-189	-135	540	162
36	162	162	1944	162
0	-135	-189	-54	162
11	0	27	18	36
27	-135	-54	270	162
27	-54	-135	-	162
11	27	0	27	36
				18
				11
				0
				76

6.8. HIGHER ORDER ELEMENTS

Table 6.7 (Cont.) Table of T Matrix for $n = 1$ to 4

$n = 4$	Common denominator: 56700	290	160	160	-80	160	-80	0	-160	-160	0	-27	-112	-112	-27
290	160	2560	1280	-1280	1280	-960	768	256	-256	512	0	512	64	256	-112
160	1280	2560	-960	1280	-1280	512	-256	256	256	-112	256	64	512	0	512
-80	-1280	-960	3168	384	48	-1280	384	-768	64	-80	-960	48	64	-12	-12
160	1280	1280	384	10752	384	256	-1536	-1536	256	-160	-256	-768	-256	-160	-160
-80	-960	-1280	48	384	3168	64	-768	384	-1280	-12	64	48	-960	-80	-80
0	768	512	-1280	256	64	2560	1280	-256	256	160	1280	-960	512	-112	-112
-160	256	-256	384	-1536	-768	1280	10752	-1536	-256	160	1280	384	256	-160	-160
-160	-256	256	-768	-1536	384	-256	-1536	10752	1280	-160	256	384	1280	160	160
0	512	768	64	256	-1280	256	-256	1280	2560	-112	512	-960	1280	160	160
-27	0	-112	-80	-160	-12	160	-160	-112	290	160	-80	0	-27	0	-27
-112	512	256	-960	-256	-960	512	256	1280	1280	0	768	-1280	2560	160	160
-27	-112	0	-12	-160	-80	-112	-160	160	160	-27	0	-80	160	290	0

We notice that matrix C depends on the triangle shape, whereas the matrices $Q^{(q)}$ do not. The $Q^{(1)}$ matrices for $n = 1$ to 4 are tabulated in Table 6.8. The following properties of Q matrices should be noted:

(a) they are symmetric;

(b) the row and column sums of any Q matrix are zero, i.e., $\sum_{i=1}^m Q_{ij}^{(q)} = 0 = \sum_{j=1}^m Q_{ij}^{(q)}$

so that the C matrix is singular.

$Q^{(2)}$ and $Q^{(3)}$ are easily obtained from $Q^{(1)}$ by row and column permutations so that the matrix C for any triangular element is constructed easily if $Q^{(1)}$ is known. One approach [47] involves using a rotation matrix R similar to that in Silvester and Ferrari [4], which is essentially a unit matrix with elements rearranged to correspond to one rotation of the triangle about its centroid in a counterclockwise direction. For example, for $n = 1$, the rotation matrix is basically derived from Figure 6.26 as

$$R = \begin{bmatrix} 0 & 0 & 1 \\ 1 & 0 & 0 \\ 0 & 1 & 0 \end{bmatrix} \quad (6.116)$$

where $R_{ij} = 1$ if node i is replaced by node j after one counterclockwise rotation, or $R_{ij} = 0$ otherwise. Table 6.9 presents the R matrices for $n = 1$ to 4. Note that each

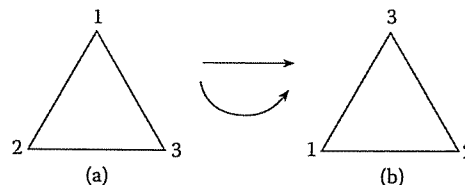


Figure 6.26

One counterclockwise rotation of the triangle in (a) gives the triangle in (b).

row or column of R has only one nonzero element since R is essentially a unit matrix with rearranged elements.

Once the R is known, we obtain

$$Q^{(2)} = R Q^{(1)} R^t \quad (6.117a)$$

$$Q^{(3)} = R Q^{(2)} R^t \quad (6.117b)$$

where R^t is the transpose of R .

Table 6.8 Table of Q Matrices for $n = 1$ to 4 (Continued)

$n = 1$	Common denominator: 2	$n = 2$	Common denominator: 6	$n = 3$	Common denominator: 80
	$\begin{pmatrix} 0 & 0 & 0 \\ 0 & 1 & -1 \\ 0 & -1 & 1 \end{pmatrix}$		$\begin{pmatrix} 0 & 0 & 0 & 0 \\ 0 & 8 & -8 & 0 \\ 0 & -8 & 8 & 0 \\ 0 & 0 & 0 & 0 \end{pmatrix}$		$\begin{pmatrix} 0 & 0 & 0 & 0 & 0 \\ 0 & 0 & 0 & 0 & 0 \\ 0 & 0 & 0 & 0 & 0 \\ 0 & 0 & 0 & 0 & 0 \\ 0 & 0 & 0 & 0 & 0 \end{pmatrix}$
			$\begin{pmatrix} 0 & 0 & 0 & 0 & 0 \\ 0 & 0 & 0 & 0 & 0 \\ 0 & 0 & 0 & 0 & 0 \\ 0 & 0 & 0 & 0 & 0 \\ 0 & 0 & 0 & 0 & 0 \end{pmatrix}$		$\begin{pmatrix} 0 & 0 & 0 & 0 & 0 \\ 0 & 0 & 0 & 0 & 0 \\ 0 & 0 & 0 & 0 & 0 \\ 0 & 0 & 0 & 0 & 0 \\ 0 & 0 & 0 & 0 & 0 \end{pmatrix}$
			$\begin{pmatrix} 0 & 0 & 0 & 0 & 0 \\ 0 & 0 & 0 & 0 & 0 \\ 0 & 0 & 0 & 0 & 0 \\ 0 & 0 & 0 & 0 & 0 \\ 0 & 0 & 0 & 0 & 0 \end{pmatrix}$		$\begin{pmatrix} 0 & 0 & 0 & 0 & 0 \\ 0 & 0 & 0 & 0 & 0 \\ 0 & 0 & 0 & 0 & 0 \\ 0 & 0 & 0 & 0 & 0 \\ 0 & 0 & 0 & 0 & 0 \end{pmatrix}$

Table 6.8 (Cont.) Table of Q Matrices for $n = 1$ to 4

$n = 4$ Common denominator: 1890											
0	0	0	0	0	0	0	0	0	0	0	0
0	3968	-3968	-1440	0	1440	640	0	-640	-80	0	0
0	-3968	3968	1440	0	-1440	-640	0	640	80	0	0
0	-1440	1440	4632	-5376	744	-1248	768	-288	80	-128	96
0	0	0	-5376	10752	-5376	1536	-1536	1536	-160	256	-192
0	1440	-1440	744	-5376	4632	-288	768	-1248	80	-128	96
0	640	-640	-1248	1536	-288	3456	-4608	1536	-384	240	-256
0	0	0	768	-1536	768	-4608	10752	-7680	1536	-160	256
0	0	0	768	-1536	768	1536	-7680	10752	-4608	-160	256
0	-640	640	-288	1536	-1248	-384	1536	-4608	3456	80	-256
0	-80	80	-160	80	240	-160	-160	80	705	-1232	884
0	0	0	-128	256	-128	-256	256	-256	-1232	3456	-464
0	0	0	96	-192	96	192	-192	192	884	-3680	5592
0	0	0	-128	256	-128	-256	256	-256	-464	1920	-3680
0	80	-80	80	-160	80	80	-160	-160	240	107	-464

6.8. HIGHER ORDER ELEMENTS

Table 6.9 R Matrix for $n = 1$ to 4

$n = 1$	$\begin{bmatrix} 0 & 0 & 1 \\ 1 & 0 & 0 \\ 0 & 1 & 0 \end{bmatrix}$
$n = 2$	$\begin{bmatrix} 0 & 0 & 0 & 0 & 1 \\ 0 & 0 & 1 & 0 & 0 \\ 0 & 0 & 0 & 0 & 1 \\ 1 & 0 & 0 & 0 & 0 \\ 0 & 1 & 0 & 0 & 0 \\ 0 & 0 & 0 & 1 & 0 \end{bmatrix}$
$n = 3$	$\begin{bmatrix} 0 & 0 & 0 & 0 & 0 & 0 & 0 & 0 & 1 \\ 0 & 0 & 0 & 0 & 0 & 1 & 0 & 0 & 0 \\ 0 & 0 & 0 & 0 & 0 & 0 & 0 & 1 & 0 \\ 0 & 0 & 1 & 0 & 0 & 0 & 0 & 0 & 0 \\ 0 & 0 & 0 & 0 & 1 & 0 & 0 & 0 & 0 \\ 0 & 0 & 0 & 0 & 0 & 0 & 0 & 1 & 0 \\ 0 & 0 & 0 & 0 & 0 & 0 & 0 & 0 & 0 \\ 1 & 0 & 0 & 0 & 0 & 0 & 0 & 0 & 0 \\ 0 & 1 & 0 & 0 & 0 & 0 & 0 & 0 & 0 \\ 0 & 0 & 1 & 0 & 0 & 0 & 0 & 0 & 0 \\ 0 & 0 & 0 & 1 & 0 & 0 & 0 & 0 & 0 \end{bmatrix}$
$n = 4$	$\begin{bmatrix} 0 & 0 & 0 & 0 & 0 & 0 & 0 & 0 & 0 & 0 & 0 & 1 \\ 0 & 0 & 0 & 0 & 0 & 0 & 0 & 0 & 0 & 1 & 0 & 0 \\ 0 & 0 & 0 & 0 & 0 & 0 & 0 & 0 & 0 & 0 & 0 & 0 \\ 0 & 0 & 0 & 0 & 0 & 0 & 0 & 0 & 0 & 0 & 0 & 0 \\ 0 & 0 & 0 & 0 & 0 & 0 & 0 & 0 & 0 & 0 & 0 & 0 \\ 0 & 0 & 0 & 0 & 0 & 0 & 0 & 0 & 0 & 0 & 0 & 0 \\ 0 & 0 & 0 & 0 & 0 & 0 & 0 & 0 & 0 & 0 & 0 & 0 \\ 0 & 0 & 0 & 0 & 0 & 0 & 0 & 0 & 0 & 0 & 0 & 0 \\ 0 & 0 & 0 & 0 & 0 & 0 & 0 & 0 & 0 & 0 & 0 & 0 \\ 0 & 0 & 0 & 0 & 0 & 0 & 0 & 0 & 0 & 0 & 0 & 0 \\ 0 & 0 & 0 & 0 & 0 & 0 & 0 & 0 & 0 & 0 & 0 & 0 \\ 0 & 0 & 0 & 0 & 0 & 0 & 0 & 0 & 0 & 0 & 0 & 0 \end{bmatrix}$

Example 6.5

For $n = 2$, calculate $Q^{(1)}$ and obtain $Q^{(2)}$ from $Q^{(1)}$ using Equation (6.117a). \square

Solution

By definition,

$$Q_{ij}^{(1)} = \iint \left(\frac{\partial \alpha_i}{\partial \xi_2} - \frac{\partial \alpha_i}{\partial \xi_3} \right) \left(\frac{\partial \alpha_j}{\partial \xi_2} - \frac{\partial \alpha_j}{\partial \xi_3} \right) d\xi_1 d\xi_2$$

For $n = 2$, $i, j = 1, 2, \dots, 6$, and α_i are given in terms of the local coordinates in Table 6.6. Since $Q^{(1)}$ is symmetric, only some of the elements need be calculated. Substituting for α_ℓ from Table 6.6 and applying Equations (6.104e) and (6.104f), we obtain

$$Q_{1j} = 0, \quad j = 1 \text{ to } 6,$$

$$Q_{i1} = 0, \quad i = 1 \text{ to } 6,$$

$$Q_{22} = \frac{1}{2A} \iint (4\xi_1)^2 d\xi_1 d\xi_2 = \frac{8}{6},$$

$$Q_{23} = \frac{1}{2A} \iint (4\xi_1)(-4\xi_1) d\xi_1 d\xi_2 = -\frac{8}{6},$$

$$Q_{24} = \frac{1}{2A} \iint (4\xi_1)(4\xi_1 - 1) d\xi_1 d\xi_2 = 0 = Q_{26},$$

$$Q_{25} = \frac{1}{2A} \iint (4\xi_1)(4\xi_3 - 4\xi_2) d\xi_1 d\xi_2 = 0,$$

$$Q_{33} = \frac{1}{2A} \iint (-4\xi_1)^2 d\xi_1 d\xi_2 = \frac{8}{6},$$

$$Q_{34} = \frac{1}{2A} \iint (-4\xi_1)(4\xi_2 - 1) d\xi_1 d\xi_2 = 0 = Q_{36},$$

$$Q_{35} = \frac{1}{2A} \iint (-4\xi_1)(4\xi_3 - 4\xi_2) d\xi_1 d\xi_2 = 0,$$

$$Q_{44} = \frac{1}{2A} \iint (4\xi_2 - 1)^2 d\xi_1 d\xi_2 = \frac{3}{6},$$

$$Q_{45} = \frac{1}{2A} \iint (4\xi_2 - 1)(4\xi_3 - 4\xi_2) d\xi_1 d\xi_2 = -\frac{4}{6},$$

$$Q_{46} = \frac{1}{2A} \iint (4\xi_2 - 1)(4\xi_3 - 1)(-1) d\xi_1 d\xi_2 = \frac{1}{6},$$

$$Q_{55} = \frac{1}{2A} \iint (4\xi_3 - 4\xi_2)^2 d\xi_1 d\xi_2 = \frac{8}{6},$$

$$Q_{56} = \frac{1}{2A} \iint (4\xi_3 - 4\xi_2)(-1)(4\xi_3 - 1) d\xi_1 d\xi_2 = -\frac{4}{6},$$

$$Q_{66} = \frac{1}{2A} \iint (-1)(4\xi_3 - 1)^2 d\xi_1 d\xi_2 = \frac{3}{6}$$

6.9. THREE-DIMENSIONAL ELEMENTS

Hence

$$Q^{(1)} = \frac{1}{6} \begin{bmatrix} 0 & 0 & 0 & 0 & 0 & 0 \\ 0 & 8 & -8 & 0 & 0 & 0 \\ 0 & -8 & 8 & 0 & 0 & 0 \\ 0 & 0 & 0 & 3 & -4 & 1 \\ 0 & 0 & 0 & -4 & 8 & -4 \\ 0 & 0 & 0 & 1 & -4 & 3 \end{bmatrix}$$

We now obtain $Q^{(2)}$ from

$$\begin{aligned} Q^{(2)} &= R Q^{(1)} R^T \\ &= \frac{1}{6} R \begin{bmatrix} 0 & 0 & 0 & 0 & 0 & 0 \\ 0 & 8 & -8 & 0 & 0 & 0 \\ 0 & -8 & 8 & 0 & 0 & 0 \\ 0 & 0 & 0 & 3 & -4 & 1 \\ 0 & 0 & 0 & -4 & 8 & -4 \\ 0 & 0 & 0 & 1 & -4 & 3 \end{bmatrix} \begin{bmatrix} 0 & 0 & 0 & 1 & 0 & 0 \\ 0 & 0 & 0 & 0 & 1 & 0 \\ 0 & 1 & 0 & 0 & 0 & 0 \\ 0 & 0 & 0 & 0 & 0 & 1 \\ 0 & 0 & 1 & 0 & 0 & 0 \\ 1 & 0 & 0 & 0 & 0 & 0 \end{bmatrix} \\ &= \frac{1}{6} \begin{bmatrix} 0 & 0 & 0 & 0 & 0 & 1 \\ 0 & 0 & 1 & 0 & 0 & 0 \\ 0 & 0 & 0 & 0 & 1 & 0 \\ 1 & 0 & 0 & 0 & 0 & 0 \\ 0 & 1 & 0 & 0 & 0 & 0 \\ 0 & 0 & 0 & 1 & 0 & 0 \end{bmatrix} \begin{bmatrix} 0 & 0 & 0 & 0 & 0 & 0 \\ 0 & -8 & 0 & 0 & 8 & 0 \\ 0 & 8 & 0 & 0 & -8 & 0 \\ 1 & 0 & -4 & 0 & 0 & 3 \\ -4 & 0 & 8 & 0 & 0 & -4 \\ 3 & 0 & 4 & 0 & 0 & 1 \end{bmatrix} \\ Q^{(2)} &= \frac{1}{6} \begin{bmatrix} 3 & 0 & -4 & 0 & 0 & 1 \\ 0 & 8 & 0 & 0 & -8 & 0 \\ -4 & 0 & 8 & 0 & 0 & -4 \\ 0 & 0 & 0 & 0 & 0 & 0 \\ 0 & -8 & 0 & 0 & 8 & 0 \\ 1 & 0 & -4 & 0 & 0 & 3 \end{bmatrix} \end{aligned}$$

6.9 Three-Dimensional Elements

The finite element techniques developed in the previous sections for two-dimensional elements can be extended to three-dimensional elements. One would expect three-dimensional problems to require a large total number of elements to achieve an accurate result and demand a large storage capacity and computational time. For the sake of completeness, we will discuss the finite element analysis of Helmholtz's equation in three dimensions, namely,

$$\nabla^2 \Phi + k^2 \Phi = g \quad (6.118)$$

We first divide the solution region into tetrahedral or hexahedral (rectangular prism) elements as in Figure 6.27. Assuming a four-node tetrahedral element, the function

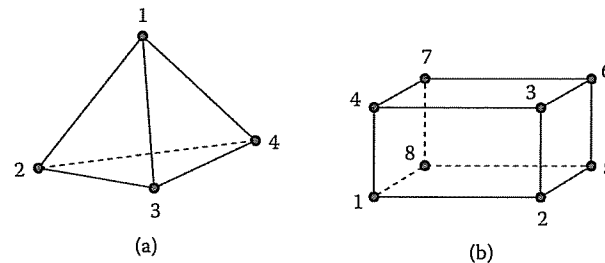


Figure 6.27

Three-dimensional elements: (a) Four-node or linear-order tetrahedral, (b) eight-node or linear-order hexahedral.

Φ is represented within the element by

$$\Phi_e = a + bx + cy + dz \quad (6.119)$$

The same applies to the function g . Since Equation (6.119) must be satisfied at the four nodes of the tetrahedral elements,

$$\Phi_{ei} = a + bx_i + cy_i + dz_i, \quad i = 1, \dots, 4 \quad (6.120)$$

Thus we have four simultaneous equations (similar to Equation (6.5)) from which the coefficients a, b, c , and d can be determined. The determinant of the system of equations is

$$\det = \begin{vmatrix} 1 & x_1 & y_1 & z_1 \\ 1 & x_2 & y_2 & z_2 \\ 1 & x_3 & y_3 & z_3 \\ 1 & x_4 & y_4 & z_4 \end{vmatrix} = 6v, \quad (6.121)$$

where v is the volume of the tetrahedron. By finding a, b, c , and d , we can write

$$\boxed{\Phi_e = \sum_{i=1}^4 \alpha_i(x, y) \Phi_{ei}} \quad (6.122)$$

where

$$\alpha_1 = \frac{1}{6v} \begin{vmatrix} 1 & x & y & z \\ 1 & x_2 & y_2 & z_2 \\ 1 & x_3 & y_3 & z_3 \\ 1 & x_4 & y_4 & z_4 \end{vmatrix}, \quad (6.123a)$$

$$\alpha_2 = \frac{1}{6v} \begin{vmatrix} 1 & x_1 & y_1 & z_1 \\ 1 & x & y & z \\ 1 & x_3 & y_3 & z_3 \\ 1 & x_4 & y_4 & z_4 \end{vmatrix}, \quad (6.123b)$$

6.9. THREE-DIMENSIONAL ELEMENTS

with α_3 and α_4 having similar expressions. For higher order approximation, the matrices for α_s become large in size and we resort to local coordinates. Another motivation for using local coordinates is the existence of integration equations which simplify the evaluation of the fundamental matrices T and Q .

For the tetrahedral element, the local coordinates are ξ_1, ξ_2, ξ_3 , and ξ_4 , each perpendicular to a side. They are defined at a given point as the ratio of the distance from that point to the appropriate apex to the perpendicular distance from the side to the opposite apex. They can also be interpreted as volume ratios, i.e., at a point P

$$\xi_i = \frac{v_i}{v} \quad (6.124)$$

where v_i is the volume bound by P and face i . It is evident that

$$\sum_{i=1}^4 \xi_i = 1 \quad (6.125a)$$

or

$$\xi_4 = 1 - \xi_1 - \xi_2 - \xi_3 \quad (6.125b)$$

The following properties are useful in evaluating integration involving local coordinates [48]:

$$dv = 6v \, d\xi_1 \, d\xi_2 \, d\xi_3, \quad (6.126a)$$

$$\iiint f \, dv = 6v \int_0^1 \left[\int_0^{1-\xi_3} \left(\int_0^{1-\xi_2-\xi_3} f \, d\xi_1 \right) d\xi_2 \right] d\xi_3, \quad (6.126b)$$

$$\iiint \xi_1^i \xi_2^j \xi_3^k \xi_4^\ell \, dv = \frac{i! j! k! \ell!}{(i+j+k+\ell+3)!} 6v \quad (6.126c)$$

In terms of the local coordinates, an arbitrary function $\Phi(x, y, z)$ can be approximated within an element in terms of a complete n th order polynomial as

$$\boxed{\Phi_e(x, y, z) = \sum_{i=1}^m \alpha_i(x, y, z) \Phi_{ei}} \quad (6.127)$$

where $m = \frac{1}{6}(n+1)(n+2)(n+3)$ is the number of nodes in the tetrahedron or the number of terms in the polynomial. The terms in a complete three-dimensional polynomial may be arrayed as shown in Figure 6.28.

Each point in the tetrahedral element is represented by four integers i, j, k , and ℓ which can be used to determine the local coordinates $(\xi_1, \xi_2, \xi_3, \xi_4)$. That is at P_{ijkl} ,

$$(\xi_1, \xi_2, \xi_3, \xi_4) = \left(\frac{i}{n}, \frac{j}{n}, \frac{k}{n}, \frac{\ell}{n} \right) \quad (6.128)$$

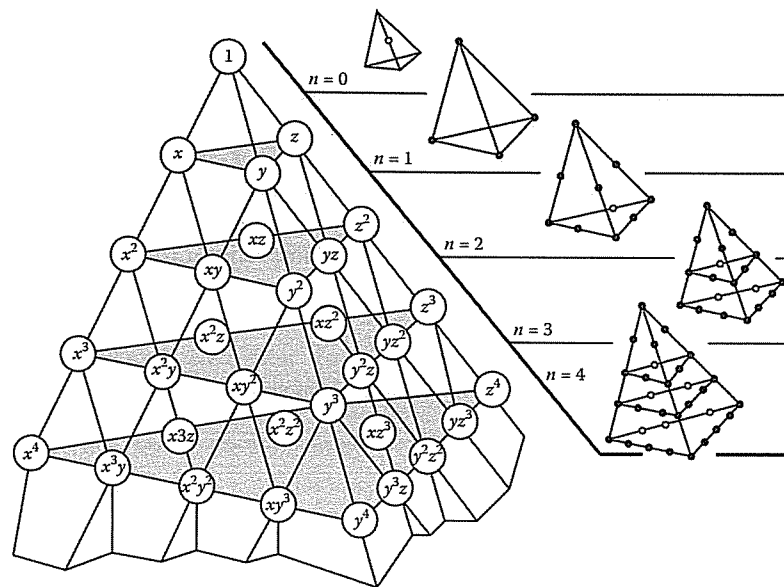


Figure 6.28

Pascal tetrahedron and associated array of terms.

Hence at each node,

$$\alpha_q = \alpha_{ijkl} = p_i(\xi_1) p_j(\xi_2) p_k(\xi_3) p_l(\xi_4), \quad (6.129)$$

where $q = 1, 2, \dots, m$ and p_r is defined in Equation (6.108) or (6.109). The relationship between the node numbers q and $ijkl$ is illustrated in Figure 6.29 for the second order tetrahedron ($n = 2$). The shape functions obtained by substituting Equation (6.108) into Equation (6.129) are presented in Table 6.10 for $n = 1$ to 3.

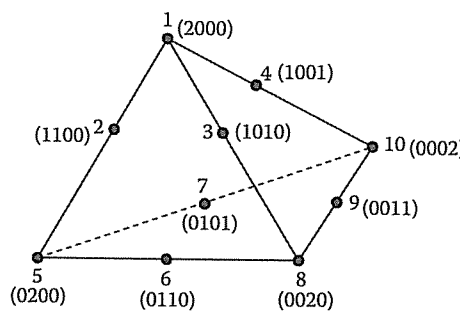


Figure 6.29

Numbering scheme for second-order tetrahedron.

Table 6.10 Shape Functions $\alpha_q(\xi_1, \xi_2, \xi_3, \xi_4)$ for $n = 1$ to 3

$n = 1$	$n = 2$	$n = 3$
$\alpha_1 = \xi_1$	$\alpha_1 = \xi_1(2\xi_2 - 1)$	$\alpha_1 = \frac{1}{2}\xi_1(3\xi_1 - 2)(3\xi_1 - 1)$
$\alpha_2 = \xi_2$	$\alpha_2 = 4\xi_1\xi_2$	$\alpha_2 = \frac{9}{2}\xi_1(3\xi_1 - 1)\xi_2$
$\alpha_3 = \xi_3$	$\alpha_3 = 4\xi_1\xi_3$	$\alpha_3 = \frac{9}{2}\xi_1(3\xi_1 - 1)\xi_3$
$\alpha_4 = \xi_4$	$\alpha_4 = 4\xi_1\xi_4$	$\alpha_4 = \frac{9}{2}\xi_1(3\xi_1 - 1)\xi_4$
	$\alpha_5 = \xi_2(2\xi_2 - 1)$	$\alpha_5 = \frac{9}{2}\xi_1(3\xi_3 - 1)\xi_2$
	$\alpha_6 = 4\xi_2\xi_3$	$\alpha_6 = 27\xi_1\xi_2\xi_3$
	$\alpha_7 = 4\xi_2\xi_4$	$\alpha_7 = 27\xi_1\xi_2\xi_4$
	$\alpha_8 = \xi_2(2\xi_3 - 1)$	$\alpha_8 = \frac{9}{2}\xi_1(3\xi_3 - 1)\xi_3$
	$\alpha_9 = 4\xi_3\xi_4$	$\alpha_9 = 27\xi_1\xi_3\xi_4$
	$\alpha_{10} = \xi_4(2\xi_4 - 1)$	$\alpha_{10} = \frac{9}{2}\xi_1(3\xi_4 - 1)\xi_4$
		$\alpha_{11} = \frac{1}{2}\xi_2(3\xi_2 - 1)(3\xi_2 - 2)$
		$\alpha_{12} = \frac{9}{2}\xi_2(3\xi_2 - 1)\xi_3$
		$\alpha_{13} = \frac{9}{2}\xi_2(3\xi_2 - 1)\xi_4$
		$\alpha_{14} = \frac{9}{2}\xi_2(3\xi_3 - 1)\xi_3$
		$\alpha_{15} = 27\xi_2\xi_3\xi_4$
		$\alpha_{16} = \frac{9}{2}\xi_2(3\xi_3 - 1)\xi_3$
		$\alpha_{17} = \frac{1}{2}\xi_3(3\xi_3 - 1)(3\xi_3 - 2)$
		$\alpha_{18} = \frac{9}{2}\xi_3(3\xi_3 - 1)\xi_4$
		$\alpha_{19} = \frac{9}{2}\xi_3(3\xi_4 - 1)\xi_4$
		$\alpha_{20} = \frac{1}{2}\xi_4(3\xi_4 - 1)(3\xi_4 - 2)$

The expressions derived from the variational principle for the two-dimensional problems in Sections 6.2 to 6.4 still hold except that the fundamental matrices $[T]$ and $[Q]$ now involve triple integration. For Helmholtz equation (6.56), for example, Equation (6.68) applies, namely,

$$[C_{ff} - k^2 T_{ff}] \Phi_f = 0 \quad (6.130)$$

except that

$$\begin{aligned} C_{ij}^{(e)} &= \int_v \nabla \alpha_i \cdot \nabla \alpha_j dv \\ &= \int_v \left(\frac{\partial \alpha_i}{\partial x} \frac{\partial \alpha_j}{\partial x} + \frac{\partial \alpha_i}{\partial y} \frac{\partial \alpha_j}{\partial y} + \frac{\partial \alpha_i}{\partial z} \frac{\partial \alpha_j}{\partial z} \right) dv, \end{aligned} \quad (6.131)$$

$$T_{ij}^{(e)} = \int_v \alpha_i \alpha_j dv = v \iiint \alpha_i \alpha_j d\xi_1 d\xi_2 d\xi_3 \quad (6.132)$$

For further discussion on three-dimensional elements, one should consult Silvester and Ferrari [4]. Applications of three-dimensional elements to EM-related problems can be found in [49]–[53].

6.10 Finite Element Methods for Exterior Problems

Thus far in this chapter, the FEM has been presented for solving interior problems. To apply the FEM to exterior or unbounded problems such as open-type transmission lines (e.g., microstrip), scattering, and radiation problems poses certain difficulties. To overcome these difficulties, several approaches [54]–[82] have been proposed, all of which have strengths and weaknesses. We will consider three common approaches: the infinite element method, the boundary element method, and absorbing boundary condition.

6.10.1 Infinite Element Method

Consider the solution region shown in Figure 6.30(a). We divide the entire domain into a near field (n.f.) region, which is bounded, and a far field (f.f.) region, which is unbounded. The n.f. region is divided into finite triangular elements as usual, while the f.f. region is divided into *infinite elements*. Each infinite element shares two nodes with a finite element. Here we are mainly concerned with the infinite elements.

Consider the infinite element in Figure 6.30(b) with nodes 1 and 2 and radial sides intersecting at point (x_o, y_o) . We relate triangular polar coordinates (ρ, ξ) to the global Cartesian coordinates (x, y) as [62]

$$\begin{aligned} x &= x_o + \rho [(x_1 - x_o) + \xi (x_2 - x_1)] \\ y &= y_o + \rho [(y_1 - y_o) + \xi (y_2 - y_1)] \end{aligned} \quad (6.133)$$

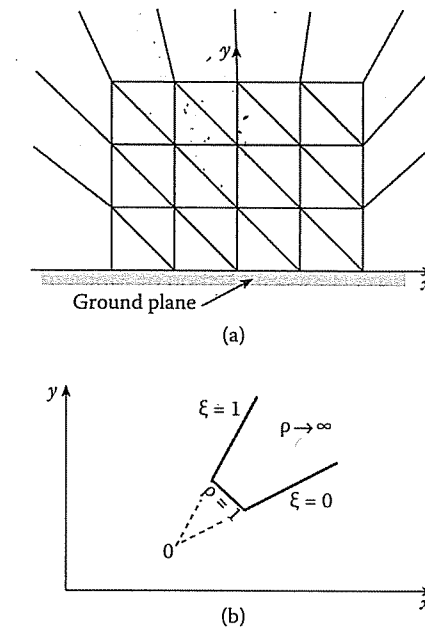


Figure 6.30

(a) Division of solution region into finite and infinite elements; (b) typical infinite element.

where $1 \leq \rho < \infty$, $0 \leq \xi \leq 1$. The potential distribution within the element is approximated by a linear variation as

$$V = \frac{1}{\rho} [V_1(1 - \xi) + V_2\xi] \quad (6.134)$$

or

$$V = \sum_{i=1}^2 \alpha_i V_i \quad (6.134)$$

where V_1 and V_2 are potentials at nodes 1 and 2 of the infinite elements, α_1 and α_2 are the interpolation or shape functions, i.e.,

$$\alpha_1 = \frac{1 - \xi}{\rho}, \quad \alpha_2 = \frac{\xi}{\rho} \quad (6.135)$$

The infinite element is compatible with the ordinary first order finite element and satisfies the boundary condition at infinity. With the shape functions in Equation (6.135), we can obtain the $[C^{(e)}]$ and $[T^{(e)}]$ matrices. We obtain solution for the exterior problem by using a standard finite element program with the $[C^{(e)}]$ and $[T^{(e)}]$ matrices of the infinite elements added to the $[C]$ and $[T]$ matrices of the n.f. region.

6.10.2 Boundary Element Method

A comparison between the finite element method (FEM) and the method of moments (MOM) is shown in Table 6.11. From the table, it is evident that the two methods have properties that complement each other. In view of this, hybrid methods have been proposed. These methods allow the use of both MOM and FEM with the aim of exploiting the strong points in each method.

Table 6.11 Comparison Between Method of Moments and Finite Element Method [83]

Method of Moments	Finite Element Method
Conceptually easy	Conceptually involved
Requires problem-dependent Green's functions	Avoids difficulties associated with singularity of Green's functions
Few equations; $O(n)$ for 2-D, $O(n^2)$ for 3-D	Many equations; $O(n^2)$ for 2-D, $O(n^3)$ for 3-D
Only boundary is discretized	Entire domain is discretized
Open boundary easy	Open boundary difficult
Fields by integration	Fields by differentiation
Good representation of far-field condition	Good representation of boundary conditions
Full matrices result	Sparse matrices result
Nonlinearity, inhomogeneity difficult	Nonlinearity, inhomogeneity easy

One of these hybrid methods is the so-called boundary element method (BEM). It is a finite element approach for handling exterior problems [68]–[80]. It basically involves obtaining the integral equation formulation of the boundary value problem [84] and solving this by a discretization procedure similar to that used in regular finite element analysis. Since the BEM is based on the boundary integral equivalent to the governing differential equation, only the surface of the problem domain needs to be modeled. Thus the dimension of the problem is reduced by one as in MOM. For 2-D problems, the boundary elements are taken to be straight line segments, whereas for 3-D problems, they are taken as triangular elements. Thus the shape or interpolation functions corresponding to subsectional bases in the MOM are used in the finite element analysis.

6.10.3 Absorbing Boundary Condition

To apply the finite element approach to open region problems such as for scattering or radiation, an artificial boundary is introduced in order to bound the region and limit the number of unknowns to a manageable size. One would expect that as the boundary approaches infinity, the approximate solution tends to the exact one. But the closer the boundary to the radiating or scattering object, the less computer memory is required. To avoid the error caused by this truncation, an *absorbing boundary condition* (ABC)

is imposed on the artificial boundary S , as typically portrayed in Figure 6.31. The ABC minimizes the nonphysical reflections from the boundary. Several ABCs have been proposed [85]–[91]. The major challenge of these ABCs is to bring the truncation boundary as close as possible to the object without sacrificing accuracy and to absorb the outgoing waves with little or no reflection. A popular approach is the PML-based ABC discussed in Section 3.8.3 for FDTD. The finite element technique is used in enforcing the condition as a tool for mesh truncation [87].

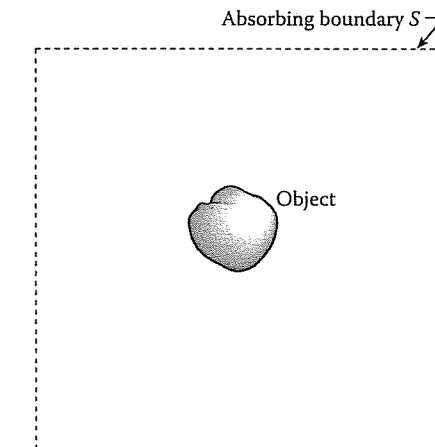


Figure 6.31
A radiating (or scattering) object surrounded by an absorbing boundary.

Another popular ABC-derived Bayliss, Gunzburger, and Turkel (BGT) employs asymptotic analysis [91]. For example, for the solution of a three-dimensional problem, an expansion of the scalar Helmholtz equation is [90]:

$$\Phi(r, \theta, \phi) = \frac{e^{-jkr}}{kr} \sum_{i=0}^{\infty} \frac{F_i(\theta, \phi)}{(kr)^i} \quad (6.136)$$

The sequence of BGT operators is obtained by the recursion relation

$$\begin{aligned} B_1 &= \left(\frac{\partial}{\partial r} + jk + \frac{1}{r} \right) \\ B_m &= \left(\frac{\partial}{\partial r} + jk + \frac{2m-1}{r} \right) B_{m-1}, \quad m = 2, 3, \dots \end{aligned} \quad (6.137)$$

Since Φ satisfies the higher-order radiation condition

$$B_m \Phi = O(1/r^{2m+1}) \quad (6.138)$$

imposing the m th-order boundary condition

$$B_m \Phi = 0 \quad \text{on } S \quad (6.139)$$

will compel the solution Φ to match the first $2m$ terms of the expansion in Equation (6.136). Equation (6.139) along with other appropriate equations is solved for Φ using the finite element method.

6.11 Finite-Element Time-Domain Method

Traditionally, frequency domain methods have dominated computational electromagnetics, while time domain computation is a novelty. The trend is to solve Maxwell's equations directly in the time domain. (It is much easier to get frequency domain results from time domain data than the other way around.) To date, finite-difference time-domain (FDTD) techniques have received the greatest attention due to their algorithmic simplicity. In recent years, finite-element time-domain (FETD) algorithms have increased in popularity because of their ability to approximate physical boundaries. The FDTD method is the method of choice when modeling geometries of low complexity, while FETD methods are most appropriate when complicated geometries need to be modeled. Since FETD formulations have not received as much attention as FDTD schemes, they are lacking in both maturity and variety of applications.

Numerous FETD methods have been proposed for electromagnetic computation [91–99]. These methods can be classified into two categories. One class of approaches directly solves Maxwell's equations and operates in a leapfrog fashion similar to the FDTD technique. The approaches are conditionally stable. Another class of FETD methods tackles the second-order vector wave equation obtained by eliminating one of the field variables from Maxwell's equations. We follow the approach in [91].

Consider Maxwell's equations in space-time:

$$\nabla \times E = -\mu \frac{\partial H}{\partial t} \quad (6.140a)$$

$$\nabla \times H = J + \epsilon \frac{\partial E}{\partial t} \quad (6.140b)$$

where E and H are electric field intensity and magnetic field intensity, respectively, and J is the current density. From Equation (6.140), we can derive an initial value problem in terms of the magnetic field H .

$$\nabla \times \frac{1}{\epsilon} \nabla \times H + \frac{\mu \sigma}{\epsilon} \frac{\partial H}{\partial t} + \mu \frac{\partial^2 H}{\partial t^2} = \frac{1}{\epsilon} \nabla \times J \quad (6.141)$$

where σ is the conductivity, $\epsilon = \epsilon_r \epsilon_0$ and $\mu = \mu_r \mu_0$ are respectively the permittivity and permeability of the medium. For 2-D region, the scalar wave equation for the

6.12 FINITE-ELEMENT TIME-DOMAIN METHOD

longitudinal component of the magnetic field is

$$\frac{1}{\epsilon_r \epsilon_0} \nabla^2 H_z - \sigma \frac{\mu_r \mu_0}{\epsilon_r \epsilon_0} \frac{\partial H_z}{\partial t} - \mu_r \mu_0 \frac{\partial^2 H_z}{\partial t^2} = -\frac{1}{\epsilon_r \epsilon_0} (\nabla \times J)_z \quad (6.142)$$

By defining the carrier frequency ω_c , the field component and the current density can be written as

$$\begin{aligned} H_z(t) &= V(t) e^{j\omega_c t} \\ J(t) &= j(t) e^{j\omega_c t} \end{aligned} \quad (6.143)$$

Where $V(t)$ is the time-varying complex envelope of the field at the carrier frequency. The application of Galerkin's process (global weak formulation) produces a set of ordinary differential equations

$$[T] \frac{d^2 v}{dt^2} + [B] \frac{dv}{dt} + [G]v + [F] = 0 \quad (6.144)$$

where v is the coefficient vector of V . Matrices $[T]$, $[B]$, and $[G]$ are time-independent and are given by

$$T_{ij} = \int \int_S \frac{\mu_r}{c^2} W_i W_j dS \quad (6.145a)$$

$$B_{ij} = \int \int_S \frac{\mu_r}{c^2} (2j\omega_c + \alpha) W_i W_j dS \quad (6.145b)$$

$$G_{ij} = \int \int_S \frac{1}{\epsilon_r} \nabla W_i \cdot \nabla W_j - \frac{\mu_r}{c^2} (\omega_c^2 - j\alpha\omega_c) W_i W_j dS \quad (6.145c)$$

$$F_i = \int \int_S \frac{1}{\epsilon_r} W_i \cdot (\nabla \times j)_z dS \quad (6.145d)$$

where c is the speed of light in free space, $\alpha = \sigma/\epsilon_r \epsilon_0$ is a constant, W_j are 2-D FEM basis functions, and S is a 2-D area bounded by the boundary Γ .

In order to solve Equation (6.144), the time derivatives must be discretized.

$$\frac{d^2 v}{dt^2} = \frac{1}{\Delta t^2} [v(n+1) - 2v(n) + v(n-1)] \quad (6.146a)$$

$$\frac{dv}{dt} = \frac{1}{2\Delta t} [v(n+1) - v(n-1)] \quad (6.146b)$$

$$v(n) = \beta v(n+1) + (1-2\beta)v(n) + \beta v(n-1) \quad (6.146c)$$

where $v(n) = v(n\Delta t)$ is the discrete-time version of $v(t)$ and β is a constant that determines the stability and the accuracy of the scheme. It is recommended that $\beta = \frac{1}{4}$ which results in an unconditionally stable scheme. Thus, Equation (6.144) becomes

$$\left(\frac{[T]}{\Delta t^2} + \frac{B}{2\Delta t} + \frac{G}{4} \right) v(n+1) = \left(\frac{2[T]}{\Delta t^2} - \frac{[G]}{2} \right) v(n) + \left(-\frac{[T]}{\Delta t^2} + \frac{B}{2\Delta t} - \frac{[G]}{4} \right) v(n-1) - f(n) \quad (6.147)$$

To solve these equations, we need to invert the matrix on the left-hand side. Since this matrix is time independent, it needs to be filled and solved only once.

6.12 Concluding Remarks

An introduction to the basic concepts and applications of the finite element method has been presented. It is by no means an exhaustive exposition of the subject. However, we have given the flavor of the way in which the ideas may be developed; the interested reader may build on this by consulting the references. Several introductory texts have been published on FEM. Although most of these texts are written for civil or mechanical engineers, the texts by Sylvester and Ferrari [4], Chari and Sylvester [41], Steele [100], Hoole [101], and Itoh [102] are for electrical engineers.

Due to its flexibility and versatility, the finite element method has become a powerful tool throughout engineering disciplines. It has been applied with great success to numerous EM-related problems. Such applications include the following:

- transmission line problems [103]–[105],
- optical and microwave waveguide problems [8]–[17], [106]–[111],
- electric machines [41], [112]–[114],
- scattering problems [71, 72, 75, 115],
- human exposition to EM radiation [116]–[119], and
- others [120]–[123].

For other issues on FEM not covered in this chapter, one is referred to introductory texts on FEM such as [2, 4, 36, 41, 48], [92]–[94], [124]–[133]. The issues of edge elements and absorbing boundary are covered in [126]. Estimating error in finite element solution is discussed in [52, 124, 125]. The reader may benefit from the numerous finite element codes that are commercially available. An extensive description of these systems and their capabilities can be found in [127, 134]. Although the codes were developed for one field of engineering or another, they can be applied to problems in a different field with little or no modification.

References

- [1] R. Courant, “Variational methods for the solution of problems of equilibrium and vibrations,” *Bull. Am. Math. Soc.*, vol. 49, 1943, pp. 1–23.
- [2] C.S. Desai and J.F. Abel, *Introduction to the Finite Element Method: A Numerical Approach for Engineering Analysis*. New York: Van Nostrand Reinhold, 1972.

REFERENCES

- [3] M.N.O. Sadiku, “A simple introduction to finite element analysis of electromagnetic problems,” *IEEE Trans. Educ.*, vol. 32, no. 2, May 1989, pp. 85–93.
- [4] P.P. Sylvester and R.L. Ferrari, *Finite Elements for Electrical Engineers*. Cambridge University Press, New York: 3rd ed., 1996.
- [5] O.W. Andersen, “Laplacian electrostatic field calculations by finite elements with automatic grid generation,” *IEEE Trans. Power App. Syst.*, vol. PAS-92, no. 5, Sept./Oct. 1973, pp. 1485–1492.
- [6] S. Nakamura, *Computational Methods in Engineering and Science*. New York: John Wiley, 1977, pp. 446, 447.
- [7] B.S. Garbow, *Matrix Eigensystem Routine—EISPACK Guide Extension*. Berlin: Springer-Verlag, 1977.
- [8] S. Ahmed and P. Daly, “Finite-element methods for inhomogeneous waveguides,” *Proc. IEEE*, vol. 116, no. 10, Oct. 1969, pp. 1661–1664.
- [9] Z.J. Csendes and P. Sylvester, “Numerical solution of dielectric loaded waveguides: I—Finite-element analysis,” *IEEE Trans. Micro. Theo. Tech.*, vol. MTT-18, no. 12, Dec. 1970, pp. 1124–1131.
- [10] Z.J. Csendes and P. Sylvester, “Numerical solution of dielectric loaded waveguides: II—Modal approximation technique,” *IEEE Trans. Micro. Theo. Tech.*, vol. MTT-19, no. 6, June 1971, pp. 504–509.
- [11] M. Hano, “Finite-element analysis of dielectric-loaded waveguides,” *IEEE Trans. Micro. Theo. Tech.*, vol. MTT-32, no. 10, Oct. 1984, pp. 1275–1279.
- [12] A. Konrad, “Vector variational formulation of electromagnetic fields in anisotropic media,” *IEEE Trans. Micro. Theo. Tech.*, vol. MTT-24, Sept. 1976, pp. 553–559.
- [13] M. Koshiba et al., “Improved finite-element formulation in terms of the magnetic field vector for dielectric waveguides,” *IEEE Trans. Micro. Theo. Tech.*, vol. MTT-33, no. 3, March 1985, pp. 227–233.
- [14] M. Koshiba et al., “Finite-element formulation in terms of the electric-field vector for electromagnetic waveguide problems,” *IEEE Trans. Micro. Theo. Tech.*, vol. MTT-33, no. 10, Oct. 1985, pp. 900–905.
- [15] K. Hayata et al., “Vectorial finite-element method without any spurious solutions for dielectric waveguiding problems using transverse magnetic-field component,” *IEEE Trans. Micro. Theo. Tech.*, vol. MTT-34, no. 11, Nov. 1986.
- [16] K. Hayata et al., “Novel finite-element formulation without any spurious solutions for dielectric waveguides,” *Elect. Lett.*, vol. 22, no. 6, March 1986, pp. 295, 296.
- [17] S. Dervain, “Finite element analysis of inhomogeneous waveguides,” M.S. thesis, Department of Electrical and Computer Engineering, Florida Atlantic University, Boca Raton, April 1987.

- [18] J.R. Winkler and J.B. Davies, "Elimination of spurious modes in finite element analysis," *J. Comp. Phys.*, vol. 56, no. 1, Oct. 1984, pp. 1-14.
- [19] M.N.O. Sadiku et al., "A further introduction to finite element analysis of electromagnetic problems," *IEEE Trans. Educ.*, vol. 34, no. 4, Nov. 1991, pp. 322-329.
- [20] The IMSL Libraries: Problem-solving software systems for numerical FORTRAN programming, IMSL, Houston, TX, 1984.
- [21] M. Kono, "A generalized automatic mesh generation scheme for finite element method," *Inter. J. Num. Method Engr.*, vol. 15, 1980, pp. 713-731.
- [22] J.C. Cavendish, "Automatic triangulation of arbitrary planar domains for the finite element method," *Inter. J. Num. Meth. Engr.*, vol. 8, 1974, pp. 676-696.
- [23] A.O. Moscardini et al., "AGTHOM—Automatic generation of triangular and higher order meshes," *Inter. J. Num. Meth. Engr.*, vol. 19, 1983, pp. 1331-1353.
- [24] C.O. Frederick et al., "Two-dimensional automatic mesh generation for structured analysis," *Inter. J. Num. Meth. Engr.*, vol. 2, no. 1, 1970, pp. 133-144.
- [25] E.A. Heighway, "A mesh generation for automatically subdividing irregular polygon into quadrilaterals," *IEEE Trans. Mag.*, vol. MAG-19, no. 6, Nov. 1983, pp. 2535-2538.
- [26] C. Kleinstreuer and J.T. Holdeman, "A triangular finite element mesh generator for fluid dynamic systems of arbitrary geometry," *Inter. J. Num. Meth. Engr.*, vol. 15, 1980, pp. 1325-1334.
- [27] A. Bykat, "Automatic generation of triangular grid. I—Subdivision of a general polygon into convex subregions. II—Triangulation of convex polygons," *Inter. J. Num. Meth. Engr.*, vol. 10, 1976, pp. 1329-1342.
- [28] N.V. Phai, "Automatic mesh generator with tetrahedron elements," *Inter. J. Num. Meth. Engr.*, vol. 18, 1982, pp. 273-289.
- [29] F.A. Akyuz, "Natural coordinates systems—An automatic input data generation scheme for a finite element method," *Nuclear Engr. Design*, vol. 11, 1970, pp. 195-207.
- [30] P. Girdinio et al., "New developments of grid optimization by the grid iteration method," in Z.J. Csendes (ed.), *Computational Electromagnetism*. New York: North-Holland, 1986, pp. 3-12.
- [31] M. Yokoyama, "Automated computer simulation of two-dimensional electrostatic problems by finite element method," *Inter. J. Num. Meth. Engr.*, vol. 21, 1985, pp. 2273-2287.
- [32] G.F. Carey, "A mesh-refinement scheme for finite element computations," *Comp. Meth. Appl. Mech. Engr.*, vol. 7, 1976, pp. 93-105.

REFERENCES

- [33] K. Preiss, "Checking the topological consistency of a finite element mesh," *Inter. J. Meth. Engr.*, vol. 14, 1979, pp. 1805-1812.
- [34] W.C. Thacker, "A brief review of techniques for generating irregular computational grids," *Inter. J. Num. Meth. Engr.*, vol. 15, 1980, pp. 1335-1341.
- [35] E. Hinton and D.R. Owen, *An Introduction to Finite Element Computations*. Swansea, U.K.: Pineridge Press, 1979, pp. 247, 328-346.
- [36] P. O. Persson and G. Strang, "A simple mesh generator in MATLAB," *SIAM Review*, vol. 46, 2004, pp. 329-345.
- [37] R.J. Collins, "Bandwidth reduction by automatic renumbering," *Inter. J. Num. Meth. Engr.*, vol. 6, 1973, pp. 345-356.
- [38] E. Cuthill and J. McKee, "Reducing the bandwidth of sparse symmetric matrices," *ACM Nat. Conf.*, San Francisco, 1969, pp. 157-172.
- [39] G.A. Akhras and G. Dhatt, "An automatic node relabelling scheme for minimizing a matrix or network bandwidth," *Inter. J. Num. Meth. Engr.*, vol. 10, 1976, pp. 787-797.
- [40] F.A. Akyuz and S. Utku, "An automatic node-relabelling scheme for bandwidth minimization of stiffness matrices," *J. Amer. Inst. Aero. Astro.*, vol. 6, no. 4, 1968, pp. 728-730.
- [41] M.V.K. Chari and P.P. Silvester (eds.), *Finite Elements for Electrical and Magnetic Field Problems*. Chichester: John Wiley, 1980, pp. 125-143.
- [42] P. Silvester, "Construction of triangular finite element universal matrices," *Inter. J. Num. Meth. Engr.*, vol. 12, 1978, pp. 237-244.
- [43] P. Silvester, "High-order polynomial triangular finite elements for potential problems," *Inter. J. Engr. Sci.*, vol. 7, 1969, pp. 849-861.
- [44] G.O. Stone, "High-order finite elements for inhomogeneous acoustic guiding structures," *IEEE Trans. Micro. Theory Tech.*, vol. MTT-21, no. 8, Aug. 1973, pp. 538-542.
- [45] A. Konrad, "High-order triangular finite elements for electromagnetic waves in anisotropic media," *IEEE Trans. Micro. Theory Tech.*, vol. MTT-25, no. 5, May 1977, pp. 353-360.
- [46] P. Daly, "Finite elements for field problems in cylindrical coordinates," *Inter. J. Num. Meth. Engr.*, vol. 6, 1973, pp. 169-178.
- [47] M. Sadiku and L. Agba, "News rules for generating finite elements fundamental matrices," *Proc. IEEE Southeastcon*, 1989, pp. 797-801.
- [48] C.A. Brebbia and J.J. Connor, *Fundamentals of Finite Element Technique*. London: Butterworth, 1973, pp. 114-118, 150-163, 191.

- [49] R.L. Ferrari and G.L. Maile, "Three-dimensional finite element method for solving electromagnetic problems," *Elect. Lett.*, vol. 14, no. 15, 1978, pp. 467, 468.
- [50] M. de Pourcq, "Field and power-density calculation by three-dimensional finite elements," *IEEE Proc.*, vol. 130, Pt. H, no. 6, Oct. 1983, pp. 377-384.
- [51] M.V.K. Chari et al., "Finite element computation of three-dimensional electrostatic and magnetostatic field problems," *IEEE Trans. Mag.*, vol. MAG-19, no. 16, Nov. 1983, pp. 2321-2324.
- [52] O.A. Mohammed et al., "Validity of finite element formulation and solution of three dimensional magnetostatic problems in electrical devices with applications to transformers and reactors," *IEEE Trans. Pow. App. Syst.*, vol. PAS-103, no. 7, July 1984, pp. 1846-1853.
- [53] J.S. Savage and A.F. Peterson, "Higher-order vector finite elements for tetrahedral cells," *IEEE Trans. Micro. Theo. Tech.*, vol. 44, no. 6, June 1996, pp. 874-879.
- [54] J.F. Lee and Z.J. Cendes, "Transfinite elements: A highly efficient procedure for modeling open field problems," *J. Appl. Phys.*, vol. 61, no. 8, April 1987, pp. 3913-3915.
- [55] B.H. McDonald and A. Wexler, "Finite-element solution of unbounded field problems," *IEEE Trans. Micro. Theo. Tech.*, vol. MTT-20, no. 12, Dec. 1972, pp. 841-847.
- [56] P.P. Silvester et al., "Exterior finite elements for 2-dimensional field problems with open boundaries," *Proc. IEEE*, vol. 124, no. 12, Dec. 1977, pp. 1267-1270.
- [57] S. Washizu et al., "Extension of finite-element method to unbounded field problems," *Elect. Lett.*, vol. 15, no. 24, Nov. 1979, pp. 772-774.
- [58] P. Silvester and M.S. Hsieh, "Finite-element solution of 2-dimensional exterior-field problems," *Proc. IEEE*, vol. 118, no. 12, Dec. 1971, pp. 1743-1747.
- [59] Z.J. Csendes, "A note on the finite-element solution of exterior-field problems," *IEEE Trans. Micro. Theo. Tech.*, vol. MTT-24, no. 7, July 1976, pp. 468-473.
- [60] T. Corzani et al., "Numerical analysis of surface wave propagation using finite and infinite elements," *Alta Frequenza*, vol. 51, no. 3, June 1982, pp. 127-133.
- [61] O.C. Zienkiewicz et al., "Mapped infinite elements for exterior wave problems," *Inter. J. Num. Meth. Engr.*, vol. 21, 1985.
- [62] F. Medina, "An axisymmetric infinite element," *Int. J. Num. Meth. Engr.*, vol. 17, 1981, pp. 1177-1185.

- [63] S. Pissanetzky, "A simple infinite element," *Int. J. Comp. Math. Electr. Engr.*, (COMPEL), vol. 3, no. 2, 1984, pp. 107-114.
- [64] Z. Pantic and R. Mittra, "Quasi-TEM analysis of microwave transmission lines by the finite-element method," *IEEE Trans. Micro. Theo. Tech.*, vol. MTT-34, no. 11, Nov. 1986, pp. 1096-1103.
- [65] K. Hayata et al., "Self-consistent finite/infinite element scheme for unbounded guided wave problems," *IEEE Trans. Micro. Theo. Tech.*, vol. MTT-36, no. 3, Mar. 1988, pp. 614-616.
- [66] P. Petre and L. Zombory, "Infinite elements and base functions for rotationally symmetric electromagnetic waves," *IEEE Trans. Ant. Prop.*, vol. 36, no. 10, Oct. 1988, pp. 1490, 1491.
- [67] Z.J. Csendes and J.F. Lee, "The transfinite element method for modeling MMIC devices," *IEEE Trans. Micro. Theo. Tech.*, vol. 36, no. 12, Dec. 1988, pp. 1639-1649.
- [68] K.H. Lee et al., "A hybrid three-dimensional electromagnetic modeling scheme," *Geophys.*, vol. 46, no. 5, May 1981, pp. 796-805.
- [69] S.J. Salon and J.M. Schneider, "A hybrid finite element-boundary integral formulation of Poisson's equation," *IEEE Trans. Mag.*, vol. MAG-17, no. 6, Nov. 1981, pp. 2574-2576.
- [70] S.J. Salon and J. Peng, "Hybrid finite-element boundary-element solutions to axisymmetric scalar potential problems," in Z.J. Csendes (ed.), *Computational Electromagnetics*. New York: North-Holland/Elsevier, 1986, pp. 251-261.
- [71] J.M. Lin and V.V. Liepa, "Application of hybrid finite element method for electromagnetic scattering from coated cylinders," *IEEE Trans. Ant. Prop.*, vol. 36, no. 1, Jan. 1988, pp. 50-54.
- [72] J.M. Lin and V.V. Liepa, "A note on hybrid finite element method for solving scattering problems," *IEEE Trans. Ant. Prop.*, vol. 36, no. 10, Oct. 1988, pp. 1486-1490.
- [73] M.H. Lean and A. Wexler, "Accurate field computation with boundary element method," *IEEE Trans. Mag.*, vol. MAG-18, no. 2, Mar. 1982, pp. 331-335.
- [74] R.F. Harrington and T.K. Sarkar, "Boundary elements and the method of moments," in C.A. Brebbia et al. (eds.), *Boundary Elements*. Southampton: CML Publ., 1983, pp. 31-40.
- [75] M.A. Morgan et al., "Finite element-boundary integral formulation for electromagnetic scattering," *Wave Motion*, vol. 6, no. 1, 1984, pp. 91-103.
- [76] S. Kagami and I. Fukai, "Application of boundary-element method to electromagnetic field problems," *IEEE Trans. Micro. Theo. Tech.*, vol. 32, no. 4, Apr. 1984, pp. 455-461.

- [77] Y. Tanaka et al., "A boundary-element analysis of TEM cells in three dimensions," *IEEE Trans. Elect. Comp.*, vol. EMC-28, no. 4, Nov. 1986, pp. 179–184.
- [78] N. Kishi and T. Okoshi, "Proposal for a boundary-integral method without using Green's function," *IEEE Trans. Micro. Theo. Tech.*, vol. MTT-35, no. 10, Oct. 1987, pp. 887–892.
- [79] D.B. Ingham et al., "Boundary integral equation analysis of transmission-line singularities," *IEEE Trans. Micro. Theo. Tech.*, vol. MTT-29, no. 11, Nov. 1981, pp. 1240–1243.
- [80] S. Washizu et al., "An analysis of unbounded field problems by finite element method," *Electr. Comm. Japan*, vol. 64-B, no. 1, 1981, pp. 60–66.
- [81] T. Yamabuchi and Y. Kagawa, "Finite element approach to unbounded Poisson and Helmholtz problems using hybrid-type infinite element," *Electr. Comm. Japan*, Pt. I, vol. 68, no. 3, 1986, pp. 65–74.
- [82] K.L. Wu and J. Litva, "Boundary element method for modelling MIC devices," *Electr. Lett.*, vol. 26, no. 8, April 1990, pp. 518–520.
- [83] M.N.O. Sadiku and A.F. Peterson, "A comparison of numerical methods for computing electromagnetic fields," *Proc. IEEE Southeastcon*, April 1990, pp. 42–47.
- [84] P.K. Kythe, *An Introduction to Boundary Element Methods*. Boca Raton, FL: CRC Press, 1995, p. 2.
- [85] J.M. Jin et al., "Fictitious absorber for truncating finite element meshes in scattering," *IEEE Proc. H*, vol. 139, Oct. 1992, pp. 472–476.
- [86] R. Mittra and O. Ramahi, "Absorbing bounding conditions for direct solution of partial differential equations arising in electromagnetic scattering problems," in M.A. Morgan (ed.), *Finite Element and Finite Difference Methods in Electromagnetics*. New York: Elsevier, 1990, pp. 133–173.
- [87] U. Pekel and R. Mittra, "Absorbing boundary conditions for finite element mesh truncation," in T. Itoh et al. (eds.), *Finite Element Software for Microwave Engineering*. New York: John Wiley & Sons, 1996, pp. 267–312.
- [88] U. Pekel and R. Mittra, "A finite element method frequency domain application of the perfectly matched layer (PML) concept," *Micro. Opt. Tech. Lett.*, vol. 9, pp. 117–122.
- [89] A. Boag and R. Mittra, "A numerical absorbing boundary condition for finite difference and finite element analysis of open periodic structures," *IEEE Trans. Micro. Theo. Tech.*, vol. 43, no. 1 Jan. 1995, pp. 150–154.
- [90] P.P. Silvester and G. Pelosi (eds.), *Finite Elements for Wave Electromagnetics: Methods and Techniques*. New York: IEEE Press, 1994, pp. 351–490.

- [91] Y. Wang and T. Itoh, "Envelope-finite-element (EVFE) technique – a more efficient time-domain scheme," *IEEE Trans. Micro. Theo. Tech.*, vol. 49, no. 12, Dec. 2001, pp. 2241–2247.
- [92] J. F. Lee, R. Lee, and A. Cangellaris, "Time-domain finite-element methods," *IEEE Trans. Ant. Prop.*, vol. 45, no. 3, March 1997, pp. 430–442.
- [93] D. Jiao et al., "A fast time-domain finite element-boundary integral method for electromagnetic analysis," *IEEE Trans. Ant. Prop.*, vol. 49, no. 10, Oct. 2001.
- [94] D. Jiao and J. M. Jin, "A general approach for the stability analysis of the time-domain finite-element method for electromagnetic simulations," *IEEE Trans. Ant. Prop.*, vol. 50, no. 11, Nov. 2002, pp. 1624–1632.
- [95] J. Jin, *The Finite Element Method in Electromagnetics*, 2nd ed. New York: John Wiley & Sons, 2002, Chapter 12, pp. 529–584.
- [96] S. Pernet, X. Ferrieres, and G. Cohen, "High spatial order finite element method to solve Maxwell's equations in time domain," *IEEE Trans. Ant. Prop.*, vol. 53, no. 9, Sept. 2005, pp. 2889–2899.
- [97] J.F. Lee, "WETD – a finite element time-domain approach for solving Maxwell's equations," *IEEE Micro. Guided Wave Lett.*, vol. 4, no. 1, Jan. 1994, pp. 11–13.
- [98] A.C. Cangellaris, C. C. Lin, and K. K. Mei, "Point-matched time domain finite element methods for electromagnetic radiation and scattering," *IEEE Trans. Ant. Prop.*, vol. AP-35, no. 10, Oct. 1987, pp. 1160–1173.
- [99] S. Benhassine, L. Pichon, and W. Tabbara, "An efficient finite-element time-domain method for the analysis of the coupling between wave and shielded enclosure," *IEEE Trans. Mag.*, vol. 38, no. 2, March 2002, pp. 709–712.
- [100] C.W. Steele, *Numerical Computation of Electric and Magnetic Fields*. New York: Van Nostrand Reinhold, 1987.
- [101] S.R. Hoole, *Computer-Aided Analysis and Design of Electromagnetic Devices*. New York: Elsevier, 1989.
- [102] T. Itoh (ed.), *Numerical Technique for Microwave and Millimeterwave Passive Structure*. New York: John Wiley, 1989.
- [103] R.L. Khan and G.I. Costache, "Finite element method applied to modeling crosstalk problems on printed circuits boards," *IEEE Trans. Elect. Comp.*, vol. 31, no. 1, Feb. 1989, pp. 5–15.
- [104] P. Daly, "Upper and lower bounds to the characteristic impedance of transmission lines using the finite method," *Inter. J. Comp. Math. Elect. Engr.*, (COMPEL), vol. 3, no. 2, 1984, pp. 65–78.

- [105] A. Khebir et al., "An absorbing boundary condition for quasi-TEM analysis of microwave transmission lines via the finite element method," *J. Elect. Waves Appl.*, vol. 4, no. 2, 1990, pp. 145–157.
- [106] N. Mabaya et al., "Finite element analysis of optical waveguides," *IEEE Trans. Micro. Theo. Tech.*, vol. MTT-29, no. 6, June 1981, pp. 600–605.
- [107] M. Ikeuchi et al., "Analysis of open-type dielectric waveguides by the finite-element iterative method," *IEEE Trans. Micro. Theo. Tech.*, vol. MTT-29, no. 3, Mar. 1981, pp. 234–239.
- [108] C. Yeh et al., "Single model optical waveguides," *Appl. Optics*, vol. 18, no. 10, May 1979, pp. 1490–1504.
- [109] J. Katz, "Novel solution of 2-D waveguides using the finite element method," *Appl. Optics*, vol. 21, no. 15, Aug. 1982, pp. 2747–2750.
- [110] B.A. Rahman and J.B. Davies, "Finite-element analysis of optical and microwave waveguide problems," *IEEE Trans. Micro. Theo. Tech.*, vol. MTT-32, no. 1, Jan. 1984, pp. 20–28.
- [111] X.Q. Sheng and S. Xu, "An efficient high-order mixed-edge rectangular-element method for lossy anisotropic dielectric waveguide," *IEEE Micro. Theo. Tech.*, vol. 45, no. 7, July 1997, pp. 1009–1013.
- [112] C.B. Rajanathan et al., "Finite-element analysis of the Xi-core levitator," *IEEE Proc.*, vol. 131, Pt. A, no. 1, Jan. 1984, pp. 62–66.
- [113] T.L. Ma and J.D. Lavers, "A finite-element package for the analysis of electromagnetic forces and power in an electric smelting furnace," *IEEE Trans. Indus. Appl.*, vol. IA-22, no. 4, July/Aug. 1986, pp. 578–585.
- [114] C.O. Obiozor and M.N.O. Sadiku, "Finite element analysis of a solid rotor induction motor under stator winding effects," *Proc. IEEE Southeastcon*, 1991, pp. 449–453.
- [115] J.L. Mason and W.J. Anderson, "Finite element solution for electromagnetic scattering from two-dimensional bodies," *Inter. J. Num. Meth. Engr.*, vol. 21, 1985, pp. 909–928.
- [116] A. Chiba et al., "Application of finite element method to analysis of induced current densities inside human model exposed to 60 Hz electric field," *IEEE Trans. Power App. Sys.*, vol. PAS-103, no. 7, July 1984, pp. 1895–1902.
- [117] Y. Yamashita and T. Takahashi, "Use of the finite element method to determine epicardial from body surface potentials under a realistic torso model," *IEEE Trans. Biomed. Engr.*, vol. BME-31, no. 9, Sept. 1984, pp. 611–621.
- [118] M.A. Morgan, "Finite element calculation of microwave absorption by the cranial structure," *IEEE Trans. Biomed. Engr.*, vol. BME-28, no. 10, Oct. 1981, pp. 687–695.

- [119] D.R. Lynch et al., "Finite element solution of Maxwell's equation for hyperthermia treatment planning," *J. Comp. Phys.*, vol. 58, 1985, pp. 246–269.
- [120] J.R. Brauer et al., "Dynamic electric fields computed by finite elements," *IEEE Trans. Ind. Appl.*, vol. 25, no. 6, Nov./Dec. 1989, pp. 1088–1092.
- [121] C.H. Chen and C.D. Lien, "A finite element solution of the wave propagation problem for an inhomogeneous dielectric slab," *IEEE Trans. Ant. Prop.*, vol. AP-27, no. 6, Nov. 1979, pp. 877–880.
- [122] T.L.W. Ma and J.D. Lavers, "A finite-element package for the analysis of electromagnetic forces and power in an electric smelting furnace," *IEEE Trans. Ind. Appl.*, vol. IA-22, no. 4, July/Aug., 1986, pp. 578–585.
- [123] M.A. Kolbehdari and M.N.O. Sadiku, "Finite element analysis of an array of rods or rectangular bars between ground," *J. Franklin Inst.*, vol. 335B, no. 1, 1998, pp. 97–107.
- [124] J. Cushman, "Difference schemes or element schemes," *Int. J. Num. Meth. Engr.*, vol. 14, 1979, pp. 1643–1651.
- [125] A.J. Baker and M.O. Soliman, "Utility of a finite element solution algorithm for initial-value problems," *J. Comp. Phys.*, vol. 32, 1979, pp. 289–324.
- [126] J.N. Reddy, *An Introduction to the Finite Element Method*, 2nd ed. New York: McGraw-Hill, 1993, pp. 293–403.
- [127] C.A. Brebbia (ed.), *Applied Numerical Modelling*, New York: John Wiley, 1978, pp. 571–586.
- [128] C.A. Brebbia (ed.), *Finite Element Systems: A Handbook*. Berlin: Springer-Verlag, 1985.
- [129] O.C. Zienkiewicz, *The Finite Element Method*. New York: McGraw-Hill, 1977.
- [130] A.J. Davies, *The Finite Element Method: A First Approach*. Oxford: Clarendon, 1980.
- [131] C. Martin and G.F. Carey, *Introduction to Finite Element Analysis: Theory and Application*. New York: McGraw-Hill, 1973.
- [132] T.J. Chung, *Finite Element Analysis in Fluid Dynamics*. New York: McGraw-Hill, 1978.
- [133] D.H. Norris and G. deVries, *An Introduction to Finite Element Analysis*. New York: Academic Press, 1978.
- [134] T. Itoh et al. (eds.), *Finite Element Software for Microwave Engineering*. New York: John Wiley & Sons, 1996.

Problems

- 6.1 For the triangular elements in Figure 6.32, determine the element coefficient matrices.

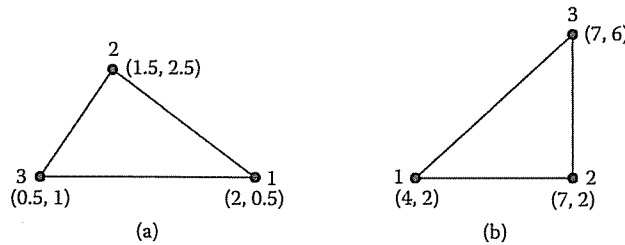


**Figure 6.32
For Problem 6.1.**

- 6.2 Find the coefficient matrix for the two-element mesh of Figure 6.33. Given that $V_2 = 10$ and $V_4 = -10$, determine V_1 and V_3 .

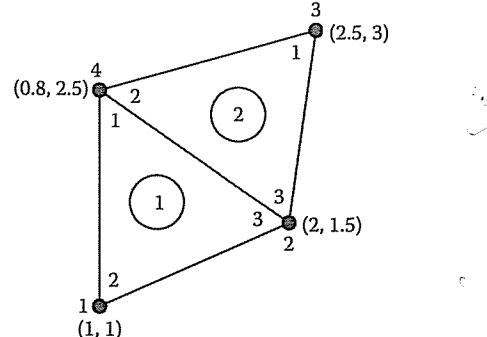


**Figure 6.33
For Problem 6.2.**

- 6.3 Determine the shape functions α_1 , α_2 , and α_3 for the element in Figure 6.34.
- 6.4 A triangular element has nodes at $(0,1)$, $(1,0)$, and $(0,1)$. Construct the shape function α_1 .

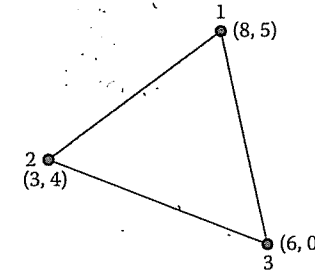


**Figure 6.34
For Problem 6.3.**

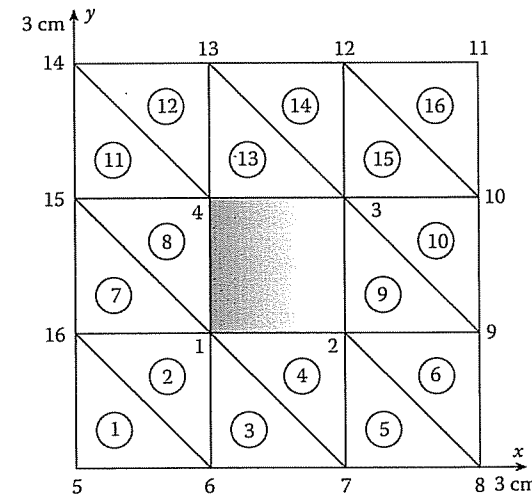


**Figure 6.35
For Problem 6.6.**

- 6.5 Show that the shape function α_1 evaluates to unity at node 1 and to zero at all other nodes for the first-order elements.
- 6.6 Consider the mesh shown in Figure 6.35. The shaded region is conducting and has no finite elements. Calculate the global elements $C_{3,10}$ and $C_{3,3}$.
- 6.7 With reference to the finite element in Figure 6.36, calculate the energy per unit length associated with the element.
- 6.8 Consider the element whose sides are parallel to the x and y axis, as shown in Figure 6.37. Verify that the potential distribution within the elements can be expressed as

$$V(x, y) = \alpha_1 V_1 + \alpha_2 V_2 + \alpha_3 V_3 + \alpha_4 V_4$$

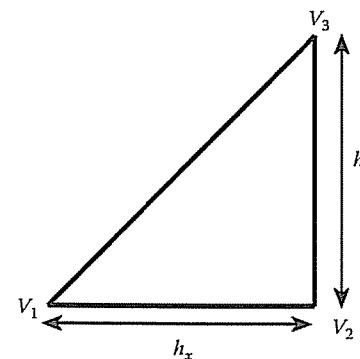


Figure 6.36
For Problem 6.7.

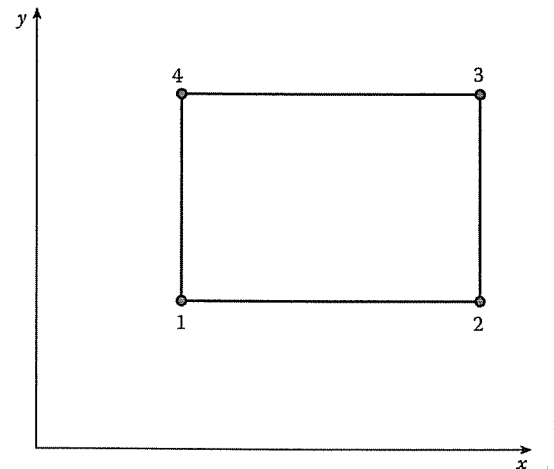


Figure 6.37
For Problem 6.8.

where V_i are the nodal potentials and α_i are local interpolating functions defined as

$$\alpha_1 = \frac{(x - x_2)(y - y_4)}{(x_1 - x_2)(y_1 - y_4)}$$

$$\alpha_2 = \frac{(x - x_1)(y - y_3)}{(x_2 - x_1)(y_2 - y_3)}$$

$$\alpha_3 = \frac{(x - x_4)(y - y_2)}{(x_3 - x_4)(y_3 - y_2)}$$

$$\alpha_4 = \frac{(x - x_3)(y - y_1)}{(x_4 - x_3)(y_4 - y_1)}$$

PROBLEMS

- 6.9 The cross section of an infinitely long rectangular trough is shown in Figure 6.38; develop a program using FEM to find the potential at the center of the cross section. Take $\epsilon_r = 4.5$.

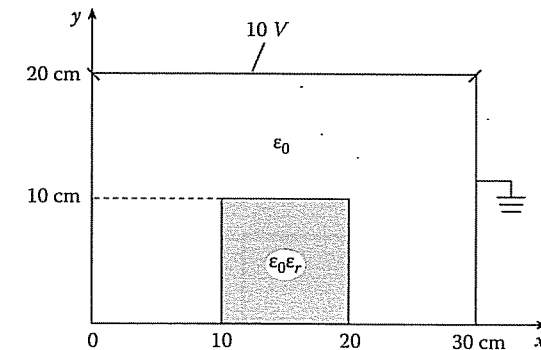


Figure 6.38
For Problem 6.9.

- 6.10 Solve the problem in Example 3.3 using the finite element method.
6.11 Once the potential distribution is obtained, the electric field intensity can be obtained from

$$\mathbf{E}(x, y) = E_x \mathbf{a}_x + E_y \mathbf{a}_y = -\nabla V(x, y)$$

For each triangular element, show that

$$E_x = -\frac{1}{2A} [(y_j - y_k)V_i + (y_k - y_i)V_j + (y_i - y_j)V_k]$$

$$E_y = -\frac{1}{2A} [(x_k - x_j)V_i + (x_i - x_k)V_j + (x_j - x_i)V_k]$$

Where A is the area of the element and $V_{i,j,k}$ represent the electric potentials of three nodes (i, j, k) of each element.

- 6.12 A potential field is defined over a triangular three-node element by

Node i	$V_i(V)$	x_i (cm)	y_i (cm)
1	40	4	6
2	-10	2	2
3	20	6	2

Calculate the potential and potential gradient at (4,4)cm.

- 6.13 Modify the program in Figure 6.10 to calculate the electric field intensity \mathbf{E} at any point in the solution region.

- 6.14 The program in Figure 6.10 applies the iteration method to determine the potential at the free nodes. Modify the program and use the band matrix method to determine the potential. Test the program using the data in Example 6.2.
- 6.15 A grounded rectangular pipe with the cross section in Figure 6.39 is half-filled with hydrocarbons ($\epsilon = 2.5\epsilon_0$, $\rho_o = 10^{-5}$ C/m³). Use FEM to determine the potential along the liquid-air interface. Plot the potential versus x .

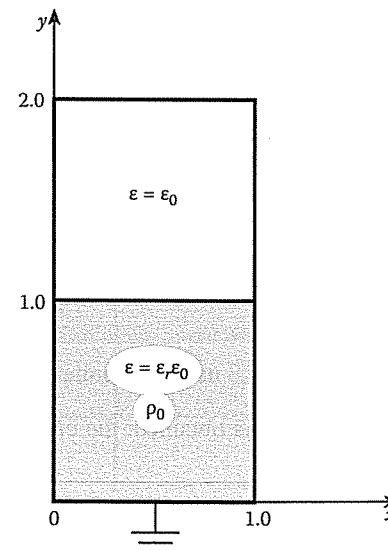


Figure 6.39
For Problem 6.15.

- 6.16 Solve the problem in Example 3.4 using the finite element method.
- 6.17 The cross section of an isosceles right-triangular waveguide is discretized as in Figure 6.40. Determine the first 10 TM cutoff wavelengths of the guide.
- 6.18 Using FEM, determine the first 10 cutoff wavelengths of a rectangular waveguide of cross section 2 cm by 1 cm. Compare your results with exact solution. Assume the guide is air-filled.
- 6.19 Use the mesh generation program in Figure 6.16 to subdivide the solution regions in Figure 6.41. Subdivide into as many triangular elements as you choose.

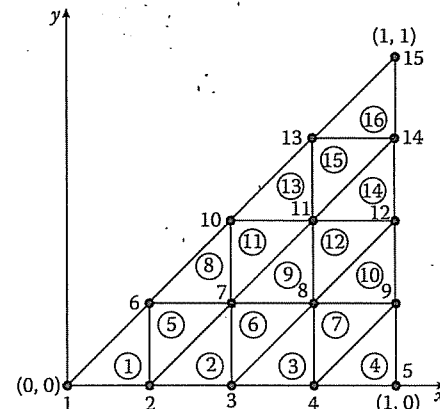


Figure 6.40
For Problem 6.17.

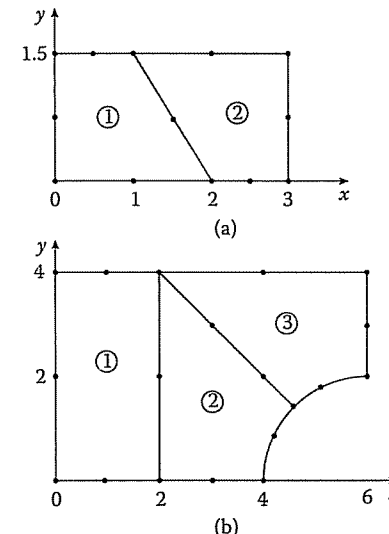


Figure 6.41
For Problem 6.19.

- 6.20 Determine the semi-bandwidth of the mesh shown in Figure 6.42. Renumber the mesh so as to minimize the bandwidth.
- 6.21 Find the semi-bandwidth B of the mesh in Figure 6.43. Renumber the mesh to minimize B and determine the new value of B .

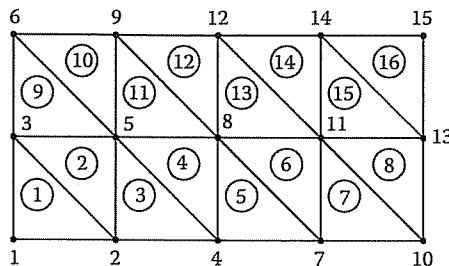


Figure 6.42

For Problem 6.20.

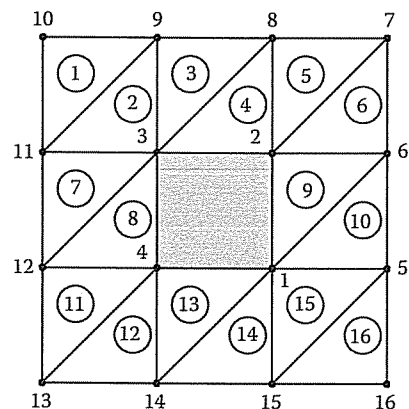


Figure 6.43

For Problem 6.21.

- 6.22 Rework Problem 3.20 using the FEM.

Hint: After calculating V at all free nodes with ϵ lumped with C_{ij} , use Equation (6.19) to calculate W , i.e.,

$$W = \frac{1}{2} [V]^T [C] [V]$$

Then find the capacitance from

$$C = \frac{2W}{V_d^2}$$

where V_d is the potential difference between inner and outer conductors.

- 6.23 Using the area coordinates
- (ξ_1, ξ_2, ξ_3)
- for the triangular element in Figure 6.3, evaluate

PROBLEMS

- (a) $\int_S x dS$
 (b) $\int_S x^2 dS$
 (c) $\int_S xy dS$

- 6.24 Evaluate the following integrals:

- (a) $\int_S \alpha_2^3 dS$
 (b) $\int_S \alpha_1 \alpha_5 dS$
 (c) $\int_S \alpha_1 \alpha_2 \alpha_3 dS$

- 6.25 Evaluate the shape functions
- $\alpha_1, \dots, \alpha_6$
- for the second-order elements in Figure 6.44.

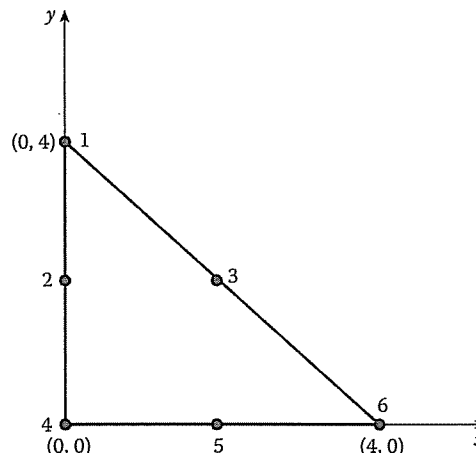


Figure 6.44

For Problem 6.25.

- 6.26 Derive matrix
- T
- for
- $n = 2$
- .

- 6.27 By hand calculation, obtain
- $Q^{(2)}$
- and
- $Q^{(3)}$
- for
- $n = 1$
- and
- $n = 2$
- .

- 6.28 The
- $D^{(q)}$
- matrix is an auxilliary matrix used along with the
- T
- matrix to derive other fundamental matrices. An element of
- D
- is defined in [43] as the partial derivative of
- α_i
- with respect to
- ξ_q
- evaluated at node
- P_j
- , i.e.,

$$D_{ij}^{(q)} = \left. \frac{\partial \alpha_i}{\partial \xi_q} \right|_{P_j}, \quad i, j = 1, 2, \dots, m$$

where $q \in \{1, 2, 3\}$. For $n = 1$ and 2, derive $D^{(1)}$. From $D^{(1)}$, derive $D^{(2)}$ and $D^{(3)}$.

- 6.29 (a) The matrix $K^{(pq)}$ can be defined as

$$K_{ij}^{(pq)} = \iint \frac{\partial \alpha_i}{\partial \xi_p} \frac{\partial \alpha_j}{\partial \xi_q} dS$$

where $p, q = 1, 2, 3$. Using the $D^{(q)}$ matrix of the previous problem, show that

$$K^{(pq)} = D^{(p)} T D^{(q)'}^t$$

where t denotes transposition.

- (b) Show that the $Q^{(q)}$ matrix can be written as

$$Q^{(q)} = [D^{(q+1)} - D^{(q-1)}] T [D^{(q+1)} - D^{(q-1)}]^t$$

Use this formula to derive $Q^{(1)}$ for $n = 1$ and 2.

- 6.30 Verify the interpolation function for the 10-node tetrahedral element.

- 6.31 The (x, y, z) coordinates of nodes 1, 2, 3, and 4 of a three-dimensional simplex element are $(0, 0, 0)$, $(2, 4, 2)$, $(4, 0, 0)$, and $(2, 0, 6)$, respectively. Determine the shape functions of the element.

- 6.32 Using the volume coordinates for a tetrahedron, evaluate

$$\int z^2 dv$$

Assume that the origin is located at the centroid of the tetrahedron.

- 6.33 Obtain the T matrix for the first-order tetrahedral element.

- 6.34 For the tetrahedral cell, obtain the matrix M whose elements are defined by

$$M_{ij} = \frac{1}{v} \int_v \xi_i \xi_j dv$$

- 6.35 For the two-dimensional problem, the BGI sequence of operators are defined by the recurrence relation

$$B_m = \left(\frac{\partial}{\partial \rho} + jk + \frac{4m-3}{2\rho} \right) B_{m-1}$$

where $B_0 = 1$. Obtain B_1 and B_2 .

Chapter 7

Transmission-Line-Matrix Method

The way to get things done is not to mind who gets the credit of doing them.

- Benjamin Jowett

7.1 Introduction

The link between field theory and circuit theory has been exploited in developing numerical techniques to solve certain types of partial differential equations arising in field problems with the aid of equivalent electrical networks [1]. There are three ranges in the frequency spectrum for which numerical techniques for field problems in general have been developed. In terms of the wavelength λ and the approximate dimension ℓ of the apparatus, these ranges are [2]:

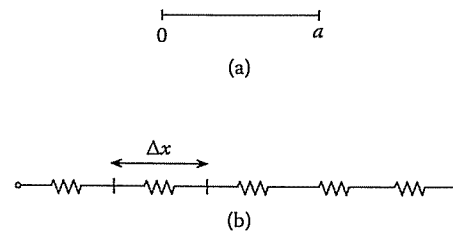
$$\lambda >> \ell$$

$$\lambda \approx \ell$$

$$\lambda << \ell$$

In the first range, the special analysis techniques are known as *circuit theory*; in the second, as *microwave theory*; and in the third, as *geometric optics* (frequency independent). Hence the fundamental laws of circuit theory can be obtained from Maxwell's equations by applying an approximation valid when $\lambda >> \ell$. However, it should be noted that circuit theory was not developed by approximating Maxwell's equations, but rather was developed independently from experimentally obtained laws. The connection between circuit theory and Maxwell equations (summarizing field theory) is important; it adds to the comprehension of the fundamentals of electromagnetics. According to Silvester and Ferrari, circuits are mathematical abstractions of physically real fields; nevertheless, electrical engineers at times feel they understand circuit theory more clearly than fields [3].

The idea of replacing a complicated electrical system by a simple equivalent circuit goes back to Kirchhoff and Helmholtz. As a result of Park's [4], Kron's [5, 6] and Schwinger's [7, 8] works, the power and flexibility of equivalent circuits become more

**Figure 7.1**

(a) One-dimensional conducting system, (b) discretized equivalent.

obvious to engineers. The recent applications of this idea to scattering problems, originally due to Johns and Beurle [9], has made the method more popular and attractive.

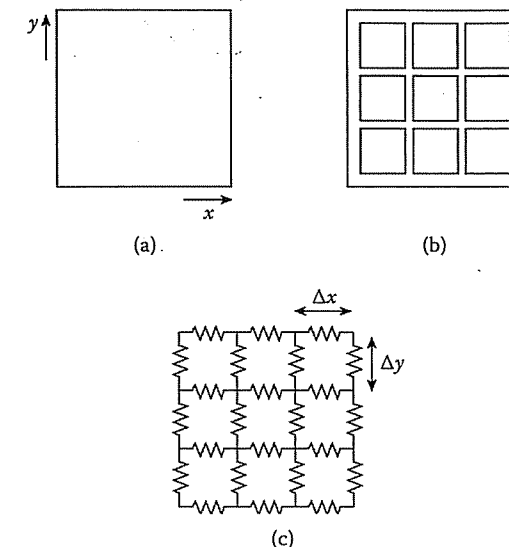
Transmission-line modeling (TLM), otherwise known as the *transmission-line-matrix method*, is a numerical technique for solving field problems using circuit equivalent. It is based on the equivalence between Maxwell's equations and the equations for voltages and currents on a mesh of continuous two-wire transmission lines. The main feature of this method is the simplicity of formulation and programming for a wide range of applications [10, 11]. As compared with the lumped network model, the transmission-line model is more general and performs better at high frequencies where the transmission and reflection properties of geometrical discontinuities cannot be regarded as lumped [7].

Like other numerical techniques, the TLM method is a discretization process. Unlike other methods such as finite difference and finite element methods, which are mathematical discretization approaches, the TLM is a physical discretization approach. In the TLM, the discretization of a field involves replacing a continuous system by a network or array of lumped elements. For example, consider the one-dimensional system (a conducting wire) with no energy storage as in Figure 7.1(a). The wire can be replaced by a number of lumped resistors providing a discretized equivalent in Figure 7.1(b). The discretization of the two-dimensional, distributed field is shown in Figure 7.2. More general systems containing energy-reservoir elements as well as dissipative elements will be considered later.

The TLM method involves dividing the solution region into a rectangular mesh of transmission lines. Junctions are formed where the lines cross forming impedance discontinuities. A comparison between the transmission-line equations and Maxwell's equations allows equivalences to be drawn between voltages and currents on the lines and electromagnetic fields in the solution region. Thus, the TLM method involves two basic steps [12]:

- replacing the field problem by the equivalent network and deriving analogy between the field and network quantities and
- solving the equivalent network by iterative methods.

7.2. TRANSMISSION-LINE EQUATIONS

**Figure 7.2**

(a) Two-dimensional conductive sheet, (b) partially discretized equivalent, (c) fully discretized equivalent.

Before we apply the method, it seems fit to briefly review the basic concepts of transmission lines and then show how the TLM method can be applied to a wide range of EM-related problems.

7.2 Transmission-Line Equations

Consider an elemental portion of length $\Delta\ell$ of a two-conductor transmission line. We intend to find an equivalent circuit for this line and derive the line equations. An equivalent circuit of a portion of the line is shown in Figure 7.3, where the line parameters R , L , G , and C are resistance per unit length, inductance per unit length, conductance per unit length, and capacitance per unit length of the line, respectively. The model in Figure 7.3 may represent any two-conductor line. The model is called the T-type equivalent circuit; other types of equivalent circuits are possible, but we end up with the same set of equations. In the model of Figure 7.3, we assume without loss of generality that wave propagates in the $+z$ direction, from the generator to the load.

By applying Kirchhoff's voltage law to the left loop of the circuit in Figure 7.3, we obtain

$$V(z, t) = R \frac{\Delta\ell}{2} I(z, t) + L \frac{\Delta\ell}{2} \frac{\partial I}{\partial t}(z, t) + V(z + \Delta\ell/2, t)$$

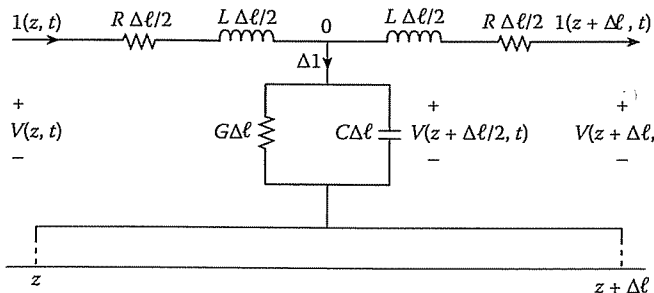


Figure 7.3

T-type equivalent circuit model of a differential length of a two-conductor transmission line.

or

$$-\frac{V(z + \Delta\ell/2, t) - V(z, t)}{\Delta\ell/2} = RI(z, t) + L\frac{\partial I}{\partial t}(z, t) \quad (7.1)$$

Taking the limit of Equation (7.1) as $\Delta\ell \rightarrow 0$ leads to

$$-\frac{\partial V(z, t)}{\partial z} = RI(z, t) + L\frac{\partial I}{\partial t}(z, t) \quad (7.2)$$

Similarly, applying Kirchhoff's current law to the main node of the circuit in Figure 7.3 gives

$$\begin{aligned} I(z, t) &= I(z + \Delta\ell, t) + \Delta I \\ &= I(z + \Delta\ell, t) + G\Delta\ell V(z + \Delta\ell/2, t) + C\Delta\ell\frac{\partial V}{\partial t}(z + \Delta\ell/2, t) \end{aligned}$$

or

$$-\frac{I(z + \Delta\ell, t) - I(z, t)}{\Delta\ell} = GV(z + \Delta\ell/2, t) + C\frac{\partial V}{\partial t}(z + \Delta\ell/2, t) \quad (7.3)$$

As $\Delta\ell \rightarrow 0$, Equation (7.3) becomes

$$-\frac{\partial I}{\partial z}(z, t) = GV(z, t) + C\frac{\partial V}{\partial t}(z, t) \quad (7.4)$$

Differentiating Equation (7.2) with respect to z and Equation (7.4) with respect to t , the two equations become

$$-\frac{\partial^2 V}{\partial z^2} = R\frac{\partial I}{\partial z} + L\frac{\partial^2 I}{\partial z \partial t} \quad (7.2a)$$

and

$$-\frac{\partial^2 I}{\partial t \partial z} = G\frac{\partial V}{\partial t} + C\frac{\partial^2 V}{\partial t^2} \quad (7.4a)$$

7.2. TRANSMISSION-LINE EQUATIONS

Substituting Equations (7.4) and (7.4a) into Equation (7.2a) gives

$$\frac{\partial^2 V}{\partial z^2} = LC\frac{\partial^2 V}{\partial t^2} + (RC + GL)\frac{\partial V}{\partial t} + RGV \quad (7.5)$$

Similarly, we obtain the equation for current I as

$$\frac{\partial^2 I}{\partial z^2} = LC\frac{\partial^2 I}{\partial t^2} + (RC + GL)\frac{\partial I}{\partial t} + RGI \quad (7.6)$$

Equations (7.5) and (7.6) have the same mathematical form, which in general may be written as

$$\frac{\partial^2 \Phi}{\partial z^2} = LC\frac{\partial^2 \Phi}{\partial t^2} + (RC + GL)\frac{\partial \Phi}{\partial t} + RG\Phi \quad (7.7)$$

where $\Phi(z, t)$ has replaced either $V(z, t)$ or $I(z, t)$.

Ignoring certain transmission-line parameters in Equation (7.7) leads to the following special cases [13]:

(a) $L = C = 0$ yields

$$\frac{\partial^2 \Phi}{\partial z^2} = k_1 \Phi \quad (7.8)$$

where $k_1 = RG$. Equation (7.8) is the one-dimensional elliptic partial differential equation called Poisson's equation.

(b) $R = C = 0$ or $G = L = 0$ yields

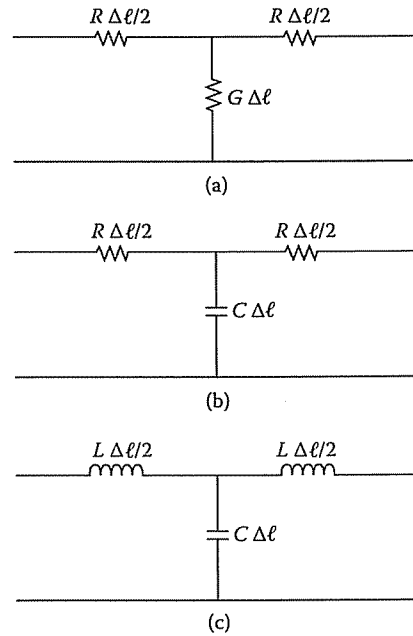
$$\frac{\partial^2 \Phi}{\partial z^2} = k_2 \frac{\partial \Phi}{\partial t} \quad (7.9)$$

where $k_2 = GL$ or RC . Equation (7.9) is the one-dimensional parabolic partial differential equation called the diffusion equation.

(c) $R = G = 0$ (lossless line) yields

$$\frac{\partial^2 \Phi}{\partial z^2} = k_3 \frac{\partial^2 \Phi}{\partial t^2} \quad (7.10)$$

where $k_3 = LC$. This is the one-dimensional hyperbolic partial differential equation called the Helmholtz equation, or simply the wave equation. Thus, under certain conditions, the one-dimensional transmission line can be used to model problems involving an elliptic, parabolic, or hyperbolic partial differential equation (PDE). The transmission line of Figure 7.3 reduces to those in Figure 7.4 for these three special cases.

**Figure 7.4**

Transmission-line equivalent models for: (a) elliptic PDE, Poisson's equation, (b) parabolic PDE, diffusion equation, (c) hyperbolic PDE, wave equation.

Apart from the equivalent models, other transmission-line parameters are of interest. A detailed explanation of these parameters can be found in standard field theory texts, e.g., [14]. We briefly present these important parameters. For the lossless line in Figure 7.4(c), the characteristic resistance

$$R_o = \sqrt{\frac{L}{C}}, \quad (7.11a)$$

the wave velocity

$$u = \frac{1}{\sqrt{LC}}, \quad (7.11b)$$

and the reflection coefficient at the load

$$\Gamma = \frac{R_L - R_o}{R_L + R_o}, \quad (7.11c)$$

where R_L is the load resistance.

The generality of the TLM method has been demonstrated in this section. In the following sections, the method is applied specifically to diffusion [15, 16] and wave propagation problems [10]–[13], [17, 18].

7.3 Solution of Diffusion Equation

We now apply the TLM method to the diffusion problem arising from current density distribution within a wire [15]. If the wire has a circular cross section with radius a and is infinitely long, then the problem becomes one-dimensional. We will assume sinusoidal source or harmonic fields (with time factor $e^{j\omega t}$).

The analytical solution of the problem has been treated in Example 2.3. For the TLM solution, consider the equivalent network of the cylindrical problem in Figure 7.5, where $\Delta\ell$ is the distance between nodes or the mesh size. Applying Kirchhoff's laws to the network in Figure 7.5 gives

$$\frac{\partial I_\rho}{\partial \rho} = -j\omega C V_\phi \quad (7.12a)$$

$$\frac{\partial V_\phi}{\partial \rho} = -R I_\rho \quad (7.12b)$$

where R and C are the resistance and capacitance per unit length.

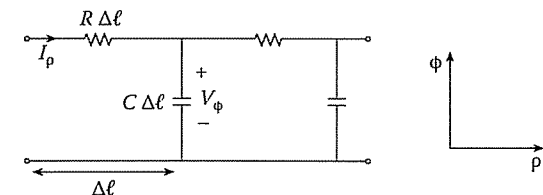


Figure 7.5
RC equivalent network.

Within the conductor, Maxwell's curl equations ($\sigma >> \omega\epsilon$) are

$$\nabla \times \mathbf{E} = -j\omega\mu\mathbf{H} \quad (7.13a)$$

$$\nabla \times \mathbf{H} = \sigma \mathbf{E} \quad (7.13b)$$

where \mathbf{E} and \mathbf{H} are assumed to be in phasor forms. In cylindrical coordinates, Equation (7.13) becomes

$$\begin{aligned} -\frac{\partial E_z}{\partial \rho} &= -j\omega\mu H_\phi \\ \frac{1}{\rho} \frac{\partial}{\partial \rho} (\rho H_\phi) &= \sigma E_z \end{aligned}$$

These equations can be written as

$$\frac{\partial E_z}{\partial \rho} = j\omega(\mu/\rho)(\rho H_\phi) \quad (7.14a)$$

$$\frac{\partial}{\partial \rho} (\rho H_\phi) = (\sigma\rho)E_z \quad (7.14b)$$

Comparing Equation (7.12) with Equation (7.14) leads to the following analogy between the network and field quantities:

$$I_\rho \equiv -E_z \quad (7.15a)$$

$$V_\phi \equiv \rho H_\phi \quad (7.15b)$$

$$C \equiv \mu/\rho \quad (7.15c)$$

$$R \equiv \sigma\rho \quad (7.15d)$$

Therefore, solving the impedance network is equivalent to solving Maxwell's equations.

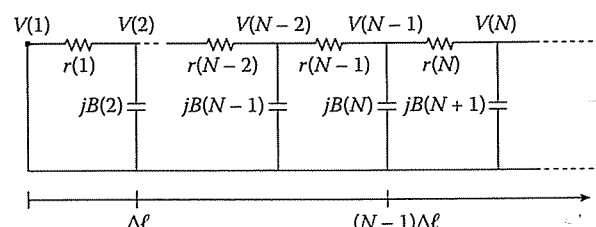


Figure 7.6
The overall equivalent network.

We can solve the overall impedance network in Figure 7.6 by an iterative method. Since the network in Figure 7.6 is in the form of a ladder, we apply the *ladder* method. By applying Kirchhoff's current law, the N th nodal voltage ($N > 2$) is related to ($N - 1$)th and ($N - 2$)th voltages according to

$$V(N) = \frac{r(N-1)}{r(N-2)} [V(N-1) - V(N-2)] + jB(N-1)r(N-1)V(N-1) + V(N-1) \quad (7.16)$$

where the resistance r and susceptance B are given by

$$r(N) = R\Delta\ell = \sigma(N-0.5)(\Delta\ell)^2, \quad (7.17a)$$

$$B(N) = \omega C \Delta\ell = \frac{\omega\mu\Delta\ell}{(N-1)\Delta\ell} = \frac{\omega\mu}{N-1} \quad (7.17b)$$

7.3. SOLUTION OF DIFFUSION EQUATION

We note that $V(1) = 0$ because the magnetic field at the center of the conductor ($\rho = 0$) is zero. Also $V(2) = I(1) \cdot r(1)$, where $I(1)$ can be arbitrarily chosen, say $I(1) = 1$. Once $V(1)$ and $V(2)$ are known, we can use Equation (7.16) to scan all nodes in Figure 7.6 once from left to right to determine all nodal voltages ($\equiv \rho H_\phi$) and currents ($\equiv E_z = J_z/\sigma$).

Example 7.1

Develop a computer program to determine the relative (or normalized) current density $J_z(\rho)/J_z(a)$ in a round copper wire operated at 1 GHz. Plot the relative current density against the radial position ρ/a for cases $a/\delta = 1, 2$, and 4 . Take $\Delta\ell/\delta = 0.1$, $\mu = \mu_0$, $\sigma = 5.8 \times 10^7$ S/m. \square

Solution

The computer program is presented in Figure 7.7. It calculates the voltage at each node using Equations (7.16) and (7.17). The current on each $r(N)$ is found from Figure 7.7 as

$$I(N-1) = \frac{V(N) - V(N-1)}{r(N-1)}$$

Since $J = \sigma E$, we obtain $J_z(\rho)/J_z(a)$ as the ratio of $I(N)$ and $I(N MAX)$, where $I(N MAX)$ is the current at $\rho = a$.

To verify the accuracy of the TLM solution, we also calculate the exact $J_z(\rho)/J_z(a)$ using Equation (2.120). (For further details, see Example 2.3.) Table 7.1 shows a comparison between TLM results and exact results for the case $a/\delta = 4.0$. It is noticed that the percentage error is maximum (about 8%) at the center of the wire and diminishes to zero as we approach the surface of the wire. Figure 7.8 portrays the plot of the relative current density versus the radial position for cases $a/\delta = 1, 2$, and 4 . \square

```
%=====
% USING THE TLM METHOD, THIS PROGRAM CALCULATES THE RELATIVE
% CURRENT DENSITY JR IN A ROUND COPPER WIRE
% THE EXACT SOLUTION JRE IS ALSO INCLUDED
% =====

clear

% SPECIFY INPUT DATA

F = 1.0E+9;
SIGMA = 5.8E+7;
PIE = 4.0*atan(1.0);
MIU = 4.0*PIE*1.0E-7;
OMEGA = 2.0*PIE*F;
```

Figure 7.7
Computer program for Example 7.1 (Continued).

```

DELTA = sqrt( 2.0/(SIGMA*MIU*OMEGA) );
H = 0.1*DELTA;
A = 4.0*DELTA;
NMAX = A/H;

% INITIALIZE AND CALCULATE RELATIVE CURRENT DENSITY JR USING TLM

V(1) = 0;
V(2) = 0.1*(SIGMA*( (1) - 0.5 )*(H^2));

for N = 3:NMAX+1
    V(N) = (SIGMA*(N-1-0.5)*H^2)/(SIGMA*(N-2-0.5)*H^2)*(V(N-1) - V(N-2))...
        + i*((OMEGA*MIU/(N-2)))*(SIGMA*(N-1-0.5)*H^2)*V(N-1) + V(N-1);
end

N = 2:NMAX+1;
I = ( V(N) - V(N-1) )./(SIGMA*(N-1-0.5)*H^2);
JR = abs(I/I(NMAX));

% CALCULATE THE CURRENT DENSITY JRE FROM THE EXACT SOLUTION

K = 0:20;
NRO = 1:NMAX;
X = ( (NRO)/(NMAX) )*A*sqrt(2.0)/DELTA;
[K2,X2] = meshgrid(K,X);

FB = ( (X2/2).^(2*K2) )./(factorial(K2).^2);
BEO = FB*exp(i*K*pi/2).'';

JRE = abs(BEO);
JRE = JRE/JRE(NMAX); % RELATIVE CURRENT DENSITY

RHO = (1:NMAX)/(NMAX);

%Output Result

disp(sprintf('\n%s %s %s','RADIAL POSITION','TLM J','EXACT J'));

for N=4:4:NMAX
    s2 = sprintf('%10g %16g %12g',RHO(N), JR(N), JRE(N));
    disp(s2)
end

figure(1),plot(RHO,JR,RHO,JRE)
ylabel('Relative current Density');
xlabel('Radial position')

```

Figure 7.7
(Cont.) Computer program for Example 7.1.

7.3. SOLUTION OF DIFFUSION EQUATION

Table 7.1 Comparison of Relative Current Density Obtained from TLM and Exact Solutions ($a/\delta = 4.0$)

Radial Position (ρ/a)	TLM Result	Exact Result
0.1	0.11581	0.10768
0.2	0.11765	0.11023
0.3	0.12644	0.12077
0.4	0.14953	0.14612
0.5	0.19301	0.19138
0.6	0.26150	0.26082
0.7	0.36147	0.36115
0.8	0.50423	0.50403
0.9	0.70796	0.70786
1.0	1.0	1.0

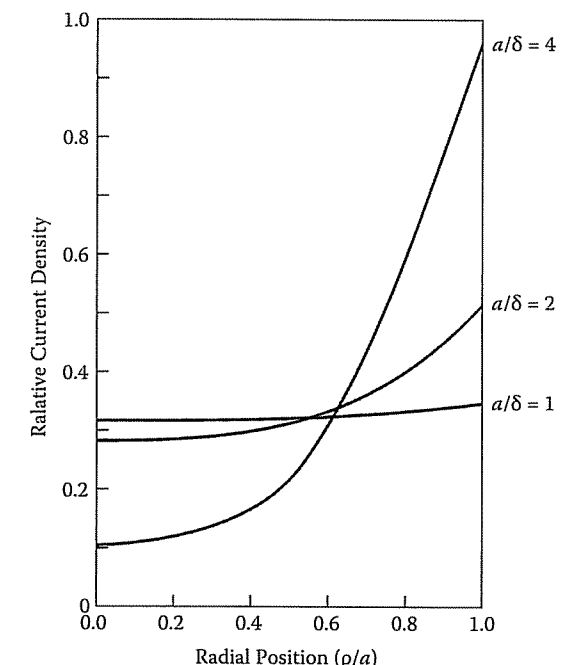


Figure 7.8
Relative current density versus radial position.

7.4 Solution of Wave Equations

In order to show how Maxwell's equations may be represented by the transmission-line equations, the differential length of the lossless transmission line between two nodes of the mesh is represented by lumped inductors and capacitors as shown in Figure 7.9 for two-dimensional wave propagation problems [17, 18]. At the nodes, pairs of transmission lines form impedance discontinuity. The complete network of transmission-line matrix is made up of a large number of such building blocks as depicted in Figure 7.10. Notice that in Figure 7.10 single lines are used to represent a transmission-line pair. Also, a uniform internodal distance of $\Delta\ell$ is assumed throughout the matrix (i.e., $\Delta\ell = \Delta x = \Delta z$). We shall first derive equivalences between network and field quantities.

7.4.1 Equivalence Between Network and Field Parameters

We refer to Figure 7.9 and apply Kirchhoff's current law at node O to obtain

$$I_x(x - \Delta\ell/2) - I_x(x + \Delta\ell/2) + I_z(z - \Delta\ell/2) - I_z(z + \Delta\ell/2) = 2C\Delta\ell \frac{\partial V_y}{\partial t}$$

Dividing through by $\Delta\ell$ gives

$$\frac{I_x(x - \Delta\ell/2) - I_x(x + \Delta\ell/2)}{\Delta\ell} + \frac{I_z(z - \Delta\ell/2) - I_z(z + \Delta\ell/2)}{\Delta\ell} = 2C \frac{\partial V_y}{\partial t}$$

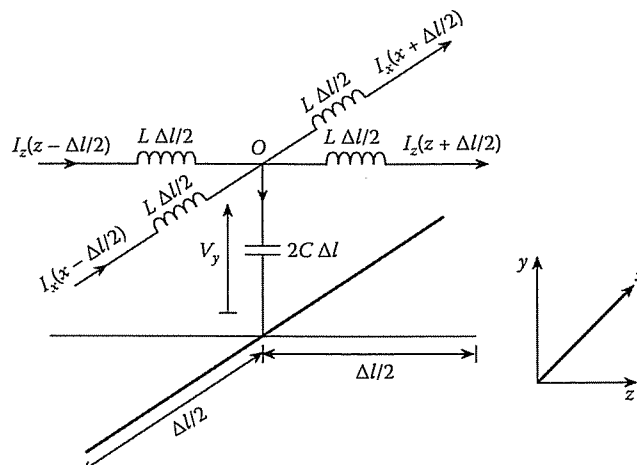


Figure 7.9

Equivalent network of a two-dimensional TLM shunt node.

7.4. SOLUTION OF WAVE EQUATIONS

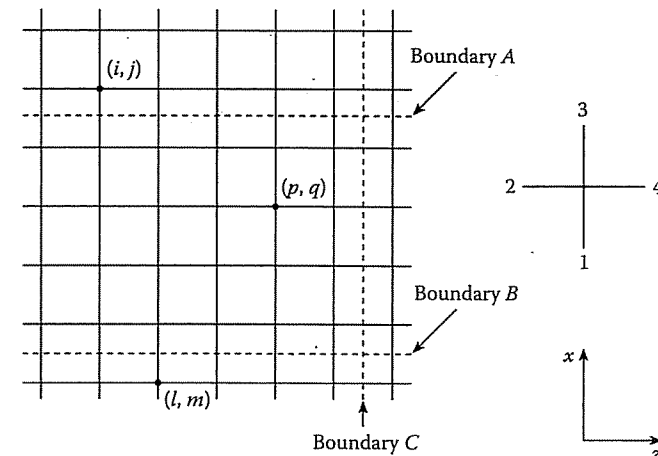


Figure 7.10
Transmission-line matrix and boundaries.

Taking the limit as $\Delta\ell \rightarrow 0$ results in

$$-\frac{\partial I_z}{\partial z} - \frac{\partial I_x}{\partial x} = 2C \frac{\partial V_y}{\partial t} \quad (7.18a)$$

Applying Kirchhoff's voltage law around the loop in the $x - y$ plane gives

$$V_y(x - \Delta\ell/2) - L\Delta\ell/2 \frac{\partial I_x(x - \Delta\ell/2)}{\partial t} - L\Delta\ell/2 \frac{\partial I_x(x + \Delta\ell/2)}{\partial t} - V_y(x + \Delta\ell/2) = 0$$

Upon rearranging and dividing by $\Delta\ell$, we have

$$\frac{V_y(x - \Delta\ell/2) - V_y(x + \Delta\ell/2)}{\Delta\ell} = \frac{L}{2} \frac{\partial I_x(x - \Delta\ell/2)}{\partial t} + \frac{L}{2} \frac{\partial I_x(x + \Delta\ell/2)}{\partial t}$$

Again, taking the limit as $\Delta\ell \rightarrow 0$ gives

$$\frac{\partial V_y}{\partial x} = -L \frac{\partial I_x}{\partial t} \quad (7.18b)$$

Taking similar steps on the loop in the $y - z$ plane yields

$$\frac{\partial V_y}{\partial z} = -L \frac{\partial I_z}{\partial t} \quad (7.18c)$$

These equations will now be combined to form a wave equation. Differentiating Equation (7.18a) with respect to t , Equation (7.18b) with respect to x , and Equation (7.18c)

with respect to z , we have

$$-\frac{\partial^2 I_z}{\partial z \partial t} - \frac{\partial^2 I_x}{\partial x \partial t} = 2C \frac{\partial^2 V_y}{\partial t^2} \quad (7.19a)$$

$$\frac{\partial^2 V_y}{\partial x^2} = -L \frac{\partial^2 I_x}{\partial t \partial x} \quad (7.19b)$$

$$\frac{\partial^2 V_y}{\partial z^2} = -L \frac{\partial^2 I_z}{\partial t \partial z} \quad (7.19c)$$

Substituting Equations (7.19b) and (7.19c) into Equation (7.19a) leads to

$$\frac{\partial^2 V_y}{\partial x^2} + \frac{\partial^2 V_y}{\partial z^2} = 2LC \frac{\partial^2 V_y}{\partial t^2} \quad (7.20)$$

Equation (7.20) is the Helmholtz wave equation in two-dimensional space.

In order to show the field theory equivalence of Equations (7.19) and (7.20), consider Maxwell's equations

$$\nabla \times \mathbf{E} = -\mu \frac{\partial \mathbf{H}}{\partial t} \quad (7.21a)$$

and

$$\nabla \times \mathbf{H} = \epsilon \frac{\partial \mathbf{E}}{\partial t} \quad (7.21b)$$

Expansion of Equation (7.21) in the rectangular coordinate system yields

$$\frac{\partial E_z}{\partial y} - \frac{\partial E_y}{\partial z} = -\mu \frac{\partial H_x}{\partial t}, \quad (7.22a)$$

$$\frac{\partial E_x}{\partial z} - \frac{\partial E_z}{\partial x} = -\mu \frac{\partial H_y}{\partial t}, \quad (7.22b)$$

$$\frac{\partial E_y}{\partial x} - \frac{\partial E_x}{\partial y} = -\mu \frac{\partial H_z}{\partial t}, \quad (7.22c)$$

$$\frac{\partial H_z}{\partial y} - \frac{\partial H_y}{\partial z} = \epsilon \frac{\partial E_x}{\partial t}, \quad (7.22d)$$

$$\frac{\partial H_x}{\partial z} - \frac{\partial H_z}{\partial x} = \epsilon \frac{\partial E_y}{\partial t}, \quad (7.22e)$$

$$\frac{\partial H_y}{\partial x} - \frac{\partial H_x}{\partial y} = \epsilon \frac{\partial E_z}{\partial t} \quad (7.22f)$$

Consider the situation for which $E_x = E_z = H_y = 0$, $\frac{\partial}{\partial y} = 0$. It is noticed at once that this mode is a transverse electric (TE) mode with respect to the z -axis but a transverse magnetic (TM) mode with respect to the y -axis. Thus by the principle of duality, the network in Figure 7.9 can be used for E_y, H_x, H_z fields as well as for

7.4. SOLUTION OF WAVE EQUATIONS

E_x, E_z, H_y fields. A network capable of reproducing TE waves is also capable of reproducing TM waves. For TE waves, Equation (7.22) reduces to

$$\frac{\partial H_x}{\partial z} - \frac{\partial H_z}{\partial x} = \epsilon \frac{\partial E_y}{\partial t}, \quad (7.23a)$$

$$\frac{\partial E_y}{\partial x} = -\mu \frac{\partial H_z}{\partial t}, \quad (7.23b)$$

$$\frac{\partial E_y}{\partial z} = \mu \frac{\partial H_x}{\partial t} \quad (7.23c)$$

Taking similar steps on Equations (7.23a)–(7.23c) as were taken for Equations (7.18a)–(7.18c) results in another Helmholtz equation

$$\frac{\partial^2 E_y}{\partial x^2} + \frac{\partial^2 E_y}{\partial z^2} = \mu \epsilon \frac{\partial^2 E_y}{\partial t^2} \quad (7.24)$$

Comparing Equations (7.23) and (7.24) with Equations (7.18) and (7.20) yields the following equivalence between the parameters

$E_y \equiv V_y$
$H_x \equiv -I_z$
$H_z \equiv I_x$
$\mu \equiv L$
$\epsilon \equiv 2C$

(7.25)

Thus in the equivalent circuit:

- the voltage at shunt node is E_y ,
- the current in the z direction is $-H_x$,
- the current in the x direction is H_z ,
- the inductance per unit length represents the permeability of the medium,
- twice the capacitance per unit length represents the permittivity of the medium.

7.4.2 Dispersion Relation of Propagation Velocity

For the basic transmission line in the TLM which has $\mu_r = \epsilon_r = 1$, the inductance and capacitance per unit length are related by [8]

$$\frac{1}{\sqrt{(LC)}} = \frac{1}{\sqrt{(\mu_0 \epsilon_0)}} = c \quad (7.26)$$

where $c = 3 \times 10^8$ m/s is the speed of light in vacuum. Notice from Equation (7.26) that for the equivalence made in Equation (7.25), if voltage and current waves on each transmission line component propagate at the speed of light c , the complete network

of intersecting transmission lines represents a medium of relative permittivity twice that of free space. This implies that as long as the equivalent circuit in Figure 7.9 is valid, the propagation velocity in the TLM mesh is $1/\sqrt{2}$ of the velocity of light. The manner in which wave propagates on the mesh is now derived.

If the ratio of the length of the transmission-line element to the free-space wavelength of the wave is $\theta/2\pi = \Delta\ell/\lambda$ (θ is called the *electrical length* of the line), the voltage and current at node i are related to those at node $i+1$ by the transfer-matrix equation (see Problem 7.2) given as [19]

$$\begin{bmatrix} V_i \\ I_i \end{bmatrix} = \begin{bmatrix} V_{i+1} \\ I_{i+1} \end{bmatrix} \quad (7.27)$$

$$\begin{bmatrix} (\cos\theta/2) & (j\sin\theta/2) \\ (j\sin\theta/2) & (\cos\theta/2) \end{bmatrix} \begin{bmatrix} 1 & 0 \\ (2j\tan\theta/2) & 1 \end{bmatrix} \begin{bmatrix} (\cos\theta/2) & (j\sin\theta/2) \\ (j\sin\theta/2) & (\cos\theta/2) \end{bmatrix} \begin{bmatrix} V_{i+1} \\ I_{i+1} \end{bmatrix}$$

If the waves on the periodic structure have a propagation constant $\gamma_n = \alpha_n + j\beta_n$, then

$$\begin{bmatrix} V_i \\ I_i \end{bmatrix} = \begin{bmatrix} e^{\gamma_n \Delta\ell} & 0 \\ 0 & e^{\gamma_n \Delta\ell} \end{bmatrix} \begin{bmatrix} V_{i+1} \\ I_{i+1} \end{bmatrix} \quad (7.28)$$

Solution of Equations (7.27) and (7.28) gives

$$\cosh(\gamma_n \Delta\ell) = \cos(\theta) - \tan(\theta/2) \sin(\theta) \quad (7.29)$$

This equation describes the range of frequencies over which propagation can take place (passbands), i.e.,

$$|\cos(\theta) - \tan(\theta/2) \sin(\theta)| < 1, \quad (7.30a)$$

and the range of frequencies over which propagation cannot occur (stop-bands), i.e.,

$$|\cos(\theta) - \tan(\theta/2) \sin(\theta)| > 1 \quad (7.30b)$$

For the lowest frequency propagation region,

$$\gamma_n = j\beta_n \quad (7.31a)$$

and

$$\theta = \frac{2\pi \Delta\ell}{\lambda} = \frac{\omega}{c} \Delta\ell \quad (7.31b)$$

Introducing Equation (7.31) in Equation (7.29), we obtain

$$\cos(\beta_n \Delta\ell) = \cos\left(\frac{\omega \Delta\ell}{c}\right) - \tan\left(\frac{\omega \Delta\ell}{2c}\right) \sin\left(\frac{\omega \Delta\ell}{c}\right) \quad (7.32)$$

7.4. SOLUTION OF WAVE EQUATIONS

Applying trigonometric identities

$$\sin(2A) = 2\sin(A)\cos(A)$$

and

$$\cos(2A) = 1 - 2\sin^2(A)$$

to Equation (7.32) results in

$$\sin\left(\frac{\beta_n \Delta\ell}{2}\right) = \sqrt{2} \sin\left(\frac{\omega \Delta\ell}{2c}\right) \quad (7.33)$$

which is a transcendental equation. If we let r be the ratio of the velocity u_n of the waves on the network to the free-space wave velocity c , then

$$r = u_n/c = \frac{\omega}{\beta_n c} = \frac{2\pi}{\lambda \beta_n} \quad (7.34a)$$

or

$$\beta_n = \frac{2\pi}{\lambda r} \quad (7.34b)$$

Substituting Equations (7.34) into Equation (7.33), the transcendental equation becomes

$$\sin\left(\frac{\pi}{r} \cdot \frac{\Delta\ell}{\lambda}\right) = \sqrt{2} \sin\left(\frac{\pi \Delta\ell}{\lambda}\right) \quad (7.35)$$

By selecting different values of $\Delta\ell/\lambda$, the corresponding values of $r = u_n/c$ can be obtained numerically as in Figure 7.11 for two-dimensional problems. From Figure 7.11, we conclude that the TLM can represent Maxwell's equations only over the range of frequencies from zero to the first network cutoff frequency, which occurs at $\omega \Delta\ell/c = \pi/2$ or $\Delta\ell/\lambda = 1/4$. Over this range, the velocity of the waves behaves according to the characteristic of Figure 7.11. For frequencies much smaller than the network cutoff frequency, the propagation velocity approximates to $1/\sqrt{2}$ of the free-space velocity.

Following the same procedure, the dispersion relation for three-dimensional problems can be derived as

$$\sin\left(\frac{\pi}{r} \cdot \frac{\Delta\ell}{\lambda}\right) = 2 \sin\left(\pi \frac{\Delta\ell}{\lambda}\right) \quad (7.36)$$

Thus for low frequencies ($\Delta\ell/\lambda < 0.1$), the network propagation velocity in three-dimensional space may be considered constant and equal to $c/2$.

7.4.3 Scattering Matrix

If kV_n^i and kV_n^r are the voltage impulses incident upon and reflected from terminal n of a node at time $t = k\Delta\ell/c$, we derive the relationship between the two quantities as

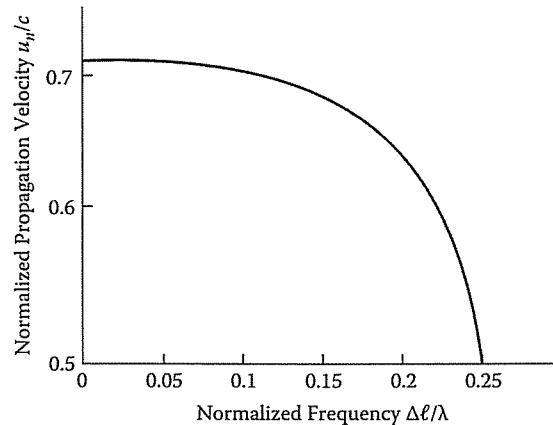


Figure 7.11

Dispersion of the velocity of waves in a two-dimensional TLM network.

follows. Let us assume that a voltage impulse function of unit magnitude is launched into terminal 1 of a node, as shown in Figure 7.12(a), and that the characteristic resistance of the line is normalized. A unit-magnitude delta function of voltage and current will then travel toward the junction with unit energy ($S_i = 1$). Since line 1 has three other lines joined to it, its effective terminal resistance is $1/3$. With the knowledge of its reflection coefficient, both the reflected and transmitted voltage impulses can be calculated. The reflection coefficient is

$$\Gamma = \frac{R_L - R_o}{R_L + R_o} = \frac{1/3 - 1}{1/3 + 1} = -\frac{1}{2} \quad (7.37)$$

so that the reflected and transmitted energies are

$$S_r = S_i \Gamma^2 = \frac{1}{4} \quad (7.38a)$$

$$S_t = S_i (1 - \Gamma^2) = \frac{3}{4} \quad (7.38b)$$

where subscripts i , r , and t indicate incident, reflected, and transmitted quantities, respectively. Thus a voltage impulse of $-1/2$ is reflected back in terminal 1, while a voltage impulse of $1/2$ is $[\frac{3}{4} / 3]^{1/2}$ will be launched into each of the other three terminals as shown in Figure 7.12(b).

The more general case of four impulses being incident on four branches of a node can be obtained by applying the superposition principle to the previous case of a single pulse. Hence, if at time $t = k\Delta\ell/c$, voltage impulses ${}_kV_1^i$, ${}_kV_2^i$, ${}_kV_3^i$, and ${}_kV_4^i$ are incident on lines 1 to 4, respectively, at any node as in Figure 7.12(c), the combined voltage reflected along line 1 at time $t = (k+1)\Delta\ell/c$ will be [9, 10]

$${}_{k+1}V_1^r = \frac{1}{2} \langle {}_kV_2^i + {}_kV_3^i + {}_kV_4^i - {}_kV_1^i \rangle \quad (7.39)$$

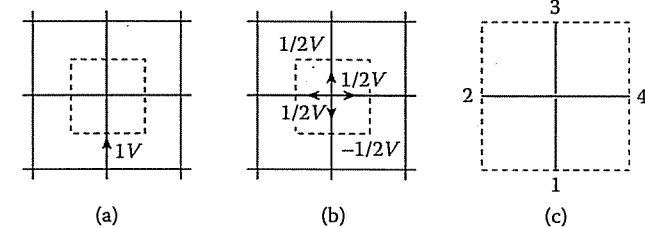


Figure 7.12

The impulse response of a node in a matrix.

In general, the total voltage impulse reflected along line n at time $t = (k+1)\Delta\ell/c$ will be

$${}_{k+1}V_n^r = \frac{1}{2} \left[\sum_{m=1}^4 {}_kV_m^i \right] - {}_kV_n^i, \quad n = 1, 2, 3, 4 \quad (7.40)$$

This idea is conveniently described by a *scattering matrix* equation relating the reflected voltages at time $(k+1)\Delta\ell/c$ to the incident voltages at the previous time step $k\Delta\ell/c$:

$$\begin{bmatrix} V_1 \\ V_2 \\ V_3 \\ V_4 \end{bmatrix}_{k+1}^r = \frac{1}{2} \begin{bmatrix} -1 & 1 & 1 & 1 \\ 1 & -1 & 1 & 1 \\ 1 & 1 & -1 & 1 \\ 1 & 1 & 1 & -1 \end{bmatrix}_k \begin{bmatrix} V_1 \\ V_2 \\ V_3 \\ V_4 \end{bmatrix}_k^i \quad (7.41)$$

Also an impulse emerging from a node at position (z, x) in the mesh (reflected impulse) becomes automatically an incident impulse at the neighboring node. Hence

$$\begin{aligned} {}_{k+1}V_1^i(z, x + \Delta\ell) &= {}_{k+1}V_3^r(z, x) \\ {}_{k+1}V_2^i(z + \Delta\ell, x) &= {}_{k+1}V_4^r(z, x) \\ {}_{k+1}V_3^i(z, x - \Delta\ell) &= {}_{k+1}V_1^r(z, x) \\ {}_{k+1}V_4^i(z - \Delta\ell, x) &= {}_{k+1}V_2^r(z, x) \end{aligned} \quad (7.42)$$

Thus by applying Equations (7.41) and (7.42), the magnitudes, positions, and directions of all impulses at time $(k+1)\Delta\ell/c$ can be obtained at each node in the network provided that their corresponding values at time $k\Delta\ell/c$ are known. The impulse response may, therefore, be found by initially fixing the magnitude, position, and direction of travel of impulse voltages at time $t = 0$, and then calculating the state of the network at successive time intervals. The scattering process forms the basic algorithm of the TLM method [10, 17].

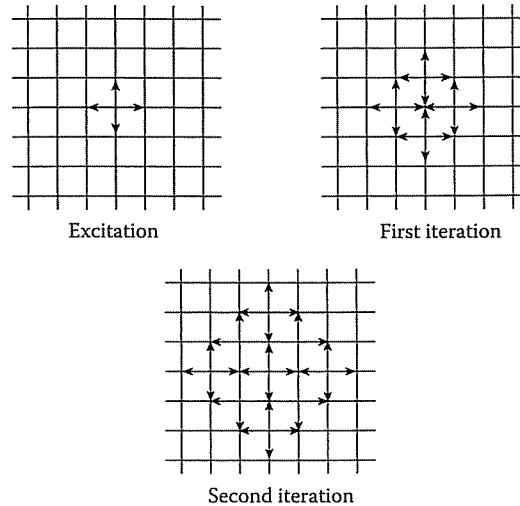


Figure 7.13
Scattering in a two-dimensional TLM network excited by a Dirac impulse.

The propagating of pulses in the TLM model is illustrated in Figure 7.13, where the first two iterations following an initial excitation pulse in a two-dimensional shunt-connected TLM are shown. We have assumed free-space propagation for the sake of simplicity.

7.4.4 Boundary Representation

Boundaries are usually placed halfway between two nodes in order to ensure synchronism. In practice, this is achieved by making the mesh size $\Delta\ell$ an integer fraction of the structure's dimensions.

Any resistive load at boundary C (see Figure 7.10) may be simulated by introducing a reflection coefficient Γ

$${}_{k+1}V_4^i(p, q) = {}_kV_2^r(p + 1, q) = \Gamma [{}_kV_4^r(p, q)] \quad (7.43)$$

where

$$\Gamma = \frac{R_s - 1}{R_s + 1} \quad (7.44)$$

and R_s is the surface resistance of the boundary normalized by the line characteristic impedance. If, for example, a perfectly conducting wall ($R_s = 0$) is to be simulated along boundary C, Equation (7.44) gives $\Gamma = -1$, which represents a short circuit, and

$${}_{k+1}V_4^i(p, q) = - {}_kV_4^r(p, q) \quad (7.45)$$

is used in the simulation. For waves striking the boundary at arbitrary angles of incidence, a method for modeling free-space boundaries is discussed in [20].

7.4.5 Computation of Fields and Frequency Response

We continue with the TE mode of Equation (7.23) as our example and calculate E_y , H_x , and H_z . E_y at any point corresponds to the node voltage at the point, H_z corresponds to the net current entering the node in the x direction [see Equation (7.25)], while H_x is the net current in the negative z direction. For any point ($z = m, x = n$) on the grid of Figure 7.10, we have for each k th transient time

$${}_kE_y(m, n) = \frac{1}{2} [{}_kV_1^i(m, n) + {}_kV_2^i(m, n) + {}_kV_3^i(m, n) + {}_kV_4^i(m, n)] \quad (7.46)$$

$$- {}_kH_x(m, n) = {}_kV_2^i(m, n) - {}_kV_4^i(m, n), \quad (7.47)$$

and

$${}_kH_z(m, n) = {}_kV_3^i(m, n) - {}_kV_1^i(m, n) \quad (7.48)$$

Thus, a series of discrete delta function of magnitudes E_y , H_x , and H_z corresponding to time intervals of $\Delta\ell/c$ are obtained by the iteration of Equations (7.41) and (7.42). (Notice that reflections at the boundaries A and B in Figure 7.10 will cancel out, thus $H_z = 0$.) Any point in the mesh can serve as an output or observation point. Equations (7.46) to (7.48) provide the output-impulse functions for the point representing the response of the system to an impulsive excitation. These output functions may be used to obtain the output waveform. For example, the output waveform corresponding to a pulse input may be obtained by convolving the output-impulse function with the shape of the input pulse.

Sometimes we are interested in the response to a sinusoidal excitation. This is obtained by taking the Fourier transform of the impulse response. Since the response is a series of delta functions, the Fourier transform integral becomes a summation, and the real and imaginary parts of the output spectrum are given by [9, 10]

$$\text{Re}[F(\Delta\ell/\lambda)] = \sum_{k=1}^N {}_kI \cos\left(\frac{2\pi k \Delta\ell}{\lambda}\right) \quad (7.49a)$$

$$\text{Im}[F(\Delta\ell/\lambda)] = \sum_{k=1}^N {}_kI \sin\left(\frac{2\pi k \Delta\ell}{\lambda}\right) \quad (7.49b)$$

where $F(\Delta\ell/\lambda)$ is the frequency response, ${}_kI$ is the value of the output-impulse response at time $t = k \Delta\ell/c$, and N is the total number of time intervals for which the calculation is made. Henceforth, N will be referred to as the number of iterations.

7.4.6 Output Response and Accuracy of Results

The output-impulse function, in terms of voltage or current, may be taken from any point in the TLM mesh. It consists of a train of impulses of varying magnitude in the time domain separated by a time interval $\Delta\ell/c$. Thus, the frequency response obtained

by taking the Fourier transform of the output response consists of series of delta functions in the frequency domain corresponding to the discrete modal frequencies for which a solution exists. For practical reasons, the output response has to be truncated, and this results in a spreading of the solution delta function $\sin x/x$ type of curves.

To investigate the accuracy of the result, let the output response be truncated after N iterations. Let $V_{out}(t)$ be the output-impulse function taken within $0 < t < N\Delta\ell/c$. We may regard $V_{out}(t)$ as an impulse function $V_\infty(t)$, taken within $0 < t < \infty$, multiplied by a unit pulse function $V_p(t)$ of width $N\Delta\ell/c$, i.e.,

$$V_{out}(t) = V_\infty(t) \times V_p(t) \quad (7.50)$$

where

$$V_p = \begin{cases} 1, & 0 \leq t \leq N\Delta\ell/c \\ 0, & \text{elsewhere} \end{cases} \quad (7.51)$$

Let $S_{out}(f)$, $S_\infty(f)$, and $S_p(f)$ be the Fourier transform of $V_{out}(t)$, $V_\infty(t)$, and $V_p(t)$, respectively. The Fourier transform of Equation (7.50) is the convolution of $S_\infty(f)$ and $S_p(f)$. Hence

$$S_{out}(f) = \int_{-\infty}^{\infty} S_\infty(\alpha) S_p(f - \alpha) d\alpha \quad (7.52)$$

where

$$S_p(f) = \frac{N\Delta\ell}{c} \frac{\sin \frac{\pi N\Delta\ell f}{c}}{\frac{\pi N\Delta\ell f}{c}} e^{-(\pi N\Delta\ell f)/c} \quad (7.53)$$

which is of the form $\sin x/x$. Equations (7.52) and (7.53) show that $S_p(f)$ is placed in each of the positions of the exact response $S_\infty(f)$. Since the greater the number of iterations N the sharper the maximum peak of the curve, the accuracy of the result depends on N . Thus the solution of a wave equation by TLM method involves the following four steps [21]:

1. Space discretization: The solution region is divided into a number of blocks to fit the geometrical and frequency requirements. Each block is replaced by a network of transmission lines interconnected to form a "node." Transmission lines from adjacent nodes are connected to form a mesh describing the entire solution region.
2. Excitation: This involves imposing the initial conditions and source terms.
3. Scattering: With the use of the scattering matrix, pulses propagate along transmission lines toward each node. At each new time step, a multiple of propagation time δt , scattered pulses from each node become incident on adjacent nodes. The scattering and connection processes may be repeated to simulate propagation for any desired length of time.

7.4. SOLUTION OF WAVE EQUATIONS

4. Output: At any time step, voltages and currents on transmission lines are available. These represent the electric and magnetic fields corresponding to the particular problem and excitation. The quantities available at each time step are the solution in the time domain — there is no need for an iterative solution procedure. If desired, frequency-domain information may be obtained by using Fourier transform techniques.

The following examples are taken from Johns's work [9, 18].

Example 7.2

The MATLAB program in Figure 7.14 is for the numerical calculations of one-dimensional TEM wave problems. It should be mentioned that the computer program in this example and the following ones are modified versions of those in Agba [22]. The calculations were carried out on a 25 by 11 rectangular matrix. TEM field-continuation boundaries were fixed along $x = 2$ and $x = 10$, producing boundaries, in effect, along the lines $x = 1.5$ and $x = 10.5$. The initial impulse excitation was on all points along the line $z = 4$, and the field along this line was set to zero at all subsequent time intervals. In this way, interference from boundaries to the left of the excitation line was avoided. Calculations in the z direction were terminated at $z = 24$, so that no reflections were received from points at $z = 25$ in the matrix, and the boundary C in Figure 7.10, situated at $z = 24.5$, was therefore matched to free space. The output-impulse response for E_y and H_x was taken at the point $z = 14, x = 6$, which is 10.5 mesh points away from the boundary C, for 100, 150, and 200 iterations.

Since the velocity of waves on the matrix is less than that in free space by a factor u_n/c (see Figure 7.11), the effective intrinsic impedance presented by the network matrix is less by the same factor. The magnitude of the wave impedance on the matrix, normalized to the intrinsic impedance of free space, is given by $Z = |E_y|/|H_x|$ and is tabulated in Table 7.2, together with $\text{Arg}(Z)$, for the various numbers of iterations made. A comparison is made with the exact impedance values [14]. \square

Table 7.2 Normalized Impedance of a TEM Wave with Free-Space Discontinuity

$\Delta\ell/\lambda$ Number of Iterations	TLM Results			Exact Results		
	Z	Arg(Z)	Z	Arg(Z)	Z	Arg(Z)
0.002	0.9789	-0.1368	0.9730	-0.1396	0.9781	-0.1253
0.004	0.9028	-0.2432	0.8980	-0.2322	0.9072	-0.2400
0.006	0.8114	-0.3068	0.8229	-0.2979	0.8170	-0.3046
0.008	0.7238	-0.3307	0.7328	-0.3457	0.7287	-0.3404
0.010	0.6455	-0.3201	0.6367	-0.3350	0.6396	-0.3281
0.012	0.5783	-0.2730	0.5694	-0.2619	0.5742	-0.2680
0.014	0.5272	-0.1850	0.5313	-0.1712	0.5266	-0.1797
0.016	0.4993	-0.0609	0.5043	-0.0657	0.5009	-0.0538
0.018	0.5002	-0.0790	0.4987	-0.0748	0.5057	-0.0785

```

clear
% ****
% THIS PROGRAM APPLIES THE TLM METHOD TO SOLVE
% ONE-DIMENSIONAL WAVE PROBLEMS. THE SPECIFIC EXAMPLE
% SOLVED HERE IS DESCRIBED AS FOLLOWS:-
%
% THE TEM WAVES ON A 25 x 11 MATRIX
% THE BOUNDARIES ARE AT X = 2 AND X = 10
% INITIAL IMPULSE EXCITATION IS ALONG Z=4 AT t = 0
% AND SUBSEQUENTLY THIS LINE IS SET TO ZERO. THE GRID
% IS TERMINATED AT Z=25. OUTPUT IS TAKEN AT Z = 14,
% X = 6 FOR Ey AND Hx FOR 100,150,200 ITERATIONS
% VI(IT,I,J,K) -- ARRAY FOR INCIDENT VOLTAGE
% VR(IT,I,J,K) -- ARRAY FOR REFLECTED VOLTAGE
% IT = 1 -- FOR PREVIOUS PULSE VALUE
% IT = 2 -- FOR CURRENT PULSE VALUE
% I,J -- CORRESPOND TO NODE LOCATION (Z,X)
% K = 1..4 -- FOR TERMINALS
% NX -- INDEX OF NODES IN X-DIRECTION
% NZ -- INDEX OF NODES IN Z-DIRECTION
% NX/NZ B,E -- INDEX OF BEGINNING, END NODE
% NX/NX O -- INDEX OF OUTPUT NODE
% GAMMA -- REFLECTION COEFFICIENT AT THE BOUNDARY C
% DELTA -- MESH SIZE DIVIDED BY LAMBA
% ITRATE -- NO. OF ITERATIONS
% *****

VI = zeros(2,25,11,4); VR = zeros(2,25,11,4);
EFI = zeros(1,20); EFR = zeros(1,20);
HFI = zeros(1,20); HFR = zeros(1,20);

CEF = zeros(1,20); CHF = zeros(1,20);
OUT = zeros(20,9);

NXB=2;NXE=10;NZB=4;NZE=24;NT=4;ITRATE=200;
NXO=6;NZO=14;PIE=3.1415927;GAMMA=0;DELTA=.002;

% STEP #1 *****
% INSERT INITIAL PUSLE EXCITATION ALONG LINE Z = 4

VI(1,NZB+1,NXB:NXE,2) = 1.0;

% STEP #2 *****
% Using EQUATIONS (7.40) TO (7.42), CALCULATE THE
% REFLECTED VOLTAGE AND SUBMIT IT DIRECTLY
% TO THE NEIGHBORING NODE.

K = 1:20; II = 0;
DEL = DELTA:DELTA:DELTA*20;
OUT(:,1) = DEL;

```

Figure 7.14

Computer program for Example 7.2 (*Continued*).

```

for ITIME = 1: ITRATE
    IT = 2;
    for I = (NZB+1):NZE
        for J = NXB:NXE

            VR(IT,I,J,1:NT) = 0.5*sum(VI(IT-1,I,J,1:NT)) - VI(IT-1,I,J,1:NT);
            VI(IT,I,J-1,3) = VR(IT,I,J,1);
            VI(IT,I-1,J,4) = VR(IT,I,J,2);
            VI(IT,I,J+1,1) = VR(IT,I,J,3);
            VI(IT,I+1,J,2) = VR(IT,I,J,4);

            % STEP #3 *****
            % Using EQUATIONS (7.43) AND (7.44), INSERT BOUNDARY CONDITIONS

            if (J==NXE), VI(IT,I,NXE,3) = VR(IT,I,NXE,1); end
            if (J==NXB), VI(IT,I,NXB,1) = VR(IT,I,NXB,3); end
            if (I==NZE), VI(IT,NZE,J,4) = GAMMA*VR(IT,NZE,J,4); end
        end
    end

    % STEP #4 *****
    % Using EQUATIONS (7.46) - (7.49), CALCULATE IMPULSE RESPONSE
    % OF Ey and Hx AT Z=NZO,X=NXO

    EI = sum(VI(IT,NZO,NXO,1:NT)) * 0.5;
    HI = VI(IT,NZO,NXO,2) - VI(IT,NZO,NXO,4);

    % SUM THE FREQUENCY RESPONSE FOR DIFFERENT VALUES OF MESH-SIZE DIVIDED
    % BY WAVELENGTH

    CEF = CEF + EI*exp(j*2*pi*ITIME*DEL); %Complex E Field
    CHF = CHF + HI*exp(j*2*pi*ITIME*DEL); %Complex H Field

    % SAVE THE CURRENT PULSE MAGNITUDE FOR NEXT ITERATION
    VI(IT-1,:,:,:) = VI(IT,:,:,:);
    VR(IT-1,:,:,:) = VR(IT,:,:,:);

    IT = ITIME;
    if((IT==100)|| (IT==150)|| (IT==200))
        II = II + 2;
    % STEP #5 *****
    % CALCULATE MAGNITUDE & ARGUMENT OF IMPEDANCE
    OUT(K,II) = abs(CEF)./abs(CHF); % MAGNITUDE
    ZARG = CEF./CHF;
    OUT(K,II+1) = -atan(imag(ZARG)./real(ZARG));
    end
end

```

Figure 7.14

(Cont.) Computer program for Example 7.2.

```
% STEP #6 ****
% CALCULATE EXACT VALUE OF IMPEDANCE [REF. 13]

R2 = 1./(pi*DEL./.(asin(sqrt(2).*sin(pi*DEL))));
R3 = tan(21.0*R2*pi.*DEL);
CNUM = R2+R3*i;
CDEM = 1 + j*real(CNUM).*imag(CNUM);
OUT(K,8) = abs(CNUM)./(abs(CDEM).*real(CNUM));
ZARG = CNUM./CDEM;
OUT(K,9) = atan(imag(ZARG)./real(ZARG));
END

% disp('Compare to Table 7.2')
% disp(OUT(1:9,:))

hdr2 = {'','|z|','Arg(z)','|z|','Arg(z)','|z|','Arg(z)','|z|','Arg(z)'};
hdr3 = {'iteration','100','','150','','200','','Exact',''};
disp([hdr2;hdr3;num2cell(OUT(1:9,:))])
```

Figure 7.14

(Cont.) Computer program for Example 7.2.

Example 7.3

The second example was on a rectangular waveguide with a simple load. The MATLAB program used for the numerical analysis was basically similar to that of one-dimensional simulation. A 25×11 matrix was used for the numerical analysis of the waveguide. Short-circuit boundaries were placed at $x = 2$ and $x = 10$, the width between the waveguide walls thus being 9 mesh points. The system was excited at all points along the line $z = 2$, and the impulse function of the output was taken from the point ($x = 6, z = 12$). The C boundary at $z = 24$ represented an abrupt change to the intrinsic impedance of free space. The minor changes in the program of Figure 7.14 are shown in Figure 7.15. The cutoff frequency for the waveguide occurs [19] at $\Delta\ell/\lambda_n = 1/18$, λ_n is the network-matrix wavelength, which corresponds to $\Delta\ell/\lambda = \sqrt{2}/18$ since

$$\frac{\lambda_n}{\lambda} = \frac{u_n}{c} = \frac{\sqrt{\mu_o \epsilon_o}}{\sqrt{\mu_n \epsilon_n}} = \frac{\sqrt{LC}}{\sqrt{2LC}} = \frac{1}{\sqrt{2}}$$

A comparison between the results for the normalized guide impedance using this method is made with exact results in Table 7.3. \square

7.5 Inhomogeneous and Lossy Media in TLM

In our discussion on the transmission-line-matrix (TLM) method in the last section, it was assumed that the medium in which wave propagates was homogeneous and lossless. In this section, we consider media that are inhomogeneous or lossy

```
:
:
:

0034      DATA HXB,HXE,HZB,HZE,IT,ITRATE/2,10,2,24,4,200/
0035      DATA HX0,HZ0,PIE,GAMMA,DELTA/6,12,3.1415927,0,.02/
:
:
:
0064      C STEP #3 ****
0065      C USING EQS. (7.43) AND (7.44), INSERT BOUNDARY CONDITIONS
0066      C
0067      IF(J .EQ. HXE)VI(IT,I,HXE,3)=-VR(IT,I,HXE,1)
0068      IF(J .EQ. HXB)VI(IT,I,HXB,1)=VR(IT,I,HXB,1)
0069      IF(I .EQ. HZE)VI(IT,HZE,J,4)=GAMMA*VR(IT,HZE,J,4)
:
:
:
0095      70      DEL = DEL + 0.001
:
:
:
```

Figure 7.15

Modification in the program in Figure 7.14 for simulating waveguide problem in Example 7.3.

Table 7.3 Normalized Impedance of a Rectangular Waveguide with Simple Load

$\Delta\ell/\lambda$	TLM Results		Exact Results	
	$ Z $	$\text{Arg}(Z)$	$ Z $	$\text{Arg}(Z)$
0.020	1.9391	0.8936	1.9325	0.9131
0.021	2.0594	0.6175	2.0964	0.6415
0.022	1.9697	0.3553	2.0250	0.3603
0.023	1.7556	0.1530	1.7800	0.1438
0.024	1.5173	0.0189	1.5132	0.0163
0.025	1.3036	-0.0518	1.2989	-0.0388
0.026	1.1370	-0.0648	1.1471	-0.0457
0.027	1.0297	-0.0350	1.0482	-0.0249
0.028	0.9776	0.0088	0.9900	0.0075
0.029	0.9620	0.0416	0.9622	0.0396
0.030	0.9623	0.0554	0.9556	0.0632

or both. This necessitates that we modify the equivalent network of Figure 7.9 and the corresponding transmission-line matrix of Figure 7.10. Also, we need to draw the corresponding equivalence between the network and Maxwell's equations and derive the scattering matrix. We will finally consider how lossy boundaries are represented.

7.5.1 General Two-Dimensional Shunt Node

To account for the inhomogeneity of a medium (where ϵ is not constant), we introduce additional capacitance at nodes to represent an increase in permittivity [17], [23]–[25]. We achieve this by introducing an additional length of line or stub to the node as shown in Figure 7.16 (a). The stub of length $\Delta\ell/2$ is open circuited at the

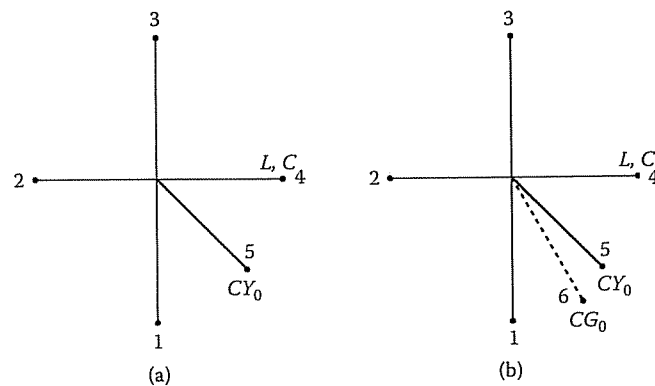


Figure 7.16
A two-dimensional node with: (a) Permittivity stub, (b) permittivity and loss stub.

end and is of variable characteristic admittance Y_o relative to the unity characteristic admittance assumed for the main transmission line. At low frequencies, the effect of the stub is to add to each node an additional lumped shunt capacitance $CY_o\Delta\ell/2$, where C is the shunt capacitance per unit length of the main lines that are of unity characteristic admittance. Thus at each node, the total shunt capacitance becomes

$$C' = 2C\Delta\ell + CY_o\Delta\ell/2$$

or

$$C' = 2C\Delta\ell(1 + Y_o/4) \quad (7.54)$$

To account for the loss in the medium, we introduce a power-absorbing line at each node, lumped into a single resistor, and this is simulated by an infinite or matched line of characteristic admittance G_o normalized to the characteristic impedance of the main lines as illustrated in Figure 7.16 (b).

Due to these additional lines, the equivalent network now becomes that shown in Figure 7.17. (Compare Figure 7.17 with Figure 7.9). Applying Kirchhoff's current law to shunt node O in the x - z plane in Figure 7.17 and taking limits as $\Delta\ell \rightarrow 0$ result in

$$-\frac{\partial I_z}{\partial z} - \frac{\partial I_x}{\partial x} = \frac{G_o V_y}{Z_o \Delta\ell} + 2C(1 + Y_o/4) \frac{\partial V_y}{\partial t} \quad (7.55)$$

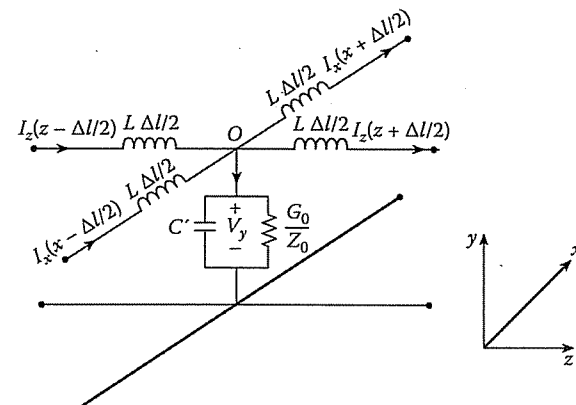


Figure 7.17
General two-dimensional shunt node.

Expanding Maxwell's equations $\nabla \times \mathbf{E} = -\mu \frac{\partial \mathbf{H}}{\partial t}$ and $\nabla \times \mathbf{H} = \sigma \mathbf{E} + \epsilon \mathbf{E}$ for $\partial/\partial y \equiv 0$ leads to

$$\frac{\partial H_x}{\partial z} - \frac{\partial H_z}{\partial x} = \sigma E_y + \epsilon_o \epsilon_r \frac{\partial E_y}{\partial t} \quad (7.56)$$

This may be considered as denoting TE _{$m0$} modes with field components H_z , H_x , and E_y . From Equations (7.55) and (7.56), the following equivalence between the TLM equations and Maxwell's equations can be drawn:

$E_y \equiv V_y$
$H_x \equiv -I_z$
$H_z \equiv I_x$
$\epsilon_o \equiv 2C$
$\epsilon_r \equiv \frac{4+Y_o}{4}$
$\sigma \equiv \frac{G_o}{Z_o \Delta\ell}$

(7.57)

where $Z_o = \sqrt{L/C}$. From Equation (7.57), the normalized characteristic admittance G_o of the loss stub is related to the conductivity of the medium by

$$G_o = \sigma \Delta\ell Z_o \quad (7.58)$$

Thus losses on the matrix can be varied by altering the value of G_o . Also from Equation (7.57), the variable characteristic admittance Y_o of the permittivity stub is related to the relative permittivity of the medium as

$$Y_o = 4(\epsilon_r - 1) \quad (7.59)$$

7.5.2 Scattering Matrix

We now derive the impulse response of the network comprising the interconnection of many generalized nodes such as that in Figure 7.17. As in the previous section, if $kV_n(z, x)$ is unit voltage impulse reflected from the node at (z, x) into the n th coordinate direction ($n = 1, 2, \dots, 5$) at time $k\Delta\ell/c$, then at node (z, x) ,

$$\begin{bmatrix} V_1(z, x) \\ V_2(z, x) \\ V_3(z, x) \\ V_4(z, x) \\ V_5(z, x) \end{bmatrix}_{k+1}^r = [S] \begin{bmatrix} V_3(z, x - \Delta\ell) \\ V_4(z - \Delta\ell, x) \\ V_1(z, x + \Delta\ell) \\ V_2(z + \Delta\ell, x) \\ V_5(z, x + \Delta\ell) \end{bmatrix}_k^i \quad (7.60)$$

where $[S]$ is the scattering matrix given by

$$[S] = \frac{2}{Y} \begin{bmatrix} 1 & 1 & 1 & 1 & Y_o \\ 1 & 1 & 1 & 1 & Y_o \\ 1 & 1 & 1 & 1 & Y_o \\ 1 & 1 & 1 & 1 & Y_o \\ 1 & 1 & 1 & 1 & Y_o \end{bmatrix} - [I] \quad (7.61)$$

$[I]$ is a unit matrix and $Y = 4 + Y_o + G_o$. The coordinate directions 1, 2, 3, and 4 correspond to $-x$, $-z$, $+x$, and $+z$, respectively (as in the last section), and 5 refers to the permittivity stub. Notice that the voltage V_6 (see Figure 7.16) scattered into the loss stub is dropped across G_o and not returned to the matrix. We apply Equation (7.60) just as Equation (7.41).

As in the last section, the output-impulse function at a particular node in the mesh can be obtained by recording the amplitude and the time of the stream of pulses as they pass through the node. By taking the Fourier transform of the output-impulse function using Equation (7.49), the required information can be extracted.

The dispersion relation can be derived in the same manner as in the last section. If $\gamma_n = \alpha_n + j\beta_n$ is the network propagation constant and $\gamma = \alpha + j\beta$ is the propagation constant of the medium, the two propagation constants are related as

$$\frac{\beta}{\beta_n} = \frac{\theta/2}{\sin^{-1} [\sqrt{2(1 + Y_o/4)} \sin \theta/2]} \quad (7.62a)$$

$$\frac{\alpha}{\alpha_n} = \frac{\sqrt{1 - 2(1 + Y_o/4) \sin^2 \theta/2}}{\sqrt{2(1 + Y_o/4)} \cos \theta/2} \quad (7.62b)$$

where $\theta = 2\pi \Delta\ell/\lambda$ and

$$\alpha = \frac{G_o}{8\Delta\ell(1 + Y_o/4)} \quad (7.63)$$

In arriving at Equation (7.62), we have assumed that $\alpha_n \Delta\ell \ll 1$. For low frequencies, the attenuation constant α_n and phase constant β_n of the network are fairly constant

7.5. INHOMOGENEOUS AND LOSSY MEDIA IN TLM

so that Equation (7.62) reduces to

$$\gamma_n = \sqrt{2(1 + Y_o/4)} \gamma \quad (7.64)$$

From this, the network velocity $u_n (= \omega/\beta_n = \beta c/\beta_n)$ of waves on the matrix is readily obtained as

$$u_n^2 = \frac{c^2}{2(1 + Y_o/4)} \quad (7.65)$$

where c is the free-space velocity of waves.

7.5.3 Representation of Lossy Boundaries

The above analysis has incorporated conductivity σ of the medium in the TLM formulation. To account for a lossy boundary [25]–[27], we define the reflection coefficient

$$\Gamma = \frac{Z_s - Z_o}{Z_s + Z_o} \quad (7.66)$$

where $Z_o = \sqrt{\mu_o/\epsilon_o}$ is the characteristic impedance of the main lines and Z_s is the surface impedance of the lossy boundary given by

$$Z_s = \sqrt{\frac{\mu\omega}{2\sigma_c}} (1 + j) \quad (7.67)$$

where μ and σ_c are the permeability and conductivity of the boundary. It is evident from Equations (7.66) and (7.67) that the reflection coefficient Γ is in general complex. However, complex Γ implies that the shape of the pulse functions is altered on reflection at the conducting boundary, and this cannot be accounted for in the TLM method [22]. Therefore, assuming that Z_s is small compared with Z_o and that the imaginary part of Γ is negligible,

$$\Gamma \simeq -1 + \sqrt{\frac{2\epsilon_o\omega}{\sigma_c}} \quad (7.68)$$

where $\mu = \mu_o$ is assumed. We notice that Γ is slightly less than -1 . Also, we notice that Γ depends on the frequency ω and hence calculations involving lossy boundaries are only accurate for the specific frequency; calculations must be repeated for a different value of $\Delta\ell/\lambda$. The following example is taken from Akhtarzad and Johns [24].

Example 7.4

Consider the lossy homogeneous filled waveguide shown in Figure 7.18. The guide is 6 cm wide and 13 cm long. It is filled with a dielectric of relative permittivity $\epsilon_r = 4.9$ and conductivity $\sigma = 0.05$ mhos/m and terminated in an open circuit discontinuity. Calculate the normalized wave impedance. \square

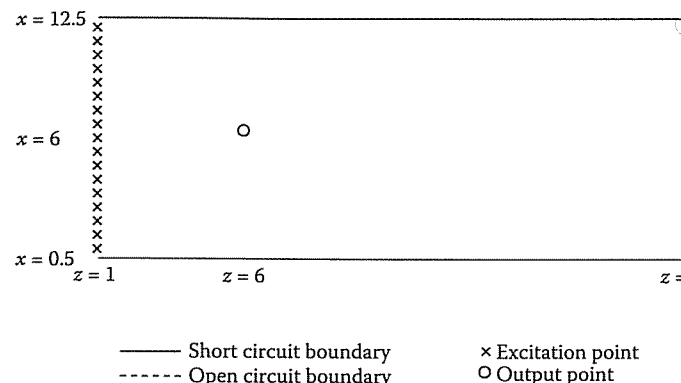


Figure 7.18
A lossy homogeneously filled waveguide.

Solution

The computer program for this problem is in Figure 7.19. It is an extension of the program in Figure 7.14 with the incorporation of new concepts developed in this section. Enough comments are added to make it self-explanatory. The program is suitable for a two-dimensional TE_{m0} mode.

The waveguide geometry shown in Figure 7.18 is simulated on a matrix of 12×26 nodes. The matrix is excited at all points along line $z = 1$ with impulses corresponding to E_y . The impulse function of the output at point $(z, x) = (6, 6)$ is taken after 700 iterations. Table 7.4 presents both the TLM and theoretical values of the normalized wave impedance and shows a good agreement between the two. ■

Table 7.4 Impedance of a Homogeneously Filled Waveguide with Losses

$\Delta\ell/\lambda$	TLM Results		Exact Results	
	$ Z $	$\text{Arg}(Z)$	$ Z $	$\text{Arg}(Z)$
0.003	0.0725	1.5591	0.0729	1.5575
0.006	0.1511	1.5446	0.1518	1.5420
0.009	0.2446	1.5243	0.2453	1.5205
0.012	0.3706	1.4890	0.3712	1.4840
0.015	0.5803	1.4032	0.5792	1.3977
0.018	1.0000	1.0056	0.9979	1.0065
0.021	1.1735	0.5156	1.1676	0.5121
0.024	0.5032	-0.1901	0.5093	-0.2141
0.027	0.6766	0.6917	0.6609	0.6853
0.030	0.8921	-0.3869	0.8921	-0.4185

```

clear
%
% THIS PROGRAM SOLVES A TYPICAL TWO-DIMENSIONAL
% WAVE PROPAGATION PROBLEM AT STATED BELOW:
% A WAVE GUIDE 6cm X 13cm IS FILLED WITH A
% DIELECTRIC OF RELATIVE PERMITTIVITY EQUAL TO 4.9
% AND CONDUCTIVITY 0.05 MHO/M. THIS GEOMETRY IS
% BEING SIMULATED ON A MATRIX OF 12 X 26 NODES
% THE MATRIX WAS EXCITED AT ALL POINTS ALONG THE
% LINE Z = 1 WITH IMPULSES CORRESPONDING TO Ey.
% THE IMPULSE FUNCTION OF THE OUTPUT WAS TAKEN FROM
% THE POINT (Z = 6, X=6) AFTER 750 ITERATIONS.
% THE BOUNDARIES WERE SHORT CIRCUITED AT X = 0.5
% AND X = 12.5 AND TERMINATED AT Z = 26.5 IN AN
% OPEN CIRCUIT DISCONTINUITY.
% VI -- ARRAY FOR INCIDENT VOLTAGE
% VR -- ARRAY FOR REFLECTED VOLTAGE
% NX -- INDEX OF NODES IN X-DIRECTION
% NZ -- INDEX OF NODES IN Z-DIRECTION
% RO -- REFLECTION COEFFICIENT
% DELTA -- MESH SIZE (SPACING)

```

```

VI=zeros(2,27,13,5);
VR=zeros(2,27,13,5);
EFI=zeros(1,50);
EFR=zeros(1,50);
HFI=zeros(1,50);
HFR=zeros(1,50);
NXB=1;
NZE=12;
NZB=1;
NZE=26;
NT=5;
ITRATE=750;
NXI=0;
NZI=1;
NXO=6;
NZO=6;
RoS=-1;
RoC=1;
Eo=8.854E-12;
Er=4.9;
SIGMA=0.05;
DELTA=0.005;

Yo = 4.0 * (Er/2 - 1);
Ur = 1.0;
Uo = 4.0 * pi * 1.0E-07;
Go = SIGMA * DELTA * sqrt( Uo/Eo );
Y = 4.0 + Yo + Go;

```

Figure 7.19
Computer program for Example 7.4 (Continued).

```
% SINCE REFLECTION COEFFICIENT, RO, DEPENDS ON
% FREQUENCY, THE ITERATIONS MUST BE REPEATED FOR
% EACH VALUE OF THE MESH-SIZE DIVIDED BY WAVELENGTH.

DELTA = 0.0;
for L = 1:10
    DELTA = DELTA + 0.003;

% INITIALIZE ALL NODES (BOTH FREE AND FIXED)
VI = zeros(2,NZE,NXE,NT);
VR = zeros(2,NZE,NXE,NT);

% START THE ITERATION
for ITime = 0: IT RATE

    IT = 1;
    for I = NZB: NZE
        for J = NXB: NXE
            SUM = 0.0;
            for K = 1:4
                SUM = SUM + VI(IT-1+1,I,J,K);
            end
            SUM = (SUM + Yo*VI(IT-1+1,I,J,5)) * 2/Y;
            % INSERT THE INITIAL CONDITION AT I = 1
            if ((ITime==0)&&(I==NZI)), SUM = 1.0; end
            for K = 1: NT
                VR(IT+1,I,J,K) = SUM - VI(IT-1+1,I,J,K);
            end
            if (J==NXB), VI(IT+1,I,J-1,3) = VR(IT+1,I,J,1);end
            if (I==NZB), VI(IT+1,I-1,J,4) = VR(IT+1,I,J,2);end
            if (J==NZE), VI(IT+1,I,J+1,1) = VR(IT+1,I,J,3);end
            if (I==NZE), VI(IT+1,I+1,J,2) = VR(IT+1,I,J,4);end
            VI (IT+1,I,J,5) = VR(IT+1,I,J,5);

            % INSERT THE BOUNDARY CONDITIONS
            % FOR THE SHORT CIRCUIT AT X = 0.5
            if (J==NXB), VI(IT+1,I,1,1) = RoS*VR(IT+1,I,1,1);end
            % FOR THE SHORT CIRCUIT AT X = 12.5
            if (J==NZE), VI(IT+1,I,J,3) = RoS*VR(IT+1,I,J,3);end
            % FOR THE OPEN CIRCUIT DISCONTINUITY AT Z = 26.5
            if (I==NZE), VI(IT+1,I,J,4) = RoC*VR(IT+1,I,J,4);end
        end
    end
end
```

Figure 7.19
(Cont.) Computer program for Example 7.4.

7.6. THREE-DIMENSIONAL TLM MESH

```
% IN ORDER TO CONSERVE SPACE, THE ARRAYS
% HAVE TO BE UPDATED

VI(IT-1+1,1:NZE,1:NXE,1:NT) = VI(IT+1,1:NZE,1:NXE,1:NT);
VR(IT-1+1,1:NZE,1:NXE,1:NT) = VR(IT+1,1:NZE,1:NXE,1:NT);

% CALCULATE IMPULSE RESPONCE AT Z=NZO, X=NXO
EI = (sum(VI(IT+1,NZO,NXO,1:4)) + Yo * VI(IT+1,NZO,NXO,5)) * 2.0/Y;
HI = -(VI(IT+1,NZO,NXO,2)-VI(IT+1,NZO,NXO,4));

% SUM THE FREQUENCY RESPONSE (imaginary and
% real parts) FOR DIFFERENT VALUES OF
% MESH-SIZE DIVIDED BY WAVELENGTH

T = (ITime);
EFI(L) = EFI(L)+EI*sin(2.0 * pi * T * DELTA);
EFR(L) = EFR(L)+EI*cos(2.0 * pi * T * DELTA);
HFI(L) = HFI(L)+HI*sin(2.0 * pi * T * DELTA);
HFR(L) = HFR(L)+HI*cos(2.0 * pi * T * DELTA);
OUT(L,1) = DELTA;
if (ITime==ITRATE)
    CEF = EFR(L)+EFI(L)*i;
    CHF = HFR(L)+HFI(L)*i;
    OUT(L,2) = abs(CEF)/abs(CHF);

    % CALCULATE ARGUMENT Z

    ZARG = CEF/CHF;
    XZ = real(ZARG);
    YZ = imag(ZARG);
    XYZ = YZ / XZ;
    OUT(L,3) = -atan(XYZ);
end
format short g
disp('      DELTA      |z|      Arg(z)')
disp(OUT)
```

Figure 7.19
(Cont.) Computer program for Example 7.4.

7.6 Three-Dimensional TLM Mesh

The TLM mesh considered in Sections 7.4 and 7.5 is two-dimensional. The choice of shunt-connected nodes to represent the two-dimensional wave propagation was quite arbitrary; the TLM mesh could have equally been made up of series-connected

nodes. To represent a three-dimensional space, however, we must apply a hybrid TLM mesh consisting of three shunt and three series nodes to simultaneously describe all the six field components. First of all, we need to understand what a series-connected node is.

7.6.1 Series Nodes

Figure 7.20 portrays a lossless series-connected node that is equipped with a short-circuited stub called the permeability stub. The corresponding network representation is illustrated in Figure 7.21. The input impedance of the short-circuited stub is

$$Z_{in} = j Z_o \sqrt{\frac{L}{C}} \tan\left(\frac{\omega \Delta\ell}{2c}\right) \simeq j \omega L Z_o \Delta\ell / 2 \quad (7.69)$$

where Equation (7.26) has been applied. This represents an impedance with inductance

$$L' = L \frac{\Delta\ell}{2} Z_o \quad (7.70)$$

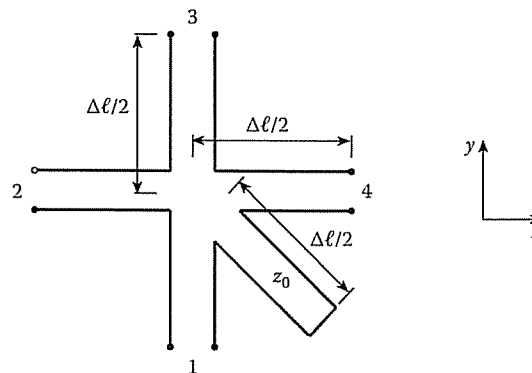


Figure 7.20
A lossless series connected node with permeability stub.

Hence the total inductance on the side in which the stub is inserted is $L \Delta\ell(1 + Z_o)/2$ as in Figure 7.21. We now apply Kirchhoff's voltage law around the series node of Figure 7.21 and obtain

$$V_z + L \frac{\Delta\ell}{2} (1 + Z_o) \frac{\partial I_x}{\partial t} + V_y + \frac{\partial V_y}{\partial z} \Delta\ell - \left(V_z + \frac{\partial V_z}{\partial y} \Delta\ell \right) + 3L \frac{\Delta\ell}{2} \frac{\partial I_x}{\partial t} - V_y = 0$$

Dividing through by $\Delta\ell$ and rearranging terms leads to

$$\frac{\partial V_z}{\partial y} - \frac{\partial V_y}{\partial z} = 2L(1 + Z_o/4) \frac{\partial I_x}{\partial t} \quad (7.71)$$

7.6. THREE-DIMENSIONAL TLM MESH

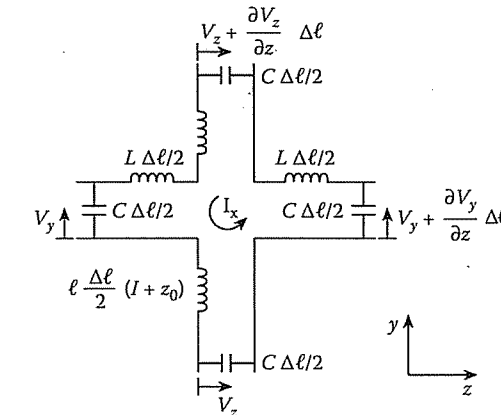


Figure 7.21
Network representation of a series node.

Note that the series node is oriented in the y - z plane. Equations for series nodes in the x - y and x - z planes can be obtained in a similar manner as

$$\frac{\partial V_y}{\partial x} - \frac{\partial V_x}{\partial y} = 2L(1 + Z_o/4) \frac{\partial I_z}{\partial t} \quad (7.72)$$

and

$$\frac{\partial V_x}{\partial z} - \frac{\partial V_z}{\partial x} = 2L(1 + Z_o/4) \frac{\partial I_y}{\partial t}, \quad (7.73)$$

respectively.

Comparing Equations (7.71) to (7.73) with Maxwell's equations in Equation (7.22), the following equivalences can be identified:

$E_x \equiv V_x$
$E_z \equiv V_z$
$\mu_o \equiv 2L$
$\mu_r \equiv \frac{4 + Z_o}{4}$

(7.74)

A series-connected two-dimensional TLM mesh is shown in Figure 7.22 (a), while the equivalent one-dimensional mesh is in Figure 7.22 (b). A voltage impulse incident on a series node is scattered in accordance with Equation (7.60), where the scattering matrix is now

$$[S] = \frac{2}{Z} \begin{bmatrix} -1 & 1 & 1 & -1 & -1 \\ 1 & -1 & -1 & 1 & 1 \\ 1 & -1 & -1 & 1 & 1 \\ -1 & 1 & 1 & -1 & -1 \\ -Z_o & Z_o & Z_o & -Z_o & -Z_o \end{bmatrix} + [I] \quad (7.75)$$

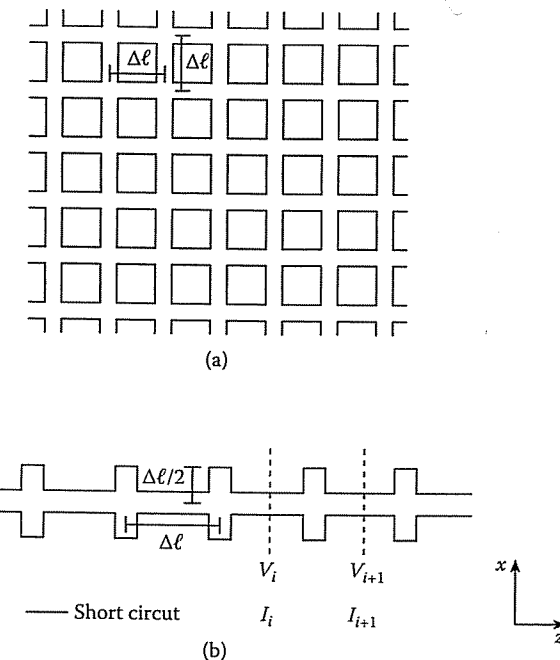


Figure 7.22

(a) A two-dimensional series-connected TLM mesh. (b) A one-dimensional series-connected TLM mesh.

where $Z = 4 + Z_o$, and $[I]$ is the unit matrix. The velocity characteristic for the two-dimensional series matrix is the same as for the shunt node [24]. For low frequencies ($\Delta\ell/\lambda < 0.1$) the velocity of the waves on the matrix is approximately $1/\sqrt{2}$ of the free-space velocity. This is due to the fact that the stubs have twice the inductance per unit length, while the capacitance per unit length remains unchanged. This is the dual of the two-dimensional shunt case in which the capacitance was doubled and the inductance was unchanged.

7.6.2 Three-Dimensional Node

A three-dimensional TLM node [27] consists of three shunt nodes in conjunction with three series nodes. The voltages at the three shunt nodes represent the three components of the \mathbf{E} field, while the currents of the series nodes represent the three components of the \mathbf{H} field. In the x - z plane, for example, the voltage-current equations

7.6. THREE-DIMENSIONAL TLM MESH

for the shunt node are

$$\frac{\partial I_x}{\partial z} - \frac{\partial I_z}{\partial x} = 2C \frac{\partial V_y}{\partial t} \quad (7.76a)$$

$$\frac{\partial V_y}{\partial x} = -L \frac{\partial I_x}{\partial t} \quad (7.76b)$$

$$\frac{\partial V_y}{\partial z} = -L \frac{\partial I_z}{\partial t} \quad (7.76c)$$

and for the series node in the x - z plane, the equations are

$$\frac{\partial V_x}{\partial z} - \frac{\partial V_z}{\partial x} = 2L \frac{\partial I_y}{\partial t} \quad (7.77a)$$

$$\frac{\partial I_y}{\partial x} = -C \frac{\partial V_z}{\partial t} \quad (7.77b)$$

$$\frac{\partial I_y}{\partial z} = -C \frac{\partial V_x}{\partial t} \quad (7.77c)$$

Maxwell's equations $\nabla \times \mathbf{E} = \frac{\partial \mathbf{B}}{\partial t}$ and $\nabla \times \mathbf{H} = \epsilon \frac{\partial \mathbf{E}}{\partial t}$ for $\frac{\partial}{\partial y} \equiv 0$ give

$$\frac{\partial H_x}{\partial z} - \frac{\partial H_z}{\partial x} = \epsilon \frac{\partial E_y}{\partial t} \quad (7.78a)$$

$$\frac{\partial E_y}{\partial x} = \mu \frac{\partial H_x}{\partial t} \quad (7.78b)$$

$$\frac{\partial E_y}{\partial z} = -\mu \frac{\partial H_z}{\partial t} \quad (7.78c)$$

and

$$\frac{\partial E_x}{\partial z} - \frac{\partial E_z}{\partial x} = -\mu \frac{\partial H_y}{\partial t} \quad (7.79a)$$

$$\frac{\partial H_y}{\partial x} = -\epsilon \frac{\partial E_x}{\partial t} \quad (7.79b)$$

$$\frac{\partial H_y}{\partial z} = -\epsilon \frac{\partial E_z}{\partial t} \quad (7.79c)$$

A similar analysis for shunt and series nodes in the x - y and y - z planes will yield the voltage-current equations and the corresponding Maxwell's equations. The three sets of two-dimensional shunt and series nodes oriented in the x - y , y - z , and z - x planes form a three-dimensional model. The two-dimensional nodes must be connected in

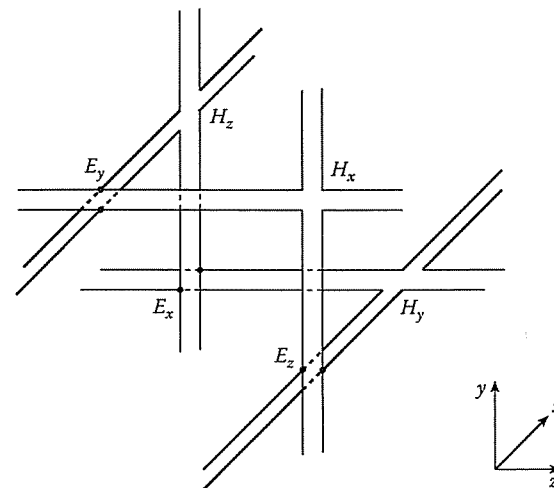


Figure 7.23

A three-dimensional node consisting of three shunt nodes and three series nodes.

such a way as to correctly describe Maxwell's equations at each three-dimensional node. Each of the shunt and series nodes has a spacing of $\Delta\ell/2$ so that like nodes are spaced $\Delta\ell$ apart.

Figure 7.23 illustrates a three-dimensional node representing a cubical volume of space $\Delta\ell/2$ long in each direction. A close examination shows that if the voltage between lines represents the \mathbf{E} field and the current in the lines represents the \mathbf{H} field, then the following Maxwell's equations are satisfied:

$$\frac{\partial H_x}{\partial z} - \frac{\partial H_z}{\partial x} = \epsilon \frac{\partial E_y}{\partial t} \quad (7.80a)$$

$$\frac{\partial E_z}{\partial y} - \frac{\partial E_y}{\partial z} = -\mu \frac{\partial H_x}{\partial t} \quad (7.80b)$$

$$\frac{\partial E_y}{\partial x} - \frac{\partial E_x}{\partial y} = -\mu \frac{\partial H_z}{\partial t} \quad (7.80c)$$

$$\frac{\partial E_x}{\partial z} - \frac{\partial E_z}{\partial x} = -\mu \frac{\partial H_y}{\partial t} \quad (7.80d)$$

$$\frac{\partial H_z}{\partial y} - \frac{\partial H_y}{\partial z} = \epsilon \frac{\partial E_x}{\partial t} \quad (7.80e)$$

$$\frac{\partial H_y}{\partial x} - \frac{\partial H_x}{\partial y} = \epsilon \frac{\partial E_z}{\partial t} \quad (7.80f)$$

In the upper half of the node in Figure 7.23, we have a shunt node in the x - z plane [representing Equation (7.80a)] connected to a series node in the y - z plane [representing Equation (7.80b)] and a series node in the x - y plane [representing

7.6. THREE-DIMENSIONAL TLM MESH

Equation (7.80c)]. In the lower half of the node, a series node in the x - z plane [representing Equation (7.80d)] is connected to a shunt node in the y - z plane [representing Equation (7.80e)] and a shunt node in the x - y plane [representing Equation (7.80f)]. Thus Maxwell's equations are completely satisfied at the three-dimensional node. A three-dimensional TLM mesh is obtained by stacking similar nodes in x , y , and z directions (see Figure 7.25, for example).

The wave characteristics of the three-dimensional mesh are similar to those of the two-dimensional mesh with the difference that low-frequency velocity is now $c/2$ instead of $c/\sqrt{2}$.

Figure 7.24 illustrates a schematic diagram of a three-dimensional node using single lines to represent pairs of transmission lines. It is more general than the representation in Figure 7.23 in that it includes the permittivity, permeability, and loss stubs. Note that the dotted lines making up the corners of the cube are guidelines and do not represent transmission lines or stubs. It can be shown that for the general node the

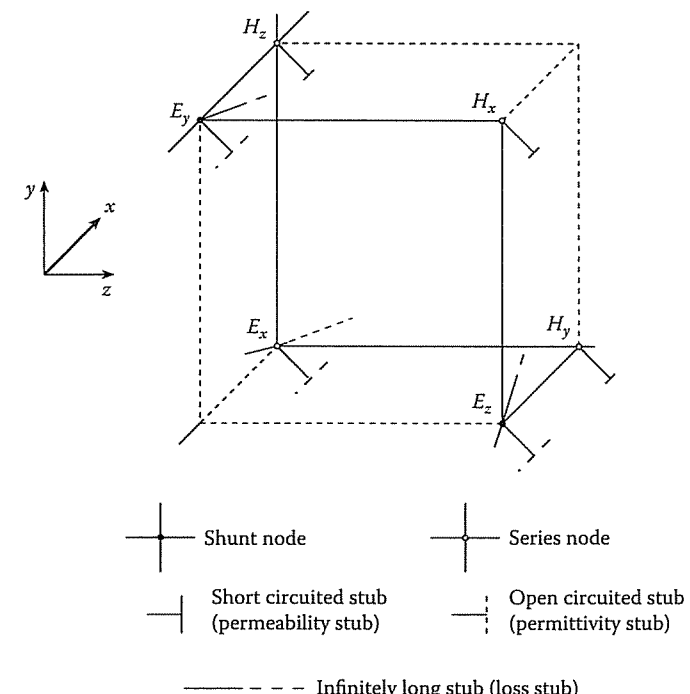


Figure 7.24

A general three-dimensional node.

following equivalences apply [28]:

$$\begin{aligned}
 E_x &\equiv \text{the common voltage at shunt node } E_x \\
 E_y &\equiv \text{the common voltage at shunt node } E_y \\
 E_z &\equiv \text{the common voltage at shunt node } E_z \\
 H_x &\equiv \text{the common current at series node } H_x \\
 H_y &\equiv \text{the common current at series node } H_y \\
 H_z &\equiv \text{the common current at series node } H_z \\
 \epsilon_0 &\equiv C \text{ (the capacitance per unit length of lines)} \\
 \epsilon_r &\equiv 2(1 + Y_o/4) \\
 \mu_o &\equiv L \text{ (the inductance per unit length of lines)} \\
 \mu_r &\equiv 2(1 + Z_o/4) \\
 \sigma &\equiv \frac{G_o}{\Delta\ell \frac{L}{C}}
 \end{aligned} \tag{7.81}$$

where Y_o , Z_o , and G_o remain as defined in Sections 7.4 and 7.5. Interconnection of many of such three-dimensional nodes forms a TLM mesh representing any inhomogeneous media. The TLM method for three-dimensional problems is therefore concerned with applying Equation (7.60) in conjunction with Equations (7.61) and (7.75) and obtaining the impulse response. Any of the field components may be excited initially by specifying initial impulses at the appropriate nodes. Also, the response at any node may be monitored by recording the pulses that pass through the node.

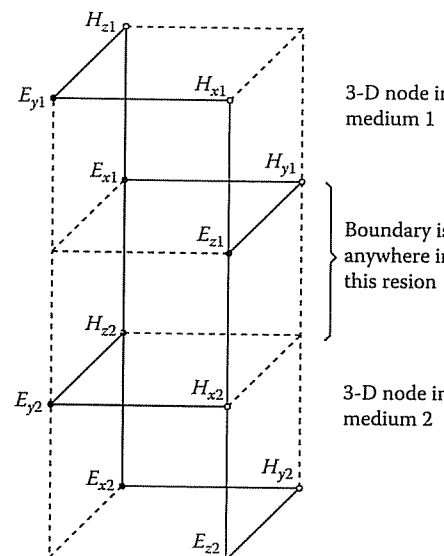


Figure 7.25
A dielectric/dielectric boundary in TLM mesh.

7.6. THREE-DIMENSIONAL TLM MESH

507

7.6.3 Boundary Conditions

Boundary conditions are simulated by short-circuiting shunt nodes (electric wall) or open-circuiting series nodes (magnetic wall) situated on a boundary. The tangential components of \mathbf{E} must vanish in the plane of an electric wall, while the tangential components of \mathbf{H} must be zero in the plane of a magnetic wall. For example, to set E_x and E_y equal to zero in a particular plane, all shunt nodes E_x and E_y lying in that plane are shorted. Similarly, to set H_y and H_z equal to zero in some plane, the series nodes H_y and H_z in that plane are simply open-circuited.

The continuity of the tangential components of \mathbf{E} and \mathbf{H} fields across a dielectric/dielectric boundary is automatically satisfied in the TLM mesh. For example, for a dielectric/dielectric boundary in the x - z plane such as shown in Figure 7.25, the following equations valid for a transmission-line element joining the nodes on either side of the boundaries are applicable:

$$\begin{aligned}
 E_{z1} &= E_{z2} + \frac{\partial E_{z2}}{\partial y} \Delta\ell \\
 E_{x1} &= E_{x2} + \frac{\partial E_{x2}}{\partial y} \Delta\ell \\
 H_{x1} &= H_{x2} + \frac{\partial H_{x2}}{\partial y} \Delta\ell \\
 H_{z1} &= H_{z2} + \frac{\partial H_{z2}}{\partial y} \Delta\ell
 \end{aligned} \tag{7.82}$$

Finally, wall losses are included by introducing imperfect reflection coefficients as discussed in Section 7.5. The three-dimensional TLM mesh will be applied in solving the three-dimensional problems of resonant cavities in the following examples, taken from Akhtarzad and Johns [27].

Example 7.5

Determine the resonant frequency of an $a \times b \times d$ empty rectangular cavity using the TLM method. Take $a = 12\Delta\ell$, $b = 8\Delta\ell$, and $d = 6\Delta\ell$. \square

Solution

The exact solution [13, 14] for TE_{mnp} or TM_{mnp} mode is

$$f_r = \frac{c}{2} \sqrt{(m/a)^2 + (n/b)^2 + (p/d)^2}$$

from which we readily obtain

$$k_c = \frac{w_r}{c} = \frac{2\pi f_r}{c} = \pi \sqrt{(m/a)^2 + (n/b)^2 + (p/d)^2}$$

The TLM program, the modified version of the program in [22], is shown in Figure 7.26. The program initializes all field components by setting them equal to

```

0001 C*****
0002 C THIS PROGRAM ANALYZES THREE-DIMENSIONAL WAVE PROBLEMS
0003 C USING THE TLM METHOD
0004 C THE SPECIFIC EXAMPLE SOLVED HERE IS THE DETERMINATION
0005 C OF THE TM DOMINANT MODE OF RECTANGULAR LOSSLESS CAVITY
0006 C OF DIMENSION 12 X 8 X 6
0007 C E ... E - field
0008 C H ... H - field
0009 C X ... X - component
0010 C Y ... Y - component
0011 C Z ... Z - component
0012 C I ... incident impulse
0013 C R ... reflected impulse
0014 C NX ... number of nodes in X-direction
0015 C NY ... number of nodes in Y-direction
0016 C NZ ... number of nodes in Z-direction
0017 C SHUNT and SERIES ... scattering matrix
0018 C DELTA = DELTA/LAMBDA (FREE SPACE)
0019
0020      IMPLICIT REAL*8(A,B,D-H,O-Z),COMPLEX*8(C),
0021      INTEGER*2(I-N)
0022      DIMENSION EXR(2,7,9,13,5), EXI(2,7,9,13,5),
0023      1   EYR(2,7,9,13,5), EYI(2,7,9,13,5),
0024      2   EZR(2,7,9,13,5), EZI(2,7,9,13,5),
0025      3   HXR(2,7,9,13,5), HXI(2,7,9,13,5),
0026      4   HYR(2,7,9,13,5), HYI(2,7,9,13,5),
0027      5   HZR(2,7,9,13,5), HZI(2,7,9,13,5),
0028      6   EX(2,1000), EY(2,1000), EZ(2,1000),
0029      7   HX(2,1000), HY(2,1000), HZ(2,1000),
0030      8   OUT(12,1000), SHUNT(5,5), SERIES(5,5)
0031
0032      COMMON / PART1 / NT, NXB, NXE, NYB, NYE, NZB, NZE, IT
0033      SQMAG(CM) = ( CABS(CM) ) ** 2
0034      DATA ITRATE, NXB, NXE, NYB, NYE, NZB, NZE, NT, DELTA
0035      1   /1000, 1, 12, 1, 8, 1, 6, 4, 1.0/
0036      DATA NXI, NYI, NZI, NXO, NYO, NZO, RoH, HUMPT, DEL
0037      1   /11, 7, 0, 2, 2, 2, -1.0, 1000, 0.0001/
0038      DATA PI, Eo, Er, Ur, SIGMA, DELTA
0039      1   /3.1415927, 8.854E-12, 1.0, 1.0, 0.0, 0.01 /
0040      DATA SERIES /-1.0, 1.0, 1.0, -1.0, -1.0,
0041      1   1.0, -1.0, -1.0, 1.0, 1.0,
0042      2   1.0, -1.0, -1.0, 1.0, 1.0,
0043      3   -1.0, 1.0, 1.0, -1.0, -1.0,
0044      4   -1.0, 1.0, 1.0, -1.0, -1.0/
0045      DATA SHUNT / 1.0, 1.0, 1.0, 1.0, 1.0,
0046      1   1.0, 1.0, 1.0, 1.0, 1.0,
0047      2   1.0, 1.0, 1.0, 1.0, 1.0,
0048      3   1.0, 1.0, 1.0, 1.0, 1.0,
0049      4   1.0, 1.0, 1.0, 1.0, 1.0/
0050
0051      Uo = 4.0 * PI * 1.0E-07
0052      Yo = 4.0 * (Er - 1.0)
0053      Zo = 4.0 * (Ur - 1.0)
0054      Go = SIGMA * DELTA * SQRT(Uo/Eo)
0055      Y = 4.0 + Yo + Go
0056      Z = 4.0 + Zo
0057      DO 5 I = 1,5
0058      SHUNT(I,5) = SHUNT(I,5) * Yo
0059      SERIES(5,I) = SERIES(5,I) * Zo
0060      5  CONTINUE
0061      C

```

Figure 7.26

Computer program for Example 7.5 (Continued).

7.6. THREE-DIMENSIONAL TLM MESH

```

0062      C INITIALIZE ALL THE NODES
0063      C
0064      DO 10 IT = 1,2
0065      DO 10 K = NZB, NZE
0066      DO 10 J = NYB, NYE
0067      DO 10 I = NYB, NYE
0068      DO 10 L = 1, NT
0069      EXI(IT,K,J,I,L) = 0.0
0070      EYI(IT,K,J,I,L) = 0.0
0071      EZI(IT,K,J,I,L) = 0.0
0072      HXI(IT,K,J,I,L) = 0.0
0073      HYI(IT,K,J,I,L) = 0.0
0074      HZI(IT,K,J,I,L) = 0.0
0075      EXR(IT,K,J,I,L) = 0.0
0076      EYR(IT,K,J,I,L) = 0.0
0077      EZR(IT,K,J,I,L) = 0.0
0078      HXR(IT,K,J,I,L) = 0.0
0079      HYR(IT,K,J,I,L) = 0.0
0080      1G      HZR(IT,K,J,I,L) = 0.0
0081      C
0082      C INSERT THE INITIAL EXCITATION
0083      C
0084      DO 15 K = NZB, NZE
0085      DO 15 L = 1, 4
0086      EZR(2,K,NYI,NXI,L) = 1.0
0087      15  CONTINUE
0088      IT = 2
0089      C
0090      C START ITERATION
0091      C
0092      DO 60 ITIME = 1, ITRATE
0093      IF(ITIME .EQ. 1) GOTO 25
0094      C
0095      C COMPUTE THE REFLECTED E-FIELD AT ALL NODES
0096      C
0097      ISIGN = -1
0098      CALL COMPUTE(EXR,EYR,EZR,SHUNT
0099      1           ,Y,EXI,EYI,EZI,ISIGN)
0100      C
0101      C RE-INITIALIZE MATRIX AND FORCE TANGENTIAL
0102      C E-FIELD TO ZERO AT BOUNDARY
0103
0104      DO 20 K = NZB, NZE
0105      DO 20 J = NYB, NYE
0106      DO 20 I = NYB, NYE
0107      DO 20 L = 1, NT
0108      HXI(IT-1,K,J,I,L) = 0.0
0109      HYI(IT-1,K,J,I,L) = 0.0
0110      HZI(IT-1,K,J,I,L) = 0.0
0111      IF(I .EQ. NXB) THEN
0112          EYR(IT,K,J,I,L) = 0.0
0113          EZR(IT,K,J,I,L) = 0.0
0114          HXR(IT,K,J,I,L) = 0.0
0115      END IF
0116      IF(J .EQ. NYB) THEN
0117          EXR(IT,K,J,I,L) = 0.0
0118          EZR(IT,K,J,I,L) = 0.0
0119          HYR(IT,K,J,I,L) = 0.0
0120      END IF
0121      IF(K .EQ. NZB) THEN
0122          EXR(IT,K,J,I,L) = 0.0
0123          EYR(IT,K,J,I,L) = 0.0
0124          HZR(IT,K,J,I,L) = 0.0

```

Figure 7.26

(Cont.) Computer program for Example 7.5.

```

0125      END IF
0126 20    CONTINUE
0127 25    CONTINUE
0128      DO 30 K = HZB, HZE
0129      DO 30 J = HYB, HYE
0130      DO 30 I = HXB, HXE
0131      IF(J .NE. HYB)HZI(IT-1,K,J-1,I,4)=EXR(IT,K,J,I,1)
0132      IF(K .NE. HZB)HYI(IT-1,K-1,J,I,4)=EXR(IT,K,J,I,2)
0133          HZI(IT-1,K,J,I,2) =EXR(IT,K,J,I,3)
0134          HYI(IT-1,K,J,I,2) =EXR(IT,K,J,I,4)
0135      IF(I .NE. HXB)HZI(IT-1,K,J-1,I,3)=EYR(IT,K,J,I,1)
0136      IF(K .NE. HZB)HXI(IT-1,K,J-1,I,4)=EYR(IT,K,J,I,2)
0137          HZI(IT-1,K,J,I,1) =EYR(IT,K,J,I,3)
0138          HXI(IT-1,K,J,I,2) =EYR(IT,K,J,I,4)
0139      IF(I .NE. HXB)HYI(IT-1,K,J,I-1,3)=EZR(IT,K,J,I,1)
0140      IF(J .NE. HYB)HXI(IT-1,K,J-1,I,3)=EZR(IT,K,J,I,2)
0141          HYI(IT-1,K,J,I,1) =EZR(IT,K,J,I,3)
0142          HXI(IT-1,K,J,I,1) =EZR(IT,K,J,I,4)
0143 30    CONTINUE
0144 C
0145 C INSERT THE BOUNDARY CONDITIONS AT ALL BOUNDARIES
0146 C
0147      DO 35 K = HZB, HZE
0148      DO 35 J = HYB, HYE
0149      DO 35 I = HXB, HXE
0150      IF(I .EQ. HXB)THEN
0151          HYI(IT-1,K,J,I,1) = RoH * HYR(IT,K,J,I,1)
0152          HZI(IT-1,K,J,I,1) = RoH * HZR(IT,K,J,I,1)
0153      END IF
0154      IF(I .EQ. HXE)THEN
0155          HZI(IT-1,K,J,I,3) = RoH * HZR(IT,K,J,I,3)
0156          HYI(IT-1,K,J,I,3) = RoH * HYR(IT,K,J,I,3)
0157      END IF
0158      IF(J .EQ. HYB)THEN
0159          HXI(IT-1,K,J,I,1) = RoH * HXR(IT,K,J,I,1)
0160          HZI(IT-1,K,J,I,2) = RoH * HZR(IT,K,J,I,2)
0161      END IF
0162      IF(J .EQ. HYE)THEN
0163          HXI(IT-1,K,J,I,3) = RoH * HXR(IT,K,J,I,3)
0164          HZI(IT-1,K,J,I,4) = RoH * HZR(IT,K,J,I,4)
0165      END IF
0166      IF(K .EQ. HZB)THEN
0167          HXI(IT-1,K,J,I,2) = RoH * HXR(IT,K,J,I,2)
0168          HYI(IT-1,K,J,I,2) = RoH * HYR(IT,K,J,I,2)
0169      END IF
0170      IF(K .EQ. HZE)THEN
0171          HXI(IT-1,K,J,I,4) = RoH * HXR(IT,K,J,I,4)
0172          HYI(IT-1,K,J,I,4) = RoH * HYR(IT,K,J,I,4)
0173      END IF
0174 35    CONTINUE
0175 C
0176 C COMPUTE THE H-FIELDS AT ALL THE NODES
0177 C
0178      ISIGN = 1
0179      CALL COMPUTE(HXR,HYR,HZR,SERIES,
0180      1           Z,HXI,HYI,HZI,ISIGN)
0181 C
0182 C RE-INITIALIZE ALL THE NODES
0183 C
0184      DO 40 K = HZB, HZE
0185      DO 40 J = HYB, HYE
0186      DO 40 I = HXB, HXE
0187      DO 40 L = 1, MT

```

Figure 7.26

(Cont.) Computer program for Example 7.5.

7.6. THREE-DIMENSIONAL TLM MESH

```

0188      EXI(IT-1,K,J,I,L) = 0.0
0189      EYI(IT-1,K,J,I,L) = 0.0
0190      EZI(IT-1,K,J,I,L) = 0.0
0191 40    CONTINUE
0192      DO 45 K = HZB, HZE
0193      DO 45 J = HYB, HYE
0194      DO 45 I = HXB, HXE
0195          EZI(IT-1,K,J,I,4) =HXR(IT,K,J,I,1)
0196          EYI(IT-1,K,J,I,4) =HXR(IT,K,J,I,2)
0197      IF(J .NE. HYE)EZI(IT-1,K,J+1,I,2)=HXR(IT,K,J,I,3)
0198      IF(K .NE. HZE)EYI(IT-1,K+1,J,I,2)=HXR(IT,K,J,I,4)
0199          EZI(IT-1,K,J,I,3) =HYR(IT,K,J,I,1)
0200          EXI(IT-1,K,J,I,4) =HYR(IT,K,J,I,2)
0201      IF(I .NE. HXE)EZI(IT-1,K,J,I+1,I)=HYR(IT,K,J,I,3)
0202      IF(K .NE. HZE)EXI(IT-1,K+1,J,I,2)=HYR(IT,K,J,I,4)
0203          EYI(IT-1,K,J,I,3) =HZR(IT,K,J,I,1)
0204          EXI(IT-1,K,J,I,3) =HZR(IT,K,J,I,2)
0205      IF(I .NE. HXE)EYI(IT-1,K,J,I+1,I)=HZR(IT,K,J,I,3)
0206      IF(J .NE. HYE)EXI(IT-1,K,J+1,I,1)=HZR(IT,K,J,I,4)
0207 45    CONTINUE
0208 C
0209 C CALCULATE THE IMPULSE RESPONSE AT HXO, HYO, HZO
0210 C
0211      EXT = 0.0
0212      EYT = 0.0
0213      EZT = 0.0
0214      HXT = 0.0
0215      HYT = 0.0
0216      HZT = 0.0
0217      DO 50 L = 1, MT
0218          EXT = EXT + EXI(IT-1,HZO,HYO,HXO,L) * (2.0/Y)
0219          EYT = EYT + EYI(IT-1,HZO,HYO,HXO,L) * (2.0/Y)
0220          EZT = EZT + EZI(IT-1,HZO,HYO,HXO,L) * (2.0/Y)
0221          HXT = HXT + HXI(IT-1,HZO,HYO,HXO,L) * (2.0/Y)
0222          HYT = HYT + HYI(IT-1,HZO,HYO,HXO,L) * (2.0/Y)
0223 50    HZT = HZT + HZI(IT-1,HZO,HYO,HXO,L) * (2.0/Y)
0224 C
0225 C SUM THE FREQUENCY RESPONSE(imaginary and real
0226 C parts) FOR DIFFERENT VALUES OF MESH-SIZE DIVIDED
0227 C BY WAVELENGTH BUT FIRST CONVOLVE IMPULSE RESPONSE
0228 C WITH HANNING PROFILE
0229 C
0230      DIHCR = DELTA
0231      DO 55 L = 1, HUMPT
0232          T = DFLOAT(ITIME)
0233          AMT = DFLOAT(ITRATE)
0234          EXTH = EXT * (1.0 + DCOS(PI * T/AMT)) * 0.5
0235          EYTH = EYT * (1.0 + DCOS(PI * T/AMT)) * 0.5
0236          EZTH = EZT * (1.0 + DCOS(PI * T/AMT)) * 0.5
0237          HXTH = HXT * (1.0 + DCOS(PI * T/AMT)) * 0.5
0238          HYTH = HYT * (1.0 + DCOS(PI * T/AMT)) * 0.5
0239          HZTH = HZT * (1.0 + DCOS(PI * T/AMT)) * 0.5
0240      EX(1,L) = EX(1,L) + EXTH * DCOS(2.0*PI*T*DINCR)
0241      EI(2,L) = EI(2,L) + EXTH * DSIN(2.0*PI*T*DINCR)
0242      EY(1,L) = EY(1,L) + EYTH * DCOS(2.0*PI*T*DINCR)
0243      EI(2,L) = EI(2,L) + EYTH * DSIN(2.0*PI*T*DINCR)
0244      EZ(1,L) = EZ(1,L) + EZTH * DCOS(2.0*PI*T*DINCR)
0245      EZ(2,L) = EZ(2,L) + EZTH * DSIN(2.0*PI*T*DINCR)
0246      HX(1,L) = HX(1,L) + HXTH * DCOS(2.0*PI*T*DINCR)
0247      HX(2,L) = HX(2,L) + HXTH * DSIN(2.0*PI*T*DINCR)
0248      HY(1,L) = HY(1,L) + HYTH * DCOS(2.0*PI*T*DINCR)
0249      HY(2,L) = HY(2,L) + HYTH * DSIN(2.0*PI*T*DINCR)

```

Figure 7.26

(Cont.) Computer program for Example 7.5.

```

0250      HZ(1,L) = HZ(1,L) + HZTH * DCOS(2.0*PI*T*DINCR)
0251      HZ(2,L) = HZ(2,L) + HZTH * DSIN(2.0*PI*T*DINCR)
0252          OUT(1,L) = DINCR
0253  55      DINCR = DINCR + DEL
0254  60      CONTINUE
0255          DO L = 1, HUMPT
0256              CEX = CMPLX(EX(1,L),EX(2,L))
0257              CEY = CMPLX(EY(1,L),EY(2,L))
0258              CEZ = CMPLX(EZ(1,L),EZ(2,L))
0259              CHX = CMPLX(HX(1,L),HX(2,L))
0260              CHY = CMPLX(HY(1,L),HY(2,L))
0261              CHZ = CMPLX(HZ(1,L),HZ(2,L))
0262              OUT(2,L) = CABS(CEX)
0263              OUT(3,L) = CABS(CEY)
0264              OUT(4,L) = CABS(CEZ)
0265              OUT(5,L) = CABS(CHX)
0266              OUT(6,L) = CABS(CHY)
0267              OUT(7,L) = CABS(CHZ)
0268              OUT(8,L)=SQRT(SQMAG(CEX)+SQMAG(CEY)+SQMAG(CEZ))
0269              OUT(9,L)=SQRT(SQMAG(CHX)+SQMAG(CHY)+SQMAG(CHZ))
0270          END DO
0271
C  C PICK THE MODES
0272
C
0273      DO 65 L = 2, 9
0274      DO 65 K = 1, HUMPT
0275          IF(K .NE. 1 .AND. K .NE. HUMPT) THEN
0276              IF(OUT(L,K) .GT. OUT(L,K-1) .AND.
0277  1                  OUT(L,K) .GT. OUT(L,K+1)) THEN
0278                  WRITE(6,80) L,K,(OUT(J,K),J=1,9)
0279          END IF
0280      END IF
0281
0282  65      CONTINUE
0283
C  C WRITE OUT DATA FOR PLOTTING
0284
C
0285      DO 70 L = 2, 9
0286      DO 70 K = 1, HUMPT
0287          WRITE(6,75) K, OUT(1,K), OUT(L,K)
0288  70      CONTINUE
0289  75      FORMAT(I5,4F15.8)
0290  80      FORMAT(2I5,10F8.4)
0291      STOP
0292
0293      END
0001
0002  ***** THIS SUBROUTINE COMPUTES THE REFLECTED PULSES
0003
C
0004      SUBROUTINE COMPUTE(AXR,AYR,AZR,SCATTER,
0005  1          W,AXI,AYI,AZI,ISIGH)
0006
0007      IMPLICIT REAL*8(A-B,O-Z), INTEGER*2(I-H)
0008      DIMENSION AXR(2,HzE,HyE,HxE,WT),
0009  1          AYR(2,HzE,HyE,HxE,WT), SCATTER(5,5),
0010  2          AZR(2,HzE,HyE,HxE,WT), AXI(2,HzE,HyE,HxE,WT),
0011  3          AYI(2,HzE,HyE,HxE,WT), AZI(2,HzE,HyE,HxE,WT)
0012
0013      COMMON / PART1 / WT,HyB,HxE,HyE,HzB,HzE,IT
0014
0015      DO 20 K = HzB, HzE
0016          DO 20 J = HyB, HyE
0017  C      DO 20 I = HxB, HxE
0018          C  INSERT FEW LINES HERE FOR INHOMOGENEOUS CAVITY
0019          DO 15 L = 1, WT

```

Figure 7.26

(Cont.) Computer program for Example 7.5.

7.6. THREE-DIMENSIONAL TLM MESH

```

0019          AXRS = 0.0
0020          AYRS = 0.0
0021          AZRS = 0.0
0022          DO 10 M = 1, WT
0023              AXRS = AXRS+2./W*SCATTER(L,M)*AXI(IT-1,K,J,I,M)
0024              AYRS = AYRS+2./W*SCATTER(L,M)*AYI(IT-1,K,J,I,M)
0025  10          AZRS = AZRS+2./W*SCATTER(L,M)*AZI(IT-1,K,J,I,M)
0026          CONTINUE
0027          AXR(IT,K,J,I,L)=AXRS+ISIGH*AXI(IT-1,K,J,I,L)
0028          AYR(IT,K,J,I,L)=AYRS+ISIGH*AYI(IT-1,K,J,I,L)
0029          AZR(IT,K,J,I,L)=AZRS+ISIGH*AZI(IT-1,K,J,I,L)
0030  15          CONTINUE
0031  20          CONTINUE
0032          RETURN
0033          END

```

Figure 7.26

(Cont.) Computer program for Example 7.5.

Table 7.5 Resonant Wavenumber ($k_c a$) of an Empty Rectangular Cavity, Where $k_c a = 4\pi a/c$ and λ Is the Free-Space Wavelength

Modes	Exact Results	TLM Results	Error %
TM ₁₁₀	5.6636	5.6400	0.42
TE ₁₀₁	7.0249	6.9819	0.61
TM ₂₁₀ , TE ₀₁₁	7.8540	7.8112	0.54

zero at all nodes in the $12\Delta\ell \times 6\Delta\ell \times 6\Delta\ell$ TLM mesh and exciting one field component. With subroutine COMPUTE, it applies Equation (7.60) in conjunction with Equation (7.61) and (7.75) to calculate the reflected \mathbf{E} and \mathbf{H} field components at all nodes. It applies the boundary conditions and calculates the impulse response at a particular node in the mesh.

The results of the computation along with the exact analytical values for the first few modes in the cavity are shown in Table 7.5. ■

Example 7.6

Modify the TLM program in Figure 7.26 to calculate the resonant wavenumber $k_c a$ of the inhomogeneous cavities in Figure 7.27. Take $\epsilon_r = 16$, $a = \Delta\ell$, $b = 3a/10$, $d = 4a/10$, $s = 7a/12$. ■

Solution

The main program in Figure 7.26 can be used to solve this example. Only the subroutine COMPUTE requires slight modification to take care of the inhomogeneity of the cavity. The modifications in the subprogram for the cavities in Figure 7.27 (a) and (b) are shown in Figure 7.28 (a) and (b), respectively. For each modification, the few lines in Figure 7.28 are inserted in between lines 15 and 17 in subroutine COMPUTE of Figure 7.26. The results are shown in Table 7.6 for TE₁₀₁ mode. ■

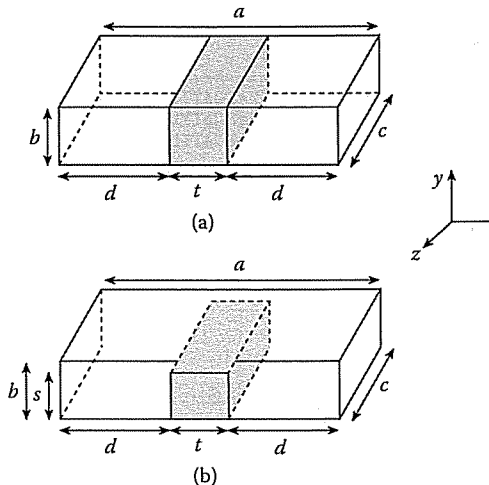


Figure 7.27

Rectangular cavity loaded with dielectric slab.

```

0001  *****
0002  C THIS SUBROUTINE COMPUTES THE REFLECTED PULSES
0003  C
0004  SUBROUTINE COMPUTE(AXR,AYR,AZR,SCATTER,
0005      1           WW,AXI,AYI,AZI,ISIGN)

:
:
:

0017  C INSERT FEW LINES HERE FOR INHOMOGENEOUS CAVITY
0018  IF ((I.GE.9).AND.(I.LE.13)
0019      1           .AND.(ISIGN.EQ.-1)) THEN
0020      HT = 5
0021      W = WW
0022  ELSE
0023      HT = 4
0024      W = 4.0
0025  END IF
:
```

Figure 7.28

(a) Modification in subroutine COMPUTE for the inhomogeneous cavity of Figure 7.27(a) (Continued).

7.7. ERROR SOURCES AND CORRECTION

```

0001  *****
0002  C THIS SUBROUTINE COMPUTES THE REFLECTED PULSES
0003  C
0004  SUBROUTINE COMPUTE(AXR,AYR,AZR,SCATTER,
0005      1           WW,AXI,AYI,AZI,ISIGN)

:
:
:

0017  C INSERT FEW LINES HERE FOR INHOMOGENEOUS CAVITY
0018  IF ((J.GT.4) GO TO 5
0019  IF ((I.GE.9).AND.(I.LE.13)
0020      1           .AND.(ISIGN.EQ.-1)) THEN
0021      HT = 5
0022      W = WW
0023  GO TO 6
0024  END IF
0025  5  CONTINUE
0026      HT = 4
0027      W = 4.0
0028  6  CONTINUE
0029  DO 15 L = 1, HT
:
```

Figure 7.28

(Cont.) (b) Modification in subroutine COMPUTE for the inhomogeneous cavity of Figure 7.27(b).

Table 7.6 Resonant Wavenumber ($k_c a$) for TE_{101} Mode of Inhomogeneous Rectangular Cavities, Where $k_c a = 4\pi a/c$, and λ Is the Free-Space Wavelength

Modes	Exact Results	TLM Results	Error %
Figure 7.27 (a)	2.589	2.5761	0.26
Figure 7.27 (b)	(none)	3.5387	

7.7 Error Sources and Correction

As in all approximate solutions such as the TLM technique, it is important that the error in the final result be minimal. In the TLM method, four principal sources of error can be identified [10, 28, 29]:

- truncation error,
- coarseness error,

- velocity error,
- misalignment error.

Each of these sources of error and ways of minimizing it will be discussed.

7.7.1 Truncation Error

The truncation error is due to the need to truncate the impulse response in time. As a result of the finite duration of the impulse response, its Fourier transform is not a line spectrum but rather a superposition of $\sin x/x$ functions, which may interfere with each other and cause a slight shift in their maxima. The maximum truncation error is given by

$$e_T = \frac{\Delta S}{\Delta \ell / \lambda_c} = \frac{3\lambda_c}{SN^2\pi^2\Delta\ell} \quad (7.83)$$

where λ_c is the cutoff wavelength to be calculated, ΔS is the absolute error in $\Delta \ell / \lambda_c$, S is the frequency separation (expressed in terms of $\Delta \ell / \lambda_c$, λ_c being the free-space wavelength) between two neighboring peaks as shown in Figure 7.29, and N is the number of iterations. Equation (7.83) indicates that e_T decreases with increasing N and increasing S . It is therefore desirable to make N large and suppress all unwanted modes close to the desired mode by carefully selecting the input and output points in the TLM mesh. An alternative way of reducing the truncation error is to use a Hanning window in the Fourier transform. For further details on this, one should consult [10, 31].

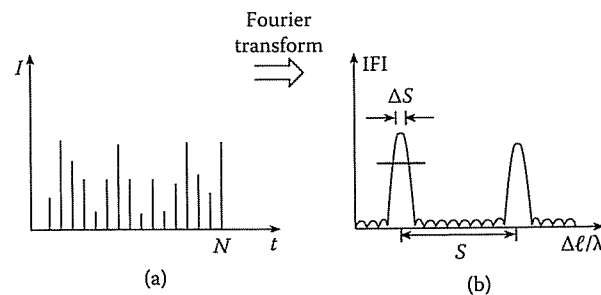


Figure 7.29
Source of truncation error: (a) Truncated output-impulse, (b) resulting truncation error in the frequency domain.

7.7.2 Coarseness Error

This occurs when the TLM mesh is too coarse to resolve highly nonuniform fields as can be found at corners and edges. An obvious solution is to use a finer mesh

7.8. ABSORBING BOUNDARY CONDITIONS

($\Delta\ell \rightarrow 0$), but this would lead to large memory requirements and there are limits to this refinement. A better approach is to use variable mesh size so that a higher resolution can be obtained in the nonuniform field region [71]. This approach requires more complicated programming.

7.7.3 Velocity Error

This stems from the assumption that propagation velocity in the TLM mesh is the same in all directions and equal to $u_n = u/\sqrt{2}$, where u is the propagation velocity in the medium filling the structure. The assumption is only valid if the wavelength λ_n in the TLM mesh is large compared with the mesh size $\Delta\ell$ ($\Delta\ell/\lambda_n < 0.1$). Thus the cutoff frequency f_{cn} in the TLM mesh is related to the cutoff frequency f_c of the real structure according to $f_c = f_{cn}\sqrt{2}$. If $\Delta\ell$ is comparable with λ_n , the velocity of propagation depends on the direction and the assumption of constant velocity results in a velocity error in f_c . Fortunately, a measure to reduce the coarseness error takes care of the velocity error as well.

7.7.4 Misalignment Error

This error occurs in dielectric interfaces in three-dimensional inhomogeneous structures such as microstrip or fin line. It is due to the manner in which boundaries are simulated in a three-dimensional TLM mesh; dielectric interfaces appear halfway between nodes, while electric and magnetic boundaries appear across such nodes. If the resulting error is not acceptable, one must make two computations, one with recessed and one with protruding dielectric, and take the average of the results.

7.8 Absorbing Boundary Conditions

Just like FDTD and FEM, the TLM method requires absorbing boundary conditions (ABCs) at the limit of the solution region. Several ABCs have been proposed for TLM simulations [32]–[37]. It has been recognized that the perfectly matched-layer (PML) technique, discussed for FDTD in Section 3.9, has excellent absorbing performances that are significantly superior to other techniques. So only PML will be discussed here.

Consider the PML region and the governing Maxwell's equations. Each field component is split into two. For example, $E_x = E_{xy} + E_{xz}$. In 3-D, Maxwell's equations become twelve [38]:

$$\mu_o \frac{\partial H_{xy}}{\partial t} + \sigma_y^* H_{xy} = -\frac{\partial(E_{zx} + E_{zy})}{\partial y} \quad (7.84a)$$

$$\mu_o \frac{\partial H_{xz}}{\partial t} + \sigma_z^* H_{xz} = \frac{\partial(E_{yx} + E_{yz})}{\partial z} \quad (7.84b)$$

$$\mu_o \frac{\partial H_{yz}}{\partial t} + \sigma_z^* H_{yz} = -\frac{\partial(E_{xy} + E_{xz})}{\partial z} \quad (7.84c)$$

$$\mu_o \frac{\partial H_{yx}}{\partial t} + \sigma_x^* H_{yx} = \frac{\partial(E_{zx} + E_{zy})}{\partial x} \quad (7.84d)$$

$$\mu_o \frac{\partial H_{zx}}{\partial t} + \sigma_x^* H_{zx} = -\frac{\partial(E_{yx} + E_{yz})}{\partial x} \quad (7.84e)$$

$$\mu_o \frac{\partial H_{zy}}{\partial t} + \sigma_y^* H_{zy} = \frac{\partial(E_{xy} + E_{xz})}{\partial y} \quad (7.84f)$$

$$\epsilon_o \frac{\partial E_{xy}}{\partial t} + \sigma_y E_{xy} = \frac{\partial(H_{zx} + H_{zy})}{\partial y} \quad (7.84g)$$

$$\epsilon_o \frac{\partial E_{xz}}{\partial t} + \sigma_z E_{xz} = -\frac{\partial(H_{yx} + H_{yz})}{\partial z} \quad (7.84h)$$

$$\epsilon_o \frac{\partial E_{yz}}{\partial t} + \sigma_z E_{yz} = \frac{\partial(H_{xy} + H_{xz})}{\partial z} \quad (7.84i)$$

$$\epsilon_o \frac{\partial E_{yx}}{\partial t} + \sigma_x E_{yx} = -\frac{\partial(H_{zx} + H_{zy})}{\partial x} \quad (7.84j)$$

$$\epsilon_o \frac{\partial E_{zx}}{\partial t} + \sigma_x E_{zx} = \frac{\partial(H_{yx} + H_{yz})}{\partial x} \quad (7.84k)$$

$$\epsilon_o \frac{\partial E_{zy}}{\partial t} + \sigma_y E_{zy} = -\frac{\partial(H_{xy} + H_{xz})}{\partial y} \quad (7.84l)$$

in which (σ_i, σ_i^*) where $i \in \{x, y, z\}$ are, respectively, the electric and magnetic conductivities of the PML region and they satisfy

$$\frac{\sigma_i}{\epsilon_o} = \frac{\sigma_i^*}{\mu_o} \quad (7.85)$$

Using the usual Yees's notation, the field samples are expressed as

$$\begin{aligned} E_x^n(i, j, k) &= E_x[(i + 1/2)\delta, j\delta, k\delta, (n + 1/2)\delta t] \\ E_y^n(i, j, k) &= E_y[i\delta, (j + 1/2)\delta, k\delta, (n + 1/2)\delta t] \\ E_z^n(i, j, k) &= E_z[i\delta, j\delta, (k + 1/2)\delta, (n + 1/2)\delta t] \\ H_x^n(i, j, k) &= H_x[i\delta, (j + 1/2)\delta, (k + 1/2)\delta, n\delta t] \\ H_y^n(i, j, k) &= H_y[(i + 1/2)\delta, j\delta, (k + 1/2)\delta, n\delta t] \\ H_z^n(i, j, k) &= H_z[(i + 1/2)\delta, (j + 1/2)\delta, k\delta, n\delta t] \end{aligned} \quad (7.86)$$

where $\delta = \Delta x = \Delta y = \Delta z = \Delta \ell$. Without loss of generality, we set $\delta t = \delta/2c$. Since we want to interface the FDTD algorithm with the TLM, we express the fields in

7.9. CONCLUDING REMARKS

terms of voltages. For a cubic cell,

$$V_{ers}^n(i, j, k) = \delta E_{rs}^n(i, j, k) \quad \text{with } r \in \{x, y\}, s \in \{x, z\} \quad (7.87a)$$

$$V_{ms}^n(i, j, k) = \sqrt{\frac{\mu_o}{\epsilon_o}} \delta H_s^n(i, j, k) \quad \text{with } s \in \{y, z\} \quad (7.87b)$$

where the subscripts e and m denote electric and magnetic, respectively. By applying the central-difference scheme to Equation (7.84), we obtain, after some algebraic manipulations,

$$\begin{aligned} V_{exy}^n(i, j, k) &= \left(\frac{4 - G_{ey}}{4 + G_{ey}} \right) V_{exy}^{n-1}(i, j, k) \\ &\quad + \left(\frac{2}{4 + G_{ey}} \right) (V_{mz}^n(i, j, k) - V_{mz}^n(i, j - 1, k)) \end{aligned} \quad (7.88a)$$

$$\begin{aligned} V_{exz}^n(i, j, k) &= \left(\frac{4 - G_{ez}}{4 + G_{ez}} \right) V_{exz}^{n-1}(i, j, k) \\ &\quad - \left(\frac{2}{4 + G_{ez}} \right) (V_{my}^n(i, j, k) - V_{my}^n(i, j, k - 1)) \end{aligned} \quad (7.88b)$$

$$V_{ex}^n(i, j, k) = V_{exy}^n(i, j, k) + V_{exz}^n(i, j, k) \quad (7.88c)$$

where $G_{es} = \delta \sigma_s(i, j, k) \sqrt{\mu_o \epsilon_o}$ with $s \in \{y, z\}$. Applying this TLM FDTD-PML algorithm has been found to yield excellent performance with reflection level below -55 dB [37].

7.9 Concluding Remarks

This chapter has described the TLM method which is a modeling process rather than a numerical method for solving differential equations. The flexibility, versatility, and generality of the time-domain method have been demonstrated. Our discussion in this chapter has been introductory, and one is advised to consult [10], [39]–[41] for a more in-depth treatment. A generalized treatment of TLM in the curvilinear coordinate system is presented in [42], while a theoretical basis of TLM is derived in [43]. Further developments in TLM can be found in [44]–[50].

Although the application of the TLM method in this chapter has been limited to diffusion and wave propagation problems, the method has a wide range of applications. The technique has been applied to other problems including:

- cutoff frequencies in fin lines [29, 30],
- transient analysis of striplines [51, 52],
- linear and nonlinear lumped networks [53]–[58],

- microstrip lines and resonators [17, 59, 60],
- diffusion problems [61]–[63],
- electromagnetic compatibility problems [21], [64]–[67],
- antenna problems [43, 53, 68, 69],
- induced currents in biological bodies exposed to EM fields [70],
- cylindrical and spherical waves [53, 71, 72], and
- others [73]–[78].

A major advantage of the TLM method, as compared with other numerical techniques, is the ease with which even the most complicated structures can be analyzed. The great flexibility and versatility of the method reside in the fact that the TLM mesh incorporates the properties of EM fields and their interaction with the boundaries and material media. Hence, the EM problem need not be formulated for every new structure. Thus a general-purpose program such as in [79] can be developed such that only the parameters of the structure need be entered for computation. Another advantage of using the TLM method is that certain stability properties can be deduced by inspection of the circuit. There are no problems with convergence, stability or spurious solutions. The method is limited only by the amount of memory storage required, which depends on the complexity of the TLM mesh. Also, being an explicit numerical solution, the TLM method is suitable for nonlinear or inhomogeneous problems since any variation of material properties may be updated at each time step.

Perhaps the best way to conclude this chapter is to compare the TLM method with the finite difference method, especially FDTD [80]–[86]. While TLM is a physical model based on Huygens' principle using interconnected transmission lines, the FDTD is an approximate mathematical model directly based on Maxwell's equations. In the two-dimensional TLM, the magnetic and electric field components are located at the same position with respect to space and time, whereas in the corresponding two-dimensional FDTD cell, the magnetic field components are shifted by half an interval in space and time with respect to the electric field components. Due to this displacement between electric and magnetic field components in Yee's FDTD, Chen et al. [83] derived a new FDTD and demonstrated that the new FDTD formulation is exactly equivalent to the symmetric condensed node model used in the TLM method. This implies that the TLM algorithm can be formulated in FDTD form and vice versa. However, both algorithms retain their unique advantages. For example, the FDTD model has a simpler algorithm where constitutive parameters are directly introduced, while the TLM has certain advantages in the modeling of boundaries and the partitioning of the solution region. Furthermore, the FDTD requires less than one-half of the CPU time spent by the equivalent TLM program under identical conditions. While the TLM scheme requires 22 real memory stores per node, the FDTD method requires only seven real memory stores per 3-D node in an isotropic dielectric medium [81]. Although both are time-domain schemes, the quantities available at each time step

are the solution in TLM model and there is no need for an iterative procedure. The dispersion relations for TLM and FDTD are identical for 2-D but are different for 3-D problems. The comparison is summarized in Table 7.7. According to Johns, the two methods complement each other rather than compete with each other [80].

Table 7.7 A Comparison of TLM and FDTD Methods

FDTD	TLM
A mathematical model based on Maxwell's equations	A physical model based on Huygen's principle
E and H are shifted with respect to space and time	E and H are calculated at the same time and position
Requires less memory and one-half the CPU time	Needs more memory and more CPU time
Provides solution at each time step	Requires some iterative procedure

References

- [1] G. Kron, "Numerical solution of ordinary and partial differential equations by means of equivalent circuits," *J. Appl. Phys.*, vol. 16, Mar. 1945, pp. 172–186.
- [2] C.H. Durney and C.C. Johnson, *Introduction to Modern Electromagnetics*. New York: McGraw-Hill, 1969, pp. 286–287.
- [3] P.P. Silvester and F.L. Ferrari, *Finite Elements for Electrical Engineers*. New York: Cambridge University Press, 1983, p. 24.
- [4] R.H. Park, "Definition of an ideal synchronous machine and formulators for armature flux linkages," *Gen. Elect. Rev.*, vol. 31, 1928, pp. 332–334.
- [5] G. Kron, "Equivalent circuit of the field equations of Maxwell," *Proc. IRE*, May 1944, pp. 289–299.
- [6] G. Kron, *Equivalent Circuits of Electrical Machinery*. New York: John Wiley, 1951.
- [7] N. Marcovitz and J. Schwinger, "On the reproduction of the electric and magnetic fields produced by currents and discontinuity in wave guides, I," *J. Appl. Phys.*, vol. 22, no. 6, June 1951, pp. 806–819.
- [8] J. Schwinger and D.S. Saxon, *Discontinuities in Waveguides*. New York: Gordon and Breach, 1968.

- [9] P.B. Johns and R.L. Beurle, "Numerical solution of 2-dimensional scattering problems using a transmission line matrix," *Proc. IEEE*, vol. 118, no. 9, Sept. 1971, pp. 1203–1208.
- [10] W.J.R. Hoefer, "The transmission-line matrix method—theory and applications," *IEEE Trans. Microwave Theory Tech.*, vol. MTT-33, no. 10, Oct. 1985, pp. 882–893.
- [11] C. Christopoulos, *The Transmission-Line Modeling Method (TLM)*. New York: IEEE Press, 1995.
- [12] M.N.O. Sadiku and L.C. Agba, "A simple introduction to the transmission-line modeling," *IEEE Trans. Cir. Sys.*, vol. CAS-37, no. 8, Aug. 1990, pp. 991–999.
- [13] B.J. Ley, *Computer Aided Analysis and Design for Electrical Engineers*. New York: Holt, Rinehart and Winston, 1970, pp. 815–817.
- [14] M.N.O. Sadiku, *Elements of Electromagnetics*, 4th ed. New York: Oxford Univ. Press, 2007.
- [15] C.C. Wong, "Solution of the network analog of one-dimensional field equations using the ladder method," *IEEE Trans. Educ.*, vol. E-28, no. 3, Aug. 1985, pp. 176–179.
- [16] C.C. Wong and W.S. Wong, "Multigrid TLM for diffusion problems," *Int. J. Num. Model.*, vol. 2, no. 2, 1989, pp. 103–111.
- [17] G.E. Marike and G. Yek, "Dynamic three-dimensional T.L.M. analysis of microstrip lines on anisotropic substrate," *IEEE Trans. Micro. Theo. Tech.*, vol. MTT-33, no. 9, Sept. 1985, pp. 789–799.
- [18] P.B. Johns, "Applications of the transmission-line matrix method to homogeneous waveguides of arbitrary cross-section," *Proc. IEEE*, vol. 119, no. 8, Aug. 1972, pp. 1086–1091.
- [19] R.A. Waldron, *Theory of Guided Electromagnetic Waves*. London: Van Nostrand Reinhold Co., 1969, pp. 157–172.
- [20] N.R.S. Simons and E. Bridges, "Method for modeling free space boundaries in TLM situations," *Elec. Lett.*, vol. 26, no. 7, March 1990, pp. 453–455.
- [21] C. Christopoulos and J.L. Herring, "The application of the transmission-line modeling (TLM) to electromagnetic compatibility problems," *IEEE Trans. Elect. Magn. Comp.*, vol. 35, no. 2, May 1993, pp. 185–191.
- [22] L.C. Agba, "Transmission-line-matrix modeling of inhomogeneous rectangular waveguides and cavities," M.Sc. thesis, Department of Electrical and Computer Engineering, Florida Atlantic University, Boca Raton, Aug. 1987.
- [23] P.B. Johns, "The solution of inhomogeneous waveguide problems using a transmission line matrix," *IEEE Trans. Micro. Theo. Tech.*, vol. MTT-22, no. 3, Mar. 1974, pp. 209–215.

REFERENCES

- [24] S. Akhtarzad and P.B. Johns, "Generalized elements for t.l.m. method of numerical analysis," *Proc. IEEE*, vol. 122, no. 12, Dec. 1975, pp. 1349–1352.
- [25] S. Akhtarzad and P.B. Johns, "Numerical solution of lossy waveguides: T.L.M. computer programs," *Elec. Lett.*, vol. 10, no. 15, July 25, 1974, pp. 309–311.
- [26] S. Akhtarzad and P.B. Johns, "Transmission line matrix solution of waveguides with wall losses," *Elec. Lett.*, vol. 9, no. 15, July 1973, pp. 335–336.
- [27] S. Akhtarzad and P.B. Johns, "Solution of Maxwell's equations in three space dimensional and time by the T.L.M. method of numerical analysis," *Proc. IEEE*, vol. 122, no. 12, Dec. 1975, pp. 1344–1348.
- [28] S. Akhtarzad and P.B. Johns, "Three-dimensional transmission-line matrix computer analysis of microstrip resonators," *IEEE Trans. Micro. Theo. Tech.*, vol. MTT-23, no. 12, Dec. 1975, pp. 990–997.
- [29] Y.C. Shih and W.J.R. Hoefer, "The accuracy of TLM analysis of finned rectangular waveguides," *IEEE Trans. Micro. Theo. Tech.*, vol. MTT-28, no. 7, July 1980, pp. 743–746.
- [30] Y.C. Shih and W.J.R. Hoefer, "Dominant and second-order mode cutoff frequencies in fin lines calculated with a two-dimensional TLM program," *IEEE Trans. Micro. Theo. Tech.*, vol. MTT-28, no. 12, Dec. 1980, pp. 1443–1448.
- [31] N. Yoshida, et al., "Transient analysis of two-dimensional Maxwell's equations by Bergeron's method," *Trans. IECE (Japan)*, vol. J62B, June 1979, pp. 511–518.
- [32] J.A. Morente, J.A. Porti, and M. Khalladi, "Absorbing boundary conditions for the TLM method," *IEEE Trans. Micro. Theo. Tech.*, vol. 40, no. 11, Nov. 1992, pp. 2095–2099.
- [33] S.C. Pomeroy, G. Zhang, and C. Wykes, "Variable coefficient absorbing boundary condition for TLM," *Elec. Lett.*, vol. 29, no. 13, June 1993, pp. 1198–1200.
- [34] C. Eswarappa and W.J.R. Hoefer, "One-way equation absorbing boundary conditions for 3-D TLM analysis of planar and quasi-planar structures," *IEEE Trans. Micro. Theo. Tech.*, vol. 42, no. 9, Sept. 1994, pp. 1669–1677.
- [35] N. Kukutsu and R. Konno, "Super absorption boundary conditions for guided waves in the 3-D TLM simulation," *IEEE Micro. Guided Wave Lett.*, vol. 5, Sept. 1995, pp. 299–301.
- [36] N. Pena and M.M. Ney, "A new TLM node for Berenger's perfectly matched layer (PML)," *IEEE Micro. Guided Wave Lett.*, vol. 6, Nov. 1996, pp. 410–412.
- [37] N. Pena and M.M. Ney, "Absorbing-boundary conditions using perfectly matched-layer (PML) technique for three-dimensional TLM simulations," *IEEE Trans. Micro. Theo. Tech.*, vol. 45, no. 10, Oct. 1997, pp. 1749–1755.

- [38] A. Taflove, *Computational Electrodynamics*. Boston: Artech House, 1995, pp. 189–190.
- [39] P.B. Johns, “Numerical modeling by the TLM method,” in A. Wexler (ed.), *Large Engineering Systems*. Oxford: Pergamon, 1977.
- [40] T. Itoh (ed.), *Numerical Techniques for Microwave and Millimeterwave Passive Structure*. New York: John Wiley, 1989, pp. 496–591.
- [41] P.B. Johns, “Simulation of electromagnetic wave interactions by transmission-line modeling (TLM),” *Wave Motion*, vol. 10, no. 6, 1988, pp. 597–610.
- [42] A.K. Bhattacharyya and R. Garg, “Generalized transmission line model for microstrip patches,” *IEEE Proc.*, vol. 132, Pt. H, no. 2, April 1985, pp. 93–98.
- [43] M. Krumpholz and P. Russer, “A field theoretical derivation of TLM,” *IEEE Trans. Micro. Theo. Tech.*, vol. 42, no. 9, Sept. 1994, pp. 1660–1668.
- [44] P. Naylor and C. Christopoulos, “A comparison between the time-domain and the frequency-domain diakopic methods of solving field problems by transmission-line modeling,” *Int. J. Num. Model.*, vol. 2, no. 1, 1989, pp. 17–30.
- [45] P. Saguet, “The 3-D transmission-line matrix method theory and comparison of the processes,” *Int. J. Num. Model.*, vol. 2, 1989, pp. 191–201.
- [46] W.J.R. Hoefer, “The discrete time domain Green’s function or Johns’ matrix — a new powerful concept in transmission line modeling (TLM),” *Int. J. Num. Model.*, vol. 2, no. 4, 1989, pp. 215–225.
- [47] L.R.A.X. de Menezes and W.J.R. Hoefer, “Modeling of general constitutive relationship in SCN TLM,” *IEEE Trans. Micro. Theo. Tech.*, vol. 44, no. 6, June 1996, pp. 854–861.
- [48] V. Trenkic, C. Christopoulos, and T.M. Benson, “Simple and elegant formulation of scattering in TLM nodes,” *Elec. Lett.*, vol. 29, no. 18, Sept. 1993, pp. 1651–1652.
- [49] J.L. Herring and C. Christopoulos, “Solving electromagnetic field problems using a multiple grid transmission-line modeling method,” *IEEE Trans. Ant. Prop.*, vol. 42, no. 12, Dec. 1994, pp. 1655–1658.
- [50] J.A. Porti, J.A. Morente, and M.C. Carrion, “Simple derivation of scattering matrix for TLM nodes,” *Elec. Lett.*, vol. 34, no. 18, Sept. 1998, pp. 1763–1764.
- [51] N. Yoshida, I. Fukai, and J. Fukuoka, “Transient analysis of three-dimensional electromagnetic fields by nodal equations,” *Trans. Inst. Electron. Comm. Engr. Japan*, vol. J63B, Sept. 1980, pp. 876–883.
- [52] N. Yoshida and I. Fukai, “Transient analysis of a stripline having corner in three-dimensional space,” *IEEE Trans. Micro. Theo. Tech.*, vol. MTT-32, no. 5, May 1984, pp. 491–498.

REFERENCES

- [53] W.R. Zimmerman, “Network analog of Maxwell’s field equations in one and two dimensions,” *IEEE Trans. Educ.*, vol. E-25, no. 1, Feb. 1982, pp. 4–9.
- [54] P.B. Johns and M. O’Brien, “Use of the transmission-line modeling (T.L.M.) method to solve non-linear lumped networks,” *Radio Electron. Engr.*, vol. 50, no. 1/2, Jan./Feb., 1980, pp. 59–70.
- [55] J.W. Bandler et al., “Transmission-line modeling and sensitivity evaluation for lumped network simulation and design in the time domain,” *J. Franklin Inst.*, vol. 304, no. 1, 1971, pp. 15–23.
- [56] C.R. Brewitt-Taylor and P.B. Johns, “On the construction and numerical solution of transmission line and lumped network models of Maxwell’s equations,” *Int. J. Num. Meth. Engr.*, vol. 15, 1980, pp. 13–30.
- [57] P. Saguet and W.J.R. Hoefer, “The modeling of multiaxial discontinuities in quasi-planar structures with the modified TLM method,” *Int. J. Num. Model.*, vol. 1, 1988, pp. 7–17.
- [58] E.M. El-Sayed and M.N. Morsy, “Analysis of microwave ovens loaded with lossy process materials using the transmission-line matrix method,” *Int. J. Num. Meth. Engr.*, vol. 20, 1984, pp. 2213–2220.
- [59] N.G. Alexopoulos, “Integrated-circuit structures on anisotropic substrates,” *IEEE Trans. Micro. Theo. Tech.*, vol. MTT-33, no. 10, Oct. 1985, pp. 847–881.
- [60] S. Akhatarzad and P.B. Johns, “TLMRES—the TLM computer program for the analysis of microstrip resonators,” *IEEE Trans. Micro. Theo. Tech.*, vol. 35, no. 1, Jan. 1987, pp. 60–61.
- [61] P.B. Johns, “A simple explicit and unconditionally stable numerical routine for the solution of the diffusion equation,” *Int. J. Num. Methods Engr.*, vol. 11, 1977, pp. 1307–1328.
- [62] P.B. Johns and G. Butler, “The consistency and accuracy of the TLM method for diffusion and its relationship to existing methods,” *Int. J. Num. Methods Engr.*, vol. 19, 1983, pp. 1549–1554.
- [63] P.W. Webb, “Simulation of thermal diffusion in transistors using transmission line matrix modeling,” *Electron. Comm. Engr. Jour.*, vol. 4, no. 6, Dec. 1992, pp. 362–366.
- [64] P. Naylor, C. Christopoulos, and P.B. Johns, “Coupling between electromagnetic field and wires using transmission-line modeling,” *IEEE Proc.*, Pt. A, vol. 134, no. 8, 1987, pp. 679–686.
- [65] P. Naylor and C. Christopoulos, “A new wire node for modeling thin wires in electromagnetic field problems solved by transmission line modeling,” *IEEE Trans. Micro. Theo. Tech.*, vol. 38, no. 3, March 1990, pp. 328–330.

- [66] J.A. Porti et al., "Comparison of the thin-wire models for TLM method," *Elect. Lett.*, vol. 28, no. 20, Sept. 1992, pp. 1910–1911.
- [67] A.P. Duffy et al., "New methods for accurate modeling of wires using TLM," *Elect. Lett.*, vol. 29, no. 2, Jan. 1993, pp. 224–226.
- [68] I. Palocz and N. Marcovitz, "A network-oriented approach in the teaching of electromagnetics," *IEEE Trans. Educ.*, vol. E-28, no. 3, Aug. 1985, pp. 150–154.
- [69] H. Pues and A. Van de Capelle, "Accurate transmission-line model for the rectangular microstrip antenna," *IEEE Proc.*, vol. 131, Pt. H, no. 6, Dec. 1984, pp. 334–340.
- [70] J.F. Deford and O.P. Gandhi, "An impedance method to calculate currents induced in biological bodies exposed to quasi-static electromagnetic fields," *IEEE Trans. Elect. Comp.*, vol. EMC-27, no. 3, Aug. 1985, pp. 168–173.
- [71] D.A. Al-Mukhtar and T.E. Sitch, "Transmission-line matrix method with irregularly graded space," *IEEE Proc.*, vol. 128, Pt. H, no. 6, Dec. 1981, pp. 299–305.
- [72] H.L. Thal, "Exact circuit analysis of spherical waves," *IEEE Trans. Ant. Prog.*, vol. AP-26, no. 2, Mar. 1978, pp. 282–287.
- [73] C.V. Jones and D.L. Prior, "Unification of fields and circuit theories of electrical machines," *Proc. IEEE*, vol. 119, no. 7, July 1972, pp. 871–876.
- [74] P. Hammond and G.J. Rogers, "Use of equivalent circuits in electrical-machine studies," *Proc. IEEE*, vol. 121, no. 6, June 1974, pp. 500–507.
- [75] E.M. Freeman, "Equivalent circuits from electromagnetic theory: low-frequency induction devices," *Proc. IEEE*, vol. 121, no. 10, Oct. 1974, pp. 1117–1121.
- [76] W.J. Karplus and W.W. Soroka, *Analog Methods: Computation and Simulation*. New York: McGraw-Hill, 1959.
- [77] G.L. Ragan (ed.), *Microwave Transmission Circuits*. New York: McGraw-Hill, 1948, pp. 544–547.
- [78] R.H. MacNeal, *Electric Circuit Analogies for Elastic Structures*, vol. 2. New York: John Wiley & Sons, 1962.
- [79] S. Akhtarzad, "Analysis of lossy microwave structures and microstrip resonators by the TLM method," Ph.D. thesis, University of Nottingham, England, July 1975.
- [80] P.B. Johns, "On the relationship between TLM and finite-difference methods for Maxwell's equations," *IEEE Trans. Micro. Theo. Tech.*, vol. MTT-35, no. 1, Jan. 1987, pp. 60, 61.
- [81] D.H. Choi and W.J.R. Hoefer, "The finite-difference time-domain method and its application to eigenvalue problems," *IEEE Trans. Micro. Theo. Tech.*, vol. 34, no. 12, Dec. 1986, pp. 1464–1472.

- [82] D.H. Choi, "A comparison of the dispersion characteristics associated with the TLM and FD-TD methods," *Int. J. Num. Model.*, vol. 2, 1989, pp. 203–214.
- [83] Z. Chen, M. Ney, and W.J.R. Hoefer, "A new finite-difference time-domain formulation and its equivalence with the TLM symmetrical condensed node," *IEEE Trans. Micro. Theo. Tech.*, vol. 39, no. 12, Dec. 1992, pp. 2160–2169.
- [84] M. Krumpholz and P. Russer, "Two-dimensional FDTD and TLM," *Int. J. Num. Model.*, vol. 7, no. 2, 1994, pp. 141–143.
- [85] M. Krumpholz and P. Russer, "On the dispersion of TLM and FDTD," *IEEE Trans. Micro. Theo. Tech.*, vol. 42, no. 7, July 1994, pp. 1275–1279.
- [86] M. Krumpholz, C. Huber, and P. Russer, "A field theoretical comparison of FDTD and TLM," *IEEE Trans. Micro. Theo. Tech.*, vol. 43, no. 8, Aug. 1995, pp. 1935–1950.

Problems

- 7.1 A conductor has a uniform resistance R per unit length and leakage conductance G per unit length. Show that the potential V at a point distant x from one end satisfies the differential equation

$$\frac{d^2V}{dx^2} - RGV = 0$$
- 7.2 For the two-port network in Figure 7.30 (a), the relation between the input and output variables can be written in matrix form as

$$\begin{bmatrix} V_1 \\ I_1 \end{bmatrix} = \begin{bmatrix} A & B \\ C & D \end{bmatrix} \begin{bmatrix} V_2 \\ -I_2 \end{bmatrix}$$

For the lossy line in Figure 7.30 (b), show that the ABCD matrix (also called the cascaded matrix) is

$$\begin{bmatrix} \cosh \gamma \ell & Z_0 \sinh \gamma \ell \\ \frac{1}{Z_0} \sinh \gamma \ell & \cosh \gamma \ell \end{bmatrix}$$

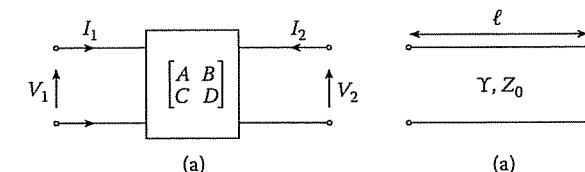
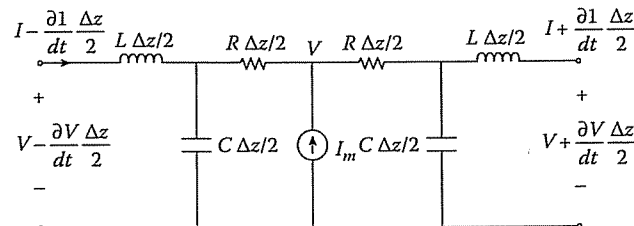


Figure 7.30
For Problem 7.2.

**Figure 7.31****For Problem 7.3.**

- 7.3 The circuit in Figure 7.31 is used to model diffusion processes and presents a Δz section of a lossy transmission line. Show that

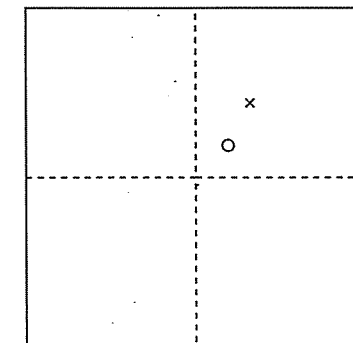
$$\frac{\partial^2 V}{\partial z^2} = -Ri + RC \frac{\partial V}{\partial t} - L \frac{\partial i}{\partial t} + LC \frac{\partial^2 V}{\partial t^2}$$

where $i = I_m / \Delta z$, the current density.

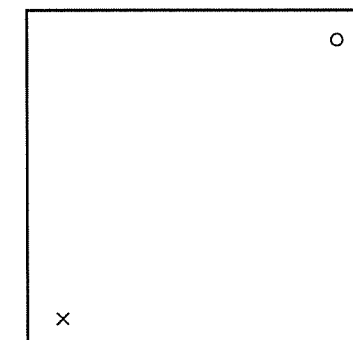
- 7.4 Consider an EM wave propagation in a lossless medium in TEM mode ($E_y = 0 = E_z = H_z = H_x$) along the z direction. Using one-dimensional TLM mesh, derive the equivalencies between network and field quantities.
- 7.5 Modify the program in Figure 7.14 to calculate the cutoff frequency (expressed in terms of $\Delta\ell/\lambda$) in a square section waveguide of size $10\Delta\ell$. Perform the calculation for the TM_{11} mode by using open-circuit symmetry boundaries to suppress even-order modes and by taking the excitation and output points as in Figure 7.32 to suppress the TM_{13} , TM_{33} , and TM_{15} modes. Use $N = 500$.
- 7.6 Repeat Problem 7.5 of higher-order modes but take excitation and output points as in Figure 7.33.
- 7.7 For the waveguide with a free space discontinuity considered in Example 7.2, plot the variation of the magnitude of the normalized impedance of the guide with $\Delta\ell/\lambda$. The plot should be for frequencies above and below the cutoff frequency, i.e., including both evanescent and propagating modes.
- 7.8 Rework Example 7.4, but take the output point at $(x = 6, z = 13)$.
- 7.9 Verify Equation (7.62).
- 7.10 For transverse waves on a stub-loaded transmission-line matrix, the dispersion relation is given by

$$\sin^2\left(\frac{\beta_n \Delta\ell}{2}\right) = 2(1 + Y_o/4) \sin^2\left(\frac{\omega \Delta\ell}{2c}\right)$$

Plot the velocity characteristic similar to that in Figure 7.11 for $Y_o = 0, 1, 2, 10, 20, 100$.



- Short circuit boundary
- - - Open circuit boundary
- Source point
- × Output point

Figure 7.32**Square cross section waveguide of Problem 7.5.**

- Short circuit boundary
- Source point
- × Output point

Figure 7.33**Square cross section waveguide of Problem 7.6.**

- 7.11 Verify Equation (7.68).

- 7.12 The transmission equation for one cell in a stub-loaded three-dimensional TLM network is

$$\begin{bmatrix} V_i \\ I_i \end{bmatrix} = T \cdot \begin{bmatrix} 1 & j(2+z_o)\tan\theta/2 \\ 0 & 1 \end{bmatrix} \cdot T \cdot T \cdot \begin{bmatrix} 1 & 0 \\ g_o + j(2+y_o)\tan\theta/2 & 1 \end{bmatrix} \cdot T \cdot \begin{bmatrix} V_{i+1} \\ I_{i+1} \end{bmatrix}$$

where

$$T = \begin{bmatrix} \cos\theta/4 & j\sin\theta/4 \\ j\sin\theta/4 & \cos\theta/4 \end{bmatrix}$$

$\theta = 2\pi\Delta\ell/\lambda$, $y_o = 4(\epsilon_r - 1)$, $z_o = 4(\mu_r - 1)$, and $g_o = \sigma\Delta\ell\sqrt{L/C}$. Assuming small losses $\alpha_n\Delta\ell \ll 1$, show that the transmission equation can be reduced to

$$\begin{bmatrix} V_i \\ I_i \end{bmatrix} = \begin{bmatrix} e^{\gamma_n\Delta\ell} & 0 \\ 0 & e^{\gamma_n\Delta\ell} \end{bmatrix} \begin{bmatrix} V_{i+1} \\ I_{i+1} \end{bmatrix}$$

where $\gamma_n = \alpha_n + j\beta_n$ is the propagation constant and

$$\begin{aligned} \cos(\beta_n\Delta\ell) &= 1 - 8(1 + y_o/4)(1 + z_o/4)\sin^2\theta/2 \\ \alpha_n\Delta\ell \sin(\beta_n\Delta\ell) &= \frac{g_o}{2}(4 + z_o)\sin\theta/2\cos\theta/2 \end{aligned}$$

- 7.13 In the y - z plane of a symmetric condensed node of the TLM mesh, the normalized characteristic impedance of the inductive stub is

$$Z_x = \frac{2\mu_r}{u_o\Delta t} \cdot \frac{\Delta y\Delta z}{\Delta x} - 4$$

Assuming that $\Delta x = \Delta y = \Delta z = 0.1$ m, determine the stubs required to model a medium with $\epsilon_r = 4$, $\mu_r = 1$, $u_o = c$, and the value of Δt for stability.

- 7.14 Consider the 61×8 rectangular matrix with boundaries at $x = 0.5$ and $x = 8.5$ as in Figure 7.34. By making one of the boundaries, say $x = 8.5$, an open circuit, a waveguide of twice the width can be simulated. For the TE_{m0} family of modes, excite the system at all points on line $z = 1$ with impulses corresponding to E_y and take the impulse function of the output at point $x = 7$, $z = 6$. Calculate the normalized wave impedance $Z = E_y/H_x$ for frequencies above cutoff, i.e., $\Delta\ell/\lambda = 0.023, 0.025, 0.027, \dots, 0.041$. Take $\sigma = 0$, $\epsilon_r = 2$, $\mu_r = 1$.
- 7.15 Repeat Problem 7.14 for a lossy waveguide with $\sigma = 278$ mhos/m, $\epsilon_r = 1$, $\mu_r = 1$.
- 7.16 Using the TLM method, determine the cutoff frequency (expressed in terms of $\Delta\ell/\lambda$) of the lowest order TE and TM modes for the square waveguide with cross section shown in Figure 7.35. Take $\epsilon_r = 2.45$.
- 7.17 For the dielectric ridge waveguide of Figure 7.36, use the TLM method to calculate the cutoff wavenumber k_c of the dominant mode. Express the result in terms of $k_c a (= \omega a/c)$ and try $\epsilon_r = 2$ and $\epsilon_r = 8$. Take $a = 10\Delta\ell$.

PROBLEMS

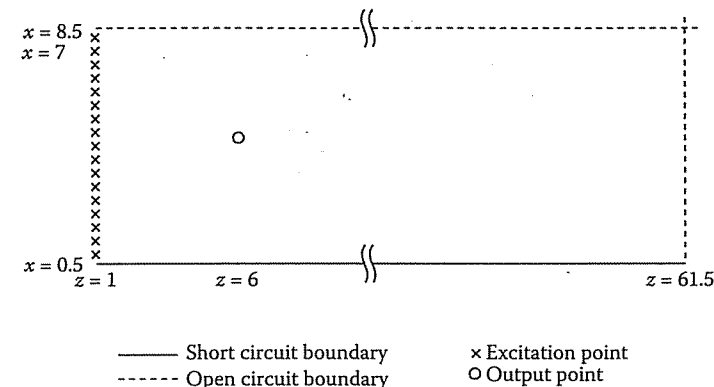


Figure 7.34
The 61×8 TLM mesh of Problem 7.14.

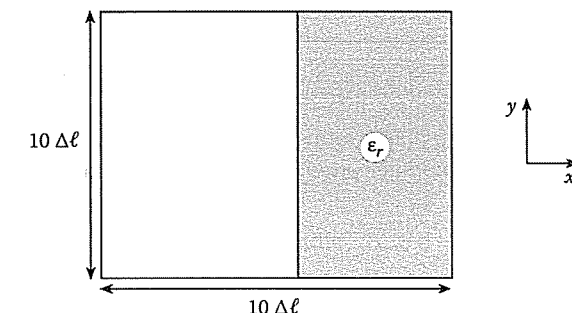


Figure 7.35
For Problem 7.16.

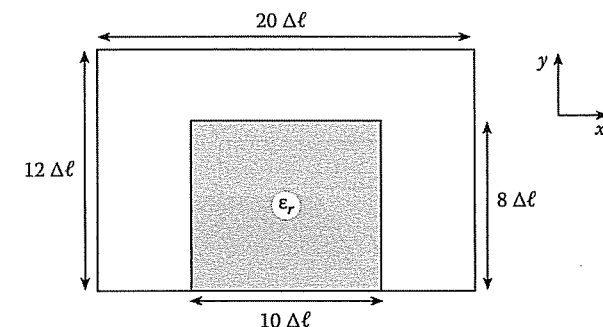


Figure 7.36
For Problem 7.17.

- 7.18 Rework Example 7.6 for the inhomogeneous cavity of Figure 7.37. Take $\epsilon_r = 16$, $a = 12\Delta\ell$, $b = 3a/10$, $d = 4a/10$, $s = 7a/12$, $u = 3d/8$.

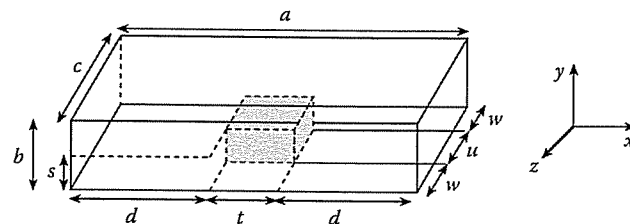


Figure 7.37

The inhomogeneous cavity of Problem 7.18.

- 7.19 Consider a single microstrip line shown in Figure 7.38. Dispersion analysis of the line by the TLM method involves resonating a section of the transmission line by placing shorting planes along the axis of propagation (the z-axis in this case). Write a TLM computer program and specify the input data as

$$\begin{aligned} E_x &= 0 = E_z \text{ along } y = 0, y = b, \\ E_x &= 0 = E_z \text{ along } x = 2a, \\ E_x &= 0 = E_z \text{ for } y = H, -W \leq x \leq W, \\ H_y &= 0 = H_z \text{ along } x = 0 \end{aligned}$$

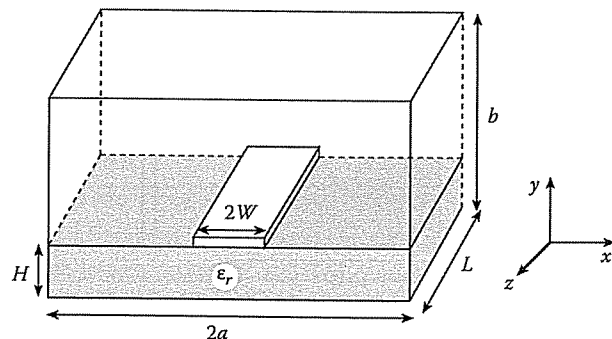


Figure 7.38

The microstrip line of Problem 7.19.

Plot the dispersion curves depicting the phase constant β as a function of frequency f for cases when the line is air-filled and dielectric-filled. The distance $L (= \pi/\beta)$ between the shorting planes is the variable. Assume the dielectric substrate and the walls of the enclosure are lossless. Take $\epsilon_r = 4.0$, $a = 2 \text{ mm}$, $H = 1.0 \text{ mm}$, $W = 1.0 \text{ mm}$, $b = 2 \text{ mm}$, $\Delta\ell = a/8$.

- 7.20 For the cubical cavity of Figure 7.39, use the TLM technique to calculate the time taken for the total power in the lossy dielectric cavity to decay to $1/e$ of its original value. Consider cases when the cavity is completely filled with dielectric material and half-filled. Take $\epsilon_r = 2.45$, $\sigma = 0.884 \text{ mhos/m}$, $\mu_r = 1$, $\Delta\ell = 0.3 \text{ cm}$, $2a = 7\Delta\ell$.

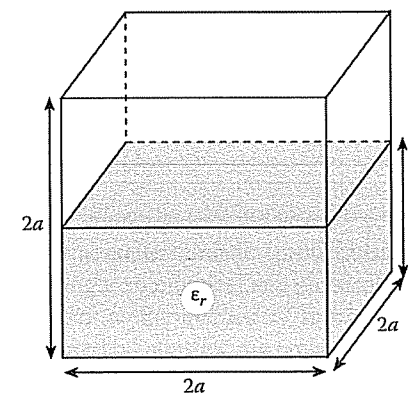


Figure 7.39

The lossy cavity of Problem 7.20.